UNIVERSIDAD AUTONOMA DE MADRID

FACULTAD DE CIENCIAS
DEPARTAMENTO DE BIOLOGÍA MOLECULAR

DISEÑO DE UNA VACUNA PARA PREVENIR LA INFECCIÓN POR EL CORONAVIRUS CAUSANTE DEL SÍNDROME RESPIRATORIO AGUDO Y GRAVE

JOSÉ ANGEL REGLA NAVA

Madrid, Julio de 2015

UNIVERSIDAD AUTÓNOMA DE MADRID

FACULTAD DE CIENCIAS

DEPARTAMENTO DE BIOLOGÍA MOLECULAR

DISEÑO DE UNA VACUNA PARA PREVENIR LA INFECCIÓN POR EL CORONAVIRUS CAUSANTE DEL SÍNDROME RESPIRATORIO AGUDO Y GRAVE

Memoria presentada por José Angel Regla Nava
para optar al grado de Doctor en Ciencias por la
Universidad Autónoma de Madrid

Madrid, Julio de 2015

Lo consiguieron porque no sabían que era imposible.

("Jean Cocteau")

A MIS PADRES Y HERMANOS

ACE2	Enzima convertidora de angiotensina 2
ALI	Daño pulmonar agudo
ARDS	Síndrome de deficiencia respiratoria aguda
ATI	Célula alveolar de tipo I
ATII	Célula alveolar de tipo II
BAC	Cromosoma artificial de bacterias
BCoV	Coronavirus bovino
BHK	Línea celular de riñón de hámster
Cap	7-metil-guanosina
CCL2	Quimioquina con motivo C-C 2
CCL3	Quimioquina con motivo C-C 3
CCL4	Quimioquina con motivo C-C 4
CCL5	Quimioquina con motivo C-C 5
cDNA	Ácido desoxirribonucleico complementario
CMV	Citomegalovirus
CoV	Coronavirus
Ct	Número de ciclos de amplificación para superar el umbral de detección
CXCL1	Quimioquina con motivo C-X-C 1
CXCL10	Quimioquina con motivo C-X-C 10
CXCL2	Quimioquina con motivo C-X-C 2
DAPI	Diclorhidrato de 4´,6-diamidino-2-fenilindol
Ddi	Días después de la infección
DMEM	Medio Eagle modificado por Dulbecco
DNA	Ácido desoxirribonucleico
dsRNA	RNAs de doble cadena
DTM	Dominio transmembrana
DTT	1,4-Ditiotreitol
EDTA	Ácido etilén-diamino-tetra-acético
ERGIC	Compartimento intermedio entre el retículo endoplasmático y el aparato de Golgi
FBS	Suero fetal bovino
FDR	Frecuencia de falsos descubrimientos
HCoV	Coronavirus humano
HCoV-229E	Coronavirus humano 299E
HCoV-HKU1	Coronavirus humano Hong Kong University 1
HCoV-NL63	Coronavirus humano NL63
HCoV-OC43	Coronavirus humano OC43
Hdi	Horas después de la infección
Hdt	Horas después de la transfección
HEPES	Ácido N-2-hidroxietilpiperazina-N´-2-etanosulfónido
HRP	Peroxidasa del rábano picante
IBV	Virus de la bronquitis infecciosa aviar
IFN	Interferón
IL	Interleuquina
IL1α	Interleuquina 1alfa
IL1β	Interleuquina 1beta
IL4	Interleuquina 4
IL5	Interleuquina 5
IL6	Interleuquina 6
IL10	Interleuquina 10
IL12B	Interleuquina 12B
IL13	Interleuquina 13
ISGs	Genes activados por IFN
kb	Kilobase
kDa	KiloDalton
LB	Medio de cultivo Luria-Bertani
MAPK	Proteína quinasa activada por mitógeno
mdi	Multiplicidad de infección
MERS	Síndrome respiratorio del Oriente Medio

MHV	Virus de la hepatitis del ratón
mRNA	Ácido ribonucleico mensajero
NF-κB	Factor nuclear potenciador de las cadenas ligeras kappa de las células B activadas
nsp	Proteína no estructural
nt	Nucleótido
ORF	Fase de lectura abierta
p38 MAPK	Proteína quinasa p38 activada por mitógeno
PAMPs	Patrones moleculares asociados a patógenos
PBM	Motivo de unión a dominios PDZ
PBS	Tampón fosfato salino
PCR	Reacción en cadena de la polimerasa
PEDV	Virus de la diarrea epidémica porcina
poliA	Tramo de poliadeninas
PRRSV	Virus del síndrome respiratorio y reproductivo porcino
RE	Retículo endoplasmático
RNA	Ácido ribonucleico
Rpm	Revoluciones por minuto
rRNA	Ácido ribonucleico ribosómico
RS	Sentido reverso
RSV	Virus respiratorio sincitial
RT	Transcripción reversa
SARS	Síndrome respiratorio agudo y grave
SARS-CoV	Virus productor del síndrome respiratorio agudo y grave
SARS-CoV-MA15	Virus SARS-CoV adaptado a ratón con 15 pases en ratón
SDS	Dodecilsulfato sódico
SDS-PAGE	Electroforesis en gel de poliacrilamida con dodecil sulfato sódico
SERCA	ATPasa de calcio del retículo sarcoplásmico
sgmRNA	RNA mensajero subgenómico
TAE	Tampón Tris-acetato-EDTA
TGEV	Virus de la gastroenteritis porcina transmisible
Tm	Temperatura de fusión
TNF	Factor de necrosis tumoral
TRS	Secuencia reguladora de la transcripción
ufp	Unidades formadoras de placas
UTR	Región no traducida
VDM	Vesícula de doble membrana
VS	Sentido viral
WT	Tipo nativo

Nomenclatura abreviada de los CoV recombinantes

rSARS-CoV-MA15	SCoV
rSARS-CoV-MA15-ΔE	SCoV-ΔE
rSARS-CoV-MA15-EMut1	SCoV-EMut1
rSARS-CoV-MA15-EΔ2	SCoV-EΔ2
rSARS-CoV-MA15-EΔ3	SCoV-EΔ3
rSARS-CoV-MA15-EΔ4	SCoV-EΔ4
rSARS-CoV-MA15-EΔ5	SCoV-EΔ5
rSARS-CoV-MA15-EΔ6	SCoV-EΔ6
rSARS-CoV-MA15-nsp1ΔA	SCoV-nspΔA
rSARS-CoV-MA15-nsp1ΔB	SCoV-nspΔB
rSARS-CoV-MA15-nsp1ΔC	SCoV-nspΔC
rSARS-CoV-MA15-nsp1ΔD	SCoV-nspΔD
rSARS-CoV-MA15-nsp1ΔD-ΔE	SCoV-nspΔD-ΔE
rSARS-CoV-MA15-nsp1ΔD-EΔ3	SCoV-nspΔD-EΔ3

ÍNDICE

I. ÍNDICE

ÍNDICE DE FIGURAS

ÍNDICE DE TABLAS

RESUMEN EN INGLÉS

Coronavirus such as the severe acute respiratory syndrome coronavirus (SARS-CoV) and the Middle East respiratory syndome virus (MERS-CoV) cause high case fatality rates and remain as major human public health threats. No specific therapy for any human coronavirus is available, making vaccine development critical for protection against these viruses. Previously, we demonstrated that a mouse-adapted SARS-CoV (SARS-CoV-MA15) lacking the envelope (E) protein (rSARS-CoV-MA15-ΔE) is attenuated *in vivo*. To identify E protein regions and host responses that contribute to rSARS-CoV-MA15-ΔE attenuation, several mutants (rSARS-CoV-MA15-E*) containing point mutations or deletions in the amino-terminal or the carboxy-terminal regions of the E protein were generated. We showed that small deletions and modifications within E protein led to virus attenuation, causing minimal lung injury, limited neutrophil influx to the lungs, reduced expression of proinflammatory cytokines, increased anti-inflammatory cytokine levels, and enhanced $CD4^+$ and $CD8^+$ T cell counts *in vivo*. These data suggests that the described mutant phenotype contributed to virus attenuation. The attenuated mutants fully protected mice from challenge with virulent virus. A major problem of using live attenuated viruses as vaccines is the possibility of reversion to virulence. To overcome this limitation, we introduced additional attenuating mutations into the nsp1 protein to generate a safer vaccine candidate. Nsp1 gene was selected as a target because it is located at a distal position (>20kb) from that of E gene in the viral genome, making the generation of a virulent virus through a single recombination event with circulating coronaviruses highly unlikely. To identify nsp1 protein regions that contribute to rSARS-CoV-MA15 attenuation, several mutants (rSARS-CoV-MA15-nsp1*) containing small deletions in of the nsp1 protein were generated. Deletion of 121 to 129 and 154 to 165 aminoacids in the carboxy terminal region of nsp1 protein led to virus attenuation. Immunization with single SARS-CoV mutants protected mice against challenge with the lethal parental virus. A recombinat virus including safety guards in E and nsp1 genes was generated. This mutant virus was in general genetically stable *in vitro* and *in vivo*, completely attenuated, and protected mice against challenge with the lethal parental virus, indicating that this virus is promising vaccine candidate.

INTRODUCCIÓN

1. ORIGEN DE LA EPIDEMIA DEL SÍNDROME RESPIRATORIO AGUDO Y GRAVE

El primer caso de neumonía atípica se detectó en el estado de Guandong, China en noviembre de 2002 (Zhao, 2007). La enfermedad se propagó a Hong Kong y Vietnam a finales de febrero de 2003, y luego rápidamente a otros países debido a los viajes por medios aéreos o terrestres de personas infectadas. La Organización Mundial de la Salud declaró el estado de alerta global de la enfermedad en marzo de 2003. En días posteriores la enfermedad se denominó síndrome respiratorio agudo y grave (SARS). Un nuevo coronavirus (CoV) se identificó como el agente causal de la enfermedad en abril de 2003 (Drosten et al., 2003; Rota et al., 2003). La epidemia se dio por terminada el 5 de Julio de 2003 con el establecimiento de programas de vigilancia médica, medidas de cuarentena y el aislamiento de los individuos infectados. La epidemia del SARS dejó 8273 personas infectadas y 775 muertes (http://www.who.int/csr/sars/en/).

2. CLASIFICACIÓN Y CARACTERÍSTICAS DE LOS CoVs

2.1. Taxonomía de los CoVs

Los CoVs son virus con envuelta y con genoma RNA polaridad positiva. Los CoVs pertenecen a la familia *Coronaviridae,* que junto a las familias *Arteriviridae*, *Roniviridae* y *Mesoniviridae* componen el orden de los *Nidovirales* (**Figura 1**). Este orden hace referencia a la producción de mRNAs subgenómicos 3´ coterminales (Carstens, 2010; de Groot et al., 2012; Enjuanes et al., 2008b). La familia *Arteriviridae*, constituida por el género *Arterivirus*, incluye especies de virus que afectan a mamíferos, como el virus del síndrome respiratorio y reproductivo porcino (PRRSV) de alta relevancia económica (Lunney et al., 2010; Snijder and Spaan, 1995). Las familias *Roniviridae* y *Mesoniviridae* infectan a organismos invertebrados como gambas y mosquitos, respectivamente (Lauber et al., 2012; Walker et al., 2005). La familia *Coronaviridae* alberga a las subfamilias *Torovirinae*, compuesta por los géneros *Torovirus* y *Bafinivirus*, y *Coronavirinae* formada a su vez por los géneros *Alfacoronavirus, Betacoronavirus, Gammacoronavirus* y *Deltacoronavirus (de Groot et al., 2012).*

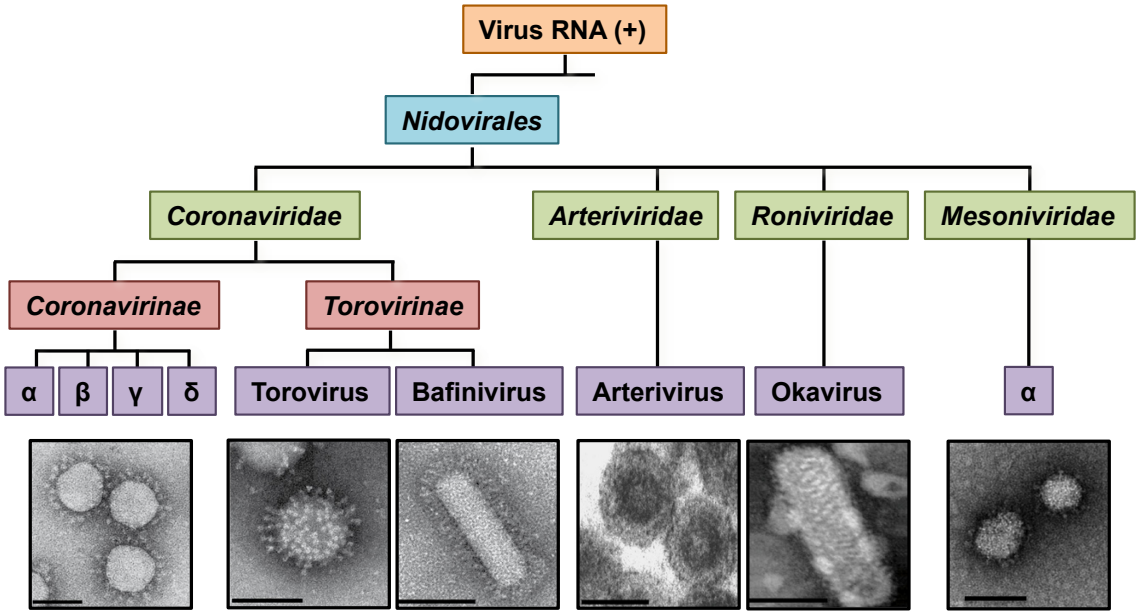

Figura 1. Taxonomía del orden *Nidovirales*. La figura muestra las familias (rectángulos verdes), subfamilias (rectángulos rojos) y géneros (rectángulos morados) que componen el orden *Nidovirales*. En la parte inferior se muestran micrografías electrónicas de virus representativos de los distintos géneros. Barra 100 nm.

2.2. Epidemiología

Los CoVs son patógenos que infectan a animales vertebrados causando principalmente enfermedades respiratorias, entéricas, hepáticas y cerebrales de diversa consideración. Muchos de estos virus son los responsables de grandes pérdidas humanas y económicas a nivel mundial. El virus de la diarrea epidémica porcina (PEDV), el virus de la gastroenteritis porcina transmisible (TGEV) y un nuevo *Deltacoronavirus* del cerdo (SCDV) son los responsables de diversas patologías en el ganado porcino (Huang et al., 2013; Saif and Wesley, 1992; Zhang, 2014). Otros CoVs como el bovino (BCoV) y el virus de la bronquitis infecciosa (IBV) afectan a las explotaciones bovinas y aviares, respectivamente (Cavanagh, 2005; Fukutomi et al., 1999). Estos patógenos también pueden causar enfermedades severas en animales de compañía (CoVs felino y canino) y en animales de experimentación (CoVs murinos) (Perlman and Netland, 2009).

Los CoVs humanos son responsables del 10-20% de los catarros comunes, y de enfermedades respiratorias más graves, como las producidas por el SARS-CoV, y se

han clasificado dentro de los géneros α y β (Chu et al., 2006; McIntosh et al., 1969; Poon et al., 2005). El género α incluye el CoV humano (HCoV) 229E (HCoV-229E), el cual está asociado con catarros comunes, y el CoV HCoV-NL63 que es el causante de enfermedades más severas del tracto respiratorio inferior (Fouchier et al., 2004). Los CoVs humanos pertenecientes al género β incluyen el virus HCoV-OC43, que producen catarros comunes, y el CoV HKU1, identificado en adultos con neumonía (Woo et al., 2005). La importancia de estos virus aumentó con la aparición del virus causante del síndrome respiratorio agudo y grave (SARS-CoV) en el año 2002 (Drosten et al., 2003; Rota et al., 2003), y con la aparición en el año 2012 de un nuevo CoV productor del síndrome respiratorio en Oriente Medio (MERS-CoV) (Assiri et al., 2013).

La epidemia del SARS fomentó la búsqueda del reservorio animal del virus. Estos estudios llevaron a la identificación de CoVs muy similares a SARS-CoV en mapaches (*Nyctereutes procyonoides*), hurones (*Melogale moschata*), y principalmente en civetas (*Paguma larvata*), animales comercializados en los mercados presentes en las regiones de China donde se originó la epidemia. Sin embargo, no se detectaron CoVs similares al SARS-CoV en ejemplares silvestres. El análisis de la secuencia de diferentes aislados virales mostró que este evolucionaba muy rápidamente, lo que indicaba que el virus se estaba adaptando rápidamente a las civetas y que estos animales eran un hospedador intermedio y no el reservorio natural del patógeno (Kan et al., 2005; Song et al., 2005),. Virus filogenéticamente similares a los SARS-CoVs identificados en civetas y humanos fueron detectados también en murciélagos en 2005 (Lau et al., 2005; Li et al., 2005). Estos hallazgos sugieren fuertemente que el virus habría pasado desde los murciélagos al hombre directamente o a través de las civetas. Diversos análisis de muestras de murciélagos repartidos por varias zonas del mundo han permitido identificar otros CoVs causantes de diversas patologías humanas o animales, sugiriendo que los CoVs de murciélago son los antecesores comunes recientes de los virus de los géneros α y β (Annan et al., 2013; Chu et al., 2008; Drexler et al., 2010; Falcon et al., 2011; Graham et al., 2013; Muller et al., 2007; Quan et al., 2010).

Las más de 1100 especies de murciélagos distribuidas por todo el planeta representan el reservorio fundamental de los CoVs. Estos murciélagos facilitan un ambiente propicio para que ocurran fenómenos de recombinación entre distintos CoVs. La rápida evolución de los CoVs facilita la aparición de nuevos virus potencialmente peligrosos capaces de infectar a los humanos o a otros animales. En Arabia Saudita se identificó un nuevo CoV (MERS-CoV), que emergió de los murciélagos (Annan et al., 2013). Este virus infecta a humanos causando neumonías graves que son acompañadas ocasionalmente de patología renal (Assiri et al., 2013). Este CoV ha infectado a 1102 personas en diferentes partes del planeta, causando la muerte de 416 de ellos hasta el 9 de Abril 2015 (http://www.who.int/csr/disease/coronavirus_infections/en/). Por ello, el estudio de los mecanismos implicados en la virulencia de estos virus y el desarrollo de nuevas terapias y vacunas efectivas son de gran relevancia para el control de estas patologías.

2.3. Estructura del genoma y expresión génica en CoVs

Los CoVs son virus esféricos con una envuelta lipídica y un diámetro de entre 70 y 120 nm. Su genoma consiste en una cadena de RNA sencilla y de polaridad positiva de aproximadamente 30 kb de longitud, lo que representa el genoma RNA viral conocido de mayor tamaño (de Groot et al., 2012; Enjuanes et al., 2008b). En la envuelta viral se inserta la proteína de la espícula (S), la cual confiere a la partícula viral apariencia de corona, de donde se deriva el nombre de la familia *Coronoviridae* (Delmas and Laude, 1990). Además en la envuelta del virus se insertan las proteínas de membrana (M), de la envuelta (E) y, en ciertos casos, otras proteínas específicas de especie (**Figura 2**).

La proteína S es una glicoproteína de membrana de tipo I, con una masa molecular de 200 kDa. Su función es la de mediar la unión al receptor celular, y promover la fusión de las membranas celular y viral, permitiendo la entrada del virus en la célula. Esta proteína confiere a los virus la especificidad de tejido y especie, e induce anticuerpos neutralizantes en el huésped (Gallagher and Buchmeier, 2001; Jimenez et al., 1986; Sui et al., 2004). La proteína M es el componente más

abundante en la envuelta viral. Esta proteína tiene una masa molecular de 29 kDa en SARS-CoV y tres dominios transmembrana, que participan en los procesos de morfogénesis y ensamblaje viral (Nguyen and Hogue, 1997). La proteína M, al igual que la proteína S, también induce anticuerpos neutralizantes, pero en menor proporción que la proteína S (Escors et al., 2001).

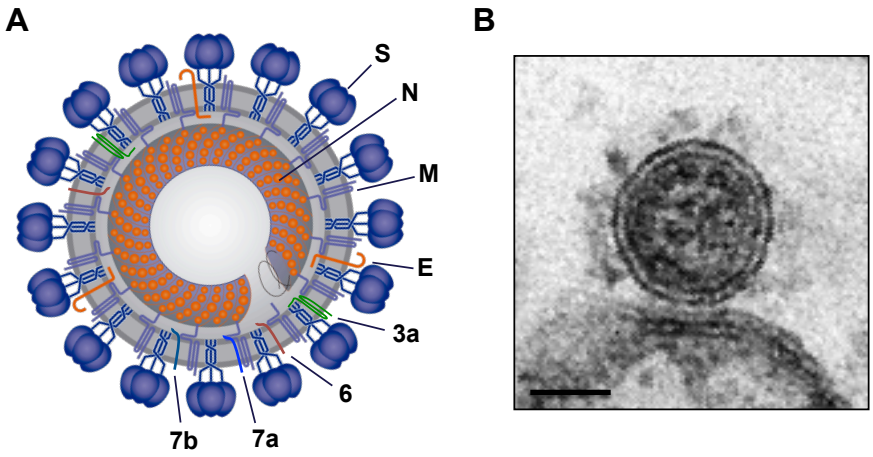

Figura 2. Estructura del virión del SARS-CoV. (A) Esquema grafico de un virión del SARS-CoV. En la envuelta lipídica se insertan las proteínas S, M, y E, que son comunes en todos los CoVs y además las proteínas 3a, 6, 7a y 7b, que son específicas del SARS-CoV. En el interior del virus se muestra la nucleocápsida, que es una estructura helicoidal formada por el genoma viral asociado a la proteína N. **(B)** Micrografía electrónica de un virión del SARS-CoV después de la gemación celular. Barra 50 nm.

La proteína E, o de la envuelta, es una proteína transmembrana de pequeño tamaño, que está presente en los viriones en bajo número de copias (20 moléculas por virión). Sin embargo, se expresa abundantemente durante la infección, participando en la morfogénesis viral junto con la proteína M (Nguyen and Hogue, 1997; Ruch and Machamer, 2012). Además, en la envuelta del SARS-CoV se encuentran las proteínas 3a, 6, 7a y 7b (Huang et al., 2006; Schaecher et al., 2007; Shen et al., 2005). El interior del virión contiene una cápsida helicoidal compuesta por la asociación entre el genoma del virus y la nucleoproteína (N). La proteína N, es una fosfoproteína de 40 kDa, que se une al RNA genómico promoviendo su encapsidación. Esta proteína participa en la síntesis de RNAs virales, posee actividad chaperona de RNA y funciona como antagonista de la respuesta antiviral

mediada por interferón (IFN) de tipo I (Almazan et al., 2004; Lu et al., 2011; Thiel et al., 2003; Ye et al., 2007b; Zuñiga et al., 2007)

La estructura del genoma de CoV se asemeja a los mRNAs celulares, dado que posee una estructura cap en el extremo 5' y una cola de poliA en el extremo 3'. En los extremos 5´ y 3´ del genoma de CoV se encuentran regiones no traducidas (5´UTR y 3´UTR) de entre 210 y 530 nucleótidos de longitud **(Figura 3)**.

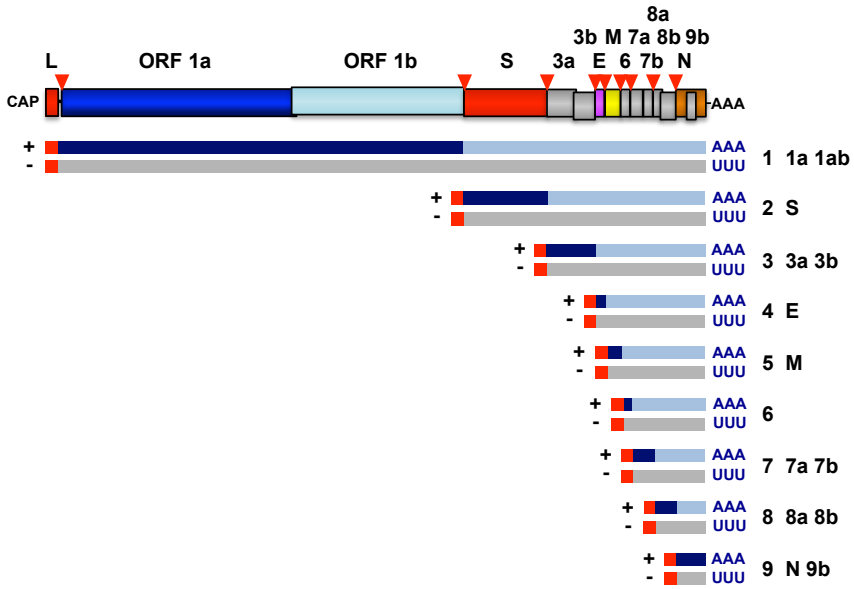

Figura 3. Expresión génica en el SARS-CoV. Esquema del genoma del SARS-CoV (parte superior) donde se muestra la estructura cap (CAP), la secuencia líder (L), los genes virales (ORF 1a, ORF 1b, S, 3a, 3b, E, M, 6, 7a, 7b, 8a, 8b, N y 9b), el poliA (AAA) y la posición de las secuencias reguladoras de la transcripción o TRS (triángulos rojos invertidos). La polimerasa viral genera durante el ciclo infectivo una serie de RNAs virales (parte inferior), numerados del 1 al 9, de polaridad positiva (+) y otros complementarios de polaridad negativa (-). En cada caso se indica los genes que codifican, las secuencias líder y antilíder (rojo), la secuencia codificante traducida (azul oscuro) y la secuencia codificante no traducida (azul claro).

Los dos tercios 5´ terminales del genoma codifican la replicasa viral, la cual está constituida por dos fases de lectura (ORFs) solapantes, 1a y 1b, que se traducen directamente a partir del RNA genómico al comienzo de la infección. La traducción da origen a dos largas poliproteínas, pp1a y pp1ab, las cuales incluyen los genes de la replicasa. Estas poliproteínas se procesan proteolíticamente por proteasas virales para generar 15 o 16 (16 en el caso del SARS-CoV) proteínas no

estructurales (nsps), las cuales están implicadas en la replicación y transcripción (Gorbalenya et al., 1989; Ziebuhr, 2005; Ziebuhr et al., 2000). El tercio 3´ terminal del genoma contiene los genes estructurales S, E, M y N, además de varias proteínas accesorias cuyo número y secuencia varían entre las distintas especies de CoVs. En el caso del SARS-CoV las proteínas accesorias son 3a, 3b, 6, 7a, 7b, 8a 8b, y 9b (Narayanan et al., 2008b).

Los CoVs se replican en el citoplasma celular, y codifican un conjunto de RNAs mensajeros subgenómicos (sgm RNAs) 5´ y 3´ coterminales de diferentes tamaños. De estos mRNAs generalmente solo se traduce la ORF situada más cerca del extremo 5´ del RNA **(Figura 3)**. Estos sgmRNAs incluyen una secuencia líder de 72 nucleótidos en su extremo 5´ en el caso de SARS-CoV. Esta secuencia líder también se encuentra en el extremo 5´ del genoma viral, y se incorpora a los sgmRNAs por un proceso de síntesis discontinua del RNA, en el que se generan moléculas intermedias de polaridad negativa. Este mecanismo está liderado por las secuencias reguladoras de la transcripción (TRS), que se localizan al final de la secuencia líder, precediendo a cada uno de los genes (**Figura 3**) (Enjuanes et al., 2006; Sola et al., 2005; Zuñiga et al., 2004).

2.4. Ciclo infectivo viral

Los CoVs infectan principalmente a las células del tracto entérico y respiratorio (Miura and Holmes, 2009). La infección con CoV comienza con la unión de la proteína S, presente en la superficie de los viriones, al receptor celular. En el caso del SARS-CoV el receptor celular es la enzima convertidora de angiotensina 2 humana (hACE-2) (Li et al., 2003; Wong et al., 2004b). Esta unión induce la entrada del virus en la célula mediante endocitosis **(Figura 4)**. La membrana viral se fusiona con la membrana del endosoma, dando como resultado la liberación de la nuclelocápside en el citoplasma de la célula. Las poliproteínas pp1a y pp1ab son procesadas principalmente por proteasas virales, originando las proteínas del complejo de replicación-transcripción (Ziebuhr, 2005). Este complejo se une a vesículas de doble membrana originadas a partir del retículo endoplasmático celular (RE) (Knoops et al., 2008), llevando a cabo la replicación del genoma viral y

la síntesis de los sgmRNAs a través de moléculas de RNA intermediarias de polaridad negativa (Enjuanes et al., 2006; Sawicki and Sawicki, 1990; Zuñiga et al., 2010). Las proteínas M, S y E se sintetizan e insertan en la membrana del RE. La proteína M recluta a la proteína S en su transporte hacia el compartimiento intermedio celular (ERGIC), y además se une a la proteína E (de Haan et al., 1999; Lim and Liu, 2001; Nguyen and Hogue, 1997). Al mismo tiempo, la proteína N se asocia con el RNA genómico viral, dando lugar a la nucleocápsida. Esta se incorpora en las partículas virales por medio de la interacción entre las proteínas N y M durante un proceso de gemación intracelular que tiene lugar en las membranas del ERGIC (Narayanan et al., 2000). Una vez que los viriones están ensamblados se acumulan en vesículas y maduran conforme progresan a través de la ruta secretora. Por último, las vesículas cargadas de virus se fusionan con la membrana plasmática celular, liberando la progenie viral al medio extracelular (Tooze et al., 1987).

3. GENÉTICA REVERSA EN CoV

La manipulación del genoma de CoVs mediante genética reversa estuvo limitada por su gran tamaño y por la presencia de regiones de carácter tóxico en el gen de la replicasa, que impedían la clonación y crecimiento en bacterias de un DNA complementario (cDNA) infectivo. Por ello, inicialmente los estudios genéticos de CoVs estaban limitados al análisis de mutantes termosensibles o de RNAs defectivos o minigenomas. Estos últimos requerían un virus complementador para replicarse (Izeta et al., 1999; Repass and Makino, 1998). El primer clon infectivo de CoV se construyó en nuestro laboratorio para el TGEV y se basó en el clonaje de un cDNA infectivo, bajo el control de un promotor de citomegalovirus (CMV), en un cromosoma artificial de bacterias (BAC) (Almazan et al., 2000). El uso de BACs limita la cantidad de vector por bacteria a una o dos copias, reduciendo así la toxicidad, y permitiendo su propagación y amplificación de una forma eficiente y estable. Cuando el BAC entra en el núcleo de la célula huésped, la RNA polimerasa II celular transcribe el RNA genómico viral, dado que este último está situado bajo el control de un promotor de CMV. A continuación, el RNA genómico se transloca hacia el citoplasma, iniciándose el ciclo infectivo del virus. Clones infectivos para el

SARS-CoV (Almazan et al., 2006; Fett et al., 2013) y MERS-CoV (Almazan et al., 2013) se desarrollaron en nuestro laboratorio basándose en esta tecnología.

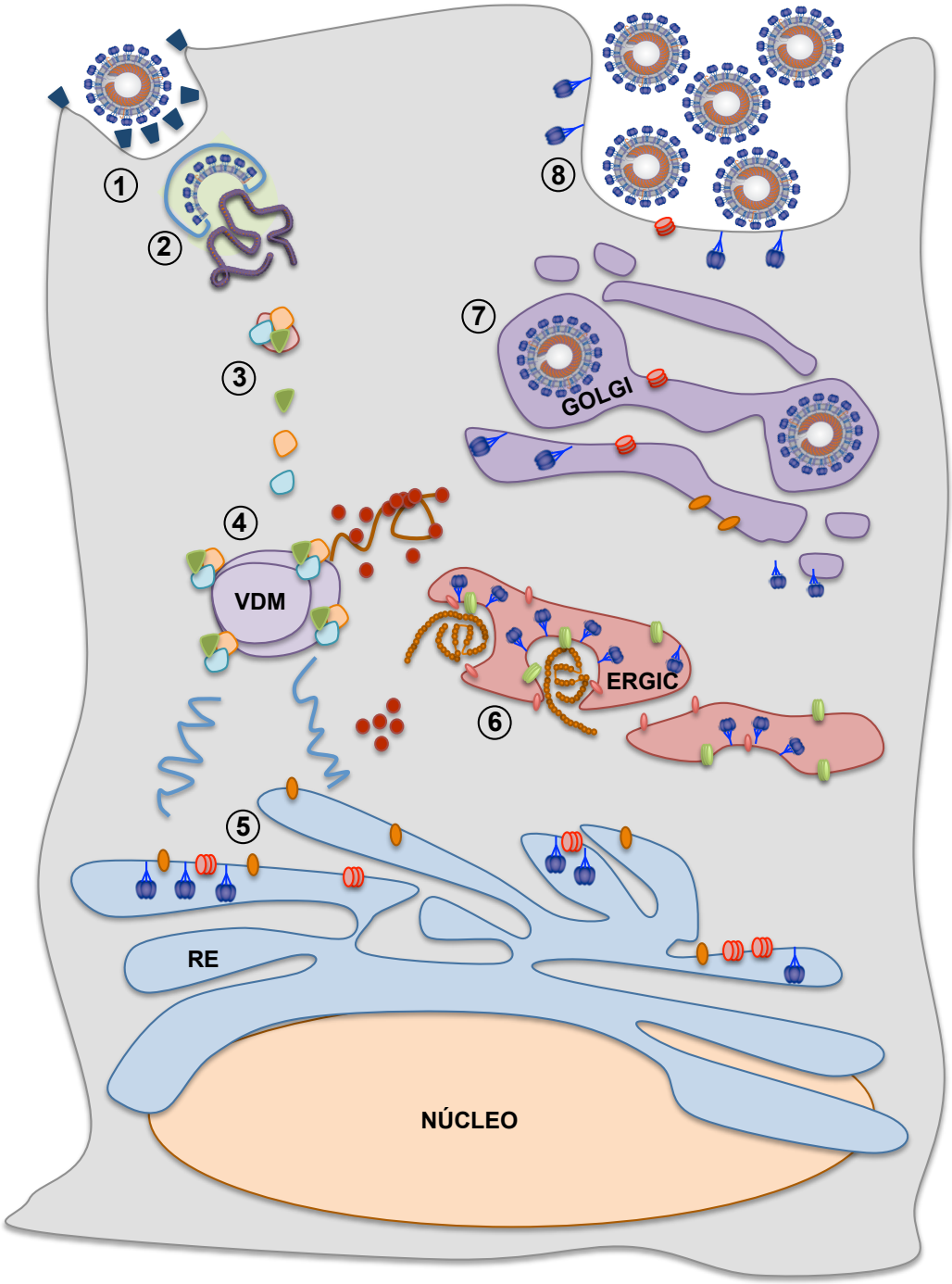

Figura 4. Ciclo infectivo de los CoVs. Esquema de la infección por SARS-CoV, en la cual se indican los siguientes pasos: (1) Interacción del virión con el receptor celular y endocitosis. (2) Fusión de membranas viral y celular, y liberación de la nucleocápsida. (3) Traducción y procesamiento proteolítico de las poliproteínas pp1a y pp1ab. (4) Asociación de los componentes de la replicasa viral en vesículas de doble membrana (VDM) y síntesis de RNAs virales. (5) Traducción de los RNAs virales y generación, entre otros componentes, de la proteína N (círculos rojos), que se asocia al

genoma viral, y de las proteínas M (elipses naranjas), S (estructura azul) y E (elipse roja), que se insertan en RE. (6) Gemación del virus en el ERGIC. (7) Maduración de los viriones. (8) Fusión de las vesículas con la membrana plasmática y liberación de la progenie viral.

Una estrategia alternativa en la generación de clones infectivos se basa en la ligación *in vitro* de fragmentos cDNA, que incluyen el genoma viral completo bajo el control del promotor del fago T7. El cDNA ensamblado se inserta finalmente en el genoma del virus de la vacuna para su propagación o, alternativamente, se transcribe *in vitro* generándose el RNA infectivo viral. Este sistema se ha utilizado para la construcción de diversos clones infectivos de distintos CoVs como HCoV-229E (Thiel et al., 2001), HCoV-NL63 (Donaldson et al., 2008), virus de la hepatitis de ratón (MHV) (Coley et al., 2005; Yount et al., 2002), IBV (Casais et al., 2001), SARS-CoV (Yount et al., 2003) y MERS-CoV (Scobey et al., 2013).

4. PROTEÍNA E DE LOS CoVs

4.1. Estructura, localización subcelular y topología

La proteína E de los CoVs es una proteína transmembrana de 76 a 109 aminoácidos de longitud (Ruch and Machamer, 2012). Las proteínas E de los CoVs no presentan un alto grado de homología entre sí. Sin embargo, incluyen regiones estructurales de características similares. Estas proteínas están formadas por un dominio amino terminal hidrofílico de entre 7 y 12 aminoácidos, un dominio transmembrana de 25 aminoácidos mayoritariamente hidrofóbicos con estructura en alfa hélice, y una región carboxilo terminal, que posee zonas relevantes para la interacción con otras proteínas, como el motivo de unión a dominios PDZ (PBM) (Jimenez-Guardeño et al., 2014) (**Figura 5**).

La proteína E de los diferentes CoVs se localiza fundamentalmente entre las membranas del RE y el aparato de Golgi, participando en el proceso de ensamblaje y gemación del virus (Lim and Liu, 2001; Nal et al., 2005; Raamsman et al., 2000; Ruch and Machamer, 2012). La proteína E del SARS-CoV, tanto expresada aisladamente, como en el contexto de la infección, se localiza mayoritariamente en el ERGIC de la célula (Nieto-Torres et al., 2011). La proteína E de los diferentes

CoVs adquiere distintas conformaciones topológicas dependiendo de la especie. Las proteínas E del SARS-CoV y TGEV establecen un único paso transmembrana, situando su extremo amino terminal hacia el lumen de vesiculas intracelulares y el dominio carboxilo terminal hacia el citosol (Godet et al., 1992; Nieto-Torres et al., 2011).

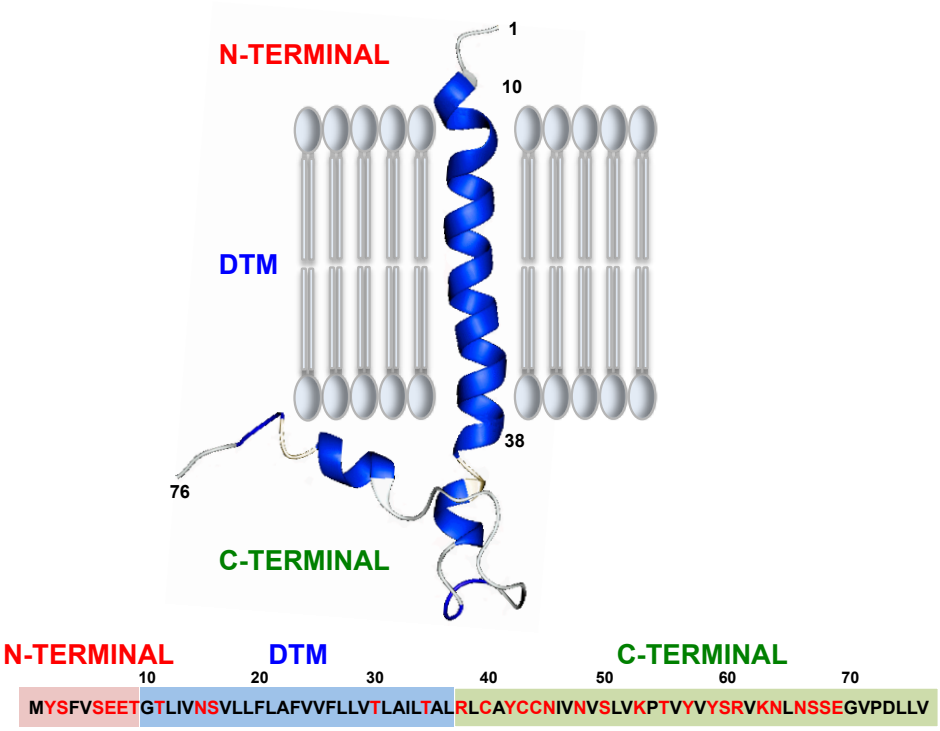

Figura 5. Secuencia y motivos estructurales y funcionales de la proteína E del SARS-CoV. Esquema gráfico de la proteína E del SARS-CoV insertada en una membrana lipídica (parte superior). Se indican los dominios amino-terminal (N-terminal), transmembrana (DTM) y carboxilo-terminal (C-terminal), así como los aminoácidos que comprenden cada dominio. Los dominios que conforman esta proteína de 76 aminoácidos se muestran en la parte inferior. Los aminoácidos apolares se representan en letras negras y los polares en letras rojas. Las posiciones de aminoácidos 73 al 76 (DLLV) constituyen el dominio PBM.

Aparentemente ocurre lo contrario con la proteína E del IBV, donde el extremo amino terminal se orienta hacia el citosol y el carboxilo terminal hacia el lumen de los orgánulos (Corse and Machamer, 2000). En la proteína E de MHV ambos dominios amino y carboxilo terminal se orientan hacia el citoplasma (Raamsman et al., 2000).

4.2. Relevancia de la proteína E en la morfogénesis y virulencia de los CoVs

La proteína E participa en el proceso de ensamblaje y liberación de los CoVs junto con las proteínas M y N (de Haan and Rottier, 2005; Masters, 2006). Sin embargo, su requerimiento varía dependiendo de la especie de CoV. Una característica de gran importancia de esta proteína es que solo una pequeña fracción de la misma sintetiza durante la infección por CoV, se incorpora en la partícula viral (Ruch and Machamer, 2012). La proteína E del TGEV es esencial para la maduración y secreción de virus infecciosos (Ortego et al., 2007; Ortego et al., 2002). De forma similar la eliminación de la proteína E del MERS-CoV, genera virus competentes en replicación pero deficientes en propagación, que se pueden diseminar al expresar la proteína E en *trans* (Almazan et al., 2013). Sin embargo, las proteínas E del MHV y SARS-CoV, no son esenciales para la liberación de virus infecciosos, aunque se aprecian bajadas en el título viral de 100 veces para MHV (Kuo and Masters, 2013) y de entre 20 y 200 veces para el SARS-CoV cuando se elimina esta proteína (DeDiego et al., 2007; DeDiego et al., 2008).

En el laboratorio se ha demostrado que la proteína E es un factor de virulencia, ya que virus recombinantes que carecen de esta proteína (SCoV-ΔE) muestran un fenotipo atenuado en tres modelos animales distintos. Además, la inmunización con el virus atenuado SCoV-ΔE protege frente a la infección con el virus nativo (DeDiego et al., 2007; DeDiego et al., 2008; Fett et al., 2013; Lamirande et al., 2008; Netland et al., 2010). La realización de estudios detallados con el recombinante SCoV-ΔE han permitido conocer algunas funciones y rutas de señalización celulares que contribuyen a la atenuación de este virus. El análisis de la expresión génica diferencial en células infectadas con el virus que carece de la proteína E, con respecto a células infectadas con el virus nativo, permitió identificar que la proteína E disminuye el estrés celular inducido por la infección por SARS-CoV y otros virus, como el virus respiratorio sincitial (RSV), y por drogas como la tapsigargina, que inhibe la actividad ATPasa de Ca^{++} del retículo sarcoplasmático (SERCA), o la tunicamicina, cuya función es la de inhibir la glicosilación de proteínas (DeDiego et al., 2011). Además, la ausencia de la proteína E lleva asociada una disminución en la respuesta pro-inflamatoria inducida en la infección

por SARS-CoV. Esta respuesta pro-inflamatoria se encuentra mediada principalmente por el factor de transcripción NF-κB, dado que cuando la ruta de señalización de NF-κB se inhibe con drogas, se reduce la respuesta pro-inflamatoria, observándose un aumento en la supervivencia de los animales infectados (DeDiego et al., 2014).

Una función notable de las proteínas E de los CoVs es que poseen actividad canal iónico (Liao et al., 2004; Madan et al., 2005; Torres et al., 2006; Verdia-Baguena et al., 2012; Wilson et al., 2004). Dado que el virus SCoV-ΔE esta atenuado, se estudió la relevancia de la actividad canal iónico de la proteína E en la patogénesis del virus. Para ello, se generaron mutantes de SARS-CoV con mutaciones puntuales en la proteína E que abolían la actividad canal iónico. Se identificó que la actividad canal iónico de la proteína E confiere una ventaja selectiva al virus (Nieto-Torres et al., 2014). Además, se determinó que la actividad canal iónico contribuye a la inducción de una respuesta inflamatoria exacerbada en el parénquima pulmonar de ratones infectados promoviendo la virulencia de SARS-CoV (Nieto-Torres et al., 2014).

La relevancia del motivo PBM de la proteína E se basa en que potencialmente podría interaccionar con aproximadamente 400 dominios PDZ presentes en más de 800 proteínas celulares. Ello hizo que la influencia de este motivo estructural sobre la virulencia del SARS-CoV se estudiase por nuestro grupo (Jimenez-Guardeño et al., 2014). Se identificó que el dominio PBM de la proteína E contribuye a la patogénesis de SARS-CoV (Jimenez-Guardeño et al., 2014). La proteína E de SARS-CoV se une a la proteína celular sintenina, que incluye dos dominios PDZ, a través del dominio PBM. Esta unión favorece la activación de la quinasa p38 activada por mitógenos (MAPK p38), promoviendo una respuesta pro-inflamatoria exacerbada y por tanto el aumento en la patogénesis viral (Jimenez-Guardeño et al., 2014). En nuestro laboratorio se mostró que el uso de inhibidores específicos de la ruta de señalización de la MAPK p38, aumentó la supervivencia de ratones infectados con SARS-CoV. Estos inhibidores eran por tanto buenos antivirales para prevenir la enfermedad causada por el virus (Jimenez-Guardeño et al., 2014).

En esta Tesis Doctoral, se ha profundizado en el estudio de dominios y funciones de la proteína E del SARS-CoV que pudieran estar implicados en la virulencia del virus. Para ello, se generaron virus mutantes que contenían mutaciones puntuales en el dominio amino terminal o distintas deleciones en la región carboxilo terminal de la proteína E, y se analizó la virulencia y la respuesta del huésped a la infección por los mutantes virales construidos, utilizando como modelo de ratones BALB/c.

5. LA REPLICASA DE CoV

El gen de la replicasa codifica la mayor parte de las actividades virales implicadas en la replicación y transcripción de CoV. La traducción se lleva a cabo al inicio de la infección, produciéndose las poliproteínas pp1a y pp1ab. Esta segunda se sintetiza mediante un salto de fase del ribosoma. Ambas poliproteínas se autoprocesan de una forma perfectamente regulada en el tiempo, lo que da lugar a 15 o 16 proteínas no estructurales (nsps) (Schiller et al., 1998). Las proteínas maduras originadas por el procesamiento de las poliproteínas pp1a (nsp1-nsp11) son comunes con las originadas por el procesamiento de la pp1ab (nsp1-10 y nsp12-nsp16) con la excepción de la proteína nsp11, la cual solo se produce en ausencia del salto de fase del ribosoma.

5.1. Estructura y localización de la proteína nsp1 de los CoVs

La proteína nsp1 es la primera proteína madura procesada a partir de la poliproteína por la acción de la proteinasa viral papaína (PL^{pro}) (Baker et al., 1989; Denison and Perlman, 1987; Ziebuhr, 2005). De los cuatro géneros de CoV, solo los géneros α y β codifican la proteína nsp1. Los géneros γ y δ carecen de ella, por lo que su genoma codifica solo 15 nsps (nsp2 a nsp16). La proteína nsp1 en los CoVs α tiene una longitud de 110 aminoácidos. En los CoVs β, como el MHV y el CoVs humano OC43 la proteína nsp1 posee 245 aminoácidos (Brockway and Denison, 2005). La proteína nsp1 del SARS-CoV (perteneciente al género β) y la de sus equivalentes en murciélagos tiene un tamaño de 179 aminoácidos (Gorbalenya et al., 2006; Gorbalenya et al., 2004; Snijder et al., 2003). La proteína nsp1 del virus TGEV se distribuye entre el núcleo y el citoplasma, tal como se observó en células

embrionarias de riñón humano. Esta proteína, en principio, puede pasar libremente del citoplasma al núcleo debido a su pequeño tamaño de 9 kDa, que es el límite de exclusión del complejo que forma el poro nuclear (Gorlich, 1998; Silver, 1991).

5.2. Funciones de la proteína nsp1 de los CoVs

La proteína nsp1 de CoV inhibe la expresión génica del huésped (Huang et al., 2011; Kamitani et al., 2006; Narayanan et al., 2008a; Zust et al., 2007), mediante el aumento de la degradación específica de los RNAs mensajeros celulares (Kamitani et al., 2009; Kamitani et al., 2006; Tanaka et al., 2012). En el caso del SARS-CoV, la proteína nsp1 se une a la subunidad 40S ribosomal, suprimiendo así la expresión génica del huésped (Kamitani et al., 2006). La proteína nsp1 de MHV promueve la parada del ciclo celular en la fase G0/G1 en células transfectadas (Chen and Makino, 2004). Mutantes puntuales en el sitio de escisión proteolítico entre la proteína nsp1 y nsp2 del virus de TGEV bloquean la liberación de la proteína nsp1 causando una reducción en el crecimiento del virus (Galan et al., 2005). De forma similar, mutantes de MHV en los que la liberación de la proteína nsp1 está afectada, muestran una replicación tardía, disminución de los títulos virales, placas de lisis pequeñas y una reducción de la síntesis de RNA comparados con el virus nativo (Denison et al., 2004). Estas observaciones ponen de relieve la importancia del sitio de escisión de la proteína nsp1 en la síntesis óptima de RNA viral, sugiriendo la importancia de esta proteína en los complejos de replicación de CoV. La proteína nsp1 del SARS-CoV es un potente inductor de la expresión de las citoquinas CCL5, CXCL10 y CCL3 en células epiteliales de pulmón humano, mediante la activación de la vía de señalización NF-kB (Law et al., 2007). La proteína nsp1 del virus MHV interacciona con las proteínas p10 y p15, correspondientes a las proteínas nsp7 y nsp10 del SARS-CoV, respectivamente (Brockway et al., 2004). Además, la proteína nsp1 de SARS-CoV interacciona con las proteínas E y 3a, tal como se ha determinado utilizando las técnicas de doble híbrido y coimmunoprecipitación (von Brunn et al., 2007).

5.3. Relevancia de la proteína nsp1 en la virulencia de los CoVs

La proteína nsp1 de CoV es un factor de virulencia. Esta proteína posee muchas funciones. Además de inhibir la expresión génica del huésped, como se ha indicado anteriormente, interfiere eficientemente en la producción y señalización mediada por IFN tipo I (Narayanan et al., 2014; Zust et al., 2007). Estudios con virus MHV recombinantes que contienen deleciones en la proteína nsp1 mostraron que esta proteína afecta a la vía de producción y señalización de IFN I, originando virus atenuados en ratón. Estos virus protegen frente al desafío con un virus silvestre (Lei et al., 2013; Zust et al., 2007), por lo tanto, modificaciones en la proteína nsp1 son una posible diana para el diseño de vacunas basadas en virus con virulencia disminuida.

6. SÍNDROME RESPIRATORIO AGUDO Y GRAVE

6.1. Transmisión del SARS-CoV

El SARS-CoV se transmite fundamentalmente mediante la producción de pequeñas partículas en suspensión, generadas durante el proceso de la respiración (Dwosh et al., 2003). Su transmisibilidad es moderada, produciéndose alrededor de tres infecciones secundarias por cada paciente infectado (Riley et al., 2003). El contagio del virus en ciertas circunstancias también se puede llevar a cabo por contacto directo o indirecto con secreciones respiratorias, heces o animales portadores (Ng, 2003; Tsang et al., 2003). El sitio de replicación en el organismo es el tracto respiratorio inferior y superior, alcanzando los mayores títulos virales en el tracto respiratorio superior a los 10 días posteriores a la infección, cuando los síntomas de la enfermedad son más evidentes (Peiris et al., 2003). La estabilidad del SARS-CoV es mayor a temperatura ambiente que la observada para otros CoVs (Sizun et al., 2000). El virus mantiene su capacidad infectiva durante 2 o 4 días en superficies plásticas y heces respectivamente. Su detección se puede realizar mediante RT-PCR y el virus infectado se puede aislar de muestras de secreciones respiratorias, heces, orina y muestras de pulmón de pacientes infectados (Chan et al., 2004; Peiris et al., 2003).

6.2. Patología causada por el SARS-CoV

El SARS-CoV se caracteriza por una neumonía atípica que deriva en fallo respiratorio progresivo. La infección por este virus alcanza una tasa de mortalidad del 10% en los individuos infectados con edades entre 20 y 50 años, y superiores al 50% en personas mayores de 65 años (Donnelly et al., 2003). La enfermedad se manifiesta inicialmente con fiebre, mialgia, malestar general, escalofríos, estornudos y esporádicamente diarrea (Zhao et al., 2003). La linfopenia es común y algunos pacientes tienen bajos los niveles de plaquetas. Un tercio de los pacientes se recuperan, mientras que los otros dos tercios sufren fiebres persistentes, fallos respiratorios, taquipnea y diarrea (Peiris et al., 2003). En algunos casos los pacientes requieren el internamiento en una unidad de cuidados intensivos y respiración asistida. En la etapa tardía de la enfermedad, algunos pacientes desarrollan fallo respiratorio severo, fallo multiorgánico, infarto agudo de miocardio y sepsis, lo cual conduce a la muerte. El análisis histopatológico de autopsias de pulmón de pacientes fallecidos a causa de la infección por SARS-CoV reveló la presencia de daño alveolar difuso, descamación de los epitelios pulmonares, formación de membranas hialinas y acumulación de edema (Franks et al., 2003; Nicholls et al., 2003; Peiris et al., 2003). Estos signos son característicos de las patologías conocidas como daño pulmonar agudo (ALI) y su forma más severa, el síndrome de deficiencia respiratoria aguda (ARDS). El ARDS aparece por infecciones de origen viral, entre otras causas, originando una mortalidad de alrededor del 40% (Matthay et al., 2002). La enfermedad se origina por una acumulación de edema en las vías respiratorias, desencadenada por una salida de líquido hacia los espacios alveolares. Esta patología provoca un intercambio gaseoso deficiente y eventualmente la muerte del paciente. El SARS-CoV infecta células bronquiales y bronquiolares, células alveolares de tipo I y II y, de forma menos productiva, macrófagos alveolares (Frieman et al., 2008; Hsiao et al., 2005; Shieh et al., 2005; Ye et al., 2007a). Los epitelios pulmonares infectados provocan una respuesta inflamatoria mediada por la producción de citoquinas, amplificada por los macrófagos. Las citoquinas atraen quimiotácticamente células leucocitarias, principalmente neutrófilos, liberando compuestos oxidantes, proteasas, leucotrienos y otras moléculas pro-inflamatorias. Esto provoca daño de

los vasos sanguíneos, permitiendo la salida de líquido hacia el epitelio pulmonar (Matthay and Zemans, 2011). Además, la infección por SARS-CoV provoca la destrucción de las células del epitelio pulmonar, lo cual hace que estas células sean incapaces de retirar el exceso de líquido y restos celulares de los espacios aéreos, originando un ineficiente intercambio gaseoso (**Figura 6**).

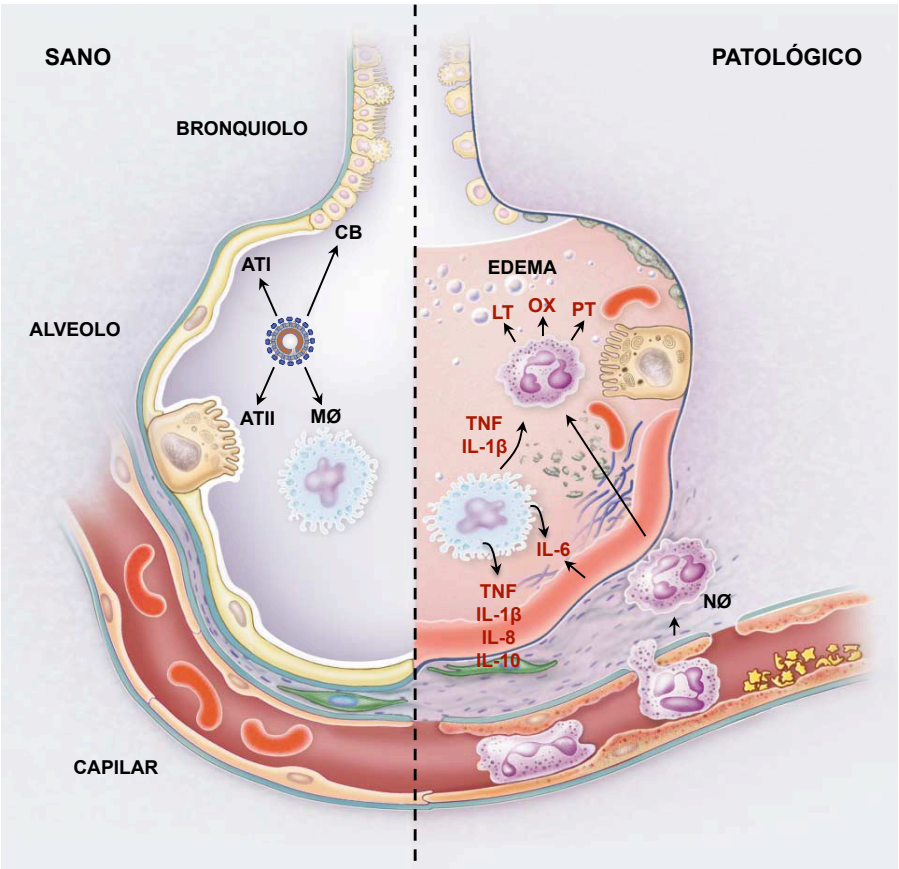

Figura 6. Patología pulmonar causada por el SARS-CoV. Esquema de la evolución de las vías aéreas antes y después de la infección por el virus del SARS-CoV. El virus infecta las células bronquiolares (CB) y células alveolares de tipo I (ATI); responsables del intercambio gaseoso, células alveolares de tipo II (ATII): que están implicadas en la secreción del surfactante pulmonar y en la proliferación del reemplazo de los epitelios dañados, y macrófagos alveolares (MØ), implicados en el proceso de defensa frente a sustancias extrañas. Los epitelios pulmonares son destruidos durante la infección, promoviendo una respuesta inflamatoria amplificada por los macrófagos alveolares. Como resultado, los neutrófilos (NØ) se extravasan desde los capilares sanguíneos a los espacios aéreos donde liberan: leucotrienos (LT), compuestos oxidantes (OX) y proteasas (PT), aumentando la respuesta inflamatoria. El aumento de la permeabilidad de los epitelios y endotelios causa la acumulación de edema en las vías aéreas.

7. SARS-CoV E INMUNIDAD

7.1. Respuesta inmune innata

La respuesta inmune innata es la primera línea de defensa antiviral desarrollada por el huésped. Esta respuesta se desencadena por una serie de eventos que se promueven tanto en las células infectadas como en las células vecinas. Estos eventos incluyen la inhibición de la síntesis proteica, la activación transcripcional de interferón (IFN), y de genes activados por este (ISGs) y otras citoquinas pro-inflamatorias y, en última instancia, la inducción de muerte celular. La respuesta antiviral se inicia mediante el reconocimiento de receptores celulares, específicos de patrones moleculares asociados a patógenos (PAMPs). Estos son generados durante el ciclo viral, e incluyen los RNAs de doble cadena (dsRNA) que se producen en las infecciones virales, y los intermediarios RNA de replicación o transcripción (Andrejeva et al., 2004; Thompson and Locarnini, 2007; Yoneyama et al., 2004).

7.1.1. Interferón

Los interferones constituyen una gran familia de citoquinas que combaten las infecciones virales y promueven la respuesta inmune adaptativa (Medzhitov and Janeway, 1997). Existen al menos tres tipos: IFN tipo I, que comprende las especies IFN α, β, ω, ε y τ, IFN de tipo II, que incluye la especie IFNγ, y el IFN tipo III que comprende las especies IFN-λ1, λ2 y λ3 (Kotenko et al., 2003), también llamados IL-29, IL-28A e IL-28B, respectivamente (Sheppard et al., 2003).

El IFN de tipo I se induce en la mayoría de los tipos celulares. Durante una infección viral, las células infectadas secretan mayoritariamente IFN β como respuesta inicial a la infección. En una fase más tardía se secreta IFNα durante la fase de amplificación de la respuesta de IFN (Marie et al., 1998). El IFN tipo II es secretado mayoritariamente por linfocitos CD4 Th1, linfocitos CD8 citotóxicos y células *natural killer* (NK) después de varios tipos de estímulos, incluyendo los mitógenos (Young, 1996). El IFN de tipo III se expresa como respuesta a las infecciones virales, fundamentalmente en células epiteliales, complementando a la

respuesta antiviral de una manera similar al IFN tipo I, pero independiente de este (Kotenko et al., 2003).

En las infecciones virales, las moléculas de dsRNA se unen a los sensores citoplasmáticos, *retinoic acid-inducible gene 1* (RIG-1) y *melanoma differentiation-associated protein 5* (MDA-5), y a los sensores endosomales o de superficie celular *toll-like receptors* (TLRs), dando como resultado la activación de los factores de transcripción IRF3/IRF7, AP-1 y NF-κB, reguladores principales de la expresión de IFNα/β y citoquinas pro-inflamatorias (Haller et al., 2006; Kawai et al., 2005) (**Figura 7**).

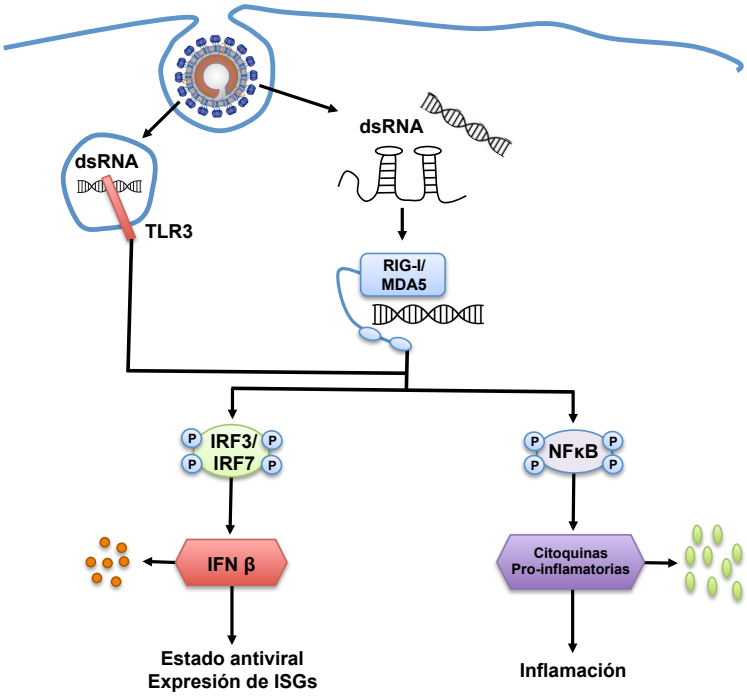

Figura 7. Respuesta antiviral activada por dsRNA. Esquema del reconocimiento de dsRNA y las rutas celulares que se activan. A la izquierda se muestra la ruta de producción de IFN β. A la derecha se muestra la ruta de la producción de las citoquinas pro-inflamatorias.

7.1.1.1. Acción del IFN

Los IFNs actúan de forma autocrina y paracrina. Los IFNs de tipo I se unen a los receptores de IFN de tipo I formados por las subunidades IFNAR1 e IFNAR2 localizadas en la membrana plasmática de la célula (Brierley and Fish, 2002; Darnell et al., 1994; Platanias, 2005; Uze et al., 1990). Los IFNs de tipo III se unen a

los receptores de IFN tipo III, localizados en la superficie celular y formados por las subunidades IL10R2 y IFNLR1. La unión de los IFN tipo I y III a sus receptores celulares activa las quinasas *Janus Kinase* (JAK1) y tirosin-quinasa 2 (TYK2), las cuales están localizadas próximas al dominio citoplásmico del receptor. Como consecuencia estas quinasas catalizan la fosforilación de los factores de transcripción STAT1 y STAT2. Los factores STAT1 y STAT2 fosforilados se unen al factor IRF9, formando el complejo *IFN stimulated gene factor 3* (ISGF3). El complejo ISGF3 se transloca al núcleo de las células, e induce la transcripción de más de 100 genes activados por IFN (ISGs) que contienen elementos de respuesta estimulados por IFN (ISRE). Entre estos genes se encuentran genes con función antiviral tales como PKR, 2´-5´-OAS, IFIT y Mx (Chawla-Sarkar et al., 2003; Garcia-Sastre and Biron, 2006).

Los IFNs de tipo II se unen a los receptores compuestos por las subunidades IFNG1 e IFNG2, activando las quinasas JAK1 y JAK2. Estas quinasas fosforilan el factor STAT1, que homodimeriza y se transloca al núcleo, activando la transcripción de genes que contienen sitios activados por IFNγ (GAS). Estos genes activan la respuesta inmune adaptativa, la respuesta inflamatoria, y retroalimentan la respuesta de IFN tipo I, manteniendo la respuesta antiviral (Kotenko et al., 2003)

7.1.2. Antagonistas del IFN en CoV

El tratamiento con IFN inhibe el crecimiento de CoV en células en cultivo y en distintos modelos animales (Barnard et al., 2006; Dahl et al., 2004; Fuchizaki et al., 2003; Haagmans et al., 2004; Kumaki et al., 2011; Mahlakoiv et al., 2012; Sainz et al., 2004; Stroher et al., 2004; Zheng et al., 2004). Por ello, los CoVs, han desarrollado distintas estrategias para inhibir la activación de los sistemas que desencadenan la producción de IFN, y para contrarrestar tanto la producción como la señalización mediada por IFN.

Diversas proteínas virales participan como antagonistas del IFN. La proteína N de MHV y SARS-CoV inhibe la producción de IFN, pero no la cascada de señalización derivada del tratamiento de las células con esta citoquina (Kopecky-Bromberg et

al., 2007; Lu et al., 2011; Ye et al., 2007b). La proteína nsp3 de MHV y SARS-CoV regula negativamente la producción de IFN inhibiéndose la activación del factor IRF3, a través de los dominios PLP2 y PLP1 de nsp3, respectivamente (Frieman et al., 2009; Wang et al., 2011). Además, el dominio PLP1 de la proteína nsp3 de SARS-CoV también inhibe la ruta de señalización mediada por el factor NF-κB (Frieman et al., 2009). Se ha sugerido que el dominio ADP-ribosa-1-fosfatasa de la nsp3 del SARS-CoV y del HCoV-229E, actúa como antagonista del IFN, dado que la eliminación de este dominio aumentó la sensibilidad de estos virus a IFNα (Kuri et al., 2011). La proteína nsp16 previene la producción de IFN de tipo I y disminuye la sensibilidad a IFN de CoV a través de la 2´-O-metilación de la estructura Cap de los mRNAs virales (Zust et al., 2011). La proteína nsp1 estudiada en esta tesis, y descrita con anterioridad, inhibe la ruta de señalización activada por el IFN mediante la inhibición de la fosforilación de STAT1 (Wathelet et al., 2007; Zust et al., 2007).

La proteína 6 de SARS-CoV, que es específica de especie, previene la translocación del factor STAT-1 al núcleo de la célula mediante la retención de las proteínas carioferina α1 y β1 en las membranas del ER/Golgi, que están implicadas en el transporte nuclear (Frieman et al., 2008). La proteína específica de especie 3b de SARS-CoV inhibe la producción y la señalización del IFN (Kopecky-Bromberg et al., 2007). Finalmente, se ha descrito que las proteínas ns2 y 5a del MHV actúan como antagonistas del IFN, dado que su eliminación da lugar a fenotipos atenuados más sensibles al IFN que los virus silvestres (Koetzner et al., 2010; Roth-Cross et al., 2009; Zhao et al., 2011).

7.2. Inflamación

Durante la infección viral, el reconocimiento de los PAMPs mediante receptores celulares dispara la transcripción de diversos genes pro-inflamatorios a través de la activación de factores de transcripción como el NF-κB (Bonjardim et al., 2009). El proceso inflamatorio lleva asociada la producción y secreción de citoquinas, quimioquinas y otros mediadores de la inflamación, y se manifiesta por la aparición de un aumento de la temperatura, dolor, enrojecimiento e hinchazón en

zonas localizadas. La inflamación promueve el aumento en la permeabilidad de los capilares, aumentando el flujo sanguíneo y la salida de líquido hacia los tejidos afectados. Las células del tejido, en el inicio de la infección viral, secretan citoquinas pro-inflamatorias específicas como: TNF, CCL2, CCL4 o CCL5 (RANTES) (Kohlmeier and Woodland, 2009; Strieter et al., 2002). El IFNγ, IL-1, IL-6 e IL-12 se mantienen elevados al menos durante dos semanas después de la aparición de SARS. A su vez los altos niveles de las quimioquinas IL-8, CCL2 y CXCL10 se asocian con una infección aguda del SARS-CoV (Wong et al., 2004a). La sobreexpresión de CXCL10, CXCL9 e IL-8 están asociadas a finales adversos de la enfermedad de SARS (Tang et al., 2005). Además, altos niveles de IFNγ, IL-6 y CCL2 son relevantes durante la fase aguda de SARS (Huang et al., 2005).

Una gran variedad de estas citoquinas favorecen el reclutamiento y la diferenciación de células de la línea blanca de la sangre. Estas células incluyen a los monocitos, granulocitos y células dendríticas. Los monocitos, cuando se internan en los tejidos, se diferencian a macrófagos, los cuales junto con los macrófagos residentes, son las principales células fagocíticas del sistema inmune innato. Las células granulocíticas se dividen en basófilos, eosinófilos y neutrófilos, que después de la extravasación aumentan en número durante la respuesta inmune. Los basófilos y eosinófilos están implicados en la defensa contra parásitos y con las inflamaciones alérgicas respectivamente. Además, estas ultimas células participan en la secreción de moléculas que aumentan la permeabilidad de los vasos sanguíneos. Los neutrófilos tienen una función fagocítica y son los granulocitos más abundantes durante las infecciones virales. Por lo tanto, los macrófagos y los neutrófilos son los responsables de fagocitar y destruir a las células infectadas. El reclutamiento de células de la línea blanca en tejidos inflamados amplifica la señal pro-inflamatoria, dado que los macrófagos y neutrófilos activados producen y secretan nuevas citoquinas y quimioquinas.

Un equilibrio en las infecciones virales está proporcionado por el balance entre los mecanismos pro- y anti-inflamatorios. La combinación de estos mecanismos lleva a la eliminación del virus y a la adquisición de protección frente a nuevas reinfecciones, con mínimo daño en el tejido huésped. Una activación excesiva de los mecanismos pro-inflamatorios puede dar origen a la eliminación del virus, pero

causando excesivo daño en el tejido (Rouse and Sehrawat, 2010). De hecho muchos de los virus que producen hipervirulencia, lo hacen mediante la respuesta inmune que producen, y no debida a su propia replicación en el tejido infectado (Peiris et al., 2010; Zampieri et al., 2007).

7.3. Linfocitos T $CD4^+$ y $CD8^+$

En pacientes con enfermedades respiratorias, como es el caso de los pacientes de SARS, se observan parámetros hematológicos anormales (Wong et al., 2003). La presencia de linfopenia se asocian con la severidad de la enfermedad en general. De hecho, una reducción en la cantidad de células T $CD4^+$ y $CD8^+$ en sangre son el reflejo de la severidad de la enfermedad causada por el virus del SARS (Channappanavar et al., 2014; Wong et al., 2003). Por lo tanto, el recuento de células T es buen marcador para monitorizar la severidad de la enfermedad por SARS. La reducción de los linfocitos se explica por el efecto de varias citoquinas asociadas a las células T, dado que los linfocitos T no se infectan por el SARS-CoV (Maury and Lahdevirta, 1990; Van Campen et al., 1989).

8. MODELOS ANIMALES PARA ESTUDIAR LA PATOLOGIA PRODUCIDA POR EL SARS-CoV

El virus del SARS-CoV replica en múltiples cepas de ratones (BALB/c, C57BL/6, 129 S), hurones, hámsteres, gatos y varias especies de monos (*cynomolgus*, macacos *rhesus*, mono verde africano y titíes) (Subbarao and Roberts, 2006). Sin embargo, estos modelos animales no reproducen fielmente la enfermedad, tal como se da en humanos.

El modelo de ratón tiene múltiples ventajas sobre otros modelos animales debido a su pequeño tamaño, bajo coste, por la posibilidad de ser manipulados genéticamente para la generación de ratones *knock-out* y *knock-in.* Además se obtienen reactivos inmunológicos para el estudio de la patogénesis con facilidad. Sin embargo, ninguno de los modelos de ratones no transgénicos, excepto los ratones viejos o inmunodeprimidos (Stat-/-), desarrollan una enfermedad clínica

significativa, patología y letalidad. En la actualidad el mejor modelo animal para estudiar el SARS, es la infección de ratones convencionales con virus adaptados a crecer en ratón (Day et al., 2009; Roberts et al., 2007; Tseng et al., 2007). Este modelo reproduce la enfermedad (mortalidad y morbilidad) y los síntomas clínicos tal como se dan en humanos. Por ello, en esta tesis doctoral el virus adaptado a ratón SARS-CoV-MA15 (SCoV) se utilizó, como punto de partida en el desarrollo de distintos recombinantes virales (Roberts et al., 2007).

9. VACUNAS PARA PREVENIR EL SARS-CoV

La vacunación basada en el uso de virus inactivados es uno de los métodos más usados para la inmunización y se aplica a un gran número de virus, incluyendo el de la polio o el de la rabia (Montagnon, 1989). En este tipo de vacunas las posibilidades de reversión a un fenotipo virulento son nulas, dado que no se utilizan virus infectivos. En el caso del SARS-CoV se ha descrito que la inmunización con virus inactivados induce protección frente al desafío con el virus nativo en ratones y monos (Kong et al., 2005; Marshall and Enserink, 2004; Qin et al., 2006; Spruth et al., 2006; Zhou et al., 2005). Sin embargo, la inmunización con este tipo de virus podría causar efectos adversos si la inactivación no es completa. En el caso del SARS-CoV se han probado además otras fórmulas vacúnales basadas en vacunas de subunidades, DNA, proteínas virales, vectores virales y virus vivos atenuados, estas últimas con buenos resultados (Enjuanes et al., 2008a; Graham et al., 2013). Por lo general, las vacunas basadas en virus atenuados son más efectivas que otros tipos vacúnales debido a su capacidad para replicar en el huésped, dando lugar a una estimulación antigénica continua y a una alta respuesta inmune de larga duración (Fett et al., 2013). En nuestro laboratorio se generó la primera vacuna para SARS utilizando el virus atenuado SCoV-ΔE. La inmunización con este virus confirió protección en hámsteres, ratones transgénicos hACE2, y en ratones BALB/c de edad avanzada (Fett et al., 2013; Lamirande et al., 2008; Netland et al., 2010). El SCoV-ΔE indujo la producción de altos títulos de anticuerpos neutralizantes así como una respuesta eficiente de células T $CD4^+$ y $CD8^+$, resultando en una disminución del daño pulmonar, la inflamación, la acumulación de edema y la replicación viral después del desafío con el virus nativo. Sin

embargo, el principal inconveniente de las vacunas vivas atenuadas es que, debido a su capacidad para replicar en el huésped, la atenuación puede no ser estable en el tiempo y el virus pueda revertir a un fenotipo patogénico. De hecho, la alta frecuencia de recombinación descrita en los CoVs, tanto en cultivos celulares como en animales (Liao and Lai, 1992) hace del análisis de la estabilidad de cualquier candidato a vacuna un asunto crucial. Por ello, uno de los objetivos de esta tesis fue aumentar la seguridad de la vacuna basada en virus atenuados con deleciones en la proteína E, o mediante la deleción de la proteína nsp1, implicada en la virulencia del virus. Los genes E y nsp1 se encuentran en regiones distantes del genoma (>20 kb), minimizando las posibilidades de reversión a un fenotipo virulento por fenómenos de recombinación. Ambas deleciones introducidas en los respectivos genes, tanto individualmente como de forma conjunta, dieron lugar a virus completamente atenuados que inducían protección en ratones frente al desafío con la cepa virulenta nativa (Jimenez-Guardeño et al., 2015; Regla-Nava et al., 2015). Además, se ha determinado que los virus con deleciones en los dos genes a la vez son estables en cultivos celulares y en ratón, siendo candidatos vacúnales bioseguros para inducir protección por sí mismos o como punto de partida para generar vacunas inactivadas. Este modelo, puede ser aplicable al desarrollo de candidatos vacúnales para otros CoVs altamente patogénicos como el MERS-CoV o nuevos virus emergentes.

OBJETIVOS

Los coronavirus humanos son importantes patógenos zoonóticos. El SARS-CoV infecta a humanos causando aproximadamente un 10% de muertes en los individuos. Actualmente no existe ninguna terapia disponible para los coronavirus humano. Por lo tanto, el entendimiento de los mecanismos de la virulencia del virus SARS-CoV así como el desarrollo de vacunas eficaces son de alta importancia para la prevención de epidemias causadas por este o por otros coronavirus. El objetivo principal de esta Tesis consiste en analizar los mecanismos responsables de la virulencia de SARS-CoV. Asimismo, se propone construir virus atenuados mediante la deleción del gen E y de genes distantes al gen E, incrementando la seguridad de los posibles candidatos a vacunas. Los objetivos específicos que se abordan en esta memoria fueron los siguientes:

1. Generación de una línea celular de ratón susceptible a la infección por SARS-CoV, como herramienta para estudiar la atenuación en cultivos celulares de los SARS-CoVs recombinantes.

2. Análisis de los mecanismos responsables de la atenuación de un SARS-CoV en el que se ha modificado la proteína E mediante la introducción de pequeñas deleciones en los extremos amino y carboxi-terminal de la proteína, y análisis de la inducción de protección conferida por estos virus.

3. Análisis de la estabilidad del SARS-CoV-ΔE candidato a vacuna, y diseño de mutantes atenuados del SARS-CoV bioseguros basados en deleciones en los genes E y nsp1 que protejan frente al síndrome respiratorio agudo y grave.

MATERIALES Y MÉTODOS

1. CÉLULAS EUCARIOTAS

1.1. Líneas celulares

La línea celular Vero E6, derivada de riñón de mono verde africano (*Cercopithecus aethiops*), fue cedida por Eric Snijder (Centro Médico de la Universidad de Leiden, Holanda). La línea celular BHK-pAPN, derivada de la línea epitelial de riñón de hámster BHK-21, que expresa la aminopeptidasa-N porcina, fue cedida por el Dr. H. Laude (Unité de Virologie Immunologie Moléculaires, Jouy-en-Josas, Francia). La línea celular Huh 7.5.1, clon derivado de la línea celular derivada de hepatocarcinoma humano Huh, fue cedida por F. V. Chisari (Scripps Research Institute, La Jolla, California) (Zhong et al., 2005). Las células DBT, derivadas de astrocitoma de ratón, fueron cedidas por el doctor Thomas Gallagher (Centro Médico de la Universidad de Loyola, Chicago, USA). La línea celular derivada de la anterior DBT-mACE2, que expresa establemente la enzima convertidora de angiotensina 2 murina (mACE2), el receptor para el SARS-CoV en ratón, fue generada en nuestro laboratorio (Regla-Nava et al., 2013).

1.2. Cultivo de células eucariotas

Las células se crecieron a 37ºC en una atmósfera de CO_2 al 5% y una humedad del 98% en medio *Dulbecco´s modified Eagle medium* (DMEM, GIBCO) suplementado con aminoácidos no esenciales al 1% (Sigma), 25 mM Hepes, 50 µg/ml de gentamicina (Sigma) y suero bovino fetal (FBS) al 10% (Bio-Whittaker). Las células DBT-mACE2 se crecieron en presencia del antibiótico de selección geneticina (G418) a una concentración de 800 µg/ml. Las células se almacenaron en nitrógeno líquido a una densidad de 1-2x10^6 células/ml en dimetilsulfóxido (DMSO, sigma) al 10% en FBS.

2. BACTERIAS

2.1. Cepas y cultivos de bacterias

La cepa DH10B de *Escherichia coli* (GIBCO/BRL), con fenotipo F^- *mcr*A Δ(*mrr-hsd*RMS-*mcr*BC) ∅80d*lac*ZΔM15 Δ*lac*X74 *deo*R *rec*A1 *end*A1 *ara*D139 Δ(*ara,leu*)7697 *gal*U *gal*K λ-*rps*L *nup*G, se utilizaron para el clonaje de los plásmidos de DNA.

Las bacterias se crecieron en medio líquido Luria Bertani (LB), (Sambrook and Russell, 2001). Este medio contiene 10 g/l de bactotriptona, 5 g/l de extracto de levadura y 10 g/l de NaCl. Para el aislamiento de colonias bacterianas se preparó medio sólido añadiendo agar a una concentración de 15 g/l. El medio líquido o sólido se suplementó con 100 μg/ml de ampicilina, para seleccionar bacterias con los plásmidos psl1190 y pcDNA3 o con 12.5 μg/ml de cloranfenicol, para seleccionar bacterias transformadas con los BACs. Las bacterias transformadas con los plásmidos psl1190 o pcDNA3 y BACs se crecieron a 37ºC y 30ºC, respectivamente.

2.2. Generación de bacterias competentes

Para la electroporación de DNA se utilizaron bacterias DH10B competentes preparadas a partir de una colonia aislada crecida en medio sólido. Esta colonia se creció en 1L de medio SOB (20g/l triptona, 5g/l extracto de levadura, 0.5 g/l NaCl y 0.18 g/l KCl) a 37ºC hasta alcanzar una DO_{550} de 0.7. Las bacterias se mantuvieron a 4ºC durante 20 min y se sedimentaron mediante centrifugación en un rotor GSA de centrífuga Sorvall, a 5000 rpm durante 15 min. Este sedimento se lavó tres veces con una solución de glicerol al 10% previamente enfriada a 4ºC, utilizando un volumen igual al volumen de cultivo inicial para el primer lavado. El volumen inicial se redujo en los sucesivos lavados a la mitad (0.5 y 0.25 l, respectivamente). En cada lavado las bacterias se resuspendieron a 4ºC y se centrifugaron a 4000 rpm durante 15 min. Finalmente, el sedimento se resuspendió en 3 ml de glicerol frío al 10%, y se prepararon alícuotas, que se almacenaron rápidamente a -80ºC.

2.3. Transformación de bacterias

El DNA a transformar se mezcló con 50 μl de las bacterias DH10B competentes y las células se transformaron por electroporación. Para ello, la mezcla se transfirió a una cubeta de electroporación de 0.2 cm (Bio-Rad), aplicándose un pulso eléctrico de 25 μF, 2.5 kV y 200 Ω usando un electroporador *GenePulser* (Bio-Rad). Posteriormente las células se resuspendieron en 1 ml de medio LB, se incubaron a 37ºC en agitación durante 1 hora y se sembraron en placas de medio LB-sólido suplementadas con cloranfenicol o ampicilina.

3. TECNICAS DE MANIPULACIÓN Y ANÁLISIS DEL DNA

3.1. Plásmidos

El plásmido psl1190 (Pharma Biotech), de alto número de copias, que contiene el gen de resistencia a ampicilina (*amp*), fue utilizado para los clonajes y modificaciones de cDNAs virales de hasta 10 kb.

El plásmido pBAC, de una copia por célula, contiene el gen de resistencia a cloranfenicol (*cat*), el origen de replicación del factor F de *E. Coli* (*oriS*) y los genes (*par*A, *par*B, *par*C y *rep*E). Este plásmido se utilizó para los clonajes y modificaciones de cDNAs virales de gran tamaño (Almazan et al., 2000).

El plásmido pcDNA3.1 que codifica el gen ACE2 de ratón (secuencia en el banco de genes NM_001130513.1) se encuentra fusionado al extremo 5´ a un péptido marcador myc (pcDNA3.1-myc-mACE2), fue cedido por M. Farzan (Harvard Medical School, USA) (Li et al., 2004). El plásmido además contiene un gen de resistencia a geneticina (G418).

El plásmido pcDNA3 utilizado para expresar las proteínas E y M del SARS-CoV, se obtuvo de Life technologies. Este plásmido de 5446 nucleótidos contiene genes de resistencia a ampicilina y neomicina.

3.2. Purificación de plásmidos y fragmentos de DNA

La purificación de los plásmidos psl1190 y pcDNA 3 se realizó utilizando los reactivos *Plasmid Mini Kit* (QIAGEN, partiendo de 10 ml de cultivo) *y Plasmid Midi Kit* (QIAGEN, partiendo de 100 ml de cultivo), siguiendo el protocolo del fabricante. Los cultivos se crecieron a 37ºC en medio LB suplementado con 50 μg/ml de ampicilina.

Los plásmidos pBACs se crecieron a 30ºC en un volumen de 400 ml de medio LB suplementado con 12.5 μg/ml de cloranfenicol y se purificaron con el reactivo *Large-Construct Kit* (QIAGEN).

Para la purificación de DNAs amplificados a partir de PCR y fragmentos de DNA extraídos de geles de agarosa se utilizó el reactivo *QIAquick gel extraction kit* (QIAGEN) o el reactivo *QIAEX II* (QIAGEN), en el caso de fragmentos mayores de 10 kb, siguiendo el protocolo indicado por el fabricante en cada caso.

3.3 Enzimas de restricción y ligación de DNA

Todas las enzimas de restricción, desfosforilación (fosfatasa alcalina de gamba) y de ligación (DNA ligasa del fago T4), utilizadas para realizar los clonajes, se adquirieron de New England Biolabs y Roche. Todas las reacciones se realizaron acorde a los protocolos previamente descritos (Sambrook and Russell, 2001). Todas las construcciones generadas fueron confirmadas por secuenciación utilizando un secuenciador automático 373 (Applied Biosystems).

3.4 Amplificación del DNA mediante PCR

Los fragmentos de DNA que no se utilizarían en clonajes o para secuenciar se amplificaron utilizando la enzima *AmpliTaq DNA polymerase* (Applied Biosystems) a una concentración de 2.5 U en un volumen de 50 μl. La mezcla de reacción contenía 20 pmoles de los oligonucleótidos correspondientes, deoxinucleótidos trifosfato (0.25 mM), 1.25 mM de $MgCl_2$ y tampón de PCR (10 mM Tris-HCl pH 8.3, 50 mM KCl). Se utilizaron entre 10 y 50 ng de DNA como molde para la reacción. Las condiciones de la reacción se determinaron en función de la temperatura de

fusión de los oligonucleótidos (Tm) y del tamaño del producto a amplificar. La reacción se llevó a cabo en las siguientes condiciones: (1) 94ºC, 5 min; (2) 25-35 ciclos a 94ºC, 1 min; (Tm-10ºC), 1 min; 72ºC, 1 min/Kb y (3) 72ºC, 10 min. La enzima *Platinum Pfx DNA polymerase* (Invitrogen) que tiene una mayor fidelidad por poseer actividad exonucleasa correctora 3´-5´, fue utilizada para los clonajes y para los fragmentos de DNA que se iban a secuenciar. Las condiciones de reacción fueron similares a las que se utilizaron para la enzima *AmpliTaq DNA polymerase,* a excepción de la temperatura y tiempo de elongación que fue de 68ºC y 2 min/Kb respectivamente.

3.5 Electroforesis del DNA en geles de agarosa

La separación de los fragmentos de DNA para estudios analíticos y para la purificación de bandas de DNA se realizó en geles de agarosa *D-1 Medio EEO* (Pronadisa). Las concentraciones variaron de 0.7% al 1.5% dependiendo del tamaño del fragmento a separar. La agarosa se disolvió en tampón TAE (40 mM Tris-acetato, 1 mM EDTA) y las bandas de DNA se visualizaron con *SYBR®Safe DNA gel stain* 1X (Invitrogen).

4. CONSTRUCCIÓN DE PLÁSMIDOS RECOMBINANTES

4.1. Construcción de los plásmidos pcDNA3-E y pcDNA-HA-M

Para expresar la proteína E de SARS-CoV, se clonó la secuencia de esta proteína en el plásmido pcDNA3.1, añadiendo una secuencia Kozak en el extremo 5´ de la proteína para mejorar la expresión de la misma (Nieto-Torres et al., 2014). Para la generación del plásmido pcDNA3 que contiene una deleción dentro de la proteína E (pcDNA3-E-Δ3) se utilizo el oligonucleótido sentido Δ-*EcoR*I (5-GCGCGCGCGAATTCGCCGCCATGTACTCATTCGTTTCGGAAGAAACAG-3´, que incluye la diana de restricción de la enzima *EcoRI*) y el oligonucleótido antisentido Δ-*Xho*I (5´-CGCGCTCGAGTTAGACCAGAAGATCAGGAACTCCTTCAGAAGAGTT-3´, que incluye la diana de restricción para la enzima *XhoI*) usando como molde el plásmido pBAC-SARS-CoV-MA15-Δ3, con la respectiva deleción. Posteriormente el

producto de PCR se digirió con las enzimas de restricción *EcoRI* y *XhoI* y se clonó en el plásmido pcDNA3. Se confirmó la secuencia de todos los plásmidos generados.

Para construir el plásmido que codifica la proteína M del SARS-CoV fusionada a un péptido marcador HA (pcDNA3-HA-M), la proteína M se amplificó mediante PCR a partir del cDNA infectivo viral. Para ello se utilizaron los oligonucleótidos M-*EcoR*I-HA (5´-GCGCGCCGCGAATTCGCCGCCATGTACCCATACGATGTTCCAGATTACGCTGCAGACAA CGGTACTATTACCGTTGAG-3´, que incluye el sitio de reconocimiento de la enzima de restricción *EcoR*I, la secuencia del péptido marcador HA, y el extremo 5´de la secuencia codificante de la proteína M) y el oligonucleótido antisentido M-*Xho*I (5-´CGCGCTCGAGTTACTGTACTAGCAAAGCAATATTGTC-3´, que codifica la secuencia 3´ de la proteína M y la secuencia de reconocimiento de la enzima de restricción *Xho*I). El producto de PCR se digirió con las enzimas de restricción *EcoR*I y *Xho*I y se clonó en el plásmido pcDNA3.

5. OBTENCIÓN DE SARS-CoV RECOMBINANTES

5.1. Manipulación del SARS-CoV en cultivos celulares

Todo el trabajo con virus infecciosos fue aprobado por el Ministerio de Medio Ambiente (resolución 001/36438). La manipulación del virus en cultivos celulares se realizó en un laboratorio de bioseguridad con nivel de contención 3 (CNB, CSIC). El laboratorio está perfectamente equipado con los medios e infraestructuras necesarias, incluyendo un sistema de tratamiento de aire y de inactivación biológica de efluentes líquidos. Además, el operador está permanentemente protegido con un sistema de filtración de aire *HEPA Airmate* (3M) y la vestimenta adecuada, compuesta por monos y calzas de protección (Tyvek) y varios pares de guantes.

Los virus recombinantes basados en la cepa Urbani del SARS-CoV de longitud completa rSARS-CoV y el mutante de deleción carente del gen E (SCoV-ΔE), y las correspondientes cepas virales adaptadas a ratón rSARS-CoV-MA15 (SCoV) y SCoV-ΔE respectivamente, utilizados en los experimentos de esta tesis, se

generaron y rescataron previamente en el laboratorio (Almazan et al., 2006b; DeDiego et al., 2007; DeDiego et al., 2014; Fett et al., 2013).

5.2 Construcción de cDNAs infectivos

Para identificar las regiones de la proteína E y nsp1 implicadas en la atenuación del virus, se generaron virus recombinantes con mutaciones en ambas proteínas (SCoV-E* y nsp1*). Para ello, se partió de un clon infectivo, que codifica el genoma viral del SARS-CoV-MA15 ensamblado en un BAC (pBAC-SARS-CoV-MA15) (DeDiego et al., 2014; Fett et al., 2013). Los virus recombinantes (SCoV-E*) contenían mutaciones puntuales en la región amino terminal (SCoV-EMut1) o pequeñas deleciones en la región carboxilo terminal de la proteína E (SCoV-EΔ2, -EΔ3, -EΔ4, -EΔ5 y -EΔ6). Para generar los mutantes de la región carboxilo terminal se amplificó una parte del genoma del SARS-CoV (entre los nucleótidos 26044 a 26779), que abarca la proteína E. Se realizaron reacciones de PCR (nombradas como PCR1 y PCR2), usando los oligonucleótidos mostrados en la tabla I. A continuación, los productos de PCR 1 y 2 se utilizaron como moldes en PCRs solapantes utilizando el oligonucleótido VS utilizado en la PCR1 y el oligonucleótido RS usando en la PCR2 (**Tabla I**).

Para generar un virus recombinante que contenía mutaciones puntuales en el extremo amino terminal de la proteína E, un fragmento que contenía los nucleótidos 26042 a 26782 del clon infectivo del SARS-CoV (Almazan et al., 2006b) se generó mediante síntesis química (Bio Basic, Inc). Este fragmento incluía cuatro mutaciones puntuales, generando cuatro cambios de aminoácidos: S3A (TCA a GCA), V5L (GTT a CTT), T9A (ACA a GCA), y T11A (ACG a GCG). En todos los casos se conservó el codón de iniciación de la traducción ATG, el marco de lectura de la traducción y el codón de terminación de la traducción de la proteína E. Además, estas cuatro mutaciones puntuales, eran mutaciones silenciosas para la fase de lectura abierta del gen 3b, que solapa parcialmente con el gen E. Los productos finales obtenidos por PCR o por síntesis química se digirieron con las enzimas *BamH*I y *Mfe*I y se clonaron en el plásmido intermedio psl1190+*BamH*I/*Sac*II que contiene los nucleótidos 26045 a 30091 del clon infectivo del SARS-CoV (Almazan et al., 2006a). Los plásmidos generados (psl1190-EMut1 , -EΔ2, -EΔ3, -EΔ4, -EΔ5, y

-EΔ6) se digirieron con las enzimas de restricción *BamHI* y *SacII* y los fragmentos digeridos se clonaron en el pBAC-SARS-CoV-MA15 para generar los plásmidos pBAC-SARS-CoV-MA15-E*. La integridad de los DNAs clonados se verificó mediante análisis de restricción con la enzima *HindIII* y secuenciación.

Tabla I. Oligonucleótidos usados para la generación de los mutantes de deleción SCoV-E*

E*	PCR	Oligonucleótido	Secuencia (5´-3´)
EΔ2 24 nts	PCR1	E-SARS-25871-VS	CGTTGTACATGGCTATTTCACCG
		E-SARS-26278-RS	GGTTTTACTAAACTCACGTTAACAATAAGC GCAGTAAGGATGGCTAGTGTG
	PCR2	E-SARS-26223-VS	GCGCTTATTGTTAACGTGAGTTTAGTAAAA CC
		E-SARS-28160-RS	CTGAGTGAGCTGTGAACC
EΔ3 21 nts	PCR 1	E-SARS-25871-VS	CGTTGTACATGGCTATTTCACCG
		E-SARS-26299-RS	CGCGAGTAGACGTAAACCGTTGGTTTATTGC AGCAGTACGCACACAATCG
	PCR2	E-SARS-26274-VS	AAACCAACGGTTTACGTCTACTCGCG
		E-SARS-28160-RS	CTGAGTGAGCTGTGAACC
EΔ4 18 nts	PCR 1	E-SARS-25871-VS	CGTTGTACATGGCTATTTCACCG
		E-SARS-26298-RS	CGCGAGTAGACGTAAACCACGTTAACAATA TTGCAGCAGTACGC
	PCR2	E-SARS-26248-VS	GCGTACTGCTGCAATATTGTTAACGTGGTTT ACGTCTACTCGCG
		E-SARS-28160-RS	CTGAGTGAGCTGTGAACC
EΔ5 36 nts	PCR 1	E-SARS-25871-VS	CGTTGTACATGGCTATTTCACCG
		E-SARS-26332-RS	GGAACTCCTTCAGAAGAGTTCAGTACTAAA CTCACGTTAACAATATTGC
	PCR2	E-SARS-26266-VS	GTTTAGTACTGAACTCTTCTGAAGGAGTTCC
		E-SARS-28160-RS	CTGAGTGAGCTGTGAACC
EΔ6 36 nts	PCR 1	E-SARS-25871-VS	CGTTGTACATGGCTATTTCACCG
		E-SARS-26379-RS	CCAAACAGAATAATAATAATAGTTAGTTCG TTTAATTTTTAACACGCGAGTAGACGTAAA CCG
	PCR2	E-SARS-26296-VS	CGCGTGTTAAAAATTAAACGAACTAACTAT TATTATTATTCTGTTTGG
		E-SARS-28160-RS	CTGAGTGAGCTGTGAACC

[a]nts, nucleótidos.

Los virus recombinantes (SCoV-nsp1*) que contenían pequeñas deleciones en la proteína nsp1 (SCoV-nspΔA, -nspΔB, -nspΔC, y -nspΔD), se generaron amplificando una parte del genoma del SARS-CoV (entre los nucleótidos 8142 a 9211), que abarca la proteína nsp1. Para ello se realizaron reacciones de PCR (nombradas como PCR1 y PCR2), usando los oligonucleótidos mostrados en la tabla II.

A continuación, los productos de PCR 1 y 2 se utilizaron como moldes en PCRs solapantes utilizando el oligonucleótido VS utilizado en la PCR1 y el oligonucleótido RS usando en la PCR2 (**Tabla II**).

Tabla II. Oligonucleótidos usados para la generación de los mutantes de deleción SCoV-nsp1*

nsp1*	PCR	Oligonucleótido	Secuencia (5´-3´)
nspΔA 24 nts[a]	PCR1	SARS-8142-VS	GCAGTCGATCATCAGCATACCTAGGTTTCG TCCGGGTGTGACCGAAAGGTAAGATGGAG AGCCTTGTTCTTCAACTCAGTTTGCCTGTC CTTCAGG
		SARS-9211-RS	GGCTTTCAGAAAGTCGCACGTCTGCC
nspΔB 33 nts	PCR 1	SARS-8028-VS	GGCTGCATGCCTAGTGCACCTACGC
		SARS-8471-RS	AGAACGTTTAATGAACACATAGGGCCCAT TTCTGCAACCAGCTCAAC
	PCR2	SARS-8450-VS	GTTGAGCTGGTTGCAGAAATGG
		SARS-9211-RS	GGCTTTCAGAAAGTCGCACGTCTGCC
nspΔC 27 nts	PCR 1	SARS-8028-VS	GGCTGCATGCCTAGTGCACCTACGC
		SARS-8609-RS	AACATTGCGGTATGCAATTGGGGCGATGCC ATAGCTATGACCACCGGC
	PCR2	SARS-8585-VS	GCCGGTGGTCATAGCTATGGCATCG
		SARS-9211-RS	GGCTTTCAGAAAGTCGCACGTCTGCC
nspΔD 33 nts	PCR 1	SARS-8028-VS	GGCTGCATGCCTAGTGCACCTACGC
		SARS-8713-RS	AATGGGATCAGTGCCAAGCTCGTCACCGAG TTCACGGAGTGCACCACTGCC
	PCR2	SARS-8690-VS	GGCAGTGGTGCACTCCGTGAACTC
		SARS-9211-RS	GGCTTTCAGAAAGTCGCACGTCTGCC

[a]nts, nucleótidos.

En todos los casos se conservó el codón de iniciación de la traducción ATG, el marco de lectura de la traducción y el codón de terminación de la traducción de la

proteína nsp1. Los productos finales obtenidos por PCR se digirieron con las enzimas *Avr*I y *Bst*BI y se clonaron en el plásmido intermedio pBAC+*Sfo*I/*Mlu*I, que contiene los primeros 7452 nucleótidos del genoma del SARS-CoV (Almazan et al., 2006a).

Los plásmidos generados (pBAC-ΔA, ΔB, ΔC, y ΔD) se digirieron con las enzimas de restricción *SfoI* y *MluI* y los fragmentos digeridos se clonaron en el pBAC-SARS-CoV-MA15 para generar los plásmidos pBAC-SARS-CoV-MA15-nsp1*. La integridad de los DNAs clonados se verificó mediante análisis de restricción con la enzima *HindIII* y secuenciación.

Los virus recombinantes que contenían deleciones en las proteínas E y nsp1 (ScoV-nspΔD-ΔE y SCoV-nspΔD-EΔ3) se generaron partiendo de los plásmidos finales pBAC-SARS-CoV-MA15-ΔE, y -EΔ3. Para ello estos plásmidos se digirieron con las enzimas *BamH*I y *Mfe*I y los fragmentos digeridos se clonaron en el plásmido que contenía la deleción ΔD en la proteína nsp1 (pBAC-SARS-CoV-MA15-nsp1-ΔD). La integridad de los DNAs clonados se verificó mediante análisis de restricción con la enzima *HindIII* y secuenciación.

5.3. Rescate de SARS-CoVs recombinantes

Para el rescate de los SARS-CoVs recombinantes a partir de los clones de cDNA, células BHK-pAPN crecidas al 90% de confluencia en frascos de 12.5 cm^2 se transfectaron con 6 μg de los plásmidos pBAC-SARS-CoV-MA15-E*-nsp1*, usando 12 μg de Lipofectamina 2000 (Invitrogen), de acuerdo con las instrucciones del fabricante. Después de un periodo de incubación de 6 horas a 37ºC, las células BHK-pAPN se tripsinizaron con 500 μl de tripsina-EDTA y se añadieron sobre una monocapa de células Vero E6, susceptibles a la infección viral. Las células se incubaron durante un periodo de 72 horas. A continuación, se recogió el sobrenadante y se pasó dos veces en células Vero E6 para amplificar el virus. Los virus se clonaron mediante tres pasos sucesivos de purificación de placas de lisis en medio semi-sólido que contenía 0.6% de agarosa (Pronadisa). Para la generación de lotes de los virus, células Vero E6 se crecieron en monocapas hasta el 90% de confluencia y se infectaron a una mdi de 0.0001. El sobrenadante se recogió a las 72 hdi y se almacenó en alícuotas a -80ºC hasta su utilización.

5.4. Titulación del SARS-CoV

Para titular el SARS-CoV por el método de formación de placas de lisis en medio semi-sólido, se utilizaron monocapas confluentes de células Vero E6 crecidas en placas de 6 o 12 pocillos. Se realizó una adsorción con los virus durante 45 minutos a 37°C, se retiró el medio de adsorción, y se añadió medio DMEM suplementado con 2% de FBS y agarosa al 0.6%. A las 72 hdi, las células se fijaron con formaldehído al 10% en tampón fosfato salino (PBS) durante 30 minutos a temperatura ambiente y las placas de lisis se visualizaron mediante tinción con cristal violeta al 0.1% (peso/volumen) y metanol al 20%. El límite de sensibilidad de la técnica fue de 20 unidades formadoras de placa (ufp) por ml.

Para analizar si la infección con SARS-CoV produce placas de lisis en las células DBT-mACE2, las células DBT-mACE2 sembraron a una densidad celular de 2.5 x 10^5 células/cm^2 y se infectaron con SARS-CoV-MA15. Posteriormente se retiró el medio y las células se cubrieron con medio DMEM conteniendo 0.6% de agarosa y FBS al 4%. Las células se fijaron con formaldehido al 10% en PBS a las 48 hdi y las placas se visualizaron mediante la tinción de las células con una solución de cristal violeta.

6. GENERACIÓN DE CÉLULAS DE RATÓN SUSCEPTIBLES A LA INFECCIÓN POR SARS-CoV.

Para obtener una línea de ratón susceptible a la infección por SARS-CoV-MA15, se sembraron células DBT a una densidad celular de 3 x 10^5 células/cm^2. A continuación las células se transfectaron utilizando el programa EN-158 del nucleofector 4D de Amaxa y 1 μg del plásmido pcDNA3.1-mycACE2 linearizado en buffer SG (Lonza). Después de la nucleofeción las células se sembraron en placas de 24 pocillos y se incubaron durante 10 minutos a temperatura ambiente. Transcurrido este tiempo, se agregó medio de cultivo DMEM (GIBCO) suplementado con 25 mM de HEPES, FBS al 10% (Biowhittaker) y aminoácidos esenciales al 1% (Sigma) a las células, y estas se incubaron a 37°C. 24 horas después de la transfección (hdt), se agregó el antibiótico G418 al medio de cultivo a una concentración final de 800 μg/ml, para seleccionar las células que contenían

el plásmido transfectado. El medio de selección se remplazó cada 3 o 4 días. Las células se clonaron tres veces por dilución límite (1 célula/pocillo) en presencia de G418 (800 μg/ml). Finalmente, se seleccionaron 10 clones de DBT-mACE2 y se amplificaron en la presencia del antibiótico.

Para analizar la producción viral en los diferentes clones de células DBT-mACE2, las células se crecieron a una densidad celular de 3.0 x 10^5 células/cm^2 y se infectaron a una mdi de 0.1 con los virus SARS-CoV-MA15 o SARS-CoV-urbani. Los sobrenadantes de las células se recogieron a las 72 horas después de la infección (hdi) y el título viral se determinó en células Vero E6 como se describe en el apartado 5.4. Para analizar el efecto de la mdi en la producción de virus, el clon 6 de las células DBT-mACE2, que produjo el mayor título viral, se infectó a diferentes mdi en el rango de 0.0001 a 1 ufp por célula con el SARS-CoV-MA15. Los sobrenadantes de las células se recogieron a distintos tiempos después de la infección y se titularon en células Vero E6. Para determinar el efecto de la densidad celular en la producción de virus, las células DBT-mACE2 (clon 6) se sembraron a diferentes densidades celulares y se infectaron a una mdi de 0.1. Los sobrenadantes de las células se recogieron a las 72 hdi y se titularon en células Vero E6.

7. MANIPULACIÓN Y ANÁLISIS DEL RNA

7.1. Extracción del RNA total intracelular

Para verificar la secuencia, analizar la estabilidad de los virus generados, y cuantificar la expresión de mRNAs celulares, se extrajo el RNA total de las células infectadas utilizando el reactivo *RNeasy Mini kit* (QIAGEN), según el protocolo del fabricante. El RNA purificado se cuantificó mediante espectrofotometría utilizando un *NanoDrop ND-1000* (NanoDrop Technologies, USA) y se almacenó a -80°C hasta su uso.

7.2. Generación de cDNAs mediante RT-PCR

Para la generación de cDNAs a partir de los RNAs purificados, se realizó una reacción de retrotranscripción (RT) utilizando el reactivo *High Capacity cDNA RT kit* (Applied biosystems). La reacción se llevó a cabo en un volumen de 20 µl utilizando 100 ng de RNA como molde y hexanucleótidos al azar proporcionados en el *kit*. La reacción se mantuvo durante 10 min a 25°C y 120 min a 37°C. La enzima se inactivó incubando la reacción a 85°C durante 5 segundos. Los cDNAs generados se almacenaron a -20°C.

Para verificar la secuencia de las mutaciones introducidas en el genoma viral, se utilizaron 2 µl del cDNA generado en la reacción de RT como molde en una reacción de PCR utilizando la enzima *Platinum Pfx DNA polymerase*, como se ha descrito previamente.

7.3. Cuantificación de RNAs mediante RT-PCR en tiempo real

Para analizar la expresión diferencial de genes celulares, se utilizaron 2 µl de la reacción correspondiente de RT, el reactivo *Taqman Universal PCR Master mix* (Applied Biosystems) y sondas TaqMan específicas de genes de ratón (Applied Biosystems) (**Tabla III**). Se utilizó un volumen de reacción de 20 µl de acuerdo con las especificaciones del fabricante. El análisis se realizó utilizando un equipo *ABI PRISM 7000* (Applied Biosystems) utilizando los siguientes parámetros de reacción: (A) 50°C, 2 min; 95°C, 10min; (B) 40 ciclos de 95°C, 15 seg y 60°C, 1 min. De rutina, se realizaron tres réplicas biológicas y tres réplicas técnicas de las anteriores para aumentar la fiabilidad del análisis. Los datos obtenidos, se analizaron utilizando el programa *ABI PRISM 7000 SDS, vs 1.2.3* (Applied Biosystems). Los valores correspondientes a la media del número de ciclos de corte (Ct) de cada condición experimental, se usaron para calcular los valores de expresión relativos utilizando el método $2^{-\Delta\Delta Ct}$ (Livak and Schmittgen, 2001). El RNA ribosomal (rRNA) 18S o el mRNA que codifica la proteína crecimiento transformante beta (TGB-β) se utilizaron como control, dado que se había demostrado previamente que su expresión no variaba en distintas condiciones

experimentales que implican infección por el virus SARS-CoV (Frieman et al., 2010; Sheahan et al., 2008a) y en datos de matrices de oligonucleótidos.

Para determinar los niveles de expresión de la respuesta inmune en los mutantes SCoV-nsp1*, células DBT-mACE2 se infectaron con los correspondientes virus a una mdi de 0.125. Los RNAs totales de las células infectadas se extrajeron a las 48 hdi como se ha descrito en el apartado 7.1.

Tabla III. Ensayos Taqman usados para analizar la expresión de genes celulares por RT-PCR cuantitativa

Nombre de la proteína	Ensayos Taqman *	Descripción
TNF	Mm00443258-m1	Factor de necrosis tumoral
IL-1α	Mm00439620-m1	Interleuquina 1a
IL-1β	Mm01336189-m1	Interleuquina 1b
IL-4	Mm00445259_m1	Interleuquina 4
IL-5	Mm00439646_m1	Interleuquina 5
IL-6	Mm00446190-m1	Interleuquina 6
IL-10	Mm00439614_m1	Interleuquina 10
IL-12B	Mm00434174_m1	Interleuquina 12B
IL-13	Mm00434204_m1	Interleuquina 13
CCL2/ MCP-1	Mm00441242-m1	Proteína 1 quimiotáctica de monocitos
CCL3/MIP1A	Mm00441259_g1	Proteína 1α inflamatoria de macrófagos
CCL4/(MIP1B	Mm00443111_m1	Proteína 1β inflamatoria de macrófagos
CCL5/RANTES	Mm01302428-m1	Regulación de la activación en la expresión y secreción de las células T normales
IFN-β	Mm00439552-s1	Interferón β
IFN-γ	Mm01168134-m1	Interferón g
CXCL1/NAP-3	Mm04207460-m1	Proteína 3 activadora de neutrófilos
CXCL2/MIP-2	Mm00436450-m1	Proteína 2 inflamatoria de macrófagos
CXCL10/IP-10	Mm00445235-m1	Proteína 10 inducible o proteína del interferón 10
IRF1	Mm01288580_m1	Factor regulador del IFN 1
DDX58	Mm01216853_m1	DEAD (Asp-Glu-Ala-Asp) caja de polipéptido 58
STAT1	Mm00439531_m	Factor trasductor de señal y activador de transcripción 1
TGF-β	Mm01178820_m1	Crecimiento transformante beta 1
18S	Mm03928990-g1	RNA Ribosomico 18S

Mm, significa *Mus musculus*

8. EVALUACIÓN DE PROTEÍNAS

8.1. Infectividad especifica de los virus SCoV-E*

Para determinar la infectividad especifica de las diferentes proteínas E, se infectaron células Vero E6 crecidas al 90% de confluencia, a una multiplicidad de infección de 0.3, con los virus SCoV-E*, SCoV-ΔE y SCoV. El medio de cultivo se retiró a las 8 hdi y se reemplazó con medio fresco y suplementado con 2% de FBS. A las 11 hdi se recogieron los sobrenadantes y se determinó el título viral en células Vero E6. En paralelo, se aisló el RNA viral partiendo de 400 μL de sobrenadante usando el reactivo RNA viral MagMAX™ (Life Technologies), siguiendo las instrucciones del fabricante. La cantidad de RNA genómico se midió por RT-qPCR. Para ello, los RNAs se usaron como moldes para obtener los cDNAs utilizando el kit de transcripción cDNA High Capacity (Applied Biosystems) y el oligonucleótido anti-sentido Q-SARS-2015-RS- (5´- ATGGCGTCGACAAGACGTAAT-3′). Los cDNAS se amplificaron por qPCR usando el reactivo SYBR Green PCR master mix (Applied Biosystems) y oligonucleótidos que hibridan cerca del extremo 5´de la replicasa (oligonucleótido *virus sense* Q-SARS-1931-VS 5´ ACCACTCAATTCCTGATTTGCA-3′; y el oligonucleótido anti-sentido usado para la generación de los cDNAs). La relación entre los títulos virales y la cantidad de RNA genómico representa la infectividad especifica.

8.2. Estimación de la vida media de la proteína E

Para determinar la vida media de las proteínas E de los mutantes SCoV-E*, se infectaron células Vero E6 al 90% de confluencia con los respectivos virus a una mdi de 0.3. Las células se trataron con 200 μg/ml de cicloheximida (Sigma) diluida en medio de cultivo a 12 hdi. Las células se lavaron con PBS a las 0, 2, 4, 6 y 8 horas después del tratamiento. Los extractos de proteínas de células infectadas se obtuvieron realizando un raspado celular con el tampón de lisis de proteínas que contenía 10 mM Tris/HCl, 1 mM EDTA, 150 mM NaCl, 1% IGEPAL y el inhibidor de proteasas *Complete* (Roche), pH8. Los extractos de proteínas se analizaron en geles desnaturalizantes de acrilamida-SDS de gradiente *NuPAGE® Novex 4-12% Bis/Tris*

Precast Gels (Life technologies) utilizando el tampón de carga *NuPAGE® LDS* suplementado con 1mM DTT y se realizó un *Western blot* con anticuerpos específicos frente a la proteína E y frente a la proteína celular actina. Los valores de la vida media de las diferentes proteínas se obtuvieron calculando la masa relativa de la proteína E normalizada con la masa de la proteína actina para cada tiempo.

8.3. Inmunodetección de proteínas (*Western blot*)

Las proteínas presentes en los lisados celulares se separaron mediante electroforesis en geles SDS-PAGE. Las proteínas se transfirieron a membranas de nitrocelulosa (*Hybond-C Extra nitrocellulose membrane*, GEHealthcare) mediante el sistema *Mini Protean II* (BioRad) utilizando un tampón de transferencia que contenía 25 mM Tris/HCl, 192 mM glicina, y 20% metanol pH 8.3, durante 1 hora a 110 V. Las membranas se bloquearon durante 1 hora con leche al 5% en tampón TTBS (20 mM Tris/HCl, 150 mM NaCl, 0.05% Tween-20, pH 7.5) y se incubaron con el anticuerpo primario policlonal de conejo específico para la proteína E (cedido por Shen Shuo, Instituto de Biología Molecular y Celular, Singapore, dilución 1:6000), y anticuerpos monoclonales específicos para el péptido marcador de la hemaglutinina (HA) (dilución 1:1000; Sigma) o para la β-actina (dilución 1:10000, Abcam). Los anticuerpos unidos se detectaron con anticuerpos conjugados a la peroxidasa del rábano picante (HRP), específicos para las distintas especies (dilución 1:30000, Cappel), y el sustrato *Immobilon Western* (Millipore). La intensidad de la señal se cuantificó por *phosphorimaging*.

8.4. Ensayos de inmunoprecipitación

Células Vero E6 crecidas al 90% de confluencia se cotransfectaron con un plásmido que codifica la proteína M del SARS-CoV etiquetada con un péptido marcador HA en la región amino de la proteína (pcDNA3-HA-M) en combinación con plásmidos que expresan la proteína E completa o la proteína E con una pequeña deleción (pcDNA3-E o pcDNA3-Δ3). Como controles se usaron células cotransfectadas con los plásmidos pcDNA3-HA-M y el plásmido vacío pcDNA3. Los extractos celulares se recogieron como se ha descrito anteriormente en el apartado 8.2 a las 24 hdi.

Para los ensayos de immunoprecipitación, los extractos celulares se incubaron con 75 μL de un anticuerpo anti-HA conjugado a agarosa (Sigma) durante toda la noche a 4^0C. El complejo inmune se eluyo usando 20 μL de buffer de carga 2X de SDS y calentado a 95^0C durante 3 minutos. Los complejos de la inmunoprecipitación se analizaron por SDS-PAGE seguidos de *Western blot*.

8.5. Inmunofluorescencia indirecta

Para determinar la expresión de la proteína N viral y de la proteína ACE-2 murina fusionada a un péptido marcador myc, se crecieron células DBT-mACE2 a una confluencia del 80%. Para analizar la expresión de la proteína E, se crecieron células Vero E6 a una confluencia del 70%. Ambas líneas celulares se crecieron sobre cubreobjetos de vidrio. Las células DBT-mACE2 se infectaron con SCoV, SCoV-ΔE y los diferentes mutantes de la proteína E (SCoV-E*) a una mdi de 0.3. A las 24 hdi, se retiró el medio y las células se lavaron dos veces con PBS. Las células se fijaron y se permeabilizaron con etanol frío al 100% durante 20 minutos a -20^oC o con paraformaldehído al 4% en una PBS durante 30 minutos a temperatura ambiente, para analizar las células DBT-mACE2 sin permeabilizar y para analizar la expresión de la proteína E. Las células se incubaron con los respectivos anticuerpos primarios en PBS con FBS al 10%, durante 90 minutos a temperatura ambiente. Se utilizaron los siguientes anticuerpos primarios: un anticuerpo monoclonal producido en ratón específico para la proteína N (SA46-4) que fue cedido por Yin Fang (South Dakota State University, Brookings, USA) a una dilución de 1:500, un anticuerpo de ratón anti myc (Millipore, Ref. 05-724), diluido 1:500, un anticuerpo policlonal de conejo específico para la proteína E (cedido por Shen Shuo, Institute of Molecular and Cellular Biology, Singapore) diluido 1:500, y un marcador anti-ERGIC de ratón (Alexis Biochemicals), diluido 1:200. Los cubreobjetos se lavaron dos veces con PBS y las células se incubaron con anticuerpos secundarios anti-conejo o anti-ratón conjugados a Alexa 488, para la detección de las proteínas N y E, o Alexa 594, para la detección del péptido marcador myc y del marcador para el ERGIC. Los anticuerpos secundarios se incubaron durante 45 minutos a temperatura ambiente a una dilución de 1:500 en PBS conteniendo FBS al 10%. Para la tinción de los núcleos, las muestras se

incubaron con el reactivo DAPI a una dilución de 1:200 (Sigma) durante 20 minutos. Finalmente los cubreobjetos se montaron en portaobjetos utilizando el reactivo Prolong Gold anti-fade (Invitrogen) y se analizó la fluorescencia en un microscopio confocal Leica SP5 (Leica Microsystems). El porcentaje de expresión de mACE2 y la proteína N viral se calculó analizando 10 campos aleatorios que contenían por lo menos 30 células cada uno.

8.6. Cuantificación de citoquinas en células infectadas

Para determinar los niveles de citoquinas a nivel de proteína, células DBT-mACE2 (clon 6), se infectaron a una mdi de 0.1 y los extractos celulares se recogieron a las 48 hdi en buffer de lisis de proteínas (1% NP-40, 50 mM Tris-HCl, pH 7.6, 2 mM NaCl, 2 mM EDTA e inhibidores de proteasas). Los extractos celulares se diluyeron 1:5 en el buffer de ensayo (Millipore). La expresión de las citoquinas de ratón CXCL10/IP-10 y CXCL2/proteína 2 inflamatoria de macrófagos (MIP-2) se evaluó utilizando un reactivo a base de perlas para la detección de citoquinas de ratón (Milliplex map kit; Millipore) y la tecnología del Luminex, siguiendo las instrucciones del fabricante. Se analizaron tres infecciones independientes.

9. PATOGÉNESIS VIRAL EN RATÓN

9.1. Cepa de ratón utilizada, inoculación y manejo de ratones infectados

Todos los protocolos de trabajo se aprobaron por el Comité de Ética del centro de trabajo CISA-INIA (números de permiso: 2011-009 y 2011-09), de acuerdo con el Real Decreto Español (RD 1201/2005) y las normas internacionales de la Unión Europea 2010/63/UE y la ley española 32/2007 sobre la protección y el manejo de los animales de experimentación, y por el comité de bioseguridad de cuidados de animales y bioética de la Universidad de Iowa. Para los experimentos de patogénesis del SARS-CoV se utilizaron hembras de ratones libres de patógenos específicos BALB/c OlaHsd, obtenidas de Harlan o compradas al Instituto Nacional del Cáncer, USA de 6 o 16 semanas de edad. Los ratones se anestesiaron con isofluorano (IsoFlo, Abbott Laboratories Ltd) y se inocularon intranasalmente

utilizando 100000 ufp, de los virus en un volumen de 50 µl de DMEM suplementado con 2% de FBS. Para los experimentos de protección, los ratones se inmunizaron con una dosis viral de 6000 ufp de los virus atenuados y se desafiaron con una inoculación intranasal de un virus nativo SCoV a una dosis letal de 100000 ufp a los 21 después de la inmunización. La manipulación de ratones infectados se llevó a cabo en laboratorios de nivel 3 de bioseguridad del Centro de Investigación en Sanidad Animal (CISA-INIA) o de la Universidad de Iowa, equipados con las infraestructuras de contención descritas anteriormente para el trabajo con cultivos celulares, y además, con los *rack* ventilados *Animal transport unit-Bio containment unit* (Harvard) para mantener a los animales durante el desarrollo del experimento.

9.2. Seguimiento de la enfermedad y análisis de la virulencia

La pérdida de peso, los síntomas de la enfermedad y la supervivencia de los ratones infectados intranasalmente se evaluó durante un periodo de 10 días. Los animales que durante el experimento alcanzaron pérdidas de peso superiores al 25% fueron sacrificados de acuerdo con los protocolos de eutanasia establecidos.

9.3. Producción viral en los pulmones de los ratones infectados

Para el análisis de la producción de virus, los ratones se sacrificaron por dislocación cervical y se recogieron los pulmones infectados a 2 y 4 ddi. El pulmón derecho se homogenizó en 2 ml de PBS suplementado con 100 UI/ml de penicilina, 100 µg/ml de estreptomicina, 50 µg/ml de gentamicina y 0.25 µg/ml anfotericina B utilizando un homogeneizador *gentleMACS Dissociator* (Milteny Biotec) siguiendo el protocolo descrito por el fabricante. Las muestras se centrifugaron a 3000*xg* durante 10 min a 4°C, y se recogieron los sobrenadantes para su titulación en células Vero E6, como se ha descrito anteriormente. Los títulos virales se expresaron como ufp/g de tejido.

9.4. Extracción de RNA y proteínas de pulmón

Para obtener el RNA total de pulmón, las muestras se recogieron a 2 y 4 ddi y se incubaron en el reactivo *RNAlater* (Ambion) a 4°C durante 48 horas con el fin de preservar la integridad de las moléculas de RNA. Inmediatamente las muestras se congelaron a -80°C hasta el momento de su procesamiento. Para extraer el RNA total, los pulmones se homogenizaron en 2 ml de tampón *RLT lysis buffer* (QIAGEN) suplementado con β-mercaptoetanol al 1% utilizando el sistema *gentleMACS Dissociator* (Miltenyi Biotec) siguiendo el protocolo propuesto por el fabricante. Las muestras se centrifugaron a 3000*xg* durante 10 minutos, y el RNA se purificó de los sobrenadantes utilizando el reactivo *RNeasy mini kit* (QIAGEN) como se ha descrito previamente. La expresión génica celular se analizó usando sondas TaqMan específicas para genes de ratón (Applied Biosystems) (**Tabla III**).

Para el análisis de la expresión de citoquinas a nivel de proteína en pulmón, se homogenizaron los pulmones de los ratones infectados y las proteínas de las fracciones nuclear, citoplasmática y extracelular, se extrajeron usando el reactivo de extracción de núcleos (Active Motif, Carlsbad, CA). El sobrenadante, que contiene las proteínas citoplasmáticas y extracelulares, se diluyó 1:5 en tampón de ensayo (Millipore) antes del análisis. La expresión de las citoquinas TNF, MCP-1/CCL2, KC/CXCL1, IL-5, IL-6, IL-13, IFN-γ, proteína inflamatoria de macrófagos, (MIP-1α)-1A/CCL3 y MIP-1β/CCL4 se midió utilizando la tecnología *Luminex* y los correspondientes anticuerpos específicos de ratón conjugados a bolas magnéticas (Milliplex map kit, Millipore), siguiendo las especificaciones del fabricante.

9.5. Histopatología en tejido pulmonar de ratón

Para los estudios de histopatología se extrajeron los pulmones derechos de los ratones. Los pulmones se fijaron en formalina de zinc y se embebieron en parafina. Se realizaron 3 secciones de 4 μg de grosor cada 200 μm que se tiñeron con hematoxilina y eosina en el servicio de histología del Centro Nacional de Biotecnología (CNB-CSIC, Madrid, España).

9.6. Medición de infiltrados leucocitarios en los pulmones de ratón

Para la cuantificación de las células leucocitarias, se inocularon ratones de 16 semanas con una dosis de 100000 ufp de cada virus como se ha descrito anteriormente. A los 4 ddi se recogieron los pulmones, se cortaron en trozos pequeños y se digirieron con el buffer HBSS que contenía 2% de FBS, 25 mM de HEPES, 1 mg/ml de Colagenasa D (Roche, Indianapolis, IN) y 0.1 mg/ml de DNasa (Roche), durante 30 minutos a temperatura ambiente. Los restos de materiales triturados se eliminaron con un filtro de 70 μm para obtener suspensiones de células simples. Para la identificación de los macrófagos se utilizaron los marcadores $CD45^+$ $CD11b^+$ $Ly6C^+$ $Ly6G^-$ y para la identificación de neutrófilos $CD45^+$ $CD11b^+$ $Ly6C^+$ $Ly6G^+$. Los anticuerpos monoclonales de rata anti ratón utilizados fueron CD11b (M1/70), CD16/32 (2.4G2), Ly6G (1A8) y Ly6C (AL-21) todos ellos de BD Biosciences (San Diego, CA). Además se utilizó el anticuerpo anti-ratón F4/80 (BM8) de eBioscience (San Diego, CA). Para la tinción de la superficie celular, se bloquearon 10^6 células con 1 μg del anticuerpo anti CD16/32 en suero de rata al 1%. A continuación, las células se incubaron con los anticuerpos específicos $CD11b^-$, $Ly6G^-$, $Ly6C^-$ y F4/80 y se fijaron utilizando la solución Cytofix (BD Biosciences). Para la identificación de las células $CD4^+$ y $CD8^+$ específicas frente a SARS-CoV, las células se incubaron con una solución de brefeldina A (BD Pharmingen, San Diego, CA) durante 5 horas, en la presencia o ausencia de los péptidos específicos para el SARS-CoV S366 (CD8; HNYKYRYL) y N353 (CD4; VNFNFNGL) (BioSynthesis Inc., Lewisville, TX). A continuación, se marcó la superficie celular de 10^6 células con los anticuerpos de rata anti ratón específicos frente a CD4 (RM4-5), CD8α (53-6.7) (ambos de BD Bioscience) y IFN-γ (XMG1.2) (eBioscience, San Diego). Finalmente, las células se fijaron y permeabilizaron con una solución de Cytofix/Cytoperm (BD Biosciences) y se marcaron con el anticuerpo anti IFN-γ. Todos los datos de citometría de flujo se adquirieron con un BD FACSCalibur o FACSVerse (BD Biosciences, San José, CA) y se analizaron usando el programa informático FlowJo (Tree Star, Inc).

9.7. Pases seriados en ratones

Para analizar la estabilidad del virus SCoV-nspΔD-EΔ3, los ratones se sacrificaron por dislocación cervical y se recogieron los pulmones infectados a 2 ddi. El pulmón derecho se homogenizó y se clarifico como se ha descrito previamente en el apartado 9.3. Posteriormente 100 µl de este sobrenadante fue administrado nuevamente intranasalmente a otro ratón nativo. El proceso de inoculación intranasal de ratones con sobrenadante clarificado de pulmón colectado cada 2 ddi fue repetido durante 10 veces.

9.8. Análisis estadístico

La prueba estadística t de student fue usada para analizar las diferencias de los valores promedios entre los diferentes grupos. Todos los resultados se expresaron como el promedio $\pm$ los errores de las desviaciones estándar de los promedios. Los valores $P < 0.05$ fueron considerados estadísticamente significativos.

10. TRANSCRIPTÓMICA EN RATÓN

10.1. Análisis de la expresión génica en pulmones de ratones infectados

Para analizar la expresión génica, los ratones se infectaron con 100000 ufp de los virus SCoV, SCoV-ΔE, SCoV-EΔ3 y SCoV-EΔ5 o se dejaron sin infectar, como control. A los 2 ddi, se extrajo el RNA total de los pulmones, como se ha indicado anteriormente.

10.2. Análisis de matrices de oligonucleótidos

Para los análisis de matrices de oligonucleótidos se utilizaron pulmones de ratones infectados a los 2 ddi. La integridad del RNA total se evaluó con un *Bioanalyzer 2100* (Agilent Technologies) siguiendo especificaciones del fabricante, y los datos se analizaron con el programa informático *2100 Expert* (Agilent Technologies). Para aumentar la fiabilidad y representatividad de los ensayos de genómica, se

analizaron RNAs de tres pulmones diferentes, los cuales se hibridaron independientemente en los matrices de oligonucleótidos. Para los ensayos, se utilizaron 200 ng de RNA total, que se amplificaron usando el reactivo *One Color Low Input Quick Amp Labeling Kit* (Agilent Technologies). La preparación de las sondas y las hibridaciones se desarrollaron según se describe en el manual de análisis de la expresión génica basado en matrices de oligonucleótidos (Ver. 6.5 Agilent Technologies). Para cada hibridación se utilizaron 600 ng de sonda mezclada en 5 μl de agente bloqueante 10x y 1 μl de buffer de fragmentación 25x, en un volumen total de 25 μl de agua libre de nucleasas. La mezcla se incubó a 60^0C durante 30 minutos para fragmentar el RNA. La reacción se paró utilizando 25 μl de buffer de hibridación 2x, e inmediatamente las muestras se pasaron a hielo y se cargaron cuidadosamente en los *arrays* de ratón. (Sure Print G3 Agilent 8x60K Mouse; G4852A-028005). Los arrays se hibridaron a 65^0C durante 17 horas en un horno rotatorio de hibridación. Posteriormente el *chip* se lavó una vez con el buffer 1 GE durante 1 minuto a temperatura ambiente, y otra vez con el buffer 3 GE a 37^0C durante 1 minuto. Los arrays se secaron por centrifugación a 2000 rpm durante 2 minutos. Las imágenes se capturaron con un escáner Microarray Agilent y los puntos se cuantificaron usando un programa de extracción de rasgos (Agilent Technologies). La corrección y normalización de los datos de expresión se realizó usando modelos lineales para datos de matrices de oligonucleótidos (LIMMA) (Smyth, 2004).

10.3. Análisis de datos de matrices de oligonucleótidos.

Para determinar los genes expresados diferencialmente se usaron los métodos LIMMA. Cada sonda se analizó usando el método estadístico t empírico moderado de Bayes (Benjamini and Hochberg, 1995). Para el control de la tasa de frecuencia de falsos descubiertos (FDR), los valores-p fueron corregidos usando el método de Benjamini y Hochberg. Se consideró que un gen estaba diferencialmente expresado cuando los valores de FDR fueron <0.05, y las tasas de cambio fueron >2 o <-2. Los resultados de los matrices de oligonucleótidos se depositaron en la base de datos de expresión génica Omnibus (GEO [Natiotal Center for Biotechnology Information], con el código de acceso (GSE59185).

RESULTADOS

1. GENERACIÓN DE UNA LÍNEA CELULAR MURINA ALTAMENTE SUSCEPTIBLE A LA INFECCIÓN POR SARS-CoVs ADAPTADOS A RATÓN

1.1 Estrategia para la generación de una línea celular murina susceptible a la infección por SARS-CoVs adaptados a ratón, que expresa el receptor mACE2

El modelo animal utilizado en esta tesis consiste en infectar ratones BALB/c con un virus adaptado a ratón SARS-CoV-MA15 (SCoV) (Roberts et al., 2007). Sin embargo, las células de ratón no son susceptibles a la infección por SCoV. Con el objetivo de generar una línea celular de ratón altamente susceptible a la infección por un SARS-CoV adaptado a crecer en ratón SCoV, se nucleofectaron células DBT con un plásmido que codifica el receptor del SARS-CoV, la enzima convertidora de angiotensina 2 (ACE2) murina, y un gen de resistencia a geneticina (G418) (**Figura 8**). Las células transfectadas se seleccionaron utilizando dicho antibiótico.

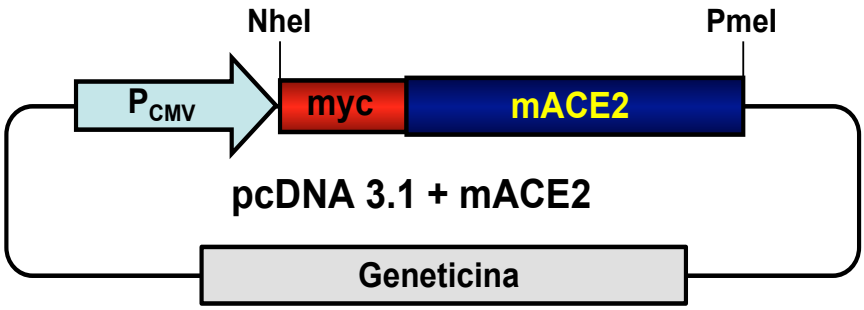

Figura 8. Plásmido pcDNA 3.1 que expresa el receptor murino de SARS-CoV. El pcDNA codifica un péptido marcador myc, fusionado a la proteína mACE2 en la región amino terminal, bajo un promotor de citomegalovirus (CMV), así como de un gen de resistencia a geneticina para seleccionar las células transfectadas.

Se generaron 10 clones celulares que se derivaron independientemente. La expresión de la proteína mACE2 en los diferentes clones se analizó mediante inmunofluorescencia usando un anticuerpo específico frente al péptido marcador myc. Myc-mACE2 se detectó en la membrana plasmática, en células no permeabilizadas, confirmando que el receptor mACE2 estaba presente en la superficie de la célula (**Figura 9**).

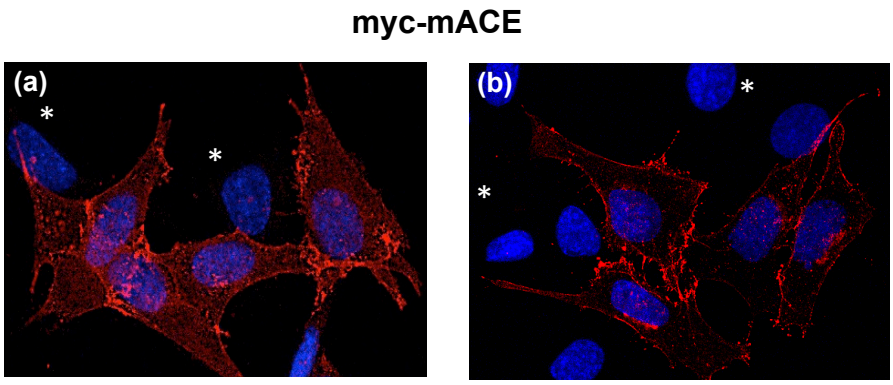

Figura 9. Expresión de myc-mACE2 en los clones de células DBT-mACE2 infectados con SCoV. Células DBT-mACE2 se infectaron a una mdi de 0.1 con el virus SCoV (WT). La expresión de myc-mACE2 se analizó por inmunofluorescencia indirecta usando anticuerpos específicos frente a myc. Se utilizo el anticuerpo secundario de ratón conjugados a A549. Los asteriscos indican células que no expresan myc-mACE2 como control. (a) células myc-mACE2 permeabilizadas y (b) células myc-mACE2 no permeabilizadas.

Como se esperaba, la expresión de myc-mACE2 no se detectó en células DBT sin transformar (**Figura 10A**). Los 10 clones seleccionados mostraron una alta expresión de la proteína myc-mACE2 en más del 70% de las células (**Figura 10B**). La expresión de myc-mACE2 fue estable en cultivos celulares durante al menos 20 pases. Para determinar el porcentaje de células infectadas, células DBT sin transformar y clones de células DBT-mACE2 se infectaron con SCoV. La expresión de la proteína N viral se detectó con un anticuerpo específico frente a la proteína N mediante inmunofluorescencia. El porcentaje de células infectadas fue mayor del 70% en todos los clones de DBT-mACE2 (**Figura 10A y B**). Para determinar si las células DBT-mACE2 son fácilmente transfectables con plásmidos de DNA, las células se nucleofectaron con un plásmido que codifica la proteína verde fluorescente (GFP). Así mismo, se observó que la eficacia de nucleofeción de estas células fue mayor al 90% (datos no mostrados).

1.2 Susceptibilidad de las células DBT-mACE2 a la infección por SARS-CoV

Para determinar si las células DBT-mACE2 eran susceptibles a la infección por SARS-CoV, los 10 clones seleccionados, células DBT sin transformar y células Vero E6 como control positivo, se infectaron con SCoV a una mdi de 0.1 y se analizaron

los títulos virales en los sobrenadantes de las células infectadas a las 72 hdi. No se detectaron virus infectivos en las células sin transformar pero si en las células transformadas y en las células Vero E6 (**Figura 11A**).

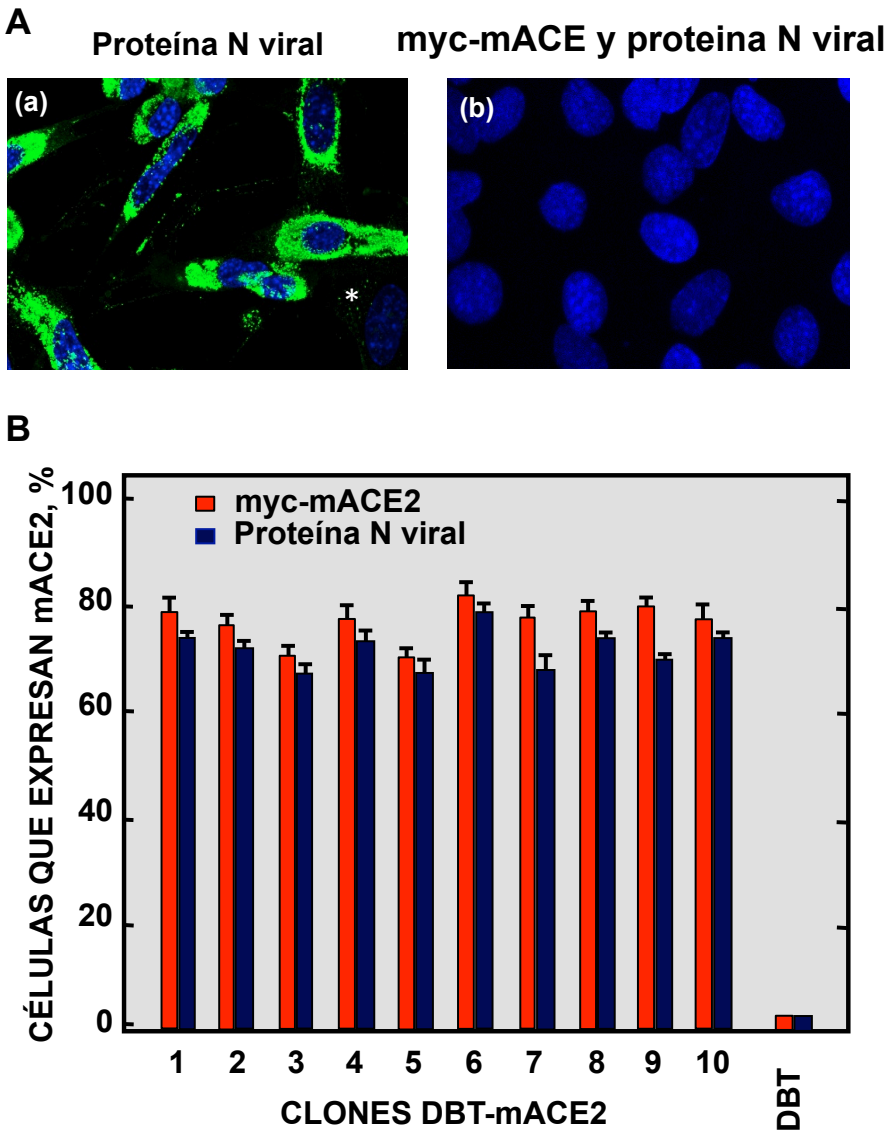

Figura 10. Expresión de la proteína N viral en los clones de células DBT-mACE2 infectados con SCoV. (A) Células DBT sin transformar y células DBT-mACE2 se infectaron a una mdi de 0.1 con el virus SCoV (WT). La expresión de myc-mACE2 y de la nucleoproteína viral N se analizó por inmunofluorescencia indirecta usando anticuerpos específicos frente a myc y específicos para la proteína N, respectivamente. Se utilizaron los anticuerpos secundarios de ratón conjugados a A549 y A488, respectivamente. Los asteriscos indican células que no expresan la proteína N viral como control. (a) proteína N viral en células permeabilizadas y (b) myc-mACE2 y proteína N viral en células DBT sin transformar. (B) El porcentaje de células positivas para myc-mACE2 y la proteína N viral se calculó analizando campos al azar que contenían por lo menos 30 células.

Para analizar si las células DBT-mACE2 eran susceptibles a la infección por una cepa de SARS-CoV no adaptada a crecer en ratón (Urbani), el clon 6 de células DBT-mACE2, que producía el mayor título viral para el recombinante SCoV, células DBT sin transformar y células Vero E6, se infectaron con SARS-CoV-Urbani. Este virus creció en células DBT-mACE2, aunque con títulos 1000 veces menores que los obtenidos para SCoV (**Figura 11A y B**). Por el contrario, en células DBT sin transformar no se recuperaron virus infecciosos. Los títulos en células Vero E6 fueron similares para los virus SCoV y SARS-CoV-Urbani (**Figura 11A y B**).

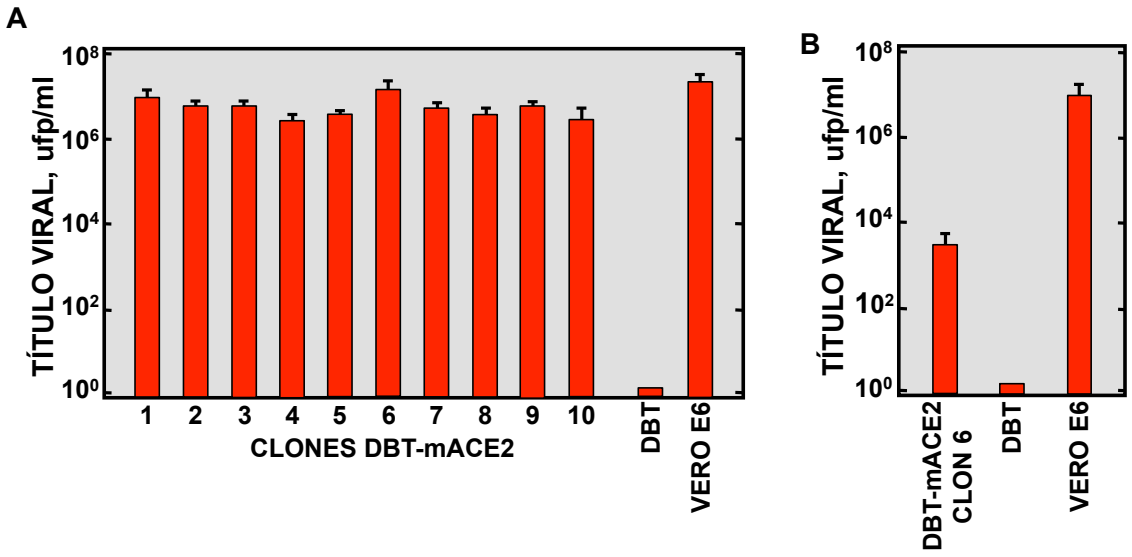

Figura 11. Producción de SARS-CoV en los clones de células DBT-mACE2. Las células se infectaron a una mdi de 0.1 con SCoV (WT) (A) ó con SARS-CoV-Urbani (WT) (B). Se determinaron los títulos virales en los sobrenadantes de las células a 72 hdi mediante ensayos de placa de lisis en células Vero E6. Las barras de error representan las desviaciones estándar de tres experimentos independientes. Todos los clones de las células transfectadas mostraron altos títulos virales a 72 hdi, que oscilaron entre 5.0 x 10^6 a 1.2 x 10^7 ufp/ml, similares a los títulos virales obtenidos en células Vero E6. Los clones 1 y 6 son los que produjeron un mayor título viral (9.2 x 10^6 y 1.2 x 10^7 ufp/ml, respectivamente).

Para identificar las variables óptimas para la producción de virus, se infectaron células a distintas mdi y densidades celulares y se evaluó el efecto en la producción viral. Para ello, células DBT-mACE2 (clon 6) se infectaron con SCoV a diferentes mdi, en el rango de 0.0001 a 1. Los títulos virales se determinaron a 0, 4, 24, 48 y 72 hdi (**Figura 12**). El mayor título viral (>10^7 ufp/ml) se obtuvo a una mdi de 0.1. Cuando las células se infectaron a una mdi de 1 el título viral disminuía

rápidamente después de 24 hdi (**Figura 12**), probablemente debido a una rápida de muerte celular, que se reflejaba en el considerable efecto citopático observado por microscopia óptica.

Para determinar el efecto de la densidad celular en la producción viral, las células DBT-mACE2 (clon 6) con diferentes densidades celulares (de 0.5 x 10^5 a 4 x 10^5 células/cm^2), se infectaron con una mdi óptima de 0.1 y los títulos virales se determinaron a 72 hdi. El mayor título viral (>10^7 ufp/ml) se observó para una densidad celular de 3 x 10^5 células/cm^2 (**Figura 13**).

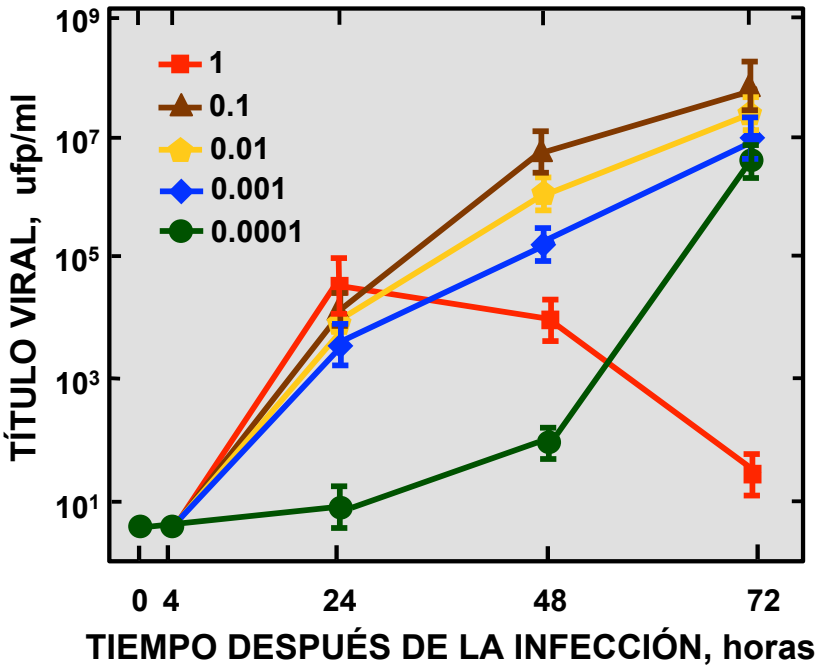

Figura 12. Efecto de la mdi en la cinética de crecimiento del SCoV en células DBT-mACE2. Células DBT-mACE2 (clon 6) se infectaron con el virus nativo (WT) a las mdi indicadas. Se determinaron los títulos virales en los sobrenadantes de las células infectadas a distintos tiempos después de la infección mediante ensayos de placa de lisis sobre células Vero E6. Las barras de error representan las desviaciones estándar de tres experimentos independientes.

La infección por SARS-CoV causa efecto citopático en células DBT-mACE2. Cuando las células se infectan a una mdi de 0.1, las células presentan una morfología redondeada y un evidente desprendimiento de la superficie de la placa de cultivo a 48 hdi, siendo casi total a las 72 hdi (**Figura 14A**). En medio sólido, la infección por el SCoV forma placas de lisis en las células DBT-mACE2, de tamaño mayor a las

observadas en células Vero E6 (**Figura 14B**), lo cual indica que estas células se pueden utilizar para titular los virus SCoV adaptados a ratón.

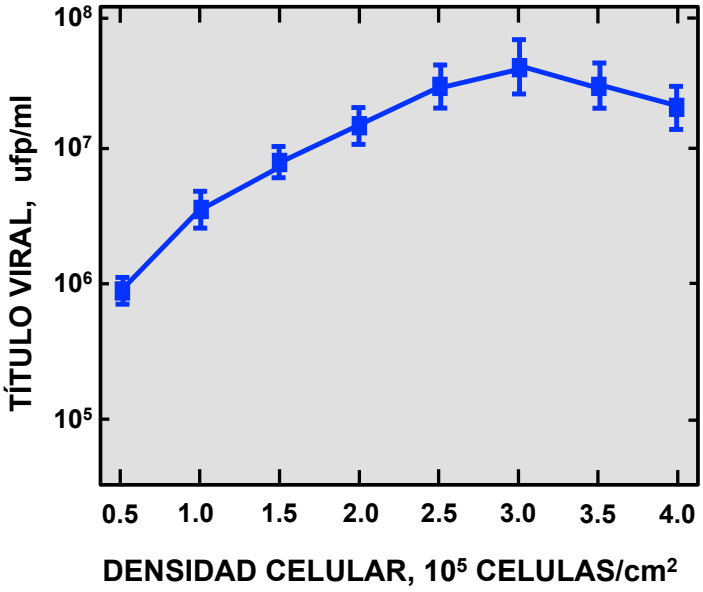

Figura 13. Efecto de la densidad celular en el crecimiento del SCoV en células DBT-mACE2. Células DBT-mACE2 se sembraron a diferentes densidades celulares y se infectaron con el virus nativo (WT) a una mdi de 0.1. Los títulos virales se determinaron en los sobrenadantes de las células infectadas a las 72 hdi. Las barras de error representan las desviaciones estándar de tres experimentos independientes.

1.3. Expresión de citoquinas pro-inflamatorias en células DBT-mACE2 infectadas con SCoV

Las citoquinas y los IFNs son importantes mediadores en la regulación de la respuesta inmune (Cameron et al., 2007; Chien et al., 2006; Jiang et al., 2005; Lam et al., 2004; Puneet et al., 2005; Smits et al., 2011; Tang et al., 2005; Wong et al., 2004). Para determinar si las células DBT-mACE2 son un buen modelo para evaluar la respuesta de IFN y la respuesta inflamatoria del huésped después de la infección por SCoV, se determinaron los niveles de expresión de los mRNAs de IFN-β e IFN-γ y de las citoquinas pro-inflamatorias CCL2/MCP-1, factor de necrosis tumoral (TNF), CXCL10/IP-10, CXCL1/proteína 3 activadora de neutrófilos (NAP-3), CXCL2/MIP-2, CCL5/RANTES, IL6, IL1B, e IL1A mediante RT-qPCR. Los niveles de expresión se compararon entre células no infectadas e infectadas con SCoV a 24,

48 y 72 hdi. Los niveles de inducción de citoquinas fueron entre 1.2 y 3 veces mayores en células infectadas a las 48 hdi, que a las 24 hdi. Se observaron niveles similares de expresión a las 48 y 72 hdi (datos no mostrados). Las citoquinas que mostraron mayores niveles de inducción a las 48 hdi fueron: CCL2/MCP-1, TNF, CXCL10/IP-10 y CXCL1/NAP-3, con incrementos de 22 a 50 veces, en relación con las células sin infectar (**Figura 15A**).

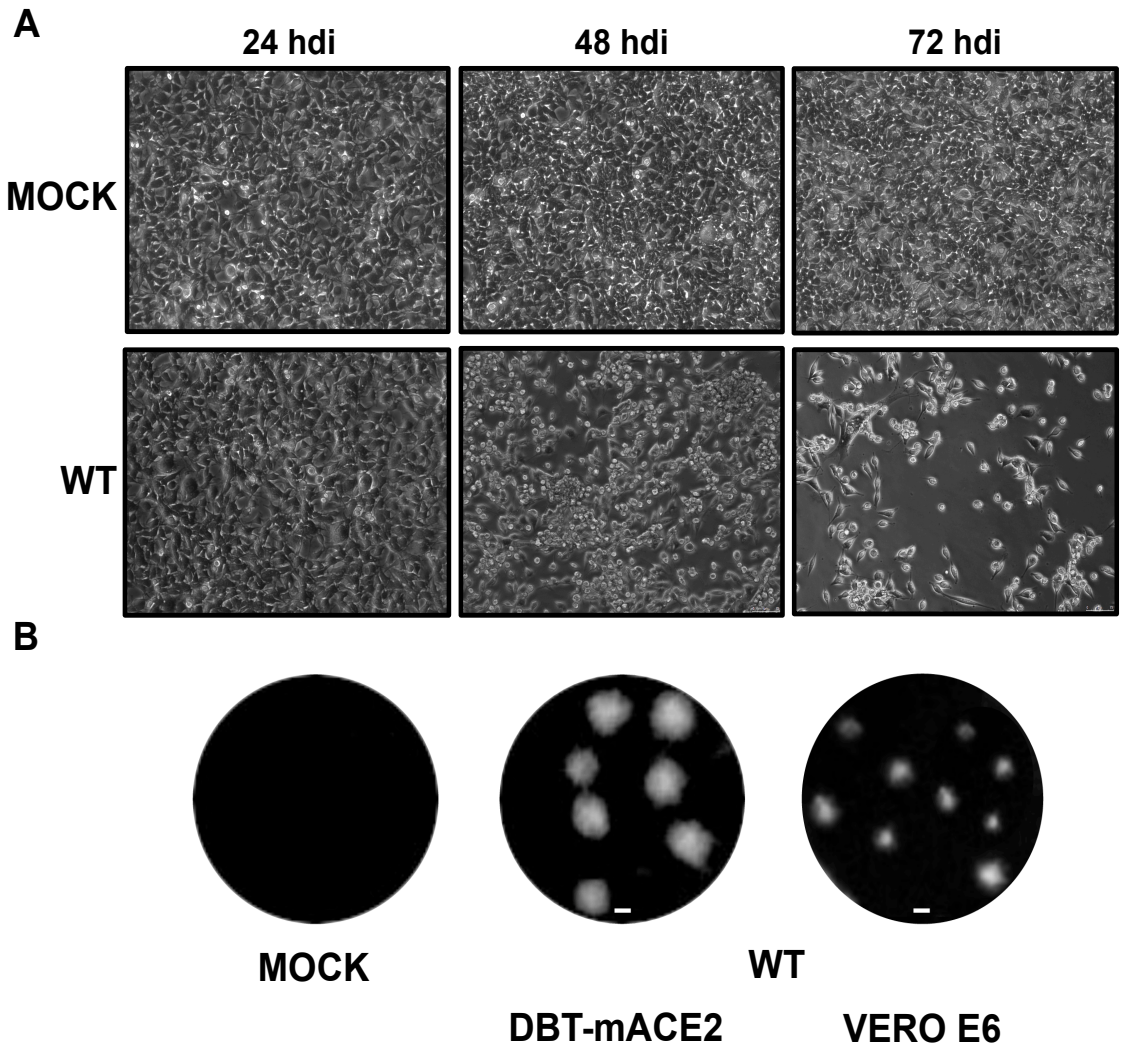

Figura 14. Efecto citopático y placas de lisis producidas por la infección de SCoV en células DBT-mACE2. (A) Células DBT-mACE2 (clon 6) se dejaron sin infectar (Mock) o se infectaron con SCoV (WT) a una mdi de 0.1. El efecto citopático se analizó a 24, 48 y 72 hdi. (B) Placas de lisis en células DBT-mACE2 y Vero E6 producidas por la infección por SCoV 2 ddi.

Después de la infección, se observó una menor inducción de las citoquinas IFN-β, CXCL2/MIP-2, CCL5/RANTES e IL6, mientras que se observaron cambios muy

limitados en las citoquinas IL1B, IL1A e IFN-γ (**Figura 15A**). Los niveles de expresión del rRNA 18S, usado como control, no variaron en células infectadas y no infectadas. Para evaluar si la inducción de citoquinas a nivel de mRNA en células DBT-mACE2 infectadas por SCoV se correlacionaba con los niveles de inducción a nivel de proteína, se determinaron los niveles de expresión de las proteínas CXCL2 y CXCL10 en células no infectadas e infectadas. La expresión de las proteínas CXCL10 y CXCL2 aumentó 3 y 1.8 veces, en células infectadas en comparación con las células sin infectar, respectivamente (**Figura 15B**). Los datos obtenidos indican que las células DBT-mACE2 son útiles para el estudio de la expresión de citoquinas pro-inflamatorias y de inducción de IFN de tipo I.

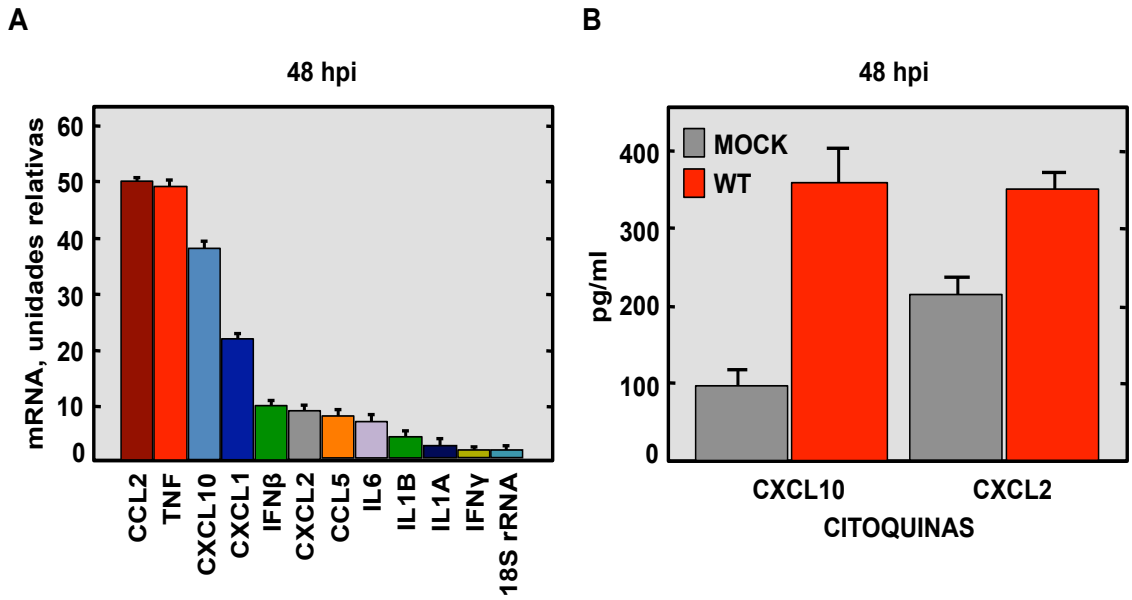

Figura 15. Expresión de citoquinas pro-inflamatorias en células DBT-mACE2 infectadas con SCoV. Se infectaron células DBT-mACE2 (clon 6) a una mdi de 0.1 con el recombinante SCoV (WT). (A) Los RNAs celulares se extrajeron a las 48 hdi. La expresión de las citoquinas indicadas, de los interferones, y el rRNA 18S usado como control se determinó mediante RT-qPCR. Los niveles de expresión de los correspondientes mRNAs se normalizaron en cada caso en relación con los niveles de expresión en células no infectadas. (B) Extractos celulares se prepararon a las 48 hdi y los niveles de expresión de las citoquinas CXCL10 y CXCL2 a nivel de proteína se evaluaron en células sin infectar (Mock) y en células DBT-mACE2 infectadas, mediante la técnica Luminex.

2. ANÁLISIS DE LOS MECANISMOS RESPONSABLES DE LA ATENUACIÓN DE UN SARS-CoV EN EL QUE SE HA ELIMINADO LA PROTEÍNA E

2.1 Generación, crecimiento y caracterización de virus mutantes de la proteína E (SCoV-E*)

Los virus que carecen de la proteína E (SCoV-ΔE) están atenuados en distintos modelos animales (DeDiego et al., 2007; DeDiego et al., 2008; Fett et al., 2013). Para identificar las regiones responsables de la atenuación del SCoV-ΔE, se generaron virus mutantes con mutaciones o pequeñas deleciones a lo largo de la proteína E (SCoV-E*) (**Figura 16A**). La región amino terminal de la proteína se modificó mediante la introducción de mutaciones puntuales (SCoV-EMut1). Esta región amino terminal no se delecionó, para mantener inalterada la secuencia primaria del gen 3b, dado que los genes 3b y E se solapan parcialmente. En la región carboxilo terminal de la proteína E se introdujeron deleciones de 6 a 12 aminoácidos (mutantes SCoV-EΔ2, -EΔ3, -EΔ4, -EΔ5 y -EΔ6, Figura 16A). Los virus generados por genética reversa se rescataron en células Vero E6, se clonaron tres veces mediante aislamiento de placa en células Vero E6 y se secuenciaron, comprobando que la estructura de su genoma era correcta.

Para analizar el efecto de las regiones de la proteína E mutadas o delecionadas en el crecimiento del virus, se realizaron cinéticas de producción de los diferentes virus mutantes SCoV-E* infectando células de mono Vero E6 y células humanas Huh7.5.1 (**Figura 16B**). Los títulos virales en todos los casos se observaron a 48 y 72 hdi en ambas líneas celulares. Los mutantes (SCoV-EMut1 y -EΔ6) mostraron los mayores títulos (>10^7 ufp/ml), similares a los observados para SCoV en ambas líneas celulares. Por el contrario, los virus (SCoV-EΔ3 y -EΔ5) mostraron títulos de alrededor de 10^6 y 10^5 ufp/ml en células Vero E6 y Huh7.5.1, respectivamente. Estos títulos fueron similares a los determinados para el virus SCoV-ΔE. El virus SCoV-EΔ4 mostró títulos intermedios con respecto a los virus nativo y SCoV-ΔE alcanzando títulos cercanos a 10^7 y 10^6 ufp/ml en células Vero E6 y Huh7.5.1 respectivamente. El virus recombinante SCoV-EΔ2 fue el que alcanzó un menor crecimiento viral (10^5 y 10^4 ufp/ml, en células Vero y Huh7.5.1 respectivamente).

Estos datos indican que las regiones 2, 3 y 5 de la proteína E se requieren para un crecimiento viral óptimo.

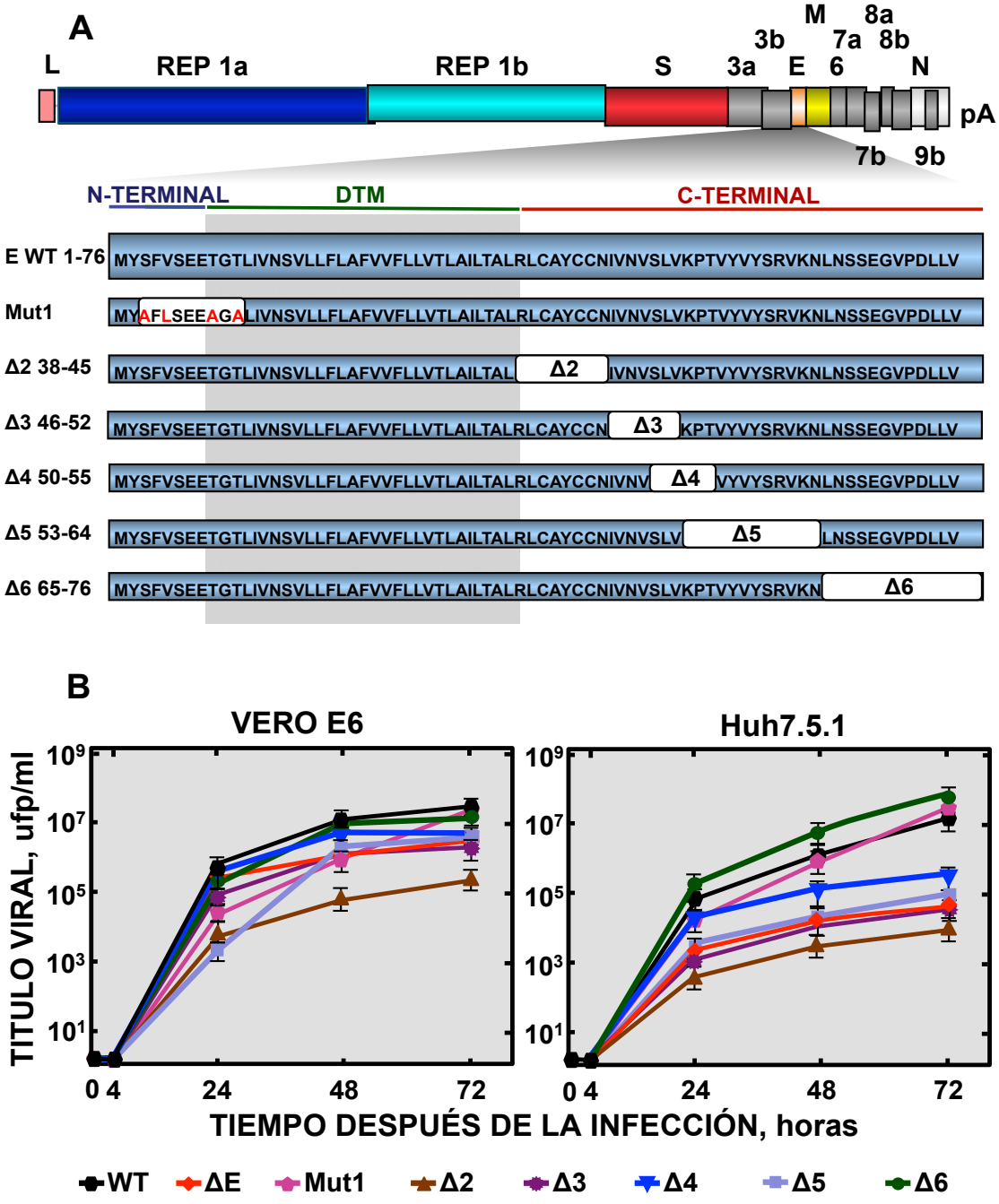

Figura 16. Esquema de mutaciones y deleciones introducidas en la proteína E del SARS-CoV y cinéticas de crecimiento de los virus mutantes SCoV-E*. (A) El genoma del SARS-CoV se muestra en la parte superior. La región expandida muestra la secuencia de la proteína E y sus diferentes regiones. Los aminoácidos de la proteína E delecionados se representan con rectángulos blancos. Los aminoácidos mutados en la región amino terminal de la proteína se indican en rojo. (B) Cinética de crecimiento de los virus recombinantes. Células Vero E6 y Huh7.5.1 se infectaron a una

mdi de 0.001 con los mutantes SCoV-E* (Mut1, SCoV-EMut1; Δ2, SCoV-EΔ2; Δ3, SCoV-EΔ3; Δ4, SCoV-EΔ4; Δ5, SCoV-EΔ5 y Δ6, SCoV-EΔ6), SCoV-ΔE y el virus nativo (WT) y la progenie viral se tituló a los tiempos indicados después de la infección, mediante ensayos de placas de lisis en células Vero E6. Las barras de error representan las desviaciones estándar de tres experimentos independientes.

Para determinar si las mutaciones o deleciones introducidas en la proteína E afectan a su localización subcelular, pudiendo afectar a su función, se infectaron células Vero E6 con los virus mutantes SCoV-E*, y se determinó su localización subcelular mediante anticuerpos específicos para la proteína E (**Figura 17**). La localización subcelular de todas las proteínas E mutadas fue similar y todas las proteínas E* colocalizaron parcialmente con el marcador de ERGIC (**Figura 17**), como se ha descrito previamente para la proteína nativa (WT) (Nieto-Torres et al., 2011). Estos datos indicaron que ninguna de las regiones delecionadas son esenciales para la localización subcelular de la proteína E, no alterando, por lo tanto, las funciones asociadas a su localización.

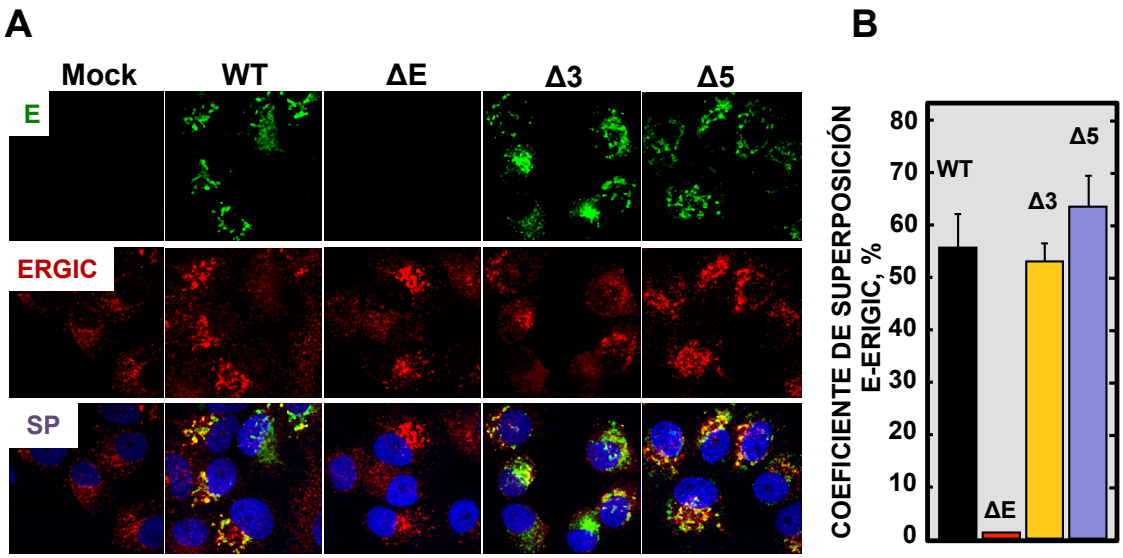

Figura 17. Localización subcelular de las proteínas E mutadas. Células Vero E6 se dejaron sin infectar, como control, o se infectaron con los virus mutantes SCoV-E* (Δ3, SCoV-EΔ3 y Δ5, SCoV-EΔ5), (ΔE, SCoV-ΔE), y el virus nativo (WT), a una mdi de 0.3. Las células se fijaron a las 24 horas después de la infección y se marcaron con anticuerpos específicos para la proteína E (verde) y un marcador de ERGIC (rojo). Los núcleos se tiñeron con DAPI (azul). SP indica la superposición de los canales verde, rojo y azul. Las imágenes se tomaron originalmente con un aumento de 126x. (B) La

gráfica representa el coeficiente de superposición entre la proteína E y el ERGIC, calculado con el programa Leica LAS AF v2.6.0.

2.1.1. Análisis de la estabilidad de los SCoV-E* en cultivos celulares

La estabilidad de los virus es esencial tanto para su caracterización como para su utilización como vacunas. Para analizar la estabilidad de los virus, los virus SCoV-E* se pasaron diariamente en células Vero E6 hasta un total de 8 veces. Posteriormente, se analizó la secuencia de todos los genes virales, excluido el gen de la replicasa (**Figura 18**). No se observaron deleciones, inserciones ni reordenamientos en los virus SCoV-E*. Solo se detectaron mutaciones puntuales en la secuencia viral, sugiriendo que estos virus fueron en general genéticamente estables, al menos en cultivos celulares (**Figura 18**).

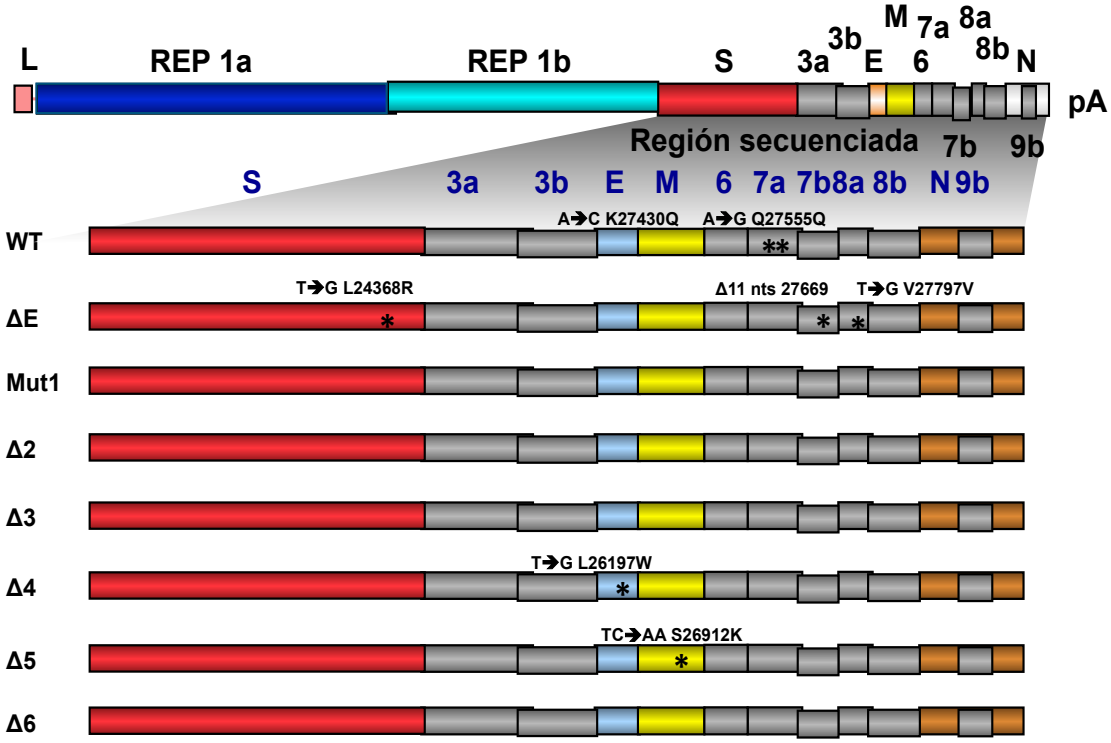

Figura 18. Estabilidad de los virus mutantes SCoV-E* después de infecciones seriadas en cultivos celulares. La secuencia de los virus SCoV-E* (Mut1, SCoV-EMut1; Δ2, SCoV-EΔ2; Δ3, SCoV-EΔ3; Δ4, SCoV-EΔ4; Δ5, SCoV-EΔ5 y Δ6, SCoV-EΔ6), (ΔE, SCoV-ΔE) y el virus nativo (WT), se evaluó después de 8 pases seriados en células Vero E6. Los asteriscos denotan la presencia de sustituciones de nucleótidos.

Para analizar si las mutaciones puntuales que incorporaron los virus después de los pases celulares se comportaban como mutaciones compensatorias, se realizaron cinéticas de crecimiento en células Vero E6 y Huh7.5.1 con los virus antes y después de ser pasados en cultivos celulares. No se encontraron diferencias significativas en la producción de virus de pase 1 (p1) y los pasados en cultivos celulares (p8) (datos no mostrados). Estos datos indicaron que las mutaciones que incorporaron los diferentes virus después de los pases celulares no afectaron al crecimiento del virus y por lo tanto, no son mutaciones compensatorias en cuanto a la producción viral.

2.1.2. Análisis de la infectividad específica y vida media de las proteínas E de los mutantes SCoV-E*

Para identificar si las diferentes deleciones introducidas en la proteína E alteran la infectividad específica del virus, se determinó el título del virus extracelular producido por los virus SCoV, SCoV-ΔE, SCoV-EΔ3 y SCoV-EΔ5. Estos títulos se compararon con los niveles de RNA genómico extracelular correspondientes. La infectividad específica de los virus con deleciones en la proteína E, SCoV-ΔE, SCoV-EΔ3 y SCoV-EΔ5 fue más baja (21%, 11%, y 17% respectivamente) que la infectividad específica del virus nativo (**Figura 19**).

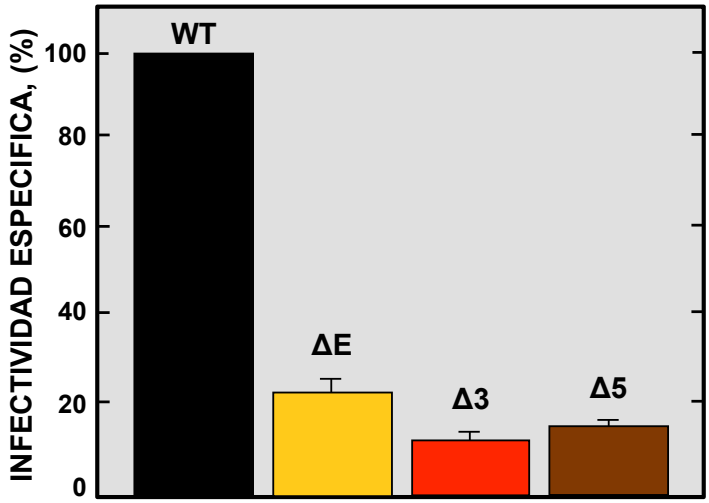

Figura 19. Infectividad específica de los mutantes SCoV-E*. Células Vero E6 se infectaron con los virus (ΔE, SCoV-ΔE; Δ3, SCoV-EΔ3 y Δ5, SCoV-EΔ5) o el virus nativo (WT) a una mdi de 0.3. El

medio de cultivo se retiró y se reemplazó con medio fresco suplementado con 2% de FBS a las 8 hdi. El sobrenadante celular se recogió a las 11 hdi y los niveles de RNA genómico y virus infectivo se determinaron por RT-qPCR y formación de placas de lisis en células Vero E6, respectivamente. La relación entre los títulos de virus infecciosos (ufp/ml) y la cantidad de RNA genómico se representa en la gráfica como porcentaje de la infectividad específica. Los promedios y desviaciones estándar muestran los resultados de 3 experimentos independientes.

Por lo tanto, la eliminación de la proteína E o la introducción de pequeñas deleciones dentro de la misma, disminuyó la infectividad de las partículas, contribuyendo probablemente a los bajos títulos observados para los mutantes (SCoV-ΔE, -EΔ3 y -EΔ5).

Para analizar si las pequeñas deleciones introducidas dentro de la proteína E alteran la estabilidad de la proteína, se inhibió la traducción celular mediante el uso de cicloheximida, y se analizó la degradación de la proteína E mediante *Western blot*. La vida media de la proteína E codificada por los virus mutantes (SCoV-EΔ3 y -EΔ5) fue mayor (3.5 h y 3.6 h respectivamente) que la vida media observada para la proteína E codificada por un virus nativo (2.4 h), análoga a la descrita previamente (Ruch and Machamer, 2012) (**Figura 20**). Estos resultados sugieren que la introducción de pequeñas deleciones dentro de la proteína E alteran modestamente la estabilidad de la proteína.

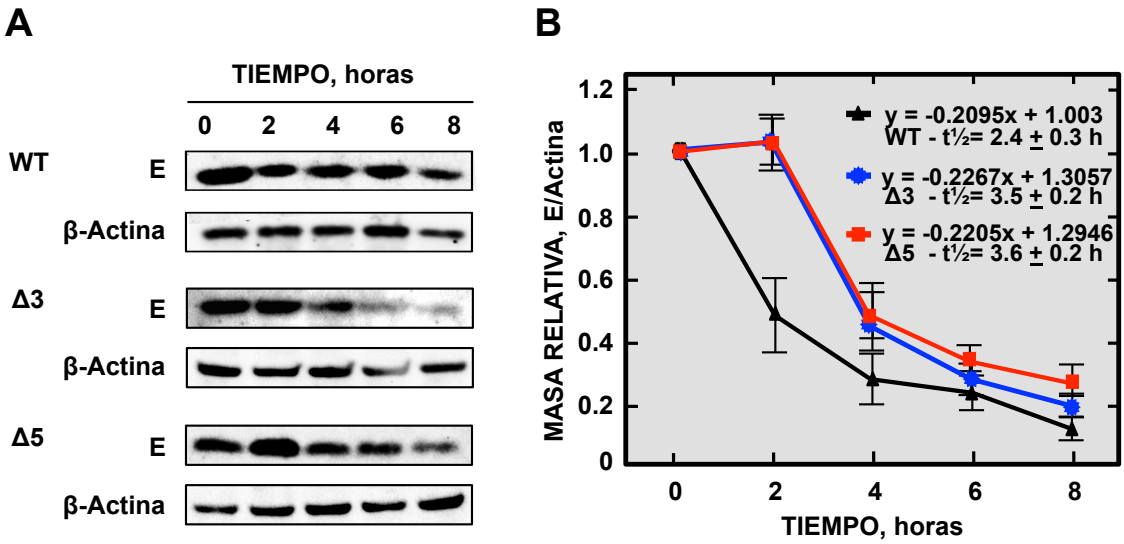

Figura 20. Vida media de las proteínas E de SCoV-E*. Células Vero E6 se infectaron con los virus (Δ3, SCoV-EΔ3 y Δ5, SCoV-EΔ5) o el virus nativo (WT) y se evaluó la estabilidad de las proteínas E mutantes en relación a la proteína E nativa. Para ello, las células se trataron con cicloheximida a las

12 hdi y se recogieron extractos celulares a los tiempos indicados. La cantidad de proteína E y de β actina, como control, se determinó mediante *Western blot*. (A) Membranas incubadas con los anticuerpos específicos para la proteína E y β actina, como control de carga. (B) La gráfica representa los valores obtenidos después del análisis de densitometría. Se muestra el porcentaje de la proteína E restante después de añadir la cicloheximida. Los promedios y desviaciones estándar muestran los resultados de 3 experimentos independientes.

2.1.3. Análisis de la interacción entre las proteínas E y M de SARS-CoV

Las interacciones entre las proteínas E y M de CoVs son esenciales en el ensamblaje de la partícula viral (Ho et al., 2004; Siu et al., 2008; Vennema et al., 1996). Teniendo en cuenta esta observación y los resultados previamente descritos que muestran que los virus SCoV-EΔ3 y SCoV-EΔ5 crecen menos eficientemente en cultivos celulares que el virus nativo, se analizó la interacción entre la proteína delecionada EΔ3 y la proteína M. Para ello, se coexpresó la proteína M fusionada a un péptido marcador HA y la proteína delecionada EΔ3, o la proteína E con longitud completa. La proteína E nativa y la mutante EΔ3 coimmunoprecipitaron con la proteína M, utilizando un anticuerpo específico para el marcador HA fusionado a la proteína M no observándose variaciones en las proporciones relativas de las dos proteínas (**Figura 21**).

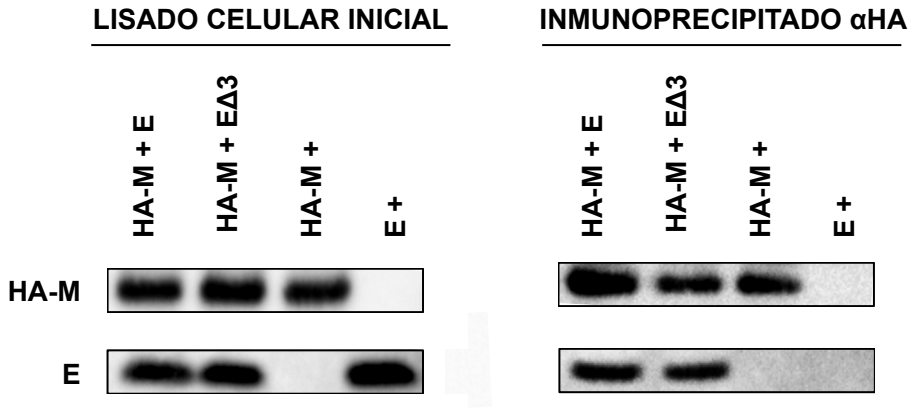

Figura 21. Interacción de la proteína EΔ3 con la proteína M del SARS-CoV. Células Vero E6 se cotransfectaron con un plásmido pcDNA3 que codifica la proteína M fusionada a un péptido marcador HA en su región amino terminal, y con plásmidos que expresan la proteína E de longitud completa o la proteína E con una pequeña deleción (EΔ3). Las cotransfeciones de un plásmido que

codifica la proteína HA-M y de un plásmido vacío se usaron como controles. Las células se lisaron y analizaron por *Western blot* con los anticuerpos específicos para las proteínas E y HA (panel izquierdo) y se realizaron inmunoprecipitaciones con el anticuerpo monoclonal específico para el péptido HA (panel derecho). La presencia de las proteínas E y M se analizó en las fracciones precipitadas usando los anticuerpos específicos contra las proteínas E y el péptido HA (panel derecho).

Estos resultados confirman que las proteínas E y M interaccionan y que la deleción introducida en la proteína E para generar el recombinante SCoV-EΔ3 no altera significativamente la unión de esta proteína a la proteína M. Por lo tanto, los menores títulos virales observados para el virus mutante SCoV-EΔ3 no se debieron a la ausencia de interacción entre las proteínas EΔ3 y M y probablemente fueron causados por una distinta interacción de la proteína EΔ3 con otras proteínas virales o celulares.

2.2. Virulencia de los mutantes SCoV-E* en el modelo de ratón

Previamente hemos descrito que el virus que carece de la proteína E SCoV-ΔE muestra un fenotipo completamente atenuado (DeDiego et al., 2007; DeDiego et al., 2014; DeDiego et al., 2008; Fett et al., 2013). Para evaluar la relevancia de las diferentes regiones de la proteína E en la patogénesis causada por estos virus se inocularon intranasalmente ratones BALB/c con el virus nativo, SCoV-ΔE, y los virus recombinantes SCoV-E*. Los animales se controlaron, durante 10 días. Los ratones infectados con el virus nativo mostraron síntomas de la enfermedad a partir del día 2 después de la inoculación, tales como una movilidad reducida y la presencia de pelo erizado (datos no mostrados). Estos ratones infectados con el virus nativo perdieron peso rápidamente y el 80% murieron antes del día 7 después de la infección (**Figura 22**). Los ratones infectados con el recombinante SCoV-EΔ6, que contiene delecionados los últimos 12 aminoácidos de la proteína E, mostraron un fenotipo muy similar al observado para los ratones inoculados con el virus nativo (**Figura 22**). Por el contrario, los ratones infectados con los virus mutantes SCoV-EΔ2; SCoV-EΔ3; SCoV-EΔ5 y SCoV-ΔE no mostraron signos clínicos de enfermedad (datos no mostrados), no experimentaron pérdida de peso, y el 100% de los ratones sobrevivieron (**Figura 22**). Los ratones infectados con los

virus SCoV-EMut1 y SCoV-EΔ4 mostraron una pérdida de peso del 15 y 10%, respectivamente, recuperándose a los 3 días después de la inoculación, y el 100% de los ratones sobrevivió (**Figura 22**). Estos datos mostraron que las regiones delecionadas 2, 3 y 5, y en menor medida las regiones 1 y 4 de la proteína E, se requieren para mantener la virulencia del SARS-CoV.

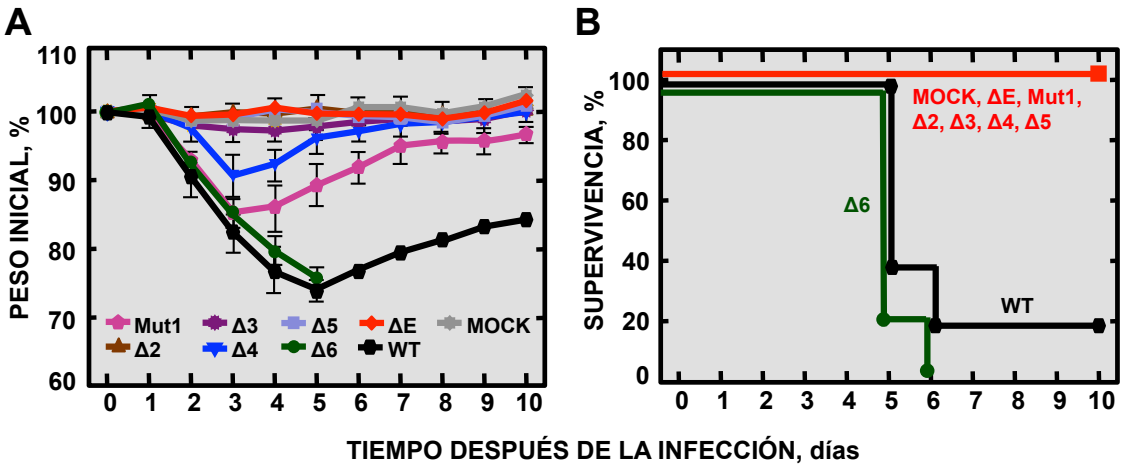

Figura 22. Patología causada por los mutantes SCoV-E* en ratones BALB/c. Grupos de cinco ratones de 16 semanas de edad se inocularon con 100000 ufp de los virus SCoV-E* (Mut1, SCoV-EMut1; Δ2, SCoV-EΔ2; Δ3, SCoV-EΔ3; Δ4, SCoV-EΔ4; Δ5, SCoV-EΔ5 y Δ6, SCoV-EΔ6), (ΔE, SCoV-ΔE), del virus nativo, o sin virus (Mock). Se analizó la pérdida de peso (A) y la supervivencia (B). Los ratones que perdieron mas del 30% de su peso inicial se sacrificaron. Las barras de error representan la desviación estándar del peso de los ratones en cada variable experimental.

2.3. Crecimiento de los virus mutantes SCoV-E* en ratones infectados

Previamente habíamos determinado que la deleción de la proteína E completa disminuye el crecimiento del virus (DeDiego et al., 2007; DeDiego et al., 2008). Para evaluar si las regiones de la proteína E delecionadas son requeridas para una óptima producción viral en ratón, se inocularon ratones BALB/c con los virus SCoV-E* generados, y los virus SCoV-ΔE o nativo. A los 2 y 4 ddi se recogieron los pulmones, se homogeneizaron y se determinó el título viral (**Figura 23**). Los mayores títulos virales se detectaron a 2 ddi, observándose una reducción considerable de 1 a 2 unidades logarítmicas a 4 ddi. El virus nativo mostró los títulos más altos (8×10^7 y 5×10^7 ufp/g de tejido a 2 y 4 ddi, respectivamente). Los

títulos virales del SCoV-ΔE disminuyeron 80 y 1000 veces a 2 y 4 ddi confirmando que el recombinante SCoV-ΔE se replica menos eficientemente en ratón. El virus mutante SCoV-EΔ6 mostró un crecimiento similar al virus nativo (7×10^7 y 10^7 ufp/g de tejido a 2 y 4 ddi, respectivamente, **Figura 23**), indicando que la región delecionada mas próximo, al extremo carboxilo terminal de la proteína E es la menos relevante en el crecimiento del virus en ratón. Los virus SCoV-EΔ2 y SCoV-EΔ5 mostraron títulos similares a los observados para el virus mutante SCoV-ΔE o incluso un poco más bajos. Por el contrario, los virus SCoV-EMut1, SCoV-EΔ3 y SCoV-EΔ4 crecieron con un título intermedio (10^7 y 10^6 ufp/g a 2 y 4 ddi, respectivamente). Estos resultados son similares a los observados previamente en cultivos celulares y muestran que las regiones 2 y 5 de la proteína E son particularmente necesarias para un óptimo crecimiento del SARS-CoV en ratón.

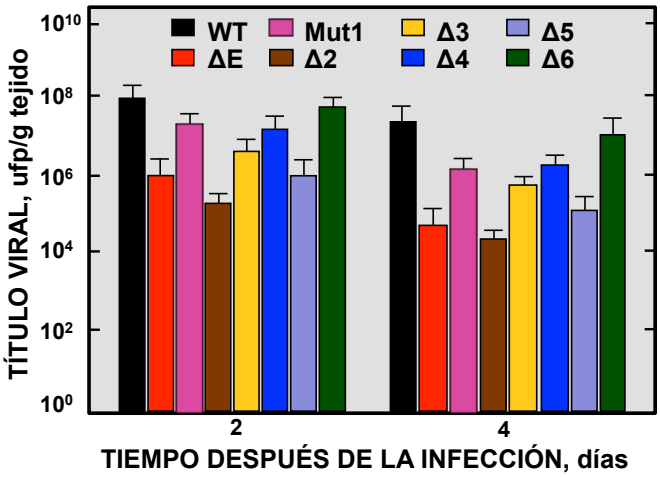

Figura 23. Crecimiento de los mutantes SCoV-E* en pulmones de ratones BALB/c. Grupos de seis ratones de 16 semanas de edad se inocularon con 100000 ufp de los virus SCoV-E* (Mut1, SCoV-EMut1; Δ2, SCoV-EΔ2; Δ3, SCoV-EΔ3; Δ4, SCoV-EΔ4; Δ5, SCoV-EΔ5 y Δ6, SCoV-EΔ6), (ΔE, SCoV-ΔE), o nativo (WT). A los 2 y 4 ddi se sacrificaron 3 ratones de cada grupo para determinar los títulos virales en pulmón. Las barras de error representan la desviación estándar de los títulos obtenidos en los pulmones de los 3 ratones utilizados para cada variable experimental.

2.4. Patología pulmonar causada por la infección con SCoV-E* en ratón

Para analizar los mecanismos por los cuales los diferentes virus generados SCoV-E* están atenuados, se analizaron macroscópica y microscópicamente los pulmones de ratones no infectados, infectados con el virus nativo, o con los virus

mutantes de la proteína E a días 2 y 4 di (**Figura 24**). Para el análisis microscópico, cortes de pulmones se tiñeron mediante hematoxilina y eosina y se analizaron los cambios histopatológicos.

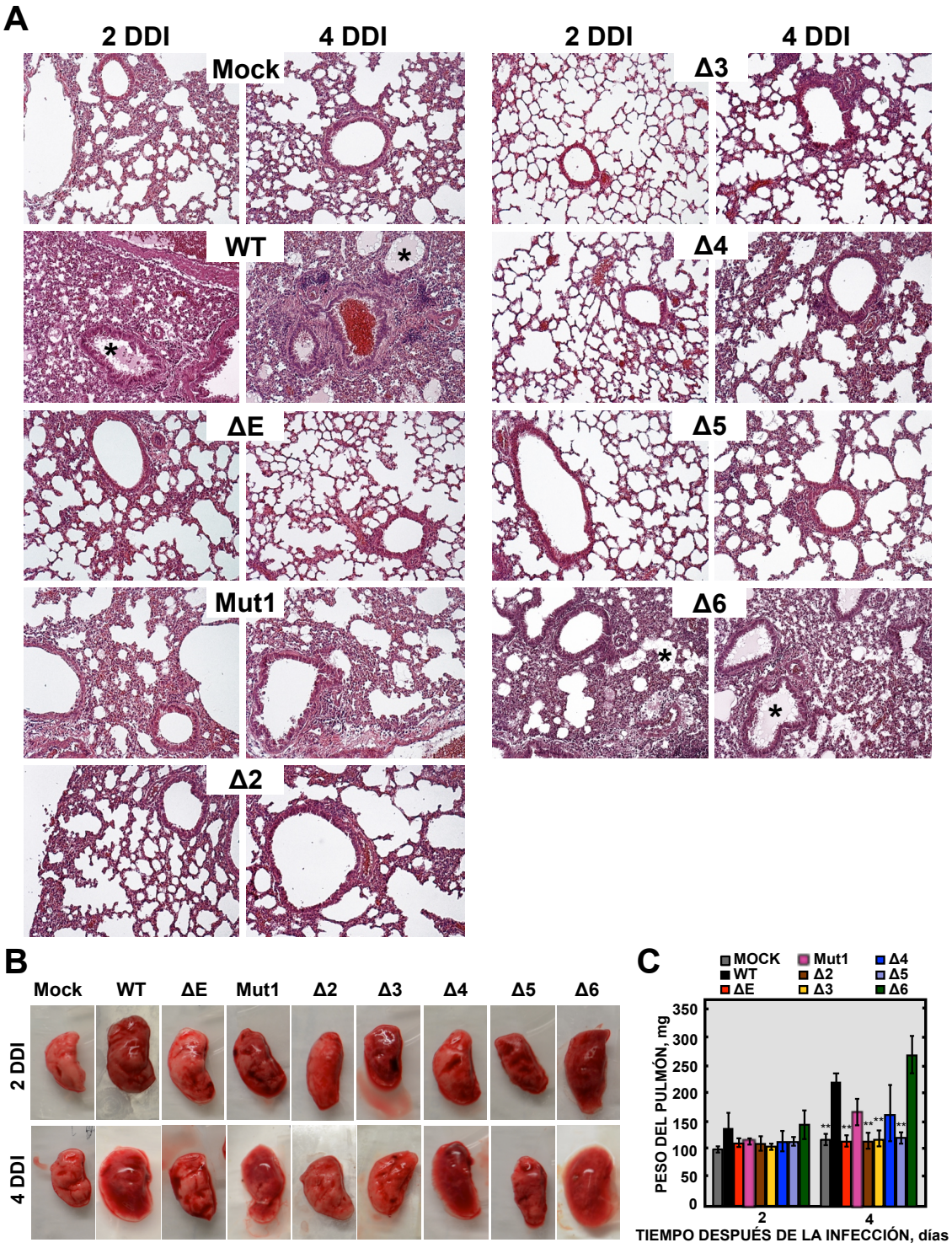

Figura 24. Patología pulmonar causada por la infección SCoV-E* en ratones. Grupos de seis ratones de 16 semanas de edad se inocularon con 100000 ufp de los virus SCoV-E* (Mut1, SCoV-

EMut1; Δ2, SCoV-EΔ2; Δ3, SCoV-EΔ3; Δ4, SCoV-EΔ4; Δ5, SCoV-EΔ5 y Δ6, SCoV-EΔ6), (ΔE, SCoV-ΔE), nativo (WT) o sin virus (Mock). A los 2 y 4 ddi se sacrificaron 3 ratones de cada grupo y se recogieron sus pulmones. (A) Los pulmones se fijaron con formalina de zinc, se incluyeron en parafina, se cortaron y se tiñeron con hematoxilina y eosina. Los asteriscos indican acumulación de edema en bronquiolos y alveolos. El aumento original utilizado fue de 20x. (B) Las imágenes muestran la patología macroscópica observada en los pulmones de ratón infectados con los distintos virus. (C) Antes de fijar los pulmones, estos se pesaron. Las barras de error indican la desviación estándar hallada para los 3 ratones de cada variable. Los datos estadísticamente significativos se indican con dos asteriscos (test de Student, p-valor <0.01).

Los pulmones de ratones no infectados presentaron las vías aéreas (alveolos y bronquiolos) despejados, y no se observó la presencia de infiltrados leucocitarios (**Figura 24A**). Por el contrario, los pulmones de los ratones infectados con los virus nativo y SCoV-EΔ6 mostraron engrosamiento de los epitelios alveolares, edema y presencia de infiltraciones leucocitarias a 2 y 4 ddi (**Figura 24A**). El análisis histológico de los pulmones de los ratones infectados con los virus (SCoV-ΔE, -EMut1, -EΔ2, -EΔ3, -EΔ4, y -EΔ5) reveló solo pequeños daños en el pulmón e infiltrados celulares. En el análisis macroscópico, los pulmones de ratones infectados con los virus nativo o SCoV-EΔ6, a diferencia de los pulmones de los ratones infectados con los virus (SCoV-ΔE, -EMut1, -EΔ2, -EΔ3, -EΔ4 y -EΔ5), mostraron un aumento del volumen pulmonar y un aspecto más rojizo, debido probablemente a procesos hemorrágicos. Además, estos pulmones presentaron un incremento del peso sobretodo a 4 ddi, posiblemente debido a la presencia de infiltraciones leucocitarias y acumulación de edema en las zonas infectadas (**Figura 24B y C**). Estos datos indican que las regiones 1, 2, 3, 4 y 5 de la proteína E contribuyen al daño pulmonar inducido por la infección por SARS-CoV.

2.5. Efecto de la infección por los virus SCoV-E* en la inducción de la respuesta celular inmune

El avance de la enfermedad ocasionada por la infección del SARS-CoV da como resultado un masivo flujo de células inflamatorias a los pulmones y una débil respuesta de las células T (Channappanavar et al., 2014; Wong et al., 2003; Zhao and Perlman, 2010; Zhao et al., 2009). Para analizar la respuesta celular inducida por los diversos mutantes, se cuantificaron distintos tipos de leucocitos en los

infiltrados pulmonares de ratones infectados con el virus nativo y con los mutantes virales SCoV-ΔE, SCoV-EΔ3 y SCoV-EΔ5 mediante citometría de flujo. El número de leucocitos totales se incrementó ligeramente en los infiltrados pulmonares observados en los ratones infectados con los virus con fenotipo atenuado (SCoV-ΔE, -EΔ3 y -EΔ5), en comparación con los ratones infectados con el virus virulento nativo (**Figura 25A**).

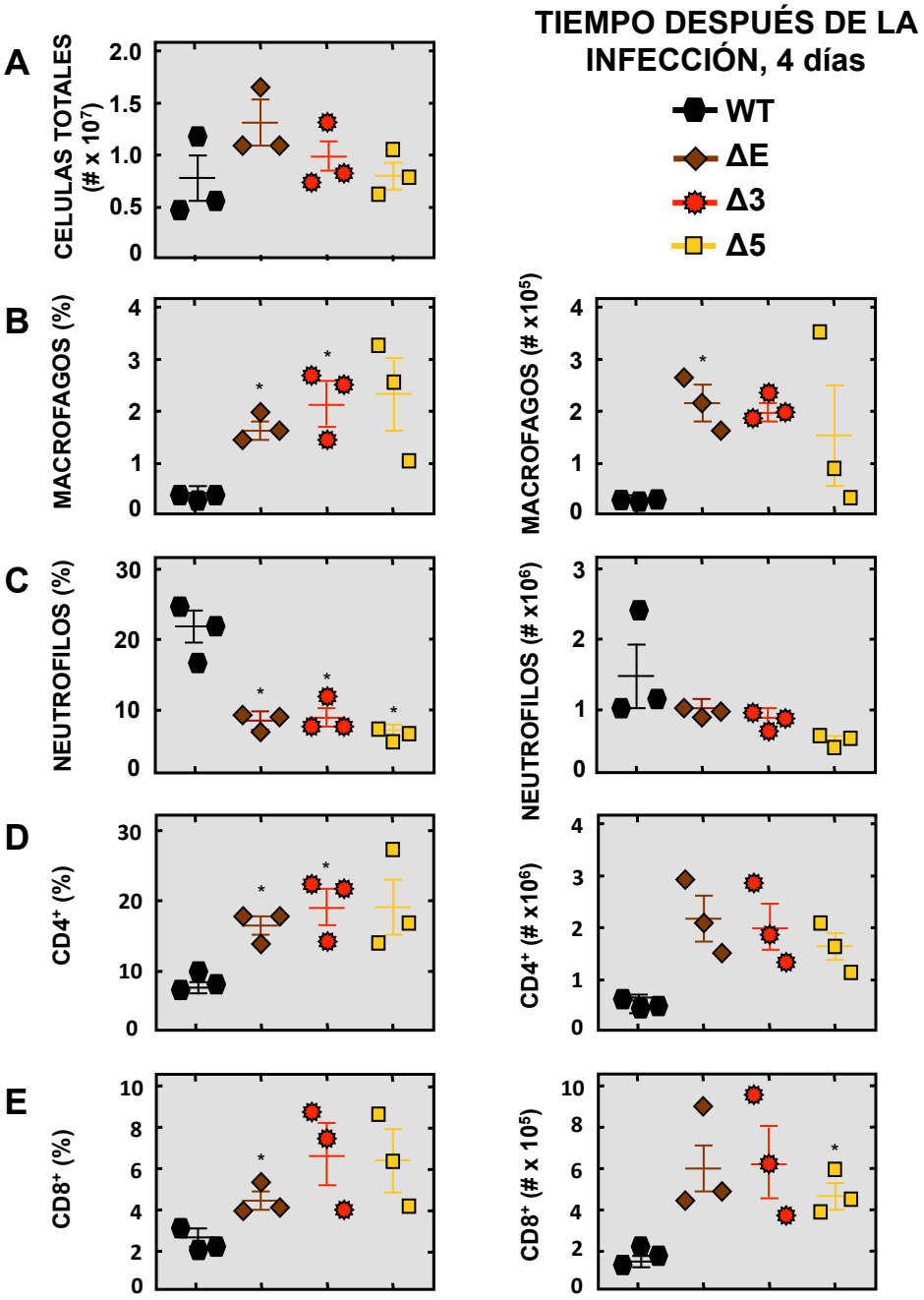

Figura 25. Presencia de células leucocitarias en infiltrados en el pulmón de ratones infectados con los virus mutantes SCoV-E*. Ratones BALB/c se infectaron intranasalmente con

100000 ufp de cada uno de los virus (ΔE, SCoV-ΔE; Δ3, SCoV-EΔ3, Δ5, SCoV-EΔ5 y nativo), y se sacrificaron a los 4 ddi. Se determinó: (A) El número de leucocitos totales. (B) Los números totales y los porcentajes de macrófagos. (C) El numero de neutrófilos. (D) El numero de células T $CD4^+$ y (E) de células T $CD8^+$. Se muestran los promedios y desviaciones estándar. Los datos representan el resultado de tres experimentos independientes (n = 3 ratones). Los datos estadísticamente significativos están indicados con un asterisco (t de Student p-valor <0.05).

Se observó un aumento del numero de macrófagos totales y también de su proporción relativa con respecto al número total de leucocitos en los infiltrados de los ratones infectados con los virus atenuados respecto a los ratones infectados con el virus nativo (**Figura 25B**). Así mismo, se observó una reducción del infiltrado pulmonar de neutrófilos, tanto en porcentaje como en número total en los ratones infectados con los virus atenuados en comparación con los infectados con el SCoV virulento (**Figura 25C**). Estos datos muestran que el fenotipo observado en los virus mutantes atenuados (SCoV-ΔE, -EΔ3 y -EΔ5) se correlacionó con una disminución de infiltración por neutrófilos y un incremento del flujo de macrófagos en los pulmones. Además, la infección por los virus mutantes atenuados (SCoV-ΔE, -EΔ3 y -EΔ5) dieron lugar a una respuesta mayor de células T, observándose un aumento en los números totales y relativos de las células $CD4^+$ y $CD8^+$ en comparación con los valores obtenidos en la respuesta T inducida en los ratones infectados con el virus nativo (**Figura 25D y E**). Estos datos indican que los ratones infectados con los virus atenuados desarrollaron una mejor respuesta de células T que la inducida por el virus nativo, contribuyendo probablemente a una eliminación del virus mas rápida y al control de la infección viral.

2.6. Efecto de la infección por los virus SCoV-E* en la expresión génica del huésped

Para analizar las respuestas celulares del huésped que contribuyan a la atenuación de los mutantes SCoV-E*, se analizaron los transcriptomas de los pulmones de ratón sin infectar o infectados con los virus SCoV-ΔE, SCoV-EΔ3, SCoV-EΔ5 y SCoV usando matrices de oligonucleótidos (**Figura 26A y Tabla IV**).

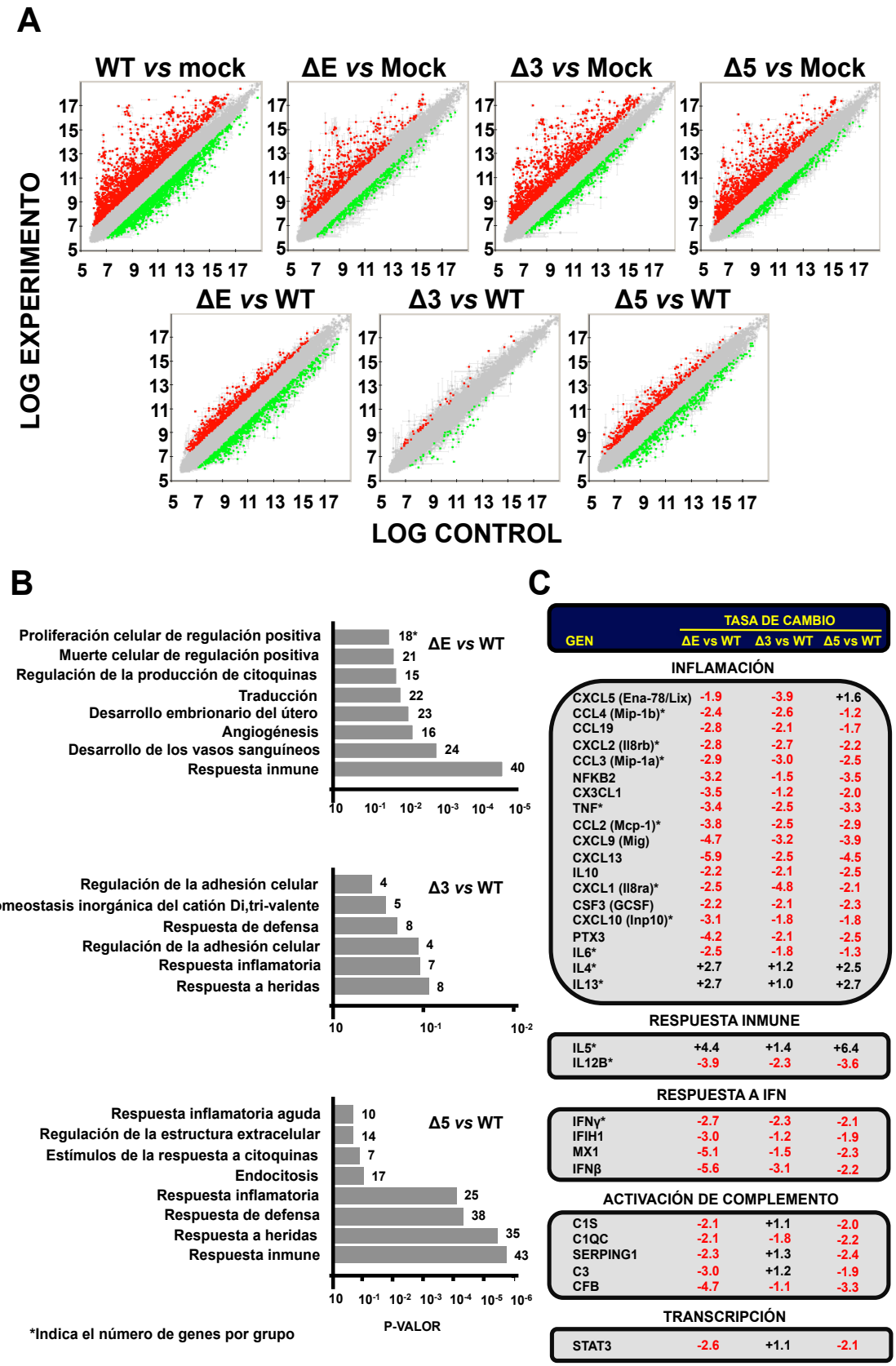

Figura 26. Expresión génica diferencial en los pulmones de los ratones infectados con los virus SCoV-E*. El RNA total de los pulmones se extrajo a los 2 ddi (n = 3 ratones). (A) La expresión

génica en los distintos ratones infectados se evaluó mediante matrices de oligonucleótidos. Solo se consideraron los genes con una tasa de frecuencia de falsos descubiertos (FDR), menor a 0.05. Los genes cuya expresión aumentó o disminuyó al menos dos veces se representan en rojo y verde, respectivamente. (B) Los genes candidatos cuya expresión aumentó o se inhibió significativamente en los pulmones de los ratones infectados con los virus (ΔE, SCoV-ΔE; Δ3, SCoV-EΔ3 y Δ5, SCoV-EΔ5), con respecto a las infecciones con el virus nativo, se agruparon de acuerdo con los procesos biológicos de *Gene-Ontology* (Ashburner et al., 2000). El eje de las abscisas indica los valores de FDR del programa bioinformático DAVID. (C) Los genes diferencialmente expresados en los pulmones de los ratones infectados con los virus (ΔE, SCoV-ΔE; Δ3, SCoV-EΔ3 y Δ5, SCoV-EΔ5) comparados con los pulmones de los ratones infectados con el virus nativo se clasificaron de acuerdo con sus principales funciones biológicas. Los genes cuya expresión aumentó y se inhibió se representan en negro y en rojo, respectivamente. Los asteriscos indican los genes cuya expresión génica se confirmó por RT-qPCR. Los números indican la tasa de cambio para cada gen en los ratones infectados con los virus (ΔE, SCoV-ΔE; Δ3, SCoV-EΔ3 y Δ5, SCoV-EΔ5), comparadas con las tasas de cambio observadas en los ratones infectados con el virus nativo (WT). En el caso de los genes que se detectaron con más de una sonda, se indican los valores de expresión génica más alta.

Los transcriptomas del tejido pulmonar de los ratones infectados con los virus SCoV-ΔE, -EΔ3 y -EΔ5 se compararon con el transcriptoma de los pulmones infectados con el virus nativo y con el de los pulmones de ratones no infectados (**Figura 26A y Tabla IV**). Los genes que variaron significativamente se agruparon de acuerdo a su función biológica mas frecuente, utilizando el programa bioinformático DAVID (Huang da et al., 2009). Cuando se compararon los genes diferencialmente expresados en los ratones infectados con los virus atenuados (SCoV-ΔE, -EΔ3 y -EΔ5), con respecto a los ratones infectados con el virus nativo virulento, los grupos de genes que mostraron mayores diferencias estadísticas se asociaron a la respuesta inmune, al dolor, a la defensa y respuesta inflamatoria (**Figura 26B**). Es de notar que, muchos de los genes cuya expresión disminuyó estaban implicados en la respuesta pro-inflamatoria. Además, la expresión de genes relacionados con la respuesta Th2 con función anti-inflamatoria, tales como IL4 e IL13, aumentó (**Figura 26C**). Estos datos se compararon con los datos de patología pulmonar y se observó que la infección con los virus atenuados (SCoV-ΔE, -EΔ3 y -EΔ5) produce menor inflamación pulmonar que la infección por el virus virulento nativo. Para validar y confirmar los resultados obtenidos por matrices de oligonucleótidos, se evaluó la expresión de genes implicados en la respuesta inflamatoria a 2 y 4 ddi mediante RT-qPCR. La expresión de todas las

citoquinas pro-inflamatorias analizadas (TNF, CCL2, CCL3, CCL4, CXCL1, CXCL2, CXCL10, IL6, IL12B e IFNγ) disminuyó en los pulmones de los ratones infectados con los virus atenuados (SCoV-ΔE, -EΔ3 y -EΔ5), con respecto a los pulmones de los ratones infectados con el virus nativo (**Figura 26C y 27A y B**). Por el contrario, las citoquinas IL4, IL5 e IL13 asociadas a la repuesta anti-inflamatoria Th2, se sobreexpresaron en los pulmones de los ratones infectados con los virus atenuados (SCoV-ΔE, -EΔ3 y -EΔ5), en comparación con la respuesta observada en los ratones infectados con SCoV (**Figura 26C y 27A y B**).

Tabla IV. Análisis de la expresión génica del huésped usando matrices de oligonucleótidos de ratón*

Comparación	Nº Total de genes diferencialmente expresados	Nº de genes aumentados	Nº de genes inhibidos
WT vs Mock	2918	1473	1445
ΔE vs Mock	957	594	363
Δ3 vs Mock	1466	1004	462
Δ5 vs Mock	1362	955	409
ΔE vs WT	1382	752	630
Δ3 vs WT	83	39	44
Δ5 vs WT	286	441	385

* Genes aumentados, tasa de cambio >2, FDR < 0.05; Genes inhibidos, tasa de cambio <-2, FDR < 0.05. (ΔE, SCoV-ΔE; Δ3, SCoV-EΔ3 y Δ5, SCoV-EΔ5).

Para analizar si estos cambios eran específicos, se estudio la expresión del rRNA 18S y del TGFβ. Este último esta implicado en la respuesta anti-inflamatoria pero su nivel de expresión fue constante (Kim et al., 1992; Martin et al., 2011). Los niveles de expresión de estos genes fueron similares en los pulmones de todos los ratones (**Figura 27B**), confirmándose que la inhibición o sobreexpresión de los genes relacionados con inflamación es específica.

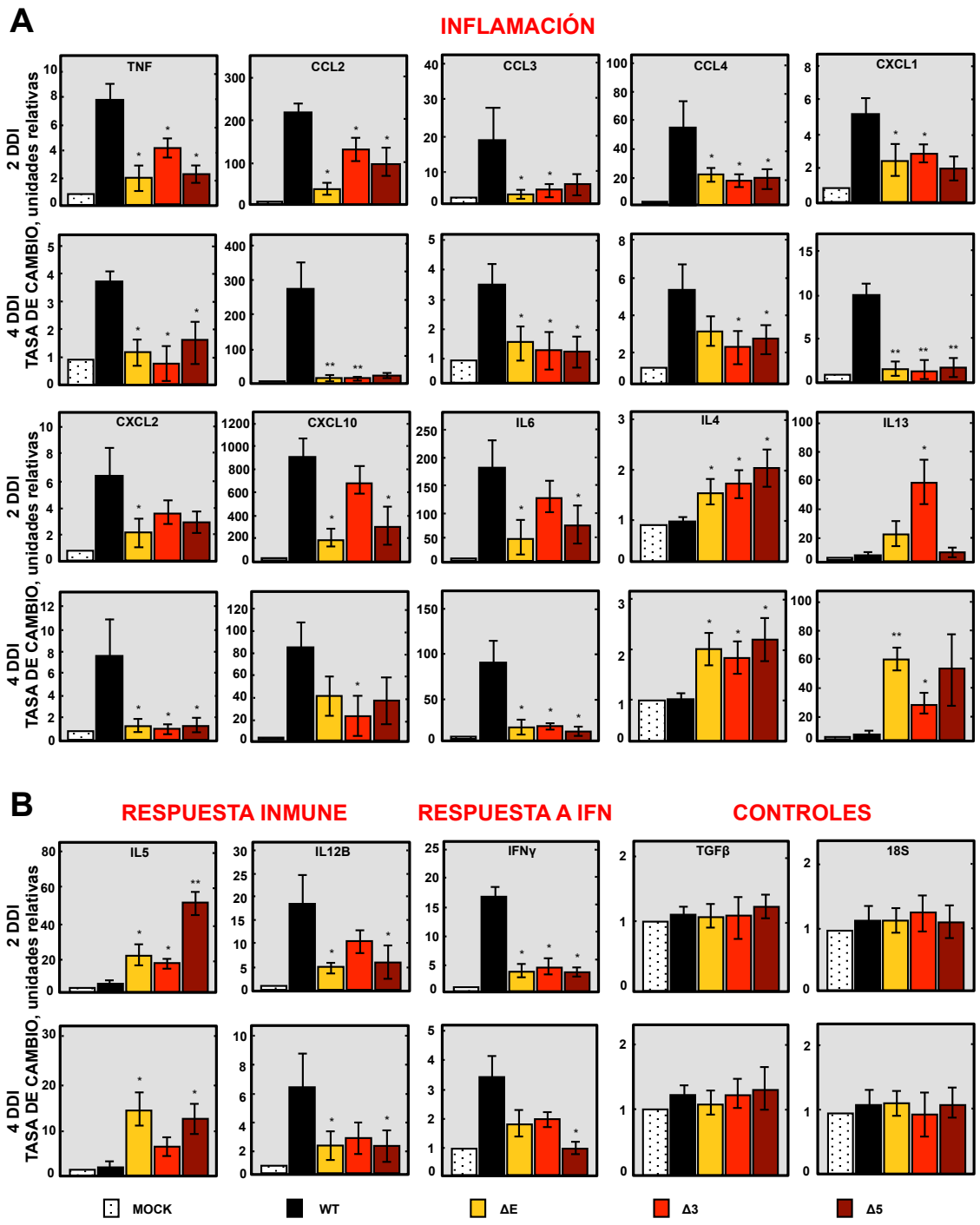

Figura 27. Expresión de citoquinas en los pulmones de ratones infectados con los virus SCoV*. Ratones BALB/c se inocularon intranasalmente con 100000 ufp de los virus (ΔE, SCoV-ΔE; Δ3, SCoV-EΔ3, Δ5, SCoV-EΔ5 y nativo). El RNA total se extrajo a los 2 y 4 ddi y la expresión de genes relacionados con inflamación (A), respuesta inmune y respuesta a IFN, TGFβ y rRNA 18S (B) se evaluó por RT-qPCR. En cada caso los niveles de expresión de estas citoquinas en los pulmones de los ratones infectados se compararon con los niveles de expresión en los pulmones de los ratones no infectados. La gráfica muestra los promedios y desviaciones estándar (n = 3 ratones por grupo).

Los datos estadísticamente significativos se indican con uno o dos asteriscos (t de Student p-valor <0.05, <0.01, respectivamente).

Para confirmar si los niveles de expresión de los genes celulares a nivel de mRNA se asociaban con la acumulación de la proteína, se cuantificaron los niveles de proteína de las citoquinas TNF, CCL2, IL5, IL6, IL13 e IFNγ. Para ello, se evaluaron los niveles de proteínas en los extractos de pulmón de ratones sin infectar o infectados con los virus SCoV, SCoV-ΔE, SCoV-EΔ3 y SCoV-EΔ5. Los niveles de los mRNAs que codificaban las distintas citoquinas evolucionan paralelamente a niveles de proteína acumulados en los ratones infectados con los mismos virus (**Figura 28**). Los resultados obtenidos indicaron que la inflamación macroscópica y microscópica presente en los pulmones de los ratones infectados se asoció con un aumento de los niveles de citoquinas pro-inflamatorias y con una disminución de la expresión de las citoquinas anti-inflamatorias.

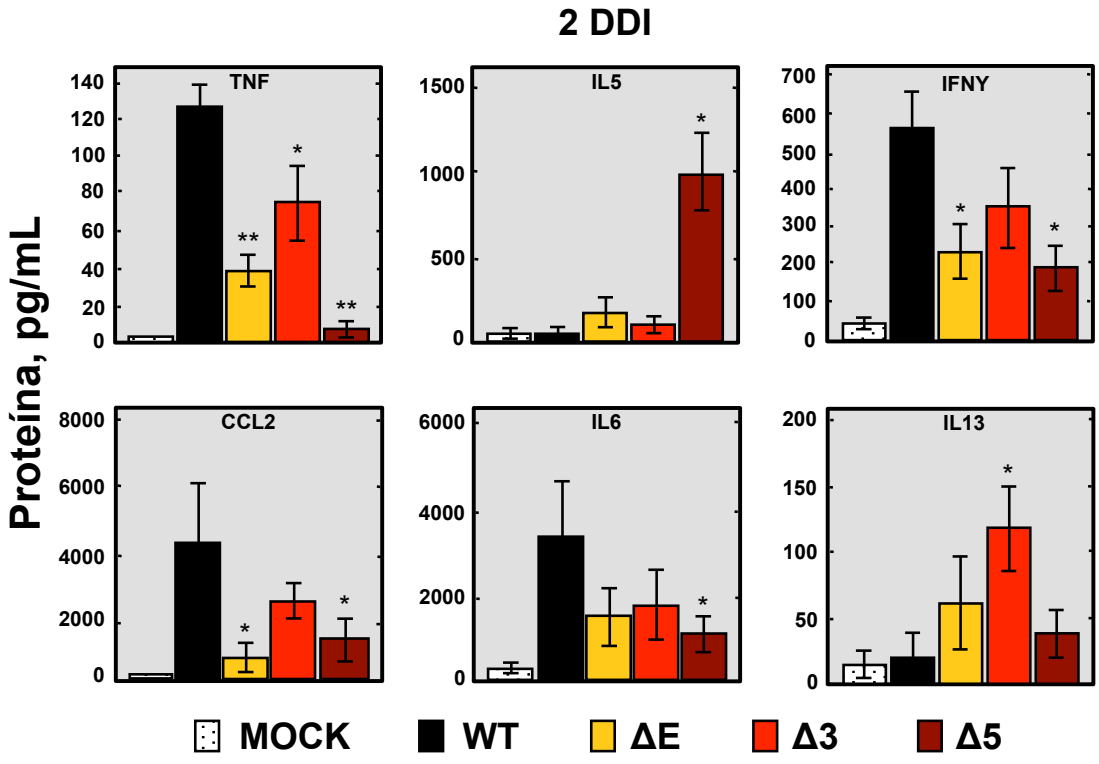

Figura 28. Expresión de citoquinas a nivel de proteínas en los pulmones de ratones infectados con los virus SCoV-E*. Ratones BALB/c se inocularon intranasalmente con 100000 ufp de los virus (ΔE, SCoV-ΔE; Δ3, SCoV-EΔ3, Δ5, SCoV-EΔ5 y nativo). Se obtuvieron extractos de proteínas de los pulmones a los 2 ddi. La acumulación de los niveles de citoquinas se analizó

mediante la técnica Luminex (Regla-Nava et al., 2013). Los resultados se expresaron en picogramos por mililitro de extracto de tejido. La gráfica muestra los promedios y desviaciones estándar (n = 3 ratones por grupo). Los datos estadísticamente significativos se indican con un asterisco (t de Student, p-valor <0.05).

2.7. Análisis de la protección conferida por los virus atenuados SCoV-E* frente al desafío con el virus virulento SCoV

Las vacunas vivas atenuadas se consideran efectivas por inducir por lo general una respuesta inmune elevada y de larga duración (Graham et al., 2013). Para determinar si los mutantes atenuados del virus SCoV eran candidatos prometedores a vacunas, se analizó la inducción de protección conferida por estos recombinantes (SCoV-EMut1, -EΔ2, -EΔ3, -EΔ4, y -EΔ5), frente al desafío con el virus virulento SCoV. Para ello, grupos de ratones no inmunizados, o inmunizados con estos virus, se desafiaron con el virus SCoV virulento 21 días después de la inmunización. Se analizó la pérdida de peso y mortalidad de los ratones durante los 14 días posteriores al desafío (**Figura 29**).

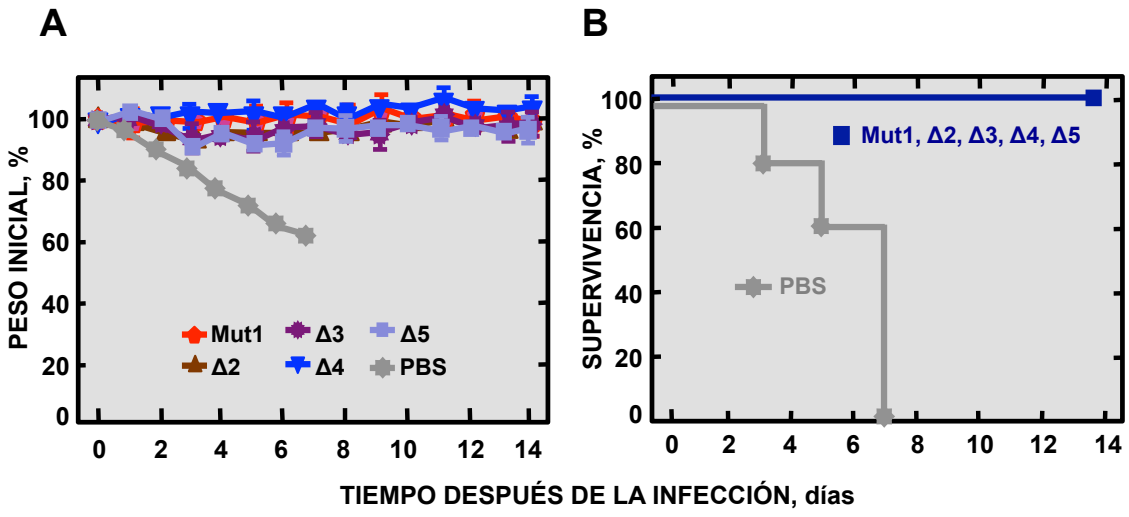

Figura 29. Protección conferida por la inmunización con los virus SCoV-E*. Ratones BALB/c de 6 semanas se dejaron sin inmunizar (PBS) o se inmunizaron con 6000 ufp de los virus (Mut1, SCoV-EMut1; Δ2, SCoV-EΔ2; Δ3, SCoV-EΔ3; Δ4, SCoV-EΔ4 y Δ5, SCoV-EΔ5). Los ratones se desafiaron con 100000 ufp del virus nativo 21 días después de la inmunización. Se evaluó la pérdida de peso (A) y la supervivencia (B) de los ratones desafiados (n = 3 ratones por grupo).

Todos los ratones no inmunizados perdieron rápidamente peso y murieron antes del día 8 después del desafío con el virus SCoV. Por el contrario, los ratones que se vacunaron con los virus atenuados, no perdieron significativamente peso, y el 100% sobrevivió (**Figura 29**). Estos datos indican que todos los virus mutantes con fenotipo atenuado inducen altos niveles de protección frente al desafío con un virus letal SCoV y por lo tanto son candidatos prometedores a vacunas.

3. ESTABILIDAD DEL SCoV-ΔE CANDIDATO A VACUNA

3.1. Generación de SCoV-ΔE con proteínas quiméricas (M_{CH}) incorporadas al genoma viral

Previamente hemos mostrado que la vacunación SCoV-ΔE induce una protección completa. Sin embargo, al analizar la estabilidad cinética de este mutante con la proteína E delecionada se observó que cuando se pasó 16 veces en cultivos celulares incorporó una proteína de membrana quimérica (M_{CH}) (**Figura 30A**). Este nuevo gen M_{CH}, esta formado por una duplicación parcial del gen M fusionado a un fragmento de la secuencia líder del SARS-CoV. El gen M_{CH} generado en el virus ΔE pasado en células DBT-mACE2 incluyó además una deleción de 7 nucleótidos de la secuencia del gen M parcialmente duplicada (**Figura 30A**). Los dos virus recombinantes que contienen la proteína M quimérica generada en células Vero E6 o DBT-mACE2 expresaron proteínas quiméricas con un dominio idéntico al de la proteína M nativa. Este dominio incluyó la región amino terminal con los tres dominios transmembrana típicos de la proteína M, en cada una de las proteínas quiméricas generadas. Es importante hacer notar que estas proteínas contienen diferentes motivos de unión al motivo PDZ (PBM) localizados al final del extremo carboxilo terminal de la proteína. Estos motivos PBM están formados por los últimos cuatro aminoácidos del carboxilo terminal de la proteína quimérica (**Figura 30B**). Estos resultados indicaron que el virus SCoV-ΔE, que carece del motivo PBM inicialmente, cuando se pasa en cultivos celulares muta hasta recuperar un motivo PBM, generando proteínas quiméricas con PBMs que no existían previamente. Estos virus nuevos mantienen su atenuación en ratón (Jimenez-Guardeño et al., 2015).

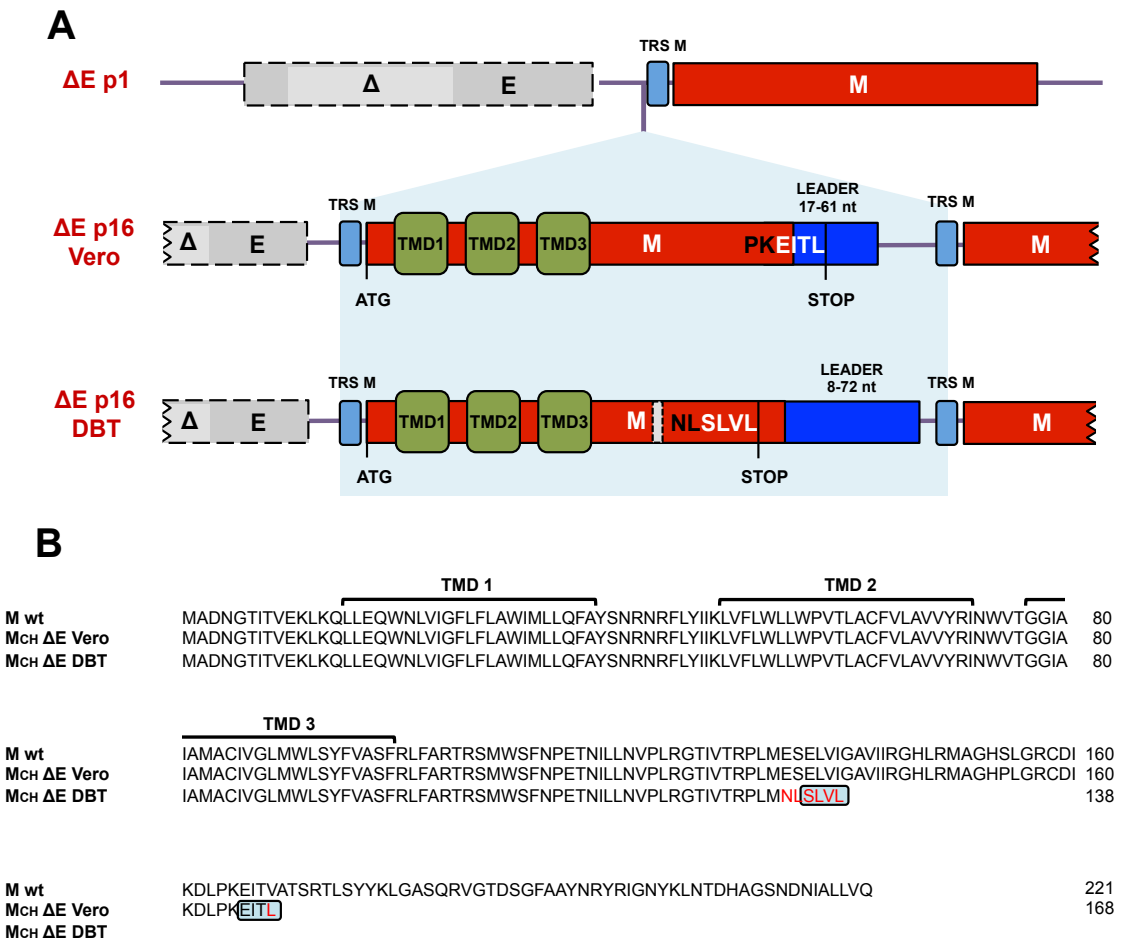

Figura 30. Generación y secuencia de aminoácidos de nuevos genes M quiméricos en SARS-CoV que carecen de la proteína E después de 16 pases seriados. (A) Esquema de la estructura de los genes M quiméricos generados después de pasar el virus SCoV-ΔE (ΔE) 16 veces en células Vero E6 y DBT-mACE2. En la parte superior, ΔE p1 representa la secuencia de los virus que no expresan la proteína E. En el recuadro gris se muestra el gen E delecionado parcialmente (Δ). La TRS de los distintos genes se representa con un recuadro azul y el gen M se muestra en color rojo. Los distintos genes M quiméricos formados después de 16 pases (p16) están formados por una duplicación parcial del gen M. Las regiones génicas que codifican los dominios transmembranas de la proteínas M quiméricas incorporadas en los pases del virus, se representan como TMD1, TMD2 y TMD3. La secuencia líder fusionada a la duplicación parcial del gen M y los nucleótidos implicados se muestran en color verde oscuro. El codón de iniciación de la nueva proteína M quimérica se representa por ATG. El codón de parada se representa por STOP. EITL y SLVL representan los cuatro últimos aminoácidos de las proteínas quiméricas, que constituyen PBMs potenciales. El recuadro gris claro de la barra inferior representa una deleción de 7 nucleótidos dentro del gen M parcialmente duplicado. (B) Se muestran las secuencias de aminoácidos de las proteínas M quiméricas generadas después de los pases. M wt, representa la secuencia de la proteína M nativa. M_{CH} ΔE Vero, representa la secuencia de la proteína M quimérica generada cuando se pasa el SCoV-ΔE 16 veces en células Vero E6. M_{CH} ΔE DBT, representa la proteína M quimérica generada después

de pasar el virus SCoV-ΔE 16 veces en células DBT-mACE2. Los dominios transmembrana de las proteínas se muestran como TMD1, TMD2 y TMD3. Los aminoácidos que difieren entre las distintas secuencias se representan en rojo. Los recuadros azules indican la presencia de los PBMs. Los números a la derecha muestran la posición de los aminoácidos.

Cuando el virus SCoV-ΔE se pasó en ratones incorporó una duplicación de 45 nucleótidos en la proteína 8a, resultando en la reversión al fenotipo virulento. Este cambio estaba asociado a la aparición de un motivo PBM en la nueva proteína 8a. Un mutante del SARS-CoV que carece de este dominio en la proteína E está atenuado en el modelo de ratón (Jimenez-Guardeño et al., 2014). Se observó que la ausencia de la proteína E en el virus SCoV-ΔE dio origen a la generación de una proteína M quimérica, cuando este virus se pasó en cultivos celulares (**Figura 30**). En base a estas observaciones se postuló que la inestabilidad de este mutante, podría ser consecuencia fundamentalmente de la eliminación del dominio PBM de la proteína E. Para ver si este era el caso, se introdujeron pequeñas deleciones en el gen E sin eliminar el motivo PBM (**Figura 31**). El conjunto de mutantes generado incluía mutaciones o deleciones de 6 a 12 aminoácidos en diferentes regiones del extremo carboxi-terminal de la proteína E. Estos mutantes se pasaron 16 veces en células Vero E6, y se determinó mediante secuenciación la posible incorporación al genoma viral de proteínas M quiméricas, y si estas incluían el motivo PBM de la proteína E (**Figura 31**). Los resultados indicaron que ninguno de los virus en los que la proteína E contenía un motivo PBM (wt, Mut1, Δ2, Δ3, Δ4, Δ5 y Δ6) en el pase 0, generó proteínas M quiméricas después de 16 pases seriados. La proteína M quimérica solo se generó cuando la proteína E se encontraba totalmente delecionada SCoV-ΔE. Estos resultados sugirieron que la proteína M quimérica se generaba para compensar la ausencia del motivo PBM de la proteína E.

3.2. Introducción de una segunda modificación en el genoma del SCoV-E* para incrementar su bioseguridad como vacuna

Para aumentar la bioseguridad del candidato a vacuna generado se introdujeron mutaciones adicionales en otra proteína viral nsp1. Para ello, se identificaron regiones de esta proteína potencialmente implicadas en la virulencia del SARS-CoV. Anteriormente que se había descrito que la proteína nsp1 aumenta la

virulencia del virus MHV (Lei et al., 2013; Zust et al., 2007). Para identificar los dominios conservados de la proteína nsp1 del SARS-CoV que pudieran estar implicados en la virulencia del virus, se realizó un alineamiento de las secuencias de las proteínas nsp1 del SARS-CoV y del MHV (**Figura 32**). El alineamiento de ambas secuencias mostró regiones conservadas entre las proteínas nsp1 de dos CoVs (**Figura 32**), sugiriendo que estas regiones podrían ser importantes para la función de la proteína. Así mismo, se tuvieron en cuenta estudios previos que habían identificado regiones de la proteína nsp1 implicadas en la producción del IFN de tipo I y la atenuación del virus (Lei et al., 2013; Narayanan et al., 2008; Zust et al., 2007). Basándonos en estas observaciones, se generaron cuatro virus mutantes (SCoV-nsp1*) con pequeñas deleciones de 8 a 11 aminoácidos a lo largo de la proteína nsp1 (SCoV-nspΔA, -nspΔB, -nspΔC y -nspΔD) (**Figura 32**). Los virus generados por genética reversa se rescataron en células Vero E6, se clonaron tres veces mediante aislamiento de placa en células Vero E6 y se secuenciaron.

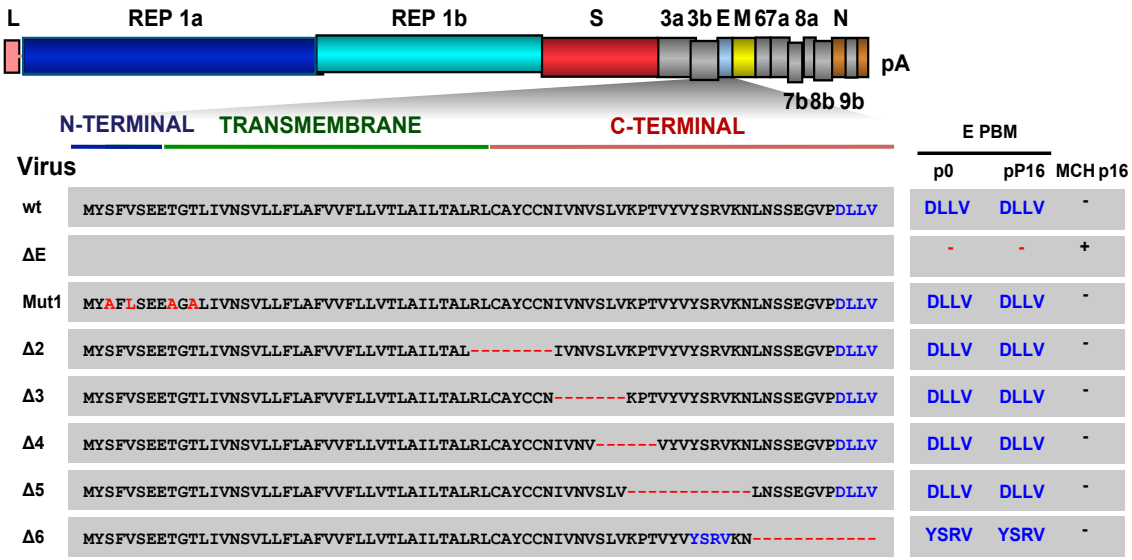

Figura 31. Dominio de la proteína E del SARS-CoV implicado en la generación de la proteína M quimérica. Conjunto de virus recombinantes con mutaciones o deleciones en distintos dominios de la proteína E utilizados para determinar las regiones relevantes en la generación de las distintas proteínas M quiméricas. Los virus recombinantes se pasaron 16 veces en células Vero E6 y posteriormente el último tercio del genoma se secuenció utilizando oligonucleótidos específicos. Se muestra la presencia y correspondiente secuencia (azul) de PBMs en las distintas proteínas E de los virus recombinantes (E PBM), en pase 0 (P0) y en pase 16 (P16). Además, se muestra la generación (+) o no (-) de una proteína M quimérica después de los pases seriados (M_{CH} P16).

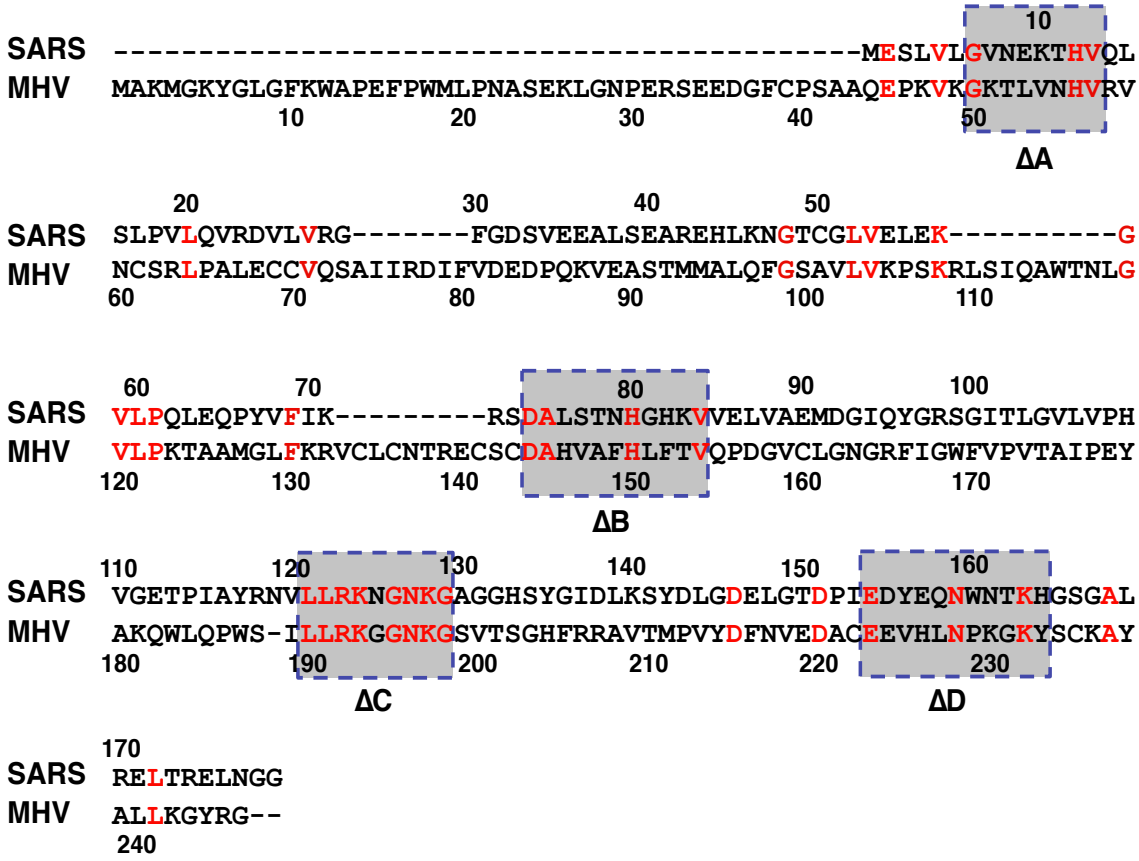

Figura 32. Alineamiento de secuencia de la proteína nsp1 de los virus SARS-CoV y MHV. Los aminoácidos que se encuentran conservados entre ambas secuencias se representan con letras rojas. Los rectángulos grises representan los aminoácidos delecionados dentro de la proteína nsp1, lo que dio lugar a la generación de los mutantes de deleción (ΔA, SCoV-nspΔA; ΔB, SCoV-nspΔB; ΔC, SCoV-nspΔC y ΔD, SCoV-nspΔD).

Para analizar el efecto de estas deleciones en la replicación viral, se estudiaron las cinéticas de crecimiento de los diferentes virus generados (SCoV-nsp1*) infectando células de mono (Vero E6) y de ratón (DBT-mACE2) (**Figura 33**). En células Vero E6, todos los mutantes de deleción mostraron títulos cercanos a 10^8 ufp/ml, similares a los títulos virales obtenidos con el virus nativo (**Figura 33**). En células DBT-mACE2 los mutantes SCoV-nspΔA y SCoV-nspΔB mostraron títulos inferiores de 10^6 ufp/ml. Sin embargo, los mutantes SCoV-nspΔC y SCoV-nspΔD crecieron con títulos de 10^7 ufp/ml similares al virus nativo (**Figura 33**). Estos datos indican que las deleciones introducidas en los mutantes ΔC y ΔD alteran significativamente la producción de virus en cultivos celulares.

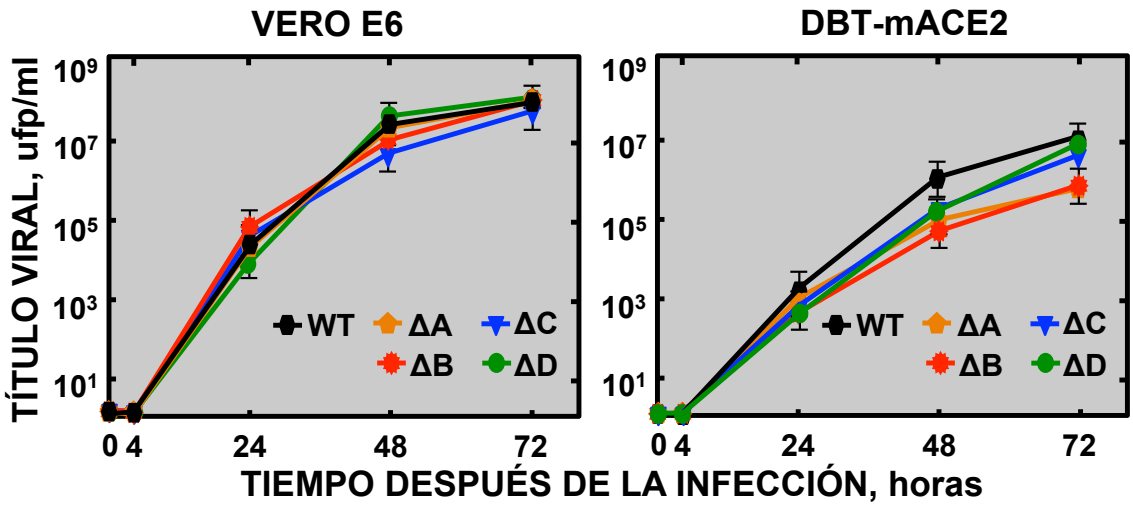

Figura 33. Cinéticas de crecimiento de los virus mutantes ScoV-nsp1*. Células Vero E6 y DBT-mACE2 se infectaron a una mdi de 0.001 con los mutantes SCoV-nsp1* (ΔA, SCoV-nspΔA; ΔB, SCoV-nspΔB; ΔC, SCoV-nspΔC y ΔD, SCoV-nspΔD), y el virus nativo (WT) y la progenie viral se tituló mediante ensayos de placas de lisis en células Vero E6 a los tiempos después de la infección indicados. Las barras de error representan las desviaciones estándar de tres experimentos independientes.

3.3. Virulencia de los mutantes SCoV-nsp1* en el modelo de ratón

Para analizar la relevancia de las distintas regiones de la proteína nsp1 en la virulencia del virus, ratones BALB/c se inocularon intranasalmente con el virus nativo o con los virus recombinantes SCoV-nsp1*. Los animales se controlaron diariamente, a lo largo de 10 días. Los ratones infectados con los virus SCoV-nspΔA y SCoV-nspΔB mostraron una pérdida de peso del 20 y 15%, respectivamente, y todos ellos recuperaron su peso, excepto dos y un ratón, respectivamente, los cuales murieron antes del día 6 después de la infección (**Figura 34**). Los ratones infectados con los virus SCoV-nspΔC y SCoV-nspΔD mostraron una pérdida de peso del 10%, recuperándose a los 3 días después de la inoculación y el 100% de los ratones sobrevivieron. Por el contrario, los ratones infectados con el virus nativo de longitud completa perdieron peso rápidamente y el 100% murieron antes del día 6 después de la infección (**Figura 34**). Estos datos indican que la deleción de las regiones C y D de la proteína nsp1 genera virus completamente atenuados,

mientras que las deleciones de las regiones A y B genera virus parcialmente atenuados.

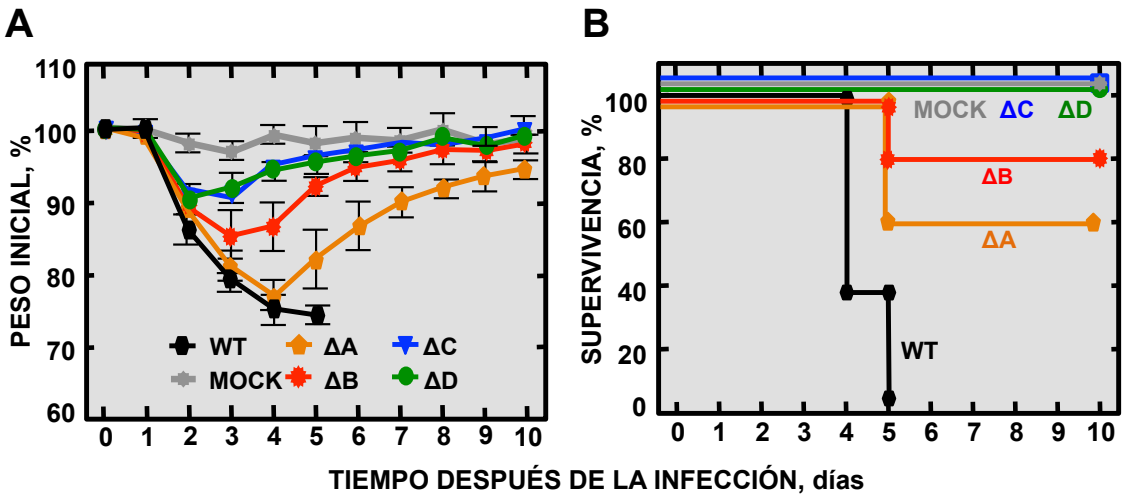

Figura 34. Patología causada por los virus SCoV-nsp1* en ratones BALB/c. Grupos de cinco ratones de 16 semanas de edad se inocularon con 100000 ufp de los virus: SCoV-nsp1* (ΔA, SCoV-nspΔA; ΔB, SCoV-nspΔB; ΔC, SCoV-nspΔC y ΔD, SCoV-nspΔD), virus nativo, o sin virus (Mock). Se analizó la pérdida de peso (A) y la supervivencia (B). Los ratones que perdieron más del 30% de su peso inicial se sacrificaron por razones éticas. Las barras de error representan la desviación estándar del peso de los ratones en cada variable experimental.

3.4. Crecimiento de los virus mutantes SCoV-nsp1* en ratones infectados

Para evaluar si las regiones de la proteína nsp1 delecionadas se requieren para el óptimo crecimiento de los virus en los pulmones de ratones infectados, ratones BALB/c se inocularon con los diferentes virus generados SCoV-nsp1*, o con el virus nativo. A los 2 y 4 ddi se recogieron los pulmones, se homogeneizaron y se determinó el título viral (**Figura 35**). El virus mutante SCoV-nspΔA mostró un crecimiento similar al virus nativo a 2 ddi, pero mostró una disminución en los títulos virales de 200 veces a 4 ddi (**Figura 35**). Los títulos virales de los virus mutantes SCoV-nspΔB y SCoV-nspΔC disminuyeron 100 y 1000 veces a 2 y 4 ddi, respectivamente, comparados con el crecimiento del virus nativo. El virus mutante SCoV-nspΔD creció 10 y 1000 veces menos, a 2 y 4 ddi, respectivamente, que el virus nativo. Estos datos indican que, aunque en distinta medida, las cuatro

regiones delecionadas en la proteína nsp1 contribuyen a disminuir el crecimiento del virus en ratón, probablemente porque las secuencias delecionadas están implicadas en antagonizar la producción del IFN en las células infectadas.

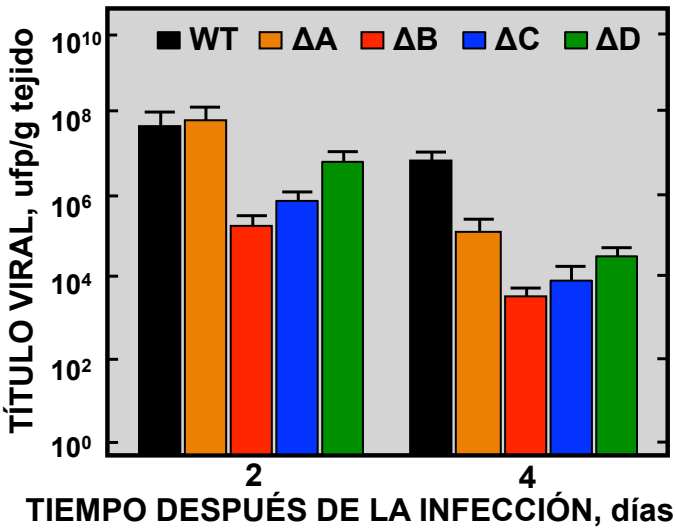

Figura 35. Crecimiento de los virus SCoV-nsp1* en pulmones de ratones BALB/c. Grupos de seis ratones de 16 semanas de edad se inocularon con 100000 ufp de los virus SCoV-nsp1* (ΔA, SCoV-nspΔA; ΔB, SCoV-nspΔB; ΔC, SCoV-nspΔC y ΔD, SCoV-nspΔD) o WT. A los 2 y 4 ddi se sacrificaron 3 ratones de cada grupo para determinar los títulos virales en pulmón. Las barras de error representan la desviación estándar de los títulos obtenidos en los pulmones de los 3 ratones utilizados para cada variable experimental.

3.5. Patología pulmonar causada por la infección con SCoV-nsp1* en ratón

Para analizar los mecanismos por los cuales los virus SCoV-nsp1* están atenuados, se estudiaron macroscópica y microscópicamente los pulmones de ratones no infectados, infectados con el virus nativo, o con los virus mutantes de la proteína nsp1, a días 2 y 4 di (**Figura 36**). En el análisis macroscópico, los pulmones de ratones infectados con el virus nativo, o en menor grado los pulmones infectados con los virus SCoV-nspΔA y SCoV-nspΔB, mostraron regiones hemorrágicas debido probablemente a la presencia de infiltraciones leucocitarias (**Figura 36A y B**). Por el contrario, los pulmones de ratones no infectados o infectados con los virus SCoV-nspΔC y SCoV-nspΔD no mostraron lesiones significativas ni cambios de peso (**Figura 36A y B**). Además, los pulmones de ratones infectados con el virus nativo

mostraron un aumento del volumen pulmonar sobre todo a 4 ddi, posiblemente debido a la acumulación de edema en las zonas infectadas (**Figura 36A y B**).

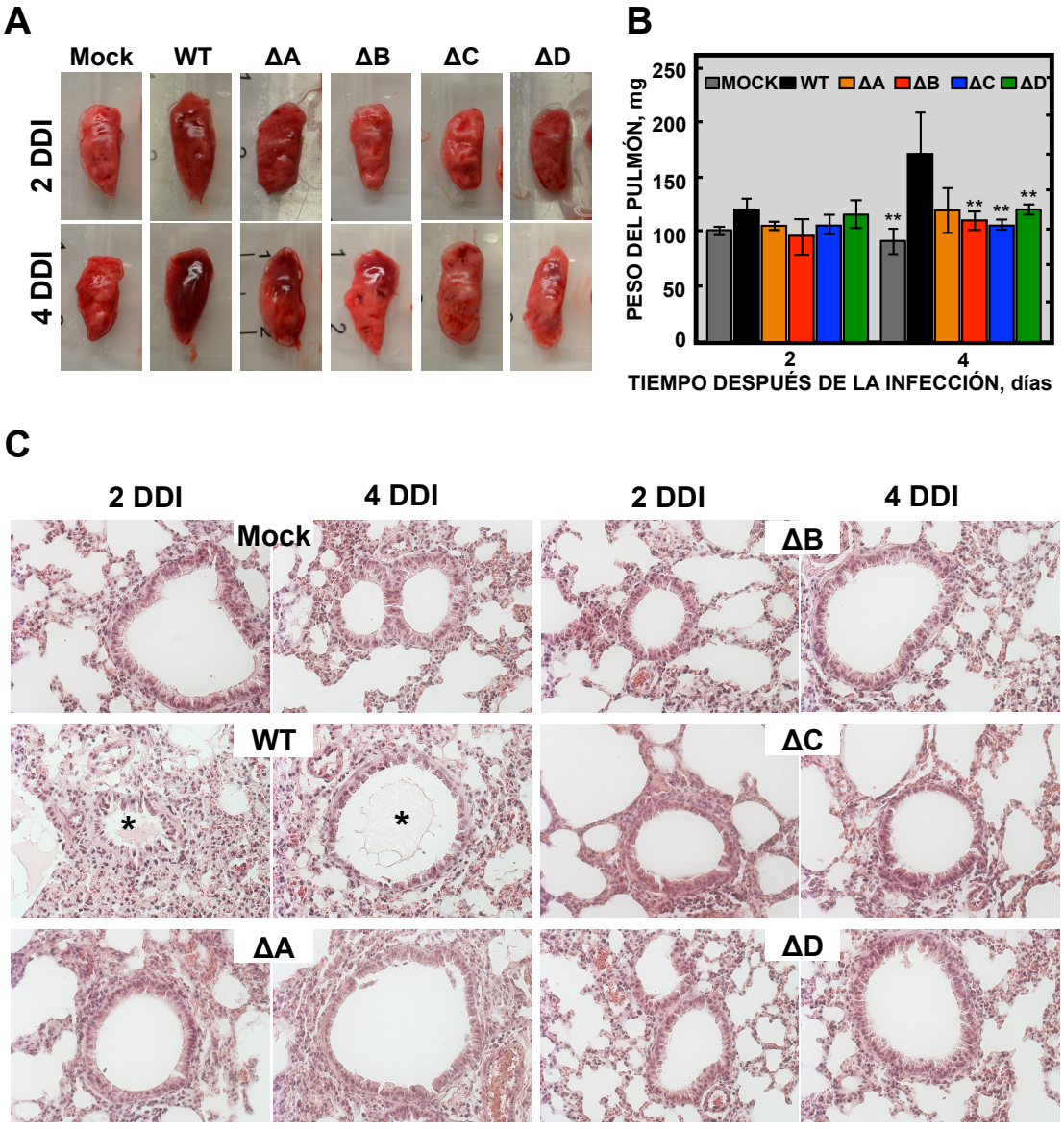

Figura 36. Patología pulmonar causada por la infección por SCoV-nsp1* en ratones. Grupos de seis ratones de 16 semanas de edad se inocularon con 100000 ufp de los virus SCoV-nsp1* (ΔA, SCoV-nspΔA; ΔB, SCoV-nspΔB; ΔC, SCoV-nspΔC y ΔD, SCoV-nspΔD), nativo (WT) o sin virus (Mock). A los 2 y 4 ddi se sacrificaron 3 ratones de cada grupo y se recogieron sus pulmones. (A) Patología macroscópica observada en los pulmones de ratón infectados con los distintos virus. (B) Antes de fijar los pulmones, estos se pesaron. Las barras de error indican la desviación estándar para los 3 ratones de cada variable experimental. Los datos estadísticamente significativos se indican con dos asteriscos (test

de Student, p-valor <0.01). (C) Los pulmones se fijaron con formalina de zinc, se incluyeron en parafina, se cortaron y se tiñeron con hematoxilina y eosina. Los asteriscos indican acumulación de edema en bronquiolos y alveolos. El aumento original utilizado fue de 20x.

Para el análisis microscópico, cortes de pulmones se tiñeron mediante hematoxilina y eosina y se analizaron los cambios histológicos. Los pulmones de ratones no infectados presentaron las vías aéreas (alveolos y bronquiolos) despejadas, y no se observó la presencia de infiltrados leucocitarios (**Figura 36C**). Por el contrario, los pulmones de los ratones infectados con el virus nativo mostraron engrosamiento de los epitelios alveolares, edema y presencia de infiltraciones leucocitarias a 2 y 4 ddi (**Figura 36C**). El análisis histológico de los pulmones de los animales infectados con los virus SCoV-nspΔA y SCoV-nspΔB mostró daños mínimos, mientras que en los pulmones de los ratones infectados con los virus SCoV-nspΔC y SCoV-nspΔD no se observarón infiltrados pulmonares (**Figura 36C**). Estos datos estaban en línea con la virulencia observada para los mutantes SCoV-nsp1*, mostrando que los virus atenuados fueron los que indujeron una menor patología pulmonar *in vivo*. Dado que los virus SCoV-nspΔC y SCoV-nspΔD estaban completamente atenuados en el modelo de ratón, los experimentos siguientes se centraron en estos virus.

3.6. Efecto de la infección por los virus SCoV-nsp1* en la inducción de la respuesta de IFN tipo I

Un virus recombinante MHV, en el que se había delecionado la proteína nsp1, creció menos eficientemente y estaba atenuado en ratón, debido a que la proteína nsp1 del MHV interfiere eficientemente con la respuesta por IFN tipo I (Narayanan et al., 2014; Zust et al., 2007). Para determinar el efecto de las regiones delecionadas en la proteína nsp1 del SARS-CoV en la respuesta del IFN del tipo I, células DBT-mACE2 se infectaron con los virus atenuados SCoV-nspΔC y SCoV-nspΔD, y con el virus virulento de longitud completa. Se analizaron los niveles de expresión del IFNβ y tres ISGs mediante RT-qPCR (**Figura 37 y Tabla III**).

Los virus atenuados SCoV-nspΔC y SCoV-nspΔD indujeron mayores niveles de expresión de IFNβ y los ISGs: IRF1, DDX58 y STAT1, con respecto a las células infectadas con el virus nativo o sin infectar (**Figura 37**). Se observó que los niveles de expresión del gen que codifica el rRNA 18S utilizado como control fueron similares en todos los casos (**Figura 37B**).

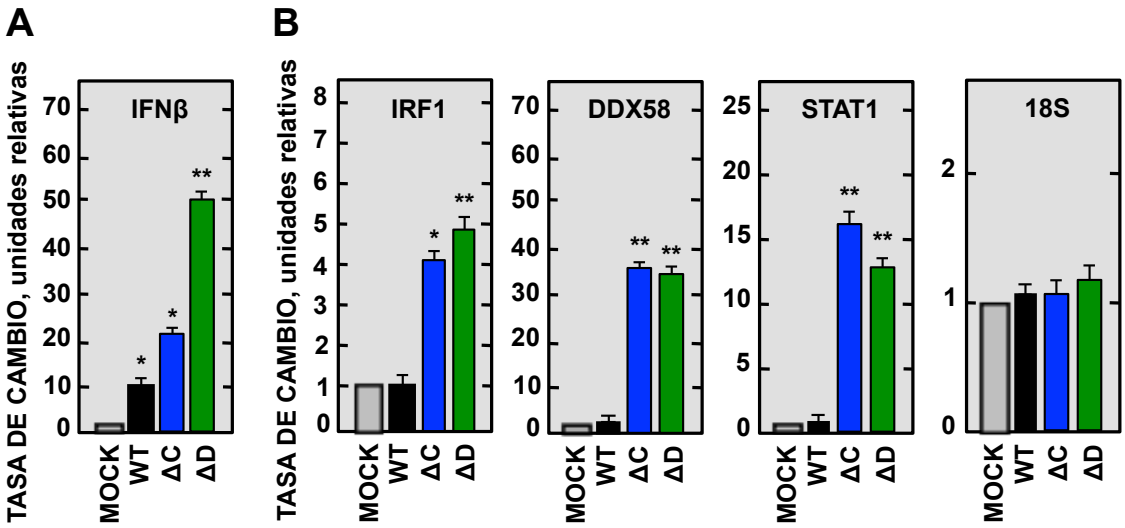

Figura 37. Expresión de IFNβ e ISGs en células DBT-mACE2 infectadas con los virus SCoV-nsp1*. Células DBT-mACE2 se infectaron con una mdi de 0.125 con los virus (ΔC, SCoV-nspΔC y ΔD, SCoV-nspΔD), nativo o se dejaron sin infectar (mock). El RNA total se extrajo a las 48 hdi y la expresión de los genes se evaluó por RT-qPCR. En cada caso los niveles de expresión de las células infectadas se compararon con los niveles de expresión de las células no infectadas. (A) IFNβ. (B) ISGs inducidos por IFN (IRF1, DDX58 y STAT1). rRNA 18S se usó como control. La gráfica muestra los promedios y desviaciones estándar de tres experimentos independientes. Los datos estadísticamente significativos se indican con uno o dos asteriscos (t de Student p-valor <0.05, <0.01, respectivamente).

Estos resultados indicaron que las regiones ΔC y ΔD delecionadas en la proteína nsp1 disminuyeron la capacidad de esta proteína para bloquear la respuesta al IFN inducida por el huésped. La mayor inducción de IFN después de la infección con los virus SCoV-nspΔC y SCoV-nspΔD, sugiere que esto es la causa de la atenuación observada en estos virus, en consonancia con lo que ocurre con otros virus (Hoffmann et al., 2015; Randall and Goodbourn, 2008; Schneider et al., 2014).

3.7. Análisis de la protección conferida por los virus atenuados SCoV-nspΔC y SCoV-nspΔD frente al desafío con el virus virulento SCoV

Para analizar si los mutantes atenuados SCoV-nspΔC y SCoV-nspΔD son candidatos prometedores a vacunas, se analizó la inducción de protección conferida por estos recombinantes frente al desafío con el virus virulento SCoV. Para ello, grupos de ratones no inmunizados, o inmunizados con los virus SCoV-nspΔC y SCoV-nspΔD, se desafiaron a los 21 días después de la inmunización con el virus SCoV. Se analizó la pérdida de peso y mortalidad de los ratones durante los 10 días posteriores al desafío (**Figura 38**). Todos los ratones no inmunizados perdieron rápidamente peso y murieron antes del día 7 después del desafío con el virus SCoV. Por el contrario, los ratones que fueron vacunados con los virus atenuados SCoV-nspΔC y SCoV-nspΔD, no perdieron significativamente peso, y el 100% de los ratones sobrevivieron (**Figura 38**). Estos datos indican que los virus mutantes con fenotipo atenuado SCoV-nspΔC y ScoV-nspΔD protegen completamente a los ratones frente al desafío con el virus letal SCoV, por lo tanto son candidatos prometedores a vacunas.

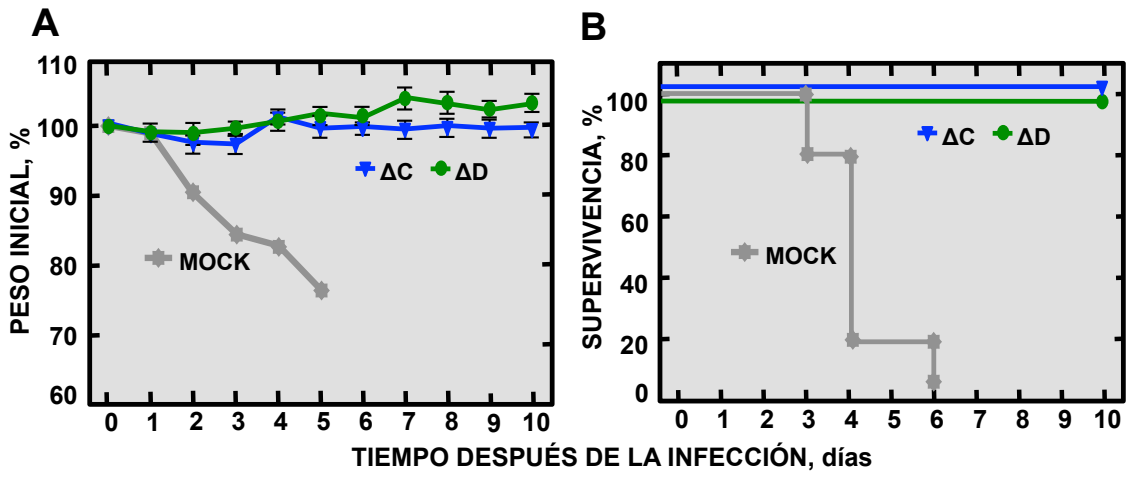

Figura 38. Protección conferida por la inmunización con los virus SCoV-nsp1*. Ratones BALB/c de 16 semanas se dejaron sin inmunizar (mock) o se inmunizaron con 6000 ufp de los virus (ΔC, SCoV-nspΔC y ΔD, SCoV-nspΔD). Los ratones se desafiaron con 100000 ufp del virus nativo 21 días después de la inmunización. Se evaluó la pérdida de peso (A) y la supervivencia (B) de los ratones desafiados (n = 3 ratones por grupo).

3.8. Generación y crecimiento de virus mutantes de SARS-CoV con deleciones en los genes nsp1 y E

Para desarrollar una vacuna basada en virus atenuados, mediante la introducción de dos medidas complementarias de bioseguridad, se generaron recombinantes virales con deleciones en los genes nsp1 y E. Para ello, se utilizaron virus recombinantes con deleciones en la proteína E completa (SCoV-ΔE) o con una pequeña deleción dentro de la proteína E (SCoV-EΔ3), dado que este virus mostró mayores títulos en ratón que el virus SCoV-ΔE (Regla-Nava et al., 2015). Estas deleciones se combinaron en un mismo virus con una segunda deleción en el gen nsp1 (SCoV-nspΔD), dado que esta modificación del virus dio lugar a mayores títulos virales que estaban completamente atenuados en ratón. Los virus SCoV-nspΔD-ΔE y SCoV-nspΔD-EΔ3 generados por genética reversa (**Figura 39**), se rescataron en células Vero E6, se clonaron tres veces mediante aislamiento de placa en estas células y se secuenciaron.

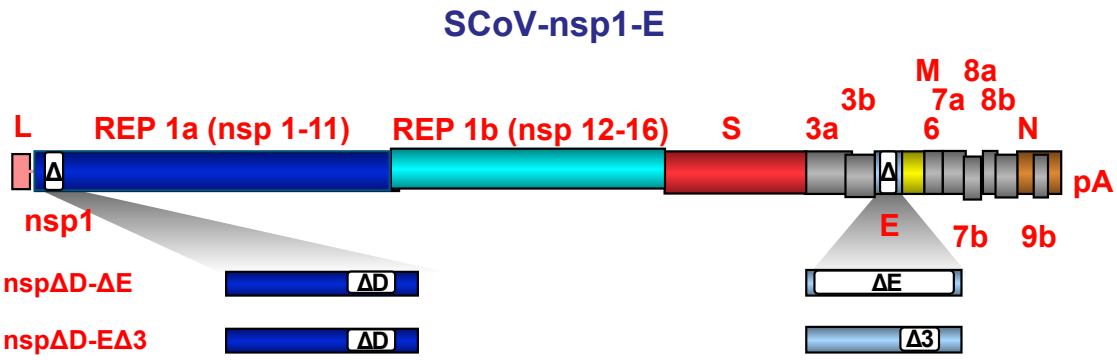

Figura 39. Esquema de la generación de virus con deleciones en las proteínas nsp1 y E del SCoV. El genoma del SARS-CoV se muestra en la parte superior. Las regiones expandidas muestran los genes donde se realizaron las respectivas deleciones.

Una característica esencial de un candidato a vacuna prometedor es que este sea estable después de pases seriados en cultivos celulares y en modelos animales. Para analizar la estabilidad de los virus, SCoV-nspΔD-ΔE y SCoV-nspΔD-EΔ3 (p1) se pasaron 10 veces en células Vero E6 (p10C). Posteriormente, se analizó la secuencia de los genes nsp1 y E para determinar si las deleciones genéticas

introducidas se mantenían. Ambas deleciones se conservaron, indicando que estos virus fueron estables en cultivos celulares. Para analizar el efecto de las dobles deleciones introducidas en los genes nsp1 y E, se estudiaron las cinéticas de crecimiento de los recombinantes SCoV-nspΔD-ΔE, y SCoV-nspΔD-EΔ3-p1 y -p10C en células Vero E6 y DBT-mACE2 (**Figura 40**). Todos los virus alcanzaron los títulos virales máximos a las 72 hdi en células Vero E6 y DBT-mACE2 (**Figura 40**). Los virus SCoV-nspΔD-ΔE y SCoV-nspΔD-EΔ3 de pase 1 crecieron aproximadamente 100 veces menos que el virus nativo, en ambas líneas celulares: Vero E6 y DBT-mACE2, a las 72 hdi, indicando que las deleciones en las proteínas nsp1 y E del SARS-CoV reducen la producción viral. Los virus de pase 10 (p10C) mostraron un ligero incremento del título viral comparado con los títulos observados para los virus recombinantes de pase 1 (**Figura 40**), sugiriendo que estos virus incorporan mutaciones compensatorias.

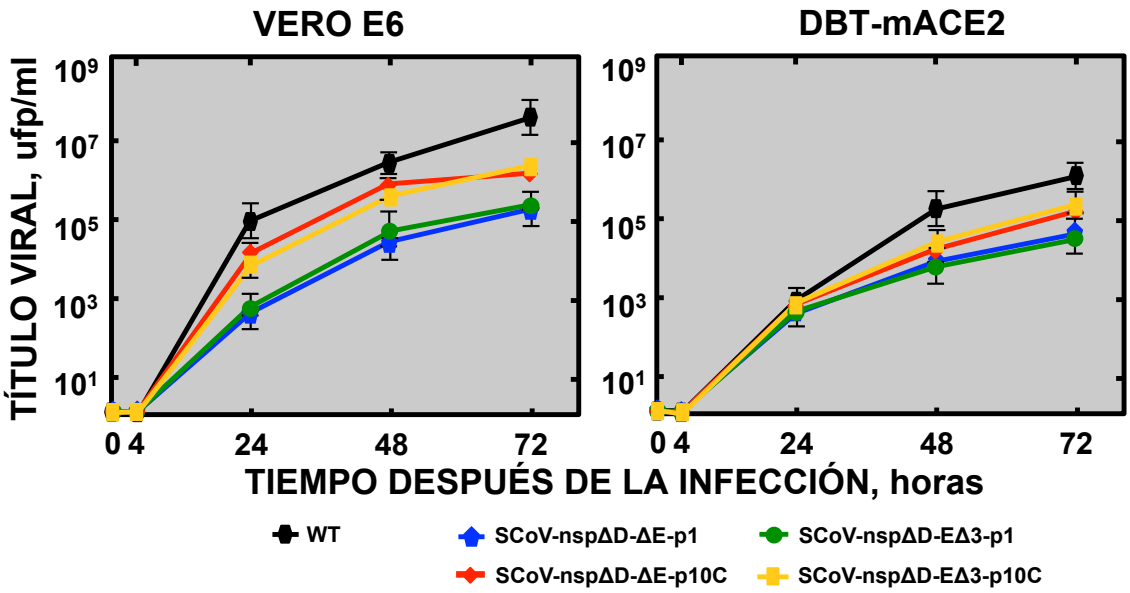

Figura 40. Cinéticas de crecimiento de los virus mutantes SCoV-nspΔD-ΔE y SCoV-nspΔD-EΔ3. Células Vero E6 y DBT-mACE2 se infectaron a una mdi de 0.001 con los mutantes SCoV-nspΔD-ΔE y SCoV-nspΔD-EΔ3 pasados solo una vez (p1) o pasados 10 veces en células Vero E6 (p10C) y con el virus nativo (WT). La progenie viral se tituló a los tiempos indicados después de la infección, mediante ensayos de placas de lisis en células Vero E6. Las barras de error representan las desviaciones estándar de tres experimentos independientes.

3.9. Virulencia de los mutantes SCoV-nspΔD-ΔE y SCoV-nspΔD-EΔ3 en el modelo de ratón

Como se ha descrito anteriormente, los virus que carecen de la proteína E completa o que incluyen pequeñas deleciones en las proteínas E y nsp1 muestran un fenotipo atenuado (DeDiego et al., 2007; DeDiego et al., 2014; DeDiego et al., 2008; Fett et al., 2013; Regla-Nava et al., 2015). Para analizar si los virus que contienen deleciones en los genes nsp1 y E mantienen su atenuación, tanto de pase 1 como después de pasarlos 10 veces en células Vero E6 (p10C), ratones BALB/c se inocularon intranasalmente con el virus nativo, o con los virus SCoV-nspΔD-ΔE y SCoV-nspΔD-EΔ3 -(p1 y p10C). Los animales se controlaron, durante 10 días. Los ratones infectados con el virus nativo mostraron signos característicos de la enfermedad descritos con anterioridad, perdieron rápidamente peso y el 100% murieron antes del día 6 di (**Figura 41**).

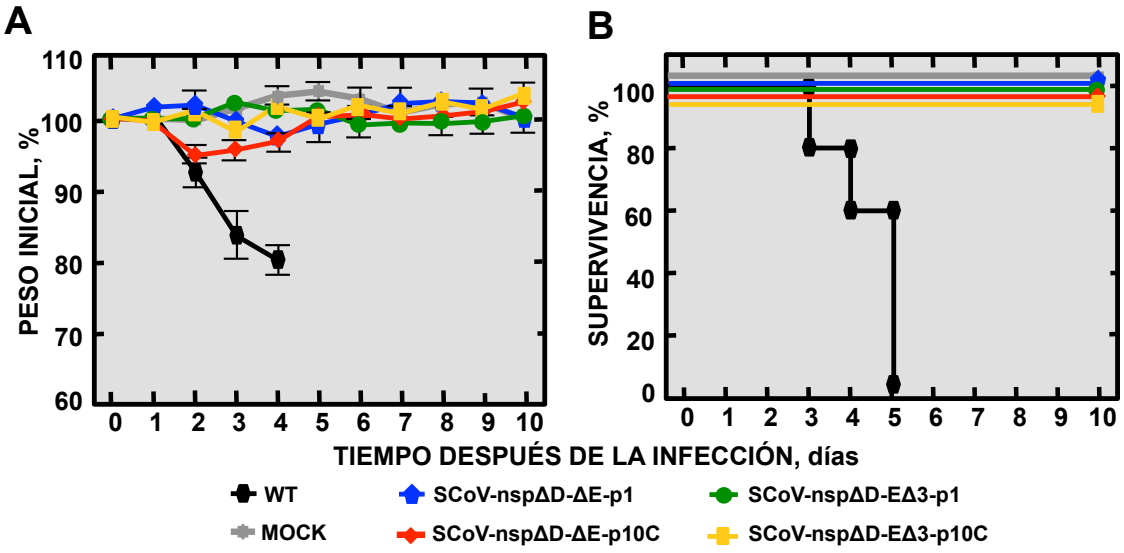

Figura 41. Patología causada por los virus SCoV-nspΔD-ΔE y SCoV-nspΔD-EΔ3 en ratones BALB/c. Grupos de cinco ratones se inocularon con 100000 ufp de los virus SCoV-nspΔD-ΔE y SCoV-nspΔD-EΔ3 en pase p1 ó p10C, con el virus nativo (WT) o sin virus (Mock). Se analizó la pérdida de peso (A) y la supervivencia (B). Los ratones que perdieron mas del 30% de su peso inicial se sacrificaron. Las barras de error representan la desviación estándar del peso de los ratones en cada variable experimental.

Por el contrario, los ratones infectados con los virus SCoV-nspΔD-ΔE y SCoV-nspΔD-EΔ3 en pase p1 ó p10C no mostraron signos clínicos de enfermedad (datos no mostrados), no experimentaron pérdida de peso, y el 100% de los ratones sobrevivieron (**Figura 41**). Estos resultados indicaron que los virus con dobles deleciones en el genoma, estaban completamente atenuados, como era de esperar. Cuando estos virus se pasaron 10 veces en células Vero E6 también mantuvieron su atenuación.

4.0. Crecimiento de los virus mutantes SCoV-nspΔD-ΔE y SCoV-nspΔD-EΔ3 en ratones

Para evaluar si las dobles deleciones introducidas en los genes nsp1 y E alteran significativamente el crecimiento del virus en ratones BALB/c, estos se inocularon con los virus SCoV-nspΔD-ΔE, SCoV-nspΔD-EΔ3 -(p1 y p10C) y con el virus nativo y se determinó el título viral en los pulmones (**Figura 42**).

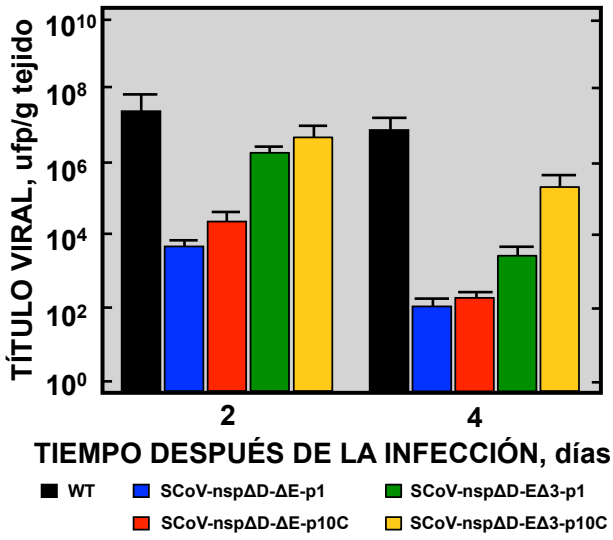

Figura 42. Crecimiento de los mutantes SCoV dobles en pulmones de ratones BALB/c. Grupos de seis ratones se inocularon con los virus SCoV-nspΔD-ΔE y SCoV-nspΔD-EΔ3-p1 y -p10C o con el virus de longitud completa (WT). A los 2 y 4 ddi se sacrificaron 3 ratones de cada grupo para determinar los títulos virales en pulmón. Las barras de error representan la desviación estándar de los títulos obtenidos en los pulmones de los 3 ratones utilizados para cada variable experimental.

Los virus SCoV-nspΔD-ΔE-p1 y -p10C crecieron con títulos muy bajos (alrededor de 10^4 y 10^2 ufp/g de tejido a 2 y 4 ddi, respectivamente) (**Figura 42**). El virus SCoV-nspΔD-EΔ3-p1 creció con títulos significativamente mayores (alrededor de 5 x 10^6 y 5 x 10^3 ufp/g de tejido a 2 y 4 ddi, respectivamente). Estos títulos se incrementaron significativamente en las infecciones con SCoV-nspΔD-EΔ3-p10C, particularmente a 4 ddi. El virus nativo mostró los títulos más altos (7 x 10^7 y 1 x 10^7 ufp/g de tejido, a 2 y 4 ddi, respectivamente) (**Figura 42**). Estos resultados mostraron que los mutantes SCoV-nspΔD-EΔ3, y especialmente el virus p10C, creció de forma más eficiente que el mutante SCoV-nspΔD-ΔE. Este resultado es consistente con los resultados previos que mostraban que el mutante sencillo SCoV-EΔ3 creció de forma más eficiente en ratones que SCoV-ΔE con la proteína E totalmente delecionada (Regla-Nava et al., 2015).

4.1. Patología pulmonar causada por la infección con SCoV-nspΔD-ΔE y SCoV-nspΔD-EΔ3 en ratón

Para analizar la patología en pulmón inducida por la infección con los dobles mutantes de pases 1 y 10, se hicieron análisis macroscópicos y microscópicos a 2 y 4 ddi (**Figura 43**). En los pulmones de los ratones infectados con los virus SCoV-nspΔD-ΔE y SCoV-nspΔD-EΔ3 de pases 1 y 10 no se observaron muestras evidentes de patología. Por el contrario los pulmones infectados con el virus nativo mostraron infiltrados y edema pulmonar, tal como se ha descrito anteriormente en esta tesis en las infecciones con virus virulentos. Estos datos refuerzan que tanto individualmente como de forma conjunta, estas deleciones dan origen a virus completamente atenuados causando mínimos daños a nivel pulmonar.

4.2. Estabilidad y patología causada por la infección con SCoV-nspΔD-EΔ3 pasado en ratón

La estabilidad de los virus infectivos durante su pase *in vivo* es una característica esencial para poder utilizarlos como vacunas atenuadas. Para analizar la estabilidad de los virus que contenían deleciones en los genes E y nsp1 *in vivo*, el

virus SCoV-nspΔD-EΔ3 se pasó diez veces en ratón (p10M), y posteriormente se secuenciaron todos los genes virales excepto el gen de la replicasa.

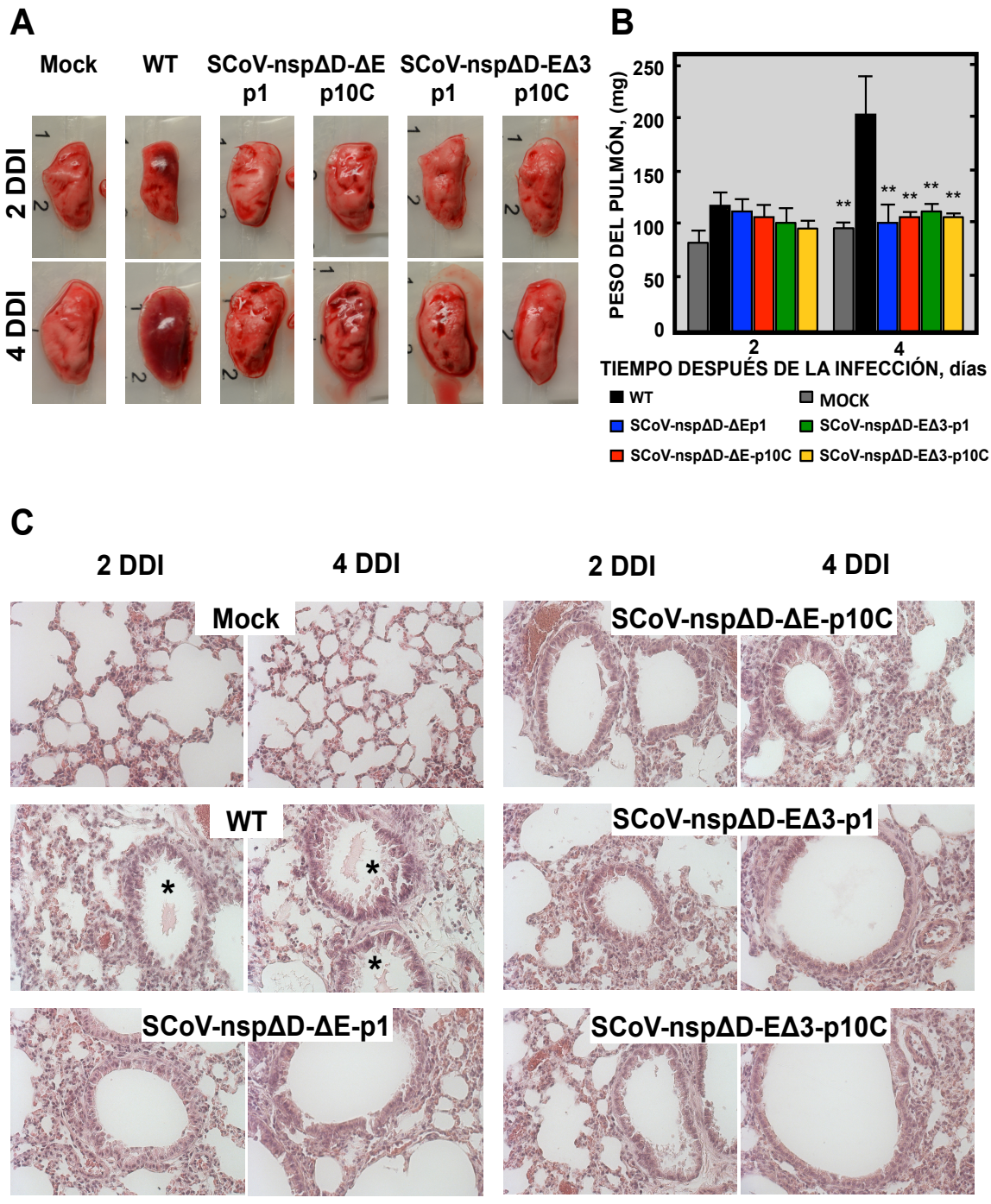

43. Patología pulmonar causada en infecciones de ratones por SCoV-nspΔD-ΔE y SCoV-nspΔD-EΔ3. Grupos de seis ratones de 16 semanas de edad se inocularon con 100000 ufp de los virus SCoV-nspΔD-ΔE y SCoV-nspΔD-EΔ3-p1 y -p10C, con el virus virulento nativo (WT), o sin virus (Mock). A los 2 y 4 ddi se sacrificaron 3 ratones de cada

grupo y se recogieron sus pulmones. (A) Las imágenes muestran la patología macroscópica observada en los pulmones de ratón infectados con los distintos virus. (B) Antes de fijar los pulmones, estos se pesaron. Las barras de error indican la desviación estándar observada para los 3 ratones de cada variable. Los datos estadísticamente significativos se indican con dos asteriscos (test de Student, p-valor <0.01). (C) Los pulmones se fijaron con formalina de zinc, se incluyeron en parafina, se prepararon microsecciones que se tiñeron con hematoxilina y eosina. Los asteriscos indican acumulación de edema en bronquiolos y alveolos. El aumento original utilizado fue de 20x.

Solo se observaron dos mutaciones puntuales en la secuencia viral, una en el gen E (26250 A→T) que generó cambio de aminoácido en la proteína (N→I), y otra en el gen M (26450 A→G) que produjo un cambio de aminoácido (Q→R). Sin embargo, las deleciones introducidas en los genes nsp1 y E se conservaron, sugiriendo que este virus era bastante estable *in vivo*. Para analizar si las mutaciones incorporadas en el virus después de los pases en ratón eran mutaciones alteraban la replicación del virus, se realizaron cinéticas de crecimiento en células Vero E6 y DBT-mACE2 con los virus antes (p1) y después de ser pasados en ratón (p10M). Los títulos virales observados para el virus SCoV-nspΔD-EΔ3-p10M fueron superiores a los títulos de los virus de pase 1 y similares a los títulos virales observados para el virus nativo (datos no mostrados), indicando que las mutaciones que los virus incorporan después de los pases aumentan la producción de virus infecciosos. Para evaluar si las mutaciones incorporadas restauraban la patogénesis del virus, ratones BALB/c se inocularon intranasalmente con el virus nativo y el virus SCoV-nspΔD-EΔ3-p10M. Los ratones infectados con el virus nativo empezaron a perder peso al día 2 di y el 100% murieron antes del día 7 di (**Figura 44**). Por el contrario, los ratones infectados con el virus mutante SCoV-nspΔD-EΔ3-p10M mostraron una pérdida de peso del 10% a los 4 ddi, sin embargo, se recuperaron a los 5 ddi y el 100% de los ratones sobrevivieron (**Figura 44**). Además, los pulmones de los ratones infectados con este doble mutante no mostraron lesiones en pulmón a nivel macroscópico ni microscópico (datos no mostrados). Estos resultados indican que a pesar de las mutaciones que el virus incorpora después de los pases en ratón, el virus mantiene su atenuación *in vivo*.

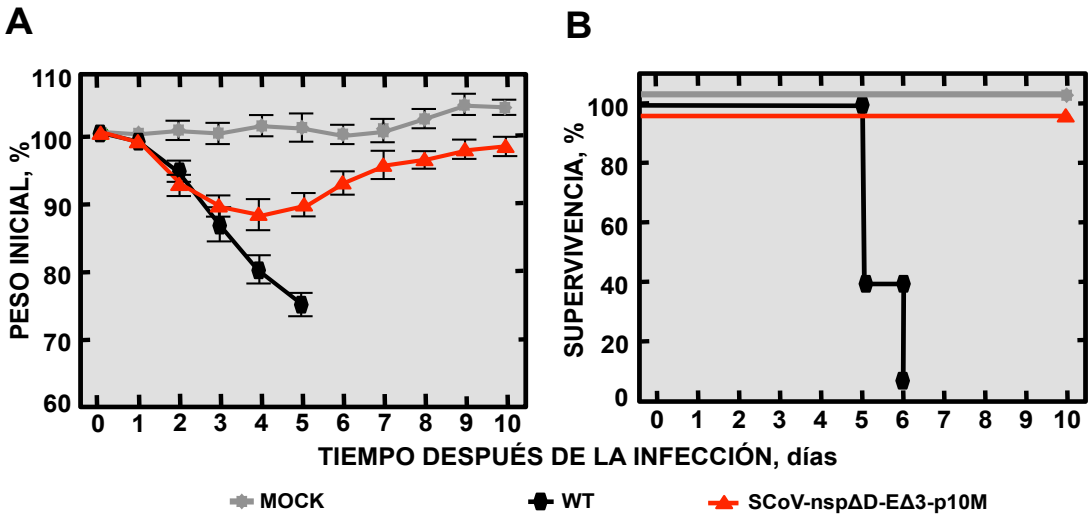

Figura 44. Patología causada por el mutante SCoV-nspΔD-EΔ3-p10M en ratones. Grupos de cinco ratones se inocularon con 100000 ufp de los virus SCoV-nspΔD-EΔ3-p10M, nativo o sin virus (mock). Se analizó la pérdida de peso (A) y la supervivencia (B). Los ratones que perdieron más del 30% de su peso inicial se sacrificaron. Las barras de error representan la desviación estándar del peso de los tres ratones inoculados.

Para evaluar el efecto de las mutaciones que se fijaron durante los pases del virus mutante SCoV-nspΔD-EΔ3-p10M en el crecimiento *in vivo*, se inocularon ratones BALB/c con este virus y se determinó su título en los pulmones (**Figura 45**). El virus creció con títulos similares a los observados para el virus nativo, a días 2 y 4 di, indicando que el virus crece eficientemente *in vivo,* debido muy probablemente a la incorporación de mutaciones compensatorias.

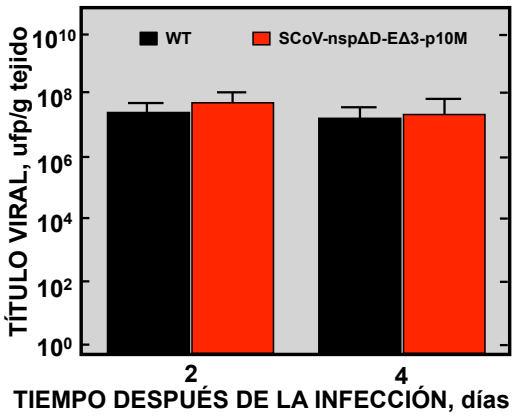

Figura 45. Crecimiento del mutante SCoV-nspΔD-EΔ3-p10M en pulmones de ratones BALB/c. Grupos de seis ratones se inocularon con 100000 ufp del virus SCoV-nspΔD-EΔ3

-p10M ó WT. Se determinaron los títulos virales en los pulmones a los 2 y 4 ddi. Las barras de error representan la desviación estándar de los títulos obtenidos en los pulmones de los 3 ratones utilizados para cada variable experimental.

4.3. Análisis de la protección conferida por el virus atenuado SCoV-nspΔD-EΔ3 frente al desafío con el virus virulento SCoV

El virus SCoV-nspΔD-EΔ3 es un candidato prometedor a vacuna dado que en él se han introducido dos medidas de seguridad complementarias, y está altamente atenuado *in vivo*, incluso después de ser pasado en cultivos celulares y en ratón. Para determinar si este virus confiere protección frente al desafío con el virus virulento SCoV, grupos de ratones no inmunizados, o inmunizados con los virus SCoV-nspΔD-EΔ3 de p1, p10C y p10M, se desafiaron con el virus SCoV a los 21 días después de la inmunización. Se analizó la pérdida de peso y la mortalidad de los ratones durante los 10 días posteriores al desafío (**Figura 46**).

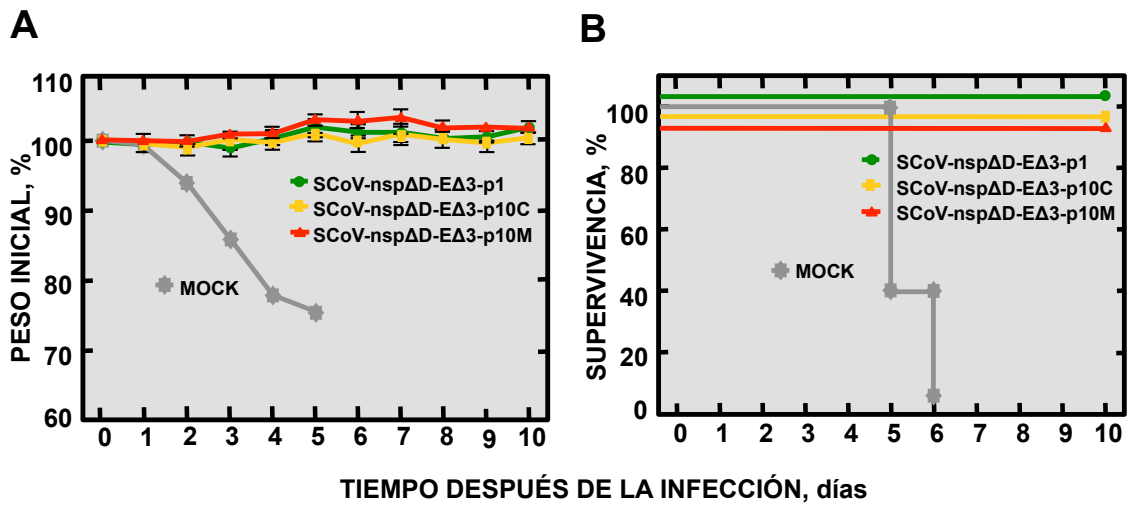

Figura 46. Protección conferida por la inmunización con los virus SCoV-nspΔD-EΔ3 -p1, -p10C y -p10M. Ratones BALB/c de 16 semanas se dejaron sin inmunizar (mock) o se inmunizaron con 6000 ufp de los virus SCoV-nspΔD-EΔ3-p1, -p10C y -p10M. Los ratones se desafiaron con 100000 ufp del virus nativo 21 después de la inmunización. Se evaluó la pérdida de peso (A) y la supervivencia (B) de los ratones desafiados (n = 3 ratones por grupo).

Todos los ratones no inmunizados perdieron rápidamente peso y murieron antes del día 7 después del desafío con el virus virulento SCoV. Por el contrario, los ratones que fueron vacunados con los virus atenuados, no perdieron peso y el 100% de los ratones sobrevivieron (**Figura 46**), indicando que este virus mutante es un candidato a vacuna muy prometedor.

DISCUSIÓN

En esta tesis doctoral se ha generado una línea celular de ratón, altamente susceptible a la infección por SARS-CoVs adaptados a ratón, que expresa establemente la proteína ACE2 murina, como herramienta fundamental para trabajar con SARS-CoVs adaptados a ratón. Asimismo, se han generado y caracterizado en cultivos celulares e *in vivo* SARS-CoVs con mutaciones y deleciones en la proteína E para identificar cuales son las bases moleculares de la virulencia de estos virus y las respuestas del huésped implicadas en la patogénesis del SARS-CoV. rSARS-CoVs adaptados a ratón que contienen deleciones en la proteína E están atenuados *in vivo* y protegen frente al desafío con el virus virulento nativo. Se ha determinado que la disminución en la expresión de citoquinas pro-inflamatorias, el aumento en la expresión de citoquinas anti-inflamatorias, de un reducido flujo de neutrófilos y de una mayor cantidad de células T en los pulmones de los ratones infectados, contribuyen a la menor patogénesis causada por los virus atenuados.

Debido a la alta tasa de recombinación de los coronavirus y la posibilidad de generar virus en los que se recupera el fenotipo virulento, se generó un candidato a vacuna más seguro como un objetivo adicional de esta tesis. Para ello se diseñaron virus con deleciones en los genes nsp1 y E. Estos virus mostraron un fenotipo altamente atenuado, y protegieron totalmente frente al desafío por SARS-CoVs virulentos. Además, estos virus mantuvieron su fenotipo atenuado *in vivo*, después de pasarlos 10 veces en cultivos celulares y en ratones, siendo candidatos prometedores a vacuna para prevenir el SARS.

1. GENERACIÓN DE CELULAS DE RATÓN QUE EXPRESAN LA PROTEÍNA mACE2, SUSCEPTIBLES A LA INFECCIÓN POR SARS-CoV

El primer objetivo de esta tesis fue el desarrollo de una línea celular de ratón estable y altamente susceptible a la infección por un virus SCoV adaptado a crecer en ratón. El modelo animal que mejor reproduce la patología causada por SARS-CoV en humanos es la infección de ratones BALB/c con SARS-CoVs adaptado a ratón (Day et al., 2009; Nagata et al., 2008; Roberts et al., 2007). Por lo tanto, la generación de una línea celular de ratón susceptible a la infección por SARS-CoV fue de interés, para poder realizar las evaluaciones en cultivos celulares e *in vivo*

con virus adaptados a ratón, en células de la misma especie, lo que previsiblemente evitaría la perdida de tropismo por el ratón.

La expresión del receptor mACE2 fue suficiente para que las células DBT, que no son susceptibles a la infección por SCoV, fueran accesibles a la infección por SCoV, produciendo altos títulos virales. Resultados similares se obtuvieron al expresar transitoriamente el gen mACE2 en células 3T3 de ratón, las cuales fueron susceptibles a la infección por SARS-CoV (Li et al., 2004). Además, existen otros estudios en los que se analiza la replicación de SARS-CoV de humanos y de civetas en células DBT que expresan el receptor ACE2 de ambas especies (Becker et al., 2008; Sheahan et al., 2008a; Sheahan et al., 2008b). La infección por SARS-CoV en ratones transgénicos que expresan el receptor humano ACE2 es mucho más virulenta que en ratones convencionales (McCray et al., 2007; Tseng et al., 2007; Yang et al., 2007). Todos estos datos indican que la expresión del receptor ACE2 se requiere para la infección por el SARS-CoV.

La infección de las células DBT-mACE2 generadas en esta tesis con SARS-CoV-Urbani no adaptado al ratón produjo títulos virales 1000 veces menores que los títulos obtenidos para SCoV. El virus SCoV posee tres cambios de aminoácidos en la proteína S, con respecto al virus Urbani (Roberts et al., 2007). Esta proteína se une al receptor celular ACE2 facilitando la entrada del virus (Li et al., 2003). Estos cambios hacen que la afinidad de unión de la proteína S del SARS-CoV-Urbani a la proteína mACE2 sea más baja que la afinidad de unión de la proteína S del SCoV, haciendo que el virus Urbani entre en la célula con una menor eficiencia (Li et al., 2004). La infección de las células DBT-mACE2 por SCoV induce efecto citopático, probablemente mediado por apoptosis. La infección por SARS-CoV también produce efecto citopático en otras líneas celulares, como por ejemplo Vero E6 (Almazan et al., 2006; Ren et al., 2005; Yan et al., 2004). Dado que también se ha observado muerte celular en las células del epitelio del tracto respiratorio en pacientes de SARS (Lang et al., 2003; Zhang et al., 2003), las células generadas son un buen sistema para analizar procesos de muerte celular inducidos por SARS-CoV. La expresión exacerbada de genes relacionados con la inflamación se ha asociado con la patología inducida por SARS-CoV (Rockx et al., 2009; Smits et al., 2010). La

expresión génica de citoquinas pro-inflamatorias, tanto a nivel de mRNA como de proteína, aumentó en células DBT-mACE2 infectadas con SCoV, comparada con la observada en células no infectadas. Estos resultados se correlacionan con los datos obtenidos en pacientes de SARS (Cameron et al., 2007; Huang et al., 2005; Jiang et al., 2005; Reghunathan et al., 2005; Tang et al., 2005; Wong et al., 2003; Zhang et al., 2004), en monos y en ratones infectados por SARS-CoV (Baas et al., 2008; de Lang et al., 2007; Smits et al., 2010; Smits et al., 2011), en los que se ha observado una alta expresión de citoquinas pro-inflamatorias. Además, la infección por SCoV indujo una limitada producción de IFNβ en las células DBT-mACE2. Esta débil inducción puede deberse al secuestro del RNA viral en las vesículas de doble membrana, en las que se produce la replicación y transcripción viral, impidiendo la detección del RNA viral por los receptores de reconocimiento de patrones (PRRs) (Gosert et al., 2002; Knoops et al., 2008). Además, la expresión de proteínas del SARS-CoV que antagonizan la respuesta innata, podría explicar la baja producción de IFNβ (Devaraj et al., 2007; Frieman et al., 2007; Kopecky-Bromberg et al., 2007; Narayanan et al., 2008; Siu et al., 2009; Sun et al., 2012; Wathelet et al., 2007).

Las células DBT-mACE2 generadas en este trabajo se pueden utilizar para analizar la adaptación del virus a receptores homólogos. Además, en las células DBT se puede crecer el virus SCoV adaptado a replicarse en ratón, con una reducida probabilidad de que se introduzcan cambios en el genoma del virus no deseados, como consecuencia del proceso de adaptación del virus al crecimiento en células de otras especies.

2. ANÁLISIS DE LOS MECANISMOS RESPONSABLES DE LA ATENUACIÓN DEL SARS-CoV EN EL QUE SE HA ELIMINADO LA PROTEÍNA E

SARS-CoVs en los que se ha delecionado el gen E están atenuados en tres modelos murinos distintos (DeDiego et al., 2007; DeDiego et al., 2008; Fett et al., 2013). Con el objetivo de analizar e identificar las regiones de la proteína E que contribuyen a la virulencia del SARS-CoV, se generó una colección de virus recombinantes con mutaciones o deleciones en esta proteína. Los virus recombinantes diseñados estaban adaptados a ratón (Roberts et al., 2007). Se adoptó este modelo porque se

ha descrito que es el que mejor reproduce los síntomas del SARS en humanos. Después de la infección de los ratones con SCoV se produce una elevada y rápida replicación del virus en los pulmones, viremia, diseminación extrapulmonar, neutrofilia, linfopenia, y cambios patológicos en los pulmones, que conduce a la muerte de los ratones (Roberts et al., 2007). La introducción de mutaciones puntuales en la región amino terminal y pequeñas deleciones a lo largo de la región carboxilo terminal de la proteína E (SCoV-EMut1, -EΔ2, -EΔ3, -EΔ4, -EΔ5) generó virus con fenotipo atenuado. Estos virus fueron similares a los obtenidos al delecionar la proteína E completa del SARS-CoV, con la excepción de la deleción introducida en el extremo carboxi-terminal de esta proteína. Los ratones infectados con los virus mutantes (SCoV-EMut1, -EΔ2, -EΔ3, -EΔ4, -EΔ5 y -ΔE) mostraron una disminución del daño pulmonar y todos los ratones sobrevivieron, en contraste con la infección con el virus nativo. Por lo tanto, las regiones delecionadas eran esenciales para la virulencia del virus. En contraste, un virus en el cual se delecionaron los últimos 12 aminoácidos de la región carboxilo terminal de la proteína E (virus SCoV-EΔ6) fue completamente virulento, indicando que no todas las pequeñas deleciones introducidas dentro de la proteína E producen virus con fenotipo atenuado. La deleción introducida dentro del SCoV-EΔ6 incluye un PBM (Jimenez-Guardeño et al., 2014; Teoh et al., 2010), y previamente se había demostrado que un mutante que carece de esta región de la proteína E está totalmente atenuado en el modelo de ratón (Jimenez-Guardeño et al., 2014). Una explicación de esta aparente discrepancia es que los últimos 6 aminoácidos (YSRVKN) de la proteína E del virus SCoV-EΔ6 (**Figura 16**), forman un dominio PBM alternativo, restaurándose así su fenotipo virulento.

El requerimiento de la proteína E en la producción viral varía en las distintas especies de CoVs. Los títulos virales obtenidos con el SCoV-EΔ6, fueron similares a los obtenidos con el virus nativo, tanto en cultivos celulares como en ratones. De forma similar, un virus al que se le habían eliminado los últimos 9 aminoácidos de la proteína E, correspondientes al dominio PBM, también crecía con títulos similares al virus nativo (Jimenez-Guardeño et al., 2014). Sin embargo, los virus SCoV-EMut1, -EΔ2, -EΔ3, -EΔ4 y -EΔ5, crecieron entre 100 y 1000 veces menos que el virus nativo. Análogamente, cuando se delecionó la proteína E completa del

SARS-CoV, los títulos virales disminuyeron en distintas líneas celulares, y también en distintos modelos animales (DeDiego et al., 2007; DeDiego et al., 2014; DeDiego et al., 2008). Para el coronavirus MHV, el gen E es no esencial para el ciclo viral, al igual que para SARS-CoV, aunque su eliminación redujo el crecimiento del virus en cultivos celulares al menos 1000 veces (Kuo and Masters, 2003). Sin embargo, en el CoV TGEV la expresión del gen E es necesaria para la salida al exterior de la célula y diseminación del virus (Ortego et al., 2002). Estos procesos se restauran cuando se expresa la proteína E en *trans* en células infectadas con el virus rTGEV-ΔE (Curtis et al., 2002; Ortego et al., 2002), lo cual permite obtener virus competentes en replicación, pero deficientes en propagación. La eliminación del gen E del MERS-CoV también genera virus competentes en replicación, pero deficientes en propagación, que se pueden crecer al expresar la proteína E en *trans* (Almazan et al., 2013).

Las mutaciones o deleciones introducidas en la proteína E podrían, afectar en principio a propiedades básicas de la proteína, como su localización subcelular, o su vida media, pudiendo alterar sus funciones dentro de la célula, lo que podría reflejarse en cambios en los títulos virales. La proteína E de CoV se acumula principalmente en las membranas del RE, el ERGIC y el aparato de Golgi, donde participa en el ensamblaje, la gemación y el tráfico de la progenie viral (Lim and Liu, 2001; Nal et al., 2005; Nieto-Torres et al., 2011; Raamsman et al., 2000). Se ha descrito que la cola citoplasmática de la proteína E contiene una señal que promueve su localización en el Golgi (Cohen et al., 2011). La proteína E de los CoVs puede alterar el trafico de proteínas (Ruch and Machamer, 2012). Por ello, se consideró de interés determinar la localización subcelular y la vida media de distintas proteínas E mutantes, lo que se analizó usando los virus recombinantes generados. Las proteínas con deleciones de pequeño tamaño (E*) de los SCoV-E***** mostraron mayoritariamente una colocalización con el marcador de ERGIC, como se había descrito anteriormente para la proteína E nativa (Nieto-Torres et al., 2011). De forma análoga, la vida media de las proteínas E mutadas no disminuyó, mostrando una vida media de 1.5 veces superior con respecto a la vida media de la proteína E nativa (Ruch and Machamer, 2012). Una de las múltiples funciones de la proteína E es participar en el proceso de morfogénesis del virus a través de su

interacción con la proteína M (Ho et al., 2004; Siu et al., 2008; Vennema et al., 1996). La interacción entre la proteína E que contenía la deleción en la región Δ3 (EΔ3) y la proteína M del SARS-CoV se conservó. Por lo tanto, la región EΔ3 de la proteína E delecionada no es esencial para su interacción con la proteína M. En contraste, la infectividad específica del resto de los mutantes con pequeñas deleciones en el extremo carboxi-terminal de la proteína E disminuyó unas 6 veces con respecto a la infectividad específica del virus nativo.

En esta tesis se ha mostrado que los virus: SCoV-EMut1, -EΔ2, -EΔ3, -EΔ4 y -EΔ5, crecen menos *in vitro* e *in vivo* y están atenuados en el modelo de ratón. Sin embargo, titulo y atenuación viral no necesariamente están ligados. En nuestro laboratorio hemos mostrado previamente que virus recombinantes con mutaciones puntuales en la proteína E que eliminaban su actividad canal iónico o eliminaban su PBM, crecían con títulos similares a los observados con el virus nativo (Jimenez-Guardeño et al., 2014; Nieto-Torres et al., 2014). Pese a ello, estos virus causaban una reducción en la inflamación y patología pulmonar mostrando un fenotipo atenuado (Jimenez-Guardeño et al., 2014; Nieto-Torres et al., 2014). Por lo tanto los mutantes de la proteína E* pueden disminuir su virulencia debido a que afectan a la respuesta específica del huésped, independientemente de sus niveles de replicación.

Para analizar la respuesta del hospedador inducida por la infección con SCoV-E*, se analizaron los transcriptomas de los pulmones de ratones infectados con estos virus. Se observó una disminución en la expresión de diversos genes pro-inflamatorios (TNF, CCL2, CCL3, CCL4, CXCL1, CXCL2, CXCL10, IL6, IL12B e IFNγ) en los pulmones de los ratones infectados con los virus atenuados (SCoV-ΔE, -EΔ3 y -EΔ5), en comparación con la expresión de estos genes en los ratones infectados con el virus virulento, lo que probablemente contribuyó a la atenuación de los virus mutantes de deleción. Anteriormente se había detectado un aumento en los niveles de citoquinas pro-inflamatorias como TNF, IL6, CXCL10, CCL2, IL8 e IL12 en los pulmones de pacientes infectados con SARS, promoviendo el desarrollo de ARDS (Cameron et al., 2007; Chien et al., 2006; Jiang et al., 2005; Lam et al., 2004; Puneet et al., 2005; Smits et al., 2011; Tang et al., 2005; Wong et al., 2004). En el

laboratorio hemos mostrado que el tratamiento de los ratones infectados con SCoV con inhibidores de NF-KB, redujeron la expresión de citoquinas pro-inflamatorias, disminuyendo la inflamación pulmonar y aumentando la supervivencia de los ratones (DeDiego et al., 2014). De forma similar, el tratamiento de ratones infectados con inhibidores de la MAPK p38, que también promueve la expresión de citoquinas pro-inflamatorias, y aumentó significativamente la supervivencia de todos los ratones infectados (Jimenez-Guardeño et al., 2014), reforzando el concepto de que la expresión exacerbada de citoquinas pro-inflamatorias contribuye a la alta virulencia del SARS-CoV. La expresión de las citoquinas IL4, IL5 e IL13, relacionadas con una respuesta inmune celular del tipo Th2 y con la respuesta anti-inflamatoria (Klein et al., 2001; Lalani et al., 1999; Marie et al., 1996; Seruga et al., 2008), se incrementó en los pulmones de ratones infectados con los virus atenuados con respecto a la respuesta observada en los pulmones de ratones infectados con el virus nativo. Ello contrastó con la expresión de citoquinas pro-inflamatorias que disminuyó en consonancia con estos resultados, se ha descrito que en ratones BALB/c jóvenes infectados con SARS-CoV, que no desarrollan la enfermedad, se produce un aumento en la expresión de la citoquina IL13, con respecto a ratones BALB/c viejos, en los que la enfermedad es más severa (Nagata et al., 2008). Todos estos datos sugieren fuertemente que la disminución en la expresión de citoquinas pro-inflamatorias y el aumento de las citoquinas anti-inflamatorias, observadas en los ratones después de la infección con los mutantes atenuados, contribuyen a la disminución de la patología y a la atenuación del virus.

Los neutrófilos desempeñan un papel muy importante en la progresión y desarrollo del ALI/ARDS (Gralinski and Baric, 2015; Grommes and Soehnlein, 2011; Lee et al., 2003; Tsui et al., 2003; Wong et al., 2003; Wygrecka et al., 2008). Se ha observado que pacientes infectados con SARS presentan altos niveles de neutrófilos en los pulmones (Grommes and Soehnlein, 2011; Lee et al., 2003; Tsui et al., 2003; Wong et al., 2003). De forma similar se ha observado un incremento del flujo de neutrófilos hacia los pulmones después de las infecciones con el virus de la gripe A y el virus respiratorio sincitial (RSV) contribuyendo a la progresión de la enfermedad (Bataki et al., 2005; Brandes et al., 2013; Narasaraju et al., 2011;

Yasui et al., 2005). El tratamiento de ratones infectados con RSV con antioxidantes redujo el flujo de neutrófilos hacia los pulmones, la expresión de citoquinas pro-inflamatorias y la gravedad del edema pulmonar (Castro et al., 2006). En los ratones infectados con los virus atenuados como SCoV-ΔE, -EΔ3 y -EΔ5 también se observó una disminución del flujo de neutrófilos en comparación con ratones infectados con el virus nativo. Así mismo, la expresión de las citoquinas CXCL1 y CXCL2 que inducen quimiotaxis de los neutrófilos (De Filippo et al., 2013; Wareing et al., 2007) aumentó en los pulmones de los ratones infectados con SCoV virulento, en comparación con los ratones infectados con los virus atenuados. Todo ello muestra la relevancia de la inflamación exacerbada en el edema pulmonar grave producido por el SARS-CoV.

Por el contrario, el número de macrófagos se incrementó en los pulmones de los ratones infectados con los virus atenuados, en comparación con los ratones infectados con el virus virulento. Los macrófagos mantienen la homeostasis fisiológica y contribuyen a la reparación de tejidos (Fujiwara and Kobayashi, 2005; Jenkins et al., 2011). Por lo tanto, un aumento de estas células durante la infección probablemente favorece la resolución de la enfermedad. Todos estos datos indican que el incremento en el número de neutrófilos, junto con la disminución de macrófagos en los pulmones, contribuye a la patogénesis causada por el SARS-CoV.
Los linfocitos T también contribuyen de forma significativa a la disminución de la replicación de SARS-CoV *in vivo* (Chen et al., 2010; Zhao and Perlman, 2010; Zhao et al., 2009). La infección por SARS-CoV produce linfopenia, y se ha determinado que los niveles bajos de células T en sangre inducidos por la infección con SARS-CoV se correlaciona con resultados adversos en los pacientes de SARS (Booth et al., 2003; He et al., 2005; Lee et al., 2003; Wong et al., 2003). Los ratones infectados con los virus atenuados (SCoV-ΔE, -EΔ3 y -EΔ5) que no mostraron síntomas clínicos de enfermedad, mostraron mayores niveles de células T $CD4^+$ y $CD8^+$ en los pulmones. Por el contrario, los niveles de células T en los ratones infectados con el virus nativo eran menores, lo que se asoció a un edema pulmonar grave que causó la muerte de los ratones.

Desde la aparición del SARS-CoV en el año 2003, se han desarrollado múltiples vacunas para prevenir la infección, sin embargo ninguna de ellas se ha aprobado para su uso en humanos (Enjuanes et al., 2008; Graham et al., 2013). El SARS-CoV podría emerger de los reservorios animales en los que se encuentra (Annan et al., 2013; Falcon et al., 2011; Muller et al., 2007; Quan et al., 2010; van Boheemen et al., 2012), por lo que el desarrollo de vacunas para SARS-CoV sigue siendo de alto interés. Las vacunas vivas atenuadas se consideran más efectivas que otros tipos de vacunas basadas en virus inactivados o en antígenos no replicativos, porque inducen una fuerte respuesta inmune de larga duración (Graham et al., 2013). En nuestro laboratorio se generó el primer candidato a vacuna para el SARS-CoV basado en un virus infectivo atenuado (SCoV-ΔE), y se determinó que este virus protege frente al desafío con el virus virulento tanto a ratones jóvenes y viejos, y en hámsteres, induciendo la generación de anticuerpos neutralizantes y células T específicas (Fett et al., 2013; Lamirande et al., 2008; Netland et al., 2010). Así mismo, todos los virus recombinantes con fenotipo atenuado generados en este trabajo (SCoV-Emut1, -EΔ2 , -EΔ3, -EΔ4 y -EΔ5) indujeron una protección completa frente al desafío por virus virulento. Los virus vacunales generados en esta tesis expresan todas las proteínas virales, con la excepción de pequeñas regiones delecionadas dentro de la proteína E, por lo que tienen un mayor potencial en la inducción de protección.

Estudios del papel de las respuestas celulares y humorales en la eliminación de la infección por SARS-CoV han mostrado que la respuesta humoral es fundamental. Así por ejemplo, la transferencia pasiva de anticuerpos neutralizantes a ratones y hurones protege a los mismos frente al desafío por el virus virulento (Subbarao et al., 2004; ter Meulen et al., 2004; Traggiai et al., 2004). Sin embargo, las respuestas T $CD4^+$ y $CD8^+$ también ayudan a proteger frente al SARS-CoV (Channappanavar et al., 2014). En ausencia de células T, el coronavirus MHV se elimina lentamente de los cerebros de los ratones infectados (Williamson and Stohlman, 1990). La inmunización con SCoV-ΔE, indujo respuestas humorales y celulares que protegieron frente al desafío con el virus virulento (Fett et al., 2013; Lamirande et al., 2008; Netland et al., 2010). Por lo tanto es muy probable en que la inmunización con los virus mutantes atenuados (SCoV-Emut1, -EΔ2, -EΔ3, -EΔ4 y -

EΔ5) que induce tanto anticuerpos neutralizantes como una respuesta de células T efectiva frente al virus, ambas ramas de la respuesta inmune contribuyen a la protección total de los ratones frente al desafío contra el virus nativo, de forma similar a lo que habíamos descrito en el caso del virus SCoV-ΔE.

En conjunto, este estudio ha mostrado que cambios en los aminoácidos de la región amino terminal, o deleciones de regiones internas de la proteína E de SARS-CoV, dieron como resultado mutantes estables con fenotipo atenuado. Estos mutantes mostraron una reducción en la infectividad específica de los virus, manteniendo la localización subcelular de la proteína E, y un ligero incremento de la vida media de la misma, comparada con la proteína sin alteraciones. La atenuación observada para los virus recombinantes (SCoV-Emut1, -EΔ2, -EΔ3, -EΔ4 y -EΔ5), se correlacionó con una patología limitada en los pulmones de los ratones infectados. Ello a sido probablemente debido a una disminución de la expresión de citoquinas pro-inflamatorias, a un aumento en los niveles de citoquinas anti-inflamatorias, a una reducción de la acumulación de neutrófilos, y a la presencia de un mayor número de células T $CD4^+$ y $CD8^+$ en los pulmones. Todos estos factores contribuyen a un mejor pronóstico en el desarrollo de la enfermedad del SARS. Estos mutantes atenuados protegen frente al desafío con un virus virulento y han constituido la base para el diseño de vacunas eficaces y seguras para combatir las infecciones por SARS-CoV.

3. ESTABILIDAD DEL SCoV-ΔE CANDIDATO A VACUNA

SARS-CoVs que carecen de la proteína E completa o de pequeñas regiones de la proteína E (SCoV-E*) tenían un fenotipo atenuado y protegieron frente al desafío con un virus nativo (DeDiego et al., 2007; DeDiego et al., 2008; Fett et al., 2013; Regla-Nava et al., 2015). Sin embargo, cuando la proteína E se delecionó en su totalidad, estos virus ΔE se mostraron inestables, incorporando de un modo reproducible proteínas quiméricas que contenían un motivo PBM. Uno de los avances mas significativos de esta tesis fue generar virus recombinantes con pequeñas deleciones dentro de la proteína E, en lugar de delecionar la proteína E completa eliminando el motivo PBM que se incluye en la misma. La presencia de

este motivo evitó la generación de nuevas proteínas quiméricas que se insertaron en el genoma viral, dando como resultado virus con una mayor estabilidad genética a la observada para el virus SCoV-ΔE, carente del motivo PBM. La hipótesis formulada del requerimiento de una proteína de membrana en el SARS-CoV para que fuese genéticamente estable se reforzó al comprobar que el pase del virus SCoV-ΔE generó además de una proteína M quimérica, la inserción de 45 nucleótidos en la proteína 8a, que incluían un motivo PBM. Estas observaciones indicaron que la inserción de la proteína M quimérica y la introducción de secuencias adicionales en el gen 8a del virus SCoV-ΔE eran modificaciones genéticas que se generaban para compensar la ausencia del motivo PBM en la proteína E. La incorporación del motivo PBM en el genoma del SARS-CoV, cuando este se ha delecionado previamente de la proteína E no es sorprendente dado que se sabe que este motivo estructural confiere a la proteína E la posibilidad de interaccionar con mas de 400 proteínas celulares que contienen motivos PDZ (Spaller, 2006). Estas interacciones pueden dar como resultado la modulación de la actividad de la célula, incrementando la activación de la p38 MAPK quinasa y la inflamación pulmonar, tal como hemos demostrado recientemente en nuestro laboratorio (Jimenez-Guardeño et al., 2014; Jimenez-Guardeño et al., 2015).

Los CoVs recombinan con alta frecuencia, haciendo posible la reversión de los virus a un fenotipo virulento (Masters, 2006; Perlman and Netland, 2009). Por esta razón, el tercer objetivo de esta tesis fue introducir una segunda alteración en el genoma de los candidatos a vacuna, para aumentar su seguridad. Por ello se seleccionó la introducción de deleciones en la proteína nsp1, utilizando como punto de partida los virus SCoV-ΔE ó SCoV-EΔ3. Se seleccionó el gen nsp1 dado que este está localizado en un sitio considerablemente alejado (>20 kb) del gen E en el genoma viral, haciendo muy improbable que la recombinación con CoVs circulantes resultase en la generación de virus con fenotipos virulentos. Otro criterio que contribuyó a la selección del gen nsp1 fue que la proteína que este codifica tiene una función importante en la patogénicidad de los CoVs. Se ha descrito que deleciones en la proteína nsp1 de MHV generan virus con fenotipo atenuado *in vivo* (Lei et al., 2013; Zust et al., 2007). La proteína nsp1 inhibe la expresión génica del huésped y contrarresta la respuesta inmune innata,

confiriendo una ventaja selectiva al virus (Kamitani et al., 2006; Narayanan et al., 2008; Wang et al., 2010; Wathelet et al., 2007). Para analizar el papel de la proteína nsp1 del SARS-CoV en la patogénesis inducida por este virus, se generaron cuatro recombinantes virales con pequeñas deleciones en esta proteína (**Figura 30**). Las deleciones de los aminoácidos 121 a 129 (SCoV-nspΔC) y 154 a 165 (SCoV-nspΔD) de la región carboxilo terminal de la proteína nsp1 dieron lugar a virus con fenotipo atenuado, indicando que la proteína nsp1 incrementa la patogénesis del virus. Estos mutantes atenuados crecieron con títulos más bajos en ratón, en comparación con el crecimiento del virus nativo, induciendo mayores niveles de IFN e ISGs que el virus nativo. Ello indicó que las regiones delecionadas son relevantes para la función de la proteína nsp1 como antagonista del IFN. La alta expresión de genes de respuesta inmune innata inducida por los virus con deleciones en la proteína nsp1, es probablemente responsable de la disminución de los títulos de los virus SCoV-nspΔC y SCoV-nspΔD observados en ratón (Emeny and Morgan, 1979). De hecho en el MHV se ha descrito que un virus en el que se había introducido una deleción en la proteína nsp1 crecía hasta niveles similares al virus wt en ratones que no expresaban receptor de IFN del tipo I (Zust et al., 2007). De forma similar, SARS-CoVs que carecían de la proteína nsp1 crecían de forma deficiente en células competentes en la producción de IFN, pero replicaban con altos títulos, de forma similar al virus nativo, en células deficientes en la producción de IFN (Wathelet et al., 2007), reforzando nuestras conclusiones.

La inmunización con virus mutantes de deleción en la proteína nsp1 protegió frente al desafío con el virus nativo, como se había mostrado previamente con MHVs que carecían de una región de la proteína nsp1 (Lei et al., 2013; Zust et al., 2007). Teniendo en cuenta estos datos, se generaron virus recombinantes que incluían dos medidas de seguridad, basadas en la deleción de regiones en los genes E y nsp1, para disminuir la probabilidad de reversión a un virus con fenotipo virulento en un solo evento de recombinación. Los virus atenuados además de recuperar su virulencia por recombinación, pueden hacerlo incorporando mutaciones adicionales en su genoma. Una característica esencial de un candidato a vacuna prometedor es que este sea estable tanto en cultivos celulares como *in vivo*. El virus SCoV-nspΔD-EΔ3 que incluía deleciones en las proteínas nsp1 y E

mantuvo la atenuación después de ser pasado 10 veces en células Vero E6 y también en ratón, indicando que este virus es un candidato a vacuna prometedor en términos de estabilidad. El virus SCoV-ΔE mantuvo su fenotipo atenuado después de ser pasado 16 veces en células Vero E6 (Netland et al., 2010). Sin embargo, cuando este virus con la proteína E delecionada se pasó 10 veces en ratones recuperó su virulencia, mostrando un fenotipo similar al observado para el virus wt (Jimenez-Guardeño et al., 2015). Estos resultados muestran uno de los avances significativos de esta tesis, que se ha contribuido a aumentar la seguridad de la vacuna recombinante para prevenir el SARS. Al introducir pequeñas deleciones en el gen E, en lugar de eliminar por completo dicho gen, el virus se atenuó, pese a que mantuvo el titulo del virus silvestre, lo que le confirió un alto potencial inmunizante. Lo más relevante fue que estos virus con la proteína E mutada evitaron la incorporación de proteínas virales que revertieron el fenotipo a virulento, aumentando la estabilidad genética del candidato a vacuna. Estos datos también refuerzan la necesidad de analizar la estabilidad de los virus *in vivo*, y de introducir más de una medida de seguridad para generar una vacuna viva atenuada segura. La inmunización con los virus que incluyen deleciones en los genes nsp1 y E protegió completamente frente a la infección con el virus nativo, indicando que estos virus son candidatos prometedores a vacunas vivas atenuadas. Esta misma estrategia puede ser aplicada para la generación de vacunas efectivas frente a otros CoVs, como el MERS-CoV.

CONCLUSIONES

1. Se ha generado una línea celular murina (DBT-mACE2) altamente susceptible a la infección con SARS-CoVs adaptados a ratón, mediante la expresión estable del receptor de SARS-CoV, la proteína mACE2. Además, se ha mostrado que esta línea celular es un buen modelo para analizar diferencias de expresión de las citoquinas inflamatorias inducidas por la infección con el SARS-CoV.

2. Regiones de la proteína E presentes en el dominio amino terminal y en la zona interna del dominio carboxilo terminal del SARS-CoV son necesarias para el crecimiento eficiente del virus *in vivo*. De hecho, mutaciones puntuales en el dominio amino terminal o deleciones en la zona interna del dominio carboxilo terminal de la proteína E del SARS-CoV dieron origen a virus con fenotipos atenuados. La infección de ratones con estos virus indujeron menor daño pulmonar, una infiltración limitada de neutrófilos en los pulmones, una reducción en la expresión de las citoquinas inflamatorias y un incremento en el número de células T $CD4^+$ y $CD8^+$ en los pulmones. El conjunto de estas características es probablemente responsable de la atenuación del virus.

3. La ausencia del motivo PBM en un virus carente de la proteína E tiende a presentar una mayor inestabilidad genética dando origen a la generación de proteínas quiméricas dentro del genoma. En contraste, pequeñas deleciones dentro de la proteína E que mantienen el motivo PBM previenen la inserción de proteínas quiméricas en el genoma viral y son responsables de una mayor estabilidad genética del SARS-CoV.

4. Deleciones en la región carboxilo terminal de la proteína nsp1 dieron origen a virus atenuados. Estos virus indujeron mayores niveles de IFN e ISGs que el virus nativo, indicando que la proteína nsp1 inhibe estas respuestas. Estos virus indujeron una protección completa frente a la infección por el SARS-CoV virulento en ratones BALB/c, por lo que son candidatos prometedores a vacunas para prevenir el SARS.

5. Se ha generado un virus recombinante que incluye deleciones en dos genes virales: nsp1 y E. Este virus mantiene su atenuación después de pasarlo en cultivos celulares y en ratón, y protege completamente frente a la infección con una dosis letal del virus virulento nativo. Todo ello indica que es un candidato a vacuna bioseguro y eficaz muy prometedor.

BIBLIOGRAFÍA

Almazan, F., DeDiego, M.L., Galan, C., Alvarez, E., Enjuanes, L., 2006a. Identification of essential genes as a strategy to select a SARS candidate vaccine using a SARS-CoV infectious cDNA. Adv. Exp. Med. Biol. 581, 579-583.

Almazan, F., DeDiego, M.L., Galan, C., Escors, D., Alvarez, E., Ortego, J., Sola, I., Zuñiga, S., Alonso, S., Moreno, J.L., Nogales, A., Capiscol, C., Enjuanes, L., 2006b. Construction of a SARS-CoV infectious cDNA clone and a replicon to study coronavirus RNA synthesis. J. Virol. 80, 10900-10906.

Almazan, F., DeDiego, M.L., Sola, I., Zuñiga, S., Nieto-Torres, J.L., Marquez-Jurado, S., Andres, G., Enjuanes, L., 2013. Engineering a replication-competent, propagation-defective Middle East respiratory syndrome coronavirus as a vaccine candidate. mBio 4, e00650-00613.

Almazan, F., Galan, C., Enjuanes, L., 2004. The nucleoprotein is required for efficient coronavirus genome replication. J. Virol. 78, 12683-12688.

Almazan, F., Gonzalez, J.M., Penzes, Z., Izeta, A., Calvo, E., Plana-Duran, J., Enjuanes, L., 2000. Engineering the largest RNA virus genome as an infectious bacterial artificial chromosome. Proc. Natl. Acad. Sci. USA 97, 5516-5521.

Andrejeva, J., Childs, K.S., Young, D.F., Carlos, T.S., Stock, N., Goodbourn, S., Randall, R.E., 2004. The V proteins of paramyxoviruses bind the IFN-inducible RNA helicase, mda-5, and inhibit its activation of the IFN-beta promoter. Proc. Natl. Acad. Sci. USA 101, 17264-17269.

Annan, A., Baldwin, H.J., Corman, V.M., Klose, S.M., Owusu, M., Nkrumah, E.E., Badu, E.K., Anti, P., Agbenyega, O., Meyer, B., Oppong, S., Sarkodie, Y.A., Kalko, E.K., Lina, P.H., Godlevska, E.V., Reusken, C., Seebens, A., Gloza-Rausch, F., Vallo, P., Tschapka, M., Drosten, C., Drexler, J.F., 2013. Human betacoronavirus 2c EMC/2012-related viruses in bats, Ghana and Europe. Emerg. Infect. Dis. 19, 456-459.

Ashburner, M., Ball, C.A., Blake, J.A., Botstein, D., Butler, H., Cherry, J.M., Davis, A.P., Dolinski, K., Dwight, S.S., Eppig, J.T., Harris, M.A., Hill, D.P., Issel-Tarver, L., Kasarskis, A., Lewis, S., Matese, J.C., Richardson, J.E., Ringwald, M., Rubin, G.M., Sherlock, G., 2000. Gene ontology: tool for the unification of biology. The Gene Ontology Consortium. Nat. Genet. 25, 25-29.

Assiri, A., McGeer, A., Perl, T.M., Price, C.S., Al Rabeeah, A.A., Cummings, D.A., Alabdullatif, Z.N., Assad, M., Almulhim, A., Makhdoom, H., Madani, H., Alhakeem, R., Al-Tawfiq, J.A., Cotten, M., Watson, S.J., Kellam, P., Zumla, A.I., Memish, Z.A., 2013. Hospital outbreak of Middle East respiratory syndrome coronavirus. N. Engl. J. Med., doi:10.1056/NEJMoa1306742.

Baas, T., Roberts, A., Teal, T.H., Vogel, L., Chen, J., Tumpey, T.M., Katze, M.G., Subbarao, K., 2008. Genomic analysis reveals age-dependent innate immune responses to severe acute respiratory syndrome coronavirus. J. Virol. 82, 9465-9476.

Baker, S.C., Shieh, C.-K., Soe, L.H., Chang, M.-F., Vannier, D.M., Lai, M.M.C., 1989. Identification of a domain required for autoproteolytic cleavage of murine coronavirus gene A polyprotein. J. Virol. 63, 3693-3699.

Barnard, D.L., Day, C.W., Bailey, K., Heiner, M., Montgomery, R., Lauridsen, L., Chan, P.K., Sidwell, R.W., 2006. Evaluation of immunomodulators, interferons and known in vitro SARS-coV inhibitors for inhibition of SARS-coV replication in BALB/c mice. Antivir. Chem. Chemother. 17, 275-284.

Bataki, E.L., Evans, G.S., Everard, M.L., 2005. Respiratory syncytial virus and neutrophil activation. Clin. Exp. Immunol. 140, 470-477.

Becker, M.M., Graham, R.L., Donaldson, E.F., Rockx, B., Sims, A.C., Sheahan, T., Pickles, R.J., Corti, D., Johnston, R.E., Baric, R.S., Denison, M.R., 2008. Synthetic recombinant bat SARS-like coronavirus is infectious in cultured cells and in mice. Proc. Natl. Acad. Sci. USA 105, 19944-19949.

Benjamini, Y., Hochberg, Y., 1995. Controlling the false discovery rate: a practical and powerful approach to multiple testing. J. Roy. Stat. Soc. B 57, 289-300.

Bonjardim, C.A., Ferreira, P.C., Kroon, E.G., 2009. Interferons: signaling, antiviral and viral evasion. Immunol. Lett. 122, 1-11.

Booth, C.M., Matukas, L.M., Tomlinson, G.A., Rachlis, A.R., Rose, D.B., Dwosh, H.A., Walmsley, S.L., Mazzulli, T., Avendano, M., Derkach, P., Ephtimios, I.E., Kitai, I., Mederski, B.D., Shadowitz, S.B., Gold, W.L., Hawryluck, L.A., Rea, E., Chenkin, J.S., Cescon, D.W., Poutanen, S.M., Detsky, A.S., 2003. Clinical features and short-term outcomes of 144 patients with SARS in the greater Toronto area. JAMA. 289, 2801-2809.

Brandes, M., Klauschen, F., Kuchen, S., Germain, R.N., 2013. A systems analysis identifies a feedforward inflammatory circuit leading to lethal influenza infection. Cell 154, 197-212.

Brierley, M.M., Fish, E.N., 2002. Review: IFN-alpha/beta receptor interactions to biologic outcomes: understanding the circuitry. J. Interferon Cytokine Res. 22, 835-845.

Brockway, S.M., Denison, M.R., 2005. Mutagenesis of the murine hepatitis virus nsp1-coding region identifies residues important for protein processing, viral RNA synthesis, and viral replication. Virology 340, 209-223.

Brockway, S.M., Lu, X.T., Peters, T.R., Dermody, T.S., Denison, M.R., 2004. Intracellular localization and protein interactions of the gene 1 protein p28 during mouse hepatitis virus replication. J. Virol. 78, 11551-11562.

Cameron, M.J., Ran, L., Xu, L., Danesh, A., Bermejo-Martin, J.F., Cameron, C.M., Muller, M.P., Gold, W.L., Richardson, S.E., Poutanen, S.M., Willey, B.M., DeVries, M.E., Fang, Y., Seneviratne, C., Bosinger, S.E., Persad, D., Wilkinson, P., Greller, L.D., Somogyi, R., Humar, A., Keshavjee, S., Louie, M., Loeb, M.B., Brunton, J., McGeer, A.J., Kelvin, D.J., 2007. Interferon-mediated immunopathological events are associated with atypical innate and adaptive immune responses in patients with severe acute respiratory syndrome. J. Virol. 81, 8692-8706.

Carstens, E.B., 2010. Ratification vote on taxonomic proposals to the International Committee on Taxonomy of Viruses (2009). Arch. Virol. 155, 133-146.

Casais, R., Thiel, V., Siddell, S.G., Cavanagh, D., Britton, P., 2001. Reverse genetics system for the avian coronavirus infectious bronchitis virus. J. Virol. 75, 12359-12369.

Castro, S.M., Guerrero-Plata, A., Suarez-Real, G., Adegboyega, P.A., Colasurdo, G.N., Khan, A.M., Garofalo, R.P., Casola, A., 2006. Antioxidant treatment ameliorates respiratory syncytial virus-induced disease and lung inflammation. Am. J. Respir. Crit. Care Med. 174, 1361-1369.

Cavanagh, D., 2005. Coronaviruses in poultry and other birds. Avian Pathol. 34, 439-448.

Chan, K.H., Poon, L.L., Cheng, V.C., Guan, Y., Hung, I.F., Kong, J., Yam, L.Y., Seto, W.H., Yuen, K.Y., Peiris, J.S., 2004. Detection of SARS coronavirus in patients with suspected SARS. Emerg. Infect. Dis. 10, 294-299.

Channappanavar, R., Zhao, J., Perlman, S., 2014. T cell-mediated immune response to respiratory coronaviruses. Immunol. Res. 59, 118-128.

Chawla-Sarkar, M., Lindner, D.J., Liu, Y.F., Williams, B.R., Sen, G.C., Silverman, R.H., Borden, E.C., 2003. Apoptosis and interferons: role of interferon-stimulated genes as mediators of apoptosis. Apoptosis 8, 237-249.

Chen, C.J., Makino, S., 2004. Murine coronavirus replication induces cell cycle arrest in G0/G1 phase. J. Virol. 78, 5658-5669.

Chen, J., Lau, Y.F., Lamirande, E.W., Paddock, C.D., Bartlett, J.H., Zaki, S.R., Subbarao, K., 2010. Cellular immune responses to severe acute respiratory syndrome coronavirus (SARS-CoV) infection in senescent BALB/c mice: CD4+ T cells are important in control of SARS-CoV infection. J .Virol. 84, 1289-1301.

Chien, J.Y., Hsueh, P.R., Cheng, W.C., Yu, C.J., Yang, P.C., 2006. Temporal changes in cytokine/chemokine profiles and pulmonary involvement in severe acute respiratory syndrome. Respirology 11, 715-722.

Chu, D.K., Peiris, J.S., Chen, H., Guan, Y., Poon, L.L., 2008. Genomic characterizations of bat coronaviruses (1A, 1B and HKU8) and evidence for co-infections in Miniopterus bats. J. Gen. Virol. 89, 1282-1287.

Chu, D.K., Poon, L.L., Chan, K.H., Chen, H., Guan, Y., Yuen, K.Y., Peiris, J.S., 2006. Coronaviruses in bent-winged bats (Miniopterus spp.). J. Gen. Virol. 87, 2461-2246.

Cohen, J.R., Lin, L.D., Machamer, C.E., 2011. Identification of a Golgi complex-targeting signal in the cytoplasmic tail of the severe acute respiratory syndrome coronavirus envelope protein. J. Virol. 85, 5794-5803.

Coley, S.E., Lavi, E., Sawicki, S.G., Fu, L., Schelle, B., Karl, N., Siddell, S.G., Thiel, V., 2005. Recombinant mouse hepatitis virus strain A59 from cloned, full-length cDNA replicates to high titers in vitro and is fully pathogenic in vivo. J. Virol. 79, 3097-3106.

Corse, E., Machamer, C.E., 2000. Infectious bronchitis virus E protein is targeted to the Golgi complex and directs release of virus-like particles. J. Virol. 74, 4319-4326.

Curtis, K.M., Yount, B., Baric, R.S., 2002. Heterologous gene expression from transmissible gastroenteritis virus replicon particles. J. Virol. 76, 1422-1434.

Dahl, H., Linde, A., Strannegard, O., 2004. In vitro inhibition of SARS virus replication by human interferons. Scand. J. Infect. Dis. 36, 829-831.

Darnell, J.E., Jr., Kerr, I.M., Stark, G.R., 1994. Jak-STAT pathways and transcriptional activation in response to IFNs and other extracellular signaling proteins. Science 264, 1415-1421.

Day, C.W., Baric, R., Cai, S.X., Frieman, M., Kumaki, Y., Morrey, J.D., Smee, D.F., Barnard, D.L., 2009. A new mouse-adapted strain of SARS-CoV as a lethal model for evaluating antiviral agents in vitro and in vivo. Virology 395, 210-222.

De Filippo, K., Dudeck, A., Hasenberg, M., Nye, E., van Rooijen, N., Hartmann, K., Gunzer, M., Roers, A., Hogg, N., 2013. Mast cell and macrophage chemokines CXCL1/CXCL2 control the early stage of neutrophil recruitment during tissue inflammation. Blood 121, 4930-4937.

de Groot, R.J., Baker, S.C., Baric, R., Enjuanes, L., Gorbalenya, A.E., Holmes, K.V., Perlman, S., Poon, L., Rottier, P.J.M., Talbot, P.J., Woo, P.C.Y., Ziebuhr, J., 2012. Coronaviridae, in: King, A.M.Q., Adams, M.J., Carstens, E.B., Lefkowitz, E.J. (Eds.), Virus Taxonomy: Ninth Report of the International Committee on Taxonomy of Viruses. Elsevier Academic Press, San Diego, pp. 774-796.

de Haan, C.A., Rottier, P.J., 2005. Molecular interactions in the assembly of coronaviruses. Adv. Virus Res. 64, 165-230.

de Haan, C.A.M., Smeets, M., Vernooij, F., Vennema, H., Pottier, P.J.M., 1999. Mapping of the coronavirus membrane protein domains involved in interaction with the spike protein. J. Virol. 73, 7441-7452.

de Lang, A., Baas, T., Teal, T., Leijten, L.M., Rain, B., Osterhaus, A.D., Haagmans, B.L., Katze, M.G., 2007. Functional genomics highlights differential induction of antiviral pathways in the lungs of SARS-CoV-infected macaques. PLoS pathogens 3, e112.

DeDiego, M.L., Alvarez, E., Almazan, F., Rejas, M.T., Lamirande, E., Roberts, A., Shieh, W.J., Zaki, S.R., Subbarao, K., Enjuanes, L., 2007. A severe acute respiratory syndrome coronavirus that lacks the E gene is attenuated in vitro and in vivo. J. Virol. 81, 1701-1713.

DeDiego, M.L., Nieto-Torres, J.L., Jimenez-Guardeño, J.M., Regla-Nava, J.A., Alvarez, E., Oliveros, J.C., Zhao, J., Fett, C., Perlman, S., Enjuanes, L., 2011. Severe acute respiratory syndrome coronavirus envelope protein regulates cell stress response and apoptosis. PLoS pathogens 7, e1002315.

DeDiego, M.L., Nieto-Torres, J.L., Regla-Nava, J.A., Jimenez-Guardeño, J.M., Fernandez-Delgado, R., Fett, C., Castaño-Rodriguez, C., Perlman, S., Enjuanes, L., 2014. Inhibition of NF-kappaB mediated inflammation in severe acute respiratory syndome coronavirus-infected mice increases survival. J. Virol. 88, 913-924.

DeDiego, M.L., Pewe, L., Alvarez, E., Rejas, M.T., Perlman, S., Enjuanes, L., 2008. Pathogenicity of severe acute respiratory coronavirus deletion mutants in hACE-2 transgenic mice. Virology 376, 379-389.

Delmas, B., Laude, H., 1990. Assembly of coronavirus spike protein into trimers and its role in epitope expression. J. Virol. 64, 5367-5375.

Denison, M., Perlman, S., 1987. Identification of putative polymerase gene product in cells infected with murine coronavirus A59. Virology 157, 565-568.

Denison, M.R., Yount, B., Brockway, S.M., Graham, R.L., Sims, A.C., Lu, X.T., Baric, R.S., 2004. Cleavage between replicase proteins p28 and p65 of mouse hepatitis virus is not required for virus replication. J. Virol., 5957-5965.

Devaraj, S.G., Wang, N., Chen, Z., Chen, Z., Tseng, M., Barretto, N., Lin, R., Peters, C.J., Tseng, C.T., Baker, S.C., Li, K., 2007. Regulation of IRF-3-dependent innate immunity by the papain-like protease domain of the severe acute respiratory syndrome coronavirus. J. Biol. Chem. 282, 32208-32221.

Donaldson, E.F., Yount, B., Sims, A.C., Burkett, S., Pickles, R.J., Baric, R.S., 2008. Systematic assembly of a full-length infectious clone of human coronavirus NL63. J. Virol. 82, 11948-11957.

Donnelly, C.A., Ghani, A.C., Leung, G.M., Hedley, A.J., Fraser, C., Riley, S., Abu-Raddad, L.J., Ho, L.-M., Thach, T.-Q., Chau, P., 2003. Epidemiological determinants of spread of causal agent of severe acute respiratory syndrome in Hong Kong. Lancet 361, 1761-1766.

Drexler, J.F., Gloza-Rausch, F., Glende, J., Corman, V.M., Muth, D., Goettsche, M., Seebens, A., Niedrig, M., Pfefferle, S., Yordanov, S., Zhelyazkov, L., Hermanns, U., Vallo, P., Lukashev, A., Muller, M.A., Deng, H., Herrler, G., Drosten, C., 2010. Genomic characterization of severe acute respiratory syndrome-related coronavirus in European bats and classification of coronaviruses based on partial RNA-dependent RNA polymerase gene sequences. J. Virol. 84, 11336-11349.

Drosten, C., Gunther, S., Preiser, W., van der Werf, S., Brodt, H.R., Becker, S., Rabenau, H., Panning, M., Kolesnikova, L., Fouchier, R.A., Berger, A., Burguiere, A.M., Cinatl, J., Eickmann, M., Escriou, N., Grywna, K., Kramme, S., Manuguerra, J.C., Muller, S., Rickerts, V., Sturmer, M., Vieth, S., Klenk, H.D., Osterhaus, A.D., Schmitz, H., Doerr, H.W., 2003. Identification of a novel coronavirus in patients with severe acute respiratory syndrome. N. Engl. J. Med. 348, 1967-1976.

Dwosh, H.A., Hong, H.H., Austgarden, D., Herman, S., Schabas, R., 2003. Identification and containment of an outbreak of SARS in a community hospital. CMAJ. 168, 1415-1420.

Emeny, J.M., Morgan, M.J., 1979. Regulation of the interferon system: evidence that Vero cells have a genetic defect in interferon production. J. Gen. Virol. 43, 247-252.

Enjuanes, L., Almazan, F., Sola, I., Zuñiga, S., Alvarez, E., Reguera, J., Capiscol, C., 2006. Biochemical aspects of coronavirus replication. Adv. Exp. Med. Biol. 581, 13-24.

Enjuanes, L., DeDiego, M.L., Alvarez, E., Deming, D., Sheahan, T., Baric, R., 2008a. Vaccines to prevent severe acute respiratory syndrome coronavirus-induced disease. Virus Res. 133, 45-62.

Enjuanes, L., Gorbalenya, A.E., de Groot, R.J., Cowley, J.A., Ziebuhr, J., Snijder, E.J., 2008b. The Nidovirales, in: Mahy, B.W.J., Van Regenmortel, M., Walker, P., Majumder-Russell, D. (Eds.), Encyclopedia of Virology, Third Edition. Elsevier Ltd., Oxford, pp. 419-430.

Escors, D., Camafeita, E., Ortego, J., Laude, H., Enjuanes, L., 2001. Organization of two transmissible gastroenteritis coronavirus membrane protein topologies within the virion and core. J. Virol. 75, 12228-12240.

Falcon, A., Vazquez-Moron, S., Casas, I., Aznar, C., Ruiz, G., Pozo, F., Perez-Brena, P., Juste, J., Ibanez, C., Garin, I., Aihartza, J., Echevarria, J.E., 2011. Detection of alpha and betacoronaviruses in multiple Iberian bat species. Arch. Virol. 156, 1883-1890.

Fett, C., DeDiego, M.L., Regla-Nava, J.A., Enjuanes, L., Perlman, S., 2013. Complete protection against severe acute respiratory syndrome coronavirus-mediated lethal respiratory disease in aged mice by immunization with a mouse-adapted virus lacking E protein. J. Virol. 87, 6551-6559.

Fouchier, R.A., Hartwig, N.G., Bestebroer, T.M., Niemeyer, B., de Jong, J.C., Simon, J.H., Osterhaus, A.D., 2004. A previously undescribed coronavirus associated with respiratory disease in humans. Proc. Natl. Acad. Sci. USA 101, 6212621-6212626.

Franks, T.J., Chong, P.Y., Chui, P., Galvin, J.R., Lourens, R.M., Reid, A.H., Selbs, E., McEvoy, C.P., Hayden, C.D., Fukuoka, J., Taubenberger, J.K., Travis, W.D., 2003. Lung pathology of severe acute respiratory syndrome (SARS): a study of 8 autopsy cases from Singapore. Hum. Pathol. 34, 743-748.

Frieman, M., Heise, M., Baric, R., 2008. SARS coronavirus and innate immunity. Virus Res. 133, 101-112.

Frieman, M., Ratia, K., Johnston, R.E., Mesecar, A.D., Baric, R.S., 2009. Severe acute respiratory syndrome coronavirus papain-like protease ubiquitin-like domain and catalytic domain regulate antagonism of IRF3 and NF-kappaB signaling. J. Virol. 83, 6689-6705.

Frieman, M., Yount, B., Heise, M., Kopecky-Bromberg, S.A., Palese, P., Baric, R.S., 2007. Severe acute respiratory syndrome coronavirus ORF6 antagonizes STAT1 function by sequestering nuclear import factors on the rough endoplasmic reticulum/Golgi membrane. J. Virol. 81, 9812-9824.

Frieman, M.B., Chen, J., Morrison, T.E., Whitmore, A., Funkhouser, W., Ward, J.M., Lamirande, E.W., Roberts, A., Heise, M., Subbarao, K., Baric, R.S., 2010. SARS-CoV pathogenesis is regulated by a STAT1 dependent but a type I, II and III interferon receptor independent mechanism. PLoS pathogens 6, e1000849.

Fuchizaki, U., Kaneko, S., Nakamoto, Y., Sugiyama, Y., Imagawa, K., Kikuchi, M., Kobayashi, K., 2003. Synergistic antiviral effect of a combination of mouse interferon-alpha and interferon-gamma on mouse hepatitis virus. J. Med. Virol. 69, 188-194.

Fujiwara, N., Kobayashi, K., 2005. Macrophages in inflammation. Curr. Drug Targets Inflamm. Allergy 4, 281-286.

Fukutomi, T., Tsunemitsu, H., Akashi, H., 1999. Detection of bovine coronaviruses from adult cows with epizootic diarrhea and their antigenic and biological diversities. Arch. Virol. 144, 997-1006.

Galan, C., Enjuanes, L., Almazan, F., 2005. A point mutation within the replicase gene differentially affects coronavirus genome versus minigenome replication. J. Virol. 79, 15016-15026.

Gallagher, T.M., Buchmeier, M.J., 2001. Coronavirus spike proteins in viral entry and pathogenesis. Virology 279, 371-374.

Garcia-Sastre, A., Biron, C.A., 2006. Type 1 interferons and the virus-host relationship: a lesson in detente. Science 312, 879-882.

Godet, M., L'Haridon, R., Vautherot, J.F., Laude, H., 1992. TGEV coronavirus ORF4 encodes a membrane protein that is incorporated into virions. Virology 188, 666-675.

Gorbalenya, A.E., Enjuanes, L., Ziebuhr, J., Snijder, E.J., 2006. Nidovirales: evolving the largest RNA virus genome. Virus Res. 117, 17-37.

Gorbalenya, A.E., Koonin, E.V., Donchenko, A.P., Blinov, V.M., 1989. Coronavirus genome: prediction of putative functional domains in the non-structural polyprotein by comparative amino acid sequence analysis. Nucleic Acids Res. 17, 4847-4861.

Gorbalenya, A.E., Snijder, E.J., Spaan, W.J., 2004. Severe acute respiratory syndrome coronavirus phylogeny: toward consensus. J. Virol. 78, 7863-7866.

Gorlich, D., 1998. Transport into and out of the cell nucleus. Embo J. 17, 2721-2727.

Gosert, R., Kanjanahaluethai, A., Egger, D., Bienz, K., Baker, S.C., 2002. RNA replication of mouse hepatitis virus takes place at double-membrane vesicles. J. Virol. 76, 3697-3708.

Graham, R.L., Donaldson, E.F., Baric, R.S., 2013. A decade after SARS: strategies for controlling emerging coronaviruses. Nat. Rev. Microbiol. 11, 836-848.

Gralinski, L.E., Baric, R.S., 2015. Molecular pathology of emerging coronavirus infections. J. Pathol. 235, 185-195.

Grommes, J., Soehnlein, O., 2011. Contribution of neutrophils to acute lung injury. Mol. Med. 17, 293-307.

Haagmans, B.L., Kuiken, T., Martina, B.E., Fouchier, R.A., Rimmelzwaan, G.F., van Amerongen, G., van Riel, D., de Jong, T., Itamura, S., Chan, K.H., Tashiro, M., Osterhaus, A.D., 2004. Pegylated interferon-alpha protects type 1 pneumocytes against SARS coronavirus infection in macaques. Nat. Med. 10, 290-293.

Haller, O., Kochs, G., Weber, F., 2006. The interferon response circuit: induction and suppression by pathogenic viruses. Virology 344, 119-130.

He, Z., Zhao, C., Dong, Q., Zhuang, H., Song, S., Peng, G., Dwyer, D.E., 2005. Effects of severe acute respiratory syndrome (SARS) coronavirus infection on peripheral blood lymphocytes and their subsets. Int. J. Infect. Dis. 9, 323-330.

Ho, Y., Lin, P.H., Liu, C.Y., Lee, S.P., Chao, Y.C., 2004. Assembly of human severe acute respiratory syndrome coronavirus-like particles. Biochem. Biophys. Res. Commun. 318, 833-838.

Hoffmann, H.H., Schneider, W.M., Rice, C.M., 2015. Interferons and viruses: an evolutionary arms race of molecular interactions. Trends Immunol. 36, 124-138.

Hsiao, C.H., Chang, M.F., Hsueh, P.R., Su, I.J., 2005. Immunohistochemical study of severe acute respiratory syndrome-associated coronavirus in tissue sections of patients. J. Formos. Med. Assoc. 104, 150-156.

Huang, C., Lokugamage, K.G., Rozovics, J.M., Narayanan, K., Semler, B.L., Makino, S., 2011. SARS coronavirus nsp1 protein induces template-dependent endonucleolytic cleavage of mRNAs: viral mRNAs are resistant to nsp1-induced RNA cleavage. PLoS pathogens 7, e1002433.

Huang, C., Narayanan, K., Ito, N., Peters, C.J., Makino, S., 2006. Severe acute respiratory syndrome coronavirus 3a protein is released in membranous structures from 3a protein-expressing cells and infected cells. J. Virol. 80, 210-217.

Huang da, W., Sherman, B.T., Lempicki, R.A., 2009. Systematic and integrative analysis of large gene lists using DAVID bioinformatics resources. Nat. Protoc. 4, 44-57.

Huang, K.J., Su, I.J., Theron, M., Wu, Y.C., Lai, S.K., Liu, C.C., Lei, H.Y., 2005. An interferon-gamma-related cytokine storm in SARS patients. J. Med. Virol. 75, 185-194.

Huang, Y.W., Dickerman, A.W., Pineyro, P., Li, L., Fang, L., Kiehne, R., Opriessnig, T., Meng, X.J., 2013. Origin, evolution, and genotyping of emergent porcine epidemic diarrhea virus strains in the United States. mBio 4, e00737-00713.

Izeta, A., Smerdou, C., Alonso, S., Penzes, Z., Mendez, A., Plana-Duran, J., Enjuanes, L., 1999. Replication and packaging of transmissible gastroenteritis coronavirus-derived synthetic minigenomes. J. Virol. 73, 1535-1545.

Jenkins, S.J., Ruckerl, D., Cook, P.C., Jones, L.H., Finkelman, F.D., van Rooijen, N., MacDonald, A.S., Allen, J.E., 2011. Local macrophage proliferation, rather than recruitment from the blood, is a signature of TH2 inflammation. Science 332, 1284-1288.

Jiang, Y., Xu, J., Zhou, C., Wu, Z., Zhong, S., Liu, J., Luo, W., Chen, T., Qin, Q., Deng, P., 2005. Characterization of cytokine/chemokine profiles of severe acute respiratory syndrome. Am. J. Respir. Crit. Care Med. 171, 850-857.

Jimenez, G., Correa, I., Melgosa, M.P., Bullido, M.J., Enjuanes, L., 1986. Critical epitopes in transmissible gastroenteritis virus neutralization. J. Virol. 60, 131-139.

Jimenez-Guardeño, J.M., Nieto-Torres, J.L., DeDiego, M.L., Regla-Nava, J.A., Fernandez-Delgado, R., Castaño-Rodriguez, C., Enjuanes, L., 2014. The PDZ-binding motif of severe acute respiratory syndrome coronavirus envelope protein Is a determinant of viral pathogenesis. PLoS pathogens 10, e1004320.

Jimenez-Guardeño, J.M., Regla-Nava, J.A., Nieto-Torres, J.L., DeDiego, M.L., Castaño-Rodríguez, C., Fernandez-Delgado, R., Perlman, S., Enjuanes, L., 2015. Identification of the mechanisms leading to virulence reversion in an attenuated SARS-CoV to optimize the design and genetic stabilization of efficient vaccines. PLoS pathogens, Submitted.

Kamitani, W., Huang, C., Narayanan, K., Lokugamage, K.G., Makino, S., 2009. A two-pronged strategy to suppress host protein synthesis by SARS coronavirus Nsp1 protein. Nat. Struct. Mol. Biol. 16, 1134-1140.

Kamitani, W., Narayanan, K., Huang, C., Lokugamage, K., Ikegami, T., Ito, N., Kubo, H., Makino, S., 2006. Severe acute respiratory syndrome coronavirus nsp1 protein suppresses host gene expression by promoting host mRNA degradation. Proc. Natl. Acad. Sci. USA 103, 12885-12890.

Kan, B., Wang, M., Jing, H., Xu, H., Jiang, X., Yan, M., Liang, W., Zheng, H., Wan, K., Liu, Q., Cui, B., Xu, Y., Zhang, E., Wang, H., Ye, J., Li, G., Li, M., Cui, Z., Qi, X., Chen, K., Du, L., Gao, K., Zhao, Y.T., Zou, X.Z., Feng, Y.J., Gao, Y.F., Hai, R., Yu, D., Guan, Y., Xu, J., 2005. Molecular evolution analysis and geographic investigation of severe acute respiratory syndrome coronavirus-like virus in palm civets at an animal market and on farms. J. Virol. 79, 11892-11900.

Kawai, T., Takahashi, K., Sato, S., Coban, C., Kumar, H., Kato, H., Ishii, K.J., Takeuchi, O., Akira, S., 2005. IPS-1, an adaptor triggering RIG-I- and Mda5-mediated type I interferon induction. Nat. Immunol. 6, 981-988.

Kim, S.J., Park, K., Koeller, D., Kim, K.Y., Wakefield, L.M., Sporn, M.B., Roberts, A.B., 1992. Post-transcriptional regulation of the human transforming growth factor-beta 1 gene. J. Biol. Chem. 267, 13702-13707.

Klein, W., Tromm, A., Griga, T., Fricke, H., Folwaczny, C., Hocke, M., Eitner, K., Marx, M., Duerig, N., Epplen, J.T., 2001. Interleukin-4 and interleukin-4 receptor gene polymorphisms in inflammatory bowel diseases. Genes Immun. 2, 287-289.

Knoops, K., Kikkert, M., Worm, S.H., Zevenhoven-Dobbe, J.C., van der Meer, Y., Koster, A.J., Mommaas, A.M., Snijder, E.J., 2008. SARS-coronavirus replication is supported by a reticulovesicular network of modified endoplasmic reticulum. PLoS Biol. 6, e226.

Koetzner, C.A., Kuo, L., Goebel, S.J., Dean, A.B., Parker, M.M., Masters, P.S., 2010. Accessory protein 5a is a major antagonist of the antiviral action of interferon against murine coronavirus. J. Virol. 84, 8262-8274.

Kohlmeier, J.E., Woodland, D.L., 2009. Immunity to respiratory viruses. Annu. Rev. Immunol. 27, 61-82.

Kong, W.P., Xu, L., Stadler, K., Ulmer, J.B., Abrignani, S., Rappuoli, R., Nabel, G.J., 2005. Modulation of the immune response to the severe acute respiratory syndrome spike glycoprotein by gene-based and inactivated virus immunization. J. Virol. 79, 13915-13923.

Kopecky-Bromberg, S.A., Martinez-Sobrido, L., Frieman, M., Baric, R.A., Palese, P., 2007. Severe acute respiratory syndrome coronavirus open reading frame (ORF) 3b, ORF 6, and nucleocapsid proteins function as interferon antagonists. J. Virol. 81, 548-557.

Kotenko, S.V., Gallagher, G., Baurin, V.V., Lewis-Antes, A., Shen, M., Shah, N.K., Langer, J.A., Sheikh, F., Dickensheets, H., Donnelly, R.P., 2003. IFN-lambdas mediate antiviral protection through a distinct class II cytokine receptor complex. Nat. Immunol. 4, 69-77.

Kumaki, Y., Ennis, J., Rahbar, R., Turner, J.D., Wandersee, M.K., Smith, A.J., Bailey, K.W., Vest, Z.G., Madsen, J.R., Li, J.K., Barnard, D.L., 2011. Single-dose intranasal administration with mDEF201 (adenovirus vectored mouse interferon-alpha) confers protection from mortality in a lethal SARS-CoV BALB/c mouse model. Antiviral Res. 89, 75-82.

Kuo, L., Masters, P.S., 2003. The small envelope protein E is not essential for murine coronavirus replication. J. Virol. 77, 4597-4608.

Kuo, L., Masters, P.S., 2013. Functional analysis of the murine coronavirus genomic RNA packaging signal. J. Virol. 87, 5182-5192.

Kuri, T., Eriksson, K.K., Putics, A., Zust, R., Snijder, E.J., Davidson, A.D., Siddell, S.G., Thiel, V., Ziebuhr, J., Weber, F., 2011. The ADP-ribose-1"-monophosphatase domains of severe acute respiratory syndrome coronavirus and human coronavirus 229E mediate resistance to antiviral interferon responses. J. Gen. Virol. 92, 1899-1905.

Lalani, T., Simmons, R.K., Ahmed, A.R., 1999. Biology of IL-5 in health and disease. Ann. Allergy Asthma Immunol. 82, 317-332; quiz 332-313.

Lam, C.W., Chan, M.H., Wong, C.K., 2004. Severe acute respiratory syndrome: clinical and laboratory manifestations. Clin. Biochem. Rev. 25, 121-132.

Lamirande, E.W., DeDiego, M.L., Roberts, A., Jackson, J.P., Alvarez, E., Sheahan, T., Shieh, W.J., Zaki, S.R., Baric, R., Enjuanes, L., Subbarao, K., 2008. A live attenuated SARS coronavirus is immunogenic and efficacious in golden Syrian hamsters. J. Virol. 82, 7721-7724.

Lang, Z.W., Zhang, L.J., Zhang, S.J., Meng, X., Li, J.Q., Song, C.Z., Sun, L., Zhou, Y.S., Dwyer, D.E., 2003. A clinicopathological study of three cases of severe acute respiratory syndrome (SARS). Pathology 35, 526-531.

Lau, S.K., Woo, P.C., Li, K.S., Huang, Y., Tsoi, H.W., Wong, B.H., Wong, S.S., Leung, S.Y., Chan, K.H., Yuen, K.Y., 2005. Severe acute respiratory syndrome coronavirus-like virus in Chinese horseshoe bats. Proc. Natl. Acad. Sci. USA 102, 14040-14045.

Lauber, C., Ziebuhr, J., Junglen, S., Drosten, C., Zirkel, F., Nga, P.T., Morita, K., Snijder, E.J., Gorbalenya, A.E., 2012. Mesoniviridae: a proposed new family in the order Nidovirales formed by a single species of mosquito-borne viruses. Arch. Virol. 157, 1623-1628.

Law, A.H., Lee, D.C., Cheung, B.K., Yim, H.C., Lau, A.S., 2007. Role for nonstructural protein 1 of severe acute respiratory syndrome coronavirus in chemokine dysregulation. J. Virol. 81, 416-422.

Lee, N., Hui, D., Wu, A., Chan, P., Cameron, P., Joynt, G., Ahuja, A., Yung, M.Y., Leung, C.B., To, K.F., Lui, S.F., Szeto, C.C., Chung, S., Sung, J.J.Y., 2003. A major outbreak of severe acute respiratory syndrome in Hong Kong. N. Engl. J. Med. 348, 1986-1994.

Lei, L., Ying, S., Baojun, L., Yi, Y., Xiang, H., Wenli, S., Zounan, S., Deyin, G., Qingyu, Z., Jingmei, L., Guohui, C., 2013. Attenuation of mouse hepatitis virus by deletion of the LLRKxGxKG region of Nsp1. PloS one 8, e61166.

Li, W., Greenough, T.C., Moore, M.J., Vasilieva, N., Somasundaran, M., Sullivan, J.L., Farzan, M., Choe, H., 2004. Efficient replication of severe acute respiratory syndrome coronavirus in mouse cells is limited by murine angiotensin-converting enzyme 2. J. Virol. 78, 11429-11433.

Li, W., Moore, M.J., Vasilieva, N., Sui, J., Wong, S.K., Berne, M.A., Somasundaran, M., Sullivan, J.L., Luzuriaga, K., Greenough, T.C., Choe, H., Farzan, M., 2003. Angiotensin-converting enzyme 2 is a functional receptor for de SARS coronavirus. Nature 426, 450-454.

Li, W., Shi, Z., Yu, M., Ren, W., Smith, C., Epstein, J.H., Wang, H., Crameri, G., Hu, Z., Zhang, H., Zhang, J., McEachern, J., Field, H., Daszak, P., Eaton, B.T., Zhang, S., Wang, L.F., 2005. Bats are natural reservoirs of SARS-like coronaviruses. Science 310, 676-679.

Liao, C.L., Lai, M.M.C., 1992. RNA recombination in a coronavirus - recombination between viral genomic RNA and transfected RNA fragments. J. Virol. 66, 6117-6124.

Liao, Y., Lescar, J., Tam, J.P., Liu, D.X., 2004. Expression of SARS-coronavirus envelope protein in Escherichia coli cells alters membrane permeability. Biochem. Biophys. Res. Commun. 325, 374-380.

Lim, K.P., Liu, D.X., 2001. The missing link in coronavirus assembly. Retention of the avian coronavirus infectious bronchitis virus envelope protein in the pre-Golgi compartments and physical interaction between the envelope and membrane proteins. J. Biol. Chem. 276, 17515-17523.

Livak, K.J., Schmittgen, T.D., 2001. Analysis of relative gene expression data using real-time quantitative PCR and the 2(-Delta Delta C(T)) Method. Methods 25, 402-408.

Lu, X., Pan, J., Tao, J., Guo, D., 2011. SARS-CoV nucleocapsid protein antagonizes IFN-beta response by targeting initial step of IFN-beta induction pathway, and its C-terminal region is critical for the antagonism. Virus genes 42, 37-45.

Lunney, J.K., Benfield, D.A., Rowland, R.R., 2010. Porcine reproductive and respiratory syndrome virus: an update on an emerging and re-emerging viral disease of swine. Virus Res. 154, 1-6.

Madan, V., Garcia Mde, J., Sanz, M.A., Carrasco, L., 2005. Viroporin activity of murine hepatitis virus E protein. FEBS Lett. 579, 3607-3612.

Mahlakoiv, T., Ritz, D., Mordstein, M., DeDiego, M.L., Enjuanes, L., Muller, M.A., Drosten, C., Staeheli, P., 2012. Combined action of type I and type III interferon restricts initial replication of SARS-Coronavirus in the lung but fails to inhibit systemic virus spread. J. Gen. Virol. 93, 2601-2605.

Marie, C., Pitton, C., Fitting, C., Cavaillon, J.M., 1996. Regulation by anti-inflammatory cytokines (IL-4, IL-10, IL-13, TGFbeta)of interleukin-8 production by LPS- and/ or TNFalpha-activated human polymorphonuclear cells. Mediators Inflamm. 5, 334-340.

Marie, I., Durbin, J.E., Levy, D.E., 1998. Differential viral induction of distinct interferon-alpha genes by positive feedback through interferon regulatory factor-7. EMBO J. 17, 6660-6669.

Marshall, E., Enserink, M., 2004. Medicine. Caution urged on SARS vaccines. Science 303, 944-946.

Martin, J., Jenkins, R.H., Bennagi, R., Krupa, A., Phillips, A.O., Bowen, T., Fraser, D.J., 2011. Post-transcriptional regulation of Transforming Growth Factor Beta-1 by microRNA-744. PloS one 6, e25044.

Masters, P.S., 2006. The molecular biology of coronaviruses. Adv. Virus Res. 66, 193-292.

Matthay, M.A., Folkesson, H.G., Clerici, C., 2002. Lung epithelial fluid transport and the resolution of pulmonary edema. Physiol. Rev. 82, 569-600.

Matthay, M.A., Zemans, R.L., 2011. The acute respiratory distress syndrome: pathogenesis and treatment. Annu. Rev. Pathol. 6, 147-163.

Maury, C.P., Lahdevirta, J., 1990. Correlation of serum cytokine levels with haematological abnormalities in human immunodeficiency virus infection. J. Intern. Med. 227, 253-257.

McCray, P.B., Jr., Pewe, L., Wohlford-Lenane, C., Hickey, M., Manzel, L., Shi, L., Netland, J., Jia, H.P., Halabi, C., Sigmund, C.D., Meyerholz, D.K., Kirby, P., Look, D.C., Perlman, S., 2007. Lethal infection of K18-hACE2 mice infected with severe acute respiratory syndrome coronavirus. J. Virol. 81, 813-821.

McIntosh, K., Kapikian, A.Z., Hardison, K.A., Hartley, J.W., Chanock, R.M., 1969. Antigenic relationships among the coronaviruses of man and between human and animal coronaviruses. J. Immunol. 102, 1109-1118.

Medzhitov, R., Janeway, C.A., Jr., 1997. Innate immunity: the virtues of a nonclonal system of recognition. Cell 91, 295-298.

Miura, T.A., Holmes, K.V., 2009. Host-pathogen interactions during coronavirus infection of primary alveolar epithelial cells. J. Leukoc. Biol. 86, 1145-1151.

Montagnon, B.J., 1989. Polio and rabies vaccines produced in continuous cell lines: a reality for Vero cell line. Dev. Biol. Stand. 70, 27-47.

Muller, M.A., Paweska, J.T., Leman, P.A., Drosten, C., Grywna, K., Kemp, A., Braack, L., Sonnenberg, K., Niedrig, M., Swanepoel, R., 2007. Coronavirus antibodies in African bat species. Emerg. Infect. Dis. 13, 1367-1370.

Nagata, N., Iwata, N., Hasegawa, H., Fukushi, S., Harashima, A., Sato, Y., Saijo, M., Taguchi, F., Morikawa, S., Sata, T., 2008. Mouse-passaged severe acute respiratory syndrome-associated coronavirus leads to lethal pulmonary edema and diffuse alveolar damage in adult but not young mice. Am. J. Pathol. 172, 1625-1637.

Nal, B., Chan, C., Kien, F., Siu, L., Tse, J., Chu, K., Kam, J., Staropoli, I., Crescenzo-Chaigne, B., Escriou, N., van der Werf, S., Yuen, K.Y., Altmeyer, R., 2005. Differential maturation and subcellular localization of severe acute respiratory syndrome coronavirus surface proteins S, M and E. J. Gen. Virol. 86, 1423-1434.

Narasaraju, T., Yang, E., Samy, R.P., Ng, H.H., Poh, W.P., Liew, A.A., Phoon, M.C., van Rooijen, N., Chow, V.T., 2011. Excessive neutrophils and neutrophil extracellular traps contribute to acute lung injury of influenza pneumonitis. Am. J. Pathol. 179, 199-210.

Narayanan, K., Huang, C., Lokugamage, K., Kamitani, W., Ikegami, T., Tseng, C.T., Makino, S., 2008a. Severe acute respiratory syndrome coronavirus nsp1 suppresses host gene expression, including that of type I interferon, in infected cells. J. Virol. 82, 4471-4479.

Narayanan, K., Huang, C., Makino, S., 2008b. SARS coronavirus accessory proteins. Virus Res. 133, 113-121.

Narayanan, K., Maeda, A., Maeda, J., Makino, S., 2000. Characterization of the coronavirus M protein and nucleocapsid interaction in infected cells. J. Virol. 74, 8127-8134.

Narayanan, K., Ramirez, S.I., Lokugamage, K.G., Makino, S., 2014. Coronavirus nonstructural protein 1: Common and distinct functions in the regulation of host and viral gene expression. Virus Res., doi:10.1016/j.virusres.2014.1011.1019.

Netland, J., DeDiego, M.L., Zhao, J., Fett, C., Alvarez, E., Nieto-Torres, J.L., Enjuanes, L., Perlman, S., 2010. Immunization with an attenuated severe acute respiratory syndrome coronavirus deleted in E protein protects against lethal respiratory disease. Virology 399, 120-128.

Ng, S.K.C., 2003. Possible role of an animal vector in the SARS outbreak at Amoy Gardens. Lancet 362, 570-572.

Nguyen, V.P., Hogue, B.G., 1997. Protein interactions during coronavirus assembly. J. Virol. 71, 9278-9284.

Nicholls, J.M., Poon, L.L., Lee, K.C., Ng, W.F., Lai, S.T., Leung, C.Y., Chu, C.M., Hui, P.K., Mak, K.L., Lim, W., Yan, K.W., Chan, K.H., Tsang, N.C., Guan, Y., Yuen, K.Y., Peiris, J.S., 2003. Lung pathology of fatal severe acute respiratory syndrome. Lancet 361, 1773-1778.

Nieto-Torres, J.L., DeDiego, M.L., Alvarez, E., Jimenez-Guardeño, J.M., Regla-Nava, J.A., Llorente, M., Kremer, L., Shuo, S., Enjuanes, L., 2011. Subcellular location and topology of severe acute respiratory syndrome coronavirus envelope protein. Virology 415, 69-82.

Nieto-Torres, J.L., Dediego, M.L., Verdia-Baguena, C., Jimenez-Guardeño, J.M., Regla-Nava, J.A., Fernandez-Delgado, R., Castaño-Rodriguez, C., Alcaraz, A., Torres, J., Aguilella, V.M., Enjuanes, L., 2014. Severe acute respiratory syndrome coronavirus envelope protein ion channel activity promotes virus fitness and pathogenesis. PLoS pathogens 10, e1004077.

Ortego, J., Ceriani, J.E., Patino, C., Plana, J., Enjuanes, L., 2007. Absence of E protein arrests transmissible gastroenteritis coronavirus maturation in the secretory pathway. Virology 368, 296-308.

Ortego, J., Escors, D., Laude, H., Enjuanes, L., 2002. Generation of a replication-competent, propagation-deficient virus vector based on the transmissible gastroenteritis coronavirus genome. J. Virol. 76, 11518-11529.

Peiris, J.S., Hui, K.P., Yen, H.L., 2010. Host response to influenza virus: protection versus immunopathology. Curr. Opin. Immunol. 22, 475-481.

Peiris, J.S.M., Chu, C.M., Cheng, V.C.C., Chan, K.S., Hung, I.F.N., Poon, L.L.M., Law, K.I., Tang, B.S.F., Hon, T.Y.W., Chan, C.S., Chan, K.H., Ng, J.S.C., Zheng, B.J., Ng, W.L., Lai, R.W.M., Guan, Y., Yuen, K.Y., 2003. Clinical progression and viral load in a community outbreak of coronavirus-associated SARS pneumonia: a prospective study. Lancet 361, 1767-1772.

Perlman, S., Netland, J., 2009. Coronaviruses post-SARS: update on replication and pathogenesis. Nat. Rev. Microbiol. 7, 439-450.

Platanias, L.C., 2005. Mechanisms of type-I- and type-II-interferon-mediated signalling. Nat. Rev. Immunol. 5, 375-386.

Poon, L.L., Chu, D.K., Chan, K.H., Wong, O.K., Ellis, T.M., Leung, Y.H., Lau, S.K., Woo, P.C., Suen, K.Y., Yuen, K.Y., Guan, Y., Peiris, J.S., 2005. Identification of a novel coronavirus in bats. J. Virol. 79, 2001-2009.

Puneet, P., Moochhala, S., Bhatia, M., 2005. Chemokines in acute respiratory distress syndrome. Am. J. Physiol. Lung Cell Mol. Physiol. 288, L3-15.

Qin, E., Shi, H., Tang, L., Wang, C., Chang, G., Ding, Z., Zhao, K., Wang, J., Chen, Z., Yu, M., Si, B., Liu, J., Wu, D., Cheng, X., Yang, B., Peng, W., Meng, Q., Liu, B., Han, W., Yin, X., Duan, H., Zhan, D., Tian, L., Li, S., Wu, J., Tan, G., Li, Y., Liu, Y., Liu, H., Lv, F., Zhang, Y., Kong, X., Fan, B., Jiang, T., Xu, S., Wang, X., Li, C., Wu, X., Deng, Y., Zhao, M., Zhu, Q., 2006. Immunogenicity and protective efficacy in monkeys of purified inactivated Vero-cell SARS vaccine. Vaccine 24, 1028-1034.

Quan, P.L., Firth, C., Street, C., Henriquez, J.A., Petrosov, A., Tashmukhamedova, A., Hutchison, S.K., Egholm, M., Osinubi, M.O., Niezgoda, M., Ogunkoya, A.B., Briese, T., Rupprecht, C.E., Lipkin, W.I., 2010. Identification of a severe acute respiratory syndrome coronavirus-like virus in a leaf-nosed bat in Nigeria. mBio 1, e00208-00210.

Raamsman, M.J.B., Locker, J.K., de Hooge, A., de Vries, A.A.F., Griffiths, G., Vennema, H., Rottier, P.J.M., 2000. Characterization of the coronavirus mouse hepatitis virus strain A59 small membrane protein E. J. Virol. 74, 2333-2342.

Randall, R.E., Goodbourn, S., 2008. Interferons and viruses: an interplay between induction, signalling, antiviral responses and virus countermeasures. J. Gen. Virol. 89, 1-47.

Reghunathan, R., Jayapal, M., Hsu, L.Y., Chng, H.H., Tai, D., Leung, B.P., Melendez, A.J., 2005. Expression profile of immune response genes in patients with Severe Acute Respiratory Syndrome. BMC Immunol. 6, 2.

Regla-Nava, J.A., Jimenez-Guardeño, J.M., Nieto-Torres, J.L., Gallagher, T.M., Enjuanes, L., DeDiego, M.L., 2013. The replication of a mouse adapted SARS-CoV in a mouse cell line stably expressing the murine SARS-CoV receptor mACE2 efficiently induces the expression of proinflammatory cytokines. J. Virol. Methods 193, 639-646.

Regla-Nava, J.A., Nieto-Torres, J.L., Jimenez-Guardeño, J.M., Fernandez-Delgado, R., Fett, C., Castaño-Rodriguez, C., Perlman, S., Enjuanes, L., DeDiego, M.L., 2015. SARS coronaviruses with mutations in E protein are attenuated and promising vaccine candidates. J. Virol. 89, 3870-3887

Ren, L., Yang, R., Guo, L., Qu, J., Wang, J., Hung, T., 2005. Apoptosis induced by the SARS-associated coronavirus in Vero cells is replication-dependent and involves caspase. DNA Cell Biol. 24, 496-502.

Repass, J.F., Makino, S., 1998. Importance of the positive-strand RNA secondary structure of a murine coronavirus defective interfering RNA internal replication signal in positive-strand RNA synthesis. J. Virol. 72, 7926-7933.

Riley, S., Fraser, C., Donnelly, C.A., Ghani, A.C., Abu-Raddad, L.J., Hedley, A.J., Leung, G.M., Ho, L.-M., Lam, T.-H., Thach, T.Q., Chau, P., Chan, K.-P., Lo, S.-V., Leung, P.-Y., Tsang, T., Ho, W., Lee, K.-H., Lau, E.M.C., Ferguson, N.M., Anderson, R.M., 2003. Transmission Dynamics of the Etiological Agent of SARS in Hong Kong: Impact of Public Health Interventions. Science 300, 1961-1966.

Roberts, A., Deming, D., Paddock, C.D., Cheng, A., Yount, B., Vogel, L., Herman, B.D., Sheahan, T., Heise, M., Genrich, G.L., Zaki, S.R., Baric, R., Subbarao, K., 2007. A mouse-adapted SARS-coronavirus causes disease and mortality in BALB/c mice. PLoS pathogens 3, 23-37.

Rockx, B., Baas, T., Zornetzer, G.A., Haagmans, B., Sheahan, T., Frieman, M., Dyer, M.D., Teal, T.H., Proll, S., van den Brand, J., Baric, R., Katze, M.G., 2009. Early upregulation of acute respiratory distress syndrome-associated cytokines promotes lethal disease in an aged-mouse model of severe acute respiratory syndrome coronavirus infection. J. Virol. 83, 7062-7074.

Rota, P.A., Oberste, M.S., Monroe, S.S., Nix, W.A., Campganoli, R., Icenogle, J.P., Peñaranda, S., Bankamp, B., Maher, K., Chen, M.-H., Tong, S., Tamin, A., Lowe, L., Frace, M., DeRisi, J.L., Chen, Q., Wang, D., Erdman, D.d., Peret, T.C.T., Burns, C., Ksiazek, T.G., Rollin, P.E., Sanchez, A., Liffick, S., Holloway, B., Limor, J., McCaustland, K., Olsen-Rassmussen, M., Fouchier, R., Gunther, S., Osterhaus, A.D.M.E., Drosten, C., Pallansch, M.A., Anderson, L.J., Bellini, W.J., 2003. Characterization of a novel coronavirus associated with severe acute respiratory syndrome. Science 300, 1394-1399.

Roth-Cross, J.K., Stokes, H., Chang, G., Chua, M.M., Thiel, V., Weiss, S.R., Gorbalenya, A.E., Siddell, S.G., 2009. Organ-specific attenuation of murine hepatitis virus strain A59 by replacement of catalytic residues in the putative viral cyclic phosphodiesterase ns2. J. Virol. 83, 3743-3753.

Rouse, B.T., Sehrawat, S., 2010. Immunity and immunopathology to viruses: what decides the outcome? Nat. Rev. Immunol. 10, 514-526.

Ruch, T.R., Machamer, C.E., 2012a. The Coronavirus E Protein: Assembly and Beyond. Viruses 4, 363-382.

Ruch, T.R., Machamer, C.E., 2012b. A single polar residue and distinct membrane topologies impact the function of the infectious bronchitis coronavirus E protein. PLoS pathogens 8, e1002674.

Saif, L.J., Wesley, R.D., 1992. Transmissible gastroenteritis, in: Leman, A.D., Straw, B.E., Mengeling, W.L., D'Allaire, S., Taylor, D.J. (Eds.), Diseases of Swine, 7th ed. Wolfe Publishing Ltd, Ames. Iowa, pp. 362-386.

Sainz, B., Jr., Mossel, E.C., Peters, C.J., Garry, R.F., 2004. Interferon-beta and interferon-gamma synergistically inhibit the replication of severe acute respiratory syndrome-associated coronavirus (SARS-CoV). Virology 329, 11-17.

Sambrook, J., Russell, D.W., 2001. Molecular cloning: A laboratory manual, 3rd ed. Cold Spring Harbor Laboratory Press, Cold Spring Harbor, New York.

Sawicki, S.G., Sawicki, D.L., 1990. Coronavirus transcription: subgenomic mouse hepatitis virus replicative intermediates function in RNA synthesis. J. Virol. 64, 1050-1056.

Schaecher, S.R., Mackenzie, J.M., Pekosz, A., 2007. The ORF7b protein of SARS-CoV is expressed in virus-infected cells and incorporated into SARS-CoV particles. J. Virol. 81, 718-731.

Schiller, J.J., Kanjanahaluethai, A., Baker, S.c., 1998. Processing of the coronavirus MHV-JHM polymerase polyprotein: identification of precursors and proteolytic products spanning 400 kilodaltons of ORF1a. Virology 242, 288-302.

Schneider, W.M., Chevillotte, M.D., Rice, C.M., 2014. Interferon-stimulated genes: a complex web of host defenses. Annu. Rev. Immunol. 32, 513-545.

Scobey, T., Yount, B.L., Sims, A.C., Donaldson, E.F., Agnihothram, S.S., Menachery, V.D., Graham, R.L., Swanstrom, J., Bove, P.F., Kim, J.D., Grego, S., Randell, S.H.,

Baric, R.S., 2013. Reverse genetics with a full-length infectious cDNA of the Middle East respiratory syndrome coronavirus. Proc. Natl. Acad. Sci. USA 110, 16157-16162.

Seruga, B., Zhang, H., Bernstein, L.J., Tannock, I.F., 2008. Cytokines and their relationship to the symptoms and outcome of cancer. Nat. Rev. Cancer 8, 887-899.

Sheahan, T., Morrison, T.E., Funkhouser, W., Uematsu, S., Akira, S., Baric, R.S., Heise, M.T., 2008a. MyD88 is required for protection from lethal infection with a mouse-adapted SARS-CoV. PLoS pathogens 4, e1000240.

Sheahan, T., Rockx, B., Donaldson, E., Corti, D., Baric, R., 2008b. Pathways of cross-species transmission of synthetically reconstructed zoonotic severe acute respiratory syndrome coronavirus. J. Virol. 82, 8721-8732.

Sheahan, T., Rockx, B., Donaldson, E., Sims, A., Pickles, R., Corti, D., Baric, R., 2008c. Mechanisms of zoonotic severe acute respiratory syndrome coronavirus host range expansion in human airway epithelium. J. Virol. 82, 2274-2285.

Shen, S., Lin, P.S., Chao, Y.C., Zhang, A., Yang, X., Lim, S.G., Hong, W., Tan, Y.J., 2005. The severe acute respiratory syndrome coronavirus 3a is a novel structural protein. Biochem. Biophys. Res. Commun. 330, 286-292.

Sheppard, P., Kindsvogel, W., Xu, W., Henderson, K., Schlutsmeyer, S., Whitmore, T.E., Kuestner, R., Garrigues, U., Birks, C., Roraback, J., Ostrander, C., Dong, D., Shin, J., Presnell, S., Fox, B., Haldeman, B., Cooper, E., Taft, D., Gilbert, T., Grant, F.J., Tackett, M., Krivan, W., McKnight, G., Clegg, C., Foster, D., Klucher, K.M., 2003. IL-28, IL-29 and their class II cytokine receptor IL-28R. Nat. Immunol. 4, 63-68.

Shieh, W.J., Hsiao, C.H., Paddock, C.D., Guarner, J., Goldsmith, C.S., Tatti, K., Packard, M., Mueller, L., Wu, M.Z., Rollin, P., Su, I.J., Zaki, S.R., 2005. Immunohistochemical, in situ hybridization, and ultrastructural localization of SARS-associated coronavirus in lung of a fatal case of severe acute respiratory syndrome in Taiwan. Hum. Pathol. 36, 303-309.

Silver, P.A., 1991. How proteins enter the nucleus. Cell 64, 489-497.

Siu, K.L., Kok, K.H., Ng, M.H., Poon, V.K., Yuen, K.Y., Zheng, B.J., Jin, D.Y., 2009. Severe acute respiratory syndrome coronavirus M protein inhibits type I interferon production by impeding the formation of TRAF3.TANK.TBK1/IKKepsilon complex. J. Biol. Chem. 284, 16202-16209.

Siu, Y.L., Teoh, K.T., Lo, J., Chan, C.M., Kien, F., Escriou, N., Tsao, S.W., Nicholls, J.M., Altmeyer, R., Peiris, J.S., Bruzzone, R., Nal, B., 2008. The M, E and N structural proteins of the SARS coronavirus are required for efficient assembly, trafficking and release of virus-like particles. J. Virol. 82, 11318-11330.

Sizun, J., Yu, M.W., Talbot, P.J., 2000. Survival of human coronaviruses 229E and OC43 in suspension and after drying onsurfaces: a possible source ofhospital-acquired infections. J. Hosp. Infect. 46, 55-60.

Smits, S.L., de Lang, A., van den Brand, J.M., Leijten, L.M., van, I.W.F., Eijkemans, M.J., van Amerongen, G., Kuiken, T., Andeweg, A.C., Osterhaus, A.D., Haagmans,

B.L., 2010. Exacerbated innate host response to SARS-CoV in aged non-human primates. PLoS pathogens 6, e1000756.

Smits, S.L., van den Brand, J.M., de Lang, A., Leijten, L.M., van Ijcken, W.F., van Amerongen, G., Osterhaus, A.D., Andeweg, A.C., Haagmans, B.L., 2011. Distinct severe acute respiratory syndrome coronavirus-induced acute lung injury pathways in two different nonhuman primate species. J. Virol. 85, 4234-4245.

Smyth, G.K., 2004. Linear models and empirical bayes methods for assessing differential expression in microarray experiments. Stat. Appl. Genet. Mol. Biol. 3, Article3.

Snijder, E.J., Bredenbeek, P.J., Dobbe, J.C., Thiel, V., Ziebuhr, J., Poon, L.L.M., Guan, Y., Rozanov, M., Spaan, W.J.M., Gorbalenya, A.E., 2003. Unique and conserved features of genome and proteome of SARS-coronavirus, an early split-off from the coronavirus group 2 lineage. J. Mol. Biol. 331, 991-1004.

Snijder, E.J., Spaan, W.J.M., 1995. The coronaviruslike superfamily, in: Siddell, S.G. (Ed.), The *Coronaviridae*. Plenum press, New York, pp. 239-252.

Sola, I., Moreno, J.L., Zuñiga, S., Alonso, S., Enjuanes, L., 2005. Role of nucleotides immediately flanking the transcription-regulating sequence core in coronavirus subgenomic mRNA synthesis. J. Virol. 79, 2506-2516.

Song, H.D., Tu, C.C., Zhang, G.W., Wang, S.Y., Zheng, K., Lei, L.C., Chen, Q.X., Gao, Y.W., Zhou, H.Q., Xiang, H., Zheng, H.J., Chern, S.W., Cheng, F., Pan, C.M., Xuan, H., Chen, S.J., Luo, H.M., Zhou, D.H., Liu, Y.F., He, J.F., Qin, P.Z., Li, L.H., Ren, Y.Q., Liang, W.J., Yu, Y.D., Anderson, L., Wang, M., Xu, R.H., Wu, X.W., Zheng, H.Y., Chen, J.D., Liang, G., Gao, Y., Liao, M., Fang, L., Jiang, L.Y., Li, H., Chen, F., Di, B., He, L.J., Lin, J.Y., Tong, S., Kong, X., Du, L., Hao, P., Tang, H., Bernini, A., Yu, X.J., Spiga, O., Guo, Z.M., Pan, H.Y., He, W.Z., Manuguerra, J.C., Fontanet, A., Danchin, A., Niccolai, N., Li, Y.X., Wu, C.I., Zhao, G.P., 2005. Cross-host evolution of severe acute respiratory syndrome coronavirus in palm civet and human. Proc. Natl. Acad. Sci. USA 102, 2430-2435.

Spaller, M.R., 2006. Act globally, think locally: systems biology addresses the PDZ domain. ACS Chem. Biol. 1, 207-210.

Spruth, M., Kistner, O., Savidis-Dacho, H., Hitter, E., Crowe, B., Gerencer, M., Bruhl, P., Grillberger, L., Reiter, M., Tauer, C., Mundt, W., Barrett, P.N., 2006. A double-inactivated whole virus candidate SARS coronavirus vaccine stimulates neutralising and protective antibody responses. Vaccine 24, 652-661.

Strieter, R.M., Belperio, J.A., Keane, M.P., 2002. Cytokines in innate host defense in the lung. J. Clin. Invest. 109, 699-705.

Stroher, U., DiCaro, A., Li, Y., Strong, J.E., Aoki, F., Plummer, F., Jones, S.M., Feldmann, H., 2004. Severe acute respiratory syndrome-related coronavirus is inhibited by interferon- alpha. J. Infect. Dis. 189, 1164-1167.

Subbarao, K., McAuliffe, J., Vogel, L., Fahle, G., Fischer, S., Tatti, K., Packard, M., Shieh, W.J., Zaki, S., Murphy, B., 2004. Prior infection and passive transfer of

neutralizing antibody prevent replication of severe acute respiratory syndrome coronavirus in the respiratory tract of mice. J. Virol. 78, 3572-3577.

Subbarao, K., Roberts, A., 2006. Is there an ideal animal model for SARS? Trends Microbiol. 14, 299-303.

Sui, J., Li, W., Murakami, A., Tamin, A., Matthews, L.J., Wong, S.K., Moore, M.J., Tallarico, A.S., Olurinde, M., Choe, H., Anderson, L.J., Bellini, W.J., Farzan, M., Marasco, W.A., 2004. Potent neutralization of severe acute respiratory syndrome (SARS) coronavirus by a human mAb to S1 protein that blocks receptor association. Proc. Natl. Acad. Sci. USA 101, 2536-2541.

Sun, L., Xing, Y., Chen, X., Zheng, Y., Yang, Y., Nichols, D.B., Clementz, M.A., Banach, B.S., Li, K., Baker, S.C., Chen, Z., 2012. Coronavirus papain-like proteases negatively regulate antiviral innate immune response through disruption of STING-mediated signaling. PloS one 7, e30802.

Tanaka, T., Kamitani, W., DeDiego, M.L., Enjuanes, L., Matsuura, Y., 2012. Severe acute respiratory syndrome coronavirus nsp1 facilitates efficient propagation in cells through a specific translational shutoff of host mRNA. J. Virol. 86, 11128-11137.

Tang, N.L., Chan, P.K., Wong, C.K., To, K.F., Wu, A.K., Sung, Y.M., Hui, D.S., Sung, J.J., Lam, C.W., 2005. Early enhanced expression of interferon-inducible protein-10 (CXCL-10) and other chemokines predicts adverse outcome in severe acute respiratory syndrome. Clin. Chem. 51, 2333-2340.

Teoh, K.T., Siu, Y.L., Chan, W.L., Schluter, M.A., Liu, C.J., Peiris, J.S., Bruzzone, R., Margolis, B., Nal, B., 2010. The SARS coronavirus E protein interacts with PALS1 and alters tight junction formation and epithelial morphogenesis. Mol. Biol. Cell. 21, 3838-3852.

ter Meulen, J., Bakker, A.B., van den Brink, E.N., Weverling, G.J., Martina, B.E., Haagmans, B.L., Kuiken, T., de Kruif, J., Preiser, W., Spaan, W., Gelderblom, H.R., Goudsmit, J., Osterhaus, A.D., 2004. Human monoclonal antibody as prophylaxis for SARS coronavirus infection in ferrets. Lancet 363, 2139-2141.

Thiel, V., Herold, J., Schelle, B., Siddell, S., 2001. Infectious RNA transcribed *in vitro* from a cDNA copy of the human coronavirus genome cloned in vaccinia virus. J. Gen. Virol. 82, 1273-1281.

Thiel, V., Ivanov, K.A., Putics, A., Hertzig, T., Schelle, B., Bayer, S., Wessbrich, B., Snijder, E.J., Rabenau, H., Doerr, H.W., Gorbalenya, A.E., Ziebuhr, J., 2003. Mechanisms and enzymes involved in SARS coronavirus genome expression. J. Gen. Virol. 84, 2305-2315.

Thompson, A.J., Locarnini, S.A., 2007. Toll-like receptors, RIG-I-like RNA helicases and the antiviral innate immune response. Immunol. Cell Biol. 85, 435-445.

Tooze, J., Tooze, S.A., Fuller, S.D., 1987. Sorting of progeny coronavirus from condensed secretory proteins at the exit from the trans-golgi network of atT20 cells. J. Cell Biol. 105, 1215-1226.

Torres, J., Parthasarathy, K., Lin, X., Saravanan, R., Liu, D.X., 2006. Model of a putative pore: the pentameric alpha-helical bundle of SARS coronavirus E protein in lipid bilayers. Biophys. J. 91, 938-947.

Traggiai, E., Becker, S., Subbarao, K., Kolesnikova, L., Uematsu, Y., Gismondo, M.R., Murphy, B.R., Rappuoli, R., Lanzavecchia, A., 2004. An efficient method to make human monoclonal antibodies from memory B cells: potent neutralization of SARS coronavirus. Nat. Med. 10, 871-875.

Tsang, K.W., Ho, P.L., Ooi, G.C., Yee, W.K., Wang, T., Chan-Yeung, M., Lam, W.K., Seto, W.H., Yam, L.Y., Cheung, T.M., Wong, P.C., Lam, B., Ip, M.S., Chan, J., Yuen, K.Y., Lai, K.N., 2003. A cluster of cases of severe acute respiratory syndrome in Hong Kong. N. Engl. J. Med. 348, 1977-1985.

Tseng, C.T., Huang, C., Newman, P., Wang, N., Narayanan, K., Watts, D.M., Makino, S., Packard, M.M., Zaki, S.R., Chan, T.S., Peters, C.J., 2007. Severe acute respiratory syndrome coronavirus infection of mice transgenic for the human Angiotensin-converting enzyme 2 virus receptor. J. Virol. 81, 1162-1173.

Tsui, P.T., Kwok, M.L., Yuen, H., Lai, S.T., 2003. Severe acute respiratory syndrome: clinical outcome and prognostic correlates. Emerg. Infect. Dis. 9, 1064-1069.

Uze, G., Lutfalla, G., Gresser, I., 1990. Genetic transfer of a functional human interferon alpha receptor into mouse cells: cloning and expression of its cDNA. Cell 60, 225-234.

van Boheemen, S., de Graaf, M., Lauber, C., Bestebroer, T.M., Raj, V.S., Zaki, A.M., Osterhaus, A.D., Haagmans, B.L., Gorbalenya, A.E., Snijder, E.J., Fouchier, R.A., 2012. Genomic characterization of a newly discovered coronavirus associated with acute respiratory distress syndrome in humans. mBio 3, e00473-00412.

Van Campen, H., Easterday, B.C., Hinshaw, V.S., 1989. Destruction of lymphocytes by a virulent avian influenza A virus. J. Gen. Virol. 70, 467-472.

Vennema, H., Godeke, G.J., Rossen, J.W.A., Voorhout, W.F., Horzinek, M.C., Opstelten, D.J., Rottier, P.J.M., 1996. Nucleocapsid-independent assembly of coronavirus-like particles by co-expression of viral envelope protein genes. EMBO J. 15, 2020-2028.

Verdia-Baguena, C., Nieto-Torres, J.L., Alcaraz, A., Dediego, M.L., Torres, J., Aguilella, V.M., Enjuanes, L., 2012. Coronavirus E protein forms ion channels with functionally and structurally-involved membrane lipids. Virology 432, 485-494.

von Brunn, A., Teepe, C., Simpson, J.C., Pepperkok, R., Friedel, C.C., Zimmer, R., Roberts, R., Baric, R., Haas, J., 2007. Analysis of Intraviral Protein-Protein Interactions of the SARS Coronavirus ORFeome. PloS one 2, 1-11.

Walker, P.J., Bonami, J.R., Boonsaeng, V., Chang, P.S., Cowley, J.A., Enjuanes, L., Flegel, T.W., Lightner, D.V., Loh, P.C., Snijder, E.J., Tang, K., 2005. *Roniviridae*, in: Fauquet, C.M., Mayo, M.A., Maniloff, J., Desselberger, U., Ball, L.A. (Eds.), Virus Taxonomy. Eighth Report of the International Committee on Taxonomy of Viruses. Academic Press, San Diego, California, pp. 975-979.

Wang, G., Chen, G., Zheng, D., Cheng, G., Tang, H., 2011. PLP2 of mouse hepatitis virus A59 (MHV-A59) targets TBK1 to negatively regulate cellular type I interferon signaling pathway. PloS one 6, e17192.

Wang, Y., Shi, H., Rigolet, P., Wu, N., Zhu, L., Xi, X.G., Vabret, A., Wang, X., Wang, T., 2010. Nsp1 proteins of group I and SARS coronaviruses share structural and functional similarities. Infect. Genet. Evol. 10, 919-924.

Wareing, M.D., Lyon, A., Inglis, C., Giannoni, F., Charo, I., Sarawar, S.R., 2007. Chemokine regulation of the inflammatory response to a low-dose influenza infection in CCR2-/- mice. J. Leukoc. Biol. 81, 793-801.

Wathelet, M.G., Orr, M., Frieman, M.B., Baric, R.S., 2007. Severe acute respiratory syndrome coronavirus evades antiviral signaling: role of nsp1 and rational design of an attenuated strain. J. Virol. 81, 11620-11633.

Williamson, J.S.P., Stohlman, S.A., 1990. Effective clearance of mouse hepatitis virus from the central nervous system requires both CD4+ and CD8+ T cells. J. Virol. 64, 4589-4592.

Wilson, L., McKinlay, C., Gage, P., 2004. SARS coronavirus E protein forms cation-selective ion channels. Virology 330, 322-331.

Wong, C.K., Lam, C.W., Wu, A.K., Ip, W.K., Lee, N.L., Chan, I.H., Lit, L.C., Hui, D.S., Chan, M.H., Chung, S.S., Sung, J.J., 2004a. Plasma inflammatory cytokines and chemokines in severe acute respiratory syndrome. Clin. Exp. Immunol. 136, 95-103.

Wong, R.S., Wu, A., To, K.F., Lee, N., Lam, C.W., Wong, C.K., Chan, P.K., Ng, M.H., Yu, L.M., Hui, D.S., Tam, J.S., Cheng, G., Sung, J.J., 2003. Haematological manifestations in patients with severe acute respiratory syndrome: retrospective analysis. BMJ 326, 1358-1362.

Wong, S.K., Li, W., Moore, M.J., Choe, H., Farzan, M., 2004b. A 193-amino acid fragment of the SARS coronavirus S protein efficiently binds angiotensin-converting enzyme 2. J. Biol. Chem. 279, 3197-3201.

Woo, P.C., Lau, S.K., Tsoi, H.W., Huang, Y., Poon, R.W., Chu, C.M., Lee, R.A., Luk, W.K., Wong, G.K., Wong, B.H., Cheng, V.C., Tang, B.S., Wu, A.K., Yung, R.W., Chen, H., Guan, Y., Chan, K.H., Yuen, K.Y., 2005. Clinical and molecular epidemiological features of coronavirus HKU1-associated community-acquired pneumonia. J. Infect. Dis. 192, 1898-1907.

Wygrecka, M., Jablonska, E., Guenther, A., Preissner, K.T., Markart, P., 2008. Current view on alveolar coagulation and fibrinolysis in acute inflammatory and chronic interstitial lung diseases. Thromb. Haemost. 99, 494-501.

Yan, H., Xiao, G., Zhang, J., Hu, Y., Yuan, F., Cole, D.K., Zheng, C., Gao, G.F., 2004. SARS coronavirus induces apoptosis in Vero E6 cells. J. Med. Virol. 73, 323-331.

Yang, X.H., Deng, W., Tong, Z., Liu, Y.X., Zhang, L.F., Zhu, H., Gao, H., Huang, L., Liu, Y.L., Ma, C.M., Xu, Y.F., Ding, M.X., Deng, H.K., Qin, C., 2007. Mice transgenic

for human angiotensin-converting enzyme 2 provide a model for SARS coronavirus infection. Comp. Med. 57, 450-459.

Yasui, K., Baba, A., Iwasaki, Y., Kubo, T., Aoyama, K., Mori, T., Yamazaki, T., Kobayashi, N., Ishiguro, A., 2005. Neutrophil-mediated inflammation in respiratory syncytial viral bronchiolitis. Pediatr. Int. 47, 190-195.

Ye, J., Zhang, B., Xu, J., Chang, Q., McNutt, M.A., Korteweg, C., Gong, E., Gu, J., 2007a. Molecular Pathology in the Lungs of Severe Acute Respiratory Syndrome Patients. Am. J. Pathol. 170, 538-545.

Ye, Y., Hauns, K., Langland, J.O., Jacobs, B.L., Hogue, B.G., 2007b. Mouse hepatitis coronavirus A59 nucleocapsid protein is a type I interferon antagonist. J. Virol. 81, 2554-2563.

Yoneyama, M., Kikuchi, M., Natsukawa, T., Shinobu, N., Imaizumi, T., Miyagishi, M., Taira, K., Akira, S., Fujita, T., 2004. The RNA helicase RIG-I has an essential function in double-stranded RNA-induced innate antiviral responses. Nat. Immunol. 5, 730-737.

Young, H.A., 1996. Regulation of interferon-gamma gene expression. J. Interferon Cytokine Res. 16, 563-568.

Yount, B., Curtis, K.M., Fritz, E.A., Hensley, L.E., Jahrling, P.B., Prentice, E., Denison, M.R., Geisbert, T.W., Baric, R.S., 2003. Reverse genetics with a full-length infectious cDNA of severe acute respiratory syndrome coronavirus. Proc. Natl. Acad. Sci. USA 100, 12995-13000.

Yount, B., Denison, M.R., Weiss, S.R., Baric, R.S., 2002. Systematic assembly of a full-length infectious cDNA of mouse hepatitis virus strain A59. J. Virol. 76, 11065-11078.

Zampieri, C.A., Sullivan, N.J., Nabel, G.J., 2007. Immunopathology of highly virulent pathogens: insights from Ebola virus. Nat. Immunol. 8, 1159-1164.

Zhang, Q.L., Ding, Y.Q., He, L., Wang, W., Zhang, J.H., Wang, H.J., Cai, J.J., Geng, J., Lu, Y.D., Luo, Y.L., 2003. Detection of cell apoptosis in the pathological tissues of patients with SARS and its significance. Di Yi Jun Yi Da Xue Xue Bao 23, 770-773.

Zhang, Y., 2014. New swine deltacoronavirus (SDCV), p. http://www.ohioagriculture.gov/addl/.

Zhang, Y., Li, J., Zhan, Y., Wu, L., Yu, X., Zhang, W., Ye, L., Xu, S., Sun, R., Wang, Y., Lou, J., 2004. Analysis of serum cytokines in patients with severe acute respiratory syndrome. Infect. Immun. 72, 4410-4415.

Zhao, G.P., 2007. SARS molecular epidemiology: a Chinese fairy tale of controlling an emerging zoonotic disease in the genomics era. Philos. Trans. R. Soc. Lond. B. Biol. Sci. 362, 1063-1081.

Zhao, J., Perlman, S., 2010. T cell responses are required for protection from clinical disease and for virus clearance in severe acute respiratory syndrome coronavirus-infected mice. J. Virol. 84, 9318-9325.

Zhao, J., Van Rooijen, N., Perlman, S., 2009. Evasion by stealth: inefficient immune activation underlies poor T cell response and severe disease in SARS-CoV-infected mice. PLoS pathogens 5, e1000636.

Zhao, L., Rose, K.M., Elliott, R., Van Rooijen, N., Weiss, S.R., 2011. Cell type-specific type I interferon antagonism influences organ tropism of murine coronavirus. J. Virol. 85, 10058-10068.

Zhao, Z., Zhang, F., Xu, M., Huang, K., Zhong, W., Cai, W., Yin, Z., Huang, S., Deng, Z., Wei, M., Xiong, J., Hawkey, P.M., 2003. Description and clinical treatment of an early outbreak of severe acute respiratory syndrome (SARS) in Guangzhou, PR China. J. Med. Microbiol. 52, 715-720.

Zheng, B., He, M.L., Wong, K.L., Lum, C.T., Poon, L.L., Peng, Y., Guan, Y., Lin, M.C., Kung, H.F., 2004. Potent inhibition of SARS-associated coronavirus (SCOV) infection and replication by type I interferons (IFN-alpha/beta) but not by type II interferon (IFN-gamma). J. Interferon Cytokine Res. 24, 388-390.

Zhong, J., Gastaminza, P., Cheng, G., Kapadia, S., Kato, T., Burton, D.R., Wieland, S.F., Uprichard, S.L., Wakita, T., Chisari, F.V., 2005. Robust hepatitis C virus infection in vitro. Proc. Natl. Acad. Sci. USA 102, 9294-9299.

Zhou, J., Wang, W., Zhong, Q., Hou, W., Yang, Z., Xiao, S.Y., Zhu, R., Tang, Z., Wang, Y., Xian, Q., Tang, H., Wen, L., 2005. Immunogenicity, safety, and protective efficacy of an inactivated SARS-associated coronavirus vaccine in rhesus monkeys. Vaccine 23, 3202-3209.

Ziebuhr, J., 2005. The coronavirus replicase, in: Enjuanes, L. (Ed.), Coronavirus replication and reverse genetics. Springer-Verlag, Berlin-Heidelberg, pp. 57-94.

Ziebuhr, J., Snijder, E.J., Gorbalenya, A.E., 2000. Virus-encoded proteinases and proteolytic processing in the *Nidovirales*. J. Gen. Virol. 81, 853-879.

Zuñiga, S., Cruz, J.L., Sola, I., Mateos-Gomez, P.A., Palacio, L., Enjuanes, L., 2010. Coronavirus nucleocapsid protein facilitates template switching and is required for efficient transcription. J. Virol. 84, 2169-2175.

Zuñiga, S., Sola, I., Alonso, S., Enjuanes, L., 2004. Sequence motifs involved in the regulation of discontinuous coronavirus subgenomic RNA synthesis. J. Virol. 78, 980-994.

Zuñiga, S., Sola, I., Moreno, J.L., Sabella, P., Plana-Duran, J., Enjuanes, L., 2007. Coronavirus nucleocapsid protein is an RNA chaperone. Virology 357, 215-227.

Zust, R., Cervantes-Barragan, L., Habjan, M., Maier, R., Neuman, B.W., Ziebuhr, J., Szretter, K.J., Baker, S.C., Barchet, W., Diamond, M.S., Siddell, S.G., Ludewig, B., Thiel, V., 2011. Ribose 2'-O-methylation provides a molecular signature for the distinction of self and non-self mRNA dependent on the RNA sensor Mda5. Nat. Immunol. 12, 137-143.

Zust, R., Cervantes-Barragan, L., Kuri, T., Blakqori, G., Weber, F., Ludewig, B., Thiel, V., 2007. Coronavirus non-structural protein 1 is a major pathogenicity factor: implications for the rational design of coronavirus vaccines. PLoS pathogens 3, e109.

ANEXO

JVI Journals.ASM.org

Severe Acute Respiratory Syndrome Coronaviruses with Mutations in the E Protein Are Attenuated and Promising Vaccine Candidates

Jose A. Regla-Nava,[a] Jose L. Nieto-Torres,[a] Jose M. Jimenez-Guardeño,[a] Raul Fernandez-Delgado,[a] Craig Fett,[b] Carlos Castaño-Rodríguez,[a] Stanley Perlman,[b] Luis Enjuanes,[a] Marta L. DeDiego[a]*

Department of Molecular and Cell Biology, Centro Nacional de Biotecnología (CNB-CSIC), Darwin 3, Campus Universidad Autónoma de Madrid, Madrid, Spain[a]; Department of Microbiology, University of Iowa, Iowa City, Iowa, USA[b]

ABSTRACT

Severe acute respiratory syndrome coronavirus (SARS-CoV) causes a respiratory disease with a mortality rate of 10%. A mouse-adapted SARS-CoV (SARS-CoV-MA15) lacking the envelope (E) protein (rSARS-CoV-MA15-ΔE) is attenuated *in vivo*. To identify E protein regions and host responses that contribute to rSARS-CoV-MA15-ΔE attenuation, several mutants (rSARS-CoV-MA15-E*) containing point mutations or deletions in the amino-terminal or the carboxy-terminal regions of the E protein were generated. Amino acid substitutions in the amino terminus, or deletion of regions in the internal carboxy-terminal region of E protein, led to virus attenuation. Attenuated viruses induced minimal lung injury, diminished limited neutrophil influx, and increased $CD4^+$ and $CD8^+$ T cell counts in the lungs of BALB/c mice, compared to mice infected with the wild-type virus. To analyze the host responses leading to rSARS-CoV-MA15-E* attenuation, differences in gene expression elicited by the native and mutant viruses in the lungs of infected mice were determined. Expression levels of a large number of proinflammatory cytokines associated with lung injury were reduced in the lungs of rSARS-CoV-MA15-E*-infected mice, whereas the levels of anti-inflammatory cytokines were increased, both at the mRNA and protein levels. These results suggested that the reduction in lung inflammation together with a more robust antiviral T cell response contributed to rSARS-CoV-MA15-E* attenuation. The attenuated viruses completely protected mice against challenge with the lethal parental virus, indicating that these viruses are promising vaccine candidates.

IMPORTANCE

Human coronaviruses are important zoonotic pathogens. SARS-CoV caused a worldwide epidemic infecting more than 8,000 people with a mortality of around 10%. Therefore, understanding the virulence mechanisms of this pathogen and developing efficacious vaccines are of high importance to prevent epidemics from this and other human coronaviruses. Previously, we demonstrated that a SARS-CoV lacking the E protein was attenuated *in vivo*. Here, we show that small deletions and modifications within the E protein led to virus attenuation, manifested by minimal lung injury, limited neutrophil influx to the lungs, reduced expression of proinflammatory cytokines, increased anti-inflammatory cytokine levels, and enhanced $CD4^+$ and $CD8^+$ T cell counts *in vivo*, suggesting that these phenomena contribute to virus attenuation. The attenuated mutants fully protected mice from challenge with virulent virus. These studies show that mutations in the E protein are not well tolerated and indicate that this protein is an excellent target for vaccine development.

Coronaviruses (CoVs) are responsible for a wide range of important veterinary and human diseases (1). Severe acute respiratory syndrome (SARS) is caused by a coronavirus (SARS-CoV) that emerged in Guangdong Province, China, causing the 2002-2003 epidemic, and infecting more than 8,000 individuals with a 10% mortality rate (1–5). A novel human coronavirus, Middle East respiratory syndrome coronavirus (MERS-CoV), was isolated from the sputum of a man with pneumonia and renal failure in Jeddah, Saudi Arabia, in 2012 (6, 7). As of 21 November 2014, the WHO confirmed 909 MERS cases, in which 36% of patients died (8). CoVs similar to SARS-CoV and MERS-CoV have been found in bats distributed across the world from which new zoonotic transmissions into human population could occur (9–15). Therefore, understanding the virulence mechanisms of these pathogens and developing efficacious vaccines and therapies are of high importance.

SARS-CoV is an enveloped virus with a single-stranded, positive-sense, 29.7-kb RNA genome (16, 17). The 5′ two-thirds of the genome comprise two overlapping open reading frames, ORF 1a and ORF 1b, encoding two polyproteins, pp1a and pp1ab. In addition, SARS-CoV encodes a set of structural proteins present in all CoVs: spike (S), membrane (M), envelope (E), nucleocapsid (N), and accessory proteins 3a, 6, 7a, 7b, 8a, 8b, and 9b (18).

SARS-CoV E protein is a small integral membrane protein of

Received 12 December 2014 **Accepted** 14 January 2015

Accepted manuscript posted online 21 January 2015

Citation Regla-Nava JA, Nieto-Torres JL, Jimenez-Guardeño JM, Fernandez-Delgado R, Fett C, Castaño-Rodríguez C, Perlman S, Enjuanes L, DeDiego ML. 2015. Severe acute respiratory syndrome coronaviruses with mutations in the E protein are attenuated and promising vaccine candidates. J Virol 89:3870–3887. doi:10.1128/JVI.03566-14.

Editor: T. S. Dermody

Address correspondence to Luis Enjuanes, L.Enjuanes@cnb.csic.es.

* Present address: Marta L. DeDiego, David H. Smith Center for Vaccine Biology and Immunology, University of Rochester Medical Center, Rochester, New York, USA.

doi:10.1128/JVI.03566-14

TABLE 1 Primers used for the generation of rSARS-CoV-MA15-E* protein deletion mutants

E* mutant	PCR no.	Primer	Sequence (5′→3′)
Δ2 mutant, 24 nt[a]	1	E-SARS-25871-VS	CGTTGTACATGGCTATTTCACCG
	1	E-SARS-26278-RS	GGTTTTACTAAACTCACGTTAACAATAAGCGCAGTAAGGATGGCTAGTGTG
	2	E-SARS-26223-VS	GCGCTTATTGTTAACGTGAGTTTAGTAAAACC
	2	E-SARS-28160-RS	CTGAGTGAGCTGTGAACC
Δ3 mutant, 21 nt	1	E-SARS-25871-VS	CGTTGTACATGGCTATTTCACCG
	1	E-SARS-26299-RS	CGCGAGTAGACGTAAACCGTTGGTTTATTGCAGCAGTACGCACACAATCG
	2	E-SARS-26274-VS	AAACCAACGGTTTACGTCTACTCGCG
	2	E-SARS-28160-RS	CTGAGTGAGCTGTGAACC
Δ4 mutant, 18 nt	1	E-SARS-25871-VS	CGTTGTACATGGCTATTTCACCG
	1	E-SARS-26298-RS	CGCGAGTAGACGTAAACCACGTTAACAATATTGCAGCAGTACGC
	2	E-SARS-26248-VS	GCGTACTGCTGCAATATTGTTAACGTGGTTTACGTCTACTCGCG
	2	E-SARS-28160-RS	CTGAGTGAGCTGTGAACC
Δ5 mutant, 36 nt	1	E-SARS-25871-VS	CGTTGTACATGGCTATTTCACCG
	1	E-SARS-26332-RS	GGAACTCCTTCAGAAGAGTTCAGTACTAAACTCACGTTAACAATATTGC
	2	E-SARS-26266-VS	GTTTAGTACTGAACTCTTCTGAAGGAGTTCC
	2	E-SARS-28160-RS	CTGAGTGAGCTGTGAACC
Δ6 mutant, 36 nt	1	E-SARS-25871-VS	CGTTGTACATGGCTATTTCACCG
	1	E-SARS-26379-RS	CCAAACAGAATAATAATAATAGTTAGTTCGTTTAATTTTTAACACGCGAGTAGACGTAAACCG
	2	E-SARS-26296-VS	CGCGTGTTAAAAATTAAACGAACTAACTATTATTATTATTCTGTTTGG
	2	E-SARS-28160-RS	CTGAGTGAGCTGTGAACC

[a] nt, nucleotides.

76 amino acids. This protein contains a short hydrophilic amino terminus, a hydrophobic region, and a hydrophilic carboxy terminus (19). The hydrophobic region forms one amphipathic α-helix that oligomerizes and displays ion channel activity (20–22). E protein is present in small amounts within viral particles but is abundantly synthesized in infected cells (23–25), where it localizes mainly in the endoplasmic reticulum Golgi intermediate compartment (ERGIC), participating in virus morphogenesis and budding (25–27). SARS-CoV lacking the E gene (rSARS-CoV-ΔE) was attenuated *in vivo* (28, 29) and protected against challenge with virulent SARS-CoV (30–32). The E protein is a virulence factor, regulating cell stress response and apoptosis and promoting inflammation (33).

SARS-CoV causes a respiratory illness characterized by acute lung injury (ALI), and its most severe pathological form is acute respiratory distress syndrome (ARDS). These pathological conditions are characterized by diffuse alveolar damage (DAD), pulmonary cellular infiltration, hyaline membrane formation, and edema accumulation, leading to hypoxemia and eventually to death (34–37). SARS-CoV infection induces migration to the lungs of immune cells, such as neutrophils and macrophages, which initiate and amplify the inflammatory response (38, 39). Accordingly, the levels of several proinflammatory cytokines, including gamma interferon (IFN-γ), IFN-inducible protein 10 (IP-10)/CXCL10, monocyte chemoattractant protein 1 (MCP-1)/CCL2, and several interleukins (IL-1β, IL-6, IL-8, and IL-12), are elevated in the lungs and peripheral blood of SARS patients (40–49). This exacerbated inflammatory process correlates with lung injury and a poor outcome. T cells are essential to resolve SARS-CoV infections. T cell responses play a crucial role in SARS-CoV clearance and in protection from clinical disease (50–52). Accordingly, one notable finding in human SARS, associated with an adverse outcome, was the rapid development of lymphopenia, with numbers of $CD4^+$ T cells more severely reduced than those of $CD8^+$ T cells during acute disease (38, 53–56).

The SARS-CoV Urbani strain virus causes no significant disease in wild-type (wt) mice (57). Passage through BALB/c mouse lungs resulted in a mouse-adapted virus (MA15 strain) (57), which upon infection reproduced many aspects of the human disease, such as high virus titers, pathological changes in lungs, viremia, neutrophilia, and lethality (57). We previously showed that rSARS-CoV-MA15-ΔE was attenuated in mice and that immunization with rSARS-CoV-MA15-ΔE completely protected young and aged BALB/c mice against challenge with a lethal dose of MA15 (32, 58). Furthermore, we showed that SARS-CoV E

TABLE 2 TaqMan assays used to analyze the expression of cellular genes by quantitative RT-PCR

Protein name	TaqMan assay[a]	Description
TNF	Mm00443258-ml	Tumor necrosis factor
IL-4	Mm00445259_ml	Interleukin 4
IL-5	Mm00439646_ml	Interleukin 5
IL-6	Mm00446190-ml	Interleukin 6
IL-10	Mm00439614_ml	Interleukin 10
IL-12B	Mm00434174_ml	Interleukin 12B
IL-13	Mm00434204_ml	Interleukin 13
CXCL1/NAP-3	Mm04207460-ml	Neutrophil-activating protein 3
CXCL2/MIP-2	Mm00436450-ml	Macrophage inflammatory protein 2
CXCL10/IP-10	Mm00445235-ml	Interferon-inducible protein 10
CCL2/MCP-1	Mm00441242-ml	Monocyte chemotactic protein 1
CCL3/MIP1A	Mm00441259_gl	Macrophage inflammatory protein 1α
CCL4/MIP1B	Mm00443111_ml	Macrophage inflammatory protein 1β
IFN-γ	Mm01168134-ml	Gamma interferon
TGF-β	Mm01178820_ml	Transforming growth factor beta 1
18S	Mm03928990-gl	Ribosomic RNA 18S

[a] Mm, *Mus musculus*.

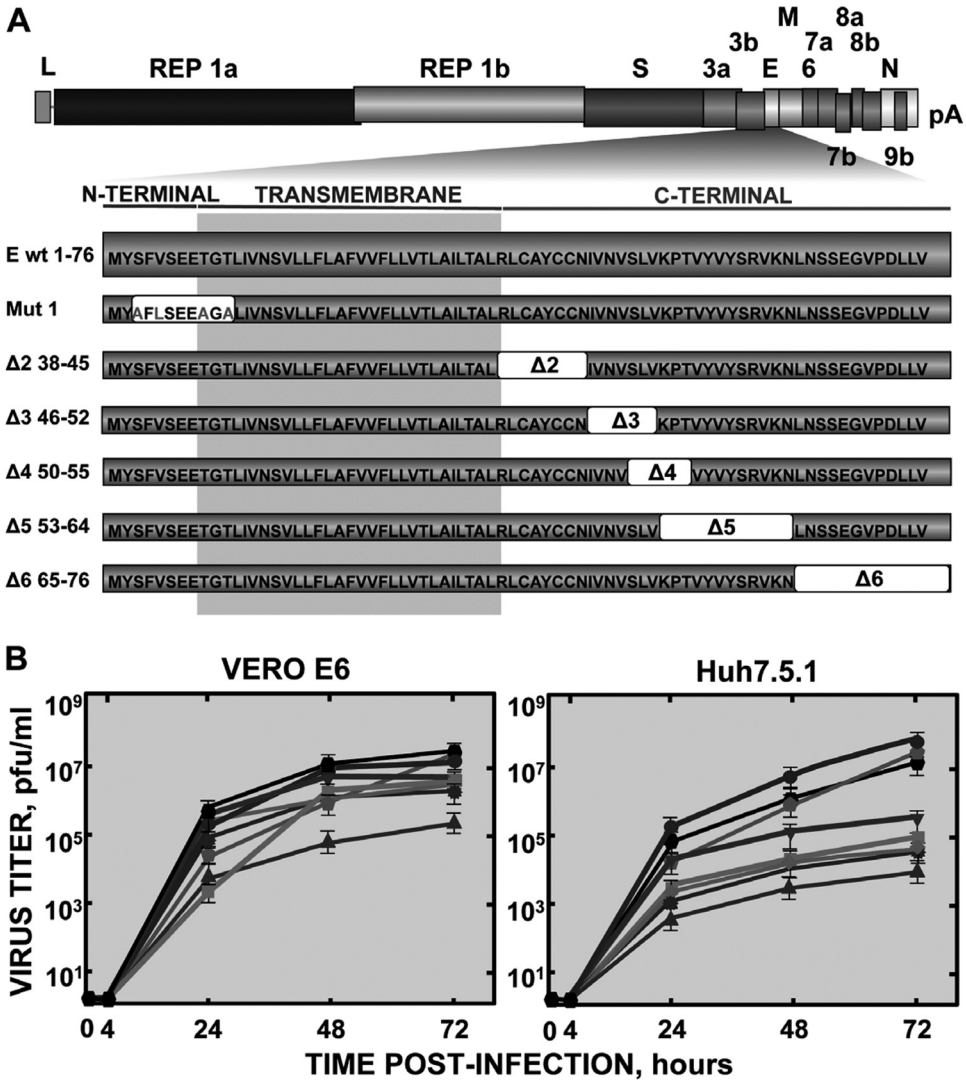

FIG 1 Schematic of mutations and deletions introduced within SARS-CoV E protein and growth kinetics of the mutant viruses (rSARS-CoV-MA15-E*). (A) The SARS-CoV genome is shown in the top, and the expanded region shows the E protein sequence and its different regions. White boxes represent the amino acids deleted within the E protein in each virus. Gray letters indicate the amino acids mutated to change the amino-terminal region of the protein. (B) Mutant virus growth kinetics. Subconfluent monolayers of Vero E6 and Huh7.5.1 cells were infected with wt, ΔE, and rSARS-CoV-MA15-E* viruses at an MOI of 0.001 on Vero E6 cells. Error bars represent standard deviations of the mean using data from three independent experiments. Hexagon, WT; diamond, ΔE; pentagon, Mut 1; triangle, Δ2; star, Δ3; inverted triangle, Δ4; square, Δ5; and circle, Δ6.

protein ion channel activity promoted virus virulence and fitness (37). To identify the E protein regions and the mechanisms leading to SARS-CoV-ΔE attenuation, several mouse-adapted virus mutants encoding amino acid substitutions in the amino terminal or small deletions located in the carboxy-terminal region of the E protein (rSARS-CoV-MA15-E*) were constructed. Amino acid substitutions in the amino terminal, or deletion of regions in the central carboxy-terminal region of E protein, resulted in virus attenuation, accompanied by reductions in lung inflammation, neutrophil influx into the lungs, and proinflammatory cytokine expression. Remarkably, the number of T cells was increased in the lungs of mice infected with the less pathogenic viruses, most probably contributing to their more rapid clearance. Importantly, the attenuated mutants protected against the challenge with the virulent wt virus.

MATERIALS AND METHODS

Cells. Vero E6, BHK, and Huh7.5.1 cells were kindly provided by E. Snijder (University of Leiden, The Netherlands), H. Laude (Unité de Virologie et Immunologie Molecularies, INRA, France), and R. Bartenschlager (Department of Molecular Virology, University of Heidelberg, Germany), respectively, and were propagated as described previously (28).

Viruses. Mouse-adapted SARS-CoV-MA15 (57) was a gift from Kanta Subbarao (National Institutes of Health, Bethesda, MD). Recombinant viruses were rescued from infectious cDNA clones generated in our laboratory (32, 58, 59).

Mice. Specific-pathogen-free BALB/c mice were purchased from the National Cancer Institute at the age of 6 or 16 weeks or from Harlan Laboratories (Holland) at the age of 8 weeks and maintained for 8 additional weeks. All experiments involving SARS-CoV were conducted in biosafety level 3 laboratories in the animal care facility at the University of Iowa or at the Center for Animal Health Research (CISA-INIA, Spain),

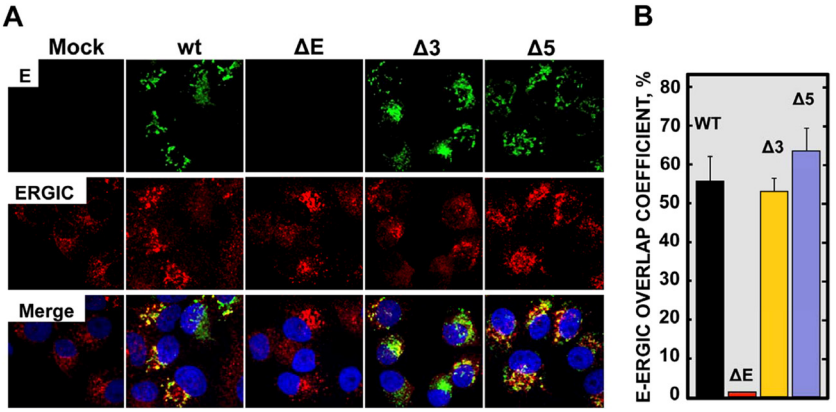

FIG 2 Subcellular localization of mutant E proteins. (A) Vero E6 cells were infected with either rSARS-CoV-MA15-ΔE, -Δ3, or -Δ5 or wt recombinant viruses, at an MOI of 0.3, and fixed at 24 hpi. E protein (green) and ERGIC (red) were labeled with specific antibodies. Nuclei were stained with DAPI (blue). Merge indicates superposition of both labels. Original magnification was ×126. (B) The panel represents the percentage of overlap coefficient between E protein and ERGIC, calculated with Leica LAS AF v2.6.0 software.

equipped with ventilated racks (animal transport unit and biocontainment unit; Allentown, Inc.) to store the animals during the experiment. All the protocols were approved by the EU, by the CISA-INIA Committees of Animal Care Biosecurity and Bioethics, or by the University of Iowa Animal Use and Care Committee. All personnel were equipped with positive-pressure air-purifying respirators (3M HEPA AirMate, St. Paul, MN).

Construction of pBAC-SARS-CoV-MA15-E* plasmids. Mutant viruses (rSARS-CoV-MA15-E*) with amino acid substitutions in the amino-terminal region (rSARS-CoV-MA15-Mut 1) or with small deletions covering different regions of the carboxy terminus of the E protein (rSARS-CoV-MA15-Δ2, -Δ3, -Δ4, -Δ5, and -Δ6) were constructed using an infectious cDNA clone. cDNA encoding the genome of the SARS-CoV-MA15 strain was assembled in a bacterial artificial chromosome (BAC) (pBAC-SARS-CoV-MA15 plasmid) (32, 58). DNA fragments containing nucleotides (nt) 26044 to 26779 of the SARS-CoV genome were generated by overlap extension PCR in the case of the carboxy-terminal mutants, using as the template the pBAC-SARS-CoV-MA15 plasmid and the primers indicated in Table 1, and by gene synthesis (Bio Basic, Inc.) in the case of the amino-terminal mutant. This last fragment included four point mutations, generating four amino acid changes: S3A (TCA to GCA), V5L (GTT to CTT), T9A (ACA to GCA), and T11A (ACG to GCG). The final PCR products or the fragments generated by gene synthesis were digested with the enzymes BamHI and MfeI and cloned into the intermediate plasmid psl1190+BamHI/SacII SARS-CoV to generate plasmids psl1190+BamHI/SacII SARS-CoV-E* (psl1190-Mut 1, Δ2, Δ3, Δ4, Δ5, and Δ6). Plasmid psl1190+BamHI/SacII SARS-CoV contains a fragment corresponding to nucleotides 26045 to 30091 of the SARS-CoV infectious cDNA clone (59) engineered into the psl1190 plasmid (Pharmacia) using unique BamHI and SacII restriction sites. Finally, these fragments were

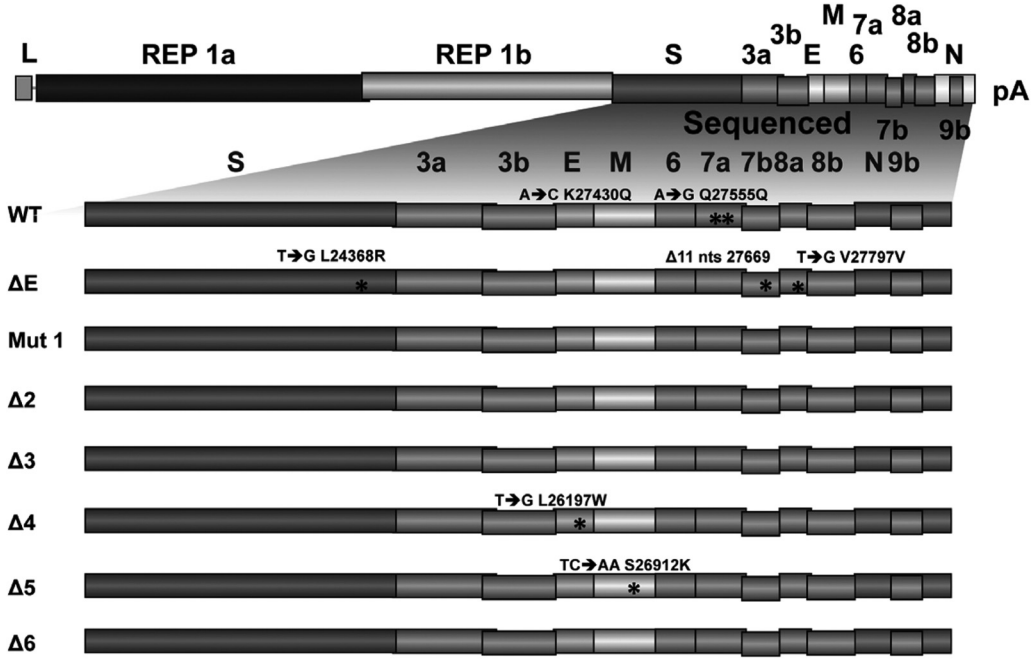

FIG 3 Stability of rSARS-CoV-MA15-E* after serial infections. The stability of rSARS-CoV-MA15-E* virus deletion mutants was examined after 8 passages in Vero E6 cells by sequence analysis. Asterisks denote the presence of nucleotide substitutions.

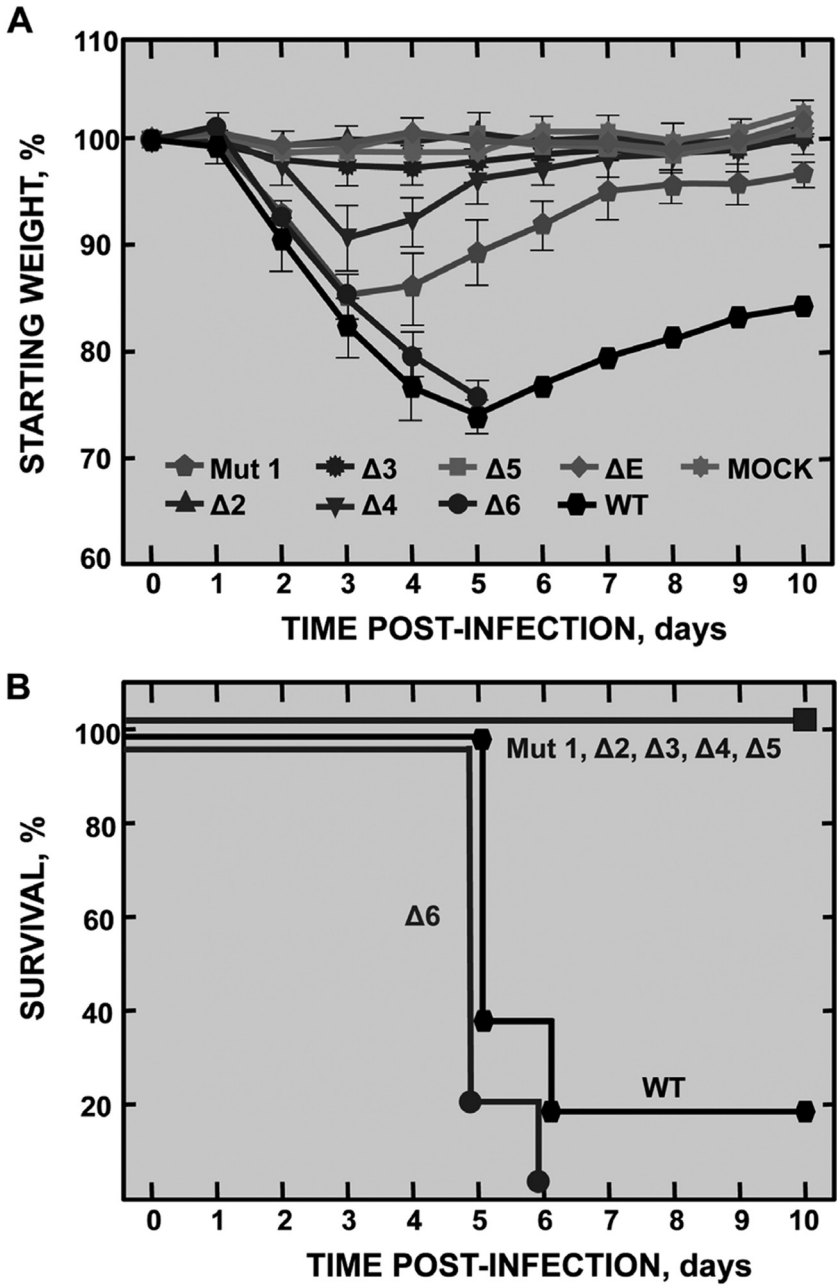

FIG 4 Weight loss and survival rate of mice inoculated with rSARS-CoV-MA15-E* mutants. BALB/c mice were intranasally infected with 1×10^5 PFU of each virus ($n = 5$ mice). Animals were monitored daily for weight loss (A) and survival (B). Animals that lost more than 30% of their initial body weight were euthanized. Differences in weight loss between attenuated and virulent viruses were statistically significant (*, $P < 0.05$).

inserted into pBAC-SARS-CoV-MA15 to generate pBAC-SARS-CoV-MA15-E* plasmids. The viruses were rescued in BHK and Vero E6 cells as previously described (28). Virus was cloned by three rounds of plaque purification.

rSARS-CoV-MA15-E* growth kinetics. Subconfluent monolayers (90% confluence) of Vero E6 or Huh7.5.1 cells were infected at a multiplicity of infection (MOI) of 0.001 with rSARS-CoV-MA15-E*, rSARS-CoV-MA15-ΔE, or rSARS-CoV-MA15. Culture supernatants were collected at the indicated times postinfection, and titers were determined on Vero E6 cells as previously described (28).

Indirect immunofluorescence microscopy. To detect viral E protein expression, Vero E6 cells were grown to 70% confluence on glass coverslips and infected with rSARS-CoV-MA15, rSARS-CoV-MA15-ΔE, and rSARS-CoV-MA15-E* at an MOI of 0.3. At 24 h postinfection (hpi), cells were fixed with 4% paraformaldehyde for 20 min at room temperature. After washing and permeabilization, primary antibody incubations were performed for 90 min at room temperature. Rabbit polyclonal antibody (Ab) specific for E protein (dilution of 1:500; kindly provided by Shen Shuo, Institute of Molecular and Cellular Biology, Singapore) and a mouse anti-ERGIC marker (dilution of 1:200; Alexis Biochemicals) were used. Secondary antibodies specific for rabbit or mice species conjugated to Alexa 488 (for detection of E protein) or Alexa 594 (for detection of ERGIC), respectively (dilution of 1:500; Invitrogen), were incubated for 45 min at room temperature. Nuclei were stained using 4′,6-diamidino-

2-phenylindole (DAPI) (dilution of 1:200; Sigma), and slides were examined on a Leica SP5 confocal microscope (Leica Microsystems).

Specific infectivity of rSARS-CoV-MA15-E* mutants. Subconfluent monolayers (90% confluence) of Vero E6 cells were infected at an MOI of 0.3 with rSARS-CoV-MA15-E*, rSARS-CoV-MA15-ΔE, or rSARS-CoV-MA15. At 8 hpi, the culture medium was harvested and replaced with fresh medium supplemented with 2% fetal bovine serum (FBS). Culture supernatants were collected at 11 hpi ("nascent virus"), and virus titer was determined on Vero E6 cells. Viral RNA was isolated from 400 μl of supernatants using a MagMAX viral RNA isolation kit (Life Technologies) according to the manufacturer's instructions, and genomic RNA was quantified by reverse transcription-quantitative PCR (RT-qPCR) analysis. cDNAs were generated using a high-capacity cDNA transcription kit (Applied Biosystems) and the reverse primer Q-SARS-2015-RS (5′-ATG GCGTCGACAAGACGTAAT-3′). The cDNAs were amplified by qPCR using SYBR green PCR master mix (Applied Biosystems) with forward primer Q-SARS-1931-VS (5′-ACCACTCAATTCCTGATTTGCA-3′) and Q-SARS-2015-RS. The ratio of infectious virus titer to genomic RNA represents the specific infectivity.

Cycloheximide chase to estimate the half-life of rSARS-CoV-MA15-E* mutants. Subconfluent monolayers (90% confluence) of Vero E6 cells were infected with the wt or rSARS-CoV-MA15-E* virus at an MOI of 0.3. At 12 hpi, the cells were treated with 200 μg/ml cycloheximide (Sigma). Cells were harvested at 0, 2, 4, 6, and 8 h, and cell extracts were prepared as previously described (60). Samples were analyzed by sodium dodecyl sulfate-polyacrylamide gel electrophoresis (SDS-PAGE) and Western blotting. In fact, E protein half-life measurements were obtained by calculating E protein relative mass normalized to actin mass for each time point.

Western blot analysis. Cell lysates were resolved by SDS-PAGE, transferred to a nitrocellulose membrane by wet immunotransfer, and processed for Western blotting. The blots were probed with a rabbit polyclonal Ab specific for E protein (dilution of 1:6,000; kindly provided by Shen Shuo, Institute of Molecular and Cellular Biology, Singapore), a monoclonal Ab specific for hemagglutinin (HA) tag (dilution of 1:1,000; Sigma), or an antibody specific for β-actin (dilution of 1:10,000; Abcam). Bound antibodies were detected with horseradish peroxidase-conjugated goat anti-rabbit or anti-mouse antibodies (dilution of 1:30,000; Cappel) and the Immobilon Western chemiluminescent substrate (Millipore). The blots were quantitated by phosphorimaging. The half-life of each E protein mutant was calculated by plotting the signal intensity (ratio of band intensity).

Plasmids. The pcDNA3-E plasmid encoding SARS-CoV E protein was used as previously described (25). To construct a pcDNA3 plasmid encoding the viral M protein fused to an HA tag (pcDNA3-HA-M), primers M-EcoRI-HA-VS (5′-GCGCGCGCGAATTCGCCGCCATGTACCC ATACGATGTTCCAGATTACGCTGCAGACAACGGTACTATTACCG TTGAG-3′, encoding an HA sequence) and M-XhoI-RS (5′-CGCGCTC GAGTTACTGTACTAGCAAAGCAATATTGTC-3′) were used. GAATTC and CTCGAG are the recognition sequences for EcoRI and XhoI, respectively. A DNA fragment encoding the SARS-CoV M protein was generated using as the template the plasmid pBAC-SARS-CoV-MA15. To generate pcDNA3 plasmids encoding the E protein with deletions (pcDNA3-E-Δ3), primers Δ-EcoRI-VS (5′-GCGCGCGCGAATTCGCCGCCATGTA CTCATTCGTTTCGGAAGAAACAG-3′) and Δ-XhoI-RS (5′-CGCGCTCGAGTTAGACCAGAAGATCAGGAACTCCTTCAGAA GAGTT-3′) were used to amplify the DNA fragment encoding the SARS-CoV E deletion proteins using as the template plasmids pBAC-SARS-CoV-MA15-E* with the appropriate deletion. After PCR, these DNA fragments were digested by restriction enzymes EcoRI and XhoI and cloned into pcDNA3-E. All expression plasmids were verified by sequencing.

Immunoprecipitation assay. Vero E6 cells were grown to 90% confluence and cotransfected with a plasmid encoding an N-terminal HA-tagged M protein (pcDNA3-HA-M), combined with plasmids expressing the full-length E protein or E protein with small deletions (pcDNA3-E or pcDNA-E-Δ3). Cells cotransfected with the plasmid pcDNA3-HA-M and the empty plasmid pcDNA3, lacking the coding region of E protein, were used as controls. Twenty-four hours later, cell extracts were collected as previously described (60). For immunoprecipitation assays, monoclonal anti-HA agarose-conjugated clone HA-7 (Sigma) was used by following the manufacturer's instructions. Briefly, 75 μl of the anti-HA agarose conjugate was incubated with the cell extracts overnight at 4°C. Immune complexes were eluted using 20 μl 2× SDS sample buffer and heating at 95°C for 3 min. Analysis of precipitated complexes was carried out by SDS-PAGE and Western blotting.

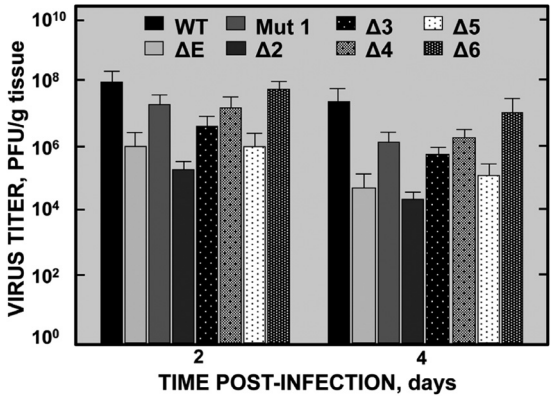

FIG 5 rSARS-CoV-MA15-E* growth in the lungs of infected mice. BALB/c mice were intranasally inoculated with 1×10^5 PFU of the indicated viruses. At 2 and 4 days p.i., lung tissue was harvested and viral titers were analyzed in Vero E6 cell monolayers. Means and standard deviations are shown ($n = 3$ mice).

Virus infection and titration in mice. BALB/c mice were anesthetized with isoflurane and intranasally inoculated with 1×10^5 PFU of virus in 50 μl of Dulbecco's modified Eagle's medium (DMEM). For protection experiments, mice were immunized intranasally with 6×10^3 PFU of the attenuated viruses and then challenged with an intranasal inoculation of 1×10^5 PFU of rSARS-CoV-MA15 at 21 days postimmunization. Mice were monitored daily for weight loss and mortality. SARS-CoV-MA15 titers were measured in Vero E6 cells as described above. Viral titers were expressed as PFU/g tissue.

Histopathologic examination of infected mouse lungs. Lungs were removed from infected mice, fixed in zinc formalin, and paraffin embedded. Sections were stained with hematoxylin and eosin.

RNA analysis by RT-qPCR. BALB/c mice were intranasally inoculated with 1×10^5 PFU of the corresponding virus or DMEM, as a control. Lungs were removed and incubated in RNAlater (Ambion) at 4°C for 24 h, prior to freezing at −80°C. Total RNA was extracted using an RNeasy minikit (Qiagen). Reverse transcription (RT) reactions were performed at 37°C for 2 h using the high-capacity cDNA transcription kit (Applied Biosystems) to generate cDNAs. qPCRs were performed using TaqMan gene expression assays (Applied Biosystems) specific for murine genes (Table 2). Quantification was achieved using the $2^{-\Delta\Delta CT}$ method (61). The data represent the average of duplicate measurements from three independent mice.

Microarray analysis. Lungs from infected mice were collected at 2 days postinfection (p.i.), and total RNA was extracted using an RNeasy minikit (Qiagen). Total RNA from three different lungs was independently hybridized for each transcriptomic comparison. A total of 200 ng of RNA was amplified using a one-color low-input Quick Amp labeling kit (Agilent Technologies) and further purified with an RNeasy minikit (Qiagen). Preparation of probes and hybridization were performed as described in *One-Color Microarray-Based Gene Expression Analysis*, version 6.5 (62). Images were captured with an Agilent microarray scanner, and spots were quantified using feature extraction software (Agilent Tech-

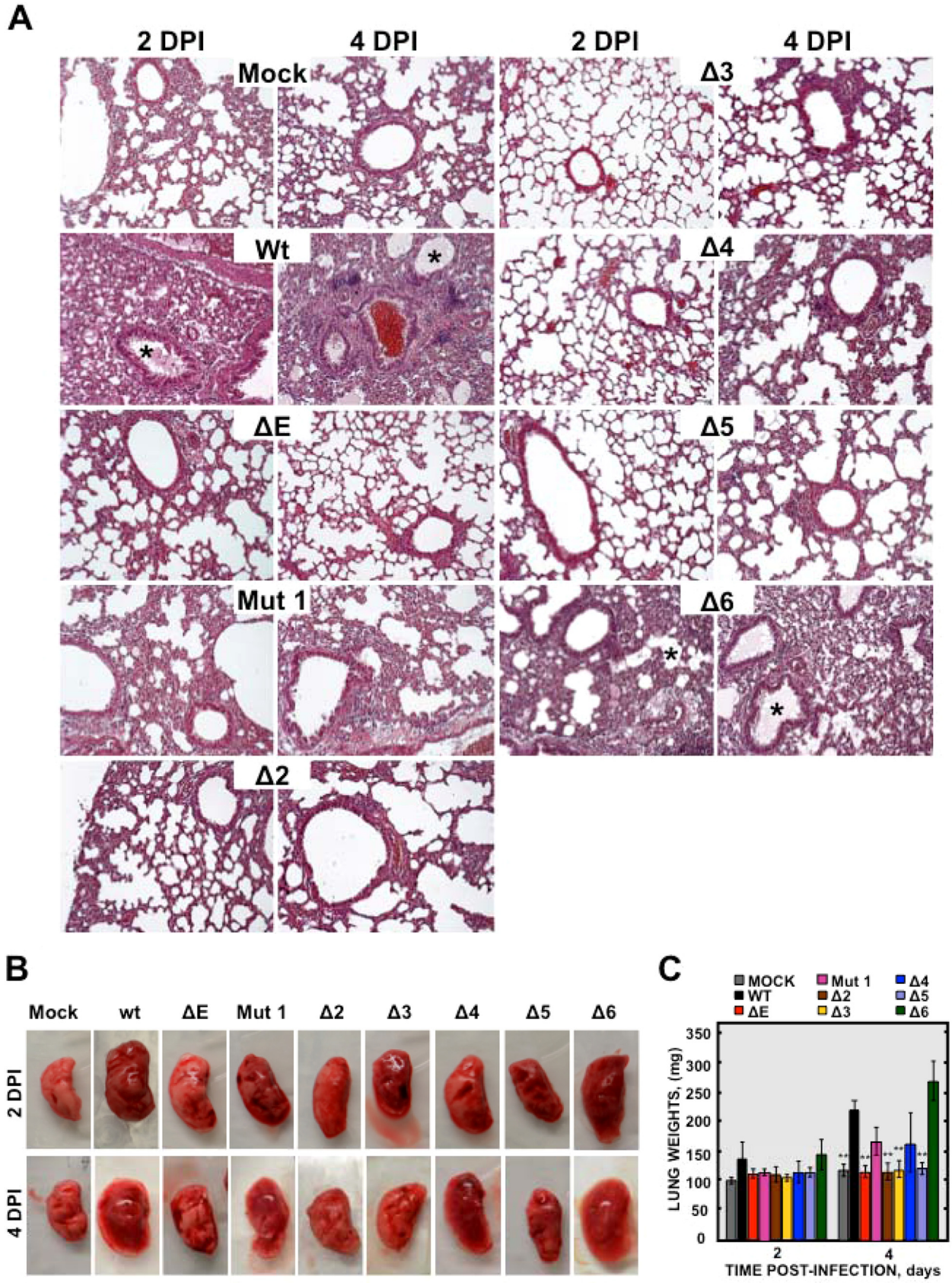

FIG 6 Lung pathology caused by infection with rSARS-CoV-MA15-E* mutants. BALB/c mice were intranasally inoculated with 1×10^5 PFU of the indicated SARS-CoV deletion mutants and sacrificed at days 2 and 4 p.i. (A) Lungs were removed and sections were prepared and stained with hematoxylin and eosin. Asterisks indicate edema accumulation in both bronchiolar and alveolar airways. Original magnification was ×20. Representative images are shown. (B) Macroscopic lung pathology in rSARS-CoV-MA15-E*-infected mice. Representative images of lung gross pathology. (C) Lung weight. Three lungs were evaluated in each case ($n = 3$ mice). Statistically significant data compared to mice infected with the wt virus are indicated (**, $P < 0.01$).

nologies). Background correction and normalization of expression data were performed using linear models for microarray data (LIMMA) (63).

Microarray data analysis. Linear model methods were used for determining differentially expressed genes. Each probe was tested for changes in expression over replicates by using an empirical Bayes moderated *t* statistic (64). To control the false discovery rate (FDR), *P* values were corrected by using the method of Benjamini and Hochberg (64). The expected false discovery rate was controlled to be less than 5%. Genes were considered differentially expressed when the FDRs were <0.05 and fold changes were >2 or <-2.

Measurement of leukocytes in the mouse lungs. Sixteen-week-old BALB/c mice were infected as indicated above with 1×10^5 PFU of each virus. Lungs were removed from mice at 4 days p.i., and cells were prepared as previously described (51). The numbers of macrophages, neutrophils, and CD4 and CD8 T cells were determined as previously described (32, 58).

Cytokine multiplex analysis. Lungs from infected mice were homogenized and nuclear, cytoplasmic, and extracellular proteins were extracted using a nuclear extract kit (Active Motif, Carlsbad, CA). Supernatant proteins (cytoplasmic and extracellular proteins) were diluted 1:5 in assay diluent (Millipore) prior to analysis. The expression of tumor necrosis factor (TNF), MCP-1/CCL2, KC/CXCL1, IL-5, IL-6, IL-13, IFN-γ, macrophage inflammatory protein 1α (MIP-1α)/CCL3, and MIP-1β/CCL4 was determined as previously described (58).

Statistical analysis. Student's *t* test was used to analyze differences in mean values between groups. All results are expressed as means ± standard errors of the means (SEM). *P* values of <0.05 were considered statistically significant.

Microarray data accession number. MIAME-compliant results of the microarrays have been deposited in the Gene Expression Omnibus database (GEO [National Center for Biotechnology Information], accession code GSE59185).

RESULTS

Generation, growth, and characterization of rSARS-CoV-MA15-E* viruses. To identify the E protein regions responsible for rSARS-CoV-ΔE attenuation, a set of mutant viruses (rSARS-CoV-MA15-E*) were generated (Fig. 1A). In rSARS-CoV-MA15-Mut 1, the E protein amino-terminal region was modified by introducing point mutations, instead of deleting amino acids, in order to maintain unaltered the primary sequence of the 3b protein, as 3b and E genes partially overlap. Sequential or partially overlapping small deletions of 6 to 12 amino acids were introduced in the carboxy-terminal region of E protein to generate rSARS-CoV-MA15-Δ2, -Δ3, -Δ4, -Δ5, and -Δ6. The engineered viruses were rescued in Vero E6 cells, cloned by three rounds of plaque purification, and sequenced to confirm the presence of the desired mutations. Mutant E* and wt proteins were similarly localized within infected cells as determined by immunofluorescence by using antibodies specific for the E protein (Fig. 2 and data not shown). All the mutant E proteins partially colocalized with the ERGIC marker as previously observed for the full-length protein (25). These data indicated that none of the regions deleted were essential for the subcellular localization of E protein and that E protein functions that were associated with its localization were not affected. SARS-CoV E protein promotes virus production since elimination of the E gene decreases virus growth from 10- to 100-fold, depending on the cell type (28). To delimit E protein regions involved in SARS-CoV production, growth kinetics of rSARS-CoV-MA15-E* were analyzed in Vero E6 and Huh7.5.1-infected cells (Fig. 1B). Maximum viral titers were observed at 48 to 72 hpi in Vero E6 cells and at 72 hpi in Huh7.5.1 cells, for all the viruses. Mut 1 and Δ6 viruses reached peak titers ($>10^7$ PFU/ml) similar to those observed for rSARS-CoV-MA15 in both cell lines. In contrast, the Δ3 and Δ5 viruses grew to lower titers (around 10^6 and 10^5 PFU/ml in Vero E6 and Huh7.5.1 cells, respectively), similar to those observed for virus lacking full-length E protein (ΔE). The Δ4 virus grew to titers intermediate between titers of the wt and ΔE viruses, reaching titers close to 10^7 and 10^6 PFU/ml in Vero E6 and Huh7.5.1 cells, respectively. The Δ2 virus showed the lowest titers (10^5 and 10^4 PFU/ml in Vero E6 and Huh7.5.1 cells, respectively). These data indicated that deletion of SARS-CoV E protein regions 2, 3, and 5 reduced virus growth to the same extent that the deletion of full-length E protein did, suggesting that these regions themselves were essential for E protein function. In a subsequent experiment, we studied the Δ3 and Δ5 viruses, because viruses grew to titers similar to those of rSARS-CoV-MA15-ΔE.

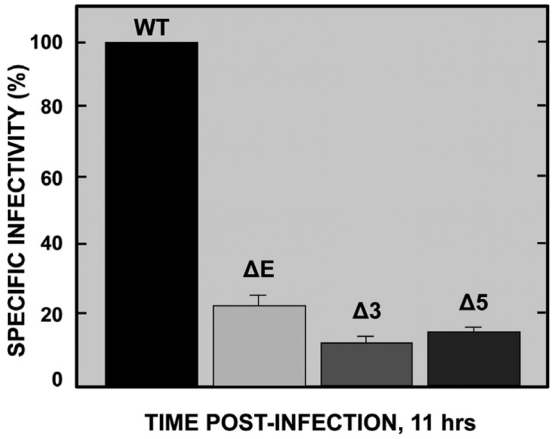

FIG 7 Specific infectivity of rSARS-CoV-MA15-E* mutants. Vero E6 cells were independently infected with each of the rSARS-CoV-MA15-ΔE, -Δ3, and -Δ5 and wt viruses, at an MOI of 0.3. At 8 hpi, the culture medium was harvested and replaced with fresh medium supplemented with 2% FBS. Cell supernatants were collected at 11 hpi ("nascent virus"), and the levels of genomic RNA and infectious virus titer were analyzed by RT-qPCR and plaque assay, respectively. The ratio of infectious virus titer (PFU/ml) to genomic RNA is depicted in the graph as percentage of specific infectivity. Means and standard deviations are shown ($n = 3$ mice).

Stability of rSARS-CoV-MA15-E* mutants in cell cultures. Prior to analyzing the virulence of rSARS-CoV-MA15-E*, their stability in cell culture was examined. The viruses were passaged daily 8 times in Vero E6 cells, followed by sequencing of the distal third of the genome, encompassing the S gene to the 3′ end. Only minor changes were detected in the viral sequences of one representative isolate, suggesting that these viruses were in general genetically stable, at least in tissue culture (Fig. 3). To analyze whether the mutations that the viruses incorporate after growing them in tissue culture cells are compensatory mutations, growth kinetics of the original and passaged viruses were compared by infecting Vero E6 and Huh7.5.1 cells and analyzing virus titers at different times postinfection. No significant differences in the production of infectious viruses were observed among the passaged viruses and the original viruses (data not shown), suggesting that the mutations that the viruses incorporate after growing them in cell culture are not compensatory mutations.

Virulence of rSARS-CoV-MA15-E* mutants. It was previously shown that a SARS-CoV lacking the full-length E protein was fully attenuated *in vivo* (28, 29, 32, 58). To evaluate the relevance of E protein regions in virus virulence, BALB/c mice were

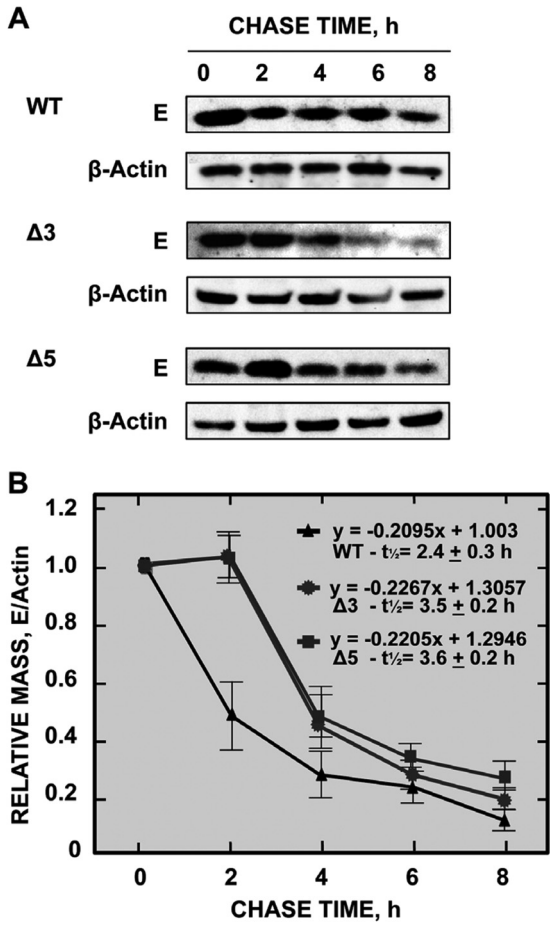

FIG 8 E protein stability of rSARS-CoV-MA15* mutants. Stability of E protein deletion mutants was evaluated in relation to that of the full-length E protein after infection of Vero E6 cells with rSARS-CoV-MA15-E* mutants. At 12 hpi, the cells were treated with cycloheximide. Cells were harvested at the indicated times, and the amount of E protein mutants was determined by Western blotting. (A) Membranes were probed with anti-E protein and with β-actin-specific antibodies as a loading control. (B) The graph represents the values obtained after densitometry analysis. The percentage of protein remaining after cycloheximide addition is represented. Bars represent standard deviations of the mean ($n = 3$ mice).

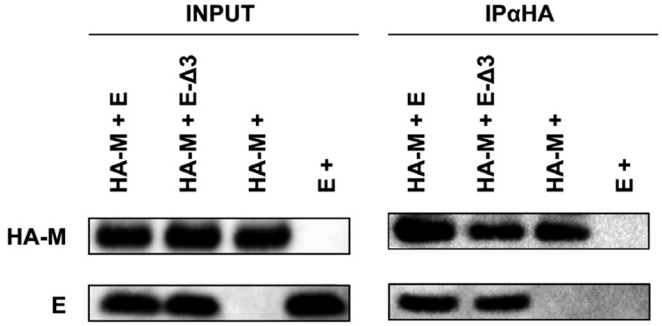

FIG 9 Interaction of SARS-CoV E protein deletion mutants with M protein. Vero E6 cells were cotransfected with a plasmid pcDNA3 encoding the N-terminal HA-tagged M protein, combined with plasmids expressing the E-wt protein or the E protein with a small deletion, E-Δ3. Cotransfections of a plasmid encoding HA-M protein and of a plasmid without E protein were used as controls. Cells were lysed and analyzed by Western blotting with specific antibodies for the E protein and HA (left) or subjected to immunoprecipitation with the monoclonal HA-specific antibody. The presence of E and M proteins was analyzed in the precipitated fractions using E- or HA-specific antibodies (right).

mock infected or infected with rSARS-CoV-MA15-E*, rSARS-CoV-MA15-ΔE, and rSARS-CoV-MA15. Clinical disease and survival were evaluated for 10 days. Mice infected with the parental virus showed disease symptoms from 2 days p.i., reflected by lethargy and ruffled fur. These mice rapidly lost weight, and 80% of them died by day 6 (Fig. 4). Animals infected with Δ6 virus, carrying a deletion in the last segment of the E protein, lost weight and died in a fashion similar to those inoculated with the wild-type virus (Fig. 4). In contrast, mice infected with Δ2, Δ3, Δ5, and ΔE viruses showed no signs of disease (data not shown), did not significantly lose weight, and uniformly survived (Fig. 4). Mice infected with the Mut 1 and Δ4 viruses lost 15% and 10% of their initial weight, respectively, but recovered from 3 days p.i., and all of them survived (Fig. 4). These data showed that E protein regions 1 and 4 and especially 2, 3, and 5 were required to maintain the optimal replication or virulence of SARS-CoV.

rSARS-CoV-MA15-E* growth *in vivo*. To evaluate whether any of the E protein regions were required for optimal virus growth *in vivo*, BALB/c mice were infected with rSARS-CoV-MA15-E*, rSARS-CoV-MA15-ΔE, or rSARS-CoV-MA15, and viral titers in lungs were determined at 2 and 4 days p.i. (Fig. 5). Peak titers were reached by all viruses at 2 days p.i. and decreased around 5- to 20-fold at 4 days p.i. in all cases. The parental virus showed the highest titers, 8×10^7 PFU/g of lung tissue at day 2 and 5×10^7 PFU/g at day 4. Titers were reduced when E protein was fully eliminated (10^6 PFU/g at day 2 and 5×10^4 PFU/g at day 4), confirming that rSARS-CoV-MA15-ΔE replicated less robustly in mice. rSARS-CoV-MA15-Δ6 grew to 7×10^7 PFU/g at 2 days p.i. and 10^7 PFU/g at 4 days p.i., similarly to the wt virus (Fig. 5), indicating that E protein carboxy terminus region 6 is the least relevant for optimal *in vivo* growth. The Δ2 and Δ5 viruses grew to titers similar to those observed for the ΔE virus, or even lower. In contrast, the Mut 1, Δ3, and Δ4 viruses grew to intermediate titers (10^7 PFU/g and 10^6 PFU/g at days 2 and 4, respectively) in lungs. These results are similar to those observed in tissue culture cells and showed that especially regions 2 and 5 of SARS-CoV E protein are required for optimal virus growth.

Lung pathology in rSARS-CoV-MA15-E*-infected mice. To analyze the mechanisms leading to rSARS-CoV-MA15-E* attenuation, macroscopic and microscopic changes in the lungs of infected mice were analyzed at 2 and 4 days p.i. (Fig. 6). The lungs from animals infected with the wt or Δ6 viruses but not ΔE, Mut 1, Δ2, Δ3, Δ4, and Δ5 viruses were increased in volume and were dusky red. Profuse areas of hemorrhage and weight increase, possibly due to leukocyte infiltration and edema accumulation, were especially evident at 4 days p.i. (Fig. 6B and C). In contrast, histological examination of lungs from ΔE, Mut 1, Δ2, Δ3, Δ4, and Δ5 virus-infected mice revealed only a small amount of lung damage and cellular infiltration, whereas examination of lungs infected with wt or Δ6 virus showed substantial lung damage characterized by peribronchial/perivascular inflammatory cell infiltration, edema, and thickening of the alveolar walls at 2 and 4 days p.i. (Fig. 6A). These data demonstrated that E protein regions 1, 2, 3, 4, and 5 contribute to the lung damage induced after SARS-CoV infection.

Specific infectivity and half-life of rSARS-CoV-MA15-E* mutants. In order to investigate whether the different small dele-

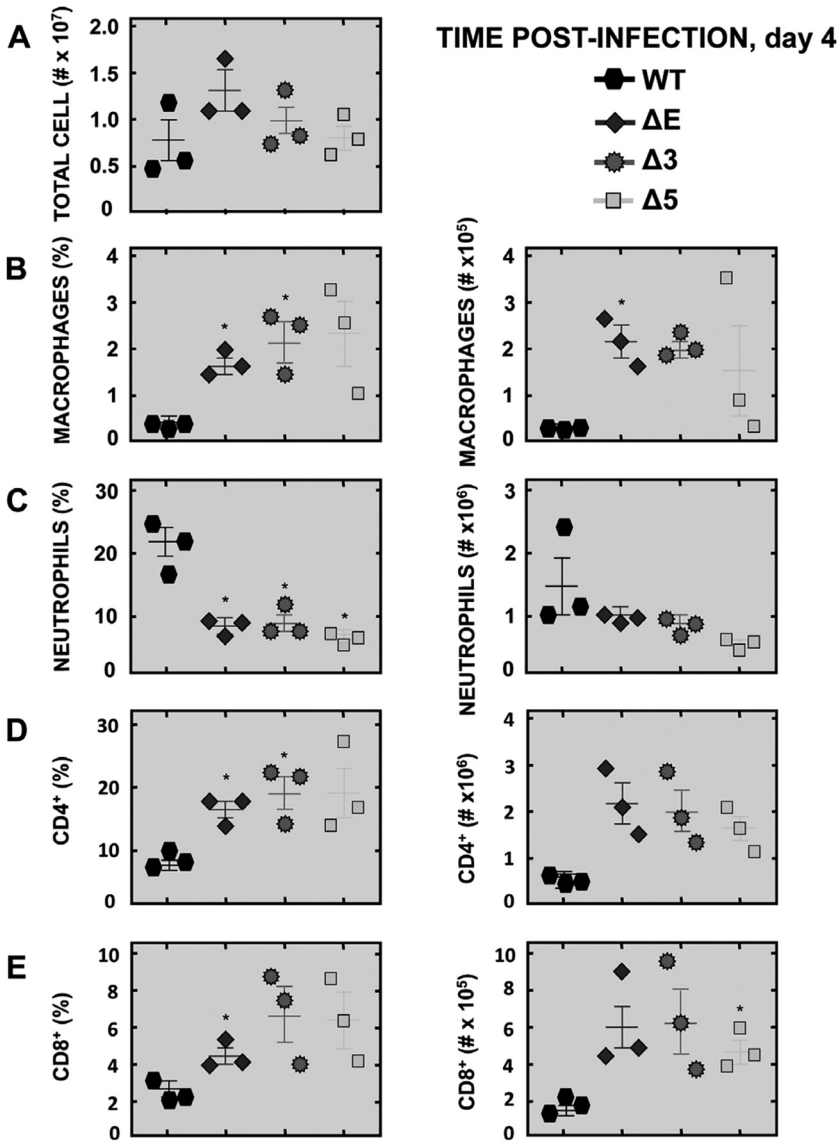

FIG 10 Leukocyte infiltrates present in the lungs of rSARS-CoV-MA15-E*-infected mice. BALB/c mice were intranasally infected with 1×10^5 PFU of the indicated SARS-CoV deletion mutants and sacrificed at 4 days p.i. The total number of leukocytes (A) and total numbers and percentages of macrophages (B), neutrophils (C), $CD4^+$ T cells (D), and $CD8^+$ T cells (E) were determined. Error bars represent the standard deviations of the means. Data are representative of three independent experiments ($n = 3$ mice). Statistically significant differences compared to infection with the wt virus are indicated (*, $P < 0.05$).

tions within the E protein altered virus-specific infectivity, the titers of extracellular rSARS-CoV-MA15-wt, -ΔE, -Δ3, and -Δ5 viruses were compared to the level of the corresponding extracellular genomic RNA. The specific infectivities of rSARS-CoV-MA15-ΔE, -Δ3, and -Δ5 mutants were lower (21%, 11%, and 17%, respectively) than that of the wt virus (Fig. 7). Thus, introducing small deletions or modifications within E protein decreases the infectivity of the particles, probably contributing to the lower titers observed for the rSARS-CoV-MA15-ΔE, -Δ3, and -Δ5 mutants.

To analyze whether the small deletions introduced in the E protein changed its stability, cellular translation was inhibited with cycloheximide, and the degradation of E protein was analyzed by Western blotting. The half-lives of the E proteins encoded by the rSARS-CoV-MA15-Δ3 and -Δ5 virus mutants were longer (3.5 h and 3.6 h, respectively) than that of the wt E protein, which had a half-life of 2.4 h, in agreement with previous results (65) (Fig. 8). The fact that wild-type E protein has a shorter half-life can be explained, because this protein is more abundantly expressed at early times compared to mutant proteins. These results suggest that the introduction of small deletions within the E protein modestly alter the stability of the protein.

Binding between E protein and M protein. The interactions between SARS-CoV E and M proteins play an essential role in the viral particle assembly (66–68). Based on this observation, and on the result showing that the rSARS-CoV-MA15-Δ3 and -Δ5 viruses grew to lower titers than those for wt virus in cell cultures, the interaction between the E-Δ3 deletion protein and the M protein was analyzed. To this end, an HA-tagged, full-length M protein and E-Δ3 deletion protein were coexpressed in Vero E6 cells by

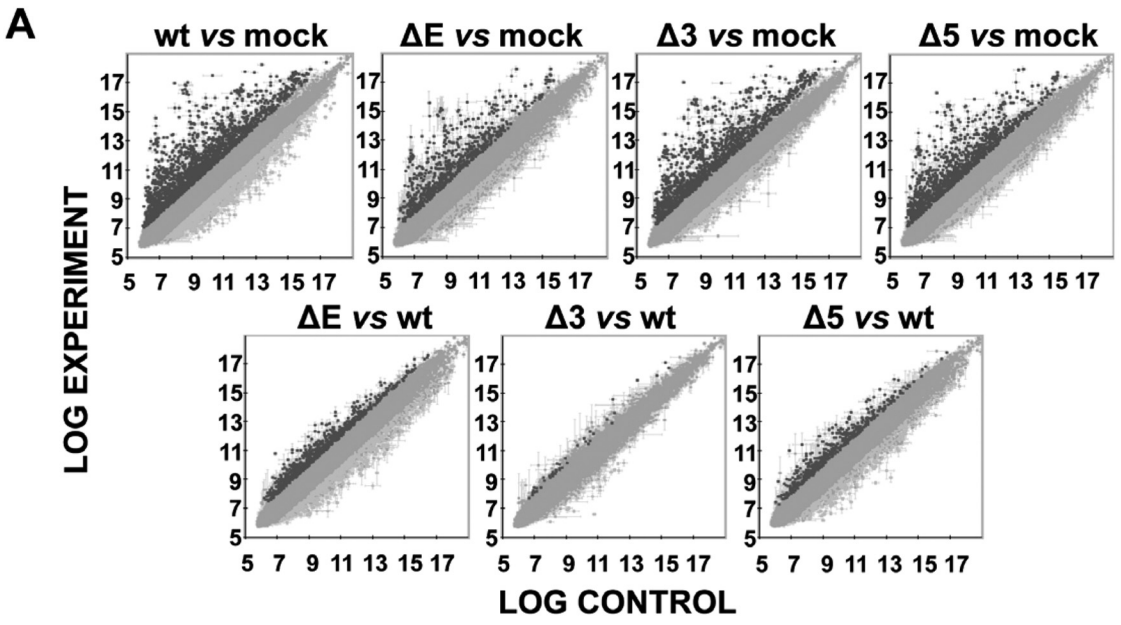

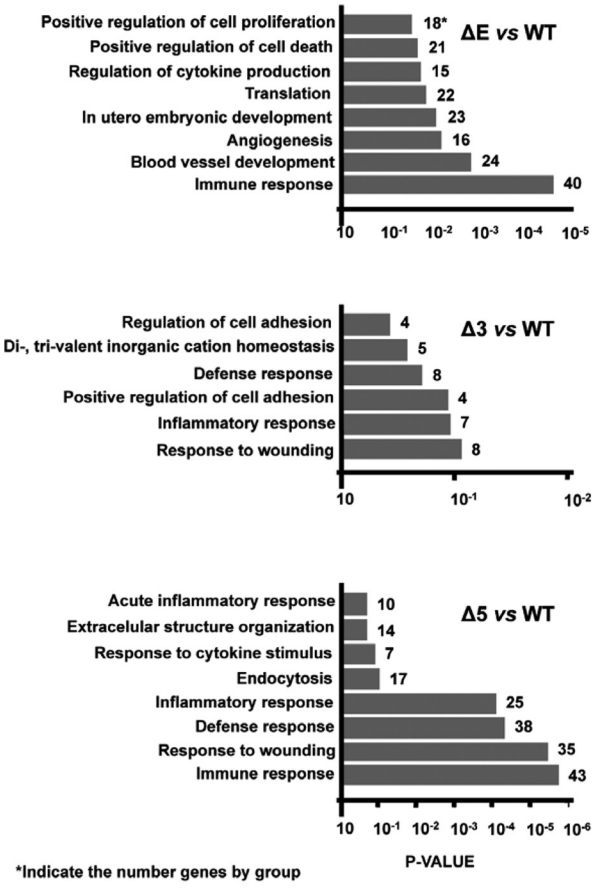

C

GENE	FOLD CHANGE ΔE vs WT	Δ3 vs WT	Δ5 vs WT
INFLAMMATION			
CXCL5 (Ena-78/Lix)	-1.9	-3.9	+1.6
CCL4 (Mip-1b)*	-2.4	-2.6	-1.2
CCL19	-2.8	-2.1	-1.7
CXCL2 (Il8rb)*	-2.8	-2.7	-2.2
CCL3 (Mip-1a)*	-2.9	-3.0	-2.5
NFKB2	-3.2	-1.5	-3.5
CX3CL1	-3.5	-1.2	-2.0
TNF*	-3.4	-2.5	-3.3
CCL2 (Mcp-1)*	-3.8	-2.5	-2.9
CXCL9 (Mig)	-4.7	-3.2	-3.9
CXCL13	-5.9	-2.5	-4.5
IL10	-2.2	-2.1	-2.5
CXCL1 (Il8ra)*	-2.5	-4.8	-2.1
CSF3 (GCSF)	-2.2	-2.1	-2.3
CXCL10 (Inp10)*	-3.1	-1.8	-1.8
PTX3	-4.2	-2.1	-2.5
IL6*	-2.5	-1.8	-1.3
IL4*	+2.7	+1.2	+2.5
IL13*	+2.7	+1.0	+2.7
IMMUNE RESPONSE			
IL5*	+4.4	+1.4	+6.4
IL12B*	-3.9	-2.3	-3.6
IFN RESPONSE			
IFNγ*	-2.7	-2.3	-2.1
IFIH1	-3.0	-1.2	-1.9
MX1	-5.1	-1.5	-2.3
IFNβ	-5.6	-3.1	-2.2
COMPLEMENT ACTIVATION			
C1S	-2.1	+1.1	-2.0
C1QC	-2.1	-1.8	-2.2
SERPING1	-2.3	+1.3	-2.4
C3	-3.0	+1.2	-1.9
CFB	-4.7	-1.1	-3.3
TRANSCRIPTION			
STAT3	-2.6	+1.1	-2.1

FIG 11 Differential gene expression in rSARS-CoV-MA15-E*-infected mice. Total lung RNA was extracted from mice infected with the indicated SARS-CoV deletion mutants at 2 days p.i. ($n = 3$ mice). (A) Differential gene expression was measured using microarrays. Only genes with an FDR less than 0.05 were considered candidate genes. Points with a differential expression higher or lower than 2-fold are represented as darker or lighter dots, respectively. (B) Candidate genes that were up- and downregulated in ΔE, Δ3, and Δ5 viruses were grouped according to Gene Ontology terms. Numbers on the *x* axis indicate DAVID FDR values. (C) Genes differentially expressed in ΔE-, Δ3-, and Δ5-infected mice compared to in wt-infected mice were classified according to their main biological functions. Black and gray lettering is used to indicate up- and downregulated genes, respectively. Asterisks indicates genes whose expression was confirmed by RT-qPCR. The numbers indicate the fold change for each gene in ΔE-, Δ3-, and Δ5-infected mice compared to in wt-infected mice. For those genes detected with more than one probe, the value corresponding to the highest upregulation or downregulation is represented.

TABLE 3 Analysis of host gene expression using mouse microarrays[a]

Comparison	Total no. of genes differentially expressed	No. of upregulated genes	No. of downregulated genes
WT vs mock	2,918	1,473	1,445
ΔE mutant vs mock	957	594	363
Δ3 mutant vs mock	1,466	1,004	462
Δ5 mutant vs mock	1,362	955	409
ΔE mutant vs WT	1,382	752	630
Δ3 mutant vs WT	83	39	44
Δ5 mutant vs WT	286	441	385

[a] Upregulated, fold change of >2, FDR of <0.05; downregulated, fold change of <−2, FDR of <0.05.

transient transfection, and coimmunoprecipitation experiments were performed. The E-wt and E-Δ3 proteins were specifically coimmunoprecipitated together with the M protein, using an antibody specific for the HA tag fused to the M protein (Fig. 9). These results confirm that E and M proteins interacted in infected cells and indicated that the Δ3 deletion introduced within the E protein did not significantly alter the binding of this protein to the M protein.

Immune cell responses in rSARS-CoV-MA15-E*-infected mice. SARS progression and disease outcomes are associated with a massive influx of inflammatory cells to the lungs and a poor T cell response (50, 51, 54, 69). Leukocyte infiltrates in the lungs of mice infected with virulent rSARS-CoV-MA15-wt or representative attenuated mutants (rSARS-CoV-MA15-ΔE, -Δ3, and -Δ5) were quantified and characterized by flow cytometry. Total leukocyte numbers were slightly increased in lung cell infiltrates of mice infected with the attenuated mutants (ΔE, Δ3, and Δ5 viruses), compared to those infected with the parental virulent virus (Fig. 10A). Higher total and relative levels of macrophages were observed in lung infiltrates of the mice infected with the attenuated viruses than in those infected with rSARS-CoV-MA15 (Fig. 10B). Interestingly, a decrease in the percentage and total number of neutrophils was observed in the mice infected with the attenuated viruses compared to those in rSARS-CoV-MA15-infected mice (Fig. 10C). These data showed that the attenuation observed for mutant viruses (ΔE, Δ3, and Δ5 viruses) correlated with a decrease in neutrophil influx and an increase in macrophage influx into the lungs. Higher total and relative numbers of $CD4^+$ and $CD8^+$ T cells were present in the lungs of ΔE, Δ3, and Δ5 virus-infected mice than in virulent rSARS-CoV-MA15-infected lungs (Fig. 10D and E). All data analyzed were statistically significant, with the exception of total leukocyte, neutrophil, and $CD4^+$ numbers. These data suggested that mice infected with the attenuated viruses develop higher T cell responses than those infected with virulent SARS-CoV, most likely contributing to virus clearance and disease attenuation.

Effect of SARS-CoV-MA15-E* virus infection on host gene expression. To analyze host responses responsible for the attenuation of the rSARS-CoV-MA15-E* mutants, the transcriptomes of rSARS-CoV-MA15-, rSARS-CoV-MA15-ΔE-, rSARS-CoV-MA15-Δ3-, rSARS-CoV-MA15-Δ5-, and mock-infected lungs were compared, using mouse microarrays (Fig. 11A and Table 3). The genes differentially expressed during SARS-CoV infection (both up- and downregulated) in rSARS-CoV-MA15-ΔE, -Δ3, and -Δ5 virus-infected mice, compared to wt-infected mice, were clustered using DAVID software (70). The most statistically significant clusters were associated with the immune response, the response to wounding, the defense response, and the inflammatory response (Fig. 11B). Based on their principal biological function, the genes downregulated in mice infected with the attenuated rSARS-CoV-MA15 mutants were involved mainly in inflammation (Fig. 11C). Interestingly, this reduction correlated with relative increase in the expression of the Th2 genes, such as those encoding IL-4 and IL-13, in comparison to that in mice infected with the parental virus.

To validate and confirm the results obtained using microarrays, several genes involved in inflammatory responses were selected for RT-qPCR analysis, and their expression was tested at 2 and 4 days p.i. A clear reduction of all the proinflammatory cytokines analyzed (TNF, CCL2, CCL3, CCL4, CXCL1, CXCL2, CXCL10, IL-6, IL-12B, and IFN-γ) was observed in the lungs of mice infected with the ΔE, Δ3, and Δ5 attenuated viruses, compared to that in wt-infected mouse lungs (Fig. 11C and 12A and B). In contrast, the expression of the Th2 cytokines IL-4, IL-5, and IL-13 was upregulated in the lungs of mice infected with the ΔE, Δ3, and Δ5 attenuated viruses, compared to those from rSARS-CoV-MA15-infected mice (Fig. 11C and 12A and B). All data analyzed were statistically significant with minor exceptions. These changes were specific, as the mRNA levels of rRNA 18S and transforming growth factor β (TGF-β), encoded by another gene involved in the anti-inflammatory response but regulated posttranscriptionally (71, 72), were the same in all mice (Fig. 12B).

To confirm that the mRNA levels correlated with protein accumulation, the levels of TNF, CCL2, CXCL1, IL-5, IL-6, IL-13, IFN-γ, CCL3, and CCL4 were evaluated in lung extracts from mice infected with the rSARS-CoV-MA15, Δ3, Δ5, and ΔE viruses or mock infected, as a control. mRNA levels of these cytokines matched with their protein levels in the mouse lungs (Fig. 13). All cytokine differences at the protein level were statistically significant, with minor exceptions in CCL3, CXCL1, and CCL4 cytokines. All together, these results indicated that the macroscopic and microscopic inflammation present in the lungs of infected mice correlated with overexpression of proinflammatory cytokines and downregulation of anti-inflammatory cytokines.

Immunization with the attenuated mutant viruses protects mice against challenge with SARS-CoV-MA15 virus. Live attenuated vaccines are considered most effective in their ability to induce a long-lived, balanced immune response. In order to determine whether the attenuated mutant viruses were good vaccine candidates, the induction of protection conferred by the attenuated viruses with point mutations or small deletions, against the challenge with virulent SARS-CoV-MA15, was studied. Groups of BALB/c mice were either mock immunized with PBS or immunized with the Mut 1, Δ2, Δ3, Δ4, and Δ5 attenuated viruses. At 21 days postimmunization, mice were challenged with rSARS-CoV-MA15, and weight loss and mortality were monitored for 14 days postchallenge (Fig. 14). All the nonimmunized mice lost weight and died by day 7 after rSARS-CoV-MA15 challenge. In contrast, vaccination with the attenuated mutant viruses completely protected mice from the lethal dose of SARS-CoV-MA15, as they showed no weight loss and all survived. These data indicated that all attenuated mutant viruses effectively induced a high level of protection against lethal rSARS-CoV-MA15 challenge in mice.

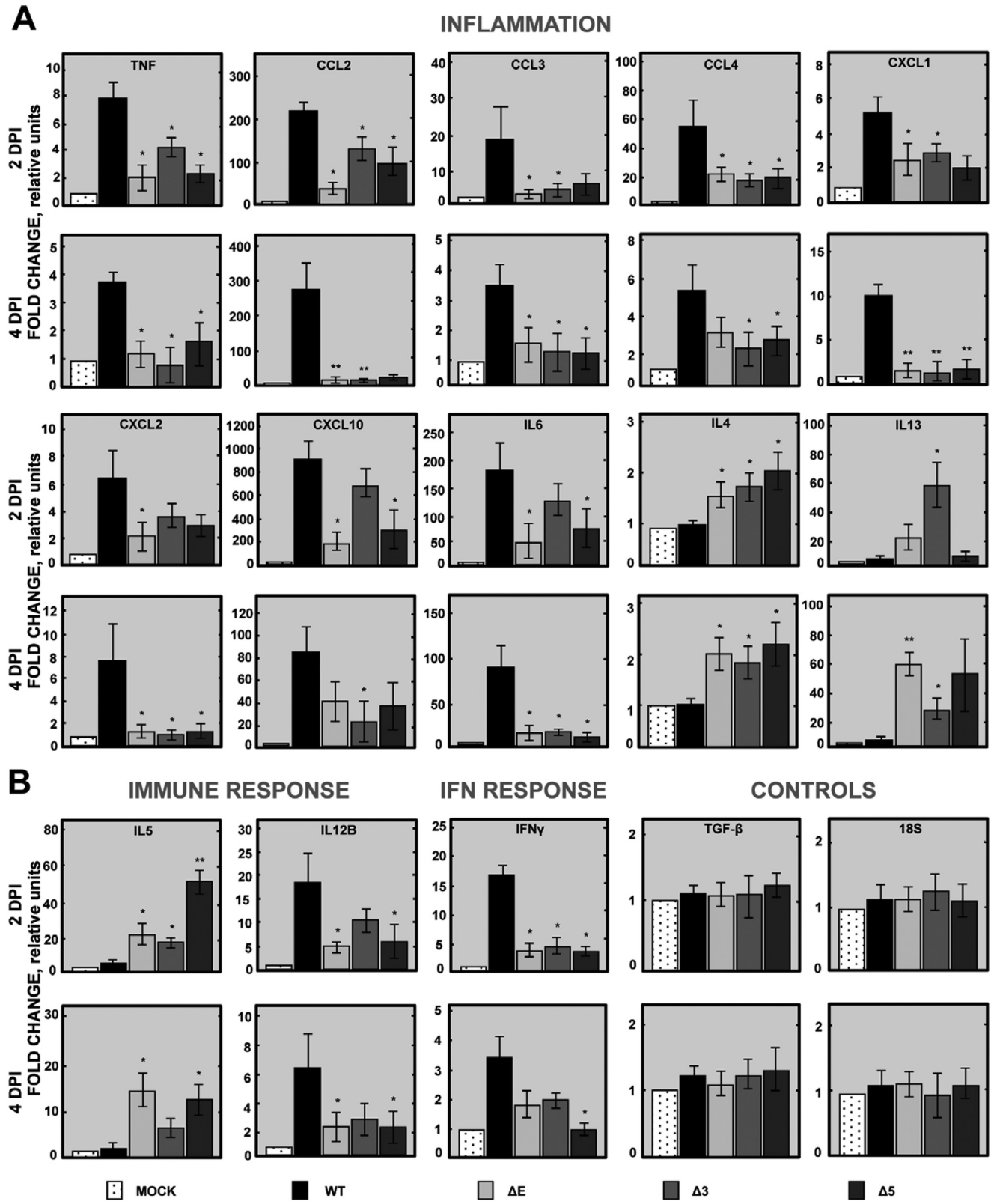

FIG 12 Effect of rSARS-CoV-MA15-E* deletion mutants on the expression of cytokine mRNAs in BALB/c mouse lung. Mice were infected with 1×10^5 PFU of rSARS-CoV-MA15-Δ3, -Δ5, and -ΔE and wt viruses, and total RNA was extracted at 2 and 4 days p.i. The expression of mRNAs encoding inflammatory genes (A) and immune response and IFN response genes encoding TGFβ and 18S rRNA (B) was measured by qRT-PCR. In each case, levels of expression in infected lungs were compared to those in mock-infected ones. Bars represent standard deviations of the mean ($n = 3$ mice). Statistically significant data compared to mice infected with the wt virus are indicated (*, $P < 0.05$; **, $P < 0.01$).

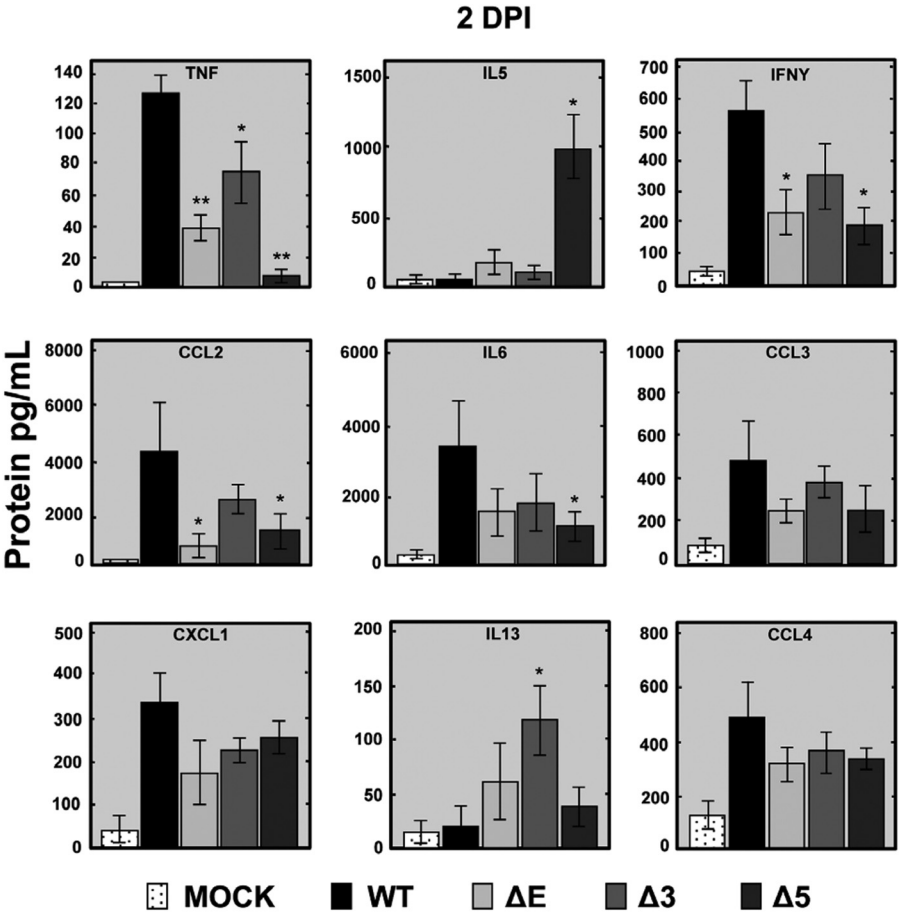

FIG 13 Expression of cytokines in rSARS-CoV-MA15-E*-infected mice. Mice were infected with 1×10^5 PFU of rSARS-CoV-MA15-wt, -Δ3, -Δ5, or -ΔE virus or were mock infected (mock). Lung proteins were extracted at 2 days p.i., and the accumulation of several cytokine proteins was measured. Protein concentration is expressed as picograms per milliliter of lung tissue extract. Means and standard deviations are shown ($n = 3$ mice). Statistically significant differences compared to mice infected with wt virus are indicated (*, $P < 0.05$).

DISCUSSION

An extensive study using a collection of recombinant viruses was performed to analyze E protein regions and host responses that contributed to the virulence of SARS-CoV. Several mutants encoding small deletions or point mutations within E protein were engineered, in the context of mouse-adapted SARS-CoV-MA15 (57). Point mutations in the amino-terminal region and small deletions in the internal carboxy-terminal region of E protein led to viruses with an attenuated phenotype, similarly to that obtained by deleting the whole E protein of SARS-CoV. Infection of mice with the rSARS-CoV-MA15-Mut 1, -Δ2, -Δ3, -Δ4, -Δ5, and -ΔE mutants led to decreased lung pathology compared to that of wt-infected mice and no mortality. Therefore, these regions are required for the virus to develop its full pathogenic potential. In contrast, virus lacking the 12 carboxy-terminal amino acids of E protein (Δ6 mutant) was fully virulent, reinforcing the idea that not all small deletions within the E protein were attenuating. The deletion within rSARS-CoV-MA15-Δ6 includes the PDZ-binding motif (PBM) (73, 74), and we previously showed that a mutant lacking this region is attenuated (73). One possible explanation for this apparent discrepancy is that the last 6 amino acids within the Δ6 virus (YSRVKN; Fig. 1) form an alternative PBM that could restore the virulent phenotype of the virus, an aspect that is currently being explored in our laboratory. Deletion or mutation of E protein regions could in principle affect basic properties of the protein, such as its subcellular localization and half-life, which could broadly disturb its major functions within the cell. The cytoplasmic tail of SARS-CoV E protein was shown to contain a signal providing Golgi localization (75). In addition, CoV E protein may impair protein trafficking depending of its half-life (65). None of these aspects was significantly altered, as mutant E proteins colocalized mainly with ERGIC markers, as described for the wt protein (25), and the half-life of E* protein mutants was slightly increased (1.5-fold) compared with that of the wt protein (65). Furthermore, the interaction between E and M proteins necessary for virus morphogenesis (66–68) was preserved despite deleting the Δ3 region. Thus, the E-Δ3 region of SARS-CoV E protein is not required to interact with M protein. In contrast, the specific infectivity of the different small deletions within the E protein was lower (6-fold) than that of the wt virus. These modifications in E protein possibly contributed to the reduced infectivity observed for E protein deletion mutants that exhibited an attenuated phenotype. However, these phenomena are not necessarily linked, because we previously demonstrated that recombinant viruses containing point mutations in the E protein that inhibited its ion channel activity or eliminated its PBM grew to titers similar to

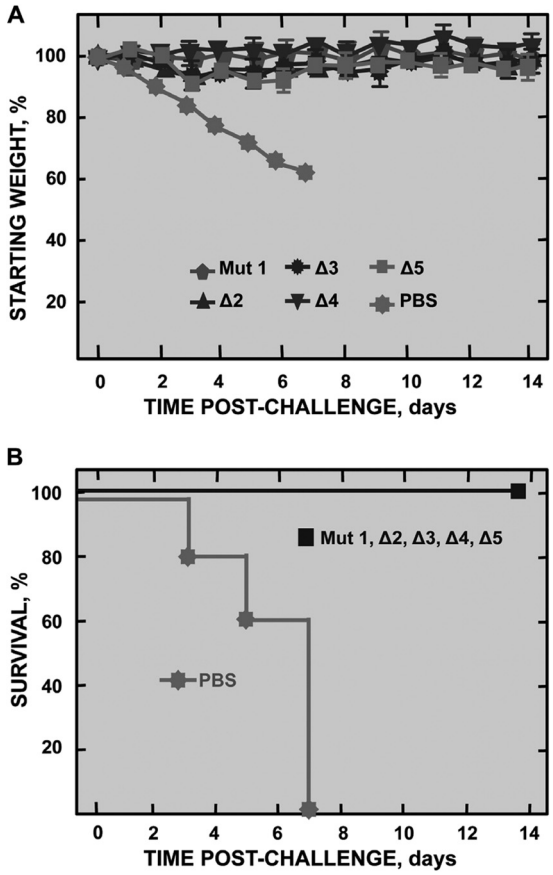

FIG 14 Protection conferred by immunization with the rSARS-CoV-MA15-E* mutants. Six-week-old BALB/c mice were mock immunized or immunized with 6,000 PFU of the SARS-CoV-MA15-E* mutants and challenged at day 21 postimmunization with 1×10^5 PFU of MA15 virus ($n = 5$ mice). Weight loss (A) and survival (B) were recorded daily.

those of the parental virus in the lungs of the infected mice (37, 73). Nevertheless, these viruses caused a reduction in lung inflammation and pathology and were attenuated (37, 73). Therefore, E* protein mutants may decrease virus virulence by affecting specific host responses, independently of effects on virus replication. Interestingly, the patterns of gene expression in infected lungs revealed that proinflammatory genes, such as those encoding TNF, CCL2, CCL3, CCL4, CXCL1, CXCL2, CXCL10, IL-6, IL-12B, and IFN-γ, were downregulated in rSARS-CoV-MA15-ΔE, -Δ3, and -Δ5-infected mice compared to in wt-infected mice, most probably contributing to viral attenuation. Notably, increased levels of proinflammatory cytokines such as TNF, IL-6, CXCL10, CCL2, IL-8, and IL-12, which play a major role in mediating and amplifying ALI/ARDS, were found in the blood and the lungs of SARS patients (40–45, 48, 76). Furthermore, the expression of the Th2 cytokines IL-4, IL-5, and IL-13 was increased in the lungs of mice infected with the attenuated viruses compared to in those infected with the virulent wt virus, possibly contributing to a better outcome. In agreement with this finding, the expression of IL-13 was increased in asymptomatic young BALB/c mice infected with a mouse-adapted SARS-CoV, compared to aged infected mice with severe respiratory disease (77). All these data strongly suggest that the lower proinflammatory cytokine expression and higher anti-inflammatory cytokine levels observed after infection with the attenuated mutants could account for the diminished lung pathology and virus attenuation.

Neutrophils play a key role in the progression of ALI/ARDS, and SARS patients with adverse outcomes presented with neutrophilia and high neutrophil counts in the lungs (38, 54, 78, 79). Similarly, massive neutrophil influx into the lungs contributed to disease after influenza A virus and respiratory syncytial virus (RSV) infections (80–83). This phenomenon was reproduced in mice infected with virulent SARS-CoV-MA15, whereas a significant reduction of neutrophils in the lungs of the mice infected with the attenuated mutants was observed. Accordingly, the expression of CXCL1 and CXCL2, key factors that induce the chemotaxis of neutrophils (84, 85), was increased when the full-length E protein was present during SARS-CoV infection.

An increase of macrophage numbers was observed in mice infected with the attenuated mutants, compared to those infected with the virulent wt virus. In addition to their role in immunity, macrophages maintain physiologic homeostasis and contribute to tissue repair (86, 87). Therefore, an increase of these cells during infection could favor disease resolution. Together, these data indicate that an increase in neutrophil numbers in conjunction with a decrease in macrophage numbers in the lungs is associated with more severe SARS-CoV pathogenesis and that the deletion of E protein carboxy-terminal regions was responsible for these changes in the phenotype of infiltrating immune cells and virus attenuation during SARS-CoV infection.

T cells are important for viral clearance and for protection from disease in primary SARS-CoV infection (50–52), and low T cell counts correlate with adverse outcomes in SARS patients (38, 53, 54, 56). Interestingly, we have shown that in rSARS-CoV-MA15-ΔE, -Δ3, and -Δ5-infected mice, which do not show a significant disease, $CD4^+$ and $CD8^+$ T cell counts are higher than those found in mice infected with the parental virus, which show adverse outcomes after infection. We were unable to measure virus-specific T cell responses, because rSARS-CoV-infected mice die before a significant T cell response develops (Fig. 4). Several anti-SARS-CoV vaccine candidates have been developed since 2003, but none has been approved for use in humans (88, 89). Live attenuated vaccines are considered most effective compared to other types of vaccines, as they induce a long-lived, balanced immune response. Remarkably, the attenuated mutants generated in this work provided full protection after challenge with the virulent wt virus. These viruses express a complete repertoire of viral proteins, except for the small regions deleted or mutated in the E protein. Therefore, it is predicted that they will elicit both antibody and T cell responses directed against the virus. The major problems of using live attenuated vaccines are the possibility that the viruses may revert to virulence. To overcome this limitation, we are introducing additional attenuating mutations into the Nsp1 protein to generate a safer vaccine candidate. The Nsp1 gene was selected as a target because it is located at a very distant site from that of the E gene in the viral genome, making the generation of a virulent virus through single recombination events with circulating coronaviruses unlikely.

In summary, we have shown that changes in the amino terminal and internal carboxy-terminal regions of E protein led to stable attenuated SARS-CoV mutants. These mutants showed a slight reduction in their specific infectivity, maintained the same E protein subcellular localization, and slightly increased their half-

life compared to the wild-type virus. Moreover, the Δ3 deletion introduced within the E protein maintained the interaction between E and M proteins. SARS-CoV attenuation correlated with limited lung pathology, mediated by decreased proinflammatory cytokine expression, increased anti-inflammatory cytokine levels, and reduced neutrophil accumulation in the lungs. In addition, higher $CD4^+$ and $CD8^+$ T cell counts in mice infected with the attenuated mutants most likely contributed to better outcomes. These attenuated mutants fully protected mice from challenge with virulent virus. These studies are the basis for the rational design of SARS-CoV vaccine candidates.

ACKNOWLEDGMENTS

This work was supported by grants from the Ministry of Science and Innovation of Spain (MICINN BIO2010-16705 and MINECO BIO2013-42869-R), the European Community's Seventh Framework Programme (FP7/2007–2013) under the project "EMPERIE" EC grant agreement number 223498, and a U.S. National Institutes of Health (NIH) project (2P01AI060699). J.A.R.-N. and C.C.-R. received a fellowship from the Fundacion La Caixa.

We thank Marga Gonzalez for her technical assistance.

REFERENCES

1. **Perlman S, Netland J.** 2009. Coronaviruses post-SARS: update on replication and pathogenesis. Nat Rev Microbiol **7:**439–450. http://dx.doi.org/10.1038/nrmicro2147.
2. **Drosten C, Gunther S, Preiser W, van der Werf S, Brodt HR, Becker S, Rabenau H, Panning M, Kolesnikova L, Fouchier RA, Berger A, Burguiere AM, Cinatl J, Eickmann M, Escriou N, Grywna K, Kramme S, Manuguerra JC, Muller S, Rickerts V, Sturmer M, Vieth S, Klenk HD, Osterhaus AD, Schmitz H, Doerr HW.** 2003. Identification of a novel coronavirus in patients with severe acute respiratory syndrome. N Engl J Med **348:**1967–1976. http://dx.doi.org/10.1056/NEJMoa030747.
3. **Rota PA, Oberste MS, Monroe SS, Nix WA, Campganoli R, Icenogle JP, Peñaranda S, Bankamp B, Maher K, Chen M-H, Tong S, Tamin A, Lowe L, Frace M, DeRisi JL, Chen Q, Wang D, Erdman DD, Peret TC, Burns C, Ksiazek TG, Rollin PE, Sanchez A, Liffick S, Holloway B, Limor J, McCaustland K, Olsen-Rassmussen M, Fouchier R, Gunther S, Osterhaus AD, Drosten C, Pallansch MA, Anderson LJ, Bellini WJ.** 2003. Characterization of a novel coronavirus associated with severe acute respiratory syndrome. Science **300:**1394–1399. http://dx.doi.org/10.1126/science.1085952.
4. **Kuiken T, Fouchier RAM, Schutten M, Rimmelzwaan GF, van Amerongen G, van Riel D, Laman JD, de Jong T, van Doornum G, Lim W, Ling AE, Chan PKS, Tam JS, Zambon MC, Gopal R, Drosten C, van der Werf S, Escriou N, Manuguerra J-C, Stohr K, Peiris JSM.** 2003. Newly discovered coronavirus as the primary cause of severe acute respiratory syndrome. Lancet **362:**263–270. http://dx.doi.org/10.1016/S0140-6736(03)13967-0.
5. **Marra MA, Jones SJM, Astell CR, Holt RA, Brooks-Wilson A, Butterfield YSN, Khattra J, Asano JK, Barber SA, Chan SY, Cloutier A, Coughlin SM, Freeman D, Girn N, Griffith OL, Leach SR, Mayo M, McDonald H, Montgomery SB, Pandoh PK, Petrescu AS, Robertson AG, Schein JE, Siddiqui A, Smailus DE, Stott JM, Yang GS, Plummer F, Andonov A, Artsob H, Bastien N, Bernard K, Booth TF, Bowness D, Czub M, Drebot M, Fernando L, Flick R, Garbutt M, Gray M, Grolla A, Jones S, Feldmann H, Meyers A, Kabani A, Li Y, Normand S, Stroher U, Tipples GA, Tyler S, et al.** 2003. The genome sequence of the SARS-associated coronavirus. Science **300:**1399–1404. http://dx.doi.org/10.1126/science.1085953.
6. **Zaki AM, van Boheemen S, Bestebroer TM, Osterhaus AD, Fouchier RA.** 2012. Isolation of a novel coronavirus from a man with pneumonia in Saudi Arabia. N Engl J Med **367:**1814–1820. http://dx.doi.org/10.1056/NEJMoa1211721.
7. **de Groot RJ, Baker SC, Baric RS, Brown CS, Drosten C, Enjuanes L, Fouchier RA, Galiano M, Gorbalenya AE, Memish ZA, Perlman S, Poon LL, Snijder EJ, Stephens GM, Woo PC, Zaki AM, Zambon M, Ziebuhr J.** 2013. Middle East respiratory syndrome coronavirus (MERS-CoV): announcement of the Coronavirus Study Group. J Virol **87:**7790–7792. http://dx.doi.org/10.1128/JVI.01244-13.
8. **WHO.** 2013. Middle East respiratory syndrome coronavirus (MERS-CoV)—update. WHO, Geneva, Switzerland. http://www.who.int/csr/don/2013_08_01/en/index.html.
9. **van Boheemen S, de Graaf M, Lauber C, Bestebroer TM, Raj VS, Zaki AM, Osterhaus AD, Haagmans BL, Gorbalenya AE, Snijder EJ, Fouchier RA.** 2012. Genomic characterization of a newly discovered coronavirus associated with acute respiratory distress syndrome in humans. mBio **3**(6):e00473–12. http://dx.doi.org/10.1128/mBio.00473-12.
10. **Muller MA, Paweska JT, Leman PA, Drosten C, Grywna K, Kemp A, Braack L, Sonnenberg K, Niedrig M, Swanepoel R.** 2007. Coronavirus antibodies in African bat species. Emerg Infect Dis **13:**1367–1370. http://dx.doi.org/10.3201/eid1309.070342.
11. **Chu DK, Peiris JS, Chen H, Guan Y, Poon LL.** 2008. Genomic characterizations of bat coronaviruses (1A, 1B and HKU8) and evidence for co-infections in Miniopterus bats. J Gen Virol **89:**1282–1287. http://dx.doi.org/10.1099/vir.0.83605-0.
12. **Drexler JF, Gloza-Rausch F, Glende J, Corman VM, Muth D, Goettsche M, Seebens A, Niedrig M, Pfefferle S, Yordanov S, Zhelyazkov L, Hermanns U, Vallo P, Lukashev A, Muller MA, Deng H, Herrler G, Drosten C.** 2010. Genomic characterization of severe acute respiratory syndrome-related coronavirus in European bats and classification of coronaviruses based on partial RNA-dependent RNA polymerase gene sequences. J Virol **84:**11336–11349. http://dx.doi.org/10.1128/JVI.00650-10.
13. **Quan PL, Firth C, Street C, Henriquez JA, Petrosov A, Tashmukhamedova A, Hutchison SK, Egholm M, Osinubi MO, Niezgoda M, Ogunkoya AB, Briese T, Rupprecht CE, Lipkin WI.** 2010. Identification of a severe acute respiratory syndrome coronavirus-like virus in a leaf-nosed bat in Nigeria. mBio **1**(4):e00208–10. http://dx.doi.org/10.1128/mBio.00208-10.
14. **Annan A, Baldwin HJ, Corman VM, Klose SM, Owusu M, Nkrumah EE, Badu EK, Anti P, Agbenyega O, Meyer B, Oppong S, Sarkodie YA, Kalko EK, Lina PH, Godlevska EV, Reusken C, Seebens A, Gloza-Rausch F, Vallo P, Tschapka M, Drosten C, Drexler JF.** 2013. Human betacoronavirus 2c EMC/2012-related viruses in bats, Ghana and Europe. Emerg Infect Dis **19:**456–459. http://dx.doi.org/10.3201/eid1903.121503.
15. **Falcon A, Vazquez-Moron S, Casas I, Aznar C, Ruiz G, Pozo F, Perez-Brena P, Juste J, Ibanez C, Garin I, Aihartza J, Echevarria JE.** 2011. Detection of alpha and betacoronaviruses in multiple Iberian bat species. Arch Virol **156:**1883–1890. http://dx.doi.org/10.1007/s00705-011-1057-1.
16. **Gorbalenya AE, Snijder EJ, Spaan WJ.** 2004. Severe acute respiratory syndrome coronavirus phylogeny: toward consensus. J Virol **78:**7863–7866. http://dx.doi.org/10.1128/JVI.78.15.7863-7866.2004.
17. **Snijder EJ, Bredenbeek PJ, Dobbe JC, Thiel V, Ziebuhr J, Poon LLM, Guan Y, Rozanov M, Spaan WJM, Gorbalenya AE.** 2003. Unique and conserved features of genome and proteome of SARS-coronavirus, an early split-off from the coronavirus group 2 lineage. J Mol Biol **331:**991–1004. http://dx.doi.org/10.1016/S0022-2836(03)00865-9.
18. **Enjuanes L, Gorbalenya AE, de Groot RJ, Cowley JA, Ziebuhr J, Snijder EJ.** 2008. The Nidovirales, p 419–430. *In* Mahy BWJ, Van Regenmortel M, Walker P, Majumder-Russell D (ed), Encyclopedia of virology, 3rd ed. Elsevier Ltd., Oxford, United Kingdom.
19. **Torres J, Parthasarathy K, Lin X, Saravanan R, Liu DX.** 2006. Model of a putative pore: the pentameric alpha-helical bundle of SARS coronavirus E protein in lipid bilayers. Biophys J **91:**938–947. http://dx.doi.org/10.1529/biophysj.105.080119.
20. **Verdia-Baguena C, Nieto-Torres JL, Alcaraz A, Dediego ML, Torres J, Aguilella VM, Enjuanes L.** 2012. Coronavirus E protein forms ion channels with functionally and structurally-involved membrane lipids. Virology **432:**485–494. http://dx.doi.org/10.1016/j.virol.2012.07.005.
21. **Verdia-Baguena C, Nieto-Torres JL, Alcaraz A, Dediego ML, Enjuanes L, Aguilella VM.** 2013. Analysis of SARS-CoV E protein ion channel activity by tuning the protein and lipid charge. Biochim Biophys Acta **1828:**2026–2031. http://dx.doi.org/10.1016/j.bbamem.2013.05.008.
22. **Pervushin K, Tan E, Parthasarathy K, Lin X, Jiang FL, Yu D, Vararattanavech A, Soong TW, Liu DX, Torres J.** 2009. Structure and inhibition of the SARS coronavirus envelope protein ion channel. PLoS Pathog **5:**e1000511. http://dx.doi.org/10.1371/journal.ppat.1000511.
23. **Nal B, Chan C, Kien F, Siu L, Tse J, Chu K, Kam J, Staropoli I, Crescenzo-Chaigne B, Escriou N, van der Werf S, Yuen KY, Altmeyer R.** 2005. Differential maturation and subcellular localization of severe

acute respiratory syndrome coronavirus surface proteins S, M and E. J Gen Virol **86:**1423–1434. http://dx.doi.org/10.1099/vir.0.80671-0.
24. **Maeda J, Repass JF, Maeda A, Makino S.** 2001. Membrane topology of coronavirus E protein. Virology **281:**163–169. http://dx.doi.org/10.1006/viro.2001.0818.
25. **Nieto-Torres JL, Dediego ML, Alvarez E, Jimenez-Guardeno JM, Regla-Nava JA, Llorente M, Kremer L, Shuo S, Enjuanes L.** 2011. Subcellular location and topology of severe acute respiratory syndrome coronavirus envelope protein. Virology **415:**69–82. http://dx.doi.org/10.1016/j.virol.2011.03.029.
26. **Ye Y, Hogue BG.** 2007. Role of the coronavirus E viroporin protein transmembrane domain in virus assembly. J Virol **81:**3597–3607. http://dx.doi.org/10.1128/JVI.01472-06.
27. **Ruch TR, Machamer CE.** 2012. The coronavirus E protein: assembly and beyond. Viruses **4:**363–382. http://dx.doi.org/10.3390/v4030363.
28. **DeDiego ML, Alvarez E, Almazan F, Rejas MT, Lamirande E, Roberts A, Shieh WJ, Zaki SR, Subbarao K, Enjuanes L.** 2007. A severe acute respiratory syndrome coronavirus that lacks the E gene is attenuated *in vitro* and *in vivo*. J Virol **81:**1701–1713. http://dx.doi.org/10.1128/JVI.01467-06.
29. **DeDiego ML, Pewe L, Alvarez E, Rejas MT, Perlman S, Enjuanes L.** 2008. Pathogenicity of severe acute respiratory coronavirus deletion mutants in hACE-2 transgenic mice. Virology **376:**379–389. http://dx.doi.org/10.1016/j.virol.2008.03.005.
30. **Lamirande EW, DeDiego ML, Roberts A, Jackson JP, Alvarez E, Sheahan T, Shieh WJ, Zaki SR, Baric R, Enjuanes L, Subbarao K.** 2008. A live attenuated SARS coronavirus is immunogenic and efficacious in golden Syrian hamsters. J Virol **82:**7721–7724. http://dx.doi.org/10.1128/JVI.00304-08.
31. **Netland J, DeDiego ML, Zhao J, Fett C, Alvarez E, Nieto-Torres JL, Enjuanes L, Perlman S.** 2010. Immunization with an attenuated severe acute respiratory syndrome coronavirus deleted in E protein protects against lethal respiratory disease. Virology **399:**120–128. http://dx.doi.org/10.1016/j.virol.2010.01.004.
32. **Fett C, DeDiego ML, Regla-Nava JA, Enjuanes L, Perlman S.** 2013. Complete protection against severe acute respiratory syndrome coronavirus-mediated lethal respiratory disease in aged mice by immunization with a mouse-adapted virus lacking E protein. J Virol **87:**6551–6559. http://dx.doi.org/10.1128/JVI.00087-13.
33. **DeDiego ML, Nieto-Torres JL, Jimenez-Guardeno JM, Regla-Nava JA, Alvarez E, Oliveros JC, Zhao J, Fett C, Perlman S, Enjuanes L.** 2011. Severe acute respiratory syndrome coronavirus envelope protein regulates cell stress response and apoptosis. PLoS Pathog **7:**e1002315. http://dx.doi.org/10.1371/journal.ppat.1002315.
34. **Ware LB, Matthay MA.** 2000. The acute respiratory distress syndrome. N Engl J Med **342:**1334–1349. http://dx.doi.org/10.1056/NEJM200005043421806.
35. **Gralinski LE, Bankhead A, III, Jeng S, Menachery VD, Proll S, Belisle SE, Matzke M, Webb-Robertson BJ, Luna ML, Shukla AK, Ferris MT, Bolles M, Chang J, Aicher L, Waters KM, Smith RD, Metz TO, Law GL, Katze MG, McWeeney S, Baric RS.** 2013. Mechanisms of severe acute respiratory syndrome coronavirus-induced acute lung injury. mBio **4**(4): e00271–13. http://dx.doi.org/10.1128/mBio.00271-13.
36. **Franks TJ, Chong PY, Chui P, Galvin JR, Lourens RM, Reid AH, Selbs E, McEvoy CP, Hayden CD, Fukuoka J, Taubenberger JK, Travis WD.** 2003. Lung pathology of severe acute respiratory syndrome (SARS): a study of 8 autopsy cases from Singapore. Hum Pathol **34:**743–748. http://dx.doi.org/10.1016/S0046-8177(03)00367-8.
37. **Nieto-Torres JL, Dediego ML, Verdia-Baguena C, Jimenez-Guardeno JM, Regla-Nava JA, Fernandez-Delgado R, Castano-Rodriguez C, Alcaraz A, Torres J, Aguilella VM, Enjuanes L.** 2014. Severe acute respiratory syndrome coronavirus envelope protein ion channel activity promotes virus fitness and pathogenesis. PLoS Pathog **10:**e1004077. http://dx.doi.org/10.1371/journal.ppat.1004077.
38. **Lee N, Hui D, Wu A, Chan P, Cameron P, Joynt G, Ahuja A, Yung MY, Leung CB, To KF, Lui SF, Szeto CC, Chung S, Sung JJY.** 2003. A major outbreak of severe acute respiratory syndrome in Hong Kong. N Engl J Med **348:**1986–1994. http://dx.doi.org/10.1056/NEJMoa030685.
39. **Yen YT, Liao F, Hsiao CH, Kao CL, Chen YC, Wu-Hsieh BA.** 2006. Modeling the early events of severe acute respiratory syndrome coronavirus infection *in vitro*. J Virol **80:**2684–2693. http://dx.doi.org/10.1128/JVI.80.6.2684-2693.2006.
40. **Chien JY, Hsueh PR, Cheng WC, Yu CJ, Yang PC.** 2006. Temporal changes in cytokine/chemokine profiles and pulmonary involvement in severe acute respiratory syndrome. Respirology **11:**715–722. http://dx.doi.org/10.1111/j.1440-1843.2006.00942.x.
41. **Wong CK, Lam CW, Wu AK, Ip WK, Lee NL, Chan IH, Lit LC, Hui DS, Chan MH, Chung SS, Sung JJ.** 2004. Plasma inflammatory cytokines and chemokines in severe acute respiratory syndrome. Clin Exp Immunol **136:**95–103. http://dx.doi.org/10.1111/j.1365-2249.2004.02415.x.
42. **Tang NL, Chan PK, Wong CK, To KF, Wu AK, Sung YM, Hui DS, Sung JJ, Lam CW.** 2005. Early enhanced expression of interferon-inducible protein-10 (CXCL-10) and other chemokines predicts adverse outcome in severe acute respiratory syndrome. Clin Chem **51:**2333–2340. http://dx.doi.org/10.1373/clinchem.2005.054460.
43. **Jiang Y, Xu J, Zhou C, Wu Z, Zhong S, Liu J, Luo W, Chen T, Qin Q, Deng P.** 2005. Characterization of cytokine/chemokine profiles of severe acute respiratory syndrome. Am J Respir Crit Care Med **171:**850–857. http://dx.doi.org/10.1164/rccm.200407-857OC.
44. **Cameron MJ, Ran L, Xu L, Danesh A, Bermejo-Martin JF, Cameron CM, Muller MP, Gold WL, Richardson SE, Poutanen SM, Willey BM, DeVries ME, Fang Y, Seneviratne C, Bosinger SE, Persad D, Wilkinson P, Greller LD, Somogyi R, Humar A, Keshavjee S, Louie M, Loeb MB, Brunton J, McGeer AJ, Kelvin DJ.** 2007. Interferon-mediated immunopathological events are associated with atypical innate and adaptive immune responses in patients with severe acute respiratory syndrome. J Virol **81:**8692–8706. http://dx.doi.org/10.1128/JVI.00527-07.
45. **Lam CW, Chan MH, Wong CK.** 2004. Severe acute respiratory syndrome: clinical and laboratory manifestations. Clin Biochem Rev **25:**121–132.
46. **de Lang A, Baas T, Teal T, Leijten LM, Rain B, Osterhaus AD, Haagmans BL, Katze MG.** 2007. Functional genomics highlights differential induction of antiviral pathways in the lungs of SARS-CoV-infected macaques. PLoS Pathog **3:**e112. http://dx.doi.org/10.1371/journal.ppat.0030112.
47. **Smits SL, de Lang A, van den Brand JM, Leijten LM, van IWF, Eijkemans MJ, van Amerongen G, Kuiken T, Andeweg AC, Osterhaus AD, Haagmans BL.** 2010. Exacerbated innate host response to SARS-CoV in aged non-human primates. PLoS Pathog **6:**e1000756. http://dx.doi.org/10.1371/journal.ppat.1000756.
48. **Smits SL, van den Brand JM, de Lang A, Leijten LM, van Ijcken WF, van Amerongen G, Osterhaus AD, Andeweg AC, Haagmans BL.** 2011. Distinct severe acute respiratory syndrome coronavirus-induced acute lung injury pathways in two different nonhuman primate species. J Virol **85:**4234–4245. http://dx.doi.org/10.1128/JVI.02395-10.
49. **Baas T, Roberts A, Teal TH, Vogel L, Chen J, Tumpey TM, Katze MG, Subbarao K.** 2008. Genomic analysis reveals age-dependent innate immune responses to severe acute respiratory syndrome coronavirus. J Virol **82:**9465–9476. http://dx.doi.org/10.1128/JVI.00489-08.
50. **Zhao J, Perlman S.** 2010. T cell responses are required for protection from clinical disease and for virus clearance in severe acute respiratory syndrome coronavirus-infected mice. J Virol **84:**9318–9325. http://dx.doi.org/10.1128/JVI.01049-10.
51. **Zhao J, Van Rooijen N, Perlman S.** 2009. Evasion by stealth: inefficient immune activation underlies poor T cell response and severe disease in SARS-CoV-infected mice. PLoS Pathog **5:**e1000636. http://dx.doi.org/10.1371/journal.ppat.1000636.
52. **Chen J, Lau YF, Lamirande EW, Paddock CD, Bartlett JH, Zaki SR, Subbarao K.** 2010. Cellular immune responses to severe acute respiratory syndrome coronavirus (SARS-CoV) infection in senescent BALB/c mice: CD4+ T cells are important in control of SARS-CoV infection. J Virol **84:**1289–1301. http://dx.doi.org/10.1128/JVI.01281-09.
53. **Booth CM, Matukas LM, Tomlinson GA, Rachlis AR, Rose DB, Dwosh HA, Walmsley SL, Mazzulli T, Avendano M, Derkach P, Ephtimios IE, Kitai I, Mederski BD, Shadowitz SB, Gold WL, Hawryluck LA, Rea E, Chenkin JS, Cescon DW, Poutanen SM, Detsky AS.** 2003. Clinical features and short-term outcomes of 144 patients with SARS in the greater Toronto area. JAMA **289:**2801–2809. http://dx.doi.org/10.1001/jama.289.21.JOC30885.
54. **Wong RS, Wu A, To KF, Lee N, Lam CW, Wong CK, Chan PK, Ng MH, Yu LM, Hui DS, Tam JS, Cheng G, Sung JJ.** 2003. Haematological manifestations in patients with severe acute respiratory syndrome: retrospective analysis. BMJ **326:**1358–1362. http://dx.doi.org/10.1136/bmj.326.7403.1358.
55. **Chen J, Subbarao K.** 2007. The immunobiology of SARS*. Annu Rev Immunol **25:**443–472. http://dx.doi.org/10.1146/annurev.immunol.25.022106.141706.

56. **He Z, Zhao C, Dong Q, Zhuang H, Song S, Peng G, Dwyer DE.** 2005. Effects of severe acute respiratory syndrome (SARS) coronavirus infection on peripheral blood lymphocytes and their subsets. Int J Infect Dis **9:**323–330. http://dx.doi.org/10.1016/j.ijid.2004.07.014.
57. **Roberts A, Deming D, Paddock CD, Cheng A, Yount B, Vogel L, Herman BD, Sheahan T, Heise M, Genrich GL, Zaki SR, Baric R, Subbarao K.** 2007. A mouse-adapted SARS-coronavirus causes disease and mortality in BALB/c mice. PLoS Pathog **3:**23–37. http://dx.doi.org/10.1371/journal.ppat.0030005.
58. **DeDiego ML, Nieto-Torres JL, Regla-Nava JA, Jimenez-Guardeno JM, Fernandez-Delgado R, Fett C, Castano-Rodriguez C, Perlman S, Enjuanes L.** 2014. Inhibition of NF-kappaB mediated inflammation in severe acute respiratory syndrome coronavirus-infected mice increases survival. J Virol **88:**913–924. http://dx.doi.org/10.1128/JVI.02576-13.
59. **Almazan F, DeDiego ML, Galan C, Escors D, Alvarez E, Ortego J, Sola I, Zuñiga S, Alonso S, Moreno JL, Nogales A, Capiscol C, Enjuanes L.** 2006. Construction of a SARS-CoV infectious cDNA clone and a replicon to study coronavirus RNA synthesis. J Virol **80:**10900–10906. http://dx.doi.org/10.1128/JVI.00385-06.
60. **Alvarez E, DeDiego ML, Nieto-Torres JL, Jimenez-Guardeno JM, Marcos-Villar L, Enjuanes L.** 2010. The envelope protein of severe acute respiratory syndrome coronavirus interacts with the non-structural protein 3 and is ubiquitinated. Virology **402:**281–291. http://dx.doi.org/10.1016/j.virol.2010.03.015.
61. **Livak KJ, Schmittgen TD.** 2001. Analysis of relative gene expression data using real-time quantitative PCR and the 2(-Delta Delta C(T)) method. Methods **25:**402–408. http://dx.doi.org/10.1006/meth.2001.1262.
62. **Agilent Technologies.** 2008. One-color microarray-based gene expression analysis. Agilent Technologies, Santa Clara, CA.
63. **Smyth GK.** 2004. Linear models and empirical Bayes methods for assessing differential expression in microarray experiments. Stat Appl Genet Mol Biol **3:**Article3. http://dx.doi.org/10.2202/1544-6115.1027.
64. **Benjamini Y, Hochberg Y.** 1995. Controlling the false discovery rate: a practical and powerful approach to multiple testing. J Roy Stat Soc B **57:**289–300.
65. **Ruch TR, Machamer CE.** 2012. A single polar residue and distinct membrane topologies impact the function of the infectious bronchitis coronavirus E protein. PLoS Pathog **8:**e1002674. http://dx.doi.org/10.1371/journal.ppat.1002674.
66. **Siu YL, Teoh KT, Lo J, Chan CM, Kien F, Escriou N, Tsao SW, Nicholls JM, Altmeyer R, Peiris JS, Bruzzone R, Nal B.** 2008. The M, E and N structural proteins of the SARS coronavirus are required for efficient assembly, trafficking and release of virus-like particles. J Virol **82:**11318–11330. http://dx.doi.org/10.1128/JVI.01052-08.
67. **Vennema H, Godeke GJ, Rossen JWA, Voorhout WF, Horzinek MC, Opstelten DJ, Rottier PJM.** 1996. Nucleocapsid-independent assembly of coronavirus-like particles by co-expression of viral envelope protein genes. EMBO J **15:**2020–2028.
68. **Ho Y, Lin PH, Liu CY, Lee SP, Chao YC.** 2004. Assembly of human severe acute respiratory syndrome coronavirus-like particles. Biochem Biophys Res Commun **318:**833–838. http://dx.doi.org/10.1016/j.bbrc.2004.04.111.
69. **Channappanavar R, Zhao J, Perlman S.** 2014. T cell-mediated immune response to respiratory coronaviruses. Immunol Res **59:**118–128. http://dx.doi.org/10.1007/s12026-014-8534-z.
70. **Huang da W, Sherman BT, Lempicki RA.** 2009. Systematic and integrative analysis of large gene lists using DAVID bioinformatics resources. Nat Protoc **4:**44–57. http://dx.doi.org/10.1038/nprot.2008.211.
71. **Kim SJ, Park K, Koeller D, Kim KY, Wakefield LM, Sporn MB, Roberts AB.** 1992. Post-transcriptional regulation of the human transforming growth factor-beta 1 gene. J Biol Chem **267:**13702–13707.
72. **Martin J, Jenkins RH, Bennagi R, Krupa A, Phillips AO, Bowen T, Fraser DJ.** 2011. Post-transcriptional regulation of transforming growth factor beta-1 by microRNA-744. PLoS One **6:**e25044. http://dx.doi.org/10.1371/journal.pone.0025044.
73. **Jimenez-Guardeno JM, Nieto-Torres JL, DeDiego ML, Regla-Nava JA, Fernandez-Delgado R, Castano-Rodriguez C, Enjuanes L.** 2014. The PDZ-binding motif of severe acute respiratory syndrome coronavirus envelope protein is a determinant of viral pathogenesis. PLoS Pathog **10:**e1004320. http://dx.doi.org/10.1371/journal.ppat.1004320.
74. **Teoh KT, Siu YL, Chan WL, Schluter MA, Liu CJ, Peiris JS, Bruzzone R, Margolis B, Nal B.** 2010. The SARS coronavirus E protein interacts with PALS1 and alters tight junction formation and epithelial morphogenesis. Mol Biol Cell **21:**3838–3852. http://dx.doi.org/10.1091/mbc.E10-04-0338.
75. **Cohen JR, Lin LD, Machamer CE.** 2011. Identification of a Golgi complex-targeting signal in the cytoplasmic tail of the severe acute respiratory syndrome coronavirus envelope protein. J Virol **85:**5794–5803. http://dx.doi.org/10.1128/JVI.00060-11.
76. **Puneet P, Moochhala S, Bhatia M.** 2005. Chemokines in acute respiratory distress syndrome. Am J Physiol Lung Cell Mol Physiol **288:**L3–L15. http://dx.doi.org/10.1152/ajplung.00405.2003.
77. **Nagata N, Iwata N, Hasegawa H, Fukushi S, Harashima A, Sato Y, Saijo M, Taguchi F, Morikawa S, Sata T.** 2008. Mouse-passaged severe acute respiratory syndrome-associated coronavirus leads to lethal pulmonary edema and diffuse alveolar damage in adult but not young mice. Am J Pathol **172:**1625–1637. http://dx.doi.org/10.2353/ajpath.2008.071060.
78. **Grommes J, Soehnlein O.** 2011. Contribution of neutrophils to acute lung injury. Mol Med **17:**293–307. http://dx.doi.org/10.2119/molmed.2010.00138.
79. **Tsui PT, Kwok ML, Yuen H, Lai ST.** 2003. Severe acute respiratory syndrome: clinical outcome and prognostic correlates. Emerg Infect Dis **9:**1064–1069. http://dx.doi.org/10.3201/eid0909.030362.
80. **Narasaraju T, Yang E, Samy RP, Ng HH, Poh WP, Liew AA, Phoon MC, van Rooijen N, Chow VT.** 2011. Excessive neutrophils and neutrophil extracellular traps contribute to acute lung injury of influenza pneumonitis. Am J Pathol **179:**199–210. http://dx.doi.org/10.1016/j.ajpath.2011.03.013.
81. **Brandes M, Klauschen F, Kuchen S, Germain RN.** 2013. A systems analysis identifies a feedforward inflammatory circuit leading to lethal influenza infection. Cell **154:**197–212. http://dx.doi.org/10.1016/j.cell.2013.06.013.
82. **Bataki EL, Evans GS, Everard ML.** 2005. Respiratory syncytial virus and neutrophil activation. Clin Exp Immunol **140:**470–477. http://dx.doi.org/10.1111/j.1365-2249.2005.02780.x.
83. **Yasui K, Baba A, Iwasaki Y, Kubo T, Aoyama K, Mori T, Yamazaki T, Kobayashi N, Ishiguro A.** 2005. Neutrophil-mediated inflammation in respiratory syncytial viral bronchiolitis. Pediatr Int **47:**190–195. http://dx.doi.org/10.1111/j.1442-200x.2005.02039.x.
84. **De Filippo K, Dudeck A, Hasenberg M, Nye E, van Rooijen N, Hartmann K, Gunzer M, Roers A, Hogg N.** 2013. Mast cell and macrophage chemokines CXCL1/CXCL2 control the early stage of neutrophil recruitment during tissue inflammation. Blood **121:**4930–4937. http://dx.doi.org/10.1182/blood-2013-02-486217.
85. **Wareing MD, Lyon A, Inglis C, Giannoni F, Charo I, Sarawar SR.** 2007. Chemokine regulation of the inflammatory response to a low-dose influenza infection in CCR2−/− mice. J Leukoc Biol **81:**793–801. http://dx.doi.org/10.1189/jlb.0506299.
86. **Fujiwara N, Kobayashi K.** 2005. Macrophages in inflammation. Curr Drug Targets Inflamm Allergy **4:**281–286. http://dx.doi.org/10.2174/1568010054022024.
87. **Jenkins SJ, Ruckerl D, Cook PC, Jones LH, Finkelman FD, van Rooijen N, MacDonald AS, Allen JE.** 2011. Local macrophage proliferation, rather than recruitment from the blood, is a signature of TH2 inflammation. Science **332:**1284–1288. http://dx.doi.org/10.1126/science.1204351.
88. **Enjuanes L, DeDiego ML, Alvarez E, Deming D, Sheahan T, Baric R.** 2008. Vaccines to prevent severe acute respiratory syndrome coronavirus-induced disease. Virus Res **133:**45–62. http://dx.doi.org/10.1016/j.virusres.2007.01.021.
89. **Graham RL, Donaldson EF, Baric RS.** 2013. A decade after SARS: strategies for controlling emerging coronaviruses. Nat Rev Microbiol **11:**836–848. http://dx.doi.org/10.1038/nrmicro3143.

Journal of Virological Methods 193 (2013) 639–646

Contents lists available at ScienceDirect

Journal of Virological Methods

journal homepage: www.elsevier.com/locate/jviromet

The replication of a mouse adapted SARS-CoV in a mouse cell line stably expressing the murine SARS-CoV receptor mACE2 efficiently induces the expression of proinflammatory cytokines

Jose A. Regla-Nava[a], Jose M. Jimenez-Guardeño[a], Jose L. Nieto-Torres[a], Thomas M. Gallagher[b], Luis Enjuanes[a,*], Marta L. DeDiego[a]

[a] Department of Molecular and Cell Biology, Centro Nacional de Biotecnología (CNB-CSIC), Darwin 3, Campus Universidad Autónoma de Madrid, 28049 Madrid, Spain
[b] Department of Microbiology and Immunology, Loyola University Medical Center, 2160 South First Avenue, Maywood, IL 60153, USA

Article history:
Received 7 March 2013
Received in revised form 10 July 2013
Accepted 15 July 2013
Available online 1 August 2013

Keywords:
SARS
Coronavirus
Mouse adapted
Stably transformed murine cells
SARS-CoV receptor ACE2
Proinflammatory cytokines

A B S T R A C T

Infection of conventional mice with a mouse adapted (MA15) severe acute respiratory syndrome (SARS) coronavirus (CoV) reproduces many aspects of human SARS such as pathological changes in lung, viremia, neutrophilia, and lethality. However, established mouse cell lines highly susceptible to mouse-adapted SARS-CoV infection are not available. In this work, efficiently transfectable mouse cell lines stably expressing the murine SARS-CoV receptor angiotensin converting enzyme 2 (ACE2) have been generated. These cells yielded high SARS-CoV-MA15 titers and also served as excellent tools for plaque assays. In addition, in these cell lines, SARS-CoV-MA15 induced the expression of proinflammatory cytokines and IFN-β, mimicking what has been observed in experimental animal models infected with SARS-CoV and SARS patients. These cell lines are valuable tools to perform in vitro studies in a mouse cell system that reflects the species used for in vivo studies of SARS-CoV-MA15 pathogenesis.

1. Introduction

Severe acute respiratory syndrome coronavirus (SARS-CoV) is an enveloped plus-strand RNA virus of the *Coronaviridae* family, genus β, within the *Nidovirales* order (de Groot et al., 2012; Enjuanes et al., 2008). SARS-CoV was first detected in late 2002 in Guangdong province, China and spread to more than 30 countries in a few months, causing 8000 infections and 800 deaths (Drosten et al., 2003; Fouchier et al., 2003; Ksiazek et al., 2003; Kuiken et al., 2003; Marra et al., 2003; Peiris et al., 2003; Rota et al., 2003). The spread of the virus was ultimately controlled by the isolation of infected individuals, and the WHO declared the end of the SARS epidemic in July 2003. However, SARS-like coronaviruses remain and are circulating in bats all over the world, making virus reemergence a realistic possibility (Lau et al., 2005; Li et al., 2005; Woo et al., 2006).

Coronaviruses encode two overlapping open reading frames (ORFs 1a and 1b) that are translated into two polyproteins which are processed by two viral proteases to yield 16 non-structural replicase proteins (Ziebuhr et al., 2000). These proteins are involved in genome replication and transcription of subgenomic mRNAs encoding the structural proteins nucleocapsid (N), envelope (E), membrane (M) and spike (S), as well as a set of CoV species-specific proteins. The spike protein is localized at the surface of the virion, and is responsible for the attachment to the cellular receptor, and for virus-cell membrane fusion, to facilitate virus entry (Gallagher and Buchmeier, 2001). The cellular receptor for SARS-CoV is the angiontesin convertin enzyme 2 (ACE2) (Li et al., 2003; Wong et al., 2004), although the glycoprotein CD209L (L-SIGN) may also be used as a weaker alternative receptor (Jeffers et al., 2004).

SARS-CoV infects many experimental animals such as mice, ferrets, cats, hamsters and non-human primates (cynomolgus and rhesus macaques, African green monkeys and marmosets) (Roberts et al., 2008; Subbarao and Roberts, 2006). However, none of the infection models completely reproduce human clinical disease and pathological findings. To overcome these limitations, SARS-CoV was adapted to grow in mice by passing the virus in lung for 10, 15, or 25 times (Day et al., 2009; Nagata et al., 2008; Roberts et al.,

* Corresponding author at: Department of Molecular and Cell Biology, Centro Nacional de Biotecnología (CNB-CSIC), Darwin 3, Cantoblanco, 28049 Madrid, Spain. Tel.: +34 915854555; fax: +34 915854506.
E-mail address: L.Enjuanes@cnb.csic.es (L. Enjuanes).

0166-0934/$ – see front matter © 2013 Elsevier B.V. All rights reserved.
http://dx.doi.org/10.1016/j.jviromet.2013.07.039

2007). Infection of Balb/c mice with the resulting mouse adapted (MA) viruses reproduced many aspects of human SARS, including pathological changes in the lung, viremia, neutrophilia, and lethality (Day et al., 2009; Nagata et al., 2008; Roberts et al., 2007). This inbred mouse model of human SARS disease has many advantages compared to the other animal models, such as small animal size, low cost, availability of the animals, the possibility to genetically manipulate the host animals (i.e. to develop gene knock-outs and knock-ins), and the availability of immunological and molecular biology reagents specific to the host animals.

Coronaviruses generally do not induce a high interferon response (Frieman et al., 2008). At least two mechanisms have been proposed to explain the low levels of type I interferon (IFN-α and -β) during coronavirus infections: the sequestering of viral RNA in double membrane vesicles (Gosert et al., 2002; Knoops et al., 2008), which prevents or reduces recognition by pattern recognition receptors (PRRs); and the expression of viral proteins that antagonize the innate response. In fact, SARS-CoV proteins nsp1, nsp3, 3b, 6, M and N act as interferon antagonists (Devaraj et al., 2007; Frieman et al., 2007; Kopecky-Bromberg et al., 2007; Narayanan et al., 2008; Siu et al., 2009; Sun et al., 2012; Wathelet et al., 2007). However, even with these viral strategies of defensive evasion and offensive antagonism of interferons, there are well-described host proinflammatory responses to in vivo SARS-CoV infections. Inflammatory mediators such as interleukin (IL)-1, -6, and -8, CXCL10/interferon-inducible protein (IP)-10, CCL2/monocyte chemoattractant protein (MCP)-1, CCL5/protein regulated and normal T expressed and secreted (RANTES), and CXCL9/monokine induced by interferon gamma (MIG) have been recognized in lungs of patients affected by SARS (Cameron et al., 2007; Huang et al., 2005; Jiang et al., 2005; Reghunathan et al., 2005; Tang et al., 2005; Wong et al., 2003; Zhang et al., 2004). Upregulation of genes mediating inflammation has also been described after infection with SARS-CoV in different animal models such as cynomolgus macaques and African green monkeys (de Lang et al., 2007; Smits et al., 2010, 2011) and mice (Baas et al., 2008). Accordingly, the expression of several proinflammatory genes is considered to be a strong correlate of SARS-CoV induced pathology.

Several established cell lines from different species, including monkey cells Vero E6, MA104 and FRhK-4, human cells Caco-2, CL-14, LoVo and Huh-7, pig cells PK-15, POEK and PS, and mink cells Mv 1 Lu (Chan et al., 2004; Cinatl et al., 2004; Hattermann et al., 2005; Mossel et al., 2005; Ng et al., 2003) are susceptible to SARS-CoV infection. However, not all of these cell lines possess the full complement of genes encoding innate immune signaling and response factors, and as such, some of the cell lines are not suitable for evaluating the innate host response to SARS-CoV. Mouse DBT cells have been transfected with human or civet SARS-CoV receptor ACE2 (Becker et al., 2008; Sheahan et al., 2008a,b). However, as far as we know, the susceptibility of these cell lines to a mouse adapted SARS-CoV has not been determined. In addition, mouse cell lines have never been stably transfected with the mouse ACE2, which is the natural receptor used by the mouse adapted SARS-CoV.

In this work, we established mouse cell lines stably expressing the murine SARS-CoV receptor ACE2 (Li et al., 2003; Wong et al., 2004). These cell lines were highly susceptible to mouse adapted SARS-CoV infection and were also transfectable with high efficiency. Using these cell lines, we demonstrated that a mouse adapted SARS-CoV (SARS-CoV-MA15) induced the expression of genes leading to inflammation, as shown in SARS patients and experimental animal models infected with SARS-CoV. In addition, SARS-CoV-MA15 induced a weak IFN-β response, as generally shown in coronavirus infections, preventing the robust production of type I IFNs. These mouse cell lines are valuable tools to perform in vitro studies that could be further developed in the species-homologous SARS mouse models.

2. Materials and methods

2.1. Cells

Delayed brain tumor (DBT) cells were originally obtained from an intracerebral tumor induced in an adult BALB/c mouse by intracerebral injection of Rous sarcoma virus (Kumanishi, 1967). The African green monkey kidney-derived Vero E6 cells were kindly provided by Snijder (University of Leiden, The Netherlands). Cells were cultured in Dulbecco's modified Eagle's medium (DMEM, GIBCO) supplemented with 25 mM HEPES, 10% fetal bovine serum (FBS, Biowhittaker), and 1% non-essential amino acids (SIGMA) and incubated in a 5% CO_2 atmosphere, at 37 °C.

2.2. Plasmids

The plasmid pcDNA3.1 encoding the murine ACE2 gene (GeneBank sequence NM_001130513.1) fused to 5′ myc tag codons (pcDNA3.1-myc-mACE2), and a gene providing geneticin (G418) resistance in prokaryotic and eukaryotic cells, was kindly provided by Farzan (Harvard Medical School, USA) (Li et al., 2004). SARS-CoV full-length cDNAs encoding the Urbani strain or the mouse adapted strain (MA15) were assembled in bacterial artificial chromosomes (BACs) under the control of the cytomegalovirus (CMV) immediate-early promoter to allow the expression of the viral RNA in the nucleus by cellular RNA polymerase II. At the 3′ end, these cDNAs were flanked by a 25-bp poly(A) tail, followed by the hepatitis delta virus ribozyme and the bovine growth hormone and termination and polyadenylation sequences, to generate a correct 3′ end (Almazan et al., 2006, 2000).

2.3. Viruses

SARS-CoV-Urbani and SARS-CoV-MA15 viruses (Roberts et al., 2007) were rescued from infectious cDNA clones generated (Almazan et al., 2006; Fett et al., 2013). To recover infectious viruses, BHK cells were grown to 95% confluence in a 25-cm^2 flask and transfected with the cDNA clones by using Lipofectamine 2000 (Invitrogen) according to the manufacturer's specifications. At 6 h posttransfection (hpt), cells were trypsinized, plated over a confluent monolayer of Vero E6 cells grown in a 25-cm^2 flask, and incubated at 37 °C for 72 h. After one passage in Vero E6 cells, the recovered viruses were cloned by three rounds of plaque purification. All work with infectious viruses was performed in biosafety level (BSL) 3 plus facilities. All personnel were equipped with positive-pressure air purifying respirators (3 M HEPA AirMate, St. Paul, MN).

2.4. Generation of DBT cells stably expressing mACE2

To transfect DBT-mACE2 with high efficiency, 3×10^5 DBT-mACE2 cells were transfected using the program EN-158 of Amaxa 4D-Nucleofector and 1 μg of the linearized plasmid pcDNA3.1-myc-mACE2 in buffer SG (Lonza). Nucleofected cells were seeded on 24-well plates. After nucleofection, cells were incubated for 10 min at room temperature (RT), and then the cells were added to DMEM (GIBCO) supplemented with 25 mM HEPES, 10% fetal bovine serum (FBS, Biowhittaker) and 1% non-essential amino acids (SIGMA) and incubated at 37 °C. 24 h post-nucleofection, G418 was added to the culture medium, to a final concentration of 800 μg/ml, to select for geneticin resistance. The selective medium was changed every 3–4 days for 2 weeks, and the cells were cloned three times by limiting dilution (1 cell/well) in the presence of G418

(800 μg/ml). Subsequently, ten clones of DBT-mACE2 were amplified in the presence of 800 μg/ml of G418.

2.5. Transfection of DBT-mACE2 clones

To analyze the efficiency of transfection, DBT-mACE2 cells were nucleofected as described above, using a GFP-encoding plasmid. 24 h post nucleofection GFP expression was analyzed by fluorescence activated cell sorting (FACS). DBT-mACE2 cells were transfected with an efficiency higher than 90%.

2.6. Indirect immunofluorescence microscopy

To detect viral N proteins and the myc tag fused to mACE2, DBT-mACE2 cells were grown to 80% confluence on glass coverslips and infected with rSARS-CoV-MA15 at a moi of 0.1. At 24 hpi, media were removed and cells were washed twice with PBS and fixed and permeabilized with ice-cold 100% methanol for 20 min at −20 °C or with 4% paraformaldehyde in phosphate buffered saline (PBS) for 30 min at room temperature, in the case of non-permeabilized cells. Primary antibody incubations were performed in PBS containing 10% FBS for 90 min at room temperature. The mouse mAb SA46-4 specific for N protein, kindly provided by Fang (South Dakota State University, Brookings, USA) (dilution 1:500), and a mouse anti-myc (dilution 1:500, Millipore, Ref. 05-724), were used. Coverslips were washed two times with PBS between primary and secondary antibody incubations. Secondary antibodies (Invitrogen) were Alexa 488 (for detection of N protein) or Alexa 594 (for detection of myc tag) conjugates and were incubated for 45 min at room temperature at 1:500 dilutions in PBS containing 10% FBS. Nuclei were stained using DAPI (dilution 1:200, Sigma). Coverslips were mounted in Prolong Gold anti-fade reagent (Invitrogen) and examined on a Leica SP5 confocal microscope (Leica Microsystems). The percentage of mACE2 and viral N-positive cells were calculated by analyzing 10 random fields, each one containing at least 30 cells.

2.7. Virus production in different DBT-mACE2 clones

DBT-mACE2 clones grown to densities of 3.0×10^5 cells/cm^2 were infected at a moi of 0.1 with SARS-CoV-MA15 or SARS-CoV-Urbani. Culture supernatants were collected at 72 hpi, and virus titers were determined in Vero E6 cells as previously described (DeDiego et al., 2007).

To analyze the effect of the moi on virus production, DBT-mACE2 clone 6 cells, which supported the highest viral titers, were infected at mois ranging from 0.0001 to 1 pfu per cell with the rSARS-CoV-MA15 virus. Culture supernatants were collected at the indicated times post-infection and titrated on Vero E6 cells.

To determine the effect of cell density on virus production, DBT-mACE2 clone 6 cells at different cell densities were infected at a moi of 0.1. Culture supernatants were collected at 72 hpi and titrated in Vero E6 cells.

2.8. Virus titration in DBT-mACE2 cells

DBT-mACE2 clone 6 cells at a cell density of 2.5×10^5 cells/cm^2 were infected with SARS-CoV-MA15. Cell cultures were incubated at 37 °C for 60 min for virus adsorption and then overlaid with DMEM containing 0.6% low melting agarose and 4% FBS. 48 hpi, cells were fixed with 10% formaldehyde in PBS and stained with a solution containing 0.1% (w/v) crystal violet and 20% methanol.

2.9. Expression of inflammation-related cytokines and IFN-β and -γ in rSARS-CoV-MA15 infected cells

DBT-mACE2 clone 6 cells were infected with rSARS-CoV at a moi of 0.1. Total RNAs from DBT-mACE2 infected cells were extracted at 48 hpi using the Qiagen RNeasy kit according to the manufacturer's instructions. Quantitative reverse transcription-polymerase chain reaction (qRT-PCR) reactions were performed at 37 °C for 2 h with a High Capacity cDNA transcription kit (Applied Biosystems) using 100 ng of total RNA and random hexamer oligonucleotides. Cellular gene expressions were analyzed using TaqMan gene expression assays (Applied Biosystems) specific for *Mus musculus* genes (Table 1). Data were acquired with an ABI PRISM 7000 sequence detection system (Applied Biosystems) and analyzed with ABI PRISM 7000 SDS version 1.0 software. Gene expression in mock-infected cells and rSARS-CoV-MA15-infected cells was compared. Quantification was achieved using the $2 - \Delta\Delta$Ct method, which analyzes relative changes in gene expression in qPCR experiments (Livak and Schmittgen, 2001). The results of three independent experiments were analyzed. DBT-mACE2 clone 6 cells were infected at a moi of 0.1 and cell extracts in lysis buffer (1% NP-40, 50 mM Tris–HCl, pH 7.6, 2 mM NaCl, 2 mM EDTA and protease inhibitors) were prepared at 48 hpi. Cell extracts were diluted 1:5 in assay buffer (Millipore). The expression of mouse CXCL10/IP-10 and CXCL2/macrophage inflammatory protein 2 (MIP-2) was evaluated with the Luminex technology and a mouse cytokine antibody bead kit (Milliplex map kit; Millipore), following the manufacturer's instructions. Data were collected from three independent infections.

3. Results

3.1. Generation of mouse DBT cells expressing the SARS-CoV receptor mACE2

To generate a mouse cell line susceptible to SARS-CoV infection, DBT cells were nucleofected with a plasmid encoding the SARS-CoV receptor mACE2 fused N-terminally to a myc tag (myc-mACE2) along with an antibiotic resistance marker. Transfected cells were selected by using geneticin (G418). Ten independently-derived cell clones were generated. mACE2 expression in the different clones was analyzed by immunofluorescence using an antibody specific for the myc tag. The ten selected clones showed high mACE2 expression in more than 70% of the cells (Fig. 1A and B). The myc-mACE2 expression was stable for at least 20 passages in tissue culture (data not shown). Myc-mACE2 was detected in the plasma membrane even in non-permeabilized cells, confirming that mACE2 is present at the cell surface. As expected, myc-mACE2 was undetectable in untransfected DBT cells (Fig. 1A and B). To determine whether the DBT-mACE2 clones were easily transfected with plasmid DNAs (a useful method for future studies), the cells were nucleofected with a plasmid encoding green fluorescent protein (GFP). Interestingly, the efficiency of DBT-mACE2 nucleofection was greater than 90% (data not shown).

3.2. Susceptibility of DBT-mACE2 to SARS-CoV infection

To determine whether the DBT-mACE2 cells were susceptible to SARS-CoV, the 10 selected clones, untransfected DBT cells, and positive-control Vero E6 cells were infected with the mouse adapted SARS-CoV-MA15 strain at a moi of 0.1. No infectious virus was recovered from untransfected DBT cells at 72 hpi (Fig. 2A). Interestingly, in transfected cells, all DBT-mACE2 clones showed high viral titers at 72 hpi, ranging from 5.0×10^6 to 1.2×10^7 pfu/ml, respectively. DBT-mACE2 clones 1 and 6 produced the highest virus

Table 1
Taqman assays used to analyze the expression of cellular genes by quantitative RT-PCR.

Gene name	Taqman assay[a]	Description
TNF	Mm00443258-m1	Tumor necrosis factor
IL-1α	Mm00439620-m1	Interleukin 1α
IL-1β	Mm01336189-m1	Interleukin 1β
IL-6	Mm00446190-m1	Interleukin 6
CCL2/MCP-1	Mm00441242-m1	Monocyte chemotactic protein 1
CCL5/RANTES	Mm01302428-m1	Regulated upon activation, normal T-cell expressed, and secreted
CXCL1/NAP-3	Mm04207460-m1	Neutrophil activating protein 3
CXCL2/MIP-2	Mm00436450-m1	Macrophage inflammatory protein 2
CXCL10/IP-10	Mm00445235-m1	Interferon inducible protein 10
IFN-β	Mm00439552-s1	Interferon β
IFN-γ	Mm01168134-m1	Interferon γ
18S	Mm03928990-g1	Ribosomic RNA 18S

[a] Mm, means Mus musculus.

outputs (9.2×10^6 and 1.2×10^7 pfu/ml), which were as high as those obtained in Vero E6 cells (Fig. 2A).

To analyze whether DBT-mACE2 cells were also susceptible to a non-mouse adapted SARS-CoV, the clone 6 of DBT-mACE2 cells, producing the highest SARS-CoV-MA15 titers, untransfected DBT cells and Vero E6 cells were infected with SARS-CoV-Urbani.

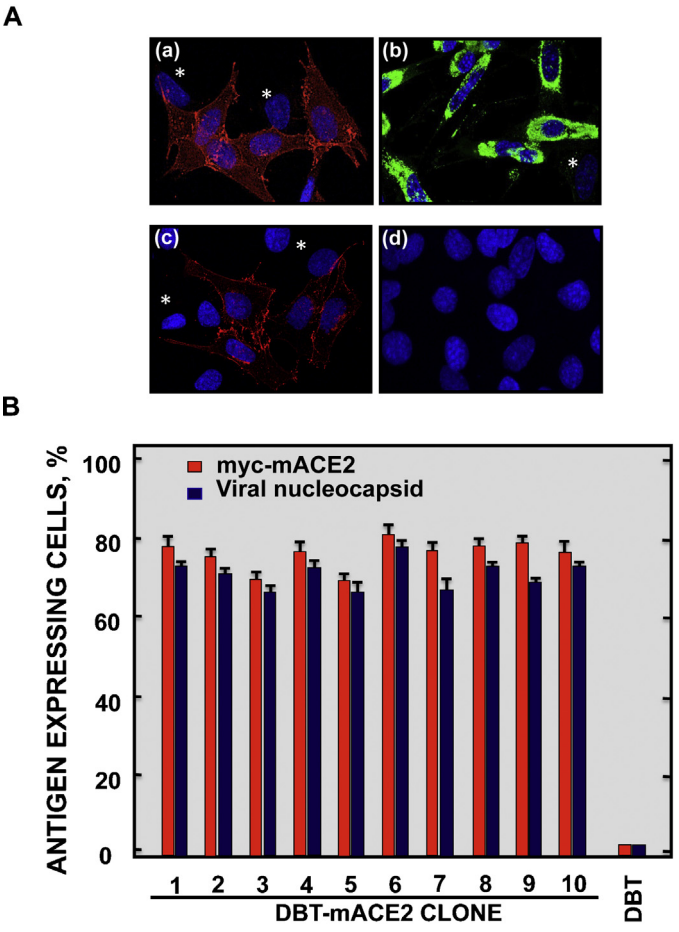

Fig. 1. Expression of myc-mACE2 and viral nucleoprotein in DBT-mACE2-infected clones. (A) Untransformed DBT and DBT-mACE2 cells were infected at a moi of 0.1 with rSARS-CoV-MA15. Myc-mACE2 and viral nucleoprotein expression was analyzed by indirect immunofluorescence using specific myc and nucleoprotein antibodies followed by A549 and A488-conjugated secondary mouse antibodies. Asterisks indicate cells that do not express myc-mACE2 or viral nucleoprotein, as controls. (a) myc-mACE2 in permeabilized cells, (b) viral nucleoprotein in permeabilized cells, (c) myc-mACE2 in non-permeabilized cells and (d) myc-mACE2 and nucleoprotein in untransformed DBT cells. (B) The percentage of myc-mACE2 positive and viral N protein-positive cells was calculated by analyzing 10 random fields, each one containing 30 cells.

Infectious viruses were also recovered in DBT-mACE2 cells, although with titers more than 10^3-fold lower than those for SARS-CoV-MA15 (Fig. 2B). In contrast, no infectious virus was recovered from untransfected DBT cells. SARS-CoV-Urbani and MA15 virus titers in Vero E6 cells were similar for both viruses (Fig. 2A and B).

To identify conditions for optimal virus production, moi and cell density parameters were varied. Firstly, DBT-mACE2 clone 6 cells were infected with SARS-CoV-MA15 at mois ranging from 0.0001 to 1. Virus titers were determined at 0, 4, 24, 48 and 72 hpi (Fig. 3). The highest viral titer (>10^7 pfu/ml) was obtained at moi of 0.1. Virus

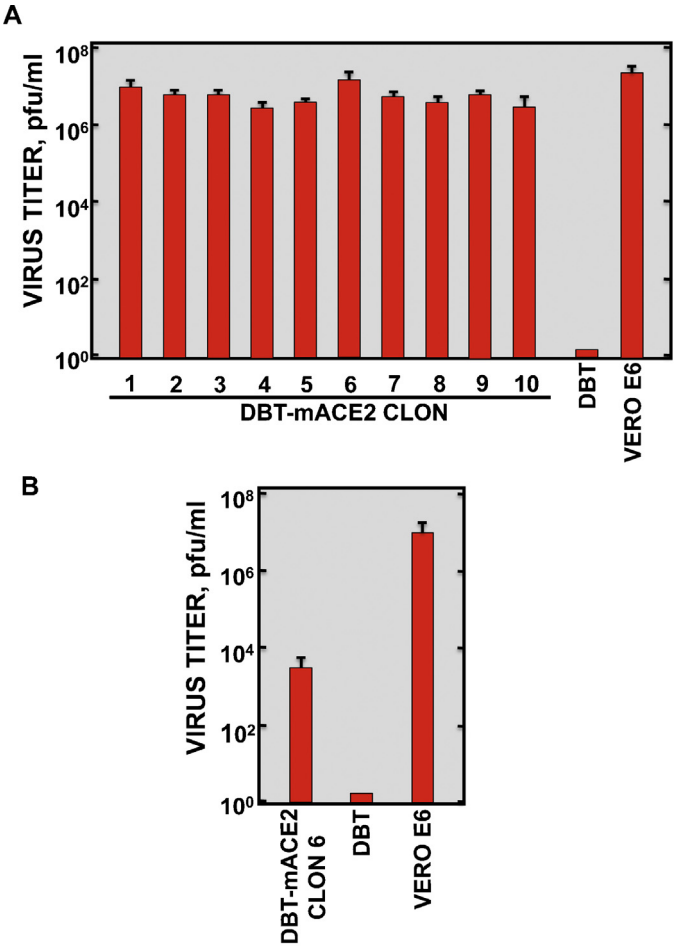

Fig. 2. SARS-CoV production in DBT-mACE2 cell clones. Cells were infected at a moi of 0.1 with rSARS-CoV-MA15 (A) or rSARS-CoV-Urbani. (B) Viral titers in cell supernatants at 72 hpi were measured using a plaque assay on Vero E6 cells. Error bars represent standard deviations of the mean from three experiments.

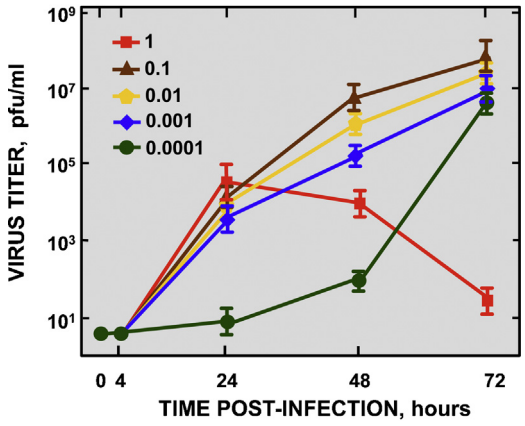

Fig. 3. Effect of moi on the growth kinetics of SARS-CoV-MA15 in DBT-mACE2 clone 6 cells. DBT-mACE2 clone 6 cells were infected at the indicated input mois. Viral titers in cell supernatants at the indicated times post-infection were measured by plaque assay on Vero E6 cells. Error bars represent standard deviations of the mean from three experiments.

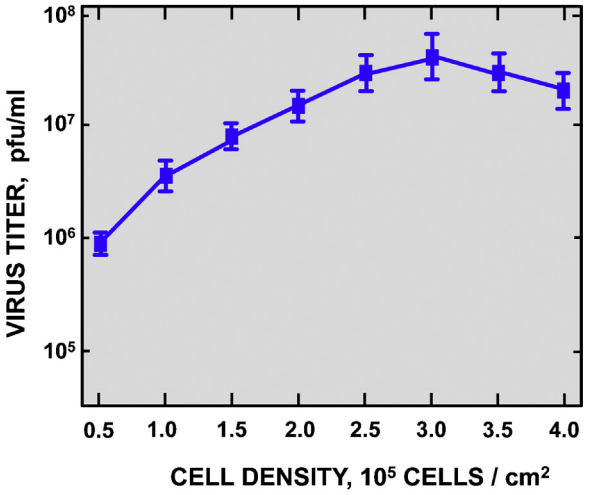

Fig. 4. Effect of cell density on the growth of SARS-CoV-MA15 in DBT-mACE2 clone 6 cells. DBT-mACE2 clone 6 cells were seeded at different cell densities and infected at a moi of 0.1. Viral titers in cell supernatants at 72 hpi were measured by plaque assay on Vero E6 cells. Error bars represent standard deviations of the mean from three experiments.

titers in cells infected with a moi of 1 rapidly decreased after 24 hpi, probably due to extensive cell death. Indeed, considerable cytopathic effect (CPE) was observed by microscopy. DBT-mACE2 clone 6 cells were also infected at cells densities ranging from 0.5×10^5 and 4×10^5 cells/cm^2, at the optimal moi of 0.1, and virus titers were determined at 72 hpi. The highest viral titers (>10^7 pfu/ml) were observed at a cell density of 3×10^5 cells/cm^2 (Fig. 4).

To determine the percentage of infected cells, untransfected DBT cells, and DBT-mACE2 clones were infected with SARS-CoV-MA15, and analyzed by immunofluorescence with an antibody specific for the viral N protein (Fig. 1A and B). The percentage of infected cells, detected by the presence of N protein, was higher than 70% in all the DBT-mACE2 transfected clones.

SARS-CoV infection caused CPE in DBT-mACE2 cells. At input mois of 0.1, cell rounding and detachment was evident at 48 hpi, being almost total at 72 hpi. Control uninfected cells showed no morphological changes (Fig. 5A). In fact, SARS-CoV-MA15 formed

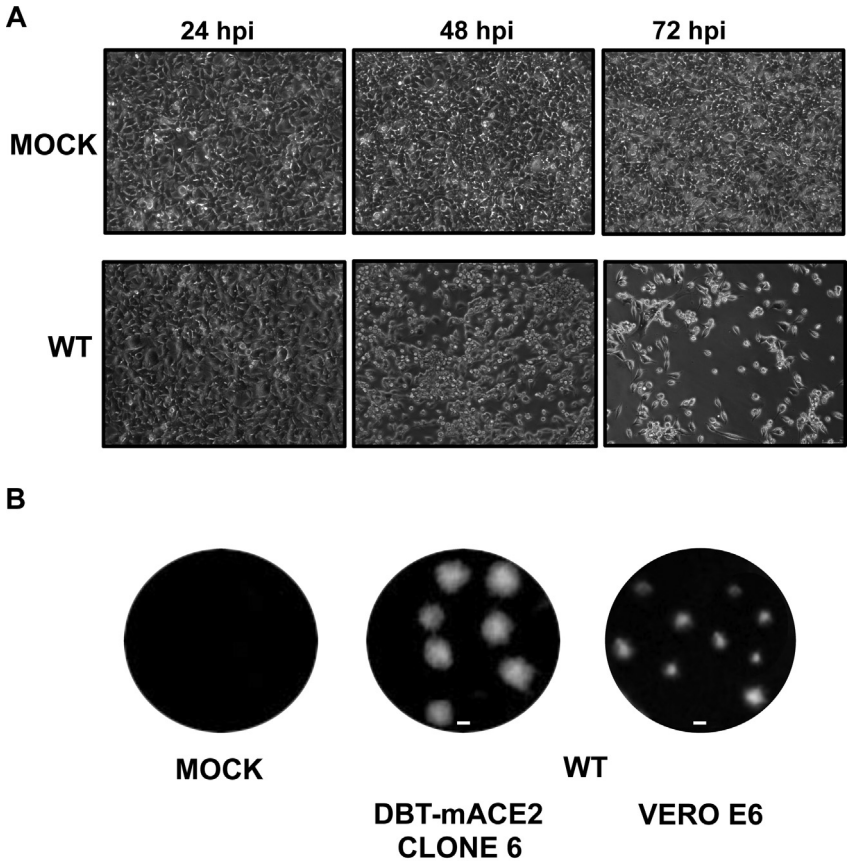

Fig. 5. Cytopathic effect and lysis plaques produced by SARS-CoV-MA15 on DBT-mACE2 clone 6 cells. (A) DBT-mACE2 clone 6 cells were mock-infected or infected with SARS-CoV-MA15 at a moi of 0.1. CPE was visualized at 24, 48, and 72 hpi. (B) Lysis plaques produced after 2 days by SARS-CoV-MA15 infection in DBT-mACE2 and Vero E6 cells.

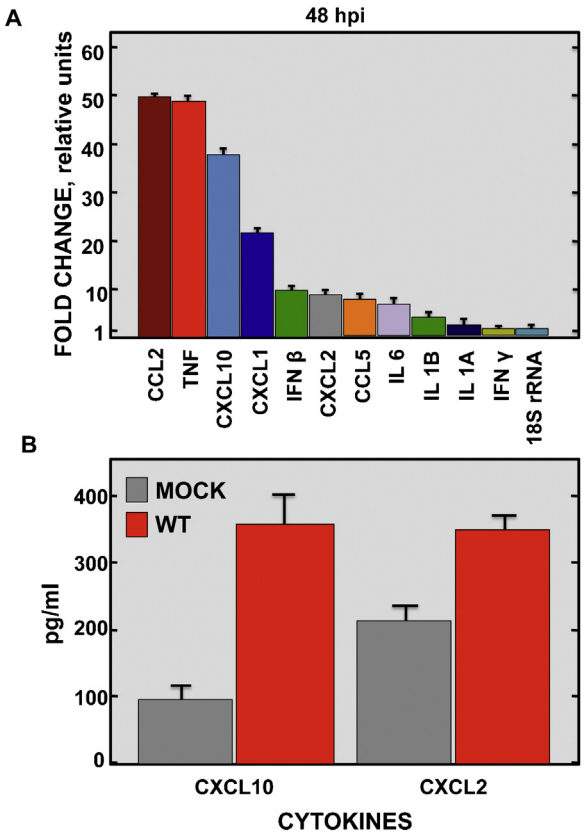

Fig. 6. Expression of proinflammatory cytokines in SARS-CoV-MA15-infected cells. DBT-mACE2 clone 6 cells were infected at a moi of 0.1 with rSARS-CoV-MA15. (A) Cellular RNAs were extracted at 48 hpi. The expression of the indicated cytokines and interferons, and that of 18S rRNA as a control, was determined by qRT-PCR. In each case, the corresponding mRNA expression levels in SARS-CoV-MA15-infected cells were plotted as fold-change relative to expression levels in uninfected cells. (B) Cell extracts were prepared at 48 hpi. Expression of the cytokines CXCL10 and CXCL2 at the protein level was evaluated in mock and DBT-mACE2-infected cells.

clear, easily identifiable plaques in DBT-mACE2 cell monolayers. Lysis plaques on DBT-mACE2 cells and Vero E6 cells were compared. Smaller plaques were observed using Vero E6 cells in comparison to DBT-mACE2 cells (Fig. 5B). Virus titers obtained by plaque assays on Vero E6 and DBT-mACE2 indicator cells were very similar (4.3×10^7 and 4.0×10^7, respectively).

3.3. Expression of inflammation related cytokines

Cytokines and IFNs are important mediators in the regulation of the immune response. To determine whether DBT-mACE2 cells are good models to evaluate the inflammatory host response to SARS-CoV infection in vitro, the mRNA expression levels of several inflammation-related cytokines and that of IFN-β and IFN-γ were analyzed by quantitative RT-PCR. Specifically, CCL2/MCP-1, tumor necrosis factor (TNF), CXCL10/IP-10, CXCL1/neutrophil activating protein 3 (NAP-3), IFN-β, CXCL2/MIP-2, CCL5/RANTES, IL6, IL1B, IL1A, and IFN-γ transcripts, and 18S rRNA, as control, were compared in both uninfected and SARS-CoV-MA15-infected cells at 24, 48 and 72 hpi. The levels of cytokine mRNAs at 24 hpi, were lower compared to 48 hpi, showing fold-increases of 1.2 to 3-fold over mock. Similar levels were observed for 48 and 72 hpi (data not shown). CCL2/MCP-1, TNF, CXCL10/IP-10 and CXCL1/NAP-3 were the most upregulated cytokines 48 h after SARS-CoV infection (between 22- and 50-fold increase; Fig. 6A). Less striking upregulations were observed for IFN-β, CXCL2/MIP-2, CCL5/RANTES and IL6, whereas more limited changes were obtained for IL 1B, IL 1A, and IFN-γ (Fig. 6A). The expression of control 18S rRNA did not change in SARS-CoV or mock-infected cells as expected (Fig. 6A).

To evaluate whether the induction of cytokine mRNAs in SARS-CoV-MA15-infected cells correlate with an induction at the protein level, the levels of CXCL10 and CXCL2 proteins were determined in mock and DBT-mACE2-infected cells. In agreement with the results obtained with the mRNAs, CXCL10 and CXCL2 were also upregulated at the protein level, showing fold-increases of 3 and 1.8-fold over mock, respectively (Fig. 6B). These data indicated that DBT-mACE2 cells were useful to study proinflammatory cytokine expression in vitro.

4. Discussion

The development of established mouse cell lines highly susceptible to mouse-adapted SARS-CoV infection is described in this study. The best current small animal model for SARS-CoV is the infection of Balb/c mice with a mouse adapted SARS-CoV (Day et al., 2009; Nagata et al., 2008; Roberts et al., 2007). The establishment of mouse cell lines susceptible to SARS-CoV was therefore of high interest, so that in vitro and in vivo evaluations with the mouse adapted SARS-CoV could take place in the same species environment and using the same cellular receptor.

The expression of mACE2 was sufficient to convert DBT cells, which were not susceptible to SARS-CoV infection, into cells producing high SARS-CoV-MA15 titers. Similarly, the transient expression of mACE2 in mouse 3T3 cells generated susceptibility to SARS-CoV infection, although these cells were not stably transformed (Li et al., 2004). In addition, the expression of civet and human ACE2 in DBT cells (Becker et al., 2008; Sheahan et al., 2008a,b), and the expression of human ACE2 in mice also led to cells susceptible to SARS-CoV and to an animal model more susceptible to the infection by a human SARS-CoV (McCray et al., 2007; Yang et al., 2007). All these data indicated that ACE2 is clearly a required SARS-CoV receptor.

SARS-CoV-Urbani titers in DBT-mACE2 cells were more than 10^3-fold lower than titers obtained for SARS-CoV-MA15. Critical mutations differentiating these two virus strains map in the gene encoding the spike protein (Roberts et al., 2007) that binds to the cellular ACE2 and facilitates virus entry (Li et al., 2003). The affinity of SARS-CoV-Urbani spike protein binding to mACE2 is lower that the affinity of SARS-CoV-MA15 spike protein binding to mACE2, making the Urbani virus entrance less efficient (Li et al., 2004).

SARS-CoV infection in DBT-mACE2 cells induced high levels of CPE, probably due to apoptosis, as it has been observed in other SARS-CoV-infected cell lines, such as Vero (DeDiego et al., 2011; Ren et al., 2005; Yan et al., 2004). This virus-induced cytopathology provides an additional experimental advantage of DBT-mACE2 cell lines, as the infection outcomes are overt and are similar to what happens to the epithelial respiratory cells in SARS patients (Lang et al., 2003; Zhang et al., 2003). Accordingly, plaque assays of SARS-CoV-MA15 were efficient in DBT-ACE2 cells.

Gene expressions leading to acute inflammation are hallmarks of SARS-CoV infection and have been associated with SARS-CoV-induced pathology (Rockx et al., 2009; Smits et al., 2010). Using genomic analysis, it has been shown that gene expressions encoding proinflammatory cytokines are increased in DBT-mACE2 cells, compared to mock-infected cells. These results correlate with the data obtained in SARS patients (Cameron et al., 2007; Huang et al., 2005; Jiang et al., 2005; Reghunathan et al., 2005; Tang et al., 2005; Wong et al., 2003; Zhang et al., 2004) and in SARS-CoV-infected monkeys and mice (Baas et al., 2008; de Lang et al., 2007; Smits et al., 2010, 2011). In addition, it has been shown that SARS-CoV-MA15 infection induced a limited IFN-β production in DBT-mACE2 cells. This weak induction could be due to the viral RNA sequestering in

double membrane vesicles described in coronaviruses (Gosert et al., 2002; Knoops et al., 2008), which prevents or reduces recognition by PRRs, and to the expression of SARS-CoV proteins that antagonize the innate response (Devaraj et al., 2007; Frieman et al., 2007; Kopecky-Bromberg et al., 2007; Narayanan et al., 2008; Siu et al., 2009; Sun et al., 2012; Wathelet et al., 2007).

The DBT-mACE2 cells generated in this work, could be used in the context of virus adaptation to a homologous receptor of another host species, such as for example hamsters or rats and in the context of mouse adaptation to the murine receptor. In addition, DBT-mACE2 cells may be useful to grow mouse adapted SARS-CoV, with reduced likelihood of undesired changes in the SARS-CoV genome that may occur during replication in non-murine cells.

Acknowledgments

This work was supported by grants from the Ministry of Science and Innovation of Spain (BIO2010-16705), the European Community's Seventh Framework Programme (FP7/2007–2013) under the project "EMPERIE" EC Grant Agreement number 223498, and U.S. National Institutes of Health (NIH) (2P01AI060699-06A1, W000306844). JAR received a fellowship from the Fundacion La Caixa. We thank Marga Gonzalez for her technical assistance.

References

Almazan, F., DeDiego, M.L., Galan, C., Escors, D., Alvarez, E., Ortego, J., Sola, I., Zuñiga, S., Alonso, S., Moreno, J.L., Nogales, A., Capiscol, C., Enjuanes, L., 2006. Construction of a SARS-CoV infectious cDNA clone and a replicon to study coronavirus RNA synthesis. Journal of Virology 80, 10900–10906.

Almazan, F., Gonzalez, J.M., Penzes, Z., Izeta, A., Calvo, E., Plana-Duran, J., Enjuanes, L., 2000. Engineering the largest RNA virus genome as an infectious bacterial artificial chromosome. Proceedings of the National Academy of Sciences of the United States of America 97, 5516–5521.

Baas, T., Roberts, A., Teal, T.H., Vogel, L., Chen, J., Tumpey, T.M., Katze, M.G., Subbarao, K., 2008. Genomic analysis reveals age-dependent innate immune responses to severe acute respiratory syndrome coronavirus. Journal of Virology 82, 9465–9476.

Becker, M.M., Graham, R.L., Donaldson, E.F., Rockx, B., Sims, A.C., Sheahan, T., Pickles, R.J., Corti, D., Johnston, R.E., Baric, R.S., Denison, M.R., 2008. Synthetic recombinant bat SARS-like coronavirus is infectious in cultured cells and in mice. Proceedings of the National Academy of Sciences of the United States of America 105, 19944–19949.

Cameron, M.J., Ran, L., Xu, L., Danesh, A., Bermejo-Martin, J.F., Cameron, C.M., Muller, M.P., Gold, W.L., Richardson, S.E., Poutanen, S.M., Willey, B.M., DeVries, M.E., Fang, Y., Seneviratne, C., Bosinger, S.E., Persad, D., Wilkinson, P., Greller, L.D., Somogyi, R., Humar, A., Keshavjee, S., Louie, M., Loeb, M.B., Brunton, J., McGeer, A.J., Kelvin, D.J., 2007. Interferon-mediated immunopathological events are associated with atypical innate and adaptive immune responses in patients with severe acute respiratory syndrome. Journal of Virology 81, 8692–8706.

Chan, P.K., To, K.F., Lo, A.W., Cheung, J.L., Chu, I., Au, F.W., Tong, J.H., Tam, J.S., Sung, J.J., Ng, H.K., 2004. Persistent infection of SARS coronavirus in colonic cells in vitro. Journal of Medical Virology 74, 1–7.

Cinatl Jr., J., Hoever, G., Morgenstern, B., Preiser, W., Vogel, J.U., Hofmann, W.K., Bauer, G., Michaelis, M., Rabenau, H.F., Doerr, H.W., 2004. Infection of cultured intestinal epithelial cells with severe acute respiratory syndrome coronavirus. Cellular and Molecular Life Sciences 61, 2100–2112.

Day, C.W., Baric, R., Cai, S.X., Frieman, M., Kumaki, Y., Morrey, J.D., Smee, D.F., Barnard, D.L., 2009. A new mouse-adapted strain of SARS-CoV as a lethal model for evaluating antiviral agents in vitro and in vivo. Virology 395, 210–222.

de Groot, R.J., Baker, S.C., Baric, R., Enjuanes, L., Gorbalenya, A.E., Holmes, K.V., Perlman, S., Poon, L., Rottier, P.J.M., Talbot, P.J., Woo, P.C.Y., Ziebuhr, J., 2012. Coronaviridae. In: King, A.M.Q., Adams, M.J., Carstens, E.B., Lefkowitz, E.J. (Eds.), Virus Taxonomy: Ninth Report of the International Committee on Taxonomy of Viruses. Elsevier Academic Press, San Diego, pp. 774–796.

de Lang, A., Baas, T., Teal, T., Leijten, L.M., Rain, B., Osterhaus, A.D., Haagmans, B.L., Katze, M.G., 2007. Functional genomics highlights differential induction of antiviral pathways in the lungs of SARS-CoV-infected macaques. PLoS Pathogens 3, e112.

DeDiego, M.L., Alvarez, E., Almazan, F., Rejas, M.T., Lamirande, E., Roberts, A., Shieh, W.J., Zaki, S.R., Subbarao, K., Enjuanes, L., 2007. A severe acute respiratory syndrome coronavirus that lacks the E gene is attenuated in vitro and in vivo. Journal of Virology 81, 1701–1713.

DeDiego, M.L., Nieto-Torres, J.L., Jimenez-Guardeno, J.M., Regla-Nava, J.A., Alvarez, E., Oliveros, J.C., Zhao, J., Fett, C., Perlman, S., Enjuanes, L., 2011. Severe acute respiratory syndrome coronavirus envelope protein regulates cell stress response and apoptosis. PLoS Pathogens 7, e1002315.

Devaraj, S.G., Wang, N., Chen, Z., Chen, Z., Tseng, M., Barretto, N., Lin, R., Peters, C.J., Tseng, C.T., Baker, S.C., Li, K., 2007. Regulation of IRF-3-dependent innate immunity by the papain-like protease domain of the severe acute respiratory syndrome coronavirus. Journal of Biological Chemistry 282, 32208–32221.

Drosten, C., Gunther, S., Preiser, W., van der Werf, S., Brodt, H.R., Becker, S., Rabenau, H., Panning, M., Kolesnikova, L., Fouchier, R.A., Berger, A., Burguiere, A.M., Cinatl, J., Eickmann, M., Escriou, N., Grywna, K., Kramme, S., Manuguerra, J.C., Muller, S., Rickerts, V., Sturmer, M., Vieth, S., Klenk, H.D., Osterhaus, A.D., Schmitz, H., Doerr, H.W., 2003. Identification of a novel coronavirus in patients with severe acute respiratory syndrome. New England Journal of Medicine 348, 1967–1976.

Enjuanes, L., Gorbalenya, A.E., de Groot, R.J., Cowley, J.A., Ziebuhr, J., Snijder, E.J., 2008. The nidovirales. In: Mahy, B.W.J., Van Regenmortel, M., Walker, P., Majumder-Russell, D. (Eds.), Encyclopedia of Virology, 3rd ed. Elsevier Ltd., Oxford, pp. 419–430.

Fett, C., DeDiego, M.L., Regla-Nava, J.A., Enjuanes, L., Perlman, S., 2013. Complete protection against severe acute respiratory syndrome coronavirus-mediated lethal respiratory disease in aged mice by immunization with a mouse-adapted virus lacking E protein. Journal of Virology 87, 6551–6559.

Fouchier, R.A., Kuiken, T., Schutten, M., van Amerongen, G., van Doornum, G.J., van den Hoogen, B.G., Peiris, M., Lim, W., Stohr, K., Osterhaus, A.D., 2003. Aetiology: Koch's postulates fulfilled for SARS virus. Nature 423, 240.

Frieman, M., Heise, M., Baric, R., 2008. SARS coronavirus and innate immunity. Virus Research 133, 101–112.

Frieman, M., Yount, B., Heise, M., Kopecky-Bromberg, S.A., Palese, P., Baric, R.S., 2007. Severe acute respiratory syndrome coronavirus ORF6 antagonizes STAT1 function by sequestering nuclear import factors on the rough endoplasmic reticulum/Golgi membrane. Journal of Virology 81, 9812–9824.

Gallagher, T.M., Buchmeier, M.J., 2001. Coronavirus spike proteins in viral entry and pathogenesis. Virology 279, 371–374.

Gosert, R., Kanjanahaluethai, A., Egger, D., Bienz, K., Baker, S.C., 2002. RNA replication of mouse hepatitis virus takes place at double-membrane vesicles. Journal of Virology 76, 3697–3708.

Hattermann, K., Muller, M.A., Nitsche, A., Wendt, S., Donoso Mantke, O., Niedrig, M., 2005. Susceptibility of different eukaryotic cell lines to SARS-coronavirus. Archives of Virology 150, 1023–1031.

Huang, K.J., Su, I.J., Theron, M., Wu, Y.C., Lai, S.K., Liu, C.C., Lei, H.Y., 2005. An interferon-gamma-related cytokine storm in SARS patients. Journal of Medical Virology 75, 185–194.

Jeffers, S.A., Tusell, S.M., Gillim-Ross, L., Hemmila, E.M., Achenbach, J.E., Babcock, G.J., Thomas Jr., W.D., Thackray, L.B., Young, M.D., Mason, R.J., Ambrosino, D.M., Wentworth, D.E., Demartini, J.C., Holmes, K.V., 2004. CD209L (L-SIGN) is a receptor for severe acute respiratory syndrome coronavirus. Proceedings of the National Academy of Sciences of the United States of America 101, 15748–15753.

Jiang, Y., Xu, J., Zhou, C., Wu, Z., Zhong, S., Liu, J., Luo, W., Chen, T., Qin, Q., Deng, P., 2005. Characterization of cytokine/chemokine profiles of severe acute respiratory syndrome. American Journal of Respiratory and Critical Care Medicine 171, 850–857.

Knoops, K., Kikkert, M., Worm, S.H., Zevenhoven-Dobbe, J.C., van der Meer, Y., Koster, A.J., Mommaas, A.M., Snijder, E.J., 2008. SARS-coronavirus replication is supported by a reticulovesicular network of modified endoplasmic reticulum. PLoS Biology 6, e226.

Kopecky-Bromberg, S.A., Martinez-Sobrido, L., Frieman, M., Baric, R.A., Palese, P., 2007. Severe acute respiratory syndrome coronavirus open reading frame (ORF) 3b, ORF 6, and nucleocapsid proteins function as interferon antagonists. Journal of Virology 81, 548–557.

Ksiazek, T.G., Erdman, D., Goldsmith, C., Zaki, S., Peret, T., Emery, S., Tong, S., Urbani, C., Comer, J.A., Lim, W., Rollin, P.E., Dowell, S., Ling, A.-E., Humphrey, C., Shieh, W.-J., Guarner, J., Paddock, C.D., Rota, P., Fields, B., DeRisi, J., Yang, J.-Y., Cox, N., Hughes, J., LeDuc, J.W., Bellini, W.J., Anderson, L.J., 2003. A novel coronavirus associated with severe acute respiratory syndrome. New England Journal of Medicine 348, 1953–1966.

Kuiken, T., Fouchier, R.A.M., Schutten, M., Rimmelzwaan, G.F., van Amerongen, G., van Riel, D., Laman, J.D., de Jong, T., van Doornum, G., Lim, W., Ling, A.E., Chan, P.K.S., Tam, J.S., Zambon, M.C., Gopal, R., Drosten, C., van der Werf, S., Escriou, N., Manuguerra, J.-C., Stohr, K., Peiris, J.S.M., 2003. Newly discovered coronavirus as the primary cause of severe acute respiratory syndrome. Lancet 362, 263–270.

Kumanishi, T., 1967. Brain tumors induced with Rous sarcoma virus, Schmidt-Ruppin strain. I. Induction of brain tumors in adult mice with Rous chicken sarcoma cells. Japanese Journal of Experimental Medicine 37, 461–474.

Lang, Z.W., Zhang, L.J., Zhang, S.J., Meng, X., Li, J.Q., Song, C.Z., Sun, L., Zhou, Y.S., Dwyer, D.E., 2003. A clinicopathological study of three cases of severe acute respiratory syndrome (SARS). Pathology 35, 526–531.

Lau, S.K., Woo, P.C., Li, K.S., Huang, Y., Tsoi, H.W., Wong, B.H., Wong, S.S., Leung, S.Y., Chan, K.H., Yuen, K.Y., 2005. Severe acute respiratory syndrome coronavirus-like virus in Chinese horseshoe bats. Proceedings of the National Academy of Sciences of the United States of America 102, 14040–14045.

Li, F., Li, W., Farzan, M., Harrison, S.C., 2005. Structure of SARS coronavirus spike receptor-binding domain complexed with receptor. Science 309, 1864–1868.

Li, W., Greenough, T.C., Moore, M.J., Vasilieva, N., Somasundaran, M., Sullivan, J.L., Farzan, M., Choe, H., 2004. Efficient replication of severe acute respiratory syndrome coronavirus in mouse cells is limited by murine angiotensin-converting enzyme 2. Journal of Virology 78, 11429–11433.

Li, W., Moore, M.J., Vasilieva, N., Sui, J., Wong, S.K., Berne, M.A., Somasundaran, M., Sullivan, J.L., Luzuriaga, K., Greenough, T.C., Choe, H., Farzan, M., 2003. Angiotensin-converting enzyme 2 is a functional receptor for de SARS coronavirus. Nature 426, 450–454.

Livak, K.J., Schmittgen, T.D., 2001. Analysis of relative gene expression data using real-time quantitative PCR and the 2(-Delta Delta C(T)) Method. Methods 25, 402–408.

Marra, M.A., Jones, S.J.M., Astell, C.R., Holt, R.A., Brooks-Wilson, A., Butterfield, Y.S.N., Khattra, J., Asano, J.K., Barber, S.A., Chan, S.Y., Cloutier, A., Coughlin, S.M., Freeman, D., Girn, N., Griffith, O.L., Leach, S.R., Mayo, M., McDonald, H., Montgomery, S.B., Pandoh, P.K., Petrescu, A.S., Robertson, A.G., Schein, J.E., Siddiqui, A., Smailus, D.E., Stott, J.M., Yang, G.S., Plummer, F., Andonov, A., Artsob, H., Bastien, N., Bernard, K., Booth, T.F., Bowness, D., Czub, M., Drebot, M., Fernando, L., Flick, R., Garbutt, M., Gray, M., Grolla, A., Jones, S., Feldmann, H., Meyers, A., Kabani, A., Li, Y., Normand, S., Stroher, U., Tipples, G.A., Tyler, S., Vogrig, R., Ward, D., Watson, B., Brunham, R.C., Krajden, M., Petric, M., Skowronski, D.M., Upton, C., Roper, R.L., 2003. The genome sequence of the SARS-associated coronavirus. Science 300, 1399–1404.

McCray Jr., P.B., Pewe, L., Wohlford-Lenane, C., Hickey, M., Manzel, L., Shi, L., Netland, J., Jia, H.P., Halabi, C., Sigmund, C.D., Meyerholz, D.K., Kirby, P., Look, D.C., Perlman, S., 2007. Lethal infection of K18-hACE2 mice infected with severe acute respiratory syndrome coronavirus. Journal of Virology 81, 813–821.

Mossel, E.C., Huang, C., Narayanan, K., Makino, S., Tesh, R.B., Peters, C.J., 2005. Exogenous ACE2 expression allows refractory cell lines to support severe acute respiratory syndrome coronavirus replication. Journal of Virology 79, 3846–3850.

Nagata, N., Iwata, N., Hasegawa, H., Fukushi, S., Harashima, A., Sato, Y., Saijo, M., Taguchi, F., Morikawa, S., Sata, T., 2008. Mouse-passaged severe acute respiratory syndrome-associated coronavirus leads to lethal pulmonary edema and diffuse alveolar damage in adult but not young mice. American Journal of Pathology 172, 1625–1637.

Narayanan, K., Huang, C., Lokugamage, K., Kamitani, W., Ikegami, T., Tseng, C.T., Makino, S., 2008. Severe acute respiratory syndrome coronavirus nsp1 suppresses host gene expression, including that of type I interferon, in infected cells. Journal of Virology 82, 4471–4479.

Ng, M.L., Tan, S.H., See, E.E., Ooi, E.E., Ling, A.E., 2003. Proliferative growth of SARS coronavirus in Vero E6 cells. Journal of General Virology 84, 3291–3303.

Peiris, J.S.M., Lai, S.T., Poon, L.L.M., Guan, Y., Yam, L.Y.C., Lim, W., Nicholls, J., Yee, W.K.S., Yan, W.W., Cheung, M.T., 2003. Coronavirus as a possible cause of severe acute respiratory syndrome. Lancet 361, 1319–1325.

Reghunathan, R., Jayapal, M., Hsu, L.Y., Chng, H.H., Tai, D., Leung, B.P., Melendez, A.J., 2005. Expression profile of immune response genes in patients with Severe Acute Respiratory Syndrome. BMC Immunology 6, 2.

Ren, L., Yang, R., Guo, L., Qu, J., Wang, J., Hung, T., 2005. Apoptosis induced by the SARS-associated coronavirus in Vero cells is replication-dependent and involves caspase. DNA and Cell Biology 24, 496–502.

Roberts, A., Deming, D., Paddock, C.D., Cheng, A., Yount, B., Vogel, L., Herman, B.D., Sheahan, T., Heise, M., Genrich, G.L., Zaki, S.R., Baric, R., Subbarao, K., 2007. A mouse-adapted SARS-coronavirus causes disease and mortality in BALB/c mice. PLoS Pathogens 3, 23–37.

Roberts, A., Lamirande, E.W., Vogel, L., Jackson, J.P., Paddock, C.D., Guarner, J., Zaki, S.R., Sheahan, T., Baric, R., Subbarao, K., 2008. Animal models and vaccines for SARS-CoV infection. Virus Research 133, 20–32.

Rockx, B., Baas, T., Zornetzer, G.A., Haagmans, B., Sheahan, T., Frieman, M., Dyer, M.D., Teal, T.H., Proll, S., van den Brand, J., Baric, R., Katze, M.G., 2009. Early upregulation of acute respiratory distress syndrome-associated cytokines promotes lethal disease in an aged-mouse model of severe acute respiratory syndrome coronavirus infection. Journal of Virology 83, 7062–7074.

Rota, P.A., Oberste, M.S., Monroe, S.S., Nix, W.A., Campganoli, R., Icenogle, J.P., Peñaranda, S., Bankamp, B., Maher, K., Chen, M.-H., Tong, S., Tamin, A., Lowe, L., Frace, M., DeRisi, J.L., Chen, Q., Wang, D., Erdman, D.d., Peret, T.C.T., Burns, C., Ksiazek, T.G., Rollin, P.E., Sanchez, A., Liffick, S., Holloway, B., Limor, J., McCaustland, K., Olsen-Rassmussen, M., Fouchier, R., Gunther, S., Osterhaus, A.D.M.E., Drosten, C., Pallansch, M.A., Anderson, L.J., Bellini, W.J., 2003. Characterization of a novel coronavirus associated with severe acute respiratory syndrome. Science 300, 1394–1399.

Sheahan, T., Rockx, B., Donaldson, E., Corti, D., Baric, R., 2008a. Pathways of cross-species transmission of synthetically reconstructed zoonotic severe acute respiratory syndrome coronavirus. Journal of Virology 82, 8721–8732.

Sheahan, T., Rockx, B., Donaldson, E., Sims, A., Pickles, R., Corti, D., Baric, R., 2008b. Mechanisms of zoonotic severe acute respiratory syndrome coronavirus host range expansion in human airway epithelium. Journal of Virology 82, 2274–2285.

Siu, K.L., Kok, K.H., Ng, M.H., Poon, V.K., Yuen, K.Y., Zheng, B.J., Jin, D.Y., 2009. Severe acute respiratory syndrome coronavirus M protein inhibits type I interferon production by impeding the formation of TRAF3.TANK.TBK1/IKKepsilon complex. Journal of Biological Chemistry 284, 16202–16209.

Smits, S.L., de Lang, A., van den Brand, J.M., Leijten, L.M., van, I.W.F., Eijkemans, M.J., van Amerongen, G., Kuiken, T., Andeweg, A.C., Osterhaus, A.D., Haagmans, B.L., 2010. Exacerbated innate host response to SARS-CoV in aged non-human primates. PLoS Pathogens 6, e1000756.

Smits, S.L., van den Brand, J.M., de Lang, A., Leijten, L.M., van Ijcken, W.F., van Amerongen, G., Osterhaus, A.D., Andeweg, A.C., Haagmans, B.L., 2011. Distinct severe acute respiratory syndrome coronavirus-induced acute lung injury pathways in two different nonhuman primate species. Journal of Virology 85, 4234–4245.

Subbarao, K., Roberts, A., 2006. Is there an ideal animal model for SARS? Trends in Microbiology 14, 299–303.

Sun, L., Xing, Y., Chen, X., Zheng, Y., Yang, Y., Nichols, D.B., Clementz, M.A., Banach, B.S., Li, K., Baker, S.C., Chen, Z., 2012. Coronavirus papain-like proteases negatively regulate antiviral innate immune response through disruption of STING-mediated signaling. PloS ONE 7, e30802.

Tang, N.L., Chan, P.K., Wong, C.K., To, K.F., Wu, A.K., Sung, Y.M., Hui, D.S., Sung, J.J., Lam, C.W., 2005. Early enhanced expression of interferon-inducible protein-10 (CXCL-10) and other chemokines predicts adverse outcome in severe acute respiratory syndrome. Clinical Chemistry 51, 2333–2340.

Wathelet, M.G., Orr, M., Frieman, M.B., Baric, R.S., 2007. Severe acute respiratory syndrome coronavirus evades antiviral signaling: role of nsp1 and rational design of an attenuated strain. Journal of Virology 81, 11620–11633.

Wong, R.S., Wu, A., To, K.F., Lee, N., Lam, C.W., Wong, C.K., Chan, P.K., Ng, M.H., Yu, L.M., Hui, D.S., Tam, J.S., Cheng, G., Sung, J.J., 2003. Haematological manifestations in patients with severe acute respiratory syndrome: retrospective analysis. BMJ 326, 1358–1362.

Wong, S.K., Li, W., Moore, M.J., Choe, H., Farzan, M., 2004. A 193-amino acid fragment of the SARS coronavirus S protein efficiently binds angiotensin-converting enzyme 2. Journal of Biological Chemistry 279, 3197–3201.

Woo, P.C., Lau, S.K., Li, K.S., Poon, R.W., Wong, B.H., Tsoi, H.W., Yip, B.C., Huang, Y., Chan, K.H., Yuen, K.Y., 2006. Molecular diversity of coronaviruses in bats. Virology 351, 180–187.

Yan, H., Xiao, G., Zhang, J., Hu, Y., Yuan, F., Cole, D.K., Zheng, C., Gao, G.F., 2004. SARS coronavirus induces apoptosis in Vero E6 cells. Journal of Medical Virology 73, 323–331.

Yang, X.H., Deng, W., Tong, Z., Liu, Y.X., Zhang, L.F., Zhu, H., Gao, H., Huang, L., Liu, Y.L., Ma, C.M., Xu, Y.F., Ding, M.X., Deng, H.K., Qin, C., 2007. Mice transgenic for human angiotensin-converting enzyme 2 provide a model for SARS coronavirus infection. Comparative Medicine 57, 450–459.

Zhang, Q.L., Ding, Y.Q., He, L., Wang, W., Zhang, J.H., Wang, H.J., Cai, J.J., Geng, J., Lu, Y.D., Luo, Y.L., 2003. Detection of cell apoptosis in the pathological tissues of patients with SARS and its significance. Di Yi Jun Yi Da Xue Xue Bao 23, 770–773.

Zhang, Y., Li, J., Zhan, Y., Wu, L., Yu, X., Zhang, W., Ye, L., Xu, S., Sun, R., Wang, Y., Lou, J., 2004. Analysis of serum cytokines in patients with severe acute respiratory syndrome. Infection and Immunity 72, 4410–4415.

Ziebuhr, J., Snijder, E.J., Gorbalenya, A.E., 2000. Virus-encoded proteinases and proteolytic processing in the *Nidovirales*. Journal of General Virology 81, 853–879.

JVI Journals.ASM.org

Inhibition of NF-κB-Mediated Inflammation in Severe Acute Respiratory Syndrome Coronavirus-Infected Mice Increases Survival

Marta L. DeDiego,[a] Jose L. Nieto-Torres,[a] Jose A. Regla-Nava,[a] Jose M. Jimenez-Guardeño,[a] Raul Fernandez-Delgado,[a] Craig Fett,[b] Carlos Castaño-Rodriguez,[a] Stanley Perlman,[b] Luis Enjuanes[a]

Department of Molecular and Cell Biology, National Center of Biotechnology, Campus Universidad Autónoma de Madrid, Madrid, Spain[a]; Department of Microbiology, University of Iowa, Iowa City, Iowa, USA[b]

Severe acute respiratory syndrome coronavirus (SARS-CoV) is the etiological agent of a respiratory disease that has a 10% mortality rate. We previously showed that SARS-CoV lacking the E gene (SARS-CoV-ΔE) is attenuated in several animal model systems. Here, we show that absence of the E protein resulted in reduced expression of proinflammatory cytokines, decreased numbers of neutrophils in lung infiltrates, diminished lung pathology, and increased mouse survival, suggesting that lung inflammation contributed to SARS-CoV virulence. Further, infection with SARS-CoV-ΔE resulted in decreased activation of NF-κB compared to levels for the wild-type virus. Most important, treatment with drugs that inhibited NF-κB activation led to a reduction in inflammation and lung pathology in both SARS-CoV-infected cultured cells and mice and significantly increased mouse survival after SARS-CoV infection. These data indicated that activation of the NF-κB signaling pathway represents a major contribution to the inflammation induced after SARS-CoV infection and that NF-κB inhibitors are promising antivirals in infections caused by SARS-CoV and potentially other pathogenic human coronaviruses.

Severe acute respiratory syndrome (SARS), caused by a coronavirus (SARS-CoV), affected approximately 8,000 individuals during the 2002-2003 epidemic and had a mortality rate of 10% (1, 2). SARS-CoV has not reappeared in humans since 2004, but SARS-like coronaviruses are present in bats circulating all over the world, making another SARS outbreak a possibility (3–6). Consistent with this prediction, a new coronavirus, Middle East respiratory syndrome coronavirus (MERS-CoV), emerged during the summer of 2012 in Saudi Arabia and is the etiological agent of severe pneumonia in patients from 10 Middle Eastern and European countries (7, 8). As of 22 October 2013, a total of 139 confirmed cases were reported, with a 43% mortality rate (http://www.cdc.gov/coronavirus/mers/). This novel coronavirus is closely related to the two bat coronaviruses Bt-CoV-HKU4 and Bt-CoV-HKU5 (8), suggesting that MERS-CoV, like SARS-CoV, originated from bats. MERS-CoV has probably been amplified in one or more intermediate hosts, including camels, and was then transmitted to humans (9). The fact that zoonotic coronaviruses frequently cross species barriers to infect humans makes the generation of vaccines and the identification of antivirals important goals.

SARS-CoV is an enveloped, positive-sense RNA virus, with a genome of 29.7 kb (10). The replicase is encoded within the 5′ two-thirds of the genome and includes two overlapping open reading frames (ORFs), named ORF1a and ORF1b. Translation of these ORFs results in the expression of two polyproteins, pp1a and pp1ab, which are processed by two viral proteinases to yield 16 nonstructural proteins (nsps) (11). These proteins participate in the replication of the viral genome and transcription of subgenomic messenger RNAs (sgmRNAs), which encode viral structural proteins (spike [S], envelope [E], membrane [M], and nucleoprotein [N]) (11). In addition, all coronaviruses encode a set of group-specific proteins whose sequence and number vary among the different coronavirus species (12). In the case of SARS-CoV, the genes 3a, 3b, 6, 7a, 7b, 8a, 8b, and 9b encode group-specific proteins (13).

SARS-CoV E protein contains 76 amino acids and is composed of a short hydrophilic amino terminus followed by a hydrophobic region and a hydrophilic carboxy terminus (14). The hydrophobic region forms at least one amphipathic α helix that oligomerizes to form an ion-conductive pore in membranes (14). The ion conductance and selectivity of this ion channel are influenced by the lipid charge of the membranes (15, 16). The requirement for E protein in virus production varies among coronaviruses. Thus, E protein is essential for the generation of propagation-competent viruses in cells infected with transmissible gastroenteritis coronavirus (TGEV) or MERS-CoV (17–20) but not for mouse hepatitis virus (MHV) or SARS-CoV (21–23). SARS-CoV lacking E protein is attenuated in hamsters, transgenic mice expressing the SARS-CoV receptor human angiotensin converting enzyme 2 (hACE2), and BALB/c mice infected with a mouse-adapted SARS-CoV (21, 22, 24). We also showed that SARS-CoV E protein reduced apoptosis and the stress response induced after SARS-CoV infection (25).

Reduced survival in SARS is associated with male gender, age over 60 years, neutrophilia, and severe biochemical abnormalities, such as the upregulation of proinflammatory cytokines (26–30). Several species of animals can be infected with SARS-CoV, but the model that best fits human SARS is infection of conventional mice with mouse-adapted SARS-CoVs (31–33). This model reproduces many aspects of the human disease, such as rapid and high viral replication in lungs, viremia, dissemination of virus to extrapulmonary sites accompanied by lymphopenia and neutrophilia, pathological changes in the lungs, and lethality (31–33). Further-

Received 5 September 2013 **Accepted** 29 October 2013
Published ahead of print 6 November 2013
Address correspondence to Luis Enjuanes, L.Enjuanes@cnb.csic.es.

doi:10.1128/JVI.02576-13

more, the disease is more severe in aged mice, as occurs in humans (28, 34).

The elevated cytokine/chemokine response in severe SARS reflects a dysregulated immune response. Activation of NF-κB is a hallmark of most infections, including those caused by viruses, leading to protective and pathological responses. Accordingly, the role of NF-κB as a potential therapeutic target in microbial diseases has been extensively studied (35), and more than 700 NF-κB inhibitors have been described (36). SARS-CoV proteins nsp1, nsp3a, nsp7a, spike, and nucleocapsid promote NF-κB activation, possibly contributing to SARS-CoV-induced pathogenesis (37–42). Aged macaques develop a more severe pathology than younger animals, with an increase in expression of genes associated with inflammation linked to a central role of NF-κB and a reduction in expression of type I interferon (IFN-β) (34).

We studied the effect of deleting SARS-CoV E protein in inflammatory responses and pathogenesis in cell cultures and mice. A mouse-adapted SARS-CoV lacking E protein induced less lung pathology, mediated by decreased expression of inflammation mediators, lower numbers of neutrophils in lung infiltrates, and limited NF-κB activation. Drugs that specifically inhibit NF-κB signaling led to a reduction in inflammation and lung pathology and increased mouse survival after infection with SARS-CoV. These results indicated that NF-κB activation is partly pathogenic in SARS and that NF-κB inhibitors are promising antivirals for treatment of this infection and perhaps for other infections caused by human coronaviruses, such as MERS-CoV.

MATERIALS AND METHODS

Reagents. The NF-κB inhibitors caffeic acid phenethyl ester (CAPE), resveratrol, Bay11-7082, and parthenolide were purchased from Tocris Biosciences, Sigma, Calbiochem, and Enzo Life Sciences, respectively.

Virus. The mouse-adapted MA15 viruses (32), recombinant SARS-CoV-MA15 (rSARS-CoV-MA15) and rSARS-CoV-MA15-ΔE were rescued from infectious cDNA clones as previously described (21, 24). All work with infectious viruses and infected animals was performed in biosafety level 3 (BSL3) facilities by personnel wearing positive-pressure air-purifying respirators (3M HEPA AirMate; 3M, St. Paul, MN).

Mice. Pathogen-free 8-week-old BALB/c Ola Hsd or BALB/c AnNCr female mice were obtained from Harlan (The Netherlands) or from the National Cancer Institute (Bethesda, MD, USA), respectively. BALB/c mice were infected at the age of 8 (AnNcr) or 16 weeks (Ola Hsd), with 6,000 PFU or 100,000 PFU, respectively. All protocols were approved by the University of Iowa Institutional Animal Care and Use Committee and by the Ethical Review Committee at the Centro de Investigación en Sanidad Animal of the Instituto Nacional de Investigaciones Agrarias (CISA-INIA). Infected mice were housed in a ventilated rack (animal transport unit-biocontainment unit [ATU-BCU], Allentown, Inc., Allentown, NJ).

Cells. African green monkey kidney-derived Vero E6 cells were kindly provided by Eric Snijder (Medical Center, University of Leiden, The Netherlands). Mouse delayed brain tumor (DBT) cells, expressing the SARS-CoV receptor mouse ACE2 (DBT-mACE2 cells), were generated in our laboratory as previously described (43). In all cases, cells were grown in Dulbecco's modified Eagle's medium (DMEM; Gibco) supplemented with 25 mM HEPES and 10% fetal bovine serum (Biowhittaker). Virus titrations were performed in Vero E6 cells following standard procedures using closed flasks or plates sealed in plastic bags, as previously described (21).

Clinical disease in BALB/c mice. Eight-week-old or 16-week-old mice were lightly anesthetized with isoflurane and inoculated intranasally with 6,000 or 100,000 PFU of rSARS-CoV-MA15 or rSARS-CoV-MA15-ΔE virus, respectively, in 50 μl of DMEM. Infected mice were examined and weighed daily.

TABLE 1 TaqMan assays used to analyze the expression of cellular genes by RT-qPCR

Gene product	TaqMan assay[a]	Description
18S	Mm03928990-g1	Ribosomal RNA 18S
TNF	Mm00443258-m1	Tumor necrosis factor
CCL2/MCP-1	Mm00441242-m1	Monocyte chemotactic protein 1
CCL5/RANTES	Mm01302428-m1	Regulated upon activation, normal T-cell expressed, and secreted
CXCL1/NAP-3	Mm04207460-m1	Neutrophil-activating protein 3
CXCL2/MIP-2	Mm00436450-m1	Macrophage inflammatory protein 2
CXCL10/IP-10	Mm00445235-m1	Interferon-inducible protein 10
IL-6	Mm00446190-m1	Interleukin-6

[a] Mm, *Mus musculus*.

Histopathological examination of lungs from infected mice. Eight-week-old or 16-week-old mice were infected as described above with 6,000 or 100,000 PFU, respectively, of rSARS-CoV-MA15 or rSARS-CoV-MA15-ΔE. Lungs were removed from mice at 2 and 4 days postinfection (dpi), fixed in zinc formalin, and processed as described previously (44). For routine histology, sections were stained with hematoxylin and eosin.

Evaluation of pulmonary infiltrates by flow cytometry. Eight-week-old or 16-week-old mice were infected as above with 6,000 or 100,000 PFU, respectively, of virus. Lungs were removed from mice at 2, 4, and 6 dpi, and cells were prepared as previously described (45). Macrophages were $CD45^+$ $CD11b^+$ $Ly6C^+$ $Ly6G^-$. Neutrophils were $CD45^+$ $CD11b^+$ $Ly6C^+$ $Ly6G^+$. The following monoclonal antibodies were used: rat anti-mouse CD11b (M1/70), rat anti-mouse CD16/32 (2.4G2), rat anti-mouse Ly6G (1A8), and rat anti-mouse Ly6C (AL-21) all from BD Biosciences (San Diego, CA), and anti-mouse F4/80 (BM8) from eBioscience (San Diego, CA). For surface staining, 10^6 cells were blocked with 1 μg of anti-CD16/32 antibody and 1% rat serum, stained with the CD11b-, Ly6G-, Ly6C-, and F4/80-specific antibodies, as indicated above, and then fixed using Cytofix Solution (BD Biosciences).

RNA analysis by RT-qPCR. Total RNA from DBT-mACE2 cells was extracted using an RNeasy Minikit (Qiagen). Mice were inoculated intranasally with 100,000 PFU of rSARS-CoV-MA15 or rSARS-CoV-MA15-ΔE in 50 μl of DMEM. Lungs were removed from mice at 2 and 4 dpi and incubated in RNA Later (Ambion) at 4°C for 24 h, prior to being frozen at −80°C. Then, lungs were thawed and homogenized in RLT buffer (Qiagen) using a gentleMACS Dissociator (Miltenyi Biotec), and total RNA was extracted using an RNeasy Minikit (Qiagen). For quantitative reverse transcription-PCR (RT-qPCR) of cellular genes, cDNA was prepared using a High-Capacity cDNA transcription kit (Applied Biosystems), followed by PCR using TaqMan gene expression assays (Applied Biosystems) specific for murine genes (Table 1). Data were acquired with an ABI Prism 7000 sequence detection system (Applied Biosystems) and analyzed using ABI Prism 7000 SDS, version 1.0, software. Gene expression relative to mock-infected samples is shown.

Cytokine multiplex analysis. Lungs were homogenized, and nuclear, cytoplasmic, and extracellular proteins were extracted using a Nuclear Extract Kit (Active Motif, Carlsbad, CA). Supernatant proteins (cytoplasmic and extracellular proteins) were diluted 1:4 in assay diluent (Millipore) prior to analysis. The expression of CCL2/MCP-1, and CXCL10/IP-10 was measured using Luminex technology and a mouse cytokine antibody bead kit (Milliplex map kit; Millipore) according to the manufacturer's instructions.

Luciferase assays. To analyze the induction of NF-κB, nuclear factor of activated T cells (NF-AT), AP-1, and the *cis*-acting replication element (CRE), luciferase reporter assays were used in DBT-mACE2 cells (Cignal Reporter Assay Kits CCS-013L for NF-κB, CCS-015L for NF-AT, CCS-011L for AP-1, and CCS-002L for CRE; Qiagen). To this end, plasmids encoding the firefly luciferase ORF under the control of the different

promoters were cotransfected with a plasmid encoding the *Renilla* luciferase to normalize levels of transfection. Separately, a plasmid encoding a noninducible firefly luciferase reporter and the plasmid encoding the *Renilla* luciferase were cotransfected as negative controls. In addition, plasmids constitutively expressing green fluorescent protein (GFP), firefly luciferase, and *Renilla* luciferase were cotransfected as positive controls.

To analyze the activation of interferon regulatory factor 3 (IRF3) and IRF7, three plasmids were cotransfected: (i) the reporter plasmid p55UASGluc encoding the firefly luciferase gene under the control of the GAL4 upstream activation sequence (UAS); (ii) plasmid pGAL4DBD-IRF3 or pGAL4DBD-IRF7, encoding the IRF3 or IRF7 transactivation domains fused to the GAL4 DNA binding domain (DBD), kindly provided by T. Fujita (Kyoto University, Kyoto, Japan) (46); and (iii) the control plasmid pRL-SV40 (where SV40 is simian virus 40), encoding *Renilla* luciferase (Promega). Firefly and *Renilla* luciferase expression levels were monitored using a Dual Glo assay luciferase system (Promega) and a luminometer.

DBT-mACE2 cells were cotransfected with the plasmids, using a three-dimensional (3D) Nucleofector (Lonza) according to the manufacturer's instructions. Then, 24 h later, the cells were infected with rSARS-CoV-MA15-ΔE or rSARS-CoV-MA15 at a multiplicity of infection (MOI) of 0.05. Firefly and *Renilla* luciferase expression levels were measured at 48 h postinfection (hpi) and normalized to *Renilla* luciferase levels.

NF-κB activity in tissue culture and *in vivo*. Cells were infected with the virus rSARS-CoV-MA15-ΔE or rSARS-CoV-MA15 at an MOI of 0.05 and collected at 48 hpi. Mice were infected intranasally as described above with 100,000 PFU of rSARS-CoV-MA15 or rSARS-CoV-MA15-ΔE virus in 50 μl of DMEM or treated with DMEM alone. Lungs were removed from mice at 2 and 4 dpi and homogenized. Nuclear extracts from infected cells and homogenized lungs were obtained using a nuclear extraction kit as described above. NF-κB DNA-binding activity in infected cells was measured using an enzyme-linked immunosorbent assay (ELISA)-based assay and a chemiluminescent kit (TransAM p65 Transcription Factor Assay kit; Active Motif). NF-κB in lung nuclear extracts was analyzed by Western blotting using antibodies specific for NF-κB (rabbit polyclonal antibody) (ab7970; Abcam) and histone H3 (rabbit polyclonal antibody) (39164; Active Motif). Bound antibodies were detected with horseradish peroxidase-conjugated goat anti-rabbit secondary antibody and the Immobilon Western chemiluminescent substrate (Millipore), according to the manufacturer's recommendations. Densitometric analysis of NF-κB and histone H3 bands from mock-, rSARS-CoV-MA15-, and rSARS-CoV-MA15-ΔE-infected mice was performed using Quantity One, version 4.5.1, software (Bio-Rad). In each case, the levels of NF-κB were normalized to the levels of histone H3. Three different experiments and appropriate gel exposures were used in all cases with similar results. In addition, different exposures of the same experiment were analyzed to ensure that data obtained were within linear range.

NF-κB inhibitor treatment of SARS-CoV-infected cells. DBT-mACE2 cells were infected at an MOI of 0.05 with rSARS-CoV-MA15-ΔE or rSARS-CoV-MA15. At 43 hpi, half of the culture medium was removed and replaced with medium containing CAPE (50 μg/ml), resveratrol (40 μg/ml), Bay11-7082 (40 μM), or parthenolide (24 μM). At 48 hpi, supernatants were collected, and total cellular RNA was extracted using an RNeasy Minikit (Qiagen). In parallel, cells were previously cotransfected with luciferase plasmids to measure NF-κB activity, as described above.

NF-κB inhibitor treatment of SARS-CoV-infected BALB/c mice. Sixteen-week-old mice were infected with 100,000 PFU of rSARS-CoV-MA15 as described above. At 4 hpi and every 24 h thereafter, from days 1 to 4, mice were treated intraperitoneally with the NF-κB inhibitors CAPE and parthenolide at 20 mg/kg of body weight/day, either alone or in combination or with vehicle (phosphate-buffered saline [PBS] containing 1.2% dimethyl sulfoxide [DMSO] and 2.5% Tween 20). Survival was analyzed in three independent experiments, with six mice per group. In addition, three mice per group were sacrificed at day 4 postinfection (p.i.), and lungs were collected to evaluate the expression of cytokines by RT-qPCR and to determine viral titers. To evaluate virus titers, right lungs were homogenized in phosphate-buffered saline (PBS) containing 100 UI/ml penicillin, 0.1 mg/ml streptomycin, 50 μg/ml gentamicin, and 0.5 μg/ml amphotericin B (Fungizone), using a gentleMACS Dissociator (Miltenyi Biotec). Virus titrations were performed in Vero E6 cells according to standard procedures using closed flasks or plates sealed in plastic bags, as previously described (21).

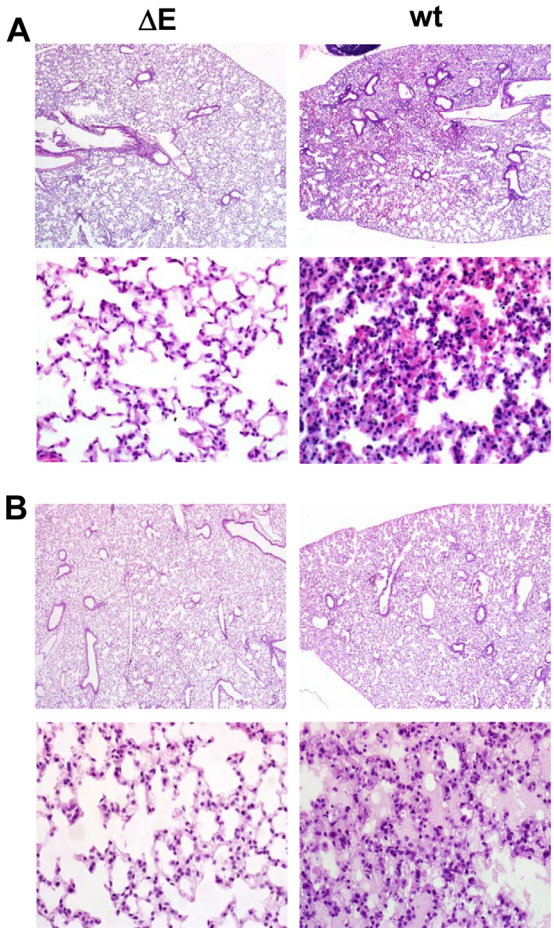

FIG 1 Lung pathology associated with rSARS-CoV-MA15-ΔE infection in BALB/c mice. Eight-week-old BALB/c mice were infected with 6,000 PFU of rSARS-CoV-MA15-ΔE (ΔE) or wild-type (wt) rSARS-CoV-MA15. After 4 (A) and 6 (B) dpi, mice were sacrificed, and lungs were processed for histopathological examination. Original magnifications were ×4 and ×40 in upper and lower images, respectively, of each panel.

RESULTS

Pathology induced by rSARS-CoV-MA15-ΔE in BALB/c mice. We previously showed that mouse-adapted rSARS-CoV-MA15-ΔE is attenuated in young (6 weeks old) and aged (12 and 18 months old) BALB/c mice, leading to no significant weight losses and no mortality (24). To identify mechanisms leading to rSARS-CoV-MA15-ΔE attenuation, pulmonary pathology associated with rSARS-CoV-MA15 and rSARS-CoV-MA15-ΔE infection was evaluated in 8-week-old mice intranasally infected with 6,000 PFU, the dose used for immunization in our previous studies (24). Infection of BALB/c mice with rSARS-CoV-MA15 caused intense lung inflammation, characterized by peribronchiolar and interstitial inflammatory infiltrates at 4 and 6 dpi (Fig. 1). In contrast,

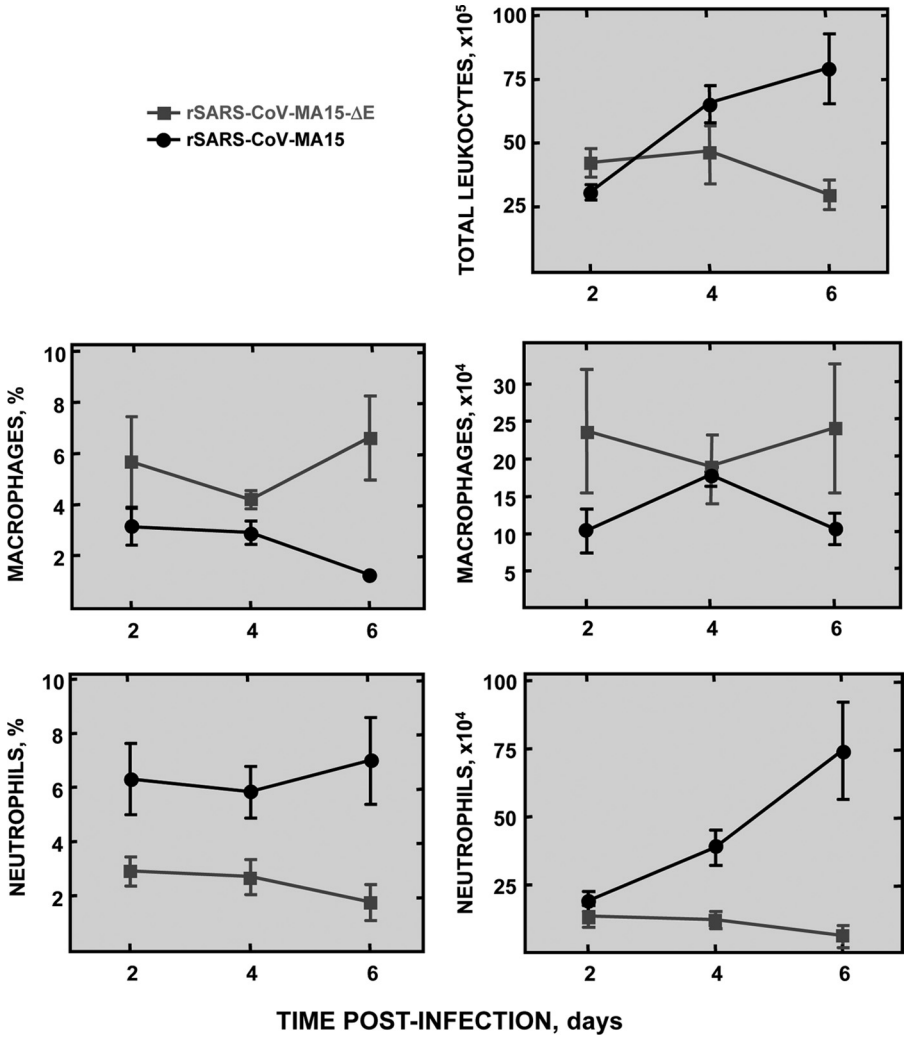

FIG 2 Analysis of lung inflammatory cell infiltrates during rSARS-CoV-MA15-ΔE infection of BALB/c mice. Leukocytes from lungs of 8-week-old BALB/c mice infected with 6,000 PFU of rSARS-CoV-MA15-ΔE or rSARS-CoV-MA15 were isolated at 2, 4, and 6 dpi, and the inflammatory cell populations were identified by flow cytometry as described in Materials and Methods. The total numbers of leukocytes, macrophages and neutrophils and the percentage of macrophages and neutrophils were determined. Error bars represent the means from six mice per group.

lung infiltrates were reduced in mice infected with rSARS-CoV-MA15-ΔE (Fig. 1), suggesting that the presence of E protein, either by a direct or an indirect effect, contributed to induce a robust inflammatory immune response. Similar results in terms of weight loss, virus titer, and pathology were obtained with 8- and 16-week-old mice infected with 6,000 and 100,000 PFU, respectively. The dose of 100,000 PFU of rSARS-CoV-MA15 was lethal in 16-week-old mice and was used in most of the experiments described below. Quantification of total lung leukocytes, macrophages, and neutrophils indicated that the total number of leukocytes and neutrophils was reduced in mice infected with either dose of rSARS-CoV-MA15-ΔE at 2, 4, and 6 dpi (Fig. 2), whereas the total number and percentage of macrophages were increased compared to amounts in mice infected with the corresponding dose of rSARS-CoV-MA15 (Fig. 2, shown for 6,000 PFU). Furthermore, the percentage of lung neutrophils was also decreased in rSARS-CoV-MA15-ΔE-infected mice. These results indicated that the presence of E protein led to a specific increase in neutrophil influx.

A property of the E protein is that it is involved in virus assembly, and we previously showed that rSARS-CoV-ΔE grew to lower titers in tissue culture cells than rSARS-CoV, reflecting this role. To determine whether rSARS-CoV-MA15-ΔE grew to lower titers in mice, 16-week-old BALB/c mice were infected with 100,000 PFU of rSARS-CoV-MA15-ΔE and rSARS-CoV-MA15, and virus titers in lungs were determined at 2 and 4 dpi. Titers were 1×10^6 PFU/g of tissue and 4×10^7 PFU/g at day 2 and 1×10^6 PFU/g and 3×10^7 PFU/g at day 4 for rSARS-CoV-MA15-ΔE and rSARS-CoV-MA15, respectively, confirming that rSARS-CoV-MA15-ΔE replicated less robustly in mice.

Proinflammatory response induced by rSARS-CoV-MA15-ΔE in BALB/c mice. To determine whether the limited inflammation induced by rSARS-CoV-MA15-ΔE was associated with a reduction in proinflammatory cytokines and with a decreased clinical disease and mortality, mice were infected with rSARS-CoV-MA15 or rSARS-CoV-MA15-ΔE. Weight loss and survival were evaluated daily (Fig. 3A). As expected, whereas mice infected with rSARS-CoV-MA15-ΔE did not significantly lose

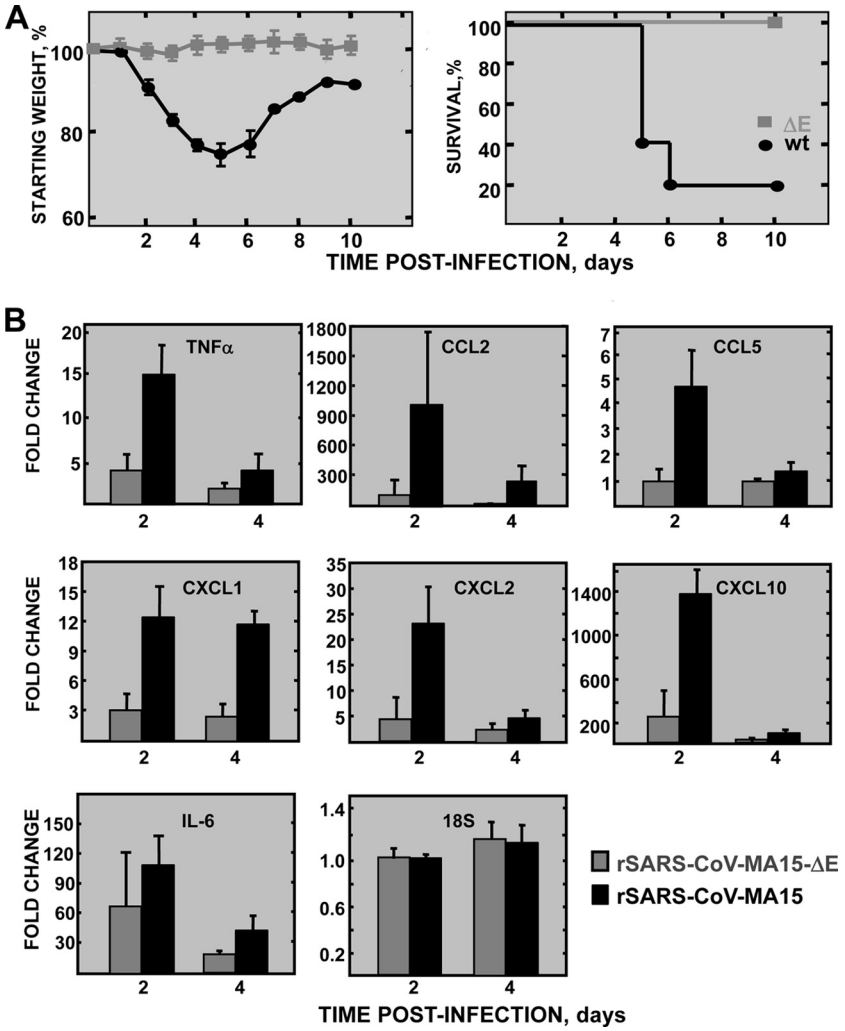

FIG 3 Effect of SARS-CoV E protein on clinical disease and proinflammatory response *in vivo*. Sixteen-week-old BALB/c mice were infected with 100,000 PFU of rSARS-CoV-MA15-ΔE or rSARS-CoV-MA15. (A) Weight loss and survival were evaluated daily in mice infected with rSARS-CoV-MA15-ΔE (ΔE) or rSARS-CoV-MA15 (wt) (10 mice per group). (B) Lung RNAs were extracted at 2 and 4 dpi, and the expression levels of cellular mRNAs corresponding to proinflammatory cytokines (CCL2, CCL5, TNF, CXCL1, CXCL2, CXCL10, and IL-6) and 18S rRNA were measured by RT-qPCR. Numbers indicate the levels of gene expression in rSARS-CoV-MA15-ΔE- or rSARS-CoV-MA15-infected mice compared to mock-infected mice. Error bars represent the means of three mice analyzed for each point.

weight and all of them survived, mice infected with wild-type rSARS-CoV-MA15 started to lose weight at day 2 p.i., and 80% of the mice died by day 6 (Fig. 3A). RNA and protein were extracted from lung samples at days 2 and 4 p.i. to measure proinflammatory cytokine mRNA levels. In rSARS-CoV-MA15-infected mice, the expression of tumor necrosis factor (TNF), CCL2/MCP-1, CCL5/RANTES, CXCL1/neutrophil activating protein-3 (NAP-3), CXCL2/MIP-2, CXCL10/IP-10, and interleukin-6 (IL-6) was clearly induced, particularly at 2 dpi, to higher levels than in mice infected with rSARS-CoV-MA15-ΔE (Fig. 3B). In fact, the induction of proinflammatory cytokines was up to 70-fold higher in mice infected with rSARS-CoV-MA15 than in those infected with the deletion mutant lacking E protein (Fig. 3B). As a control, expression levels of the gene encoding the 18S rRNA did not change in mock-, rSARS-CoV-MA15-ΔE-, and rSARS-CoV-MA15-infected mice (Fig. 3B). To evaluate whether the differential induction of cytokine mRNAs in rSARS-CoV-MA15-ΔE- and rSARS-CoV-MA15-infected mice correlated with protein levels, CCL2 and CXCL10 protein levels were determined in the lungs of control and infected mice. In agreement with the results shown in Fig. 3, CCL2 and CXCL10 protein levels were also increased in rSARS-CoV-MA15-infected mice compared to those in mice infected with rSARS-CoV-MA15-ΔE (Fig. 4).

Proinflammatory cytokines induced by rSARS-CoV-MA15-ΔE in cell culture. To analyze whether rSARS-CoV-MA15-ΔE also induced a decreased proinflammatory response in cultured cells, mouse DBT-mACE2 cells (43) were infected with rSARS-CoV-MA15-ΔE and rSARS-CoV-MA15 at MOIs of 0.5 and 0.05. The expression of the proinflammatory cytokines CCL2, CXCL1, and CXCL2 was evaluated by RT-qPCR at 24, 48, and 72 hpi (Fig. 5A). rSARS-CoV-MA15 virus induced the expression of higher levels of proinflammatory cytokines, particularly at 48 hpi (MOI of 0.5) and 48 to 72 hpi (MOI of 0.05) than the E deletion mutant. Therefore, similarly to the expression in mice lungs, rSARS-CoV-

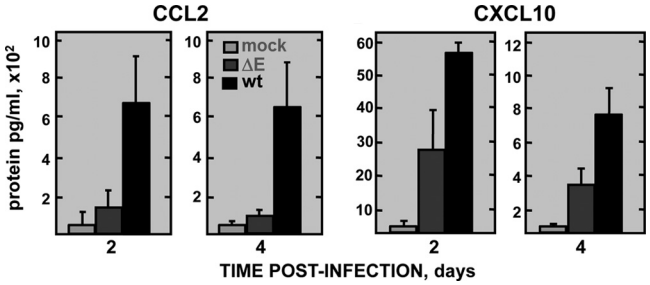

FIG 4 Expression of proinflammatory cytokines in rSARS-CoV-MA15-ΔE-infected mice. Sixteen-week-old BALB/c mice were infected with 100,000 PFU of rSARS-CoV-MA15-ΔE (ΔE) or rSARS-CoV-MA15 (wt) or were mock infected (mock). Lung proteins were extracted at 2 and 4 dpi, and the accumulation of CCL2 and CXCL10 was measured as described in Materials and Methods. Concentrations of protein are expressed as picograms per milliliter of lung tissue extract. Error bars represent the means of three mice analyzed for each point.

MA15-ΔE also induced a decreased proinflammatory response compared to that of rSARS-CoV-MA15 in infected cells (Fig. 5A). To analyze whether rSARS-CoV-MA15-ΔE growth in mouse DBT-mACE2 cells was compromised, virus titers in rSARS-CoV-MA15-ΔE- and wild-type rSARS-CoV-MA15-infected cell supernatants were compared (Fig. 5B). rSARS-CoV-MA15-ΔE grew to lower titers (from 15- to 600-fold lower than those observed for wild-type rSARS-CoV-MA15 at 24, 48, and 72 hpi), as happens in mice (Fig. 5B).

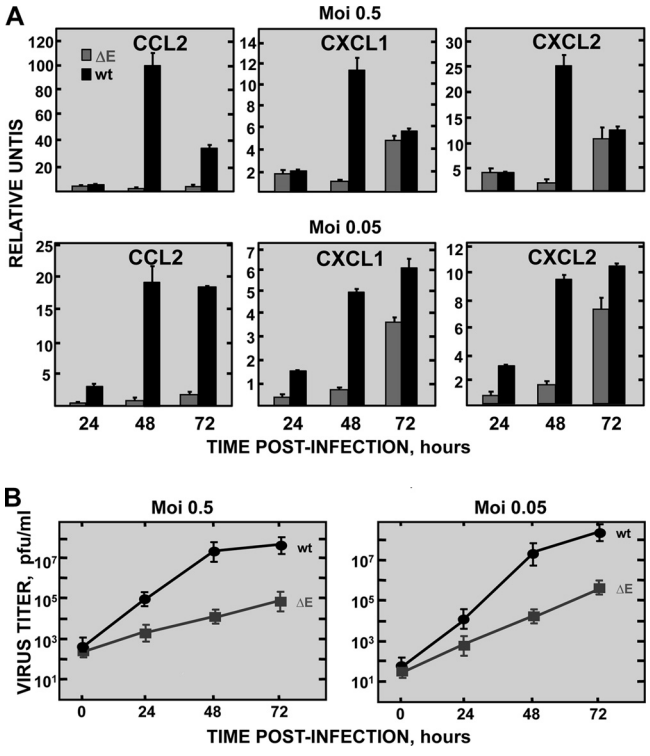

FIG 5 Expression kinetics of proinflammatory cytokines in rSARS-CoV-MA15-ΔE-infected cells. DBT-mACE2 cells were infected at MOIs of 0.5 and 0.05 with rSARS-CoV-MA15-ΔE (ΔE) and rSARS-CoV-MA15 (wt). (A) Cellular RNAs were extracted at 24, 48, and 72 hpi. The expression of the indicated cytokines was determined by RT-qPCR. In each case, the corresponding mRNA expression levels in rSARS-CoV-MA15-ΔE- or rSARS-CoV-MA15-infected cells were plotted as fold change relative to expression levels in uninfected cells. (B) Virus titers in supernatants of rSARS-CoV-MA15-ΔE-infected and rSARS-CoV-MA15-infected DBT-mACE2 cells. Error bars represent standard deviations of the means from three experiments.

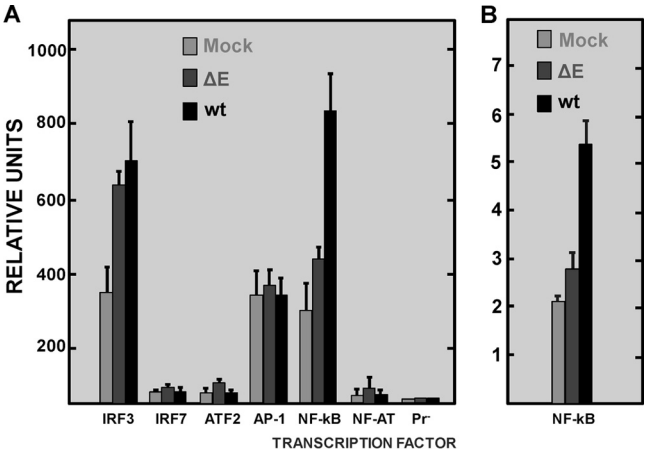

FIG 6 Activation of proinflammatory pathways in rSARS-CoV-MA15-ΔE-infected cells. (A) DBT-mACE2 cells were transfected with plasmids expressing firefly and *Renilla* luciferase, as described in Materials and Methods. Cells were mock infected (mock) or infected with rSARS-CoV-MA15-ΔE (ΔE) or rSARS-CoV-MA15 (wt) at an MOI of 0.05 at 24 h posttransfection. *Renilla* and firefly luciferase expression levels were quantified 48 h later, and the expression of firefly luciferase was normalized to that of *Renilla* luciferase. The level of firefly luciferase expression in cells transfected with a plasmid expressing the firefly luciferase under the control of a basal, noninducible promoter (Pr^{-}) was also determined. (B) Cells were infected with rSARS-CoV-MA15-ΔE or rSARS-CoV-MA15 at an MOI of 0.05. At 48 hpi, nuclear extracts were prepared, and the presence of NF-κB was quantified by ELISA as described in Materials and Methods. Error bars represent the means of three independent experiments.

rSARS-CoV-MA15 induced the activation of proinflammatory transcription factors. The most important signal transduction pathways activated by viruses leading to the expression of proinflammatory cytokines are mediated by transcription factors IRF3, IRF7, CRE, AP-1, NF-κB, and NF-AT. To analyze the mechanism by which rSARS-CoV-MA15-ΔE induced a limited proinflammatory response, DBT-mACE2 cells (43) were cotransfected with plasmids expressing the firefly luciferase under the control of each of these transcription factors and with a plasmid expressing the *Renilla* luciferase. Cells were then mock infected or infected with rSARS-CoV-MA15-ΔE or rSARS-CoV-MA15. Firefly luciferase levels were measured at 48 h postinfection (Fig. 6A) and normalized to those of *Renilla* luciferase. Transcription factors IRF3 and NF-κB were activated in rSARS-CoV-MA15-infected cells compared to levels in mock-infected cells. Interestingly, the activation of NF-κB was significantly higher (3-fold) in rSARS-CoV-MA15-infected cells than in rSARS-CoV-MA15-ΔE-infected cells, whereas IRF3 was not differentially activated (Fig. 6A). We confirmed this finding by measuring nuclear levels of NF-κB using an ELISA. The levels of p65 were measured as p50-p65 heterodimers, which are in general the most abundant forms of NF-κB (47). NF-κB was activated to higher levels in rSARS-CoV-MA15-infected cells than in rSARS-CoV-MA15-ΔE-infected cells (Fig. 6B). Virus titers at the time point the experiment was analyzed were 6×10^5 PFU/ml and 4×10^7 PFU/ml for rSARS-CoV-MA15-ΔE and wild-type rSARS-CoV-MA15 virus in

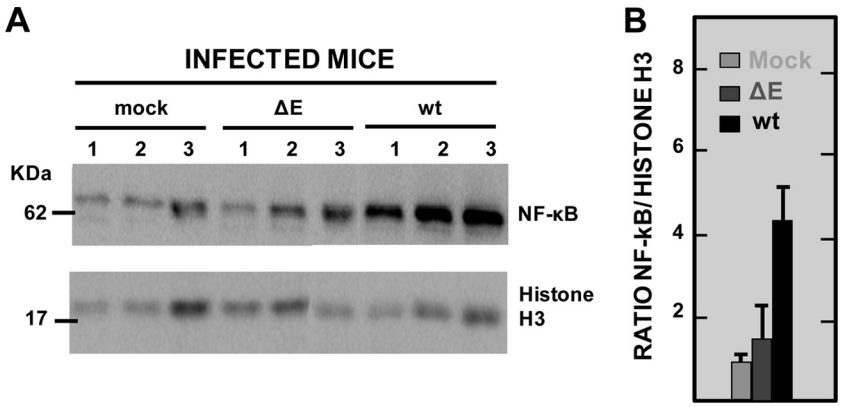

FIG 7 Activation of NF-κB in rSARS-CoV-MA15-ΔE-infected mice. BALB/c mice were infected with 100,000 PFU of rSARS-CoV-MA15-ΔE or rSARS-CoV-MA15. Nuclear lung proteins were extracted at 2 dpi. (A) The accumulation of NF-κB and histone H3 in the nucleus of three infected mice per condition was evaluated by Western blotting. (B) NF-κB and histone H3 amounts were quantified by densitometric analysis. The graph shows the NF-κB/histone H3 ratio in mock-, rSARS-CoV-MA15-ΔE (ΔE)-, and rSARS-CoV-MA15 (wt)-infected mice at 2 dpi. Error bars represent the means of three mice analyzed for each time point.

cell culture supernatants, respectively. These data suggested that transcription factors IRF3 and NF-κB were responsible for the greater inflammation observed in infected cells and mice, with NF-κB being more important in the increased inflammation observed after rSARS-CoV-MA15 infection.

NF-κB activation in the lungs of rSARS-CoV-infected mice. To determine whether NF-κB was also differentially activated in the lungs of rSARS-CoV-MA15-ΔE- and rSARS-CoV-MA15-infected mice, 16-week-old mice were infected with these viruses using 100,000 PFU and analyzed for NF-κB expression by Western blotting using a p65-specific antibody, as described in Materials and Methods. Levels of NF-κB increased about 4-fold in rSARS-CoV-MA15-infected lungs compared to mock-infected ones at day 2 p.i. (Fig. 7), with levels up to 3.1-fold higher in rSARS-CoV-MA15-infected lungs than in rSARS-CoV-MA15-ΔE-infected lungs (Fig. 7), consistent with the results observed in infected cells.

Effect of NF-κB on rSARS-CoV-induced inflammation. The results described above suggest that NF-κB is key in the differential development of inflammation in cells and in mice infected with rSARS-CoV-MA15 and rSARS-CoV-MA15-ΔE. However, virus replication was diminished by the absence of E protein in both cells and mice, possibly confounding interpretation. To address directly the role of NF-κB in inflammation, we treated rSARS-CoV-MA15-infected cells with four NF-κB inhibitors, CAPE, resveratrol, Bay11-7082, and parthenolide (48–51). Four inhibitors were used to minimize the likelihood of off-target effects. NF-κB activity decreased in both mock- and rSARS-CoV-MA15-infected cells treated with the four NF-κB inhibitors compared to activity in nontreated cells (Fig. 8A). Interestingly, none of these inhibitors affected virus titers (Fig. 8B), indicating that the treatment with the inhibitors did not compromise the cell viability and that the effect observed was due to a decrease in NF-κB activation and was not simply due to a significant inhibition of viral replication by the NF-κB inhibitors. The expression levels of TNF, CCL2, and CXCL2, which were upregulated during SARS-CoV infection and which are induced by NF-κB (52), were clearly decreased (from 2- to 5-fold) in rSARS-CoV-MA15-infected cells treated with the NF-κB inhibitors (Fig. 8C). These data indicated that NF-κB activation induces the expression of inflammatory cytokines after SARS-CoV infection.

Effect of NF-κB inhibitors on the survival of rSARS-CoV-MA15-infected mice. To determine whether NF-κB inhibitors increased survival after SARS-CoV infection, rSARS-CoV-MA15- and mock-infected mice were treated intraperitoneally with

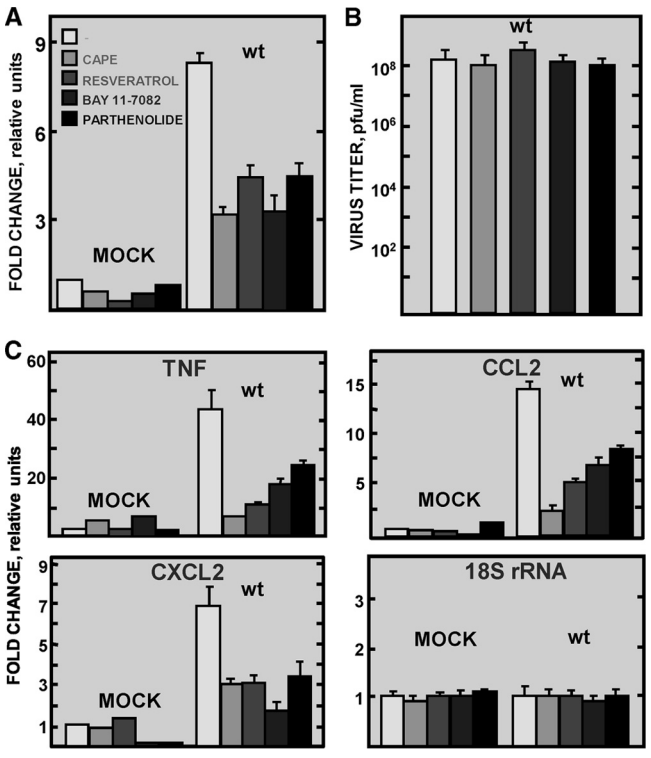

FIG 8 Effect of NF-κB on proinflammatory cytokine induction after rSARS-CoV-MA15 infection. DBT-mACE2 cells were infected at an MOI of 0.05 with rSARS-CoV-MA15 for 48 h. Mock-infected (mock) or rSARS-CoV-MA15-infected (wt) cells were treated at 43 hpi with the NF-κB inhibitors CAPE, resveratrol, Bay 11–7082, and parthenolide or left untreated (white bars). (A) NF-κB activation was analyzed in cells transfected with luciferase plasmids as described in the legend of Fig. 6. (B) Virus titers in cell culture supernatants were determined by plaque assay in Vero E6 cells. (C) Expression of TNF, CCL2, and CXCL2 and that of 18S rRNA as a control was evaluated by RT-qPCR. The expression levels of the different genes were normalized to the expression of nontreated, mock-infected cells. Error bars represent the means of three independent experiments.

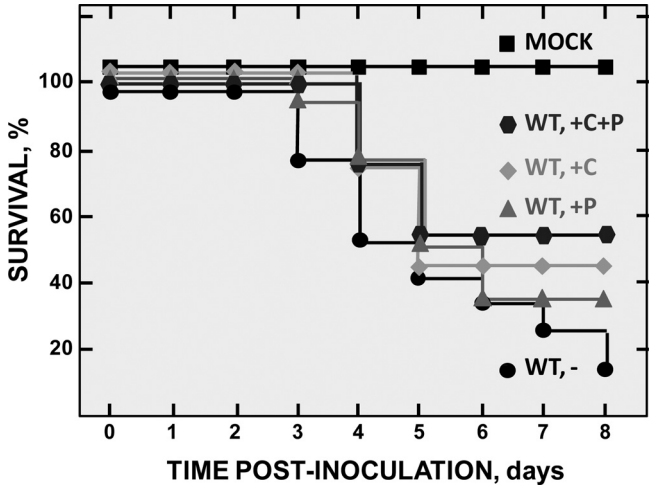

FIG 9 Effect of NF-κB inhibitors in rSARS-CoV-MA15-infected mice. Sixteen-week-old mice were intranasally infected with 100,000 PFU of rSARS-CoV-MA15 or mock infected. At 4 hpi and every 24 h from days 1 to 4, mock-infected and wild-type (wt)-infected mice were intraperitoneally injected with CAPE (wt, +C), parthenolide (wt, +P), both CAPE and parthenolide (wt, +C +P), or vehicle (wt, −). Animals were monitored daily for mortality. Data are representative of three independent experiments, comprising 6 mice per experiment and group (data for treated mock-infected mice are not shown). Differences in survival between nontreated mice and mice treated with CAPE, parthenolide, and CAPE plus parthenolide were statistically significant ($P < 0.02$).

CAPE, parthenolide, or both. All mock-infected BALB/c mice treated with inhibitors showed no signs of clinical disease or weight loss and no mortality (data not shown). Of rSARS-CoV-MA15-infected mice, 16.7% survived, whereas 44.4 and 33.3% of CAPE- and parthenolide-treated mice survived, respectively (Fig. 9). Interestingly, in the case of mice simultaneously administered both NF-κB inhibitors, survival increased to 55.6%, suggesting complementary effects of the drugs.

Effect of NF-κB inhibitors on rSARS-CoV-induced inflammation in mice. To analyze whether treatment with NF-κB inhibitors reduced the expression of proinflammatory cytokines in mouse lungs, as was observed in tissue culture cells, total lung RNA from nontreated or treated mice was extracted, and expression of TNF, CCL2, CXCL2, and a control RNA (18S rRNA) was evaluated by RT-qPCR. Levels of the three cytokine mRNAs were significantly reduced (from 2.2- to 4.5-fold) in all groups of mice treated with the different drugs compared to levels in nontreated mice. As a control, the expression of the 18S rRNA did not change in nontreated and drug-treated mice (Fig. 10A). Virus titers in lung homogenates were similar in both untreated and treated animals (Fig. 10B), suggesting that the reduction of proinflammatory cytokines after treatment with NF-κB inhibitors was not a consequence of reduced virus replication. To evaluate whether NF-κB inhibitors reduced lung pathology induced after SARS-

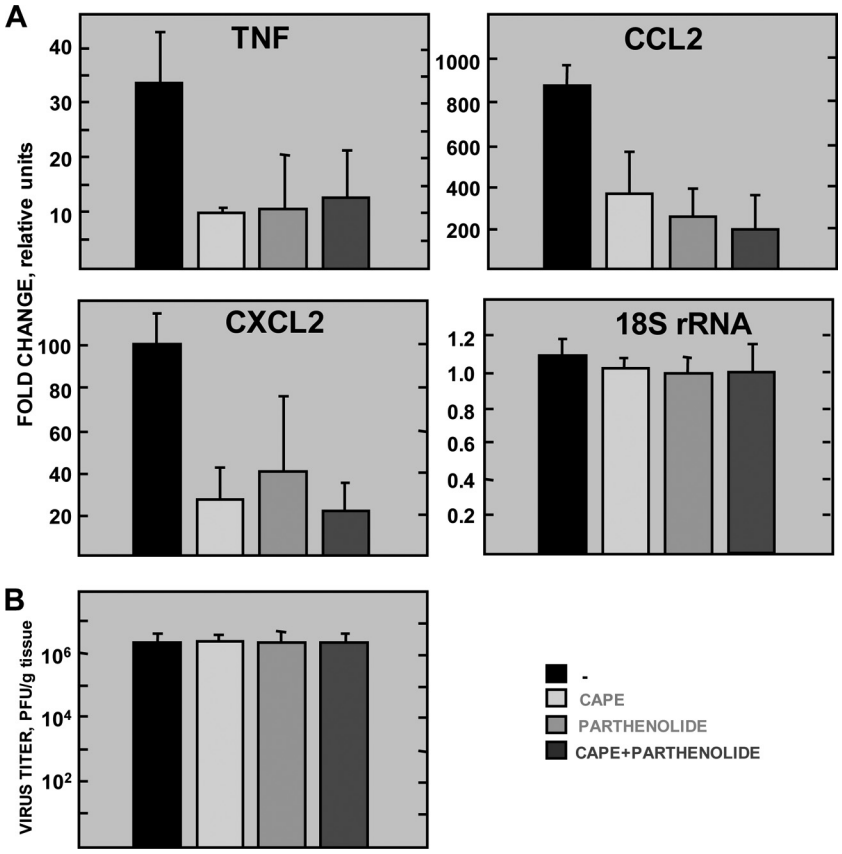

FIG 10 Effect of NF-κB inhibitors on proinflammatory cytokine induction after rSARS-CoV-MA15 infection *in vivo*. Mice were infected and treated as described in the legend of Fig. 9. (A) Four days after infection, total RNA from lungs was extracted, and the expression of TNF, CCL2, CXCL2, and 18S rRNA was quantified. The expression levels of the different genes were normalized to levels in nontreated, mock-infected mice. Error bars represent the means of three independent mice per group. (B) Four days after infection, virus titers in lung homogenates were determined. Error bars represent the means of three independent mice per group. Black bars, untreated.

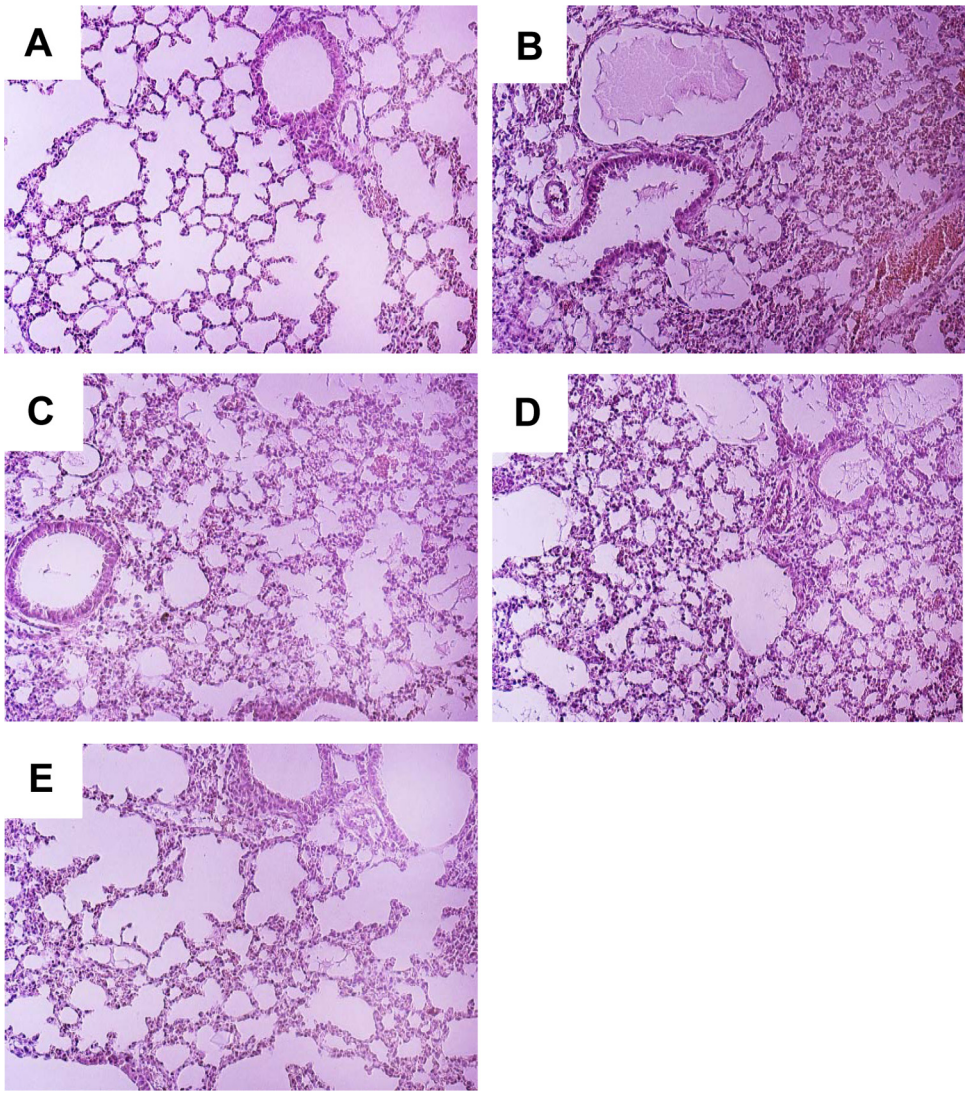

FIG 11 Lung pathology induced after rSARS-CoV-MA15 infection in the presence of NF-κB inhibitors. Mice were mock infected or infected and treated as indicated in the legend of Fig. 9. Four days after infection, lung sections from mock-infected mice (A) and from rSARS-CoV-MA15-infected mice, which were left untreated (B) or treated with CAPE (C), parthenolide (D), or both (E), were evaluated. Three independent mice per group were analyzed. Representative images are shown.

CoV infection, lung sections were analyzed (Fig. 11). In nontreated infected mice, inflammatory infiltrates and lung edema were clearly observed. Interestingly, pulmonary pathology was clearly lower in infected mice treated with each of the NF-κB inhibitors. Furthermore, higher reduction of pathology was observed in the mice treated with both inhibitors at the same time (Fig. 11). These results indicated that NF-κB inhibitors also reduced the expression of proinflammatory cytokines and lung pathology *in vivo*, suggesting that they may be useful for SARS therapy.

DISCUSSION

SARS-CoV lacking E gene is attenuated (21, 22, 24). Here, we showed that rSARS-CoV-MA15-ΔE induced less inflammation in lungs than rSARS-CoV-MA15. This decrease in inflammation correlated with decreased expression of proinflammatory mediators, such as cytokines and chemokines, with lower numbers of neutrophils in infected lungs and with a reduction in NF-κB activation. Some of the decreased inflammation observed in rSARS-CoV-MA15-ΔE-infected mice may have resulted from a reduction of virus titers after mouse infection by rSARS-CoV-MA15-ΔE compared to rSARS-CoV-MA15.

At the same time, an alternative explanation has been proposed as complementary results also suggested that E protein contributed to the extent of the inflammatory response, independently of its role in virus replication. For instance, rSARS-CoV-ΔE grew to lower titers than rSARS-CoV, but, in spite of this, it induced an increased stress response and apoptosis (25). In addition, we have shown that virus titers in the lungs of mice infected with recombinant SARS-CoVs with point mutations or small deletions in the E protein were the same as in mice infected with rSARS-CoV-MA15. However, these viruses induced limited pathological changes and were attenuated (J. L. Nieto-Torres, J. M. Jimenez-

Guardeño, J. A. Regla-Nava, M. L. DeDiego, and L. Enjuanes, unpublished results). Furthermore, SARS-CoV E protein is a viroporin with ion channel activity (15, 53), and we showed that SARS-CoV in which this activity was abrogated lost its virulence without reductions in virus titer, again indicating that an intrinsic property of E protein is responsible for virus virulence and that changes in virus titer were not necessary for increased attenuation (54). Similar results have been reported for other respiratory viruses expressing active viroporins, such as M2 and PB1-F2 of influenza virus, SH of Rous sarcoma virus (RSV), and 2B of rhinovirus. Inflammasome activation was observed in cells infected by these viruses when the viroporin displayed ion channel activity but not in its absence (55–57). Also, expression of E protein from porcine reproductive and respiratory syndrome virus (PRRSV), in the absence of virus infection, altered ion concentrations within the cell, leading to inflammasome activation, indicating that the viroporin itself was responsible for the activation (58). More importantly, when mice were infected with influenza viruses in which the ion channel activity of PB1-F2 protein was intact or abrogated, virus titers were similar, and a virulent or attenuated phenotype was observed, respectively (59). Overall, the data indicate that the intrinsic activities of these viroporins may also be responsible for virus virulence.

After infection of mice with rSARS-CoV-MA15, increases in the expression of the inflammatory cytokine TNF, of chemokines CCL2, CCL5, CXCL1, CXCL2, and CXCL10, and of IL-6 and in the migration of neutrophils to infected lungs were observed compared to levels in rSARS-CoV-MA15-ΔE-infected mice. In the lungs of human patients with fatal SARS, elevated levels of IL-6 and of chemokines such as CCL2 and CXCL10 were also detected (60–62). Similarly, during influenza virus and RSV infections, increased numbers of neutrophils in the lungs contributed to worse outcomes (63–67). Neutrophil-mediated inflammation also contributes to bronchiolitis after RSV infection, and antioxidant treatment, which reduced neutrophil influx to the lungs and proinflammatory cytokine expression, also reduced clinical illness in RSV-infected mice (68). The increase in neutrophil influx in rSARS-CoV-MA15-infected mice compared to that in mice infected with rSARS-CoV-MA15-ΔE was not associated with elevated numbers of macrophages, suggesting that the neutrophil increase was cell type specific.

NF-κB was differentially activated following rSARS-CoV-MA15-ΔE and rSARS-CoV-MA15 infection in cell cultures and *in vivo*. This transcription factor regulated the expression of proinflammatory mediators such as TNF, CCL2, and CXCL2 after SARS-CoV infection. Administration of two inhibitors of NF-κB, CAPE and parthenolide, increased mouse survival after infection and was associated with reduced expression of proinflammatory cytokines in the lungs. These drugs showed complementary effects as treatment with both of them increased survival to a higher extent than treatment with either one alone. Therefore, NF-κB inhibitors may be useful antivirals in SARS therapy. Similarly, NF-κB inhibitors may be effective as antivirals against influenza virus (69–71) and RSV (72).

NF-κB is activated following signaling events leading to activation of mitogen-activated protein kinase kinase kinases (MAP3Ks), which activate IKKα and -β, leading to IκB phosphorylation. Phosphorylated IκB is degraded through the ubiquitin-dependent 26S proteasome pathway. Degradation of IκB unmasks the nuclear NF-κB-mediated transcription. In addition to the inhibitors used in this study, other inhibitors of the signaling pathway leading to NF-κB activation could be considered to treat SARS patients. For example, inhibitors that (i) block the binding of cytokines to their receptors, such as anti-TNF antibodies, (ii) inhibit IKK activation and function, (iii) interfere with IκB degradation, such as ubiquitination and proteasome inhibitors, and (iv) impede nuclear translocation, DNA binding, and transcriptional activation of NF-κB (reviewed in references 35 and 36) could be assessed. In addition to NF-κB, IRF3 was also activated in SARS-CoV-infected cells and most probably *in vivo*. As this transcription factor is also implicated in the upregulation of proinflammatory cytokines after infection (73), IRF3 inhibitors could also be evaluated in SARS-CoV-infected mice. One advantage of antivirals that target cellular protein activity rather than that of viral proteins is that their effect is not likely to be negated by mutations in the virus genome.

In summary, we identify promising antivirals for SARS-CoV therapy by applying basic knowledge of the signaling pathways altered during infection by this virus. This strategy complements the development of candidate vaccines previously reported by our group (24, 74, 75). The next step will be to confirm the efficacy and absence of side effects in other animal models, such as macaques, which are closer to humans.

ACKNOWLEDGMENTS

This work was supported by grants from the Ministry of Science and Innovation of Spain (BIO2010-16705), the Seventh Framework Programme (FP7/2007-2013) of the European Commission (EC) under the project EMPERIE (EC grant agreement number 223498), and the U.S. National Institutes of Health (2P01AI060699-06A1 and CRIP-HHSN266200700010C). M.L.D. received a contract from the project EMPERIE (EC grant agreement number 223498), and J.A.R.-N. and C.C.-R. received a contract from Fundación La Caixa.

We thank Marga Gonzalez for technical assistance.

REFERENCES

1. **Peiris JS, Guan Y, Yuen KY.** 2004. Severe acute respiratory syndrome. Nat. Med. **10:**S88–S97. http://dx.doi.org/10.1038/nm1143.
2. **Peiris JS, Yuen KY, Osterhaus AD, Stohr K.** 2003. The severe acute respiratory syndrome. N. Engl. J. Med. **349:**2431–2441. http://dx.doi.org/10.1056/NEJMra032498.
3. **Lau SK, Woo PC, Li KS, Huang Y, Tsoi HW, Wong BH, Wong SS, Leung SY, Chan KH, Yuen KY.** 2005. Severe acute respiratory syndrome coronavirus-like virus in Chinese horseshoe bats. Proc. Natl. Acad. Sci. U. S. A. **102:**14040–14045. http://dx.doi.org/10.1073/pnas.0506735102.
4. **Li W, Shi Z, Yu M, Ren W, Smith C, Epstein JH, Wang H, Crameri G, Hu Z, Zhang H, Zhang J, McEachern J, Field H, Daszak P, Eaton BT, Zhang S, Wang LF.** 2005. Bats are natural reservoirs of SARS-like coronaviruses. Science **310:**676–679. http://dx.doi.org/10.1126/science.1118391.
5. **Lau SK, Li KS, Huang Y, Shek CT, Tse H, Wang M, Choi GK, Xu H, Lam CS, Guo R, Chan KH, Zheng BJ, Woo PC, Yuen KY.** 2010. Ecoepidemiology and complete genome comparison of SARS-related *Rhinolophus* bat coronavirus in China reveal bats as reservoir for acute, self-limiting infection that allows recombination events. J. Virol. **84:**2808–2819. http://dx.doi.org/10.1128/JVI.02219-09.
6. **Hon CC, Lam TY, Shi ZL, Drummond AJ, Yip CW, Zeng F, Lam PY, Leung FC.** 2008. Evidence of the recombinant origin of a bat severe acute respiratory syndrome (SARS)-like coronavirus and its implications on the direct ancestor of SARS coronavirus. J. Virol. **82:**1819–1826. http://dx.doi.org/10.1128/JVI.01926-07.
7. **Zaki AM, van Boheemen S, Bestebroer TM, Osterhaus AD, Fouchier RA.** 2012. Isolation of a novel coronavirus from a man with pneumonia in Saudi Arabia. N. Engl. J. Med. **367:**1814–1820. http://dx.doi.org/10.1056/NEJMoa1211721.
8. **van Boheemen S, de Graaf M, Lauber C, Bestebroer TM, Raj VS, Zaki AM, Osterhaus AD, Haagmans BL, Gorbalenya AE, Snijder EJ, Fouchier RA.** 2012. Genomic characterization of a newly discovered coronavirus associated with acute respiratory distress syndrome in humans. mBio **3**(6):e00473-12. http://dx.doi.org/10.1128/mBio.00473-12.

9. **Reusken CB, Haagmans BL, Muller MA, Gutierrez C, Godeke GJ, Meyer B, Muth D, Raj VS, Vries LS, Corman VM, Drexler JF, Smits SL, El Tahir YE, De Sousa R, van Beek J, Nowotny N, van Maanen K, Hidalgo-Hermoso E, Bosch BJ, Rottier P, Osterhaus A, Gortazar-Schmidt C, Drosten C, Koopmans MP.** 2013. Middle East respiratory syndrome coronavirus neutralising serum antibodies in dromedary camels: a comparative serological study. Lancet Infect. Dis. **13:**859–866. http://dx.doi.org/10.1016/S1473-3099(1013)70164-70166.
10. **Rota PA, Oberste MS, Monroe SS, Nix WA, Campganoli R, Icenogle JP, Peñaranda S, Bankamp B, Maher K, Chen M-H, Tong S, Tamin A, Lowe L, Frace M, DeRisi JL, Chen Q, Wang D, Erdman Dd Peret TCT, Burns C, Ksiazek TG, Rollin PE, Sanchez A, Liffick S, Holloway B, Limor J, McCaustland K, Olsen-Rassmussen M, Fouchier R, Gunther S, Osterhaus ADME, Drosten C, Pallansch MA, Anderson LJ, Bellini WJ.** 2003. Characterization of a novel coronavirus associated with severe acute respiratory syndrome. Science **300:**1394–1399. http://dx.doi.org/10.1126/science.1085952.
11. **Ziebuhr J.** 2005. The coronavirus replicase. Curr. Top. Microbiol. Immunol. **287:**57–94. http://dx.doi.org/10.1007/3-540-26765-4_3.
12. **Enjuanes L, Gorbalenya AE, de Groot RJ, Cowley JA, Ziebuhr J, Snijder EJ.** 2008. The *Nidovirales*, p 419–430. *In* Mahy BWJ, Van Regenmortel M, Walker P, Majumder-Russell D (ed), Encyclopedia of virology, 3rd ed. Elsevier Ltd., Oxford, United Kingdom.
13. **Gorbalenya AE, Snijder EJ, Spaan WJ.** 2004. Severe acute respiratory syndrome coronavirus phylogeny: toward consensus. J. Virol. **78:**7863–7866. http://dx.doi.org/10.1128/JVI.78.15.7863-7866.2004.
14. **Torres J, Parthasarathy K, Lin X, Saravanan R, Liu DX.** 2006. Model of a putative pore: the pentameric alpha-helical bundle of SARS coronavirus E protein in lipid bilayers. Biophys. J. **91:**938–947. http://dx.doi.org/10.1529/biophysj.105.080119.
15. **Verdia-Baguena C, Nieto-Torres JL, Alcaraz A, Dediego ML, Torres J, Aguilella VM, Enjuanes L.** 2012. Coronavirus E protein forms ion channels with functionally and structurally-involved membrane lipids. Virology **432:**485–494. http://dx.doi.org/10.1016/j.virol.2012.07.005.
16. **Verdia-Baguena C, Nieto-Torres JL, Alcaraz A, Dediego ML, Enjuanes L, Aguilella VM.** 2013. Analysis of SARS-CoV E protein ion channel activity by tuning the protein and lipid charge. Biochim. Biophys. Acta **1828:**2026–2031. http://dx.doi.org/10.1016/j.bbamem.2013.05.008.
17. **Curtis KM, Yount B, Baric RS.** 2002. Heterologous gene expression from transmissible gastroenteritis virus replicon particles. J. Virol. **76:**1422–1434. http://dx.doi.org/10.1128/JVI.76.3.1422-1434.2002.
18. **Ortego J, Ceriani JE, Patino C, Plana J, Enjuanes L.** 2007. Absence of E protein arrests transmissible gastroenteritis coronavirus maturation in the secretory pathway. Virology **368:**296–308. http://dx.doi.org/10.1016/j.virol.2007.05.032.
19. **Ortego J, Escors D, Laude H, Enjuanes L.** 2002. Generation of a replication-competent, propagation-deficient virus vector based on the transmissible gastroenteritis coronavirus genome. J. Virol. **76:**11518–11529. http://dx.doi.org/10.1128/JVI.76.22.11518-11529.2002.
20. **Almazan F, DeDiego ML, Sola I, Zuñiga S, Nieto-Torres JL, Marquez-Jurado S, Andres G, Enjuanes L.** 2013. Engineering a replication-competent, propagation-defective Middle East respiratory syndrome coronavirus as a vaccine candidate. mBio **4**(5):e00650–13. http://dx.doi.org/10.1128/mBio.00650-13.
21. **DeDiego ML, Alvarez E, Almazan F, Rejas MT, Lamirande E, Roberts A, Shieh WJ, Zaki SR, Subbarao K, Enjuanes L.** 2007. A severe acute respiratory syndrome coronavirus that lacks the E gene is attenuated in vitro and in vivo. J. Virol. **81:**1701–1713. http://dx.doi.org/10.1128/JVI.01467-06.
22. **DeDiego ML, Pewe L, Alvarez E, Rejas MT, Perlman S, Enjuanes L.** 2008. Pathogenicity of severe acute respiratory coronavirus deletion mutants in hACE-2 transgenic mice. Virology **376:**379–389. http://dx.doi.org/10.1016/j.virol.2008.03.005.
23. **Kuo L, Masters PS.** 2003. The small envelope protein E is not essential for murine coronavirus replication. J. Virol. **77:**4597–4608. http://dx.doi.org/10.1128/JVI.77.8.4597-4608.2003.
24. **Fett C, DeDiego ML, Regla-Nava JA, Enjuanes L, Perlman S.** 2013. Complete protection against severe acute respiratory syndrome coronavirus-mediated lethal respiratory disease in aged mice by immunization with a mouse-adapted virus lacking E protein. J. Virol. **87:**6551–6559. http://dx.doi.org/10.1128/JVI.00087-13.
25. **DeDiego ML, Nieto-Torres JL, Jimenez-Guardeno JM, Regla-Nava JA, Alvarez E, Oliveros JC, Zhao J, Fett C, Perlman S, Enjuanes L.** 2011. Severe acute respiratory syndrome coronavirus envelope protein regulates cell stress response and apoptosis. PLoS pathog. **7:**e1002315. http://dx.doi.org/10.1371/journal.ppat.1002315.
26. **Lee N, Hui D, Wu A, Chan P, Cameron P, Joynt G, Ahuja A, Yung MY, Leung CB, To KF, Lui SF, Szeto CC, Chung S, Sung JJY.** 2003. A major outbreak of severe acute respiratory syndrome in Hong Kong. N. Engl. J. Med. **348:**1986–1994. http://dx.doi.org/10.1056/NEJMoa030685.
27. **Wong RS, Wu A, To KF, Lee N, Lam CW, Wong CK, Chan PK, Ng MH, Yu LM, Hui DS, Tam JS, Cheng G, Sung JJ.** 2003. Haematological manifestations in patients with severe acute respiratory syndrome: retrospective analysis. BMJ **326:**1358–1362. http://dx.doi.org/10.1136/bmj.326.7403.1358.
28. **Nagata N, Iwata-Yoshikawa N, Taguchi F.** 2010. Studies of severe acute respiratory syndrome coronavirus pathology in human cases and animal models. Vet. Pathol. **47:**881–892. http://dx.doi.org/10.1177/0300985810378760.
29. **Leung CW, Kwan YW, Ko PW, Chiu SS, Loung PY, Fong NC, Lee LP, Hui YW, Law HK, Wong WH, Chan KH, Peiris JS, Lim WW, Lau YL, Chiu MC.** 2004. Severe acute respiratory syndrome among children. Pediatrics **113:**e535–543. http://dx.doi.org/10.1542/peds.113.6.e535.
30. **Manocha S, Walley KR, Russell JA.** 2003. Severe acute respiratory distress syndrome (SARS): a critical care perspective. Crit. Care Med. **31:**2684–2692. http://dx.doi.org/10.1097/01.CCM.0000091929.51288.5F.
31. **Day CW, Baric R, Cai SX, Frieman M, Kumaki Y, Morrey JD, Smee DF, Barnard DL.** 2009. A new mouse-adapted strain of SARS-CoV as a lethal model for evaluating antiviral agents in vitro and in vivo. Virology **395:**210–222. http://dx.doi.org/10.1016/j.virol.2009.09.023.
32. **Roberts A, Deming D, Paddock CD, Cheng A, Yount B, Vogel L, Herman BD, Sheahan T, Heise M, Genrich GL, Zaki SR, Baric R, Subbarao K.** 2007. A mouse-adapted SARS-coronavirus causes disease and mortality in BALB/c mice. PLoS Pathog. **3:**e5. http://dx.doi.org/10.1371/journal.ppat.0030005.
33. **Nagata N, Iwata N, Hasegawa H, Fukushi S, Harashima A, Sato Y, Saijo M, Taguchi F, Morikawa S, Sata T.** 2008. Mouse-passaged severe acute respiratory syndrome-associated coronavirus leads to lethal pulmonary edema and diffuse alveolar damage in adult but not young mice. Am. J. Pathol. **172:**1625–1637. http://dx.doi.org/10.2353/ajpath.2008.071060.
34. **Smits SL, de Lang A, van den Brand JM, Leijten LM, van IJcken WF, Eijkemans MJ, van Amerongen G, Kuiken T, Andeweg AC, Osterhaus AD, Haagmans BL.** 2010. Exacerbated innate host response to SARS-CoV in aged non-human primates. PLoS Pathog. **6:**e1000756. http://dx.doi.org/10.1371/journal.ppat.1000756.
35. **Vitiello M, Galdiero M, Finamore E, Galdiero S, Galdiero M.** 2012. NF-kappaB as a potential therapeutic target in microbial diseases. Mol. Biosyst. **8:**1108–1120. http://dx.doi.org/10.1039/c2mb05335g.
36. **Gilmore TD, Herscovitch M.** 2006. Inhibitors of NF-kappaB signaling: 785 and counting. Oncogene **25:**6887–6899. http://dx.doi.org/10.1038/sj.onc.1209982.
37. **Law AH, Lee DC, Cheung BK, Yim HC, Lau AS.** 2007. Role for nonstructural protein 1 of severe acute respiratory syndrome coronavirus in chemokine dysregulation. J. Virol. **81:**416–422. http://dx.doi.org/10.1128/JVI.02336-05.
38. **Kanzawa N, Nishigaki K, Hayashi T, Ishii Y, Furukawa S, Niiro A, Yasui F, Kohara M, Morita K, Matsushima K, Le MQ, Masuda T, Kannagi M.** 2006. Augmentation of chemokine production by severe acute respiratory syndrome coronavirus 3a/X1 and 7a/X4 proteins through NF-kappaB activation. FEBS Lett. **580:**6807–6812. http://dx.doi.org/10.1016/j.febslet.2006.11.046.
39. **Liao QJ, Ye LB, Timani KA, Zeng YC, She YL, Ye L, Wu ZH.** 2005. Activation of NF-κB by the full-length nucleocapsid protein of the SARS coronavirus. Acta Biochim. Biophys. Sin. **37:**607–612. http://dx.doi.org/10.1111/j.1745-7270.2005.00082.x.
40. **Zhang X, Wu K, Wang D, Yue X, Song D, Zhu Y, Wu J.** 2007. Nucleocapsid protein of SARS-CoV activates interleukin-6 expression through cellular transcription factor NF-κB. Virology **365:**324–335. http://dx.doi.org/10.1016/j.virol.2007.04.009.
41. **Wang W, Ye L, Ye L, Li B, Gao B, Zeng Y, Kong L, Fang X, Zheng H, Wu Z, She Y.** 2007. Up-regulation of IL-6 and TNF-alpha induced by SARS-coronavirus spike protein in murine macrophages via NF-κB pathway. Virus Res. **128:**1–8. http://dx.doi.org/10.1016/j.virusres.2007.02.007.
42. **Dosch SF, Mahajan SD, Collins AR.** 2009. SARS coronavirus spike protein-induced innate immune response occurs via activation of the NF-

kappaB pathway in human monocyte macrophages in vitro. Virus Res. **142:**19–27. http://dx.doi.org/10.1016/j.virusres.2009.01.005.

43. **Regla-Nava JA, Jimenez-Guardeno JM, Nieto-Torres JL, Gallagher TM, Enjuanes L, DeDiego ML.** 2013. The replication of a mouse adapted SARS-CoV in a mouse cell line stably expressing the murine SARS-CoV receptor mACE2 efficiently induces the expression of proinflammatory cytokines. J. Virol. Methods **193:**639–646. http://dx.doi.org/10.1016/j.jviromet.2013.07.039.
44. **McCray PB, Jr, Pewe L, Wohlford-Lenane C, Hickey M, Manzel L, Shi L, Netland J, Jia HP, Halabi C, Sigmund CD, Meyerholz DK, Kirby P, Look DC, Perlman S.** 2007. Lethal infection of K18-hACE2 mice infected with severe acute respiratory syndrome coronavirus. J. Virol. **81:**813–821. http://dx.doi.org/10.1128/JVI.02012-06.
45. **Zhao J, Van Rooijen N, Perlman S.** 2009. Evasion by stealth: inefficient immune activation underlies poor T cell response and severe disease in SARS-CoV-infected mice. PLoS Pathog. **5:**e1000636. http://dx.doi.org/10.1371/journal.ppat.1000636.
46. **Yoneyama M, Suhara W, Fukuhara Y, Fukuda M, Nishida E, Fujita T.** 1998. Direct triggering of the type I interferon system by virus infection: activation of a transcription factor complex containing IRF-3 and CBP/p300. EMBO J. **17:**1087–1095. http://dx.doi.org/10.1093/emboj/17.4.1087.
47. **Phelps CB, Sengchanthalangsy LL, Malek S, Ghosh G.** 2000. Mechanism of κB DNA binding by Rel/NF-κB dimers. J. Biol. Chem. **275:**24392–24399. http://dx.doi.org/10.1074/jbc.M003784200.
48. **Natarajan K, Singh S, Burke TR, Jr, Grunberger D, Aggarwal BB.** 1996. Caffeic acid phenethyl ester is a potent and specific inhibitor of activation of nuclear transcription factor NF-κB. Proc. Natl. Acad. Sci. U. S. A. **93:**9090–9095. http://dx.doi.org/10.1073/pnas.93.17.9090.
49. **Hehner SP, Hofmann TG, Droge W, Schmitz ML.** 1999. The anti-inflammatory sesquiterpene lactone parthenolide inhibits NF-κB by targeting the IκB kinase complex. J. Immunol. **163:**5617–5623.
50. **Holmes-McNary M, Baldwin AS, Jr.** 2000. Chemopreventive properties of trans-resveratrol are associated with inhibition of activation of the IκB kinase. Cancer Res. **60:**3477–3483.
51. **Pierce JW, Schoenleber R, Jesmok G, Best J, Moore SA, Collins T, Gerritsen ME.** 1997. Novel inhibitors of cytokine-induced IκBαphosphorylation and endothelial cell adhesion molecule expression show anti-inflammatory effects in vivo. J. Biol. Chem. **272:**21096–21103. http://dx.doi.org/10.1074/jbc.272.34.21096.
52. **Ali S, Mann DA.** 2004. Signal transduction via the NF-κB pathway: a targeted treatment modality for infection, inflammation and repair. Cell Biochem. Funct. **22:**67–79. http://dx.doi.org/10.1002/cbf.1082.
53. **Torres J, Maheswari U, Parthasarathy K, Ng L, Liu DX, Gong X.** 2007. Conductance and amantadine binding of a pore formed by a lysine-flanked transmembrane domain of SARS coronavirus envelope protein. Protein Sci. **16:**2065–2071. http://dx.doi.org/10.1110/ps.062730007.
54. **Nieto-Torres JL, DeDiego ML, Verdia-Baguena C, Jimenez-Guardeno JM, Regla-Nava JA, Alcaraz A, Aguilella VM, Enjuanes L.** 2013. Relevance of SARS-CoV E protein ion channel activity in virus fitness and virulence. 32nd Annu. Meet. Amer. Soc. Virol. The Pennsylvania State University, State College, PA.
55. **Triantafilou K, Kar S, Vakakis E, Kotecha S, Triantafilou M.** 2013. Human respiratory syncytial virus viroporin SH: a viral recognition pathway used by the host to signal inflammasome activation. Thorax **68:**66–75. http://dx.doi.org/10.1136/thoraxjnl-2012-202182.
56. **Triantafilou K, Kar S, van Kuppeveld FJ, Triantafilou M.** 1 July 2013. Rhinovirus-induced calcium flux triggers NLRP3 and NLRC5 activation in bronchial cells. Am. J. Respir. Cell Mol. Biol. http://dx.doi.org/10.1165/rcmb.2013-0032OC.
57. **Ichinohe T, Pang IK, Iwasaki A.** 2010. Influenza virus activates inflammasomes via its intracellular M2 ion channel. Nat. Immunol. **11:**404–410. http://dx.doi.org/10.1038/ni.1861.
58. **Zhang K, Hou Q, Zhong Z, Li X, Chen H, Li W, Wen J, Wang L, Liu W, Zhong F.** 2013. Porcine reproductive and respiratory syndrome virus activates inflammasomes of porcine alveolar macrophages via its small envelope protein E. Virology **442:**156–162. http://dx.doi.org/10.1016/j.virol.2013.04.007.
59. **McAuley JL, Tate MD, MacKenzie-Kludas CJ, Pinar A, Zeng W, Stutz A, Latz E, Brown LE, Mansell A.** 2013. Activation of the NLRP3 inflammasome by IAV virulence protein PB1-F2 contributes to severe pathophysiology and disease. PLoS Pathog. **9:**e1003392. http://dx.doi.org/10.1371/journal.ppat.1003392.
60. **Tang NL, Chan PK, Wong CK, To KF, Wu AK, Sung YM, Hui DS, Sung JJ, Lam CW.** 2005. Early enhanced expression of interferon-inducible protein-10 (CXCL-10) and other chemokines predicts adverse outcome in severe acute respiratory syndrome. Clin. Chem. **51:**2333–2340. http://dx.doi.org/10.1373/clinchem.2005.054460.
61. **Jiang Y, Xu J, Zhou C, Wu Z, Zhong S, Liu J, Luo W, Chen T, Qin Q, Deng P.** 2005. Characterization of cytokine/chemokine profiles of severe acute respiratory syndrome. Am. J. Respir. Crit. Care Med. **171:**850–857. http://dx.doi.org/10.1164/rccm.200407-857OC.
62. **Cameron MJ, Ran L, Xu L, Danesh A, Bermejo-Martin JF, Cameron CM, Muller MP, Gold WL, Richardson SE, Poutanen SM, Willey BM, DeVries ME, Fang Y, Seneviratne C, Bosinger SE, Persad D, Wilkinson P, Greller LD, Somogyi R, Humar A, Keshavjee S, Louie M, Loeb MB, Brunton J, McGeer AJ, Kelvin DJ.** 2007. Interferon-mediated immunopathological events are associated with atypical innate and adaptive immune responses in patients with severe acute respiratory syndrome. J. Virol. **81:**8692–8706. http://dx.doi.org/10.1128/JVI.00527-07.
63. **Bradley LM, Douglass MF, Chatterjee D, Akira S, Baaten BJ.** 2012. Matrix metalloprotease 9 mediates neutrophil migration into the airways in response to influenza virus-induced toll-like receptor signaling. PLoS Pathog. **8:**e1002641. http://dx.doi.org/10.1371/journal.ppat.1002641.
64. **Narasaraju T, Yang E, Samy RP, Ng HH, Poh WP, Liew AA, Phoon MC, van Rooijen N, Chow VT.** 2011. Excessive neutrophils and neutrophil extracellular traps contribute to acute lung injury of influenza pneumonitis. Am. J. Pathol. **179:**199–210. http://dx.doi.org/10.1016/j.ajpath.2011.03.013.
65. **Brandes M, Klauschen F, Kuchen S, Germain RN.** 2013. A systems analysis identifies a feedforward inflammatory circuit leading to lethal influenza infection. Cell **154:**197–212. http://dx.doi.org/10.1016/j.cell.2013.06.013.
66. **Bataki EL, Evans GS, Everard ML.** 2005. Respiratory syncytial virus and neutrophil activation. Clin. Exp. Immunol. **140:**470–477. http://dx.doi.org/10.1111/j.1365-2249.2005.02780.x.
67. **Yasui K, Baba A, Iwasaki Y, Kubo T, Aoyama K, Mori T, Yamazaki T, Kobayashi N, Ishiguro A.** 2005. Neutrophil-mediated inflammation in respiratory syncytial viral bronchiolitis. Pediatr. Int. **47:**190–195. http://dx.doi.org/10.1111/j.1442-200x.2005.02039.x.
68. **Castro SM, Guerrero-Plata A, Suarez-Real G, Adegboyega PA, Colasurdo GN, Khan AM, Garofalo RP, Casola A.** 2006. Antioxidant treatment ameliorates respiratory syncytial virus-induced disease and lung inflammation. Am. J. Respir. Crit. Care Med. **174:**1361–1369. http://dx.doi.org/10.1164/rccm.200603-319OC.
69. **Wiesener N, Zimmer C, Jarasch-Althof N, Wutzler P, Henke A.** 2011. Therapy of experimental influenza virus infection with pyrrolidine dithiocarbamate. Med. Microbiol. Immunol. **200:**115–126. http://dx.doi.org/10.1007/s00430-010-0182-x.
70. **Pinto R, Herold S, Cakarova L, Hoegner K, Lohmeyer J, Planz O, Pleschka S.** 2011. Inhibition of influenza virus-induced NF-kappaB and Raf/MEK/ERK activation can reduce both virus titers and cytokine expression simultaneously in vitro and in vivo. Antiviral Res. **92:**45–56. http://dx.doi.org/10.1016/j.antiviral.2011.05.009.
71. **Palamara AT, Nencioni L, Aquilano K, De Chiara G, Hernandez L, Cozzolino F, Ciriolo MR, Garaci E.** 2005. Inhibition of influenza A virus replication by resveratrol. J. Infect. Dis. **191:**1719–1729. http://dx.doi.org/10.1086/429694.
72. **Zang N, Xie X, Deng Y, Wu S, Wang L, Peng C, Li S, Ni K, Luo Y, Liu E.** 2011. Resveratrol-mediated gamma interferon reduction prevents airway inflammation and airway hyperresponsiveness in respiratory syncytial virus-infected immunocompromised mice. J. Virol. **85:**13061–13068. http://dx.doi.org/10.1128/JVI.05869-11.
73. **Mogensen TH, Paludan SR.** 2001. Molecular pathways in virus-induced cytokine production. Microbiol. Mol. Biol. Rev. **65:**131–150. http://dx.doi.org/10.1128/MMBR.65.1.131-150.2001.
74. **Lamirande EW, DeDiego ML, Roberts A, Jackson JP, Alvarez E, Sheahan T, Shieh WJ, Zaki SR, Baric R, Enjuanes L, Subbarao K.** 2008. A live attenuated SARS coronavirus is immunogenic and efficacious in golden Syrian hamsters. J. Virol. **82:**7721–7724. http://dx.doi.org/10.1128/JVI.00304-08.
75. **Netland J, DeDiego ML, Zhao J, Fett C, Alvarez E, Nieto-Torres JL, Enjuanes L, Perlman S.** 2010. Immunization with an attenuated severe acute respiratory syndrome coronavirus deleted in E protein protects against lethal respiratory disease. Virology **399:**120–128. http://dx.doi.org/10.1016/j.virol.2010.01.004.

JVI Journals.ASM.org

Complete Protection against Severe Acute Respiratory Syndrome Coronavirus-Mediated Lethal Respiratory Disease in Aged Mice by Immunization with a Mouse-Adapted Virus Lacking E Protein

Craig Fett,[a] Marta L. DeDiego,[b] Jose A. Regla-Nava,[b] Luis Enjuanes,[b] Stanley Perlman[a]

Department of Microbiology, University of Iowa, Iowa City, Iowa, USA[a]; Department of Molecular and Cell Biology, Centro Nacional de Biotecnologia (CNB-CSIC), Campus Universidad Autonoma, Cantoblanco, Madrid, Spain[b]

Zoonotic coronaviruses, including the one that caused severe acute respiratory syndrome (SARS), cause significant morbidity and mortality in humans. No specific therapy for any human coronavirus is available, making vaccine development critical for protection against these viruses. We previously showed that recombinant SARS coronavirus (SARS-CoV) (Urbani strain based) lacking envelope (E) protein expression (rU-ΔE) provided good but not perfect protection in young mice against challenge with virulent mouse-adapted SARS-CoV (MA15). To improve vaccine efficacy, we developed a second set of E-deleted vaccine candidates on an MA15 background (rMA15-ΔE). rMA15-ΔE is safe, causing no disease in 6-week-, 12-month-, or 18-month-old BALB/c mice. Immunization with this virus completely protected mice of three ages from lethal disease and effected more-rapid virus clearance. Compared to rU-ΔE, rMA15-ΔE immunization resulted in significantly greater neutralizing antibody and SARS-CoV-specific CD4 and CD8 T cell responses. After challenge, inflammatory cell infiltration, edema, and lung destruction were decreased in the lungs of rMA15-ΔE-immunized mice compared to those in rU-ΔE-immunized 12-month-old mice. Collectively, these results show that immunization with a species-adapted attenuated coronavirus lacking E protein expression is safe and provides optimal immunogenicity and long-term protection against challenge with lethal virus. This approach will be generally useful for development of vaccines protective against human coronaviruses as well as against coronaviruses that cause disease in domestic and companion animals.

Severe acute respiratory syndrome (SARS), caused by a novel coronavirus (SARS-CoV), was contracted by approximately 8,000 individuals during the 2002-2003 epidemic, with a consequent 10% rate of mortality (1, 2). Most strikingly, 50% of patients greater than 60 years of age succumbed to the infection, while no patient less than 24 years old died. SARS-CoV has not reappeared in human populations since 2004, but several species of coronaviruses with similarities to SARS-CoV have been identified in bat populations (3–6). A human coronavirus (Middle East respiratory syndrome coronavirus [MERS-CoV]) related to two of these bat viruses (BtCoV-HKU4 and BtCoV-HKU5) was recently isolated from several patients in the Middle East who developed severe pneumonia and renal disease (7). How these SARS-like CoVs changed host range to infect humans is not known with certainty, but the fact that they did provides the impetus for development of a SARS-CoV vaccine. Most importantly, the development of such a vaccine would provide a guide to rapid engineering and deployment of a vaccine that would be useful against a new, highly pathogenic coronavirus, even if that virus were not SARS-CoV.

Several vaccine candidates have been developed since 2003 (8, 9). Antivirus neutralizing antibodies, which are useful for protecting select populations, such as health care workers during an outbreak, have been isolated and prepared in large quantities. Several protein subunit vaccines, in which one or more SARS-CoV structural proteins are expressed by a heterologous virus or replicon, have also been developed (10). Some of these approaches will be useful in human populations, but the most-efficacious vaccines will elicit both antibody and T cell responses directed against the virus. One strategy has been to use nonreplicating Venezuelan equine encephalitis replicon particles (VRP) to induce T and B cell responses (11). However, T cell epitopes are located in both the surface glycoproteins and internal proteins, such as the nucleocapsid protein (12). An unexpected problem was that VRPs containing only the N or the N and S proteins induce an eosinophilic infiltrate in the lung after challenge with virulent virus, especially in older mice, making such vaccines not useful (11, 13).

Live attenuated vaccines are considered most effective in their ability to induce a long-lived balanced immune response. The major problems of using live attenuated vaccines relate to the possibility that viruses may revert to virulence and to the risk that even attenuated live vaccines may cause disease in immunocompromised vaccine recipients. Coronaviruses are well known to recombine (14), so any attenuated SARS-CoV should be attenuated at several sites to make the probability of reversion as close to nil as possible. Several approaches have been used to minimize the risk of reversion to virulence, including deletion of a minor structural protein, the envelope (E) protein (15–17). In addition to the N and S proteins, all coronaviruses encode at least two additional structural proteins, the E and transmembrane (M) proteins. The E protein is present in the virion in very small amounts and was initially believed to be

Received 10 January 2013 **Accepted** 25 March 2013
Published ahead of print 10 April 2013
Address correspondence to Stanley Perlman, Stanley-perlman@uiowa.edu.

doi:10.1128/JVI.00087-13

primarily a structural protein. Subsequent work suggested that E protein is involved in virus assembly and virus pathogenesis (14). Deletion of the E protein from SARS-CoV impaired replication but did not prevent release of infectious virus, although titers were lower than they were after infection with E-containing virus (17, 18). Based on these results, we previously developed a recombinant SARS-CoV (human Urbani strain) lacking the E protein (rU-ΔE) and showed that immunization with this virus completely protected hamsters and partially protected mice transgenic (Tg) for the expression of the SARS-CoV receptor human angiotensin-converting enzyme 2 (hACE2) against challenge with SARS-CoV (19, 20). hACE2-Tg mice are very sensitive to infection with SARS-CoV, developing an overwhelming encephalitis (21).

Human isolates of SARS-CoV, including the Urbani strain, cause no or mild disease in young or older wild-type mice, respectively (22, 23). To analyze the effect of vaccination with E protein-deleted virus in the context of a more severe respiratory infection, we also challenged mice with SARS-CoV that had been adapted to growth in mice by serial passage through BALB/c mice (MA15 strain) (24). MA15 causes severe pneumonia in young BALB/c mice and older mice of all strains examined (24–26). Immunization of BALB/c mice with rU-ΔE was partly protective against subsequent challenge with MA15 but induced a weak T cell and antibody response (20). Consequently, we have now engineered another virus on an MA15 background (rMA15-ΔE) with the expectation that it will be more immunogenic than rU-ΔE because it is more fit for growth in the mouse lung. We show here that this is indeed the case, with rMA15-ΔE eliciting more-potent antiviral neutralizing antibody and T cell responses than rU-ΔE but remaining highly attenuated and safe. Further, immunization with rMA15-ΔΔE fully protected 6- to 10-week-old, 12-month-old, and 18-month-old BALB/c mice from challenge with a lethal dose of MA15 and also induced long-term protection.

MATERIALS AND METHODS

Mice, virus, and cells. Specific-pathogen-free BALB/c mice with ages ranging from 6 weeks to 18 months were purchased from the National Cancer Institute. Mice were maintained in the animal care facility at the University of Iowa. All protocols were approved by the University of Iowa Institutional Animal Care and Use Committee. Mouse-adapted SARS-CoV (MA15) (24), a gift from Kanta Subbarao (National Institutes of Health, Bethesda, MD), was grown in Vero E6 cells.

Development of recombinant virus rMA15-ΔE. Mutations required for mouse adaptation were introduced into the Urbani strain of SARS-CoV using a previously described bacterial artificial chromosome (BAC)-based reverse genetics system (27). Specifically, mutations were introduced into Nsp5 (H133Y, K268N), Nsp9 (T67A), Nsp13 (A4V), S protein (Y436H), and M protein (E11K), resulting in rMA15 (24). All these amino acid substitutions except substitution K268N were previously described (24). Introduction of this additional change did not compromise the virulence of MA15 in BALB/c mice (M. L. DeDiego and L. Enjuanes, unpublished results). Virus deleted in E protein was then generated as previously described (15).

Virus infection and titration. BALB/c mice were lightly anesthetized with isoflurane and immunized intranasally with 6,000 PFU of rMA15-ΔE or phosphate-buffered saline (PBS). Some mice were then challenged with an intranasal inoculation of 10^5 PFU of MA15 (nonrecombinant virus). Mice were monitored daily for morbidity and mortality. All work with SARS-CoV was conducted in the University of Iowa biosafety level 3 (BSL3) laboratory. To obtain SARS-CoV titers, lungs were homogenized in PBS. Virus titers were determined on Vero E6 cells as previously described (15, 20). Viral titers are expressed as PFU/g of tissue for SARS-CoV.

Histology. Animals were anesthetized and transcardially perfused with PBS followed by zinc formalin. Lungs were removed, fixed in zinc formalin, and paraffin embedded. Sections were stained with hematoxylin and eosin.

Measurement of CD8 and CD4 T cell responses in the lungs. Mice were sacrificed at the indicated times after infection, and single-cell suspensions were prepared using collagenase D (Roche Applied Science, Indianapolis, IN) and 0.1 mg/ml DNase (Roche) to digest the lung (28). Virus-specific CD8 and CD4 T cells were identified by intracellular cytokine staining (ICS) for gamma interferon (IFN-γ) (28, 29). Briefly, cells were incubated for 5 h with brefeldin A (BD Pharmingen, San Diego, CA) in the presence or absence of the SARS-CoV-specific peptides S366 (CD8; HNYKYRYL) and N353 (CD4; VNFNF NGL) (BioSynthesis Inc., Lewisville, TX). A total of 10^6 cells were then labeled at 4°C for cell surface markers using rat anti-mouse CD4 (RM4-5), rat anti-mouse CD8α (53-6.7) (both from BD Bioscience), and rat anti-mouse IFN-γ (XMG1.2) (eBioscience, San Diego). Cells were then fixed/permeabilized with Cytofix/Cytoperm solution (BD Biosciences) and labeled with anti-IFN-γ antibody. All flow cytometry data were acquired on a BD FACSCalibur or FACSVerse (BD Biosciences, San Jose, CA) and were analyzed using FlowJo software (Tree Star, Inc.).

Measurement of ELISA titers. Whole blood was collected, and sera were prepared. Enzyme-linked immunosorbent assay (ELISA) titers were obtained as previously described (20). Briefly, 96-well MaxiSorp Immuno plates (Nunc) were coated with 2×10^5 PFU of formaldehyde and UV-inactivated SARS-CoV (BEI Resources, Manassas, VA). After being washed, wells were exposed to 3-fold dilutions of sera from naive or immunized mice for 1.5 h. Wells were washed and developed. The ELISA titer was defined as the highest dilution of serum that gave a 2-fold increase over the background.

Measurement of neutralizing antibody titers. A virus plaque reduction assay was used to determine serum neutralizing antibody titers (15). Sera were diluted at the indicated ratios and incubated with 50 PFU of MA15 for 30 min. The limit of detection was below 1:30.

Statistical analysis. Student's *t* test was used to analyze differences in mean values between groups. All results are expressed as means ± standard errors of the means (SEM). *P* values of <0.05 were considered statistically significant.

RESULTS

rMA15-ΔE is safe in 6-week-old and 12-month-old BALB/c mice. Previously, we showed that rU-ΔE was attenuated in hamsters, young BALB/c mice, and hACE2-Tg mice, which are highly susceptible to SARS-CoV (15, 17, 19, 20). However, this recombinant virus was constructed on the background of a human coronavirus strain that caused no disease and induced weak antivirus T cell and antibody responses in young BALB/c mice (20). Mice, even if older, develop only mild clinical disease after infection with human-adapted strains (22). In contrast, BALB/c mice of all ages infected with the mouse-adapted MA15 strain develop clinical pneumonia, with more-severe disease observed in mice greater than 20 weeks of age (24). To determine whether deletion of the E protein attenuated the MA15 strain, we infected 6-week-old BALB/c mice with 5×10^4 PFU of rMA15-ΔE. Mice developed no signs of clinical disease or weight loss, while mice infected with the same dosage of MA15 succumbed to the infection (Fig. 1A and B). Mice that are 20 weeks of age and older develop more-severe disease after infection with MA15 (25, 26). To evaluate the safety of rMA15-ΔE in older mice, we infected 12-month-old BALB/c mice with the same dosage of rMA15-ΔE. These mice also re-

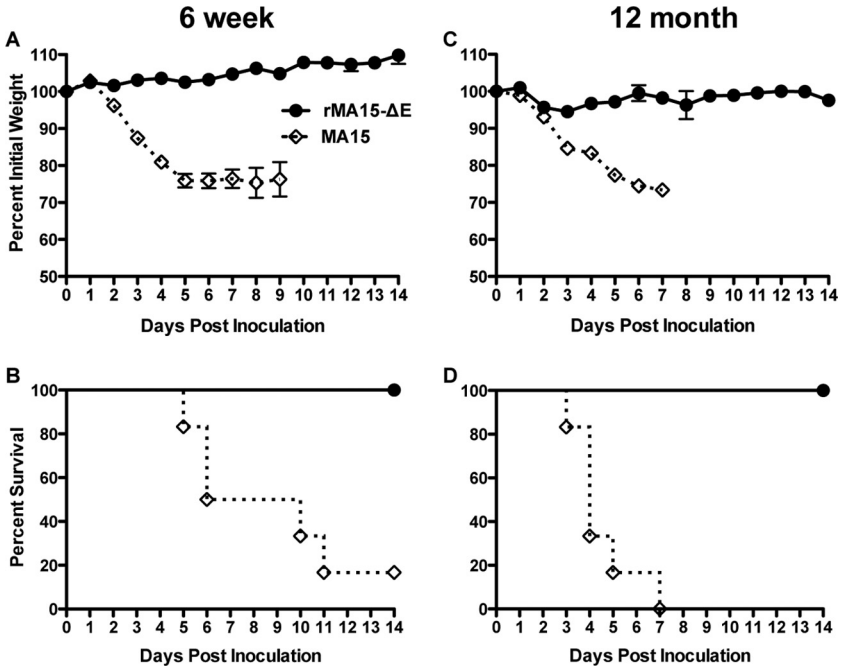

FIG 1 Weights and survival in 6-week- and 12-month-old BALB/c mice after inoculation with 5×10^4 PFU of rMA-ΔE. Six-week-old (A and B) or 12-month-old (C and D) BALB/c mice were inoculated with 5×10^4 PFU of rMA-ΔE or MA15 (nonrecombinant) and monitored for weight loss and survival. Data are from 2 independent experiments with 6 mice per group (A and B) or with 9 (rMA-ΔE) or 6 (MA15) mice per group (C and D).

mained asymptomatic and lost no weight following immunization (Fig. 1C and D).

rMA15-ΔE immunization protects 6-week-old BALB/c mice from MA15-mediated pulmonary disease. rU-ΔE immunization provides imperfect protection against challenge with MA15 (20), so we assessed the efficacy of rMA15-ΔE immunization against challenge with a lethal dose of MA15, comparing it to that of control (PBS-treated) mice. In preliminary results, we found that intranasal immunization of 6-week-old BALB/c mice with 3,000 to 12,000 PFU of rMA15-ΔE resulted in optimal CD4 and CD8 T cell responses at day 7 after immunization; we used 6,000 PFU in all subsequent experiments. Intranasal infection of 6-week-old BALB/c mice with 6,000 PFU of rMA15-ΔE resulted in a small amount of peribronchial/perivascular inflammatory cell infiltration over the first few days following immunization, as assessed on histological examination (data not shown). Infectious virus was detected at days 2, 4, and 6 after immunization in the lungs of 6-week-old mice immunized with 6,000 PFU of rMA15-ΔE but was no longer detectable by day 8 (Fig. 2A).

To evaluate the effect of rMA15-ΔE immunization on clinical disease, we immunized 6-week-old mice with rMA15-ΔE, rU-ΔE, or PBS and then challenged them with 10^5 PFU of MA15 at day 21 after immunization. We previously showed that immunization with rU-ΔE resulted in a 90% decrease in virus titer compared to immunization with PBS by day 5 postchallenge (20). rMA15-ΔE immunization was at least as effective, with virus undetectable at day 4 after challenge (Fig. 2B). All mice in the rMA15-ΔE-treated groups survived and showed no weight loss, while 100% of control mice died (Fig. 2C and D). In agreement with our previous report, immunization with rU-ΔE protected mice against death, although mice showed 10 to 15% weight loss at early times after infection (20).

Immunization with rU-ΔE induced an anti-SARS-CoV T cell response in some but not all mice at day 7 and very low (<1:10) neutralizing antibody titers at day 21 (20). To determine whether the enhanced protection afforded by rMA15-ΔE correlated with greater immunogenicity, we measured antiviral T cell and antibody responses at days 7 and 21, respectively, after immunization. Anti-SARS-CoV neutralizing antibody titers were detectable in 7 of 9 rMA15-ΔE-immunized mice, with an average titer of 1:95 ± 21 (Fig. 2E). In agreement with our previous report (20), anti-SARS-CoV neutralizing titers were below the limit of detection (1:30) in mice immunized with rU-ΔE.

Lung-specific CD4 and CD8 T cell responses were assessed at day 7 after immunization by measuring IFN-γ expression after stimulation with peptides N353 and S366, respectively. As shown in Fig. 2F, virus-specific T cell responses were barely detectable in mice inoculated with rU-ΔE. In contrast, approximately 0.4% ± 0.1% and 0.8% ± 0.1% of the CD4 and CD8 T cells, respectively, in the lungs of BALB/c mice immunized with rMA15-ΔE were virus specific.

rMA15-ΔE immunization protects 12-month-old and 18-month-old BALB/c mice after MA15 challenge. As mice age, they become progressively more susceptible to infection with SARS-CoV, so that 12- to 14-month-old BALB/c mice develop mild clinical disease and weight loss even after infection with the Urbani strain of SARS-CoV (22). We did not examine the efficacy of rU-ΔE in older mice in our previous studies. Immunization with 6,000 PFU of rMA15-ΔE caused no clinical disease in 12-month-old mice (data not shown), and histological examination of immunized lungs revealed a small amount of inflammatory cell infiltration at days 4 and 6 after inoculation (Fig. 3A to C). Almost no changes were detected in the lungs after immunization with rU-ΔE (Fig. 3D to F). The kinetics of rMA15-ΔE clearance from the lungs of 12-month-old mice was

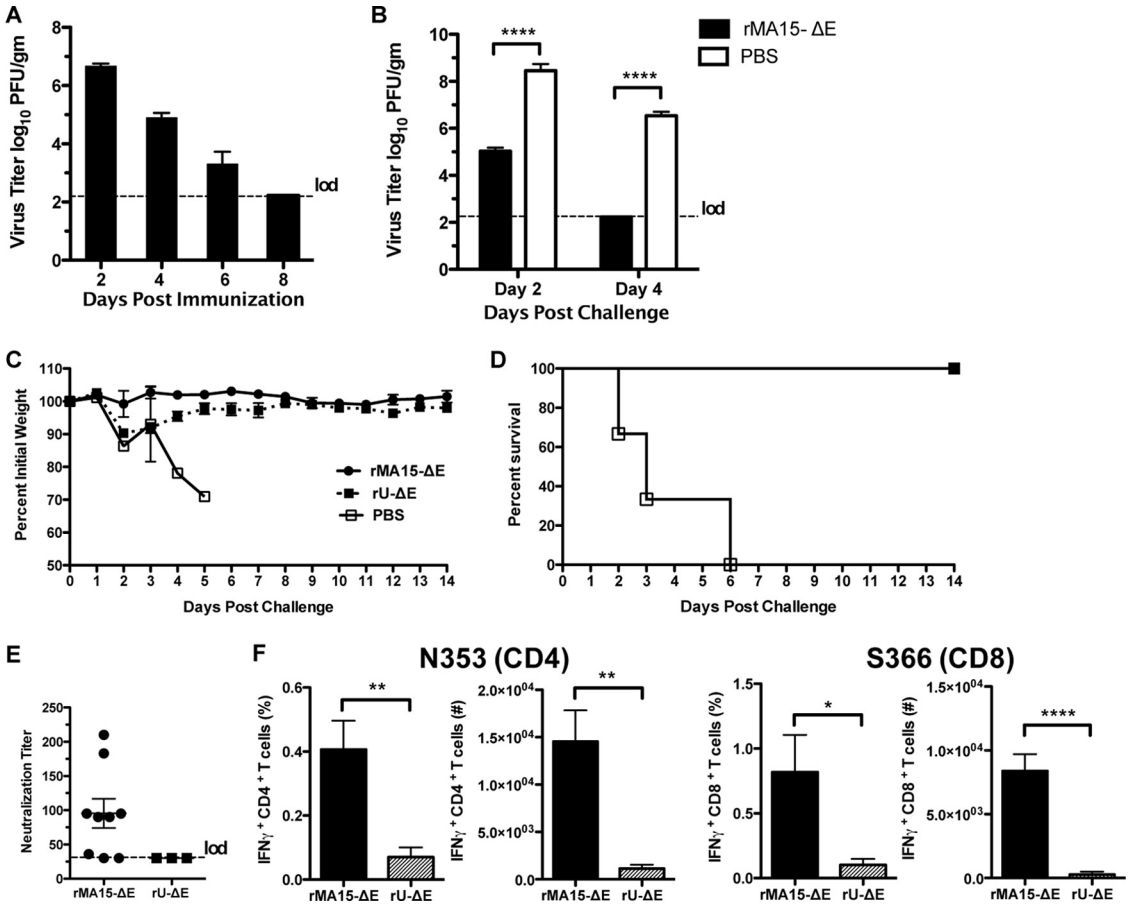

FIG 2 Immunization of 6-week-old BALB/c mice with rMA15-ΔE or rU-ΔE and challenge with MA15 at 21 days. Six-week-old mice were immunized with 6,000 PFU of rMA15-ΔE, rU-ΔE, or PBS. (A) Mice were sacrificed at days 2, 4, 6, and 8 postimmunization with rMA15-ΔE, and virus titers in the lungs were measured. (B) rMA15-ΔE-immunized mice were challenged with 10^5 PFU of MA15 at day 21 postimmunization, and lung virus titers were measured. (C and D) Mice were immunized with rMA15-ΔE, rU-ΔE, or PBS and monitored for weight loss and survival. Data are representative of 2 experiments with 4 mice/group (A) or 2 experiments with 4 to 8 mice/group (B to D). (E) Serum neutralizing antibody titers were measured at day 21 as described in Materials and Methods. (F) Virus-specific CD4 and CD8 T cell responses in the lungs of immunized mice were analyzed by intracellular IFN-γ staining at day 7 as described in Materials and Methods (see Fig. 4F for representative fluorescence-activated cell sorter [FACS] plots). Average frequencies and numbers of N353-specific CD4 and S366-specific CD8 T cells are shown. Data are representative of one of two independent experiments with 4 mice per group. *, $P < 0.05$; **, $P < 0.005$; ****, $P < 0.0001$.

delayed compared to that of rMA15-ΔE-immunized 6-week-old mice or rU-ΔE-immunized 12-month-old mice (compare Fig. 2A and 4A), with virus completely cleared by 8 days. This clearance is not due to enhanced replication of rMA15-ΔE in extrapulmonary tissues, since neither rMA15-ΔE nor rU-ΔE was detected in the liver, brain, or spleen of 12-month-old mice at day 2 postinfection (p.i.) (data not shown).

Immunization with 6,000 PFU of rMA15-ΔE, but not PBS or rU-ΔE immunization, effected rapid MA15 clearance after challenge, with virus largely cleared by day 2 (Fig. 4B). Immunization with rU-ΔE provided modest protection against lethal disease when 12-month-old mice were challenged 21 days later (Fig. 4C and D). In contrast, however, the same dose of rMA15-ΔE completely protected 12-month-old mice from challenge with 10^5 PFU of MA15. Histological examination of lungs of rU-ΔE-immunized mice or PBS-immunized mice challenged with MA15 revealed interstitial and peribronchial/perivascular inflammatory cell infiltration with edema and proteinaceous deposition in airways and alveoli (Fig. 3J to L), while the lungs of infected rMA15-ΔE-immunized mice showed minimal evidence of lung damage or cellular infiltration (Fig. 3H and I). In previous vaccine studies, inclusion of the N protein in the immunogen resulted in an eosinophilic infiltration in the lungs on subsequent challenge with SARS-CoV, suggestive of immunopathological disease (11, 13). This was especially evident in older mice. In contrast, after vaccination with rMA15-ΔE, we did not observe significant eosinophil infiltration into the lungs of 12-month-old mice after MA15 challenge.

Finally, protection correlated with higher antivirus neutralizing and ELISA antibody titers and CD4 and CD8 T cell responses in rMA15-ΔE-immunized mice than in rU-ΔE-immunized animals (Fig. 4E to H). Neutralizing antibody titers were 1:198 ± 51 in rMA15-ΔE-immunized mice, compared to low titers in two mice (1:61) or levels below the limit of detection in six rU-ΔE-immunized animals at day 21 after immunization (Fig. 4E). ELISA titers were low in all mice but significantly higher in rMA15-ΔE-immunized mice than in those immunized with rU-ΔE (Fig. 4F). Similarly, N363-specific CD4 and

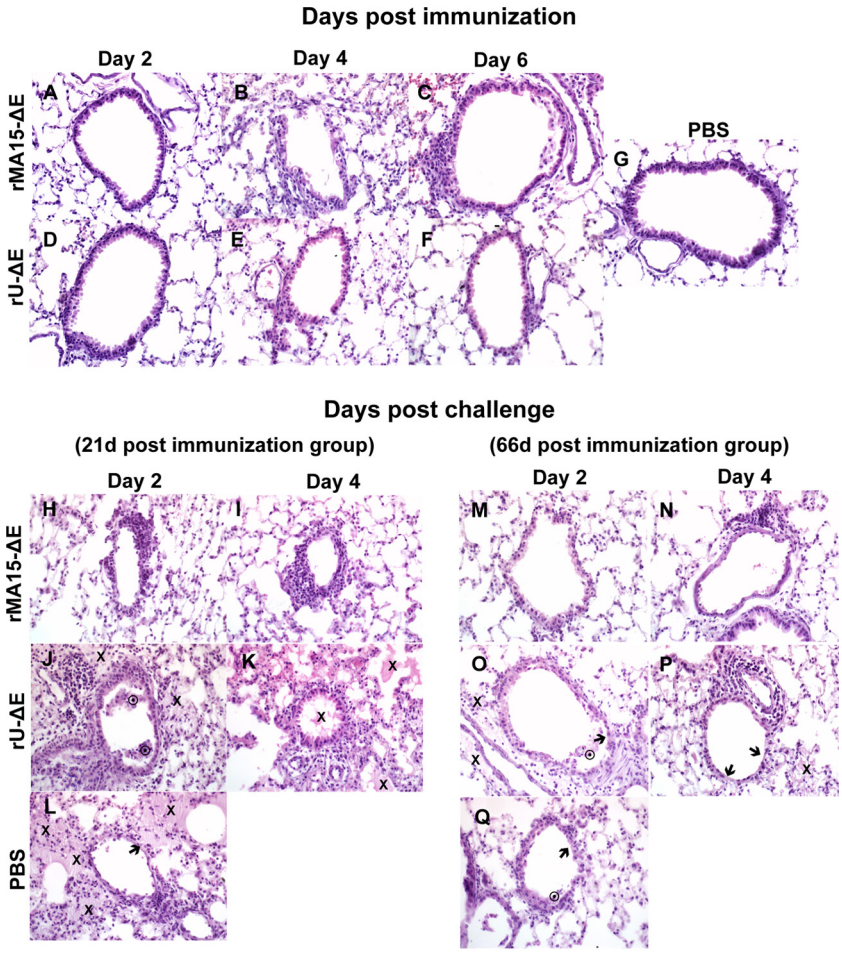

FIG 3 Histological changes observed after immunization with rMA-ΔE or rU-ΔE and challenge with MA15. Twelve-month-old BALB/c mice were immunized with 6,000 PFU of rMA15-ΔE (A to C), rU-ΔE (D to F), or PBS (G) and sacrificed at day 2, 4, or 6 postimmunization. Additional groups of mice were challenged with 10^5 PFU of MA15 at days 21 (d21) (H to L) and 66 (d66) (M to Q) after immunization. Lungs were harvested and processed for histological examination as described in Materials and Methods. Representative images are shown. X, edema; ⊙, cellular debris, ↓, denuded epithelium. Original magnification, ×40.

S366-specific CD8 T cell responses were significantly higher in rMA15-ΔE-immunized mice than in rU-immunized mice at day 7 (S366, 4.3% ± 1.1% versus 1.0% ± 0.1%, respectively; N363, 3.7% ± 0.3% versus 0.03% ± 0.03%, respectively) (Fig. 4G and H).

To determine whether immunization with rMA15-ΔE was safe and protective even in older mice, we immunized 18-month-old BALB/c mice with 6,000 PFU of rMA15-ΔE. Mice showed no signs of clinical disease and minimal weight loss after immunization (Fig. 5A). Histological examination of the lungs of rMA15-ΔE-immunized mice showed a minor amount of peribronchial and perivascular infiltration (data not shown). Next, we challenged PBS- and rMA15-ΔE-immunized 18-month-old mice with 10^5 PFU of MA15 at 21 days after immunization. Immunization with rMA15-ΔE conferred complete protection from lethal disease, with no weight loss observed, while PBS-treated mice developed rapidly fatal disease (Fig. 5B and C).

Prolonged protection against virulent challenge with MA15 after immunization with rMA15-ΔE. Vaccination must result in long-lived protection against challenge with virulent virus to be useful. To begin to address the long-term efficacy of rMA15-ΔE immunization against MA15 challenge, we immunized 6-week- and 12-month-old mice with rMA15-ΔE, rU-ΔE, or PBS and then challenged them with 10^5 MA15 at 66 days after immunization. Virus was rapidly cleared from the lungs of 6-week- and 12-month-old rMA15-ΔE-immunized mice but not from the lungs of rU-ΔE-immunized or control mice after challenge at day 66 (Fig. 6A and B). Further, all rMA15-ΔE-immunized, but not rU-ΔE- or PBS-treated, mice survived subsequent infection with MA15, had no signs of clinical illness, and exhibited virtually no weight loss (Fig. 6C to F). Anti-SARS-CoV antibody titers, whether measured in an ELISA or in a plaque reduction neutralization assay, were substantially lower in rU-ΔE-immunized mice than in rMA15-ΔE-immunized mice at day 66 after immunization in both 6-week- and 12-month-old mice (Fig. 6G to J). Notably, neutralizing antibody titers were at or below the limit of detection in both age groups after immunization with rU-ΔE, while titers measured by ELISA were present at low levels in mice immunized at 6 weeks but were not detected in those immunized at 12 months.

Histological examination of the lungs of 12-month-old mice challenged at day 66 paralleled findings observed in mice infected

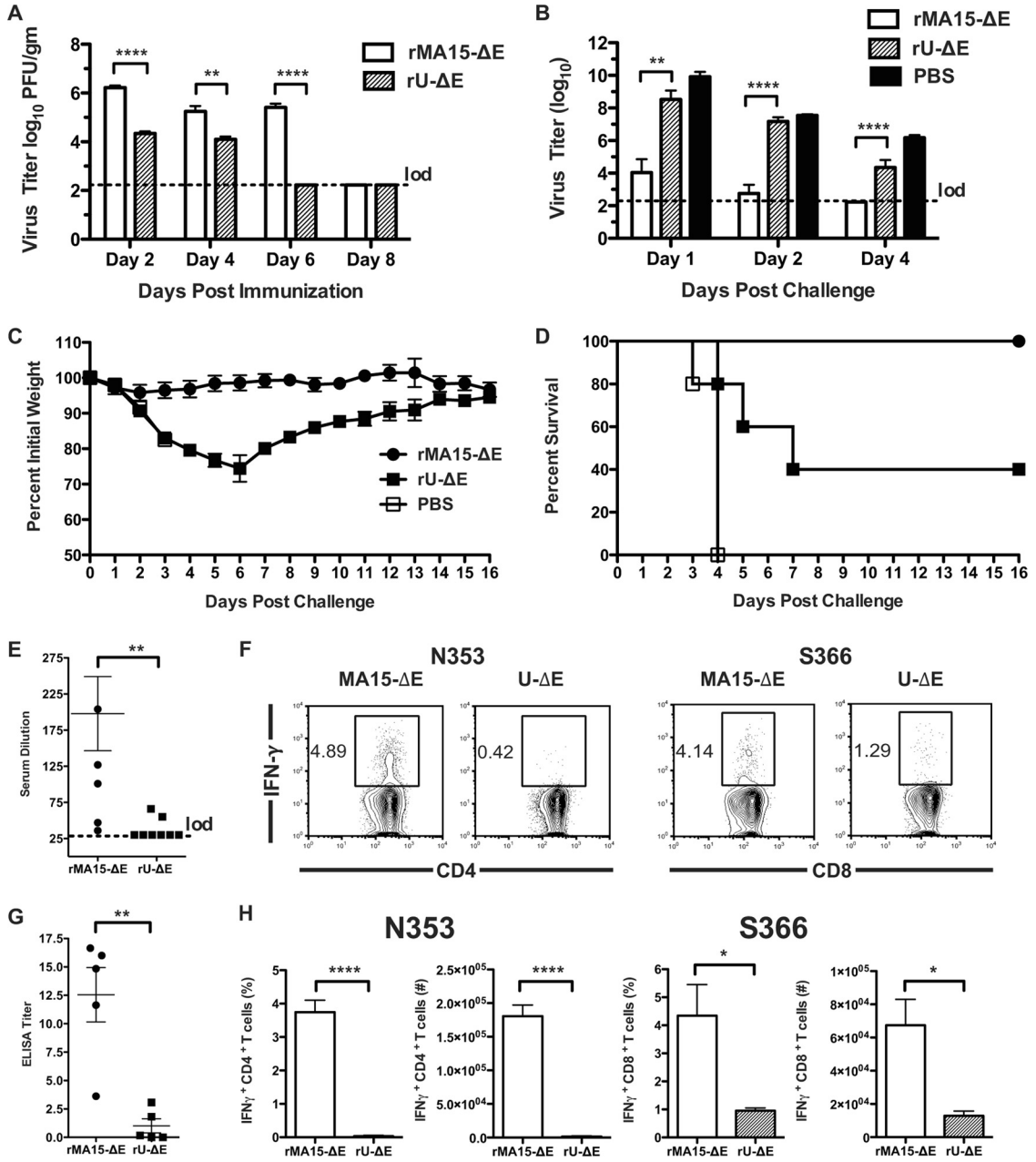

FIG 4 Immunization of 12-month-old BALB/c mice with rMA15-ΔE or rU-ΔE and challenge with MA15 at 21 days. (A to D) Twelve-month-old mice were immunized with 6,000 PFU of rMA-ΔE, rU-ΔE, or PBS. (A) Virus titers at days 2, 4, 6, and 8 postimmunization. Data are combined results from 2 experiments ($n = 4$ to 9 mice/time point/group). (B to D) Mice were challenged at 21 days postimmunization with 10^5 PFU of MA15. (B) Virus titers in the lungs were determined at days 1, 2, and 4 postchallenge ($n = 4$ to 6 mice/time point/group). (C and D) Mice were monitored for weight loss and survival. Data are representative of 1 of 2 independent experiments with 5 to 7 mice per group. (E and G) Serum neutralizing and ELISA antibody titers were measured at day 21 after immunization. (F and H) Virus-specific CD4 and CD8 T cell responses were analyzed by intracellular IFN-γ staining as described in Materials and Methods. (F) Representative flow cytometric plots of virus-specific CD4 and CD8 T cells in lungs of 12-month-old mice at day 7 after immunization. (H) Average frequency and number of N353-specific CD4 and S366-specific CD8 T cells in the lungs of 12-month-old mice. Data are representative of one of two independent experiments with 4 mice per group. *, $P < 0.05$; **, $P < 0.005$; ****, $P < 0.0001$.

21 days after immunization: we detected few changes in the lungs of rMA15-ΔE-immunized mice, with modest amounts of perivascular and peribronchial cellular infiltration and little alveolar or airway edema observed at day 2 or day 4 (Fig. 3M and N). In contrast, after challenge, PBS- and rU-ΔE-immunized mice showed airway necrosis and alveolar edema compared to rMA15-ΔE-immunized mice (Fig. 3O to Q). Few eosinophils were detected in the inflammatory infiltrate at any time point in any of the mice.

DISCUSSION

We showed that immunization of 6-week-old BALB/c mice with a recombinant version of a human strain of SARS-CoV

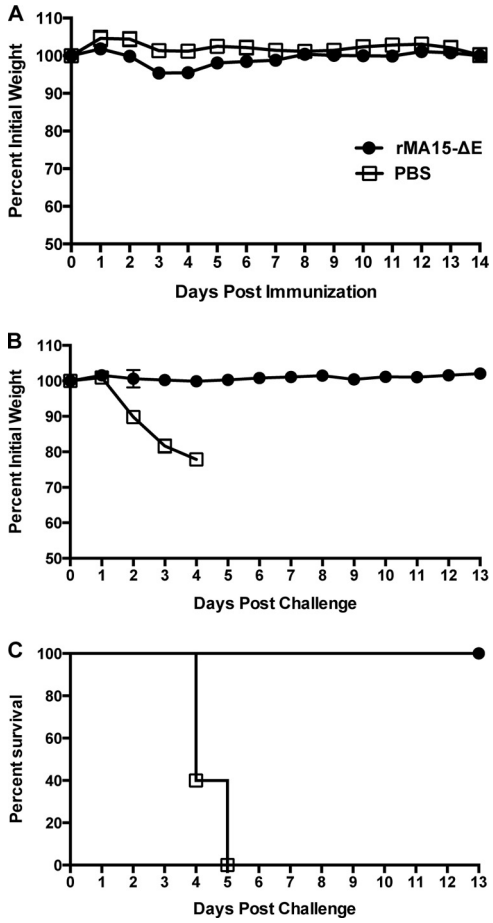

FIG 5 Immunization of 18-month-old BALB/c mice with rMA15-ΔE and challenge with MA15 at 21 days. (A) Eighteen-month-old mice were immunized with 6,000 PFU of rMA15-ΔE or PBS and monitored for weight loss. (B and C) Twenty-one days postimmunization, mice were challenged with 10^5 PFU of MA15 and monitored for weight loss and survival. Data are from 2 experiments with 5 to 6 mice per group.

lacking E protein expression provided partial protection against challenge with mouse-adapted virus (20). Here, the main objective was to investigate whether adaptation of the virus to the host species in question (mice in this case) would enhance immunogenicity. We show that this in fact occurs since mouse adaptation of the immunizing agent enhances immunogenicity and protection without compromising safety and that long-term protection was induced in 6-week- and 12-month-old mice. Our results show that mouse adaptation of the E-deleted virus augmented virus replication, resulting in detection of infectious rMA15-ΔE in the lungs of 12-month-old mice for a modestly longer time postimmunization than occurred after rU-ΔE immunization (Fig. 4A). This delay in virus clearance likely contributed to the development of a more potent antiviral immune response. This delay in virus clearance may have also contributed to the enhanced antivirus T cell response observed in 12-month-old mice compared to that in 6-week-old mice after rMA15-ΔE immunization.

Adaptation of zoonotic coronaviruses to efficient growth in human populations generally includes changes in the S glycoprotein that enhance binding to the host cell receptor as well as additional mutations that result in optimal evasion of the innate immune response. The E protein-deleted vaccines that we developed have the potential to be useful against a variety of zoonotic coronaviruses, even if these viruses mutate during adaptation, since both antivirus T cell and antibody responses are induced. T cell responses, in particular, are often induced against internal proteins, such as the nucleocapsid and transmembrane proteins (12), which are less likely to mutate without attenuating the virus. While both antivirus T cell and antibody responses have been shown to have roles in protection against SARS-CoV, more-detailed studies of immune responses in mice infected with the murine coronavirus mouse hepatitis virus (MHV) demonstrate nonoverlapping roles for both responses. In the absence of T cells or of either CD4 or CD8 T cells, virus is cleared slowly, if at all, from infected brains (29–31). On the other hand, initial virus clearance is unaffected by the absence of an antibody response, but virus recrudesces if antivirus antibodies are not produced locally in the infected brain (32).

rMA15-ΔE is very attenuated, causing no clinical disease in BALB/c mice of all ages (Fig. 1 and 5). However, even with the profound attenuation resulting from the E protein deletion, given the ability of coronaviruses to readily recombine, it will be prudent to introduce additional attenuating mutations into rMA15-ΔE to enhance safety (2, 14). In one approach to developing an attenuated vaccine, the intragenic transcription regulatory sequence (TRS) regions, critical for subgenomic RNA synthesis, were mutated to diminish the possibility that recombination with circulating coronaviruses would occur (16). This virus was also attenuated, which means that introduction of these changes into E protein-deleted virus would enhance safety. Deletion of Nsp1, a protein with functions in immune evasion and host cell RNA degradation, is also attenuating (33–35). Deletions in Nsp1 have the advantage of being located at a site distant from that of the E protein, making it less likely that recombination with circulating wild-type coronaviruses would result in the generation of a virulent virus. Mutations in another nonstructural protein, Nsp14 (a 3′ to 5′ exonuclease), result in decreased fidelity and virus attenuation *in vivo* (36). Incorporation of mutations in Nsp14 into rMA15-ΔE would minimize the risk of reversion.

We developed an E protein-deleted virus because previous work suggested that this protein was critical for optimal virus development but was not absolutely required (15, 18). The E protein is a structural protein that is present in the virion in very small amounts (37) and has an important role in virus assembly. Somewhat surprisingly, the requirement for E for the production of infectious virus is not consistent across all coronaviruses. Thus, no infectious virus is released in the absence of E from cells infected with transmissible gastroenteritis coronavirus (TGEV) (38), while virus with an abnormal morphology is released from cells infected with MHV, a betacoronavirus, like SARS-CoV (18). In the case of SARS-CoV, the virus shows normal morphology when examined by electron microscopy (15, 17). In addition to its involvement in virion morphogenesis, the E protein also has ion channel activity, although the role of this activity in the virus life cycle is not established (39–41). Recent work has shown that the E protein reduces the stress response in infected cells as well as when introduced exogenously into cells stressed chemically or by infection with a noncoronavirus (42). The E protein also interacts with several host cell proteins and modifies the expression of genes involved in signal transduction, inflammation, apoptosis, and the cell cycle, in addition to those related to stress (42). Thus, its deletion has multiple

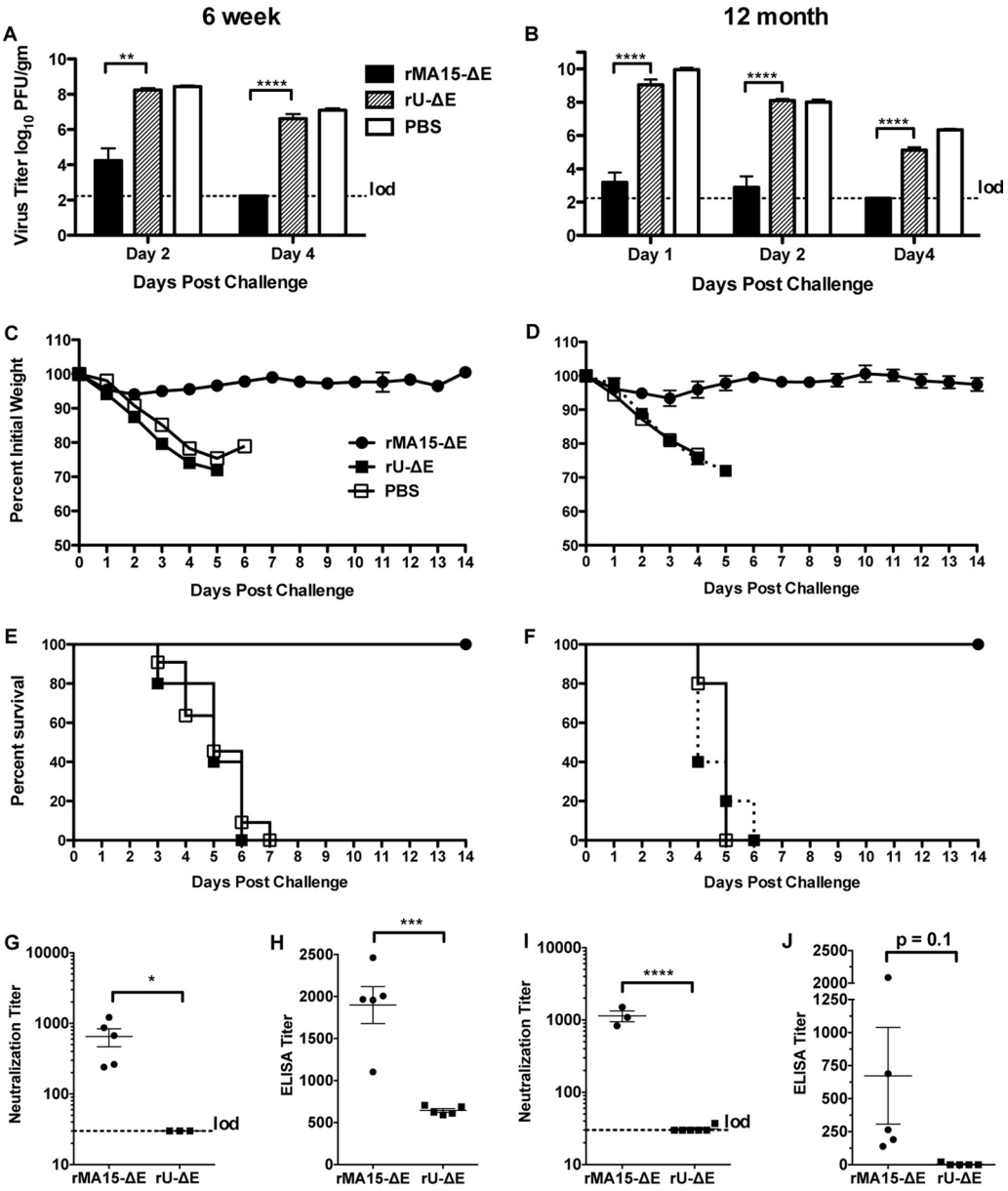

FIG 6 Immunization of 6-week- and 12-month-old BALB/c mice with rMA15-ΔE or rU-ΔE and challenge with MA15 at 66 days. Six-week-old (A, C, and E) or 12-month-old (B, D, and F) mice were immunized with 6,000 PFU of rMA15-ΔE, rU-ΔE, or PBS and challenged 66 days later with 10^5 PFU of MA15. (A to F) Mice were sacrificed for lung virus titers at the times shown postinfection ($n = 3$ to 6 mice/group/time) (A and B) or monitored for weight loss and survival ($n = 5$ mice/group) (C to F). (G to J) Neutralizing and ELISA antibody titers were measured at day 66 after immunization in 6-week-old (G and H) or 12-month-old (I and J) BALB/c mice. *, $P < 0.05$; ***, $P < 0.001$; ****, $P < 0.0001$.

effects on the infected cell, potentially attenuating the infection by a variety of mechanisms.

Currently, we are identifying domains of E protein responsible for its various roles in assembly, morphogenesis, and virulence. Our future efforts at vaccine development will be to maintain some E protein function in order to enhance immunogenicity while introducing one or more of the changes listed above in order to decrease the likelihood of recombination or reversion to wild-type virus.

ACKNOWLEDGMENTS

We thank Jincun Zhao and Rudragouda Channappanavar for critical reviews of the manuscript.

This work was supported by grants from the NIH (PO1 AI060699) and from the Ministry of Science and Innovation of Spain (BIO2010-16705) and the European Community project EMPERIE (GA223498). J.A.R.-N. was supported by a fellowship from the Fundacion La Caixa.

REFERENCES

1. **Peiris JS, Guan Y, Yuen KY.** 2004. Severe acute respiratory syndrome. Nat. Med. **10**:S88–S97.
2. **Perlman S, Netland J.** 2009. Coronaviruses post-SARS: update on replication and pathogenesis. Nat. Rev. Microbiol. **7**:439–450.
3. **Hon CC, Lam TY, Shi ZL, Drummond AJ, Yip CW, Zeng F, Lam PY, Leung FC.** 2008. Evidence of the recombinant origin of a bat severe acute respiratory syndrome (SARS)-like coronavirus and its implications on the direct ancestor of SARS coronavirus. J. Virol. **82**:1819–1826.

4. **Lau SK, Li KS, Huang Y, Shek CT, Tse H, Wang M, Choi GK, Xu H, Lam CS, Guo R, Chan KH, Zheng BJ, Woo PC, Yuen KY.** 2010. Ecoepidemiology and complete genome comparison of different strains of severe acute respiratory syndrome-related Rhinolophus bat coronavirus in China reveal bats as a reservoir for acute, self-limiting infection that allows recombination events. J. Virol. **84**:2808–2819.
5. **Lau SK, Woo PC, Li KS, Huang Y, Tsoi HW, Wong BH, Wong SS, Leung SY, Chan KH, Yuen KY.** 2005. Severe acute respiratory syndrome coronavirus-like virus in Chinese horseshoe bats. Proc. Natl. Acad. Sci. U. S. A. **102**:14040–14045.
6. **Lau SK, Woo PC, Li KS, Huang Y, Wang M, Lam CS, Xu H, Guo R, Chan KH, Zheng BJ, Yuen KY.** 2007. Complete genome sequence of bat coronavirus HKU2 from Chinese horseshoe bats revealed a much smaller spike gene with a different evolutionary lineage from the rest of the genome. Virology **367**:428–439.
7. **Zaki AM, van Boheemen S, Bestebroer TM, Osterhaus AD, Fouchier RA.** 2012. Isolation of a novel coronavirus from a man with pneumonia in Saudi Arabia. N. Engl. J. Med. **367**:1814–1820.
8. **Chen J, Subbarao K.** 2007. The immunobiology of SARS. Annu. Rev. Immunol. **25**:443–472.
9. **Enjuanes L, Dediego ML, Alvarez E, Deming D, Sheahan T, Baric R.** 2008. Vaccines to prevent severe acute respiratory syndrome coronavirus-induced disease. Virus Res. **133**:45–62.
10. **Yang ZY, Werner HC, Kong WP, Leung K, Traggiai E, Lanzavecchia A, Nabel GJ.** 2005. Evasion of antibody neutralization in emerging severe acute respiratory syndrome coronaviruses. Proc. Natl. Acad. Sci. U. S. A. **102**:797–801.
11. **Deming D, Sheahan T, Heise M, Yount B, Davis N, Sims A, Suthar M, Harkema J, Whitmore A, Pickles R, West A, Donaldson E, Curtis K, Johnston R, Baric R.** 2006. Vaccine efficacy in senescent mice challenged with recombinant SARS-CoV bearing epidemic and zoonotic spike variants. PLoS Med. **3**:e525. doi:10.1371/journal.pmed.0030525.
12. **Oh H-L, Gan S, Bertoletti A, Tan Y-J.** 2012. Understanding the T cell immune response in SARS coronavirus infection. Emerg. Microbes Infect. **1**:e23–e28.
13. **Yasui F, Kai C, Kitabatake M, Inoue S, Yoneda M, Yokochi S, Kase R, Sekiguchi S, Morita K, Hishima T, Suzuki H, Karamatsu K, Yasutomi Y, Shida H, Kidokoro M, Mizuno K, Matsushima K, Kohara M.** 2008. Prior immunization with severe acute respiratory syndrome (SARS)-associated coronavirus (SARS-CoV) nucleocapsid protein causes severe pneumonia in mice infected with SARS-CoV. J. Immunol. **181**:6337–6348.
14. **Masters PS.** 2006. The molecular biology of coronaviruses. Adv. Virus Res. **66**:193–292.
15. **DeDiego ML, Alvarez E, Almazan F, Rejas MT, Lamirande E, Roberts A, Shieh WJ, Zaki SR, Subbarao K, Enjuanes L.** 2007. A severe acute respiratory syndrome coronavirus that lacks the E gene is attenuated in vitro and in vivo. J. Virol. **81**:1701–1713.
16. **Yount B, Roberts RS, Lindesmith L, Baric RS.** 2006. Rewiring the severe acute respiratory syndrome coronavirus (SARS-CoV) transcription circuit: engineering a recombination-resistant genome. Proc. Natl. Acad. Sci. U. S. A. **103**:12546–12551.
17. **DeDiego ML, Pewe L, Alvarez E, Rejas MT, Perlman S, Enjuanes L.** 2008. Pathogenicity of severe acute respiratory coronavirus deletion mutants in hACE-2 transgenic mice. Virology **376**:379–389.
18. **Kuo L, Masters PS.** 2003. The small envelope protein E is not essential for murine coronavirus replication. J. Virol. **77**:4597–4608.
19. **Lamirande EW, DeDiego ML, Roberts A, Jackson JP, Alvarez E, Sheahan T, Shieh WJ, Zaki SR, Baric R, Enjuanes L, Subbarao K.** 2008. A live attenuated severe acute respiratory syndrome coronavirus is immunogenic and efficacious in golden Syrian hamsters. J. Virol. **82**:7721–7724.
20. **Netland J, DeDiego ML, Zhao J, Fett C, Alvarez E, Nieto-Torres JL, Enjuanes L, Perlman S.** 2010. Immunization with an attenuated severe acute respiratory syndrome coronavirus deleted in E protein protects against lethal respiratory disease. Virology **399**:120–128.
21. **McCray PB, Jr, Pewe L, Wohlford-Lenane C, Hickey M, Manzel L, Shi L, Netland J, Jia HP, Halabi C, Sigmund CD, Meyerholz DK, Kirby P, Look DC, Perlman S.** 2007. Lethal infection in K18-hACE2 mice infected with SARS-CoV. J. Virol. **81**:813–821.
22. **Roberts A, Paddock C, Vogel L, Butler E, Zaki S, Subbarao K.** 2005. Aged BALB/c mice as a model for increased severity of severe acute respiratory syndrome in elderly humans. J. Virol. **79**:5833–5838.
23. **Subbarao K, Roberts A.** 2006. Is there an ideal animal model for SARS? Trends Microbiol. **14**:299–303.
24. **Roberts A, Deming D, Paddock CD, Cheng A, Yount B, Vogel L, Herman BD, Sheahan T, Heise M, Genrich GL, Zaki SR, Baric R, Subbarao K.** 2007. A mouse-adapted SARS-coronavirus causes disease and mortality in BALB/c mice. PLoS Pathog. **3**:e5. doi:10.1371/journal.ppat.0030005.
25. **Sheahan T, Whitmore A, Long K, Ferris M, Rockx B, Funkhouser W, Donaldson E, Gralinski L, Collier M, Heise M, Davis N, Johnston R, Baric RS.** 2011. Successful vaccination strategies that protect aged mice from lethal challenge from influenza virus and heterologous severe acute respiratory syndrome coronavirus. J. Virol. **85**:217–230.
26. **Zhao J, Zhao J, Legge K, Perlman S.** 2011. Age-related increases in PGD(2) expression impair respiratory DC migration, resulting in diminished T cell responses upon respiratory virus infection in mice. J. Clin. Invest. **121**:4921–4930.
27. **Almazan F, Dediego ML, Galan C, Escors D, Alvarez E, Ortego J, Sola I, Zuniga S, Alonso S, Moreno JL, Nogales A, Capiscol C, Enjuanes L.** 2006. Construction of a severe acute respiratory syndrome coronavirus infectious cDNA clone and a replicon to study coronavirus RNA synthesis. J. Virol. **80**:10900–10906.
28. **Zhao J, Zhao J, Van Rooijen N, Perlman S.** 2009. Evasion by stealth: inefficient immune activation underlies poor T cell response and severe disease in SARS-CoV-infected mice. PLoS Pathog. **5**:e1000636. doi:10.1371/journal.ppat.1000636.
29. **Wu GF, Dandekar AA, Pewe L, Perlman S.** 2000. CD4 and CD8 T cells have redundant but not identical roles in virus-induced demyelination. J. Immunol. **165**:2278–2286.
30. **Houtman JJ, Fleming JO.** 1996. Dissociation of demyelination and viral clearance in congenitally immunodeficient mice infected with murine coronavirus JHM. J. Neurovirol. **2**:101–110.
31. **Williamson JS, Stohlman SA.** 1990. Effective clearance of mouse hepatitis virus from the central nervous system requires both $CD4^+$ and $CD8^+$ T cells. J. Virol. **64**:4589–4592.
32. **Ramakrishna C, Stohlman SA, Atkinson RD, Shlomchik MJ, Bergmann CC.** 2002. Mechanisms of central nervous system viral persistence: the critical role of antibody and B cells. J. Immunol. **168**:1204–1211.
33. **Kamitani W, Narayanan K, Huang C, Lokugamage K, Ikegami T, Ito N, Kubo H, Makino S.** 2006. Severe acute respiratory syndrome coronavirus nsp1 protein suppresses host gene expression by promoting host mRNA degradation. Proc. Natl. Acad. Sci. U. S. A. **103**:12885–12890.
34. **Narayanan K, Huang C, Lokugamage K, Kamitani W, Ikegami T, Tseng CT, Makino S.** 2008. Severe acute respiratory syndrome coronavirus nsp1 suppresses host gene expression, including that of type I interferon, in infected cells. J. Virol. **82**:4471–4479.
35. **Zust R, Cervantes-Barragan L, Kuri T, Blakqori G, Weber F, Ludewig B, Thiel V.** 2007. Coronavirus non-structural protein 1 is a major pathogenicity factor: implications for the rational design of coronavirus vaccines. PLoS Pathog. **3**:e109. doi:10.1371/journal.ppat.0030109.
36. **Graham RL, Becker MM, Eckerle LD, Bolles M, Denison MR, Baric RS.** 2012. A live, impaired-fidelity coronavirus vaccine protects in an aged, immunocompromised mouse model of lethal disease. Nat. Med. **18**:1820–1826.
37. **Yu X, Bi W, Weiss SR, Leibowitz JL.** 1994. Mouse hepatitis virus gene 5b protein is a new virion envelope protein. Virology **202**:1018–1023.
38. **Ortego J, Ceriani JE, Patino C, Plana J, Enjuanes L.** 2007. Absence of E protein arrests transmissible gastroenteritis coronavirus maturation in the secretory pathway. Virology **368**:296–308.
39. **Nieto-Torres JL, Dediego ML, Alvarez E, Jimenez-Guardeno JM, Regla-Nava JA, Llorente M, Kremer L, Shuo S, Enjuanes L.** 2011. Subcellular location and topology of severe acute respiratory syndrome coronavirus envelope protein. Virology **415**:69–82.
40. **Pervushin K, Tan E, Parthasarathy K, Lin X, Jiang FL, Yu D, Vararattanavech A, Soong TW, Liu DX, Torres J.** 2009. Structure and inhibition of the SARS coronavirus envelope protein ion channel. PLoS Pathog. **5**:e1000511. doi:10.1371/journal.ppat.1000511.
41. **Verdia-Baguena C, Nieto-Torres JL, Alcaraz A, DeDiego ML, Torres J, Aguilella VM, Enjuanes L.** 2012. Coronavirus E protein forms ion channels with functionally and structurally-involved membrane lipids. Virology **432**:485–494.
42. **DeDiego ML, Nieto-Torres JL, Jimenez-Guardeno JM, Regla-Nava JA, Alvarez E, Oliveros JC, Zhao J, Fett C, Perlman S, Enjuanes L.** 2011. Severe acute respiratory syndrome coronavirus envelope protein regulates cell stress response and apoptosis. PLoS Pathog. **7**:e1002315. doi:10.1371/journal.ppat.1002315.

OPEN ACCESS Freely available online

PLOS | PATHOGENS

The PDZ-Binding Motif of Severe Acute Respiratory Syndrome Coronavirus Envelope Protein Is a Determinant of Viral Pathogenesis

Jose M. Jimenez-Guardeño, Jose L. Nieto-Torres, Marta L. DeDiego¤, Jose A. Regla-Nava, Raul Fernandez-Delgado, Carlos Castaño-Rodriguez, Luis Enjuanes*

Department of Molecular and Cell Biology, Centro Nacional de Biotecnología (CNB-CSIC), Darwin 3, Campus Universidad Autónoma de Madrid, Madrid, Spain

Abstract

A recombinant severe acute respiratory syndrome coronavirus (SARS-CoV) lacking the envelope (E) protein is attenuated *in vivo*. Here we report that E protein PDZ-binding motif (PBM), a domain involved in protein-protein interactions, is a major determinant of virulence. Elimination of SARS-CoV E protein PBM by using reverse genetics caused a reduction in the deleterious exacerbation of the immune response triggered during infection with the parental virus and virus attenuation. Cellular protein syntenin was identified to bind the E protein PBM during SARS-CoV infection by using three complementary strategies, yeast two-hybrid, reciprocal coimmunoprecipitation and confocal microscopy assays. Syntenin redistributed from the nucleus to the cell cytoplasm during infection with viruses containing the E protein PBM, activating p38 MAPK and leading to the overexpression of inflammatory cytokines. Silencing of syntenin using siRNAs led to a decrease in p38 MAPK activation in SARS-CoV infected cells, further reinforcing their functional relationship. Active p38 MAPK was reduced in lungs of mice infected with SARS-CoVs lacking E protein PBM as compared with the parental virus, leading to a decreased expression of inflammatory cytokines and to virus attenuation. Interestingly, administration of a p38 MAPK inhibitor led to an increase in mice survival after infection with SARS-CoV, confirming the relevance of this pathway in SARS-CoV virulence. Therefore, the E protein PBM is a virulence domain that activates immunopathology most likely by using syntenin as a mediator of p38 MAPK induced inflammation.

Citation: Jimenez-Guardeño JM, Nieto-Torres JL, DeDiego ML, Regla-Nava JA, Fernandez-Delgado R, et al. (2014) The PDZ-Binding Motif of Severe Acute Respiratory Syndrome Coronavirus Envelope Protein Is a Determinant of Viral Pathogenesis. PLoS Pathog 10(8): e1004320. doi:10.1371/journal.ppat.1004320

Editor: Christopher F. Basler, Mount Sinai School of Medicine, United States of America

Received December 10, 2013; **Accepted** July 8, 2014; **Published** August 14, 2014

Funding: This work was supported by grants from the government of Spain (BIO2010-16705), the European Community's Seventh Framework Programme (FP7/2007-2013) under the project "EMPERIE" EC Gran Agreement number 223498, and U.S. National Institutes of Health (NIH) (2P01AI060699, 0258-3413/HHSN266200700010C). JMJG received a JAE fellowship from the CSIC-JAE Program co-funded by the European Social Fund. JARN and CCR received a contract from Fundación La Caixa. The funders had no role in study design, data collection and analysis, decision to publish, or preparation of the manuscript.

Competing Interests: The authors have declared that no competing interests exist.

* Email: L.Enjuanes@cnb.csic.es

¤ Current address: David H. Smith Center for Vaccine Biology and Immunology, University of Rochester Medical Center, Rochester, New York, United States of America

Introduction

Severe acute respiratory syndrome coronavirus (SARS-CoV) was identified as the etiological agent of a respiratory disease that emerged in Southeast China at the end of 2002. SARS-CoV spread to more than 30 countries within six months, infecting 8000 people with an average mortality of 10% [1]. After July 2003, only a few community and laboratory-acquired cases have been reported (http://www.who.int/csr/sars/en/). Nevertheless, coronaviruses, including those similar to the strain that caused the epidemic, are widely disseminated in bats circulating all over the world, making a future outbreak possible [2–5]. In September 2012, a novel coronavirus, named Middle East respiratory syndrome coronavirus (MERS-CoV) was identified in two persons with severe respiratory disease [6,7]. By now, 701 laboratory-confirmed MERS-CoV cases, including 249 deaths, have been diagnosed in several countries (http://www.who.int/csr/don/2014_06_16_mers/en/). Most patients reported respiratory disease symptoms, occasionally accompanied by acute renal failure [8]. A better understanding of the molecular mechanisms underlying the virulence of these highly pathogenic coronaviruses will facilitate the development of therapies to alleviate or prevent the impact of coronavirus infection on human health.

SARS-CoV belongs to the *Coronavirinae* subfamily, genus β and is an enveloped virus with a single-stranded positive sense 29.7 kb RNA genome [9]. SARS-CoV envelope (E) protein is a small integral membrane protein of 76 amino acids that contains a short hydrophilic amino-terminus followed by a hydrophobic region, and a hydrophilic carboxy-terminus [10]. The hydrophobic region forms at least one amphipathic α-helix that oligomerizes to form an ion-conductive pore in membranes [11–13]. E protein is present within virions in very small amounts, however it is abundant in the infected cells [14], and it is mainly localized in the endoplasmic reticulum Golgi intermediate compartment (ERGIC), where it actively participates in virus budding, morphogenesis and trafficking [15–17]. Interestingly, SARS-CoV lacking the E protein was attenuated in different animal models, such as hamsters, transgenic mice that expressed the SARS-CoV receptor, human angiotensin converting enzyme 2 (hACE-2), and conventional mice using a mouse adapted SARS-CoV [18–21], indicating

Author Summary

SARS-CoV caused a worldwide epidemic infecting 8000 people with a mortality of about 10%. A recombinant SARS-CoV lacking the E protein was attenuated *in vivo*. The E protein contains a PDZ-binding motif (PBM), a domain potentially involved in the interaction with more than 400 cellular proteins, which highlights its relevance in modulating host-cell behavior. To analyze the contributions of this motif to virulence, recombinant viruses with or without E protein PBM were generated. Recombinant SARS-CoVs lacking E protein PBM caused minimal lung damage and were attenuated, in contrast to viruses containing this motif, indicating that E protein PBM is a virulence determinant. E protein PBM induces the deleterious exacerbated immune response triggered during SARS-CoV infection, and interacts with the cellular protein syntenin, as demonstrated using proteomic analyses. Interestingly, syntenin redistributed from nucleus to cytoplasm during SARS-CoV infection, activating p38 MAPK and triggering the overexpression of inflammatory cytokines. Furthermore, silencing of syntenin using siRNAs led to a decrease in p38 MAPK activation. In addition, administration of a p38 MAPK inhibitor led to an increase in mice survival after SARS-CoV infection. These results indicate that syntenin and p38 MAPK are potential therapeutic targets to reduce the exacerbated immune response during SARS-CoV infection.

that SARS-CoV E gene may be a virulence factor. We have previously shown that SARS-CoV E protein increased the apoptosis and reduced the stress response induced after SARS-CoV infection [22].

Transient expression of SARS-CoV E protein in trans showed that the protein associated with *Caenorhabditis elegans* lin-7 protein 1 (PALS1), a tight junction-associated protein, is an E protein interacting partner [23]. PALS1 bound E protein through the post-synaptic density protein-95/discs Large/zonula occludens-1 (PDZ) domain of PALS1 [23], which recognized the last four carboxy-terminal amino acids of E protein that form a type II PDZ-binding motif (PBM) with the consensus sequence X-φ-X-φ_{COOH} (where X represents any amino acid and φ is a hydrophobic residue, usually V, I or L) [24]. However, the relevance of this interaction during virus infection and its impact on virulence *in vivo* was not tested.

PDZ domains are protein–protein recognition sequences, consisting of 80–90 amino acids that bind to a specific peptide sequence (PBM), usually located at the end of the carboxy-terminus of a target protein [25–27]. Proteins containing PDZ domains are typically found in the cell cytoplasm or in association with the plasma membrane and play a role in a variety of cellular processes of significance to viruses, such as cell-cell junctions, cellular polarity, and signal transduction pathways [28]. PDZ domains are found in thousands of proteins and are widespread in eukaryotes and eubacteria [29]. Just in the human genome, there are more than 900 PDZ domains in at least 400 different proteins [30]. These protein-protein interactions modulate cellular pathways influencing viral replication, dissemination in the host or pathogenesis [28].

As previously described, SARS-CoV E protein contains a PBM [23]. However, the relevance of this motif in the context of infection and its role in virus pathogenesis has not been elucidated. In this study, we have identified the SARS-CoV E protein PBM as a virulence determinant *in vivo*. Infection with recombinant viruses lacking an E protein PBM were attenuated in mice, which was accompanied by a decreased expression of inflammatory cytokines during infection, and a substantial increase of survival. In contrast, all mice infected with viruses containing E protein PBM died. We further found that the E protein PBM interacted with the cellular protein syntenin during SARS-CoV infection, affecting p38 mitogen-activated protein kinase (MAPK) activation, a protein involved in the expression of inflammatory cytokines, responsible of the pathogenicity associated to SARS-CoV infection. In addition, mice treated with a p38 MAPK inhibitor showed a significant increase in survival after infection with SARS-CoV. Together, our findings provide novel insights into how highly pathogenic viruses, such as SARS-CoV, induce virulence, suggesting potential therapeutic targets to improve the prognosis in patients.

Results

Generation of recombinant SARS-CoVs lacking E protein PBM

To evaluate the role of SARS-CoV E protein PBM in virus pathogenesis, a set of recombinant SARS-CoVs with E protein PBM mutated or truncated (SARS-CoV-E-PBMs) were generated using an infectious cDNA encoding a mouse adapted (MA15) SARS-CoV [31,32]. Infection of BALB/c mice with SARS-CoV-MA15 causes morbidity, mortality and pulmonary pathology, similar to the symptoms observed in human SARS [31]. In SARS-CoV-E-ΔPBM, abbreviated as ΔPBM, the last 9 amino acids of E protein were deleted, truncating the carboxy-terminus, and eliminating the PBM (Figure 1A). In contrast, the PBM was abolished in SARS-CoV-E-mutPBM (mutPBM) by mutating the last 4 amino acids to glycine, maintaining the full-length SARS-CoV E protein. In the last recombinant, termed SARS-CoV-E-potPBM (potPBM), four amino acids within E protein were replaced by alanine, modifying the E protein carboxy-terminal sequence while maintain the consensus PBM residues (Figure 1A).

To test whether mutation or deletion of SARS-CoV E protein PBM alters virus fitness *in vitro*, growth kinetics of SARS-CoV-E-PBM mutants were analyzed in comparison to the parental virus (wt) and the virus lacking the full-length E protein SARS-CoV-ΔE (ΔE) in monkey Vero E6 and mouse DBT-mACE2 cells [33] (Figure 1B). Despite the observed replication defects of the ΔPBM and mutPBM viruses at 24 hpi in DBT-mACE2 cells, the parental virus including native E protein or mutants lacking a PBM reached similar titers at 72 hpi, both in Vero E6 cells and in DBT-mACE2 cells (Figure 1B). In contrast, the titer of ΔE virus was reduced around 50-fold (Figure 1B). This result indicated that SARS-CoV E protein PBM was not essential for efficient virus growth in Vero E6 cells and, at late times post infection, in DBT-mACE2 cells.

Pathogenicity of SARS-CoV E protein PBM mutants in BALB/c mice

To analyze the pathogenicity of SARS-CoV-E-PBM mutants, 16 week-old female BALB/c mice were intranasally inoculated with recombinant viruses. Body weight (Figure 2A) and mortality (Figure 2B) of each mouse were monitored daily.

Mock-infected mice and those infected with a virus lacking E protein, did not lose weight and all survived. In contrast, mice infected with recombinant viruses including an E protein PBM, either the original PBM (wt) or a potential PBM (potPBM), underwent severe weight loss (Figure 2A) and developed signs of illness, including shaking, ruffling of the fur, and loss of mobility, resulting in 100% mortality by 9 days post infection (dpi) (Figure 2B). Interestingly, mice infected with the viruses in which E protein PBM was abolished (mutPBM) or deleted (ΔPBM),

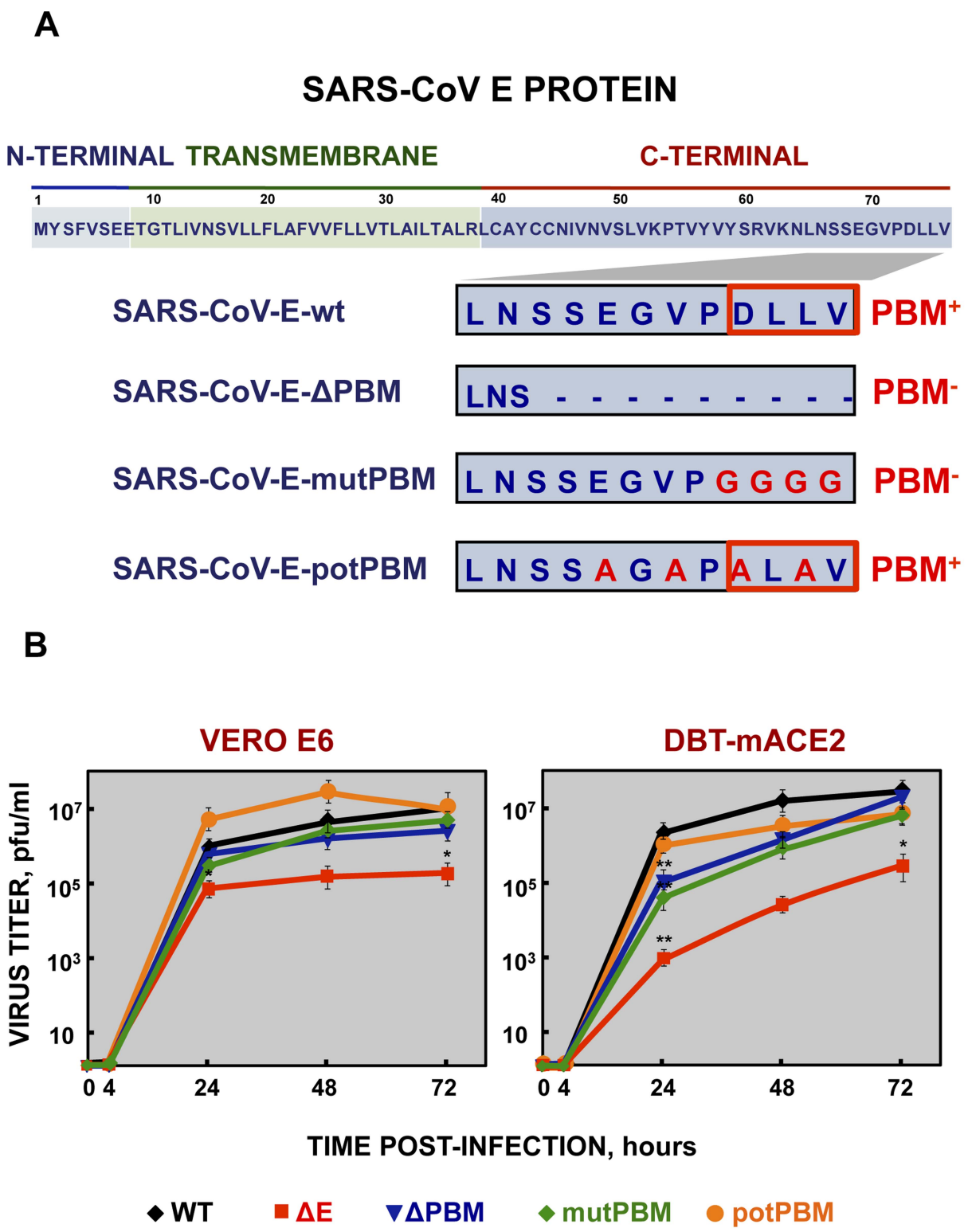

Figure 1. Generation of recombinant SARS-CoVs with E protein PBM truncated or mutated by reverse genetics and growth kinetics in cell culture. (A) Top, representation of SARS-CoV E protein sequence and its corresponding domains. Below, sequences corresponding to the end of E protein are shown in boxes for the different viruses. SARS-CoV-E-wt represents the wild type sequence. In SARS-CoV-E-ΔPBM and SARS-CoV-E-mutPBM, E protein PBM was eliminated by deletion or point mutations, reducing or maintaining the full-length protein, respectively. In SARS-CoV-E-potPBM, four amino acids of E protein were replaced to alanine, to generate a non-native new potential PBM. PBM^+ and PBM^- represent the presence or absence of a PBM within E protein sequence, respectively. Red boxes highlight PBMs within E protein. (B) Subconfluent monolayers of Vero E6 and DBT-mACE2 cells were infected with wt, ΔE, ΔPBM, mutPBM and potPBM viruses at an MOI of 0.05. Culture supernatants collected at 4, 24, 48 and 72 hpi were titrated by plaque assay. Error bars represent standard deviations of the mean of results from three experiments. Statistically significant data are indicated with one ($P<0.05$) or two ($P<0.01$) asterisks.
doi:10.1371/journal.ppat.1004320.g001

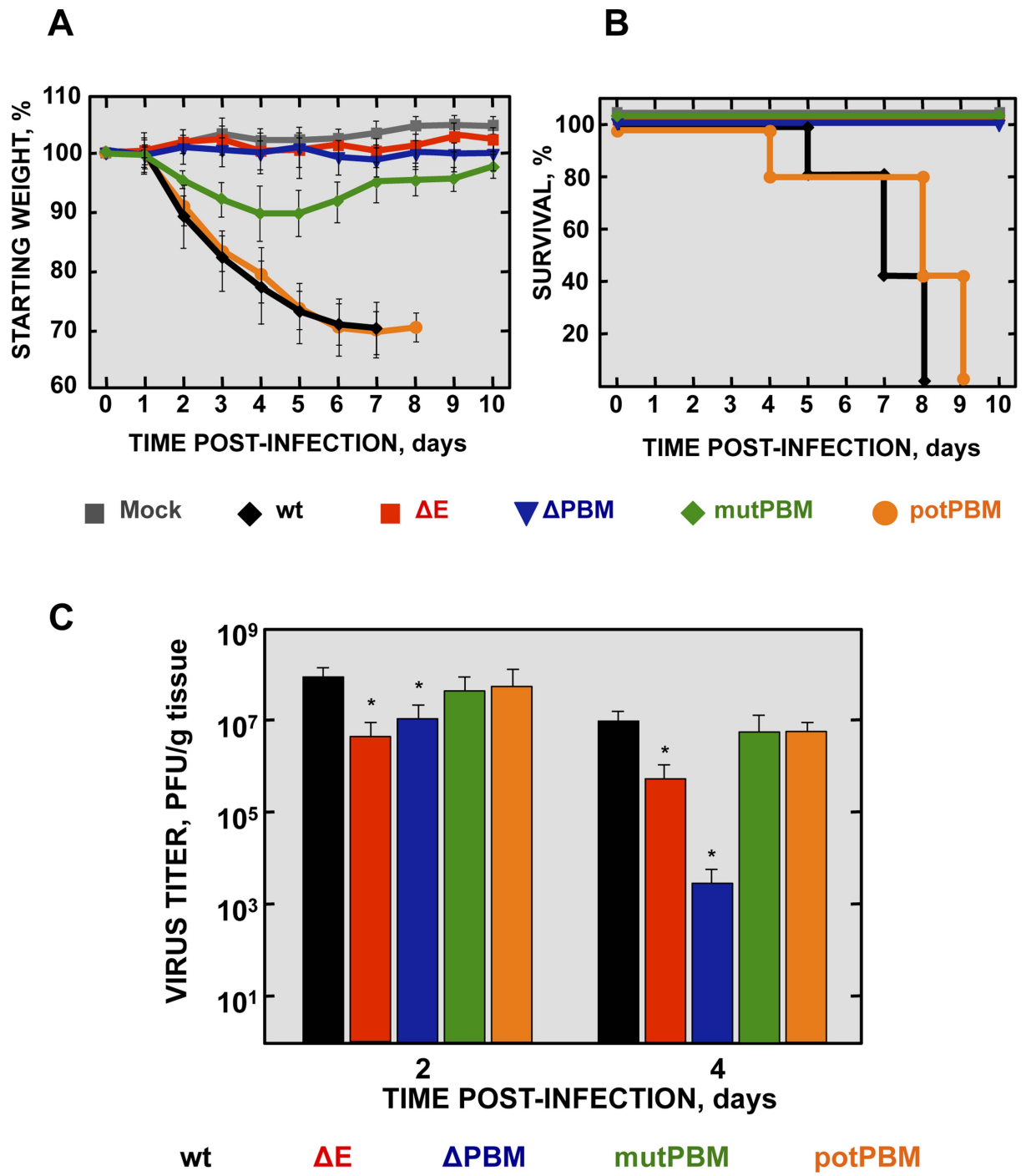

Figure 2. Virulence and viral growth of SARS-CoV-E-PBM-infected mice. 16-week-old BALB/c mice were intranasally inoculated with 100,000 pfu of wt, ΔE, ΔPBM, mutPBM and potPBM viruses. Weight loss (A) and survival (B) were monitored for 10 days. Data represent two independent experiments with 5 mice per group. Differences in weight loss between attenuated and virulent viruses were statistically significant ($P<0.01$). (C) Viral titer in lungs was determined at 2 and 4 days post infection (n = 3, each day). Error bars represent standard deviations. Statistically significant data are indicated with one ($P<0.05$) asterisk.
doi:10.1371/journal.ppat.1004320.g002

showed moderate or no weight losses, respectively, and 100% survival in both cases (Figure 2B). The fact that ΔPBM is more attenuated that mutPBM suggests the presence of sequences, outside PBM, further contributing to virus pathogenesis. These results indicated that elimination of E protein PBM led to virus attenuation *in vivo* and that the presence of a functional PBM conferred virulence, as mutant potPBM in which 4 amino acids in the carboxy-terminal domain were mutated to alanine, conserving consensus residues in the PBM was still virulent.

To evaluate the effect of the E protein PBM in virus growth *in vivo*, BALB/c mice were intranasally inoculated with recombinant viruses, and viral titers in the lung were determined at 2 and 4 dpi

(Figure 2C). Viruses ΔE and ΔPBM showed decreased titers in lungs at both 2 and 4 dpi, as compared with the wt or potPBM viruses. Mutant ΔE replicated at a higher level than ΔPBM at 4 dpi in lungs of infected mice, suggesting that the ΔPBM E protein may induce an antiviral state after infection. Interestingly, the virus lacking a functional E protein PBM but conserving a full-length E protein (mutPBM) grew to similar levels as the wt virus at 2 and 4 dpi, indicating that a virus lacking a canonical PBM in E protein, but conserving E protein full-length displayed an attenuated phenotype, although it efficiently replicated *in vivo*.

Lung pathology in mice infected with SARS-CoV E protein PBM mutants

To analyze the mechanisms by which E protein PBM confers virulence *in vivo*, lung pathology was examined in infected BALB/c mice at 2 and 4 dpi. At these time points, no obvious gross lesions or changes in weight were observed in the lungs of non-infected mice or in those from mice infected with viruses lacking functional E protein PBM (ΔE, ΔPBM and mutPBM). In contrast, at 2 and especially at 4 dpi, lungs of mice infected with SARS-CoVs with an E protein containing a functional PBM (wt and potPBM) were highly edematous, with profuse hemorrhagic areas, leading to significant lung weight increase at 4 dpi, probably due to leukocyte infiltration (Figures 3A and 3B).

To further characterize the pathology induced in BALB/c mice by the infection with SARS-CoVs with and without E protein PBM, lung sections were collected at 2 and 4 dpi, stained with hematoxylin and eosin (Figure 3C) and pulmonary histopathology scores for edema and cellular infiltrates were quantified according to previously described procedures [34] (Figures 3D and 3E). Histological examination of lungs from mock or SARS-CoV-ΔE-infected mice showed minimal evidence of damage or cellular infiltration at 2 and 4 dpi (Figure 3C, 3D and 3E). In contrast, mice infected with recombinant viruses containing functional E protein PBM (wt and potPBM) revealed interstitial and peribronchial cell infiltration and edema in both alveolar and bronchiolar airways at 2 and, mainly, at 4 dpi (Figure 3C, 3D and 3E). Interestingly, mice infected with viruses containing E protein but lacking functional PBM sequences (ΔPBM and mutPBM), showed minimal epithelial damage or lung edema and only small amounts of inflammatory cell infiltrates at 4 dpi (Figure 3C, 3D and 3E). These data indicated that the attenuation observed for viruses lacking E protein PBM correlated with decreased lung pathology.

Effect of SARS-CoV E protein PBM on host gene expression

The effect of the presence of a PBM in SARS-CoV E protein on host gene expression during BALB/c mice infection was analyzed using microarrays at 2 dpi. MIAME-compliant results of the microarrays have been deposited in the Gene Expression Omnibus database (GEO [National Center for Biotechnology Information], accession code GSE52920). A total of 922 and 640 cellular genes were differentially expressed in lung of mice infected with SARS-CoV with (wt) or without functional E protein PBM (mutPBM) as compared with mock-infected mice (Figure 4A). Remarkably, 319 genes were differentially expressed in mice infected with mutPBM compared to wt, despite a difference at only 4 amino acid positions between the two viruses. Of these, 218 genes were found to be upregulated and 101 genes were downregulated (Figure 4A). Interestingly, analysis using DAVID software [35] revealed that most of the downregulated genes in mutPBM versus wt infections clustered within wound response and inflammatory and defense response pathways (Figure 4B). The most significant genes present in at least one of these groups were serum amyloid A2 (*SAA2*), chemokine (C-C motif) ligand 3 (*CCL3*), chemokine (C-X-C motif) ligand 1 (*CXCL1*), chemokine (C-X-C motif) ligand 5 (*CXCL5*), calcitonin (*CALCA*), serum amyloid A1 (*SAA1*), chemokine (C-X-C motif) ligand 10 (*CXCL10*), chemokine (C-C motif) ligand 2 (*CCL2*), interleukin 1 beta (*IL1B*), orosomucoid 1 (*ORM1*), interleukin 6 (*IL6*), chemokine (C-C motif) ligand 4 (*CCL4*) and chemokine (C-X-C motif) ligand 9 (*CXCL9*) (Figure 4C). The differential expression of a group of cellular genes identified in the microarray (*CXCL10*, *CCL2* and *IL6*) was confirmed by RT-qPCR analysis using RNA from the lungs of mice infected with all the recombinant viruses generated, collected at 2 dpi, in relation to RNAs from mock-infected mice. *18S* ribosomal RNA (rRNA) was used to normalize the data [36,37] (Figure 4D). Using both microarray and RT-qPCR, we identified genes differentially expressed in the lungs of mice infected with viruses with or without E protein PBM (Figures 4C and 4D). Viruses lacking E protein PBM induced a decreased expression of inflammatory cytokines. These data indicated that the exacerbated host innate immune response triggered during SARS-CoV infection was reduced in the absence of SARS-CoV E protein PBM, which may explain the attenuated phenotype of these viruses.

Identification of cellular factors interacting with SARS-CoV E protein

SARS-CoVs defective in E protein PBM presented an attenuated phenotype that correlated with a decreased inflammatory response. The absence of this motif may likely imply changes in interaction patterns with cellular proteins that may explain their reduced virulence. To identify these cellular factors, a yeast two-hybrid screen was performed using the carboxy-terminal domain of SARS-CoV E protein, where amino acids 36–76 of E protein carboxy-terminus (E_{CT}) were used as bait (Figure 5A). A random-primed cDNA library from human lung was screened. One of the most prominent results of the screening was the interaction between E_{CT} and the syndecan binding protein (syntenin) (Figure 5B), with a total of 13 positive clones corresponding to this protein (GenBank accession number NM_005625.3). The interaction was classified with a high confidence score (predicted biological score of B) [38]. Syntenin is a 32 kDa protein composed of a 113 amino acid N-terminal domain (NTD) with no obvious structural motifs, followed by two adjacent tandem PDZ domains (PDZ1 and PDZ2), that could mediate its interaction with E protein and a short 24 amino acid C-terminal domain (CTD) [39] (Figure 5B). Interestingly, all 13 recovered syntenin cDNAs interacting with the E protein carboxy-terminus identified in the yeast two-hybrid platform contained the same two PDZ domains present in the cellular syntenin.

To determine whether the cellular protein syntenin is also associated with SARS-CoV E protein in infected cells, and whether this interaction was mediated through the E protein PBM, Vero E6 cells were transfected with a plasmid encoding an N-terminal HA-tagged syntenin and then infected with recombinant viruses with or without E protein PBM. Non-transfected cells infected with wt virus were used as control. Syntenin or E protein were immunoprecipitated using extracts of infected cells using an HA specific monoclonal antibody or an E protein polyclonal antibody, respectively. Inmunoblot analysis using E and HA specific antibodies revealed that E protein coprecipitated with syntenin in cells infected with recombinant viruses containing the wt or potential E protein PBM (Figure 5C). In contrast, E protein did not coprecipitate with syntenin in cells infected with viruses lacking the E protein or its PBM (Figure 5C). These results

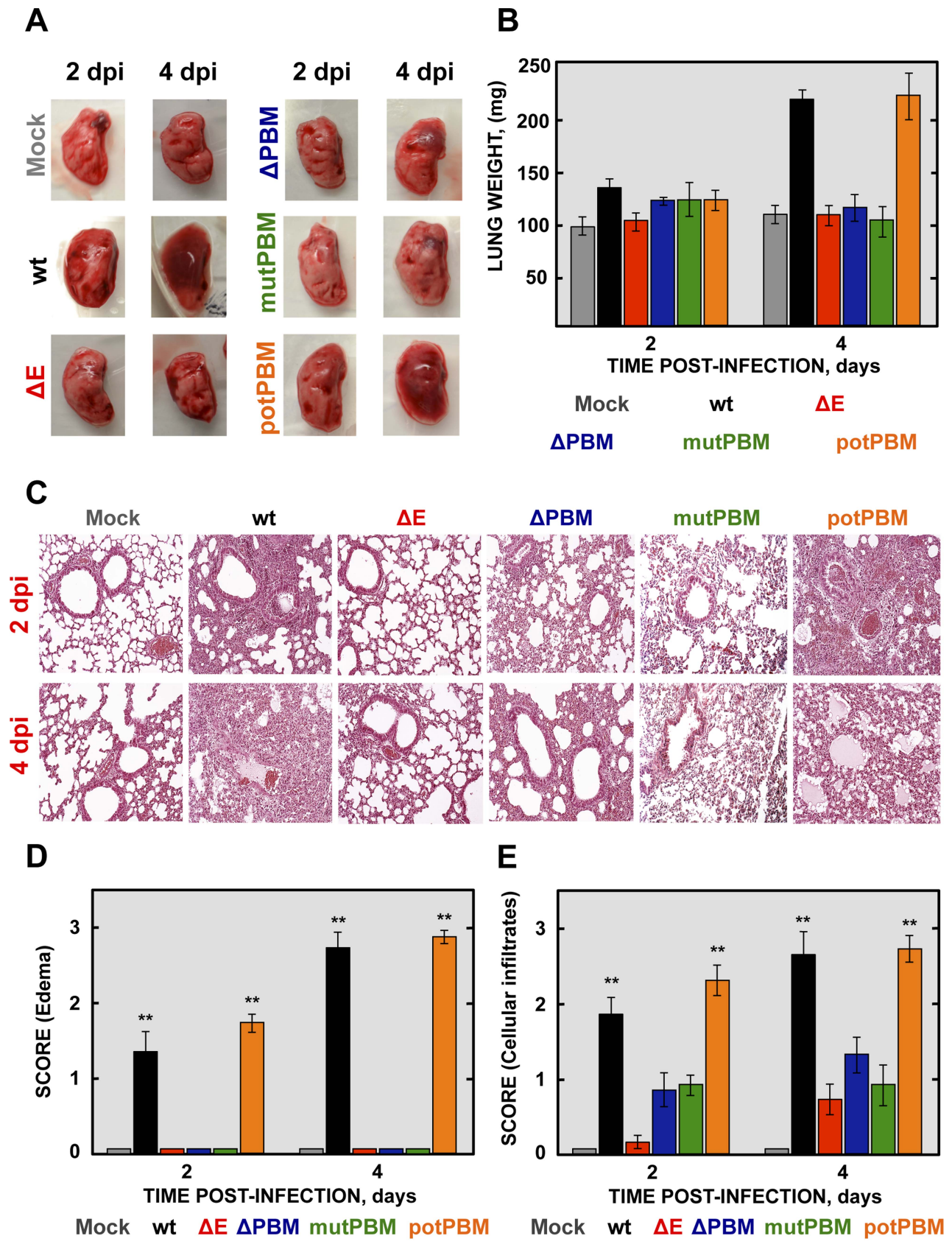

Figure 3. Lung pathology of mice infected with recombinant SARS-CoV-E-PBM mutants. 16-week-old BALB/c mice were inoculated intranasally with 100,000 pfu of wt, ΔE, ΔPBM, mutPBM and potPBM viruses. (A) Gross pathology of mouse lungs infected with recombinant viruses at 2 and 4 dpi. (B) Weight of left lungs excised from infected mice sacrificed at the indicated days (n = 3, each day). Error bars represent standard

deviations. (C) Lung tissue sections from mice infected with recombinant viruses were prepared at 2 and 4 dpi and stained with hematoxylin and eosin. Three independent mice per group were analyzed. (D and E) Pathology scoring in lung of mice infected with SARS-CoV recombinant mutants. Lungs were harvested at 2 and 4 days and scored in a blinded fashion using 3 mice per condition on a scale of 0 (none) to 3 (severe), estimated according to previously described procedures [34]. Data are presented for edema (D) and cellular infiltrates (E). Mean values are reported and statistically significant data are indicated with two ($P<0.01$) asterisks. Original magnification was 20x. Representative images are shown.
doi:10.1371/journal.ppat.1004320.g003

indicate that the last 4 amino acids of SARS-CoV E protein form a functional PBM that, in the context of virus infection, mediate its association with the cellular protein syntenin. The absence of this interaction could be playing a role in the attenuation observed in viruses lacking E protein PBM.

Colocalization of SARS-CoV E protein and syntenin in infected-cells and in cells transfected with a plasmid expressing E protein

To evaluate whether SARS-CoV E protein and syntenin colocalize during infection and to determine if syntenin localization was altered during SARS-CoV infection, mock-infected Vero E6 cells and cells infected with the wt or mutPBM virus were analyzed by confocal immunomicroscopy using specific antibodies against the cellular protein syntenin and the SARS-CoV nucleocapsid (N) and E proteins (Figure 6A). Syntenin was predominantly present in the nucleus of mock-infected cells. Upon wt infection, E protein was mainly localized at perinuclear regions as previously described [15]. Interestingly, after infection, syntenin partially colocalized with E protein in the perinuclear region and also relocalized to locations close to the plasma membrane (Figure 6A). Furthermore, infection with the mutPBM virus led to N protein cytoplasmic localization as previously described [40], and to a decrease in the relocalization of syntenin to the cytoplasm as compared with the parental virus.

To determine whether E protein was involved in syntenin relocalization during SARS-CoV infection, Vero E6 cells were transiently transfected with an empty plasmid or a plasmid expressing E protein and both, syntenin and E protein, were detected with specific antibodies (Figure 6B). As previously described with mock-infected cells, syntenin was mainly detected in the nucleus of cells transfected with an empty plasmid. However, in cells transfected with the plasmid expressing E protein, syntenin colocalized with E protein in the perinuclear region and adopted a distribution close to the plasma membrane (Figure 6B). Furthermore, the percentage of mock-infected versus virus-infected cells that showed cytoplasmic accumulation of syntenin was quantified (Figure 6C). Syntenin accumulated in the cytoplasm of 98.5% of the cells infected with the parental virus, whereas 31.2% of the mock-infected cells displayed syntenin in the cytoplasm. In cells infected with the mutPBM virus only 51.5% showed syntenin in the cytoplasm. These results indicated that syntenin partially colocalized with SARS-CoV E protein, and that it was redistributed from the nucleus to perinuclear regions, where E protein is accumulated, and also to regions close to the plasma membrane.

p38 MAPK activation in the lungs of mice infected with recombinant SARS-CoV E protein PBM mutants

Syntenin has been described as an important scaffolding protein that can initiate a signaling cascade resulting in the induction of p38 MAPK [41]. In this model, after its interaction with the extracellular matrix, syntenin induces phosphorylation and therefore, activation of p38 MAPK, a protein involved in the expression of proinflammatory cytokines [42,43]. To determine whether p38 MAPK was differentially activated in the lungs of mice infected with recombinant SARS-CoV with or without E protein PBM, 16 week-old female BALB/c mice were intranasally inoculated with these viruses. The activation of p38 MAPK was studied by Western blot analysis at 2 dpi, using a phospho-p38 MAPK (p-p38) specific antibody to detect the active form, and an antibody specifically recognizing the total endogenous p38 MAPK. Actin served as loading control. Interestingly, the levels of active p38 MAPK were increased in the lungs of mice infected with SARS-CoV containing E protein PBM, compared to those found in lungs of mice infected with viruses lacking E protein PBM (Figures 7A and 7C). To reinforce the data, p38 MAPK activation was studied in infected cells. To this end, Vero E6 cells were mock-infected or infected with recombinant viruses with an E protein with or without a PBM. Then, p38 MAPK activation was analyzed by Western blot at 24 hpi. Interestingly, an increase in p38 MAPK activation was observed during infection with viruses containing E protein PBM, similarly to what was observed in the lungs of SARS-CoV-infected mice (Figures 7B and 7D). These results indicated that the E protein PBM is involved in p38 MAPK activation in response to SARS-CoV infection.

Role of syntenin in the E protein PBM-dependent p38 MAPK activation

We have shown above that SARS-CoV E protein PBM interacted with syntenin, and that infection with SARS-CoVs containing an E protein with a functional PBM led to an increase in p38 MAPK activation. As syntenin promotes p38 MAPK activation [41], we hypothesized that syntenin relocalization from nucleus to cytoplasm during infection with SARS-CoV, containing an E protein including the PBM, may be responsible for the activation of the p38 MAPK pathway. To test this hypothesis, Vero E6 cells were mock-infected or infected with recombinant SARS-CoVs including an E protein with (wt) or without (mutPBM) E protein PBM. At 24 hpi, the cytosolic and nuclear fractions from SARS-CoV infected cells were collected, and the levels of syntenin and extent p38 MAPK activation in both fractions were determined by Western blot analysis using specific antibodies for syntenin and the non-phosphorylated and phosphorylated forms of p38 MAPK. The levels of histone H3, total p38 MAPK and actin were used as controls. Syntenin levels in the cytosol fraction were increased during wt infection. Interestingly, mutPBM virus retained the ability to mislocalize a substantial amount of syntenin to the cytoplasmic fraction, possibly due to the ability of E protein to bind SARS-CoV 3a protein, which also contains a PBM, in addition to the one present in the E protein [44,45]. Furthermore, the presence of syntenin in the cytosol correlated with the activation of p38 MAPK (Figure 8A). To determine whether syntenin relocalization from nucleus to cytoplasm mediated p38 MAPK activation, Vero E6 cells were transfected with an empty plasmid or a plasmid expressing human syntenin, and presence of this protein in the nucleus or the cytoplasm of the infected cells and the levels of p38 MAPK phosphorylation were studied by Western blot analysis using specific antibodies. The levels of histone H3, total p38 MAPK and actin were used as controls. The results showed the presence of syntenin in the nucleus of cells transfected with both plasmids. In contrast, syntenin was only detected in the cytoplasmic fraction when the syntenin was overexpressed, and failed to accumulate in

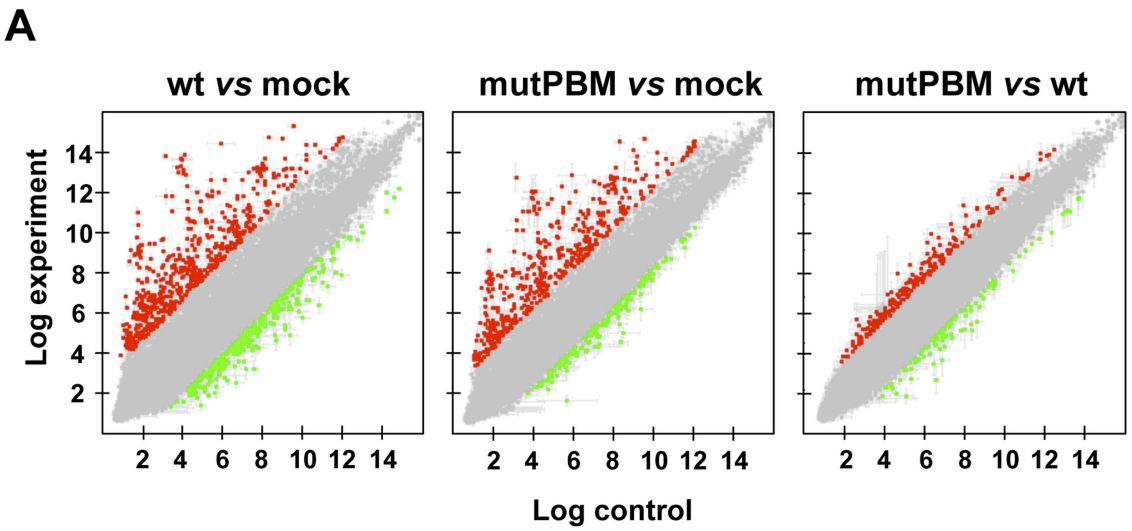

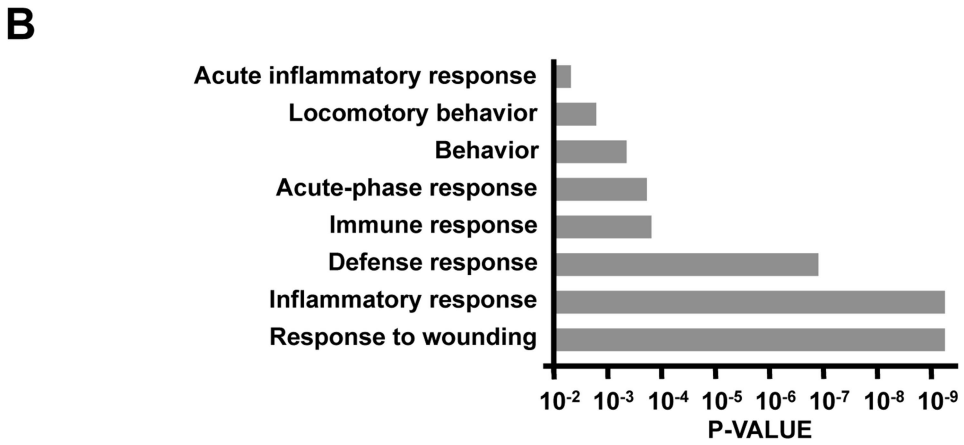

C

Gene	Fold Change	Gene	Fold Change
SAA2	-5.72	CCL2	-3.55
CCL3	-5.13	IL1B	-3.23
CXCL1	-4.62	ORM1	-3.04
CXCL5	-4.50	IL6	-2.96
CALCA	-4.35	CCL4	-2.96
SAA1	-3.77	CXCL9	-2.93
CXCL10	-3.56		

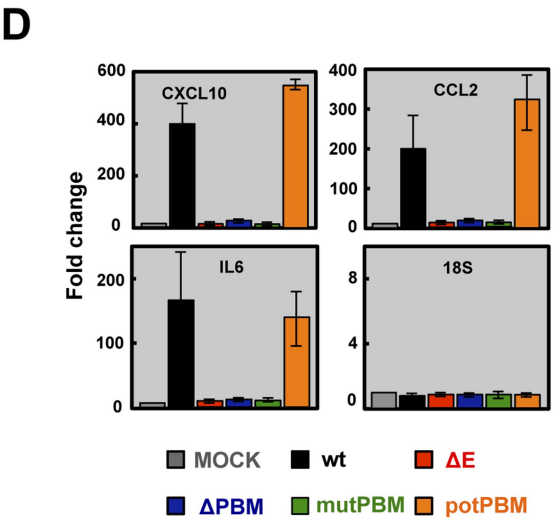

Figure 4. Effect of SARS-CoV E protein PBM on host gene expression. (A) Comparison of gene expression in lungs of infected mice using microarrays: wt versus mock-infected, mutPBM versus mock-infected and mutPBM versus wt-infected mice. Red spots indicate upregulated gene transcripts (fold change, >2) and green spots indicate downregulated gene transcripts (fold change, <−2). Only genes with a FDR of <0.01 were considered as candidate genes. (B) Candidate genes that were downregulated in mutPBM infected mice compared wt infected ones, were grouped on Gene Ontology terms. Numbers on the *x* axis indicate DAVID FDR values. (C) Selection of differentially expressed genes found in at least one functional group using DAVID software. The numbers indicate the fold change for each gene in mutPBM versus wt-infected mice. (D) Expression of inflammatory cytokines evaluated by RT-qPCR. Three independent experiments were analyzed with similar results in all cases. Error bars represent standard deviations of the mean of results from three experiments.
doi:10.1371/journal.ppat.1004320.g004

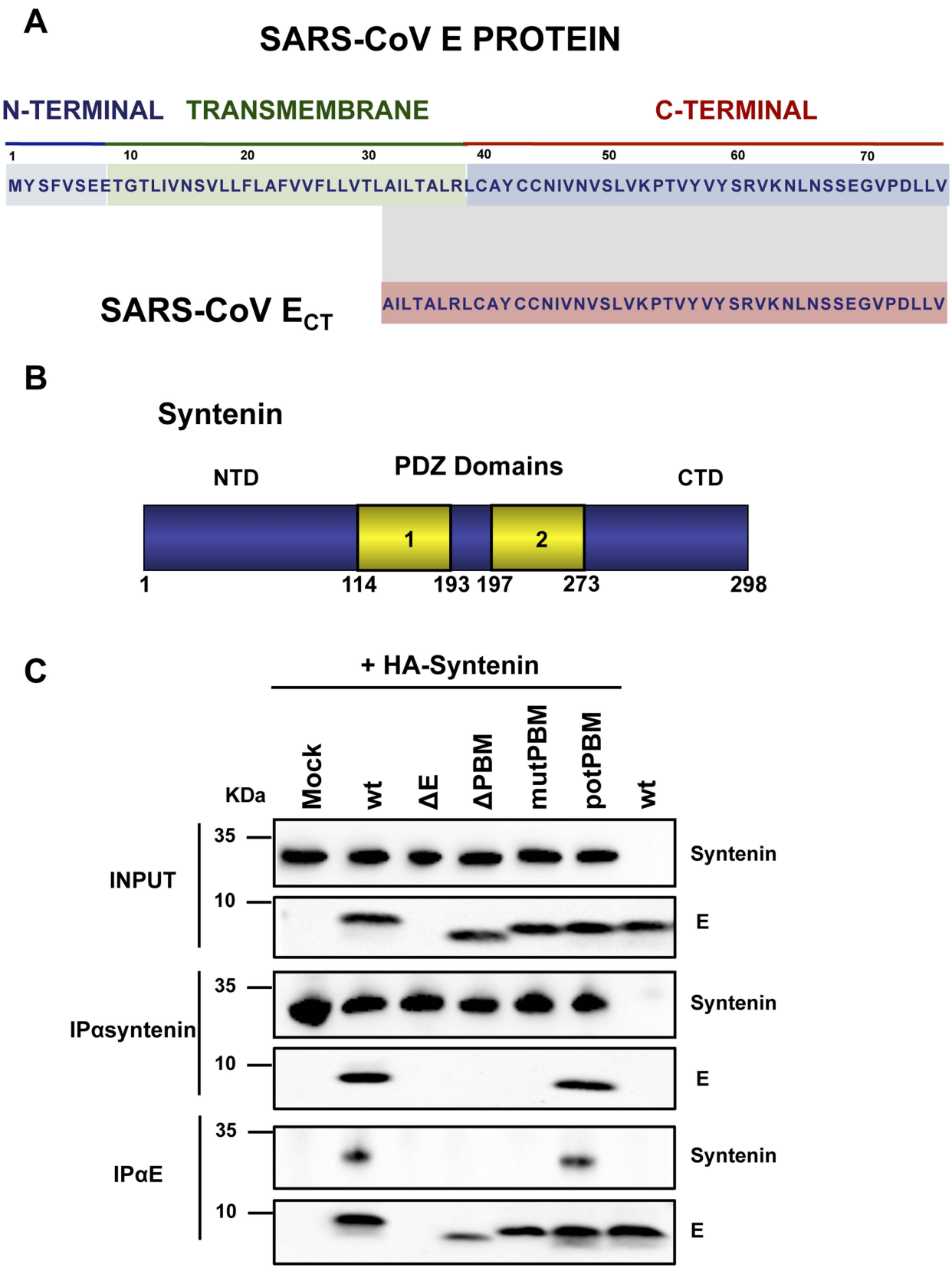

Figure 5. Interaction of SARS-CoV E protein with cellular syntenin. (A) Sequence of SARS-CoV E protein and the region containing amino acids 36–76 (SARS-CoV E_{CT}) that was used as bait for the yeast two-hybrid screening. (B) Schematic representation of syntenin. Numbers at the bottom indicate the amino acids at the beginning and the end of the different domains. NTD; N-terminal domain; CTD, C-terminal domain; PDZ 1 and 2, PDZ domains. (C) Vero E6 cells transfected with a plasmid encoding an N-terminal HA-tagged syntenin were mock-infected (mock) or infected with

recombinant viruses containing (wt and potPBM) or lacking (ΔE, PBM and mutPBM) E protein PBM, respectively. As a control, mock-transfected cells were infected with the wt virus (wt, last lane). Cells were lysed and subjected to immunoprecipitation using a monoclonal anti-HA antibody or polyclonal anti-E antibody to pulldown syntenin or E protein, respectively. The presence of E and syntenin proteins was analyzed in the precipitated fractions.
doi:10.1371/journal.ppat.1004320.g005

the nuclear fraction. This observation could be explained by the previously reported saturation of the nuclear import machinery, which leads to cytoplasmic retention of overexpressed proteins, as described for other proteins [46]. Interestingly, the presence of syntenin in the cytoplasm correlated with an increase of p38 MAPK activation (Figure 8B).

To further confirm the role of syntenin in the activation of p38 MAPK during infection by SARS-CoV with an E protein containing a functional PBM, siRNAs specifically designed to inhibit syntenin expression were used in mock-infected cells or in cells infected with the parental virus. p38 MAPK activation was analyzed by Western blot. Vero E6 cells were transfected twice by reverse transfection with either 25 nM of a validated negative control siRNA (NEG) or with similar amounts of each of two different siRNAs targeting endogenous syntenin. At 24 hpt, cells were mock-infected or infected with the parental virus at an MOI of 0.3. At 24 hpi, syntenin mRNA levels were significantly (60 to 70%) reduced in syntenin-silenced cells in relation to the cells transfected with a validated negative-control siRNA, as determined by qRT-PCR using specific Taqman gene expression assays (Figure 8C). Accordingly, syntenin levels evaluated by Western blot analysis were also significantly reduced in syntenin-silenced cells. Moreover, this silencing was found to have a higher apparent impact on the reduction of this protein in the cytoplasm, probably because that this protein accumulates more efficiently in the nucleus than the cytoplasm after protein expression. Interestingly, inhibition of syntenin expression was accompanied by a decreased in p38 MAPK activation during the infection with the parental virus (Figure 8D), whereas no changes in virus titers were observed (Figure 8E). Overall, these results support the hypothesis that the interaction of E protein PBM with syntenin facilitates the recruitment of syntenin in the cytosol and leads to p38 MAPK activation.

Effect of a p38 MAPK inhibitor on the survival of rSARS-CoV-MA15-infected mice

To analyze the contribution of SARS-CoV E protein PBM-mediated p38 MAPK activation to the disease observed during SARS-CoV infection in mice, 16 week-old female BALB/c mice were intraperitoneally administered with a control buffer or SB203580, a highly specific inhibitor of p38 MAPK, and were mock-infected or infected with the rSARS-CoV-MA15 virus. Mock-infected mice treated with the inhibitor showed 100% survival and no signs of clinical disease (Figure 9A). Interestingly, in the case of mice treated with the p38 MAPK inhibitor and infected with the parental virus, survival increased to 80% as compared with non-treated mice, with a mortality of 100%. SB203580 inhibits p38 MAPK catalytic activity by binding to the ATP-binding pocket, blocking the activation of several proteins regulated by the p38 MAPK pathway, including the heat-shock protein 27 (HSP27) [47], but does not inhibit phosphorylation of p38 MAPK by upstream kinases [48]. Therefore, to analyze whether SB203580 actually reduced p38 MAPK activity in lung tissue of virus-infected mice, the activation of HSP27 was studied by Western blot analysis at 2 dpi, using a phospho-HSP27 (p-HSP27) specific antibody to detect the active form, and an antibody specifically recognizing the total endogenous HSP27. Actin served as loading control. Results showed that the levels of active HSP27 were significantly reduced in the lungs of mice treated with SB203580 and infected with the parental virus, compared to those that were infected and non-treated (Figures 9B and 9C), indicating that p38 MAPK activity was diminished by SB203580. These results indicated that p38 MAPK activation is an important factor for SARS-CoV-induced disease.

Discussion

Cellular factors containing PDZ domains participate in a complex network of protein-protein interactions that modulate many diverse biological processes such as cell polarity, cell-cell interactions, control of proliferation, migration, immune cell recognition and signal transduction pathways [28,49,50]. Alterations of these highly regulated processes can lead to important disorders, including several types of cancer [51]. Viruses have evolved proteins containing PBM to exploit these cellular networks for their own benefit, enhancing viral replication, dissemination in the host or pathogenicity [28].

Previously, we have shown that deletion of SARS-CoV E gene leads to an attenuated virus [18,19,21]. In this study, we focused on the contributions of the E protein PBM, a motif that actively participates in protein-protein interactions with host factors [23], to the virulence of SARS-CoV. To this end, different mutant viruses containing altered or deleted E protein PBM sequences were generated using an infectious cDNA clone encoding a SARS-CoV adapted to efficiently grow in mice. Mutant viruses, with or without E protein PBM, grew in Vero E6 and DBT-mACE2 cells with titers similar to those reached by the parental virus. This result indicated that SARS-CoV E protein PBM is not essential for virus replication in cell culture.

Interestingly, recombinant SARS-CoVs lacking E protein PBM were attenuated *in vivo*, causing minimal lung damage, and no mortality in infected mice. In contrast, viruses with functional E protein PBM were highly pathogenic causing 100% mortality and inducing profuse areas of damage in the lung, indicating that E protein PBM is a determinant of pathogenicity. SARS-CoV infection induces an exacerbated immune response that potentiates both epithelial and endothelial damage within the lungs, finally leading to edema accumulation, the ultimate cause of acute lung injury (ALI) and acute respiratory distress syndrome (ARDS) [52–54]. Both the enhanced immune response, which leads to cellular infiltration, and edema accumulation leading to pulmonary failure and death, occur when conventional mice are infected with a mouse adapted SARS-CoV [55].

In SARS-CoV-infected patients and animal models, it has been shown that the observed pathology is associated with an exacerbated inflammatory response, linked to elevated levels of pro-inflammatory cytokines [54,56,57]. To understand the mechanisms leading to attenuation of viruses lacking E protein PBM, differential host gene expression in mice infected with recombinant viruses with or without an E protein PBM was analyzed using microarray analysis. The expression of genes involved in the innate immune response was significantly reduced in mice infected with SARS-CoV lacking E protein PBM, suggesting an important role of the PBM in the uncontrolled immune response triggered during SARS-CoV infection.

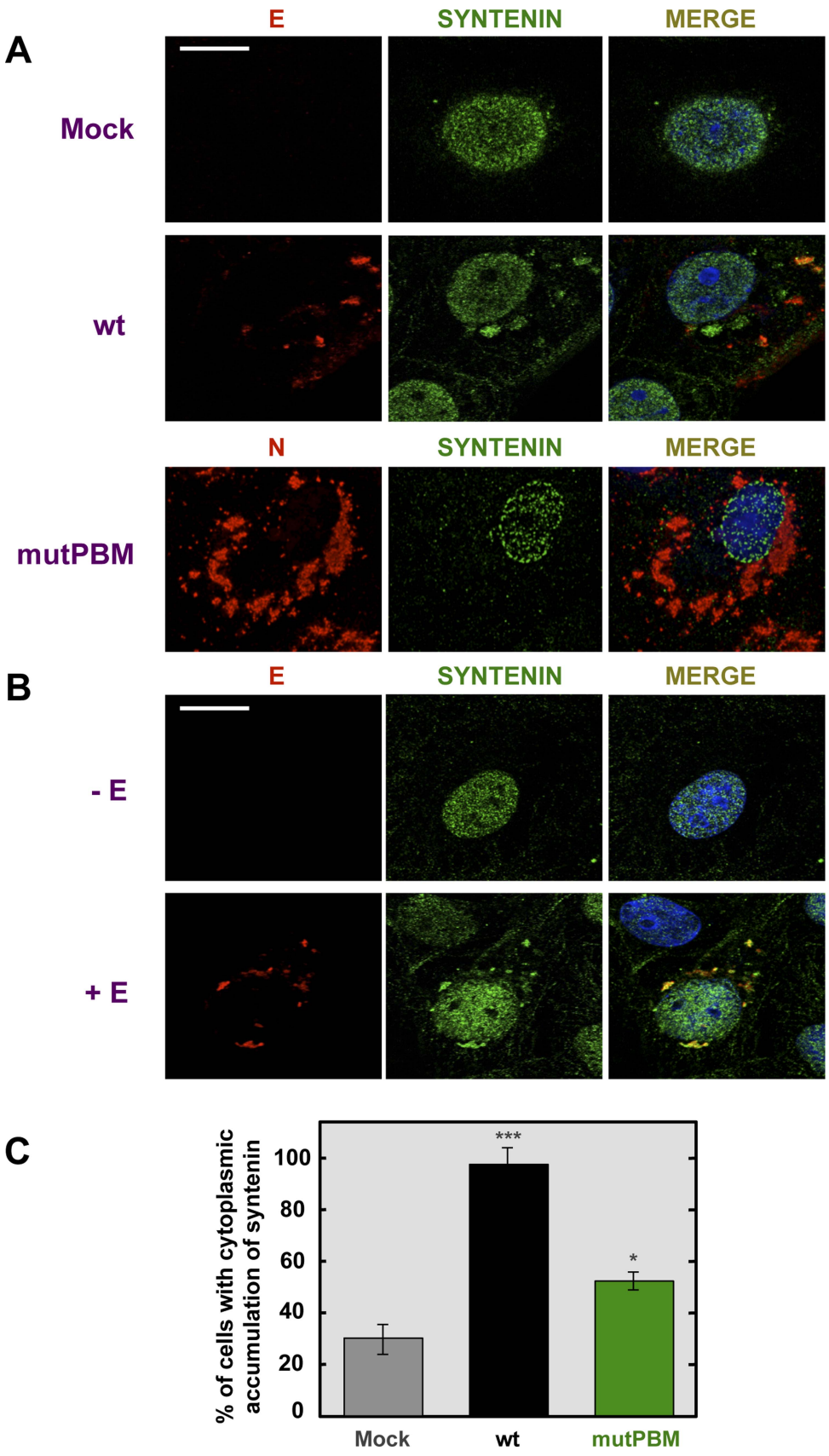

Figure 6. Colocalization of SARS-CoV E protein and syntenin in transfected and infected cells. Vero E6 were mock-infected or infected with the wt virus at an MOI of 0.3 (A) or transfected with an empty plasmid (−E) or a plasmid expressing SARS-CoV E protein (+E) (B). At 24 hpi and 24 hours post transfection (hpt) for (A) and (B), respectively, cells were fixed with 4% paraformaldehyde and E or N proteins (red) and syntenin (green)

were labeled with specific antibodies, nuclei were stained with DAPI (blue). Areas of colocalization of the two proteins appear yellow in the merged images. Scale bar = 10 μm. (C) Percentage of cells showing a cytoplasmic accumulation of syntenin after mock-infection or infected with wt or mutPBM viruses (n>50). Statistically significant data are indicated with one ($P<0.05$) or three ($P<0.001$) asterisks.
doi:10.1371/journal.ppat.1004320.g006

To further understand the molecular basis of the exacerbated immune response induced during SARS-CoV infection in the presence of SARS-CoV E protein PBM, host factors interacting with this motif were identified using a yeast two-hybrid system. One of the most prominent interactions was with the cellular protein syntenin, an important scaffolding protein containing two PDZ domains. PALS1, a protein previously associated to E protein in a similar study [23] was not identified here, probably due to the use of different cDNA libraries. In this work a human lung cDNA library was chosen to further mimic SARS-CoV infection, whereas PALS1 was identified using a human placenta cDNA collection. Coprecipitation analysis revealed that the interaction of syntenin and SARS-CoV E protein was specifically mediated by a functional PBM located in the last 4 amino acid of the E protein, which most likely associates with syntenin PDZ domains, as E protein lacking PBM did not coprecipitate with syntenin. Syntenin may participate in the activation of p38 MAPK [41], a crucial protein involved in the activation of a variety of transcription factors, controlling the expression of genes encoding inflammatory cytokines [42,43]. Indeed, we have shown an increased expression of inflammatory cytokines *in vivo* during the infection with recombinant SARS-CoVs containing E protein PBM, as compared with viruses lacking this motif, by using microarrays and RT-qPCR assays. Therefore, our results strongly suggest that the interaction of E protein with syntenin induced p38 MAPK activation leading to the inflammatory response observed after SARS-CoV infection. Interestingly, we have shown that in fact, p38 MAPK activation was significantly reduced in mice infected with viruses lacking E protein PBM as compared with mice infected with viruses containing a functional E protein PBM. This reduction in p38 MAPK activation correlated with the acquisition of an attenuated phenotype in SARS-CoV lacking the PBM. In addition, administration of one p38 MAPK inhibitor increased mouse survival after infection with the parental virus. The hypothesis that p38 MAPK is involved in CoV virulence was also postulated when patients with SARS showed augmented p38 MAPK activation [58]. It is clear that multiple host proteins and pathways may be activated through PDZ interactions with SARS-CoV E protein PBM. Interestingly, syntenin and PALS1 interaction with E protein might provide different and even complementary contributions to SARS-CoV pathogenesis, as syntenin has been described in this manuscript that activates p38 MAPK triggering an inflammatory response, whereas PALS1 affects the disruption of the lung epithelium in SARS patients [23].

In agreement with these results, proteins containing PBMs encoded by different viruses such as influenza A virus, tick-borne encephalitis virus (TBEV) and human papillomavirus (HPV) also enhanced virus pathogenesis by interacting with cellular proteins containing PDZ domains, by altering processes such as apoptosis, cell polarity or innate immune responses [28]. Our results are most likely of relevance to other coronaviruses, as the PBM is a highly conserved domain among most coronavirus E proteins, including the highly pathogenic MERS-CoV (Figure S1). Interestingly, although we demonstrated that E protein PBM was not essential for virus production after SARS-CoV infection, not all coronaviruses tolerate amino acid changes in the carboxy-terminus of E protein, as alanine substitutions in MHV E protein carboxy-terminal residues were apparently lethal, since no virus was recovered [59]. Nevertheless, it has not been excluded whether other viral proteins different from E provide alternative PBMs in the cases where the PBM does not seem to be essential.

In summary, we have shown that SARS-CoV E protein contains a functional PBM that contributes to viral pathogenesis and interacts with several cellular proteins, including syntenin. Our studies strongly suggest a causal relationship between E protein-syntenin interaction and p38 MAPK activation, leading to an increase in inflammatory cytokines expression during infection. These data identify syntenin as a potential therapeutic target to reduce the exacerbated immune response induced during SARS-CoV infection. Targeted therapies that temporarily inactivate syntenin or p38 MAPK activation during acute infection may provide a rational approach to improve the prognosis in SARS-CoV patients. In fact, we have shown that inhibition of p38 MAPK increased mice survival after infection with SARS-CoV. Accordingly to our results, *in vivo* inhibition of p38 MAPK diminished influenza virus induced cytokine expression, protecting mice from lethal disease [60]. In the future, a search for the presence of additional PDZ targets located in alternative cellular proteins, and the relevance of E protein PBM present in other coronaviruses will be pursued to better understand the influence of PDZ and PBM motifs in virus pathogenicity and in the immune responses to virus infection.

Materials and Methods

Ethics statement

Animal experimental protocols were approved by the Ethical Committee of The Center for Animal Health Research (CISA-INIA) (permit numbers: 2011-009 and 2011-09) in strict accordance with Spanish National Royal Decree (RD 1201/2005) and international EU guidelines 2010/63/UE about protection of animals used for experimentation and other scientific purposes and Spanish National law 32/2007 about animal welfare in their exploitation, transport and sacrifice and also in accordance with the Royal Decree (RD 1201/2005). Infected mice were housed in a ventilated rack (Allentown, NJ).

Cells

African Green monkey kidney-derived Vero E6 cells were kindly provided by Eric Snijder (Medical Center, University of Leiden, The Netherlands). The delayed brain tumor (DBT) cells expressing mACE2 receptor (DBT-mACE2) were generated in our laboratory [33]. Virus titrations were performed in Vero E6 cells as previously described [18].

Plasmids

The pcDNA3-E plasmid encoding SARS-CoV E protein was used as previously described [15].The N-terminal HA-tagged syntenin expression plasmid in the backbone of pMT2-HA vector was kindly provided by P.J. Coffer (University Medical Center, Utrecht, The Netherlands) [61].

Mice

8 week-old specific-pathogen-free BALB/c Ola Hsd mice females were purchased from Harlan Laboratories. BALB/c mice were infected at the age of 16 weeks with 100,000 plaque forming units (pfu).

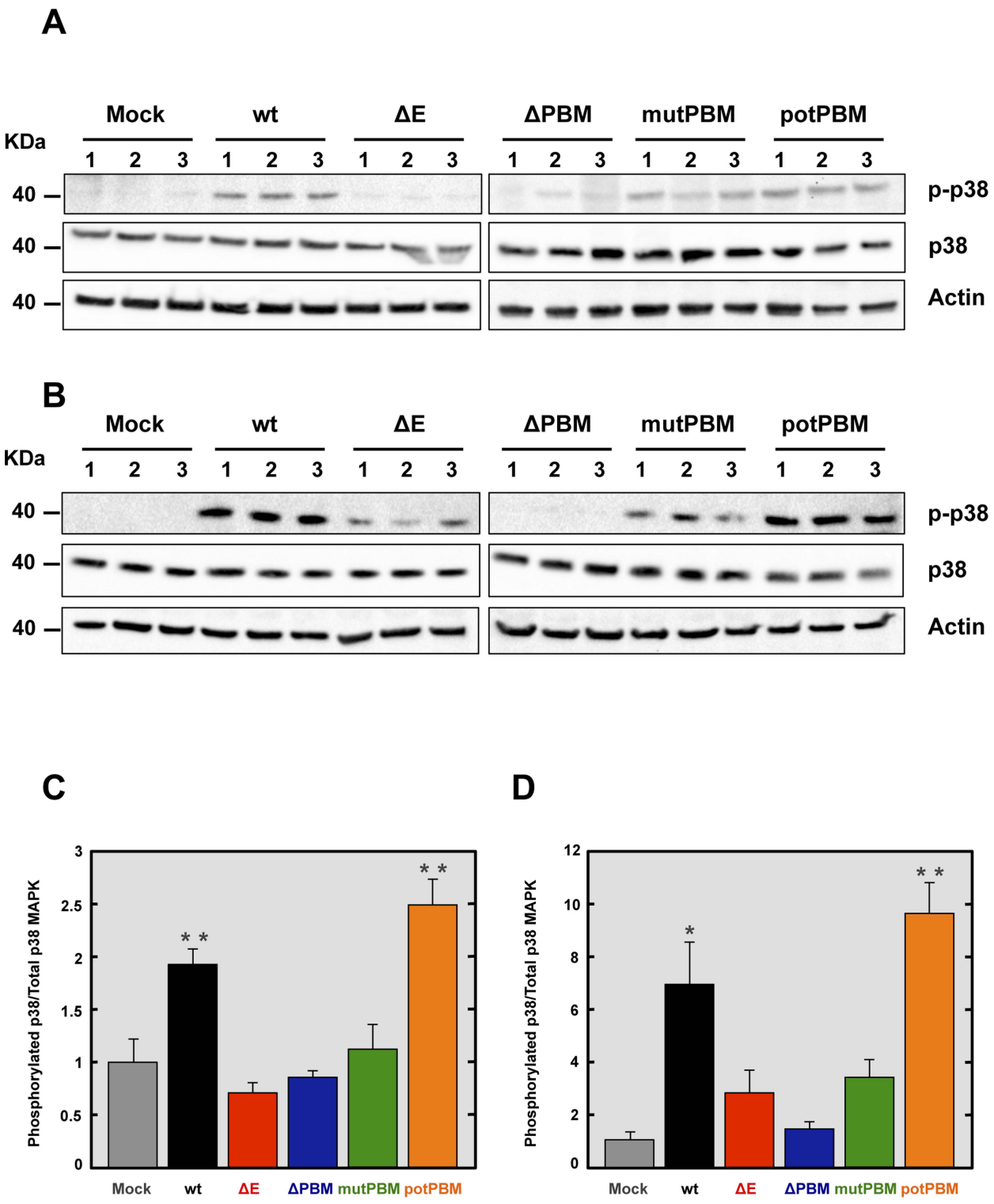

Figure 7. Activation of p38 MAPK in SARS-CoV-E-PBM mutants infected mice and cells. Lung proteins were extracted from infected mice at 2 dpi. (A) The active phosphorylated (p-p38) and total (p38) p38 MAPK in lungs of three infected mice per condition were evaluated by Western blot analysis. (B) The active phosphorylated (p-p38) and total (p38) p38 MAPK in Vero E6 infected cells were evaluated by Western blot analysis. (C and D) Phospho and total p38 MAPK amounts were quantified by densitometric analysis. The graph shows the phosphorylated p38/total p38 MAPK ratio in wt, ΔE, ΔPBM, mutPBM and potPBM infected mice at 2 dpi (C) or Vero E6 cells at 24 hpi (D). Error bars represent the means of three mice analyzed for each condition. Statistically significant data are indicated with one ($P<0.05$) or two ($P<0.01$) asterisks.
doi:10.1371/journal.ppat.1004320.g007

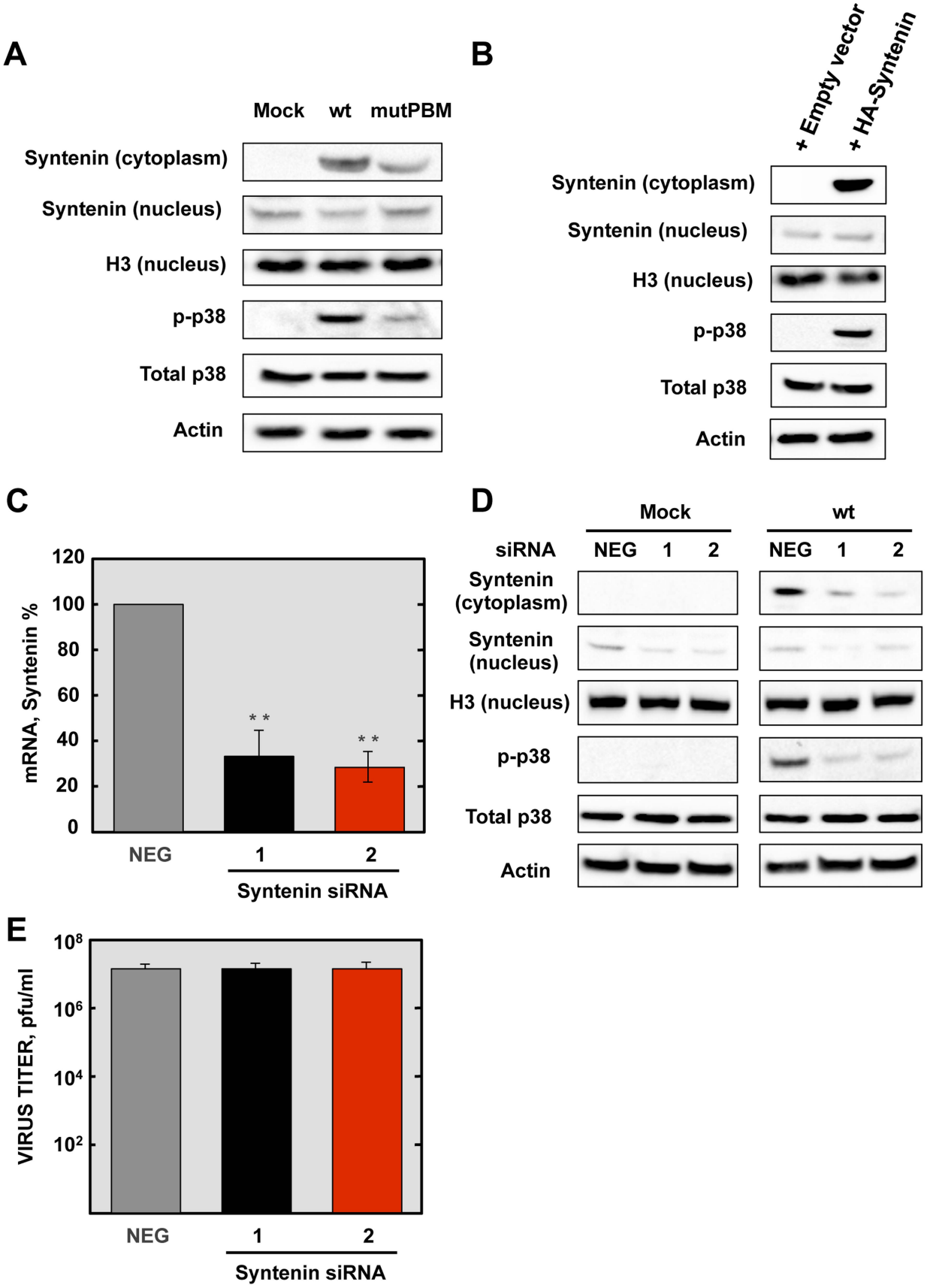
A
Mock
wt
mutPBM
Syntenin (cytoplasm)
Syntenin (nucleus)
H3 (nucleus)
p-p38
Total p38
Actin
B
+ Empty vector
+ HA-Syntenin
Syntenin (cytoplasm)
Syntenin (nucleus)
H3 (nucleus)
p-p38
Total p38
Actin
C
mRNA, Syntenin %
120
100
80
60
40
20
0
* *
* *
NEG
1
2
Syntenin siRNA
D
Mock
wt
siRNA
NEG
1
2
NEG
1
2
Syntenin (cytoplasm)
Syntenin (nucleus)
H3 (nucleus)
p-p38
Total p38
Actin
E
VIRUS TITER, pfu/ml
10^8
10^6
10^4
10^2
NEG
1
2
Syntenin siRNA

Figure 8. Role of syntenin in the E protein PBM-dependent p38 MAPK activation. (A) Vero E6 cells were mock-infected or infected with recombinant viruses containing (wt) or lacking (mutPBM) E protein PBM, and the presence of syntenin in the cytoplasm and nucleus and active p38 MAPK (p-p38) were detected by Western blot analysis at 24 hpi. As controls, histone H3 (H3), total p38 MAPK (Total p38) and actin were analyzed. (B) Vero E6 cells were transfected with an empty plasmid (empty vector) or a plasmid encoding a HA-tagged syntenin (HA-syntenin), and the presence of syntenin in the cytoplasm and nucleus, and active p38 MAPK were detected by Western blot analysis at 24 hpt. As controls, histone H3, total p38 MAPK, and actin were analyzed. (C) Quantification by qRT-PCR of syntenin mRNA in cells transfected with syntenin-specific siRNA (1 and 2) compared to reference levels from cells transfected with a validated-negative control siRNA (NEG). Mean values are reported, and statistically significant data are indicated with two ($P<0.01$) asterisks. (D) Effect of silencing syntenin expression on Vero E6 cells, mock-infected or infected with the wt virus. The presence of syntenin in the cytoplasm and nucleus and active p38 MAPK were detected by Western blot at 24 hpi. As controls, histone H3, total p38 MAPK and actin were analyzed. (E) Viral titers of wt virus in syntenin silenced Vero E6 cells were determined at 24 hpi. The experiments were performed three times, and the data represent the averages of triplicates. Standard deviations are indicated as error bars.
doi:10.1371/journal.ppat.1004320.g008

Recombinant SARS-CoV growth kinetics

Subconfluent monolayers (90% confluency) of Vero E6 and DBT-mACE2 were infected at an MOI of 0.05 with wt, ΔE, ΔPBM, mutPBM and potPBM. Culture supernatants were collected at different hpi and virus titers were determined as previously described [18].

Determination of virus titer in infected mouse lungs

Lungs harvested for virus titers were weighed and homogenized using gentleMACS Dissociator (miltenyibiotec). Virus titers were determined by plaque assay on Vero cells as previously described [18].

Histopathology

Mice were sacrificed at 2 and 4 dpi. Lungs were removed, fixed in zinc formalin and paraffin embedded. Histopathological examinations were performed on hematoxylin-eosin stained sections.

Western blot analysis

Cell lysates were resolved by sodium dodecyl sulfate-polyacrylamide gel electrophoresis (SDS-PAGE), transferred to a nitrocellulose membrane by wet immunotransfer and processed for Western blotting. The blots were probed with monoclonal antibodies specific for HA tag (dilution 1:10,000; Sigma), p38 MAPK (dilution 1:500; Cell Signaling), phospho-p38 MAPK (dilution 1:500; Cell Signaling), syntenin (dilution 1:1000; Abcam), phospho-HSP27 (dilution 1:1000, Cell Signaling) and actin (dilution 1:10000; Abcam) or polyclonal antibodies against E (dilution 1:1000), HSP27 (dilution 1:1000, Cell Signaling) and histone H3 (dilution 1:5000; Active Motif). A polyclonal antibody recognizing the carboxy-terminal domain of SARS-CoV E protein except the PBM was generated by Biogenes (Germany) using a synthetic peptide corresponding to the 49–64 residues of SARS-CoV E protein (VSLVKPTVY-VYSRVKN) as previously described [15]. Bound antibodies were detected with horseradish peroxidase-conjugated goat anti-rabbit or anti-mouse antibodies (dilution 1:30,000; Cappel) and the Immobilon Western chemiluminescent substrate (Millipore).

Confocal microscopy

Vero E6 cells were grown to 90% confluency on glass coverslips and infected with the parental virus at an MOI of 0.3. Alternatively, Vero E6 cells were grown to 70% confluency in 1 cm^2 wells and transfected with 1 μg of DNA using 1 μl of Lipofectamine 2000 (Invitrogen) according to the manufacturer's instructions. At 24 hours post infection (hpi) or post transfection (hpt), cells were fixed as previously described [15]. Primary antibody incubations were performed in PBS containing 10% FBS and 0.2% saponin for 1 h 30 min at room temperature. Immunofluorescence was performed using monoclonal antibodies specific for E (dilution 1:3000) or N (dilution 1:500) proteins [15], and polyclonal antibodies specific for syntenin (dilution 1:200, Abcam). Coverslips were washed four times with PBS between primary and secondary antibody incubations. Alexa 488- or Alexa 546-conjugated antibodies specific for the different species (dilution 1:500, Invitrogen) were incubated for 45 min at room temperature in PBS containing 10% FBS and 0.2% saponin. Nuclei were stained using DAPI (dilution 1:200, Sigma). Coverslips were mounted in ProLong Gold anti-fade reagent (Invitrogen) and examined on a Leica SP5 confocal microscope (Leica Microsystems).

Immunoprecipitation

Vero E6 were grown to 90% confluence and transfected with a N-terminal HA-tagged syntenin expression plasmid. 24 hours later, cells were infected with recombinant viruses at an MOI of 0.3. At 24 hpi, cell extracts were collected as previously described [62]. For immunoprecipitation assays, monoclonal anti-HA agarose conjugate clone HA-7 (Sigma) was used following the manufacturer's instructions. Briefly, 75 μl of the anti-HA agarose conjugate was washed five times with PBS and then incubated with the cell extracts overnight on an orbital shaker at 4°C. The samples were washed four times with PBS and then immune complexes were eluted using 20 μl 2X SDS sample buffer and heating at 95°C for 3 minutes. For reciprocal immunoprecipitation assays Protein A/G Plate IP Kit (Pierce) was used following the manufacturer's instructions as previously described [62] using polyclonal anti-E antibody. Analysis of precipitate complexes was carried out by SDS-PAGE and Western blotting.

Cytokine expression analysis from lung samples using RT-qPCR

Lung sections from infected animals were collected at 2 dpi and homogenized using gentleMACS Dissociator (Miltenyibiotec). Then, total RNA was extracted using the RNeasy purification kit (Qiagen). Reactions were performed at 37°C for 2 h using a High Capacity cDNA transcription kit (Applied Biosystems) using 100 ng of total RNA and random hexamer oligonucleotides. Cellular gene expression was analyzed using TaqMan gene expression assays (Applied Biosystems) specific for mouse genes (Table 1). Data representing the average of three independent experiments were acquired and analyzed as previously described [32]. All experiments and data analysis were MIQE compliant [63].

Yeast two-hybrid screening

Bait cloning and yeast two-hybrid screening with the carboxy-terminal (amino acids 36–76) domain of SARS-CoV E protein (E_{CT}) as bait were performed by Hybrigenics (France). E_{CT} domain was cloned into the pB27 vector, enabling its fusion with the LexA binding domain. The bait construct was transformed into the L40ΔGAL4 yeast strain [64] and then mated with the Y187 yeast strain transformed by a random-primed human lung cDNA library containing 10 million independent fragments. In the screening, 80.3 million interactions were analyzed. After selection on medium lacking leucine, tryptophan, and histidine, 268 positive clones were picked. The corresponding prey fragments were

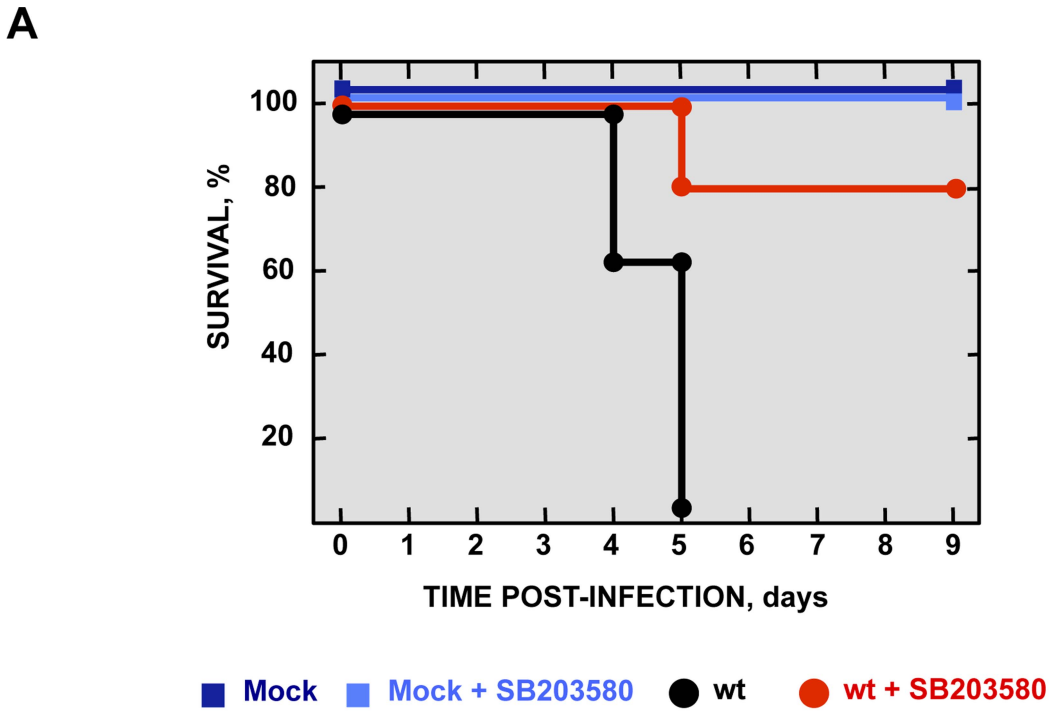

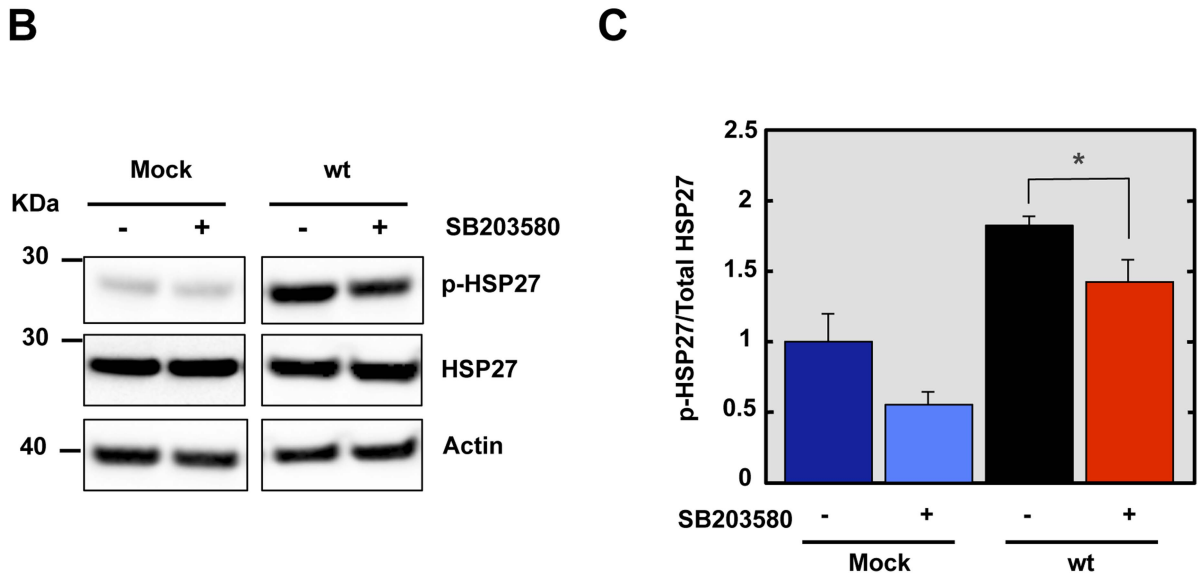

Figure 9. Effect of p38 MAPK inhibitor in rSARS-CoV-MA15-infected mice. 16-week-old BALB/c mice were mock-infected or inoculated intranasally with 100,000 pfu of wt virus. At 4 hpi and every 12 h from days 1 to 8, mock-infected and wt-infected mice were intraperitoneally injected with SB203580 (6 mg/kg of body weight/day). (A) Animals were monitored daily for mortality. Data represent three independent experiments with 5 mice per group. (B) The active phosphorylated (p-HSP27) and total HSP27 in lungs of three infected mice per condition were evaluated by Western blot analysis. (C) Phospho and total HSP27 amounts were quantified by densitometric analysis. The graph shows the phosphorylated HSP27/total HSP27 ratio at 2 dpi in lungs of mock-infected mice or mice infected with the parental virus, treated or not with SB203580. Error bars represent the means of three mice analyzed for each condition. Statistically significant data are indicated with one ($P<0.05$) asterisk.

doi:10.1371/journal.ppat.1004320.g009

subjected to PCR and sequencing. Sequences were then filtered, divided into contigs, and compared to the latest release of the GenBank database by using BLASTn (NCBI). A predicted biological score (PBS) was attributed to assess the reliability of the interaction, as described earlier [38].

p38 MAPK activation in lungs of infected mice

Lungs were removed from infected mice at 2 dpi and homogenized. Nuclear and cytoplasmic extracts from homogenized lungs were obtained using a nuclear extract kit (Active Motif, Carlsbad, CA). Levels of total and phosphorylated p38 MAPK

Table 1. Taqman assays used to analyze the expression of cellular genes by quantitative RT-PCR.

Gene name	Taqman assay*	Description
CXCL10/IP-10	Mm00445235-m1	Interferon inducible protein 10
CCL2/MCP-1	Mm00441242-m1	Monocyte chemotactic protein 1
IL-6	Mm00446190-m1	Interleukin 6
18S	Mm03928990-g1	18S rRNA
SDCBP (syntenin)	Hs01045460_g1	Syndecan binding protein (syntenin)

*Mm, means *Mus musculus*. Hs, means *Homo sapiens*.
doi:10.1371/journal.ppat.1004320.t001

were analyzed by Western blot using specific antibodies and the cytoplasmic extracts. Total and activated p38 MAPK amounts were quantified by densitometric analysis using Quantity One, version 4.5.1, software (Bio-Rad). In each case, the levels of phosphorylated p38 MAPK were normalized to the levels of total p38 MAPK. Three different experiments and appropriate gel exposures were used in all cases with similar results. In addition, different exposures of the same experiment were analyzed to assure that data obtained were within linear range.

Microarray analysis

At 2 days post infection, lungs from infected mice were collected and homogenized using the gentleMACS Dissociator (Miltenyibiotec). Then, total RNA was extracted using the RNeasy purification kit (Qiagen) according to the manufacturer's instructions. Three biological replicates were independently hybridized for each transcriptomic comparison. Total RNA (200 ng) was amplified using One Color Low Input Quick Amp Labeling Kit (Agilent Technologies) and purified with RNeasy Mini Kit (Qiagen). Preparation of probes and hybridization was performed as described in One-Color Microarray Based Gene Expression Analysis Manual Ver. 6.5, Agilent Technologies. Briefly, for each hybridization 600 ng of Cy3 probes were mixed and added to 5 ul of 10x Blocking Agent, 1 ul of 25x Fragmentation Buffer and Nuclease free water in a 25 µl reaction, incubated at 60°C for 30 minutes to fragment RNA and stopped with 25 ul of 2x Hybridization Buffer. The samples were placed on ice and quickly loaded onto arrays, hybridized at 65°C for 17 hours in a Hybridization oven rotator and then washed in GE wash buffer 1 at room temperature (1 minute) and in GE Wash Buffer 2 at 37°C (1 minute). Arrays were dried by centrifugation at 2000 rpm for 2 minutes. Slides were Sure Print G3 Agilent 8×60K Mouse (G4852A-028005)

Images were captured with an Agilent Microarray Scanner and spots quantified using Feature Extraction Software (Agilent Technologies). Background correction and normalization of expression data were performed using LIMMA [65].

Microarray data analysis

Linear model methods were used for determining differentially expressed genes. Each probe was tested for changes in expression over replicates by using an empirical Bayes moderated t-statistic [66]. To control the false discovery rate (FDR), defined as the expected proportion of false positives among the significant tests, *p-values* were corrected by using the method of Benjamini and Hochberg [66,67]. The expected false discovery rate was controlled to be less than 5% (FDR$<$0.05). Genes were considered differentially expressed when the FDR were $<$0.01. In addition, only genes with a fold change of $>$2 or of <-2 were considered for further analysis.

Viruses

The mouse-adapted (MA15) [31], parental virus (wt) and a virus lacking E gene (ΔE) were rescued from infectious cDNA clones generated in our laboratory [21].

The pBAC-SARS-CoV-E-PBM mutant plasmids encoding recombinant SARS-CoVs expressing E genes with deleted or mutated PBMs were constructed from a previously generated infectious cDNA clone (plasmid pBAC-SARS-CoV-ΔE-MA15) [21]. Deletion of the 9 most carboxy-terminal amino acids (LNS---------) or mutations (LNSSAGAPALAV) in SARS-CoV-E-ΔPBM and SARS-CoV-E-potPBM, respectively (Figure 1), were introduced by overlap extension PCR using the pBAC-SARS-CoV-ΔE-MA15 as a template and specific primers (Table 2). A fragment representing the nucleotides containing the mutations (LNSSEGVPGGGG) to generate SARS-CoV-E-mutPBM was chemically synthesized (BioBasic Inc). The final PCR products and synthesis fragments were digested with enzymes *BamHI* and *MfeI* and cloned into the intermediate plasmid psl1190+BamHI/SacII-SARS-CoV to generate the plasmids psl1190-E-ΔPBM, psl1190-E-mutPBM and psl1190-E-potPBM. The plasmid psl1190+BamHI/SacII SARS-CoV contains a fragment corresponding to nucleotides 26045 to 30091 of the SARS-CoV infectious cDNA clone [68] engineered into plasmid psl1190 (Pharmacia). These constructs were cloned in the infectious pBAC-SARS-CoV-ΔE-MA15 with the enzymes *BamHI* and *SacII*. All constructs were generated carrying a duplication of the final last nucleotides (208–231) of E gene after the stop codon of the mutated E proteins in order to avoid altering the transcription regulatory sequence (TRS) of membrane (M) gene, which overlaps with the end of E gene [69]. All viruses were rescued from infectious cDNA clones as previously described [68].

siRNA transfection

Vero E6 cells were transfected following a reverse transfection protocol. Briefly, for each well of a 24-well plate, 5×10^4 cells were incubated in suspension with 25 nM of Silencer Select siRNAs (Ambion) targeting syntenin (siRNA 1: s12641 and siRNA 2: s224582) and 2 µl of siPORT amine (Ambion) diluted in 50 µl of Opti-MEM I reduced serum medium (GibcoBRL-Invitrogen), following the manufacture's instructions. As a negative control, an irrelevant validated siRNA (Ambion, reference 4390843) was transfected. Cells were plated onto each well using DMEM with 5% heat-inactivated FBS, incubated at 37°C for 24 h. The cells were retransfected with 25 nM siRNAs at 24 h after the first transfection, and infected with the parental virus at 48 h after second transfection. At 24 hpi, total RNA, proteins and cells supernatants were collected for further analysis.

Table 2. Primers used for the generation of recombinant SARS-CoV-E-PBM mutants.

Virus	Primer	Sequence
ΔPBM	SARS-25871-VS	CGTTGTACATGGCTATTTCACCG
	SARS-ΔPBM-RS	TTAGACCAGAAGATCAGGAACTCCTTAAGAGTTCAGATTTTTAACACGC
	SARS-26325-VS	GGAGTTCCTGATCTTCTGGTCTAA
	SARS-28136-RS	GGGCACTACGTTGGTTTGATTGGGG
potPBM	SARS-25871-VS	CGTTGTACATGGCTATTTCACCG
	SARS-potPBM-RS	TTAGACCAGAAGATCAGGAACTCCTTAGACTGCAAGAGCAGGA GCTCCTGCAGAAGAGTTCAGATTTTTAACACGCG
	SARS-26325-VS	GGAGTTCCTGATCTTCTGGTCTAA
	SARS-28136-RS	GGGCACTACGTTGGTTTGATTGGGG

doi:10.1371/journal.ppat.1004320.t002

Analysis of syntenin gene expression

Syntenin gene expression was quantified by qRT-PCR. Total RNA was prepared with an RNeasy kit (Qiagen), according to the manufacturer's instructions. Reactions were performed at 37°C for 2 h using a High Capacity cDNA transcription kit (Applied Biosystems) using 100 ng of total RNA and random hexamer oligonucleotides. Syntenin gene expression was analyzed using TaqMan gene expression assays (Applied Biosystems) specific for human gene (Table 1). Data representing the average of three independent experiments were acquired and analyzed as previously described [32]. All experiments and data analysis were MIQE compliant [63].

p38 MAPK inhibitor treatment of SARS-CoV-infected BALB/c mice

16-week-old BALB/c mice were infected intranasally with 100,000 pfu of wt virus. At 4 hpi and every 12 h thereafter, from days 1 to 8, mice were treated intraperitoneally with SB203580 (Millipore) at 6 mg/kg of body weight/day with vehicle (PBS containing 2% dimethyl sulfoxide [DMSO]). Survival was analyzed in three independent experiments with 5 mice per group. To analyze p38 MAPK inhibition, lungs were removed and homogenized from mice at 2 dpi. Levels of total and phosphorylated HSP27 were analyzed by Western blot using specific antibodies and the lung extracts. Total and activated HSP27 amounts were quantified by densitometric analysis using Quantity One, version 4.5.1, software (Bio-Rad). In each case, the levels of phosphorylated HSP27 were normalized to the levels of total HSP27. Three different experiments and appropriate gel exposures were used in all cases with similar results. In addition, different exposures of the same experiment were analyzed to assure that data obtained were within linear range.

Subcellular fractionation

Vero E6 were washed twice with PBS, scraped off and pelleted by low-speed centrifugation at 2000 rpm for 2 minutes in a bench-top centrifuge. The supernatant was removed and cell pellets were lysed by repetitive pipetting with a micropipette in ice-cold lysis buffer containing 150 mM NaCl, 3 mM $MgCl_2$, 20 mM Tris/HCl (pH 7.5), 2 mM DTT and 0.5% NP-40. The lysate was incubated during 5 minutes in ice and centrifuged in a bench-top centrifuge at 3000 rpm for 2 minutes. Supernatant and pellet were saved as the cytosolic and nuclear fraction, respectively.

Scoring of lung pathology

Hematoxylin and eosin-stained lung sections were assessed using the scoring system described in the figure legends according to previously described procedures [34]. Three animals for each time point were analyzed.

Accession numbers

The UniProt (http://www.uniprot.org/) accession numbers for genes and proteins discussed in this paper are: SARS-CoV E protein, P59637; human p38 MAPK, Q16539; mouse p38 MAPK, P47811; syntenin, O00560; human ACE2, Q9BYF1; mouse ACE2, Q8R0I0; PALS1, Q8N3R9; SAA2, P05367; CCL3, P10855; CXCL1, P12850; CXCL5, P50228; CALCA, P70160; SAA1, P05366; CXCL10, P17515; CCL2, P10148; IL1B, P10749; ORM1, Q60590; IL6, P08505; CCL4, P14097; CXCL9, P18340; 18S, O35130; human actin, P60709; mouse actin, P60710; histone H3, P84243; SARS-CoV N protein, P59595; HSP27, P14602.

Supporting Information

Figure S1 Coronavirus E protein sequences representing potential PDZ-binding motifs. Top, representation of CoV E protein sequence and its corresponding domains. Below sequences corresponding to the end of several E proteins from representative genus α, β and γ CoVs are shown in boxes. Red boxes represent the presence of a potential PDZ-binding motif. (TIF)

Acknowledgments

We thank Marga Gonzalez for technical assistance.

Author Contributions

Conceived and designed the experiments: JMJG JLNT MLD LE. Performed the experiments: JMJG JLNT MLD JARN RFD. Analyzed the data: JMJG JLNT MLD JARN LE. Contributed reagents/materials/analysis tools: JMJG JLNT MLD JARN RFD CCR LE. Wrote the paper: JMJG JLNT MLD JARN CCR LE.

References

1. Peiris JS, Yuen KY, Osterhaus AD, Stohr K (2003) The severe acute respiratory syndrome. N Engl J Med 349: 2431–2441.
2. Lau SK, Woo PC, Li KS, Huang Y, Tsoi HW, et al. (2005) Severe acute respiratory syndrome coronavirus-like virus in Chinese horseshoe bats. Proc Natl Acad Sci USA 102: 14040–14045.
3. Li W, Shi Z, Yu M, Ren W, Smith C, et al. (2005) Bats are natural reservoirs of SARS-like coronaviruses. Science 310: 676–679.
4. Woo PC, Lau SK, Li KS, Poon RW, Wong BH, et al. (2006) Molecular diversity of coronaviruses in bats. Virology 351: 180–187.
5. Dominguez SR, O'Shea TJ, Oko LM, Holmes KV (2007) Detection of group 1 coronaviruses in bats in North America. Emerg Infect Dis 13: 1295–1300.
6. Zaki AM, van Boheemen S, Bestebroer TM, Osterhaus AD, Fouchier RA (2012) Isolation of a novel coronavirus from a man with pneumonia in Saudi Arabia. N Engl J Med 367: 1814–1820.
7. Bermingham A, Chand M, Brown C, Aarons E, Tong C, et al. (2012) Severe respiratory illness caused by a novel coronavirus, in a patient transferred to the United Kingdom from the Middle East, September 2012. Euro Surveill 17. pii: 20290.
8. Assiri A, McGeer A, Perl TM, Price CS, Al Rabeeah AA, et al. (2013) Hospital outbreak of Middle East respiratory syndrome coronavirus. N Engl J Med 369: 407–16.
9. Enjuanes L, DeDiego ML, Alvarez E, Capiscol C, Baric R (2008) Vaccines for severe acute respiratory syndrome virus and other coronaviruses. In: Perlman S, Gallagher TM, Snijder EJ, editors. Nidoviruses. Washington: ASM Press. pp. 379–408.
10. Torres J, Parthasarathy K, Lin X, Saravanan R, Liu DX (2006) Model of a putative pore: the pentameric alpha-helical bundle of SARS coronavirus E protein in lipid bilayers. Biophys J 91: 938–947.
11. Verdia-Baguena C, Nieto-Torres JL, Alcaraz A, Dediego ML, Torres J, et al. (2012) Coronavirus E protein forms ion channels with functionally and structurally-involved membrane lipids. Virology 432: 485–494.
12. Verdia-Baguena C, Nieto-Torres JL, Alcaraz A, Dediego ML, Enjuanes L, et al. (2013) Analysis of SARS-CoV E protein ion channel activity by tuning the protein and lipid charge. Biochim Biophys Acta 1828: 2026–2031.
13. Nieto-Torres JL, Dediego ML, Verdia-Baguena C, Jimenez-Guardeno JM, Regla-Nava JA, et al. (2014) Severe acute respiratory syndrome coronavirus envelope protein ion channel activity promotes virus fitness and pathogenesis. PLoS Pathog 10: e1004077.
14. Nal B, Chan C, Kien F, Siu L, Tse J, et al. (2005) Differential maturation and subcellular localization of severe acute respiratory syndrome coronavirus surface proteins S, M and E. J Gen Virol 86: 1423–1434.
15. Nieto-Torres JL, Dediego ML, Alvarez E, Jimenez-Guardeno JM, Regla-Nava JA, et al. (2011) Subcellular location and topology of severe acute respiratory syndrome coronavirus envelope protein. Virology 415: 69–82.
16. Ruch TR, Machamer CE (2012) A single polar residue and distinct membrane topologies impact the function of the infectious bronchitis coronavirus E protein. PLoS Pathog 8: e1002674.
17. Ye Y, Hogue BG (2007) Role of the coronavirus E viroporin protein transmembrane domain in virus assembly. J Virol 81: 3597–3607.
18. DeDiego ML, Alvarez E, Almazan F, Rejas MT, Lamirande E, et al. (2007) A severe acute respiratory syndrome coronavirus that lacks the E gene is attenuated in vitro and in vivo. J Virol 81: 1701–1713.
19. DeDiego ML, Pewe L, Alvarez E, Rejas MT, Perlman S, et al. (2008) Pathogenicity of severe acute respiratory coronavirus deletion mutants in hACE-2 transgenic mice. Virology 376: 379–389.
20. Netland J, DeDiego ML, Zhao J, Fett C, Alvarez E, et al. (2010) Immunization with an attenuated severe acute respiratory syndrome coronavirus deleted in E protein protects against lethal respiratory disease. Virology 399: 120–128.
21. Fett C, DeDiego ML, Regla-Nava JA, Enjuanes L, Perlman S (2013) Complete protection against severe acute respiratory syndrome coronavirus-mediated lethal respiratory disease in aged mice by immunization with a mouse-adapted virus lacking E protein. J Virol 87: 6551–6559.
22. DeDiego ML, Nieto-Torres JL, Jimenez-Guardeno JM, Regla-Nava JA, Alvarez E, et al. (2011) Severe acute respiratory syndrome coronavirus envelope protein regulates cell stress response and apoptosis. PLoS pathog 7: e1002315.
23. Teoh KT, Siu YL, Chan WL, Schluter MA, Liu CJ, et al. (2010) The SARS coronavirus E protein interacts with PALS1 and alters tight junction formation and epithelial morphogenesis. Mol Biol Cell 21: 3838–3852.
24. Harris BZ, Lim WA (2001) Mechanism and role of PDZ domains in signaling complex assembly. J Cell Sci 114: 3219–3231.
25. Hung AY, Sheng M (2002) PDZ domains: structural modules for protein complex assembly. J Biol Chem 277: 5699–5702.
26. Munz M, Hein J, Biggin PC (2012) The role of flexibility and conformational selection in the binding promiscuity of PDZ domains. PLoS Comput Biol 8: e1002749.
27. Gerek ZN, Keskin O, Ozkan SB (2009) Identification of specificity and promiscuity of PDZ domain interactions through their dynamic behavior. Proteins 77: 796–811.
28. Javier RT, Rice AP (2011) Emerging theme: cellular PDZ proteins as common targets of pathogenic viruses. J Virol 85: 11544–11556.
29. Ponting CP (1997) Evidence for PDZ domains in bacteria, yeast, and plants. Protein Sci 6: 464–468.
30. Spaller MR (2006) Act globally, think locally: systems biology addresses the PDZ domain. ACS Chem Biol 1: 207–210.
31. Roberts A, Deming D, Paddock CD, Cheng A, Yount B, et al. (2007) A mouse-adapted SARS-coronavirus causes disease and mortality in BALB/c mice. PLoS Pathog 3: 23–37.
32. DeDiego ML, Nieto-Torres JL, Regla-Nava JA, Jimenez-Guardeno JM, Fernandez-Delgado R, et al. (2014) Inhibition of NF-kappaB mediated inflammation in severe acute respiratory syndome coronavirus-infected mice increases survival. J Virol 88: 913–924.
33. Regla-Nava JA, Jimenez-Guardeno JM, Nieto-Torres JL, Gallagher TM, Enjuanes L, et al. (2013) The replication of a mouse adapted SARS-CoV in a mouse cell line stably expressing the murine SARS-CoV receptor mACE2 efficiently induces the expression of proinflammatory cytokines. J Virol Methods 193: 639–646.
34. Wohlford-Lenane CL, Meyerholz DK, Perlman S, Zhou H, Tran D, et al. (2009) Rhesus theta-defensin prevents death in a mouse model of severe acute respiratory syndrome coronavirus pulmonary disease. J Virol 83: 11385–11390.
35. Huang da W, Sherman BT, Lempicki RA (2009) Systematic and integrative analysis of large gene lists using DAVID bioinformatics resources. Nat Protoc 4: 44–57.
36. Frieman MB, Chen J, Morrison TE, Whitmore A, Funkhouser W, et al. (2010) SARS-CoV pathogenesis is regulated by a STAT1 dependent but a type I, II and III interferon receptor independent mechanism. PLoS Pathog 6: e1000849.
37. Sheahan T, Morrison TE, Funkhouser W, Uematsu S, Akira S, et al. (2008) MyD88 is required for protection from lethal infection with a mouse-adapted SARS-CoV. PLoS Pathog 4: e1000240.
38. Formstecher E, Aresta S, Collura V, Hamburger A, Meil A, et al. (2005) Protein interaction mapping: a Drosophila case study. Genome Res 15: 376–384.
39. Koroll M, Rathjen FG, Volkmer H (2001) The neural cell recognition molecule neurofascin interacts with syntenin-1 but not with syntenin-2, both of which reveal self-associating activity. J Biol Chem 276: 10646–10654.
40. You J, Dove BK, Enjuanes L, DeDiego ML, Alvarez E, et al. (2005) Subcellular localization of the severe acute respiratory syndrome coronavirus nucleocapsid protein. J Gen Virol 86: 3303–3310.
41. Boukerche H, Su ZZ, Emdad L, Sarkar D, Fisher PB (2007) mda-9/Syntenin regulates the metastatic phenotype in human melanoma cells by activating nuclear factor-kappaB. Cancer Res 67: 1812–1822.
42. Kumar S, Boehm J, Lee JC (2003) p38 MAP kinases: key signalling molecules as therapeutic targets for inflammatory diseases. Nat Rev Drug Discov 2: 717–726.
43. Underwood DC, Osborn RR, Bochnowicz S, Webb EF, Rieman DJ, et al. (2000) SB 239063, a p38 MAPK inhibitor, reduces neutrophilia, inflammatory cytokines, MMP-9, and fibrosis in lung. Am J Physiol Lung Cell Mol Physiol 279: L895–902.
44. Tan YJ, Teng E, Shen S, Tan THP, Goh PY, et al. (2004) A novel severe acute respiratory syndrome coronavirus protein, U274, is transported to the cell surface and undergoes endocytosis. J Virol 78: 6723–6734.
45. Yuan X, Li J, Shan Y, Yang Z, Zhao Z, et al. (2005) Subcellular localization and membrane association of SARS-CoV 3a protein. Virus Res 109: 191–202.
46. Eckmann CR, Neunteufl A, Pfaffstetter L, Jantsch MF (2001) The human but not the Xenopus RNA-editing enzyme ADAR1 has an atypical nuclear localization signal and displays the characteristics of a shuttling protein. Mol Biol Cell 12: 1911–1924.
47. Cuenda A, Rouse J, Doza YN, Meier R, Cohen P, et al. (1995) SB 203580 is a specific inhibitor of a MAP kinase homologue which is stimulated by cellular stresses and interleukin-1. FEBS Lett 364: 229–233.
48. Kumar S, Jiang MS, Adams JL, Lee JC (1999) Pyridinylimidazole compound SB 203580 inhibits the activity but not the activation of p38 mitogen-activated protein kinase. Biochem Biophys Res Commun 263: 825–831.
49. Gardiol D (2012) PDZ-containing proteins as targets in human pathologies. FEBS J 279: 3529.
50. Subbaiah VK, Kranjec C, Thomas M, Banks L (2011) PDZ domains: the building blocks regulating tumorigenesis. Biochem J 439: 195–205.
51. Roberts S, Delury C, Marsh E (2012) The PDZ protein discs-large (DLG): the 'Jekyll and Hyde' of the epithelial polarity proteins. FEBS J 279: 3549–3558.
52. Nicholls JM, Poon LL, Lee KC, Ng WF, Lai ST, et al. (2003) Lung pathology of fatal severe acute respiratory syndrome. Lancet 361: 1773–1778.
53. Rockx B, Baas T, Zornetzer GA, Haagmans B, Sheahan T, et al. (2009) Early upregulation of acute respiratory distress syndrome-associated cytokines promotes lethal disease in an aged-mouse model of severe acute respiratory syndrome coronavirus infection. J Virol 83: 7062–7074.
54. Tang NL, Chan PK, Wong CK, To KF, Wu AK, et al. (2005) Early enhanced expression of interferon-inducible protein-10 (CXCL-10) and other chemokines predicts adverse outcome in severe acute respiratory syndrome. Clin Chem 51: 2333–2340.
55. Gralinski LE, Bankhead A, 3rd, Jeng S, Menachery VD, Proll S, et al. (2013) Mechanisms of severe acute respiratory syndrome coronavirus-induced acute lung injury. MBio 4: e00271–00213.

56. Smits SL, de Lang A, van den Brand JM, Leijten LM, van IWF, et al. (2010) Exacerbated innate host response to SARS-CoV in aged non-human primates. PLoS Pathog 6: e1000756.
57. Peiris JS, Chu CM, Cheng VC, Chan KS, Hung IF, et al. (2003) Clinical progression and viral load in a community outbreak of coronavirus-associated SARS pneumonia: a prospective study. Lancet 361: 1767–1772.
58. Lee CH, Chen RF, Liu JW, Yeh WT, Chang JC, et al. (2004) Altered p38 mitogen-activated protein kinase expression in different leukocytes with increment of immunosuppressive mediators in patients with severe acute respiratory syndrome. J Immunol 172: 7841–7847.
59. Fischer F, Stegen CF, Masters PS, Samsonoff WA (1998) Analysis of constructed E gene mutants of mouse hepatitis virus confirms a pivotal role for E protein in coronavirus assembly. J Virol 72: 7885–7894.
60. Borgeling Y, Schmolke M, Viemann D, Nordhoff C, Roth J, et al. (2013) Inhibition of p38 Mitogen-activated protein kinase impairs influenza virus-induced primary and secondary host gene responses and protects mice from lethal H5N1 infection. J Biol Chem 45: 13–27.
61. Boukerche H, Aissaoui H, Prevost C, Hirbec H, Das SK, et al. (2010) Src kinase activation is mandatory for MDA-9/syntenin-mediated activation of nuclear factor-kappaB. Oncogene 29: 3054–3066.
62. Alvarez E, DeDiego ML, Nieto-Torres JL, Jimenez-Guardeno JM, Marcos-Villar L, et al. (2010) The envelope protein of severe acute respiratory syndrome coronavirus interacts with the non-structural protein 3 and is ubiquitinated. Virology 402: 281–291.
63. Bustin SA, Benes V, Garson JA, Hellemans J, Huggett J, et al. (2009) The MIQE guidelines: minimum information for publication of quantitative real-time PCR experiments. Clin Chem 55: 611–622.
64. Fromont-Racine M, Rain JC, Legrain P (1997) Toward a functional analysis of the yeast genome through exhaustive two-hybrid screens. Nat Genet 16: 277–282.
65. Smyth GK (2004) Linear models and empirical bayes methods for assessing differential expression in microarray experiments. Stat Appl Genet Mol Biol 3: Article3.
66. Benjamini Y, Hochberg Y (1995) Controlling the false discovery rate: a practical and powerful approach to multiple testing. J Roy Stat Soc B 57: 289–300.
67. Reiner A, Yekutieli D, Benjamini Y (2003) Identifying differentially expressed genes using false discovery rate controlling procedures. Bioinformatics 19: 368–375.
68. Almazan F, DeDiego ML, Galan C, Escors D, Alvarez E, et al. (2006) Construction of a SARS-CoV infectious cDNA clone and a replicon to study coronavirus RNA synthesis. J Virol 80: 10900–10906.
69. Snijder EJ, Bredenbeek PJ, Dobbe JC, Thiel V, Ziebuhr J, et al. (2003) Unique and conserved features of genome and proteome of SARS-coronavirus, an early split-off from the coronavirus group 2 lineage. J Mol Biol 331: 991–1004.

Virus Research 194 (2014) 124–137

Contents lists available at ScienceDirect

Virus Research

journal homepage: www.elsevier.com/locate/virusres

Coronavirus virulence genes with main focus on SARS-CoV envelope gene

Marta L. DeDiego[a,1], Jose L. Nieto-Torres[a], Jose M. Jimenez-Guardeño[a], Jose A. Regla-Nava[a], Carlos Castaño-Rodriguez[a], Raul Fernandez-Delgado[a], Fernando Usera[b], Luis Enjuanes[a,*]

[a] Department of Molecular and Cell Biology, National Center of Biotechnology (CNB-CSIC), Campus Universidad Autonoma de Madrid, Madrid, Spain
[b] Department of Biosafety, National Center of Biotechnology (CNB-CSIC), Campus Universidad Autonoma de Madrid, Madrid, Spain

ARTICLE INFO

Article history:
Available online 2 August 2014

Keywords:
Coronavirus
SARS-CoV
MERS-CoV
Innate immunity
Inflammation
Envelope protein

ABSTRACT

Coronavirus (CoV) infection is usually detected by cellular sensors, which trigger the activation of the innate immune system. Nevertheless, CoVs have evolved viral proteins that target different signaling pathways to counteract innate immune responses. Some CoV proteins act as antagonists of interferon (IFN) by inhibiting IFN production or signaling, aspects that are briefly addressed in this review. After CoV infection, potent cytokines relevant in controlling virus infections and priming adaptive immune responses are also generated. However, an uncontrolled induction of these proinflammatory cytokines can lead to pathogenesis and disease severity as described for SARS-CoV and MERS-CoV. The cellular pathways mediated by interferon regulatory factor (IRF)-3 and -7, activating transcription factor (ATF)-2/jun, activator protein (AP)-1, nuclear factor kappa-light-chain-enhancer of activated B cells (NF-κB), and nuclear factor of activated T cells (NF-AT), are the main drivers of the inflammatory response triggered after viral infections, with NF-κB pathway the most frequently activated. Key CoV proteins involved in the regulation of these pathways and the proinflammatory immune response are revisited in this manuscript.

It has been shown that the envelope (E) protein plays a variable role in CoV morphogenesis, depending on the CoV genus, being absolutely essential in some cases (genus α CoVs such as TGEV, and genus β CoVs such as MERS-CoV), but not in others (genus β CoVs such as MHV or SARS-CoV). A comprehensive accumulation of data has shown that the relatively small E protein elicits a strong influence on the interaction of SARS-CoV with the host. In fact, after infection with viruses in which this protein has been deleted, increased cellular stress and unfolded protein responses, apoptosis, and augmented host immune responses were observed. In contrast, the presence of E protein activated a pathogenic inflammatory response that may cause death in animal models and in humans.

The modification or deletion of different motifs within E protein, including the transmembrane domain that harbors an ion channel activity, small sequences within the middle region of the carboxy-terminus of E protein, and its most carboxy-terminal end, which contains a PDZ domain-binding motif (PBM), is sufficient to attenuate the virus. Interestingly, a comprehensive collection of SARS-CoVs in which these motifs have been modified elicited full and long-term protection even in old mice, making those deletion mutants promising vaccine candidates. These data indicate that despite its small size, E protein drastically influences the replication of CoVs and their pathogenicity. Although E protein is not essential for CoV genome replication or subgenomic mRNA synthesis, it affects virus morphogenesis, budding, assembly, intracellular trafficking, and virulence. In fact, E protein is responsible in a significant proportion of the inflammasome activation and the associated inflammation elicited by SARS-CoV in the lung parenchyma. This exacerbated inflammation causes edema accumulation leading to acute respiratory distress syndrome (ARDS) and, frequently, to the death of infected animal models or human patients.

* Corresponding author at: Department of Molecular and Cell Biology, National Center of Biotechnology (CNB-CSIC), Darwin 3, Campus Universidad Autónoma de Madrid, 28049 Madrid, Spain. Tel.: +34 91 585 4555.
E-mail addresses: L.Enjuanes@cnb.csic.es, VirusResearch@cnb.csic.es (L. Enjuanes).
[1] Present address: Center for Vaccine Biology and Immunology, University of Rochester Medical Center, 601 Elmwood Avenue, 14642 Rochester, NY, USA.

http://dx.doi.org/10.1016/j.virusres.2014.07.024
0168-1702/

Introduction

An overview of the sensors detecting virus infection is presented first, followed by a description of the mechanisms elicited by CoV proteins to counteract innate immune responses. Some CoV proteins act as antagonists of interferon (IFN) production, whereas others inhibit IFN signaling. In addition, after CoV infection, a collection of potent cytokines relevant in controlling virus infections and priming adaptive immune responses are generated (Le Bon and Tough, 2002).

Virus pathogenesis is frequently associated with an exacerbated induction of proinflammatory cytokines that is mainly driven by the activation of at least one of the following five pathways: IRF-3 and -7, ATF-2/jun, jun/fos (AP-1), NF-κB and NF-AT. Among them, the NF-κB pathway is the most frequently activated (Hatada et al., 2000; Mogensen and Paludan, 2001). NF-κB is a heterogeneous collection of dimers, composed of various combinations of members of the Rel family, which in eukaryotes include p50 (NF-κB1), p52 (NF-κB2), Rel (c-Rel), p65 (RelA) and RelB. An exacerbated immune response and a weak IFN response have been associated with virulent CoVs such as SARS-CoV and MERS-CoV (Baas et al., 2008; Lau et al., 2013; Smits et al., 2010).

The main focus of this review is the analysis of the role of the CoV envelope (E) protein in virus pathogenesis. E protein contains several active motifs despite its small size, between 76 and 109 amino acids depending on the CoV. The modification or deletion of E protein in different CoVs has led to viruses with different phenotypes and unique alteration of virus–host interactions, such as the induction of stress and unfolded protein responses, or changes in cellular ion concentrations due to the ion channel activity of E protein. All these activities have high impact on CoV pathogenesis (DeDiego et al., 2011; Nieto-Torres et al., 2014).

E protein PDZ domain-binding motif (PBM), which during SARS-CoV infection could potentially target more than 400 cellular PDZ domains present within cellular proteins, confers to E protein virus pathogenicity modulating properties. Interestingly, deletion or modification of E protein PBM and internal regions within the carboxy-terminus of E protein most frequently results in attenuated CoVs that are good vaccine candidates (Jimenez-Guardeño et al., 2014; Regla-Nava et al., 2014). In addition, the identification of signaling pathways, such as NF-κB-mediated signaling, responsible for CoV pathogenicity has led to the selection of antivirals that considerably increase the survival of infected animal models (DeDiego et al., 2014).

Coronavirus proteins inhibiting type I interferon production

IFNs are potent cytokines relevant in the control of virus infections and in the priming of adaptive immune responses (Le Bon and Tough, 2002). Treatment with type I IFN inhibits CoV growth in tissue culture and in animal models such as cynomolgus macaques and mice (Barnard et al., 2006; Dahl et al., 2004; Fuchizaki et al., 2003; Haagmans et al., 2004; Kumaki et al., 2011; Mahlakoiv et al., 2012; Sainz et al., 2004; Stroher et al., 2004; Zheng et al., 2004). To circumvent the inhibition of virus replication, many viruses, including CoVs, encode viral proteins inhibiting IFN production or signaling (Table 1). However, most of the studies describing the IFN antagonist activity of coronavirus-encoded proteins have been conducted in cells transiently expressing the viral proteins. Therefore, additional analyses in the context of the virus infection are required.

Type I IFN production is controlled by two major pathways dependent on RNA helicases or toll-like receptors (TLRs) (Arpaia and Barton, 2011; Rathinam and Fitzgerald, 2011; Sen, 2001) (Fig. 1). RNA helicases containing the cytoplasmic CARD domain, retinoic acid-inducible gene 1 (RIG-I) and melanoma differentiation-associated protein 5 (MDA5), sense pathogen-associated molecular patterns (PAMPs) in the cell cytoplasm. On the other hand, toll-like receptors detect PAMPs in the cell surface and in endosomal compartments.

The RNA helicases-dependent cytoplasmic IFN induction pathways use the adaptor molecule mitochondrial antiviral signaling protein (MAVS) (Fig. 1). MAVS promotes the activation of a complex comprising the proteins TNF receptor-associated factor 3 (TRAF-3), TRAF family member-associated NF-κB activator (TANK), TANK-binding kinase 1 (TBK-1) and IkappaB kinase ε (IKKε). Active TBK1 and IKKε directly phosphorylate the transcription factors IRF-3 and IRF-7, promoting homodimerization (Sharma et al., 2003). Then, the IRF-3 and IRF-7 dimers are imported into the nucleus, leading to IRF-3 and IRF-7-dependent transcription. In addition, MAVS triggers the NF-κB pathway through IKKα and IKKβ activation (Kawai and Akira, 2007).

The TLRs-dependent IFN induction pathways use the adaptor molecules TIR-domain-containing adapter-inducing IFN-β (TRIF) and myeloid-differentiation primary response 88 (MyD88) (Fig. 1) (Kawai and Akira, 2007). TRIF-dependent pathway leads to the activation of IRF-3 and -7, and NF-κB. The activation of IRF-3 and IRF-7 is mediated by the phosphorylation of these factors by TBK-1 and IKKε, which promote their activation, as described above. TRIF also mediates NF-κB activation through the activation of IKKα and IKKβ. MyD88-mediated pathway activates the transcription factors NF-κB, AP-1 and ATF-2/jun, through the activation of mitogen-activated protein kinases (MAPKs) (Herlaar and Brown, 1999; Whitmarsh and Davis, 1996). NF-κB is also activated in this pathway through IKKs (Kawai and Akira, 2007).

IRF-3 and IRF-7, with the help of other transcription factors like NF-κB, and AP-1, initiate the transcription of IFN-β and selected IFN-α genes. IFN-α and IFN-β proteins are then secreted from the cell and can act in either an autocrine or a paracrine fashion to amplify the IFN response (Fig. 1).

CoVs have devised a number of cell type-specific strategies to inhibit type I IFN production (Table 1; Fig. 1). These viruses encode a 2′-*O*-methylase (non-structural protein nsp16) that creates a 5′-cap structure analogous to the cellular mRNAs on the viral mRNAs, thereby escaping detection by MDA5 (Zust et al., 2011). MERS-CoV accessory protein 4a is a dsRNA binding protein that blocks IFN induction by suppressing PACT-induced activation of RIG-I and MDA5 (Niemeyer et al., 2013; Siu et al., 2014). The ORF4b encoded accessory proteins of MERS-CoV and two related bat CoVs localize to the cell nucleus and inhibit type I IFN production and NF-κB signaling pathway (Matthews et al., 2014). Interestingly, a MERS-CoV lacking 4a and 4b proteins grew about 10-fold lower than the parental virus in IFN competent infected-cells (Almazan et al., 2013). However, the specific effect of 4a and 4b proteins IFN antagonistic activity in virus growth and virulence still needs to be determined. SARS-CoV membrane (M) protein impairs the formation of TRAF3/TANK/TBK1/IKKε complex, inhibiting IFN-β production (Siu et al., 2009). SARS-CoV structural nucleocapsid (N) protein blocks IFN-β production after induction with Sendai virus and polyI:C, but not upstream of components such as RIG-I, MDA5, MAVS, IKKε, TBK1 or TRIF, indicating that N protein acts after these signaling mediators (Kopecky-Bromberg et al., 2007; Lu et al., 2011). SARS-CoV papain-like protease (PLP) domain of nsp3 inhibits RIG-I and TLR3-dependent IFN-β production, being this activity independent of the deubiquitinating and protease activities (Clementz et al., 2010), and most probably mediated by the interaction of PLP domain with the protein stimulator of IFN genes (STING), which is a protein that stimulates phosphorylation of IRF3 by the kinase TBK1 (Sun et al., 2012). The inhibition of IFN production has also been described for nsp3 PLP2 of HCoV-NL63 (Clementz et al., 2010; Sun et al., 2012), MHV (Wang et al., 2011; Zheng et al., 2008), and for the PLP domain of MERS-CoV, which blocks IFN

Table 1
Coronavirus proteins affecting innate immune responses.

Protein	CoV	Immune function	References
Nsp1	SARS-CoV	Antagonizes type I IFN production and signaling by inducing host mRNAs shut off, promoting the degradation of host mRNAs and preventing phosphorylation of STAT1	Wathelet et al. (2007), Kamitani et al. (2009), Huang et al. (2011), Tanaka et al. (2012)
		Upregulates CCL5, CXCL10, and CCL3 in human lung epithelial cells via the activation of NF-κB	Law et al. (2007)
Nsp3	SARS-CoV	Prevents IFN production by blocking IRF3 phosphorylation, most probably by interacting with STING	Devaraj et al. (2007), Frieman et al. (2009), Sun et al. (2012), Clementz et al. (2010)
	MHV	Antagonizes type I IFN	Zheng et al. (2008), Wang et al. (2011)
	MERS-CoV	Antagonizes type I IFN	Yang et al. (2014)
Nsp7	SARS-CoV	Antagonizes type I IFN	Frieman et al. (2009)
Nsp15	SARS-CoV	Antagonizes type I IFN	Frieman et al. (2009)
S	SARS-CoV	Induces the expression of IL6, IL8, CXCL10 and TNF through NF-κB activation in macrophages	Wang et al. (2007), Dosch et al. (2009)
M	SARS-CoV	Blocks IFN-β production by impairing the formation of TRAF3–TANK–TBK1/IKKε complex	Siu et al. (2009)
N	SARS-CoV	Antagonizes type I IFN production by blocking IRF-3 phosphorylation	Lu et al. (2011), Kopecky-Bromberg et al. (2007)
		Activates NF-κB and upregulates the expression of IL-6	Liao et al. (2005), Zhang et al. (2007)
		Activates AP-1	He et al. (2003)
		Induces the expression of IL8 via AP-1 activation	Chang et al. (2004)
3a	SARS-CoV	Downregulates the expression of the type I IFN receptor (IFNAR), leading to a blockade on type I IFN signaling	Minakshi et al. (2009)
		Increases NF-κB and JNK activity and upregulates TNF, IL8 and CCL5 production	Obitsu et al. (2009), Kanzawa et al. (2006)
3b	SARS-CoV	Antagonizes type I IFN production by blocking IRF-3 phosphorylation. Inhibits IFN signaling	Kopecky-Bromberg et al. (2007), Freundt et al. (2009)
		Induces transcriptional activity of AP-1, through activation of JNK and ERK pathways, leading to CCL2 upregulation	Varshney and Lal (2011), Varshney et al. (2012)
6	SARS-CoV	Antagonizes type I IFN production by blocking IRF-3 phosphorylation	Kopecky-Bromberg et al. (2007), Frieman et al. (2009)
		Inhibits IFN signaling by blocking the nuclear translocation of the transcription factor STAT1	Frieman et al. (2007)
7a	SARS-CoV	Activates NF-κB and upregulates the expression of the proinflammatory mediators IL8 and CCL5	Kanzawa et al. (2006)
Nsp3	NL63	Antagonizes type I IFN	Clementz et al. (2010)
Nsp1	MHV	Antagonizes type I IFN	Zust et al. (2007)
N	MHV	Acts as an interferon antagonist and prevents RNA degradation by inhibiting RNaseL activity	Ye et al. (2007)
2	MHV	Antagonizes type I IFN signaling and prevents activation of the cellular endoribonuclease RNase L	Zhao et al. (2011, 2012)
5a	MHV	Antagonizes type I IFN	Koetzner et al. (2010)
4a	MERS-CoV	Block interferon induction at the level of MDA5 activation presumably by direct interaction with double-stranded RNA	Niemeyer et al. (2013)
4b	MERS-CoV	Antagonizes type I IFN	Matthews et al. (2014)
7	TGEV	Reduces the expression of genes involved in the immune response, the interferon response, and inflammation	Cruz et al. (2013)
7a	FIPV	Antagonizes type I IFN	Dedeurwaerder et al. (2013)

production by inhibiting IRF3 phosphorylation and translocation into the nucleus (Yang et al., 2014). SARS-CoV nsp7 and nsp15 block IFN-β production through an unidentified mechanism (Frieman et al., 2009). SARS-CoV proteins N, 3b and 6 prevent IFN production by blocking IRF-3 phosphorylation (Devaraj et al., 2007; Freundt et al., 2009; Frieman et al., 2009; Kopecky-Bromberg et al., 2007).

TGEV protein 7 inhibits IFN production as it has been shown that a TGEV lacking protein 7 grew with similar titers than the wt virus, but induced expression of genes involved in the immune response and interferon response to a higher extent than the wt virus (Cruz et al., 2013). In addition, protein 7 prevents host translational shut off and RNA degradation through the interaction with protein phosphatase 1 (PP1) (Fig. 1) (Cruz et al., 2011).

CoV proteins inhibiting type I IFN signaling

Type I IFN signaling starts with its binding to IFNAR receptors at the cell surface, which leads to the activation of the JAK–STAT pathway (Samuel, 2001) (Fig. 2). The members of the Janus Kinase (JAK) family JAK-1 and protein tyrosine kinase 2 (TYK-2) phosphorylate the signal transducer and activators of transcription (STATs) which become activated. Phosphorylated STAT1 and STAT2 recruit IRF-9, to form the IFN stimulated gene factor 3 (ISGF3) complex. The ISGF3 heterotrimer translocates to the nucleus and triggers the transcription of IFN-stimulated genes (ISGs) that will drive the antiviral response.

Coronaviruses have developed strategies to interfere with IFN signaling at different levels. SARS-CoV affects the initial stages of the cascade by down regulating the expression of IFNAR, and inhibiting the translocation of STAT1 to the nucleus, through proteins 3a and 6, respectively (Frieman et al., 2007; Kopecky-Bromberg et al., 2007; Minakshi et al., 2009). In addition, SARS-CoV nsp1 affects STAT1 phosphorylation and induces a host translational shut off promoting the degradation of cellular mRNAs, further affecting IFN antiviral signaling (Huang et al., 2011; Jauregui et al., 2013; Kamitani et al., 2009; Tanaka et al., 2012; Wathelet et al., 2007; Zust et al., 2007). SARS-CoV protein 3b inhibits IFN signaling without inhibiting STAT1 phosphorylation (Kopecky-Bromberg et al., 2007). SARS-CoV nsp1 antagonizes type I IFN production and signaling by inducing host mRNAs shut off, promoting the degradation of cellular mRNAs and preventing phosphorylation of STAT1 (Huang et al., 2011; Kamitani et al., 2009; Tanaka et al., 2012; Wathelet et al., 2007; Zust et al., 2007). Inhibition of downstream effectors of IFN signaling pathway (ISGs) has also been described during coronavirus infection. MHV N and ns2 as well as SARS-CoV N proteins prevent the activation of RNase L, blocking viral RNA degradation (Fig. 1) (Ye et al., 2007; Zhao et al., 2012).

Other CoV proteins confer IFN-resistance, however, whether they inhibit IFN production or signaling is unknown. MHV nsp1 is

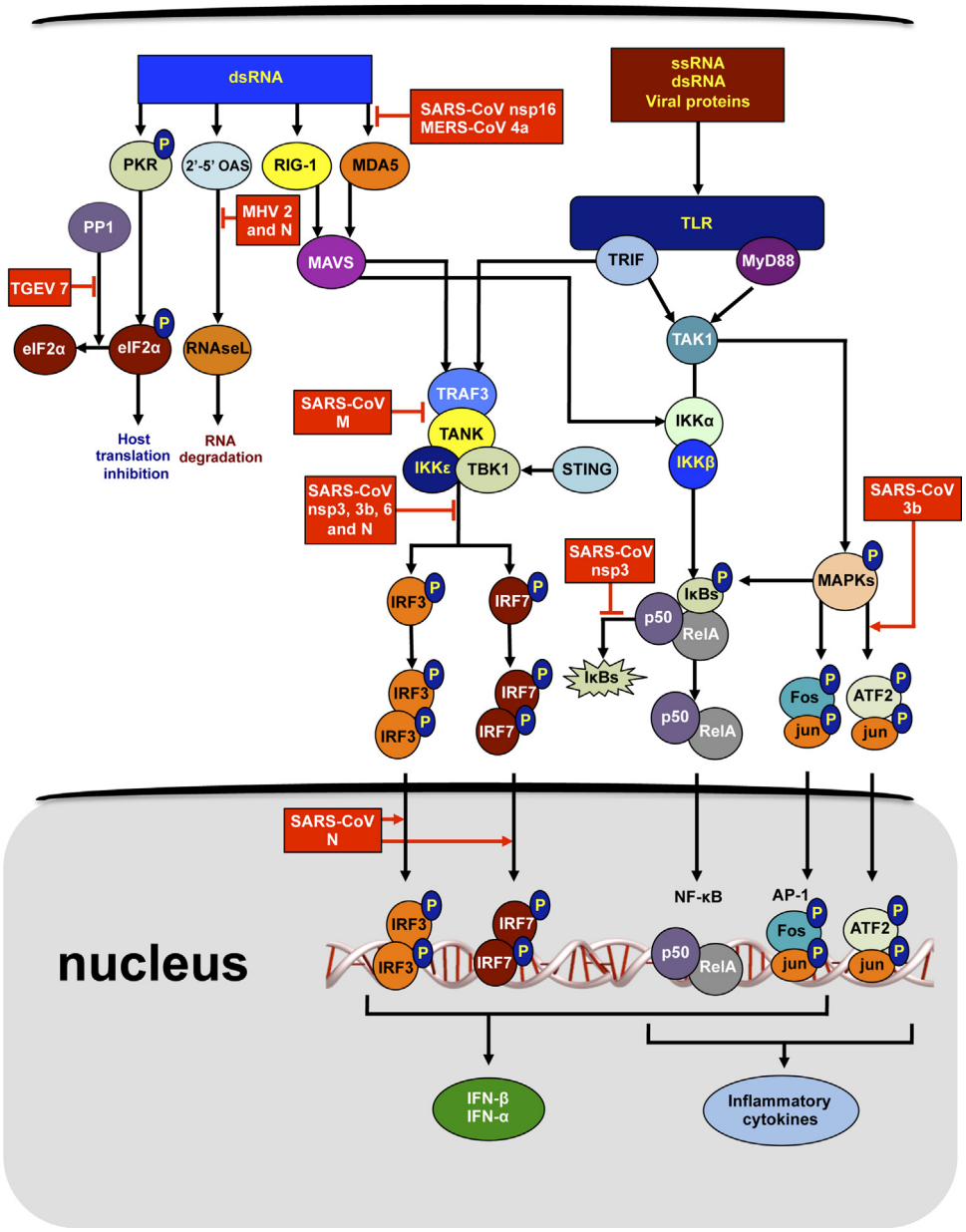

Fig. 1. Effect of coronavirus proteins on cellular signaling pathways associated with the innate immune response. PAMPs such as ssRNA, dsRNA, or viral proteins, trigger the activation of transcription factors leading to proinflammatory cytokine and type I IFN induction. PAMPs activate the PKR, leading to eIF2α phosphorylation and host translation inhibition, and 2′–5′ OAS, leading to RNase L triggering and RNA degradation. The activation of RIG-I and MDA-5 triggers the activation of IRF-3, IRF-7 and NF-κB through MAVS. In addition, TLRs activate the MyD88 and TRIF-dependent pathways, activating the transcription factors IRF-3, IRF-7, NF-κB, and AP-1. The steps inhibited or promoted by CoV proteins are indicated in red boxes. Beside these proteins, other proteins that inhibit or promote the IFN signaling and production and inflammatory cytokine expression, through an identified mechanism, are indicated in Table 1.

an efficient interferon antagonist in mice, as replication and spread of an nsp1 mutant virus were restored almost to wild-type levels in type I IFN receptor-deficient animals (Zust et al., 2007). MHV protein 5a or its homologues from related genus β coronaviruses, confer IFN-resistance to the virus (Koetzner et al., 2010). FIPV 7a protein protects the virus from the antiviral state induced by IFN, but it needs the presence of ORF3 encoded proteins to exert its antagonistic function (Dedeurwaerder et al., 2013).

Coronavirus proteins affecting the induction of proinflammatory signals

Proinflammatory cytokines and chemokines are a part of the necessary initial immune response to pathogens. However, an exacerbated immune response has been associated with the high virulence of SARS-CoV (Baas et al., 2008; Smits et al., 2010). Expression levels of proinflammatory cytokines, such as IL-1, IL-2, IL-6, and IL-8, and chemokines such as CXCL10 and CCL2 are elevated in peripheral blood and lungs of SARS patients, and associated with disease severity (Cameron et al., 2007; Chien et al., 2006; Jiang et al., 2005; Tang et al., 2005; Wong et al., 2004).

The most important signal transduction pathways activated by viruses leading to the expression of proinflammatory cytokines are mediated by factors IRF-3 and -7, ATF-2/jun, AP-1, NF-κB and NF-AT (Mogensen and Paludan, 2001). The activation of these factors has been briefly described above. NF-AT is constitutively present in the cytoplasm in a latent phosphorylated form. Increasing levels of cytoplasmic calcium activate the calmodulin-dependent phosphatase calcineurin that activates NF-AT by dephosphorylation (Crabtree, 1999).

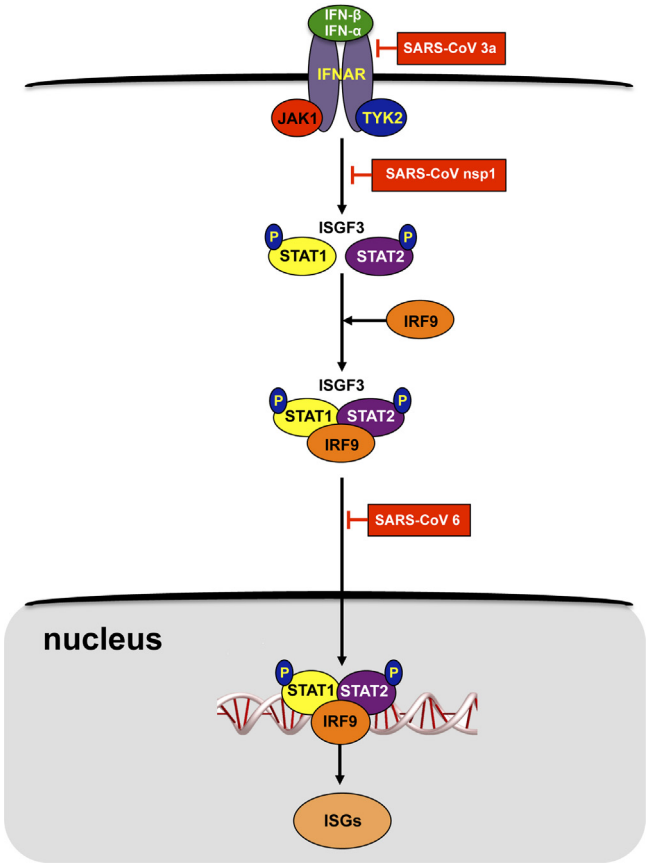

Fig. 2. Effect of coronavirus proteins on type I IFN signaling. The IFN-α and IFN-β proteins are secreted from the cell and amplify the IFN response activating the ISGF3 complex formed by STAT1, STAT2 and IRF-9, leading to the expression of the interferon-stimulated genes (ISG). The steps inhibited or promoted by CoV proteins are indicated in red boxes.

Activation of NF-κB is a hallmark of most infections including viral infections, leading to pathological outcomes. In fact, SARS-CoV-infected-aged macaques develop a more severe pathology, with an increase in differential expression of genes associated with inflammation, with NF-κB as a central player, and a reduction in the expression of type I IFN-β (Smits et al., 2010).

Several CoV-encoded proteins interfere with the production of inflammatory mediators. SARS-CoV nsp1 plays an important role in CCL5, CXCL10, and CCL3 upregulation in human lung epithelial cells via the activation of NF-κB (Law et al., 2007). The nsp3 PLP domain disrupts NF-κB signaling, most probably by inhibiting the degradation of phosphorylated IκBα, which diminishes the induction of proinflammatory cytokines, leading to virus attenuation (Frieman et al., 2009). The structural SARS-CoV N protein activates NF-κB-driven transcription and upregulates the expression of IL-6 by facilitating the translocation of NF-κB from cytosol to nucleus (Liao et al., 2005; Zhang et al., 2007). In addition, the expression of N protein, but not the M protein, activates the AP-1 pathway (He et al., 2003). Similarly, SARS-CoV S protein induces the expression of TNF, IL6, IL8, and CXCL10 through NF-κB activation in macrophages (Dosch et al., 2009; Wang et al., 2007), and the expression of IL-8 via AP-1 in lung epithelial cells (Chang et al., 2004). The accessory protein 3a upregulates mRNA and fibrinogen levels in lung epithelial cells (Tan et al., 2005). In addition, 3a protein increases NF-κB and JNK activities and upregulates the TNF, IL8 and CCL5 production in murine macrophages and lung cell lines (Kanzawa et al., 2006; Obitsu et al., 2009). Similarly, SARS-CoV 7a protein also activates NF-κB and upregulates the expression of the proinflammatory mediators IL8 and CCL5 in a lung cell line (Kanzawa et al., 2006). The accessory protein 3b induces transcriptional activity of AP-1, through activation of JNK and ERK pathways, leading to CCL2 upregulation in a human hepatoma cell line (Varshney et al., 2012; Varshney and Lal, 2011). The presence of protein 7 in TGEV reduced the expression of proinflammatory genes, compared to a virus lacking this protein, indicating that TGEV protein 7 inhibits proinflammatory cytokine expression (Cruz et al., 2013).

In summary, several structural and non-structural SARS-CoV proteins affect the expression of proinflammatory signals, most frequently by modulating the NF-κB pathway and, to a lower extent, by affecting AP-1 signaling.

Virulence of recombinant coronaviruses lacking specific viral proteins

The generation of viral mutants lacking specific proteins or domains, or containing point mutations is an invaluable tool to study the contribution of a particular protein to the virulence of the virus. These systems offer advantages in comparison to over expression systems because in this case the studies are performed in the context of infection, in the presence of the other viral proteins, in a scenario in which the only difference is the presence of a single mutated or deleted viral protein. In contrast, the over-expression of specific proteins frequently yields overwhelming amounts of protein that may result toxic to the virus–host cell interaction required for a balanced virus replication.

To study the role of SARS-CoV group specific protein 6 during viral infection two approaches have been used. In one of them, SARS-CoV protein 6 has been expressed in the context of an attenuated mouse hepatitis virus (MHV). This recombinant virus grew more rapidly and to higher titers in cell culture and in the murine central nervous system than the control virus, leading to increased mortality in mice (Hussain et al., 2008; Netland et al., 2008; Pewe et al., 2005). In the other approach, a SARS-CoV lacking protein 6 was engineered. The SARS-CoV deletion mutant grew with lower titers but essentially maintained its virulence in transgenic mice expressing the human receptor for SARS-CoV hACE-2, as it killed 100% of the mice with a delay of 1 day (Zhao et al., 2009). These data indicated that SARS-CoV protein 6, in the context of the infection by the virus of which it is a structural component (Huang et al., 2007), does not seem to have a high influence on SARS-CoV virulence.

Infection of immune suppressed hamsters with recombinant SARS-CoV viruses bearing disruptions in the gene 7 coding region showed no significant changes in replication, tissue tropism, morbidity, or mortality suggesting that the 7a and 7b proteins are not essential for virus pathogenesis (Schaecher et al., 2008). Deletion of each of genes 3a, 6, 7a, and 7b from SARS-CoV did not affect virus growth in mice to a high extent (Yount et al., 2005). A SARS-CoV lacking the group specific genes 6, 7a, 7b, 8a, 8b, and 9b grew similarly to the parental virus and induced a slightly diminished weight loss and a delay in the time of death in transgenic mice expressing hACE-2, which are highly susceptible to the disease (DeDiego et al., 2008). Although further analysis using other animal models should be performed, these data suggested that the contribution of proteins 6, 7a, 7b, 8a, 8b and 9b to the virulence of SARS-CoV is limited.

A recombinant MHV with a deletion in nsp1 (a homolog of SARS-CoV nsp1) grew normally in tissue culture, but was severely attenuated in vivo. Interestingly, replication and spread of the nsp1 deletion mutant virus was restored almost to wild-type levels in type I IFN receptor-deficient mice, indicating that nsp1 interferes efficiently with the type I IFN system in vivo (Zust et al., 2007). Similarly, a mutant virus lacking a conserved domain of MHV nsp1, showed no growth defects in cell culture, but was highly attenuated in vivo (Lei et al., 2013).

Deletion of group specific proteins ns2, HE, 4ab, and 5a from MHV led to attenuated viruses in the natural host, the mice (de

Haan et al., 2002). A MHV mutant missing protein ns2 was unable to replicate in the liver or to induce hepatitis in wild-type mice, but was highly pathogenic in RNase L deficient mice, indicating that protein ns2 increases the pathogenicity of the virus by an RNase L dependent mechanism (Zhao et al., 2011, 2012).

Genus α CoVs such as TGEV missing gene 7, or FIPV lacking at the same time genes 3abc and 7ab showed modification of the inflammatory response and virulence. TGEV 7 protein deletion mutant increased proinflammatory responses and acute tissue damage after infection, leading to a more pathogenic virus (Cruz et al., 2011, 2013). In contrast, FIPV deletion mutant was attenuated in cats and induced protection against feline infectious peritonitis (Haijema et al., 2004). In this case the effect of FIPV proteins 3abc or 7b deletion on its virulence prevailed over the deletion of FIPV protein 7a, which is the protein equivalent to TGEV protein 7.

Requirement of coronavirus E protein in coronavirus replication and morphogenesis

CoV E protein is multifunctional, affecting several steps of the viral cycle. SARS-CoV can infect mouse brain, whereas in the absence of E protein this tissue tropism has not been observed (DeDiego et al., 2008). However, in this case, the involvement of E protein in entry is not necessarily required to explain the observed difference, as the restriction could operate at a later step. E protein expression is not involved in CoV genome replication, as both SARS-CoV with and without E protein synthesize the same amounts of genomic and subgenomic mRNAs (DeDiego et al., 2011).

The requirement of E protein in CoV morphogenesis has been under debate. In fact, E protein seems necessary for virus like particle formation using some experimental systems (Ho et al., 2004; Mortola and Roy, 2004) but not others (Huang et al., 2004). Different CoVs have shown variable requirements for E protein during morphogenesis, resulting in three different phenotypes. One of them is shown by genus α coronaviruses, like TGEV, and also by genus β MERS-CoV, which in the absence of E protein are replication-competent propagation-defective viruses (Almazan et al., 2013; Curtis et al., 2002; Ortego et al., 2002, 2007). Both TGEV and MERS-CoV missing E protein were propagated in packaging cells by providing E protein in trans, leading to high virus titers. In this case, the level of recovered viruses was proportional to the amount of E protein provided by the packaging cell line (Ortego et al., 2002). A second phenotype of CoVs missing E protein, is represented by genus β MHV, with a reduction of virus titers higher than 1000-fold (Kuo and Masters, 2003). The third phenotype was observed for genus β SARS-CoV, in which deletion mutants missing E protein only reduced their replication between 20 and 200-fold, leading to viruses that replicate both in cell culture and in vivo, and display an attenuated phenotype (DeDiego et al., 2007, 2008, 2014; Enjuanes et al., 2008). The assembled viral particles could be the base for safe vaccine candidates, once additional safety guards have been incorporated at a distal position in the CoV genome.

Whereas the deletion of E protein in different CoVs may affect virus production to different extents, it is clear that for CoVs such as SARS-CoV, E protein is not essential, since SARS-CoV missing E protein can produce virus titers close to 1×10^6 pfu per ml or per gram of tissue, in Vero E6 cells or in lungs of infected BALB/c mice, respectively, in a reproducible fashion (DeDiego et al., 2007, 2008; Fett et al., 2013). Nevertheless, the presence of E protein optimizes SARS-CoV yields. The contribution of E protein to CoV morphogenesis could be mediated through its interaction with other virus structural proteins within the virus envelope (M, 3a, 3b, 6, 7b, and 9b) (Arndt et al., 2010; Boscarino et al., 2008; Chen et al., 2009; Neuman et al., 2008; Pan et al., 2008; von Brunn et al., 2007). E protein has three potential palmitoylation residues in its carboxy-terminus. The palmitoylation of these sites is essential for the formation of vesicles including E protein that contribute to CoV morphogenesis (Boscarino et al., 2008; Lopez et al., 2008). Also, the extent of E protein palmitoylation affects its interaction with M protein (Boscarino et al., 2008).

The presence of E protein in CoVs particles is very low in general (around 20 molecules per virion) (Godet et al., 1992), although this could vary depending on the species (Liu and Inglis, 1991). Interestingly, E protein is highly abundant in the cytoplasm of infected cells, what may be due to its role in virus transport and morphogenesis (Ortego et al., 2007). A role in intracellular trafficking has been described for CoV E protein. The hydrophobic domain of IBV E protein seems important for the forward trafficking of cargo to the plasma membrane. In fact, E protein alters the host secretory pathway to the apparent advantage of the virus, increasing the efficacy of infectious virus release (Ruch and Machamer, 2011, 2012). Therefore E protein seems to play a role in virus egress.

E protein oligomerizes and forms ion channels that influence the electrochemical balance in some subcellular compartments of host cells, as described below.

Effect of SARS-CoV E gene deletion on viral pathogenesis

To study the effect of SARS-CoV E protein on viral pathogenesis, a SARS-CoV lacking the full-length E gene (rSARS-CoV-ΔE) was engineered. The deleted virus was attenuated in golden Syrian hamsters, and in transgenic mice expressing the SARS-CoV receptor hACE-2 (DeDiego et al., 2007, 2008). In addition, a mouse adapted SARS-CoV lacking E gene (rSARS-CoV-MA15-ΔE) was attenuated in conventional young and aged BALB/c mice (DeDiego et al., 2014; Fett et al., 2013), indicating that the expression of E gene increases virus pathogenicity. rSARS-CoV-ΔE titers decreased *in vivo*, in comparison to parental virus titers. However, intrinsic properties of E protein, and not just a decrease in virus titers, may increase the viral pathogenesis. In fact, viral mutants lacking E protein ion channel activity and PBM, grow similarly to the wt virus, and nevertheless are attenuated (see below) (Jimenez-Guardeño et al., 2014; Nieto-Torres et al., 2014).

To identify mechanisms leading to rSARS-CoV-ΔE attenuation, gene expression was compared in cells infected with the attenuated ΔE virus and in wt virus-infected cells. Stress response genes were preferentially upregulated during infection in the absence of E gene. Interestingly, expression of E protein in trans reduced the stress response in cells infected with rSARS-CoV-ΔE or with respiratory syncytial virus, or in cells treated with drugs, such as tunicamycin and thapsigargin, that elicit cell stress by different mechanisms (DeDiego et al., 2011). In addition, SARS-CoV E protein down-regulated the signaling pathway inositol-requiring enzyme 1 (IRE-1) of the unfolded protein response, and limited cell apoptosis. The expression of proinflammatory cytokines was lower in rSARS-CoV-ΔE-infected cells compared to rSARS-CoV-infected ones, suggesting that the increase in stress responses and the reduction of inflammation in the absence of the E gene contributed to the attenuation of rSARS-CoV-ΔE (DeDiego et al., 2011). These results were confirmed in mice. A reduced expression of proinflammatory cytokines, decreased number of neutrophils in lung infiltrates, and diminished lung pathology were observed in SARS-CoV-MA15-ΔE-infected mice, compared to the wt virus-infected ones (DeDiego et al., 2014), indicating that lung inflammation contributes to SARS-CoV virulence. Furthermore, infection with rSARS-CoV-ΔE resulted in a decreased activation of the transcription factor NF-κB. Importantly, treatment with NF-κB inhibitors, led to a reduction in inflammation in both SARS-CoV-infected cultured cells and mice, and significantly diminished lung pathology. These changes increased mice survival after SARS-CoV infection (DeDiego et al., 2014). These data indicated that NF-κB activation is a major contributor to the inflammation induced after SARS-CoV

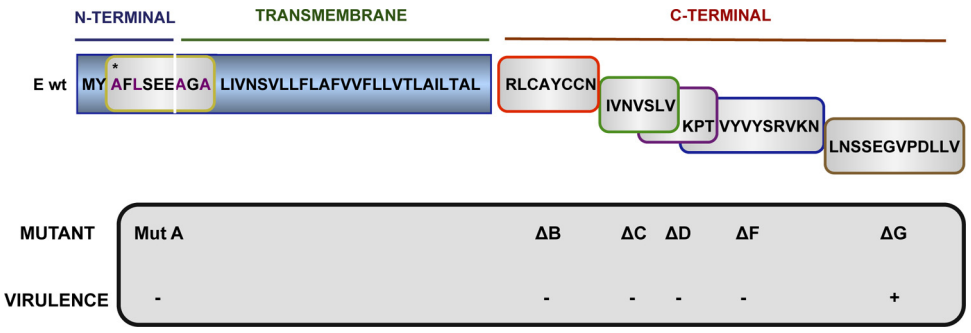

Fig. 3. Engineered rSARS-CoVs-MA15 with point mutations and deletions in E gene. The organization of E protein is shown. E protein sequence is divided into three domains: the amino terminal (N-terminal), the transmembrane and the carboxy-terminal (C-terminal). The figure illustrates the deletions and point mutations engineered within E protein. The asterisk (*) indicates mutations in the residues S3A, V5L, T9A, T11A. Gray box at the bottom indicates mutant virulence: (+) indicates a virulent phenotype and (−) indicates an attenuated phenotype.

infection, and that drugs inhibiting NF-κB activation are promising antivirals to treat SARS-CoV induced disease, and most probably the inflammation caused by other pathogenic coronaviruses, such as MERS-CoV.

Interestingly, hamsters immunized with the attenuated rSARS-CoV-ΔE developed high serum-neutralizing antibody titers, and were protected after the challenge with homologous (Urbani) and heterologous (GD03) SARS-CoV strains (Lamirande et al., 2008). In addition, SARS-CoV missing E protein partially protected transgenic mice against challenge with virulent SARS-CoVs (Netland et al., 2010). Moreover, rSARS-CoV-MA15-ΔE totally protected young and old (up to 2 years) BALB/c mice against the virulent mouse adapted virus (Fett et al., 2013), by inducing high humoral and cellular immune responses. These data indicated that the viruses lacking E gene are promising live attenuated vaccine candidates.

SARS-CoV E protein amino and carboxy-terminus modification and virus attenuation

To identify SARS-CoV E protein domains and host responses that contribute to rSARS-CoV-MA15 virulence, several mutant viruses (rSARS-CoV-MA15-E*) containing amino acid substitutions in the amino-terminal domain, or small deletions covering the carboxy-terminus region of E protein, were constructed using a mouse adapted virus (Fig. 3) (Regla-Nava et al., 2014). Interestingly, amino acid substitutions in the amino-terminus, or deletion of central domains within the carboxy-terminal region of E protein led to viruses attenuated in mice, indicating that these domains are essential for SARS-CoV pathogenesis (Regla-Nava et al., 2014). Intranasal infection of mice with these attenuated mutants resulted in minimal lung damage and cellular infiltration compared to mock-infected mice, similar to what happened with rSARS-CoV-MA15-ΔE. The lower pathology induced by the attenuated SARS-CoV-MA15 without E protein, or by the deletion mutants of this protein, including small deletions in the carboxy-terminus, was associated with a significant reduction in the expression of proinflammatory cytokines in the lungs (Regla-Nava et al., 2014). Interestingly, a reduction in the number of neutrophils, which contribute to severe inflammation, and an increase in the number of T cells, which contribute to virus clearance (Zhao and Perlman, 2010), were found in the lungs of mice infected with the attenuated mutants compared to those infected with the virulent ones (Regla-Nava et al., 2014). These results indicate that increased levels of lung inflammation, exacerbated inflammatory cytokine expression, high levels of neutrophils, and decreased levels of T cells in the lungs, contributed to SARS-CoV virulence. Interestingly, the attenuated viruses missing E protein domains, completely protected mice against challenge with lethal virus, as happened with full-length E protein deleted virus, indicating that the viruses with small deletions in the carboxy terminus may also be the basis for promising vaccines.

SARS-CoV E protein PDZ binding domain and SARS-CoV virulence

A functional PDZ domain-binding motif (PBM) has been identified at the carboxy-terminus end of E protein using in vitro and in vivo approaches (Fig. 4) (Jimenez-Guardeño et al., 2014; Teoh et al., 2010). PDZ motifs are abundant modules involved in protein–protein interaction, which consist of 80–90 amino acids that recognize a specific peptide sequence (PBM) found in the extreme C-termini of target proteins (Hung and Sheng, 2002). In the human genome, more than 900 PDZ domains are found in over 400 proteins (Spaller, 2006). It has been described that proteins containing PDZ domains can be involved in cellular processes of relevance for viruses, such as cell–cell junctions, cellular polarity and signal transduction pathways (Javier and Rice, 2011). According to this data, several viruses, such as influenza A virus (Jackson et al., 2008), tick-borne encephalitis virus (TBEV) (Melik et al., 2012), and human papillomavirus (HPV) (Kiyono et al., 1997) encode proteins with PBMs that target cellular PDZ motifs carrying proteins during infection. Through these interactions, cellular pathways influence viral replication, dissemination in the host, and pathogenesis (Javier and Rice, 2011).

To identify SARS-CoV E protein cellular targets containing PDZ domains, yeast two-hybrid based studies were undertaken. The protein associated with Lin Seven 1 (PALS1), a tight junction-associated protein, was the first PDZ protein identified as a target of E protein PBM, and this interaction was confirmed using co-immunoprecipitation studies in mammalian cells (Teoh et al., 2010). PALS1 is a key component of the complex that controls polarity establishment and tight junction formation in epithelia. Studies using Vero E6 cells infected with SARS-CoV showed that E protein relocalized PALS1 to the endoplasmic reticulum-Golgi intermediate compartment (ERGIC) and Golgi region. In addition, the ectopic expression of E protein in MDCK epithelial cells led to delayed tight junction and polarity establishment. The results suggested that hijacking of PALS1 by E protein could play an important role in the pathology observed in SARS-CoV patients by altering lung epithelia integrity (Teoh et al., 2010).

We have recently shown that SARS-CoV E protein PBM is a molecular determinant of virulence (Jimenez-Guardeño et al., 2014). In this study, recombinant viruses missing E protein PBM were generated, leading to a fully attenuated phenotype in mice. Infection of mice with the recombinant viruses lacking the E protein PBM led to a decrease in the deleterious, exacerbated immune response triggered during SARS-CoV infection and a lower expression of inflammatory cytokines, without significantly affecting

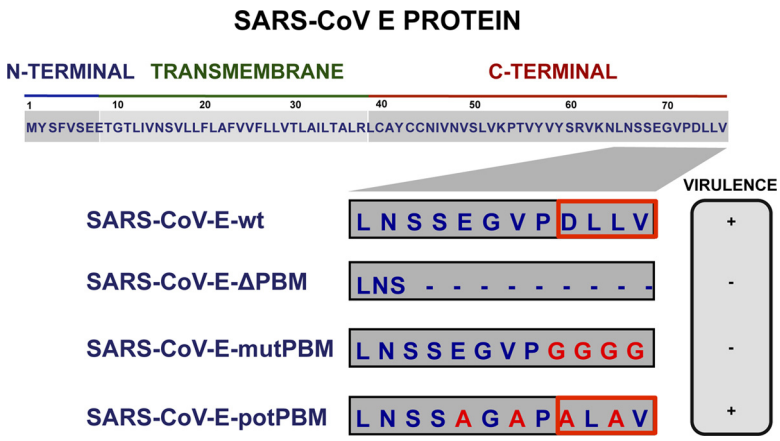

Fig. 4. Recombinant SARS-CoVs with E protein PBM truncated or mutated by reverse genetics. SARS-CoV E protein sequence and its corresponding domains are shown at the top. Below, sequences corresponding to the end of E protein are shown in boxes for the different virus mutants. SARS-CoV-E-wt, wild type sequence. In SARS-CoV-E-ΔPBM and SARS-CoV-E-mutPBM virus mutants, E protein PBM was eliminated by the introduction of deletions or point mutations, reducing or keeping the full protein length, respectively. In SARS-CoV-E-potPBM, four amino acids of E protein were replaced by alanine, to generate a new potential PBM. Red boxes highlight PBMs within E protein. Gray box on the right indicates the virulence of the mutants: (+) indicates a virulent phenotype and (−) indicates an attenuated phenotype.

virus titers in mice lungs. To understand the molecular basis of this attenuation, host factors interacting with E protein PBM were identified using proteomic studies. A specific interaction of this motif with the cellular protein syntenin, a relevant scaffolding protein that participates in the activation of p38 mitogen-activated protein kinase (MAPK), was found (Jimenez-Guardeño et al., 2014). Interestingly, activated p38 MAPK, which mediates the expression of proinflammatory cytokines (Kumar et al., 2003; Underwood et al., 2000), was specifically reduced in mice infected with viruses missing E protein PBM, as compared with viruses containing this motif. These results highlight a novel mechanism of modulation of SARS-CoV pathogenesis by E protein. The interference with this signaling pathway will allow the development of therapies to reduce the exacerbated immune response triggered during SARS-CoV infection. Interestingly, bioinformatics analysis showed that other human CoV E proteins, such as that from MERS-CoV, HCoV-229E, HCoV-NL63, HCoV-OC43 and HCoV-HKU1 also encode a PBM in its carboxy-terminus. Therefore, the antiviral strategies described above to prevent SARS-CoV, most probably also apply to the reduction of the pathogenesis induced by other human CoVs. Furthermore, the generation of human attenuated coronaviruses by deleting E protein PBM could be the basis for the development of recombinant vaccines, as those described by deleting the whole SARS-CoV E protein or internal domains of this protein (Fett et al., 2013; Lamirande et al., 2008; Netland et al., 2010; Regla-Nava et al., 2014).

Ion channel activity of SARS-CoV E, 3a and 8a proteins and virulence

A wide range of animal viruses encode hydrophobic proteins that oligomerize in host cell membranes leading to structures with ion channel (IC) activity. These proteins, named viroporins, may influence viral replication and assembly, as well as virus particle entry and release from infected cells. Viroporins have a high impact on relevant host cell physiological processes (Nieva et al., 2012). Therefore, these proteins are useful targets to counteract viral infections.

Most of the RNA viruses encoding these proteins only have one viroporin in their genome (Castaño-Rodriguez et al., 2014). However, SARS-CoV encodes three proteins with IC activity: E, 3a and 8a, which indicates that SARS-CoV is the RNA virus expressing the highest number of viroporins known up to date.

The IC activity of E protein is the most extensively characterized among the three SARS-CoV viroporins using structural, functional and physiological assays. E protein has a single transmembrane domain topology and its monomers oligomerize in a pentameric ion conductive pore, as determined by linear dichroism and NMR studies (Parthasarathy et al., 2008; Pervushin et al., 2009; Torres et al., 2006).

The first functional evidence of SARS-CoV E protein acting as a viroporin was provided after its expression in bacteria, where E protein oligomerized and modified membrane permeability (Liao et al., 2004, 2006). Direct measurement of E protein IC activity was first reported using synthetic peptides representing full-length SARS-CoV E protein or its N-terminal 40 amino acids, including the transmembrane domain, in artificial lipid membranes (Wilson et al., 2004). This IC activity was confirmed, and mutations that suppressed this function were identified (Torres et al., 2007; Verdia-Baguena et al., 2012). In addition, compounds that inhibit the SARS-CoV E protein ion conductivity were described, although their efficacy in the context of a viral infection was not reported (Pervushin et al., 2009). Initially, it was considered that SARS-CoV E protein formed an IC with an enhanced selectivity for monovalent cations over monovalent anions, and for Na^+ over K^+ ions (Wilson et al., 2004). However, recent studies showed that the selectivity of SARS-CoV E protein IC was dependent on the charge of the lipid membranes in which the pore was reconstituted, which strongly suggested that the lipid head-groups are an integral component of the channel pore (Fig. 5) (Verdia-Baguena et al., 2012, 2013). This novel finding highlights the relevance of the lipid membrane composition in the SARS-CoV ion channel structure and activity.

The influence of SARS-CoV E protein IC activity in cell ion homeostasis is highly dependent on its subcellular localization. After SARS-CoV infection, E protein mainly accumulates in the ERGIC region of the infected cells, where virus morphogenesis and budding take place (Nieto-Torres et al., 2011). In artificial membranes, mimicking the ERGIC membrane composition, where E protein is mainly inserted, E protein showed a slight selectivity for cations over anions, with no preference for a specific cation (Verdia-Baguena et al., 2012). It has been suggested that E protein could also be located at the cell plasma membrane, which could influence cell depolarization (Liao et al., 2006; Pervushin et al., 2009). Efforts done by our group to identify the presence of E protein in the cell surface, or to detect IC activity in the cell surface by using patch-clamp technology showed the absence of this activity in the plasma membrane (Nieto-Torres et al., 2011). Accordingly, an additional study indicated that E protein does not form ion channels at the cell surface (Ji et al., 2009). Therefore, we have concluded that E protein

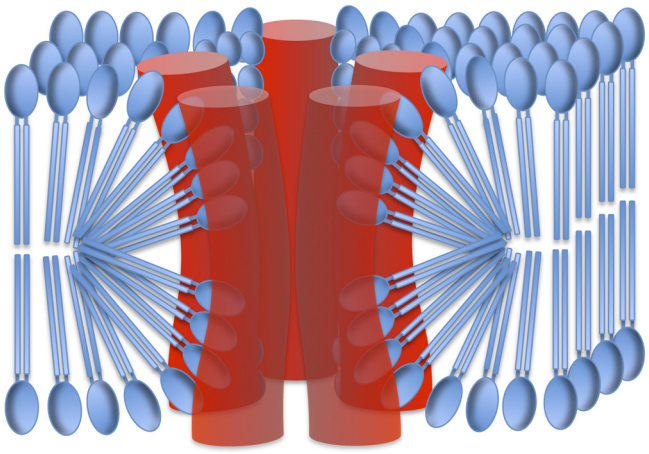

Fig. 5. Structure of SARS-CoV E protein proteolipidic ion channel. Phospholipids are represented in blue, and E protein monomers are shown as red cylinders. Note that lipid head groups (blue ellipses) also face the ion channel lumen.

ion channel activity is only shown in the intracellular structures, where E protein has been located (Nieto-Torres et al., 2011; Ruch and Machamer, 2012).

Ionic imbalances within cells can interfere with innate immunity and affect virus pathogenesis. Interestingly, disruption of ion gradients within the endoplasmic reticulum and Golgi apparatus by viral proteins with IC activity delayed protein transport preventing MHC molecules from reaching the plasma membrane (Cornell et al., 2007; de Jong et al., 2006). Recently, it has been described that ionic imbalances controlled by viroporins are sensed by the inflammasome, which triggers the activation of key pro-inflammatory cytokines such as IL-1β, a major determinant of disease progression (Ichinohe et al., 2010; Ito et al., 2012; McAuley et al., 2013; Triantafilou et al., 2013).

The introduction of point mutations that inhibited SARS-CoV E protein IC activity led to attenuated viruses, without significantly affecting virus production (Nieto-Torres et al., 2014). Furthermore, viruses in which E protein IC activity was suppressed quickly evolved by incorporating mutations that restored ion conductivity and a virulent phenotype (Nieto-Torres et al., 2014). After infection with viruses displaying E protein IC, increased damage within pulmonary epithelia and edema accumulation within lung airways (Fig. 6), the ultimate determinant of ARDS, was observed, compared to mice infected with viruses lacking E protein IC (Nieto-Torres et al., 2014). Enhanced liquid levels within lung airways avoid proper oxygen exchange leading to severe hypoxemia and eventually to death (Matthay and Zemans, 2011). Ionic balances play a central role in controlling liquid amounts present within air spaces. Lung epithelia create an osmotic gradient between the interior of the airways and the interstitial spaces. To resolve edema, a vectorial transport of Na^+ ions driven by epithelial sodium channels (ENaC) and Na^+/K^+ ATPase is established (Hollenhorst et al., 2011). Viruses displaying E protein ion channel activity caused an increased damage within pulmonary epithelia, which correlated with edema accumulation (Fig. 6) (Nieto-Torres et al., 2014). In addition, SARS-CoV E protein decreased the levels and activity of ENaC in lung epithelial cells, via the activation of distinct PKC isoforms, decreasing both ENaC exocytosis and endocytosis rates (Ji et al., 2009). These data indicated that the activation of PKC by SARS-CoV E protein, which may lead to decreased levels and activity of ENaC at the apical surface of lung epithelial cells, and the IC activity of E protein contribute to the lung edema observed after SARS-CoV infection.

Pulmonary epithelial damage is associated with a deleterious exacerbated inflammatory response triggered in the lungs after SARS-CoV infection. Evaluation of key inflammatory cytokines involved in epithelial damage and edema accumulation revealed that IL-1β, TNF and IL-6 amounts were increased in the lung airways of the mice infected with the viruses displaying E protein ion conductivity compared to the infection with the mutants lacking IC activity (Nieto-Torres et al., 2014). IL-1β is one of the most important proinflammatory cytokines involved in ARDS disease (Meduri et al., 1995; Pugin et al., 1996). IL-1β activation occurs when the inflammasome complex is stimulated by viral proteins with ion channel activity (Ichinohe et al., 2010; Ito et al., 2012; McAuley et al., 2013; Triantafilou et al., 2013). The inflammatory response elicited by IL-1β is accompanied by an increase in TNF, and both signals are amplified by the accumulation of IL-6, which are key events during ARDS progression after SARS-CoV infection (Tisoncik et al., 2012; Wang et al., 2005). We believe that this exacerbated deleterious response is a causal agent of the observed damage in the lung parenchyma of animals infected with the viruses displaying ion channel activity.

In summary, inhibition of SARS-CoV E protein IC activity, without significantly affecting virus growth, led to a virus inducing an attenuated pathogenesis. Attenuation correlated with a moderate inflammatory response leading to less epithelial damage and edema accumulation. These findings may have implications for the other viroporins encoded by SARS-CoV and, most importantly, for the identification of therapies to protect against highly pathogenic CoVs such as SARS-CoV and MERS-CoV, or other viruses encoding proteins with IC activity. For example, hexamethylene amiloride (HMA), an inhibitor of the HIV-1 Vpu protein ion channel activity, also inhibited SARS-CoV, HCoV-229E and MHV E protein ion channel conductance (Pervushin et al., 2009; Wilson et al., 2006) and, as a consequence, suppressed the replication of the wt HCoV-229E and MHV (Wilson et al., 2006). Therefore, this ion channel inhibitor may be an efficient antiviral compound to control the replication several members of the *Coronaviridae* family.

8a and 3a proteins are SARS-CoV viroporins as well, but their ion channel activities are much less studied than that of E protein. A 29 nt deletion occurred in ORF8 when the virus first infected human beings, splitting ORF8 into ORF8a and ORF8b. ORF8a encodes a 39-amino-acid-long polypeptide whose first 35 residues are identical to the N-terminal part of the ORF8 primary product (Oostra et al., 2007). ORF8a shows IC activity when reconstituted into artificial lipid bilayers (Chen et al., 2011), but this activity has not been identified in cells. A role for 8a protein in virus replication and in vitro apoptosis through a mitochondrial-dependent pathway has been suggested (Chen et al., 2007) but the experiments were performed with a HA tagged variant of 8a protein and some of the results are at variance with those previously reported (Oostra et al., 2007). A variant of SARS-CoV with a deletion of 415 nt resulting in the loss of ORF8, was isolated toward the end of the SARS epidemic and, in spite of this deletion, some of the infected patients died, suggesting that ORF8 is not essential for virus pathogenicity (Chiu et al., 2005).

3a protein is a 274 aa SARS-specific structural component of the virus with three transmembrane domains (TMDs) in its N-terminus. 3a protein forms a potassium ion channel after tetramerization via inter-monomer disulfide bridges (Cys133) (Lu et al., 2006). The IC activity of 3a protein has been characterized by the self-oligomerization of synthetic peptides corresponding to each of the three TMDs into artificial lipid bilayers. Only TMD2 and TMD3 peptides restored IC activity (Chien et al., 2013). However, additional studies are required to characterize the IC selectivity of the reconstituted viroporin. SARS-CoV 3a protein influences virus pathogenicity (McBride and Fielding, 2012). The implication of 3a protein in viral replication seems limited as deletion mutants missing this protein only show a modest reduction in virus replication (Castaño-Rodriguez et al., 2014; Yount et al., 2005). Nevertheless, the role of 3a protein in virus budding and release still warrants further investigation due to conflicting data (Akerstrom et al., 2007;

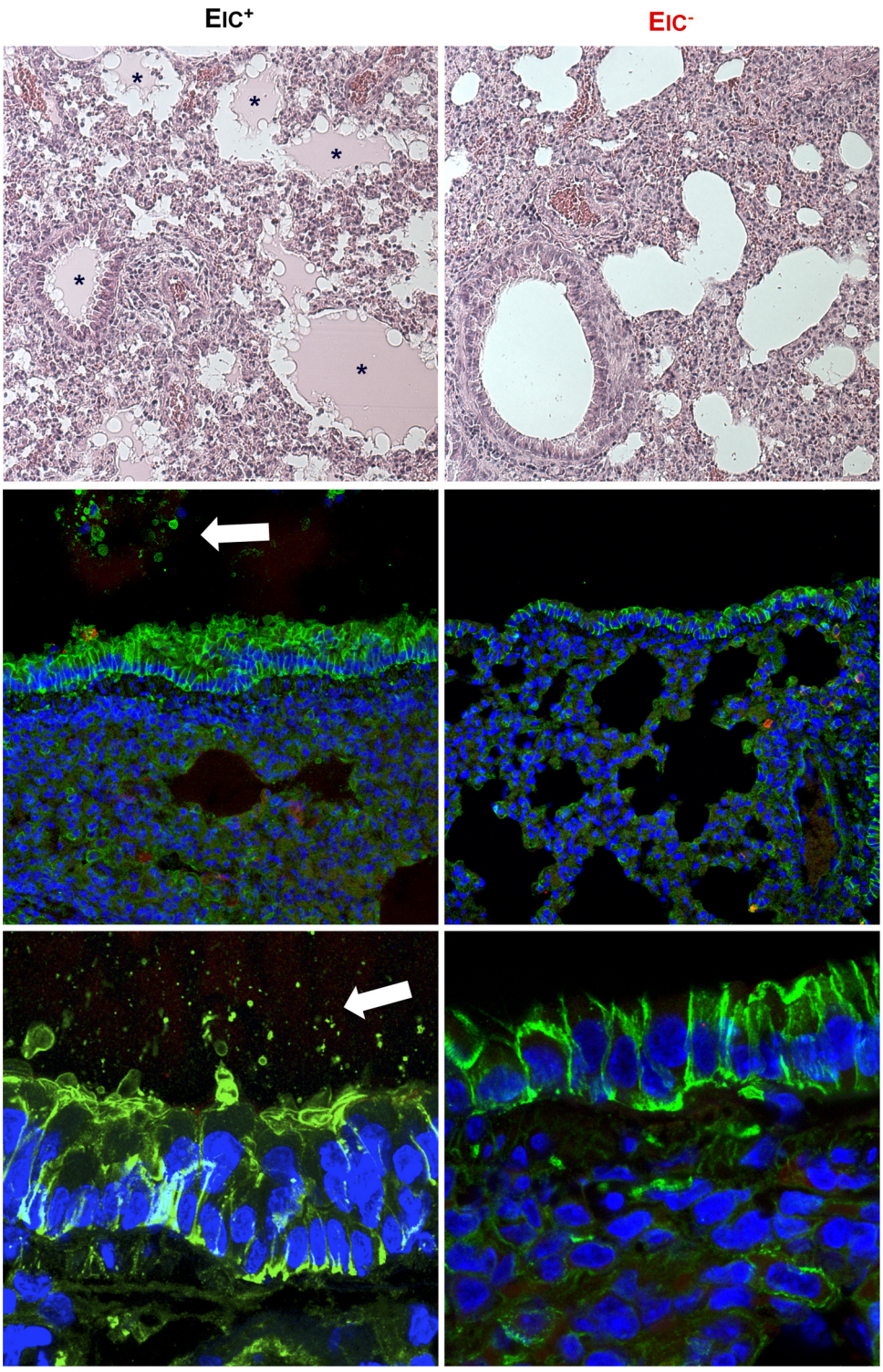

Fig. 6. Effect of SARS-CoV E protein ion channel activity in lung pathology. The lung histopathology in mice infected with a virus displaying (EIC$^+$) or lacking (EIC$^-$) E protein ion channel activity at 4 days post infection (dpi) is shown at the top. Lung sections were analyzed by hematoxylin and eosin staining at an original magnification of 20×. Airspaces where edema was accumulated are indicated with asterisks. Immunofluorescence staining of lung sections, and detail of bronchiolar epithelia at 4 dpi, at a magnification of 40× and 190×, respectively is shown at the bottom. Lung epithelia was labeled using an anti Na^+/K^+ ATPase antibody (green) and SARS-CoV infection was tracked with an anti-N protein antibody (red). Nuclei are shown in blue. Desquamated epithelial cells and cell debris are observed in lung airways after EIC$^+$ virus infection (white arrows).

Lu et al., 2006). Also, the influence of 3a protein in virus virulence requires additional studies. SARS-CoV infection induces an uncontrolled proinflammatory response leading to ARDS and respiratory failure (Smits et al., 2010, 2011). One of the most relevant functions of 3a protein in SARS-CoV virulence is the induction of a pro-inflammatory response (Kanzawa et al., 2006; Obitsu et al., 2009), similarly to what has been shown for SARS-CoV E protein (Nieto-Torres et al., 2014), and for other viroporins (Ichinohe et al., 2010; Ito et al., 2012; McAuley et al., 2013; Triantafilou et al., 2013). These data suggest that 3a protein and its IC activity could also be

responsible for the enhancement of a proinflammatory response after SARS-CoV infection. Protein 3a also induces apoptosis (Lu et al., 2006). However, this activity was elicited by a 3a protein mutant deficient in oligomerization, therefore the IC activity of 3a protein does not seem responsible for the induction of apoptosis.

Conclusions

The effect of CoVs proteins on cellular signaling pathways, in particular those affected by E protein, has been revised. It has been shown that deletion of full-length E protein or modification of active motifs present in this protein have been essential to achieve two aims, the engineering of vaccine candidates that provide full-protection against homologous and heterologous CoVs, and the identification of drugs that interfere with exacerbated pathways responsible for disease severity. These drugs increase experimental animals survival and, therefore, are good candidates as antivirals in human health.

Acknowledgments

This work was supported by grants from the Ministry of Science and Innovation of Spain (BIO2010-16705), the European Community's Seventh Framework Program (FP7/2007–2013) under the project "EMPERIE" EC Grant Agreement number 223498, and U.S. National Institutes of Health (NIH) (2P01AI060699-06A1) and CRIP-HHSN266200700010C projects. MLD received a contract from the project "EMPERIE" EC Grant Agreement number 223498. JAR and CCR received fellowships from the Fundacion La Caixa. We thank Marga Gonzalez for technical assistance.

References

Akerstrom, S., Mirazimi, A., Tan, Y.J., 2007. Inhibition of SARS-CoV replication cycle by small interference RNAs silencing specific SARS proteins, 7a/7b, 3a/3b and S. Antivir. Res. 73, 219–227.

Almazan, F., DeDiego, M.L., Sola, I., Zuniga, S., Nieto-Torres, J.L., Marquez-Jurado, S., Andres, G., Enjuanes, L., 2013. Engineering a replication-competent, propagation-defective Middle East respiratory syndrome coronavirus as a vaccine candidate. mBio 4, e00650-00613.

Arndt, A.L., Larson, B.J., Hogue, B.G., 2010. A conserved domain in the coronavirus membrane protein tail is important for virus assembly. J. Virol. 84, 11418–11428.

Arpaia, N., Barton, G.M., 2011. Toll-like receptors: key players in antiviral immunity. Curr. Opin. Virol. 1, 447–454.

Baas, T., Roberts, A., Teal, T.H., Vogel, L., Chen, J., Tumpey, T.M., Katze, M.G., Subbarao, K., 2008. Genomic analysis reveals age-dependent innate immune responses to severe acute respiratory syndrome coronavirus. J. Virol. 82, 9465–9476.

Barnard, D.L., Day, C.W., Bailey, K., Heiner, M., Montgomery, R., Lauridsen, L., Chan, P.K., Sidwell, R.W., 2006. Evaluation of immunomodulators, interferons and known in vitro SARS-coV inhibitors for inhibition of SARS-coV replication in BALB/c mice. Antivir. Chem. Chemother. 17, 275–284.

Boscarino, J.A., Logan, H.L., Lacny, J.J., Gallagher, T.M., 2008. Envelope protein palmitoylations are crucial for murine coronavirus assembly. J. Virol. 82, 2989–2999.

Cameron, M.J., Ran, L., Xu, L., Danesh, A., Bermejo-Martin, J.F., Cameron, C.M., Muller, M.P., Gold, W.L., Richardson, S.E., Poutanen, S.M., Willey, B.M., DeVries, M.E., Fang, Y., Seneviratne, C., Bosinger, S.E., Persad, D., Wilkinson, P., Greller, L.D., Somogyi, R., Humar, A., Keshavjee, S., Louie, M., Loeb, M.B., Brunton, J., McGeer, A.J., Kelvin, D.J., 2007. Interferon-mediated immunopathological events are associated with atypical innate and adaptive immune responses in patients with severe acute respiratory syndrome. J. Virol. 81, 8692–8706.

Castaño-Rodriguez, C., Nieto-Torres, J.L., DeDiego, M.L., Jimenez-Guardeno, J.M., Regla-Nava, J.A., Fernandez-Delgado, R., Torres, J., Enjuanes, L., 2014. Relevance of SARS-CoV 3a ion channel activity in virulence (unpublished results).

Chang, Y.J., Liu, C.Y., Chiang, B.L., Chao, Y.C., Chen, C.C., 2004. Induction of IL-8 release in lung cells via activator protein-1 by recombinant baculovirus displaying severe acute respiratory syndrome-coronavirus spike proteins: identification of two functional regions. J. Immunol. 173, 7602–7614.

Chen, C.C., Kruger, J., Sramala, I., Hsu, H.J., Henklein, P., Chen, Y.M., Fischer, W.B., 2011. ORF8a of SARS-CoV forms an ion channel: experiments and molecular dynamics simulations. Biochim. Biophys. Acta 1808, 572–579.

Chen, C.Y., Ping, Y.H., Lee, H.C., Chen, K.H., Lee, Y.M., Chan, Y.J., Lien, T.C., Jap, T.S., Lin, C.H., Kao, L.S., Chen, Y.M., 2007. Open reading frame 8a of the human severe acute respiratory syndrome coronavirus not only promotes viral replication but also induces apoptosis. J. Infect. Dis. 196, 405–415.

Chen, S.C., Lo, S.Y., Ma, H.C., Li, H.C., 2009. Expression and membrane integration of SARS-CoV E protein and its interaction with M protein. Virus Genes 38, 365–371.

Chien, J.Y., Hsueh, P.R., Cheng, W.C., Yu, C.J., Yang, P.C., 2006. Temporal changes in cytokine/chemokine profiles and pulmonary involvement in severe acute respiratory syndrome. Respirology 11, 715–722.

Chien, T.H., Chiang, Y.L., Chen, C.P., Henklein, P., Hanel, K., Hwang, I.S., Willbold, D., Fischer, W.B., 2013. Assembling an ion channel: ORF 3a from SARS-CoV. Biopolymers 99, 628–635.

Chiu, R.W., Chim, S.S., Tong, Y.K., Fung, K.S., Chan, P.K., Zhao, G.P., Lo, Y.M., 2005. Tracing SARS-coronavirus variant with large genomic deletion. Emerg. Infect. Dis. 11, 168–170.

Clementz, M.A., Chen, Z., Banach, B.S., Wang, Y., Sun, L., Ratia, K., Baez-Santos, Y.M., Wang, J., Takayama, J., Ghosh, A.K., Li, K., Mesecar, A.D., Baker, S.C., 2010. Deubiquitinating and interferon antagonism activities of coronavirus papain-like proteases. J. Virol. 84, 4619–4629.

Cornell, C.T., Kiosses, W.B., Harkins, S., Whitton, J.L., 2007. Coxsackievirus B3 proteins directionally complement each other to downregulate surface major histocompatibility complex class I. J. Virol. 81, 6785–6797.

Crabtree, G.R., 1999. Generic signals and specific outcomes: signaling through Ca^{2+}, calcineurin, and NF-AT. Cell 96, 611–614.

Cruz, J.L.G., Becares, M., Sola, I., Oliveros, J.C., Enjuanes, L., Zuniga, S., 2013. Alphacoronavirus protein 7 modulates host innate immune response. J. Virol. 87, 9754–9767.

Cruz, J.L.G., Sola, I., Becares, M., Alberca, B., Plana, J., Enjuanes, L., Zuniga, S., 2011. Coronavirus gene 7 counteracts host defenses and modulates virus virulence. PLoS Pathog. 7, e1002090.

Curtis, K.M., Yount, B., Baric, R.S., 2002. Heterologous gene expression from transmissible gastroenteritis virus replicon particles. J. Virol. 76, 1422–1434.

Dahl, H., Linde, A., Strannegard, O., 2004. In vitro inhibition of SARS virus replication by human interferons. Scand. J. Infect. Dis. 36, 829–831.

de Haan, C.A.M., Masters, P.S., Shen, S., Weiss, S., Rottier, P.J.M., 2002. The group-specific murine coronavirus genes are not essential, but their deletion, by reverse genetics, is attenuating in the natural host. Virology 296, 177–189.

de Jong, A.S., Visch, H.J., de Mattia, F., van Dommelen, M.M., Swarts, H.G., Luyten, T., Callewaert, G., Melchers, W.J., Willems, P.H., van Kuppeveld, F.J., 2006. The coxsackievirus 2B protein increases efflux of ions from the endoplasmic reticulum and Golgi, thereby inhibiting protein trafficking through the Golgi. J. Biol. Chem. 281, 14144–14150.

Dedeurwaerder, A., Olyslaegers, D.A., Desmarets, L.M., Roukaerts, I.D., Theuns, S., Nauwynck, H.J., 2013. The ORF7-encoded accessory protein 7a of feline infectious peritonitis virus as a counteragent against interferon-alpha induced antiviral response. J. Gen. Virol., http://dx.doi.org/10.1099/vir.1090.058743-058740.

DeDiego, M.L., Alvarez, E., Almazan, F., Rejas, M.T., Lamirande, E., Roberts, A., Shieh, W.J., Zaki, S.R., Subbarao, K., Enjuanes, L., 2007. A severe acute respiratory syndrome coronavirus that lacks the E gene is attenuated in vitro and in vivo. J. Virol. 81, 1701–1713.

DeDiego, M.L., Nieto-Torres, J.L., Jimenez-Guardeno, J.M., Regla-Nava, J.A., Alvarez, E., Oliveros, J.C., Zhao, J., Fett, C., Perlman, S., Enjuanes, L., 2011. Severe acute respiratory syndrome coronavirus envelope protein regulates cell stress response and apoptosis. PLoS Pathog. 7, e1002315.

DeDiego, M.L., Nieto-Torres, J.L., Regla-Nava, J.A., Jimenez-Guardeno, J.M., Fernandez-Delgado, R., Fett, C., Castano-Rodriguez, C., Perlman, S., Enjuanes, L., 2014. Inhibition of NF-kappaB mediated inflammation in severe acute respiratory syndome coronavirus-infected mice increases survival. J. Virol. 88, 913–924.

DeDiego, M.L., Pewe, L., Alvarez, E., Rejas, M.T., Perlman, S., Enjuanes, L., 2008. Pathogenicity of severe acute respiratory coronavirus deletion mutants in hACE-2 transgenic mice. Virology 376, 379–389.

Devaraj, S.G., Wang, N., Chen, Z., Chen, Z., Tseng, M., Barretto, N., Lin, R., Peters, C.J., Tseng, C.T., Baker, S.C., Li, K., 2007. Regulation of IRF-3-dependent innate immunity by the papain-like protease domain of the severe acute respiratory syndrome coronavirus. J. Biol. Chem. 282, 32208–32221.

Dosch, S.F., Mahajan, S.D., Collins, A.R., 2009. SARS coronavirus spike protein-induced innate immune response occurs via activation of the NF-kappaB pathway in human monocyte macrophages in vitro. Virus Res. 142, 19–27.

Enjuanes, L., DeDiego, M.L., Alvarez, E., Deming, D., Sheahan, T., Baric, R., 2008. Vaccines to prevent severe acute respiratory syndrome coronavirus-induced disease. Virus Res. 133, 45–62.

Fett, C., DeDiego, M.L., Regla-Nava, J.A., Enjuanes, L., Perlman, S., 2013. Complete protection against severe acute respiratory syndrome coronavirus-mediated lethal respiratory disease in aged mice by immunization with a mouse-adapted virus lacking E protein. J. Virol. 87, 6551–6559.

Freundt, E.C., Yu, L., Park, E., Lenardo, M.J., Xu, X.N., 2009. Molecular determinants for subcellular localization of the severe acute respiratory syndrome coronavirus open reading frame 3b protein. J. Virol. 83, 6631–6640.

Frieman, M., Ratia, K., Johnston, R.E., Mesecar, A.D., Baric, R.S., 2009. Severe acute respiratory syndrome coronavirus papain-like protease ubiquitin-like domain and catalytic domain regulate antagonism of IRF3 and NF-kappaB signaling. J. Virol. 83, 6689–6705.

Frieman, M., Yount, B., Heise, M., Kopecky-Bromberg, S.A., Palese, P., Baric, R.S., 2007. Severe acute respiratory syndrome coronavirus ORF6 antagonizes STAT1 function by sequestering nuclear import factors on the rough endoplasmic reticulum/Golgi membrane. J. Virol. 81, 9812–9824.

Fuchizaki, U., Kaneko, S., Nakamoto, Y., Sugiyama, Y., Imagawa, K., Kikuchi, M., Kobayashi, K., 2003. Synergistic antiviral effect of a combination of mouse interferon-alpha and interferon-gamma on mouse hepatitis virus. J. Med. Virol. 69, 188–194.

Godet, M., L'Haridon, R., Vautherot, J.F., Laude, H., 1992. TGEV coronavirus ORF4 encodes a membrane protein that is incorporated into virions. Virology 188, 666–675.
Haagmans, B.L., Kuiken, T., Martina, B.E., Fouchier, R.A., Rimmelzwaan, G.F., van Amerongen, G., van Riel, D., de Jong, T., Itamura, S., Chan, K.H., Tashiro, M., Osterhaus, A.D., 2004. Pegylated interferon-alpha protects type 1 pneumocytes against SARS coronavirus infection in macaques. Nat. Med. 10, 290–293.
Haijema, B.J., Volders, H., Rottier, P.J., 2004. Live, attenuated coronavirus vaccines through the directed deletion of group-specific genes provide protection against feline infectious peritonitis. J. Virol. 78, 3863–3871.
Hatada, E.N., Krappmann, D., Scheidereit, C., 2000. NF-kappaB and the innate immune response. Curr. Opin. Immunol. 12, 52–58.
He, R., Leeson, A., Andonov, A., Li, Y., Bastien, N., Cao, J., Osiowy, C., Dobie, F., Cutts, T., Ballantine, M., Li, X., 2003. Activation of AP-1 signal transduction pathway by SARS coronavirus nucleocapsid protein. Biochem. Biophys. Res. Commun. 311, 870–876.
Herlaar, E., Brown, Z., 1999. p38 MAPK signalling cascades in inflammatory disease. Mol. Med. Today 5, 439–447.
Ho, Y., Lin, P.H., Liu, C.Y., Lee, S.P., Chao, Y.C., 2004. Assembly of human severe acute respiratory syndrome coronavirus-like particles. Biochem. Biophys. Res. Commun. 318, 833–838.
Hollenhorst, M.I., Richter, K., Fronius, M., 2011. Ion transport by pulmonary epithelia. J. Biomed. Biotechnol. 2011, 174306.
Huang, C., Lokugamage, K.G., Rozovics, J.M., Narayanan, K., Semler, B.L., Makino, S., 2011. SARS coronavirus nsp1 protein induces template-dependent endonucleolytic cleavage of mRNAs: viral mRNAs are resistant to nsp1-induced RNA cleavage. PLoS Pathog. 7, e1002433.
Huang, C., Peters, C.J., Makino, S., 2007. Severe acute respiratory syndrome coronavirus accessory protein 6 is a virion-associated protein and is released from 6 protein-expressing cells. J. Virol. 81, 5423–5426.
Huang, Y., Yang, Z.Y., Kong, W.P., Nabel, G.J., 2004. Generation of synthetic severe acute respiratory syndrome coronavirus pseudoparticles: implications for assembly and vaccine production. J. Virol. 78, 12557–12565.
Hung, A.Y., Sheng, M., 2002. PDZ domains: structural modules for protein complex assembly. J. Biol. Chem. 277, 5699–5702.
Hussain, S., Perlman, S., Gallagher, T.M., 2008. Severe acute respiratory syndrome coronavirus protein 6 accelerates murine hepatitis virus infections by more than one mechanism. J. Virol. 82, 7212–7222.
Ichinohe, T., Pang, I.K., Iwasaki, A., 2010. Influenza virus activates inflammasomes via its intracellular M2 ion channel. Nat. Immunol. 11, 404–410.
Ito, M., Yanagi, Y., Ichinohe, T., 2012. Encephalomyocarditis virus viroporin 2B activates NLRP3 inflammasome. PLoS Pathog. 8, e1002857.
Jackson, D., Hossain, M.J., Hickman, D., Perez, D.R., Lamb, R.A., 2008. A new influenza virus virulence determinant: the NS1 protein four C-terminal residues modulate pathogenicity. Proc. Natl. Acad. Sci. U.S.A. 105, 4381–4386.
Jauregui, A.R., Savalia, D., Lowry, V.K., Farrell, C.M., Wathelet, M.G., 2013. Identification of residues of SARS-CoV nsp1 that differentially affect inhibition of gene expression and antiviral signaling. PLos ONE 8, e62416.
Javier, R.T., Rice, A.P., 2011. Emerging theme: cellular PDZ proteins as common targets of pathogenic viruses. J. Virol. 85, 11544–11556.
Ji, H.L., Song, W., Gao, Z., Su, X.F., Nie, H.G., Jiang, Y., Peng, J.B., He, Y.X., Liao, Y., Zhou, Y.J., Tousson, A., Matalon, S., 2009. SARS-CoV proteins decrease levels and activity of human ENaC via activation of distinct PKC isoforms. Am. J. Physiol. Lung Cell Mol. Physiol. 296, L372–L383.
Jiang, Y., Xu, J., Zhou, C., Wu, Z., Zhong, S., Liu, J., Luo, W., Chen, T., Qin, Q., Deng, P., 2005. Characterization of cytokine/chemokine profiles of severe acute respiratory syndrome. Am. J. Respir. Crit. Care Med. 171, 850–857.
Jimenez-Guardeño, J.M., Nieto-Torres, J.L., DeDiego, M.L., Regla-Nava, J.A., Fernandez-Delgado, R., Castaño-Rodriguez, C., Enjuanes, L., 2014. The PDZ-binding motif of severe acute respiratory syndrome coronavirus envelope protein is a determinant of viral pathogenesis. PLoS Pathog., http://dx.doi.org/10.1371/journal.ppat.1004320.
Kamitani, W., Huang, C., Narayanan, K., Lokugamage, K.G., Makino, S., 2009. A two-pronged strategy to suppress host protein synthesis by SARS coronavirus Nsp1 protein. Nat. Struct. Mol. Biol. 16, 1134–1140.
Kanzawa, N., Nishigaki, K., Hayashi, T., Ishii, Y., Furukawa, S., Niiro, A., Yasui, F., Kohara, M., Morita, K., Matsushima, K., Le, M.Q., Masuda, T., Kannagi, M., 2006. Augmentation of chemokine production by severe acute respiratory syndrome coronavirus 3a/X1 and 7a/X4 proteins through NF-kappaB activation. FEBS Lett. 580, 6807–6812.
Kawai, T., Akira, S., 2007. Signaling to NF-kappaB by toll-like receptors. Trends Mol. Med. 13, 460–469.
Kiyono, T., Hiraiwa, A., Fujita, M., Hayashi, Y., Akiyama, T., Ishibashi, M., 1997. Binding of high-risk human papillomavirus E6 oncoproteins to the human homologue of the *Drosophila* discs large tumor suppressor protein. Proc. Natl. Acad. Sci. U.S.A. 94, 11612–11616.
Koetzner, C.A., Kuo, L., Goebel, S.J., Dean, A.B., Parker, M.M., Masters, P.S., 2010. Accessory protein 5a is a major antagonist of the antiviral action of interferon against murine coronavirus. J. Virol. 84, 8262–8274.
Kopecky-Bromberg, S.A., Martinez-Sobrido, L., Frieman, M., Baric, R.A., Palese, P., 2007. Severe acute respiratory syndrome coronavirus open reading frame (ORF) 3b, ORF 6, and nucleocapsid proteins function as interferon antagonists. J. Virol. 81, 548–557.
Kumaki, Y., Ennis, J., Rahbar, R., Turner, J.D., Wandersee, M.K., Smith, A.J., Bailey, K.W., Vest, Z.G., Madsen, J.R., Li, J.K., Barnard, D.L., 2011. Single-dose intranasal administration with mDEF201 (adenovirus vectored mouse interferon-alpha) confers protection from mortality in a lethal SARS-CoV BALB/c mouse model. Antivir. Res. 89, 75–82.
Kumar, S., Boehm, J., Lee, J.C., 2003. p38 MAP kinases: key signalling molecules as therapeutic targets for inflammatory diseases. Nat. Rev. Drug Discov. 2, 717–726.
Kuo, L., Masters, P.S., 2003. The small envelope protein E is not essential for murine coronavirus replication. J. Virol. 77, 4597–4608.
Lamirande, E.W., DeDiego, M.L., Roberts, A., Jackson, J.P., Alvarez, E., Sheahan, T., Shieh, W.J., Zaki, S.R., Baric, R., Enjuanes, L., Subbarao, K., 2008. A live attenuated SARS coronavirus is immunogenic and efficacious in golden Syrian hamsters. J. Virol. 82, 7721–7724.
Lau, S.K., Lau, C.C., Chan, K.H., Li, C.P., Chen, H., Jin, D.Y., Chan, J.F., Woo, P.C., Yuen, K.Y., 2013. Delayed induction of proinflammatory cytokines and suppression of innate antiviral response by the novel Middle East respiratory syndrome coronavirus: implications for pathogenesis and treatment. J. Gen. Virol. 94, 2679–2690.
Law, A.H., Lee, D.C., Cheung, B.K., Yim, H.C., Lau, A.S., 2007. Role for nonstructural protein 1 of severe acute respiratory syndrome coronavirus in chemokine dysregulation. J. Virol. 81, 416–422.
Le Bon, A., Tough, D.F., 2002. Links between innate and adaptive immunity via type I interferon. Curr. Opin. Immunol. 14, 432–436.
Lei, L., Ying, S., Baojun, L., Yi, Y., Xiang, H., Wenli, S., Zounan, S., Deyin, G., Qingyu, Z., Jingmei, L., Guohui, C., 2013. Attenuation of mouse hepatitis virus by deletion of the LLRKxGxKG region of Nsp1. PLOS ONE 8, e61166.
Liao, Q.J., Ye, L.B., Timani, K.A., Zeng, Y.C., She, Y.L., Ye, L., Wu, Z.H., 2005. Activation of NF-kappaB by the full-length nucleocapsid protein of the SARS coronavirus. Acta Biochim. Biophys. Sin. 37, 607–612.
Liao, Y., Lescar, J., Tam, J.P., Liu, D.X., 2004. Expression of SARS-coronavirus envelope protein in *Escherichia coli* cells alters membrane permeability. Biochem. Biophys. Res. Commun. 325, 374–380.
Liao, Y., Yuan, Q., Torres, J., Tam, J.P., Liu, D.X., 2006. Biochemical and functional characterization of the membrane association and membrane permeabilizing activity of the severe acute respiratory syndrome coronavirus envelope protein. Virology 349, 264–265.
Liu, D.X., Inglis, S.C., 1991. Association of the infectious bronchitis virus-3c protein with the virion envelope. Virology 185, 911–917.
Lopez, L.A., Riffle, A.J., Pike, S.L., Gardner, D., Hogue, B.G., 2008. Importance of conserved cysteine residues in the coronavirus envelope protein. J. Virol. 82, 3000–3010.
Lu, W., Zheng, B.J., Xu, K., Schwarz, W., Du, L., Wong, C.K., Chen, J., Duan, S., Deubel, V., Sun, B., 2006. Severe acute respiratory syndrome-associated coronavirus 3a protein forms an ion channel and modulates virus release. Proc. Natl. Acad. Sci. U.S.A. 103, 12540–12545.
Lu, X., Pan, J., Tao, J., Guo, D., 2011. SARS-CoV nucleocapsid protein antagonizes IFN-beta response by targeting initial step of IFN-beta induction pathway, and its C-terminal region is critical for the antagonism. Virus Genes 42, 37–45.
Mahlakoiv, T., Ritz, D., Mordstein, M., DeDiego, M.L., Enjuanes, L., Muller, M.A., Drosten, C., Staeheli, P., 2012. Combined action of type I and type III interferon restricts initial replication of SARS-coronavirus in the lung but fails to inhibit systemic virus spread. J. Gen. Virol. 93, 2601–2605.
Matthay, M.A., Zemans, R.L., 2011. The acute respiratory distress syndrome: pathogenesis and treatment. Annu. Rev. Pathol. 6, 147–163.
Matthews, K.L., Coleman, C.M., van der Meer, Y., Snijder, E.J., Frieman, M.B., 2014. The ORF4b-encoded accessory proteins of Middle East respiratory syndrome coronavirus and two related bat coronaviruses localize to the nucleus and inhibit innate immune signalling. J. Gen. Virol. 95, 874–882.
McAuley, J.L., Tate, M.D., MacKenzie-Kludas, C.J., Pinar, A., Zeng, W., Stutz, A., Latz, E., Brown, L.E., Mansell, A., 2013. Activation of the NLRP3 inflammasome by IAV virulence protein PB1-F2 contributes to severe pathophysiology and disease. PLoS Pathog. 9, e1003392.
McBride, R., Fielding, B.C., 2012. The role of severe acute respiratory syndrome (SARS)-coronavirus accessory proteins in virus pathogenesis. Viruses 4, 2902–2923.
Meduri, G.U., Headley, S., Kohler, G., Stentz, F., Tolley, E., Umberger, R., Leeper, K., 1995. Persistent elevation of inflammatory cytokines predicts a poor outcome in ARDS. Plasma IL-1 beta and IL-6 levels are consistent and efficient predictors of outcome over time. Chest 107, 1062–1073.
Melik, W., Ellencrona, K., Wigerius, M., Hedstrom, C., Elvang, A., Johansson, M., 2012. Two PDZ binding motifs within NS5 have roles in tick-borne encephalitis virus replication. Virus Res. 169, 54–62.
Minakshi, R., Padhan, K., Rani, M., Khan, N., Ahmad, F., Jameel, S., 2009. The SARS coronavirus 3a protein causes endoplasmic reticulum stress and induces ligand-independent downregulation of the type 1 interferon receptor. PLoS ONE 4, e8342.
Mogensen, T.H., Paludan, S.R., 2001. Molecular pathways in virus-induced cytokine production. Microbiol. Mol. Biol. Rev. 65, 131–150.
Mortola, E., Roy, P., 2004. Efficient assembly and release of SARS coronavirus-like particles by a heterologous expression system. FEBS Lett. 576, 174–178.
Netland, J., DeDiego, M.L., Zhao, J., Fett, C., Alvarez, E., Nieto-Torres, J.L., Enjuanes, L., Perlman, S., 2010. Immunization with an attenuated severe acute respiratory syndrome coronavirus deleted in E protein protects against lethal respiratory disease. Virology 399, 120–128.
Netland, J., Meyerholz, D.K., Moore, S., Cassell, M., Perlman, S., 2008. Severe acute respiratory syndrome coronavirus infection causes neuronal death in the absence of encephalitis in mice transgenic for human ACE2. J. Virol. 82, 7264–7275.
Neuman, B.W., Adair, B.D., Yeager, M., Buchmeier, M.J., 2008. Purification and electron cryomicroscopy of coronavirus particles. Methods Mol. Biol. 454, 129–136.

Niemeyer, D., Zillinger, T., Muth, D., Zielecki, F., Horvath, G., Suliman, T., Barchet, W., Weber, F., Drosten, C., Muller, M.A., 2013. Middle East respiratory syndrome coronavirus accessory protein 4a is a type I interferon antagonist. J. Virol. 87, 12489–12495.

Nieto-Torres, J.L., Dediego, M.L., Alvarez, E., Jimenez-Guardeno, J.M., Regla-Nava, J.A., Llorente, M., Kremer, L., Shuo, S., Enjuanes, L., 2011. Subcellular location and topology of severe acute respiratory syndrome coronavirus envelope protein. Virology 415, 69–82.

Nieto-Torres, J.L., DeDiego, M.L., Verdia-Baguena, C., Jimenez-Guardeno, J.M., Regla-Nava, J.A., Fernandez-Delgado, R., Castaño-Rodriguez, C., Alcaraz, A., Torres, J., Aguilella, V.M., Enjuanes, L., 2014. Severe acute respiratory syndrome coronavirus envelope protein ion channel activity promotes virus fitness and pathogenesis. PLoS Pathog., http://dx.doi.org/10.1371/journal.ppat.1004077.

Nieva, J.L., Madan, V., Carrasco, L., 2012. Viroporins: structure and biological functions. Nat. Rev. Microbiol. 10, 563–574.

Obitsu, S., Ahmed, N., Nishitsuji, H., Hasegawa, A., Nakahama, K., Morita, I., Nishigaki, K., Hayashi, T., Masuda, T., Kannagi, M., 2009. Potential enhancement of osteoclastogenesis by severe acute respiratory syndrome coronavirus 3a/X1 protein. Arch. Virol. 154, 1457–1464.

Oostra, M., de Haan, C.A., Rottier, P.J., 2007. The 29-nucleotide deletion present in human but not in animal severe acute respiratory syndrome coronaviruses disrupts the functional expression of open reading frame 8. J. Virol. 81, 13876–13888.

Ortego, J., Ceriani, J.E., Patino, C., Plana, J., Enjuanes, L., 2007. Absence of E protein arrests transmissible gastroenteritis coronavirus maturation in the secretory pathway. Virology 368, 296–308.

Ortego, J., Escors, D., Laude, H., Enjuanes, L., 2002. Generation of a replication-competent, propagation-deficient virus vector based on the transmissible gastroenteritis coronavirus genome. J. Virol. 76, 11518–11529.

Pan, J., Peng, X., Gao, Y., Li, Z., Lu, X., Chen, Y., Ishaq, M., Liu, D., DeDiego, M.L., Enjuanes, L., Guo, D., 2008. Genome-wide analysis of protein-protein interactions and involvement of viral proteins in SARS-CoV replication. PLoS ONE 3, e3299.

Parthasarathy, K., Ng, L., Lin, X., Liu, D.X., Pervushin, K., Gong, X., Torres, J., 2008. Structural flexibility of the pentameric SARS coronavirus envelope protein ion channel. Biophys. J. 95, 39–41.

Pervushin, K., Tan, E., Parthasarathy, K., Lin, X., Jiang, F.L., Yu, D., Vararattanavech, A., Soong, T.W., Liu, D.X., Torres, J., 2009. Structure and inhibition of the SARS coronavirus envelope protein ion channel. PLoS Pathog. 5, e1000511.

Pewe, L., Zhou, H., Netland, J., Tangudu, C., Olivares, H., Shi, L., Look, D., Gallagher, T., Perlman, S., 2005. A severe acute respiratory syndrome-associated coronavirus-specific protein enhances virulence of an attenuated murine coronavirus. J. Virol. 79, 11335–11342.

Pugin, J., Ricou, B., Steinberg, K.P., Suter, P.M., Martin, T.R., 1996. Proinflammatory activity in bronchoalveolar lavage fluids from patients with ARDS, a prominent role for interleukin-1. Am. J. Respir. Crit. Care Med. 153, 1850–1856.

Rathinam, V.A., Fitzgerald, K.A., 2011. Cytosolic surveillance and antiviral immunity. Curr. Opin. Virol. 1, 455–462.

Regla-Nava, J.A., Nieto-Torres, J.L., Jimenez-Guardeno, J.M., Fernandez-Delgado, R., Fett, C., Castano-Rodriguez, C., Perlman, S., Enjuanes, L., DeDiego, M.L., 2014. Identification of host responses contributing to attenuation of severe acute respiratory syndrome coronaviruses containing mutated E protein. J. Virol. (in press).

Ruch, T.R., Machamer, C.E., 2011. The hydrophobic domain of infectious bronchitis virus E protein alters the host secretory pathway and is important for release of infectious virus. J. Virol. 85, 675–685.

Ruch, T.R., Machamer, C.E., 2012. The coronavirus E protein: assembly and beyond. Viruses 4, 363–382.

Sainz Jr., B., Mossel, E.C., Peters, C.J., Garry, R.F., 2004. Interferon-beta and interferon-gamma synergistically inhibit the replication of severe acute respiratory syndrome-associated coronavirus (SARS-CoV). Virology 329, 11–17.

Samuel, C.E., 2001. Antiviral actions of interferons. Clin. Microbiol. Rev. 14, 778–809.

Schaecher, S.R., Stabenow, J., Oberle, C., Schriewer, J., Buller, R.M., Sagartz, J.E., Pekosz, A., 2008. An immunosuppressed Syrian golden hamster model for SARS-CoV infection. Virology 380, 312–321.

Sen, G.C., 2001. Viruses and interferons. Annu. Rev. Microbiol. 55, 255–281.

Sharma, S., tenOever, B.R., Grandvaux, N., Zhou, G.P., Lin, R., Hiscott, J., 2003. Triggering the interferon antiviral response through an IKK-related pathway. Science 300, 1148–1151.

Siu, K.L., Kok, K.H., Ng, M.H., Poon, V.K., Yuen, K.Y., Zheng, B.J., Jin, D.Y., 2009. Severe acute respiratory syndrome coronavirus M protein inhibits type I interferon production by impeding the formation of TRAF3.TANK.TBK1/IKKepsilon complex. J. Biol. Chem. 284, 16202–16209.

Siu, K.L., Yeung, M.L., Kok, K.H., Yuen, K.S., Kew, C., Lui, P.Y., Chan, C.P., Tse, H., Woo, P.C., Yuen, K.Y., Jin, D.Y., 2014. Middle East respiratory syndrome coronavirus 4a protein is a double-stranded RNA-binding protein that suppresses PACT-induced activation of RIG-I and MDA5 in innate antiviral response. J. Virol., http://dx.doi.org/10.1128/JVI.03649-03613.

Smits, S.L., de Lang, A., van den Brand, J.M., Leijten, L.M., van, I.W.F., Eijkemans, M.J., van Amerongen, G., Kuiken, T., Andeweg, A.C., Osterhaus, A.D., Haagmans, B.L., 2010. Exacerbated innate host response to SARS-CoV in aged non-human primates. PLoS Pathog. 6, e1000756.

Smits, S.L., van den Brand, J.M., de Lang, A., Leijten, L.M., van Ijcken, W.F., van Amerongen, G., Osterhaus, A.D., Andeweg, A.C., Haagmans, B.L., 2011. Distinct severe acute respiratory syndrome coronavirus-induced acute lung injury pathways in two different nonhuman primate species. J. Virol. 85, 4234–4245.

Spaller, M.R., 2006. Act globally, think locally: systems biology addresses the PDZ domain. ACS Chem. Biol. 1, 207–210.

Stroher, U., DiCaro, A., Li, Y., Strong, J.E., Aoki, F., Plummer, F., Jones, S.M., Feldmann, H., 2004. Severe acute respiratory syndrome-related coronavirus is inhibited by interferon-alpha. J. Infect. Dis. 189, 1164–1167.

Sun, L., Xing, Y., Chen, X., Zheng, Y., Yang, Y., Nichols, D.B., Clementz, M.A., Banach, B.S., Li, K., Baker, S.C., Chen, Z., 2012. Coronavirus papain-like proteases negatively regulate antiviral innate immune response through disruption of STING-mediated signaling. PLOS ONE 7, e30802.

Tan, Y.J., Tham, P.Y., Chan, D.Z., Chou, C.F., Shen, S., Fielding, B.C., Tan, T.H., Lim, S.G., Hong, W., 2005. The severe acute respiratory syndrome coronavirus 3a protein up-regulates expression of fibrinogen in lung epithelial cells. J. Virol. 79, 10083–10087.

Tanaka, T., Kamitani, W., DeDiego, M.L., Enjuanes, L., Matsuura, Y., 2012. Severe acute respiratory syndrome coronavirus nsp1 facilitates efficient propagation in cells through a specific translational shutoff of host mRNA. J. Virol. 86, 11128–11137.

Tang, N.L., Chan, P.K., Wong, C.K., To, K.F., Wu, A.K., Sung, Y.M., Hui, D.S., Sung, J.J., Lam, C.W., 2005. Early enhanced expression of interferon-inducible protein-10 (CXCL-10) and other chemokines predicts adverse outcome in severe acute respiratory syndrome. Clin. Chem. 51, 2333–2340.

Teoh, K.T., Siu, Y.L., Chan, W.L., Schluter, M.A., Liu, C.J., Peiris, J.S., Bruzzone, R., Margolis, B., Nal, B., 2010. The SARS coronavirus E protein interacts with PALS1 and alters tight junction formation and epithelial morphogenesis. Mol. Biol. Cell 21, 3838–3852.

Tisoncik, J.R., Korth, M.J., Simmons, C.P., Farrar, J., Martin, T.R., Katze, M.G., 2012. Into the eye of the cytokine storm. Microbiol. Mol. Biol. Rev. 76, 16–32.

Torres, J., Maheswari, U., Parthasarathy, K., Ng, L., Liu, D.X., Gong, X., 2007. Conductance and amantadine binding of a pore formed by a lysine-flanked transmembrane domain of SARS coronavirus envelope protein. Protein Sci. 16, 2065–2071.

Torres, J., Parthasarathy, K., Lin, X., Saravanan, R., Liu, D.X., 2006. Model of a putative pore: the pentameric alpha-helical bundle of SARS coronavirus E protein in lipid bilayers. Biophys. J. 91, 938–947.

Triantafilou, K., Kar, S., Vakakis, E., Kotecha, S., Triantafilou, M., 2013. Human respiratory syncytial virus viroporin SH: a viral recognition pathway used by the host to signal inflammasome activation. Thorax 68, 66–75.

Underwood, D.C., Osborn, R.R., Bochnowicz, S., Webb, E.F., Rieman, D.J., Lee, J.C., Romanic, A.M., Adams, J.L., Hay, D.W., Griswold, D.E., 2000. SB 239063, a p38 MAPK inhibitor, reduces neutrophilia, inflammatory cytokines, MMP-9, and fibrosis in lung. Am. J. Physiol. Lung Cell Mol. Physiol. 279, L895–L902.

Varshney, B., Agnihothram, S., Tan, Y.J., Baric, R., Lal, S.K., 2012. SARS coronavirus 3b accessory protein modulates transcriptional activity of RUNX1b. PLOS ONE 7, e29542.

Varshney, B., Lal, S.K., 2011. SARS-CoV accessory protein 3b induces AP-1 transcriptional activity through activation of JNK and ERK pathways. Biochemistry 50, 5419–5425.

Verdia-Baguena, C., Nieto-Torres, J.L., Alcaraz, A., Dediego, M.L., Enjuanes, L., Aguilella, V.M., 2013. Analysis of SARS-CoV E protein ion channel activity by tuning the protein and lipid charge. Biochim. Biophys. Acta 1828, 2026–2031.

Verdia-Baguena, C., Nieto-Torres, J.L., Alcaraz, A., Dediego, M.L., Torres, J., Aguilella, V.M., Enjuanes, L., 2012. Coronavirus E protein forms ion channels with functionally and structurally-involved membrane lipids. Virology 432, 485–494.

von Brunn, A., Teepe, C., Simpson, J.C., Pepperkok, R., Friedel, C.C., Zimmer, R., Roberts, R., Baric, R., Haas, J., 2007. Analysis of intraviral protein–protein interactions of the SARS coronavirus ORFeome. PLoS ONE 2, 1–11.

Wang, C.H., Liu, C.Y., Wan, Y.L., Chou, C.L., Huang, K.H., Lin, H.C., Lin, S.M., Lin, T.Y., Chung, K.F., Kuo, H.P., 2005. Persistence of lung inflammation and lung cytokines with high-resolution CT abnormalities during recovery from SARS. Respir. Res. 6, 42.

Wang, G., Chen, G., Zheng, D., Cheng, G., Tang, H., 2011. PLP2 of mouse hepatitis virus A59 (MHV-A59) targets TBK1 to negatively regulate cellular type I interferon signaling pathway. PLoS ONE 6 (2), e17192.

Wang, W., Ye, L., Ye, L., Li, B., Gao, B., Zeng, Y., Kong, L., Fang, X., Zheng, H., Wu, Z., She, Y., 2007. Up-regulation of IL-6 and TNF-alpha induced by SARS-coronavirus spike protein in murine macrophages via NF-kappaB pathway. Virus Res. 128, 1–8.

Wathelet, M.G., Orr, M., Frieman, M.B., Baric, R.S., 2007. Severe acute respiratory syndrome coronavirus evades antiviral signaling: role of nsp1 and rational design of an attenuated strain. J. Virol. 81, 11620–11633.

Whitmarsh, A.J., Davis, R.J., 1996. Transcription factor AP-1 regulation by mitogen-activated protein kinase signal transduction pathways. J. Mol. Med. 74, 589–607.

Wilson, L., Gage, P., Ewart, G., 2006. Hexamethylene amiloride blocks E protein ion channels and inhibits coronavirus replication. Virology 353, 294–306.

Wilson, L., McKinlay, C., Gage, P., 2004. SARS coronavirus E protein forms cation-selective ion channels. Virology 330, 322–331.

Wong, C.K., Lam, C.W., Wu, A.K., Ip, W.K., Lee, N.L., Chan, I.H., Lit, L.C., Hui, D.S., Chan, M.H., Chung, S.S., Sung, J.J., 2004. Plasma inflammatory cytokines and chemokines in severe acute respiratory syndrome. Clin. Exp. Immunol. 136, 95–103.

Yang, X., Chen, X., Bian, G., Tu, J., Xing, Y., Wang, Y., Chen, Z., 2014. Proteolytic processing, deubiquitinase and interferon antagonist activities of Middle East respiratory syndrome coronavirus papain-like protease. J. Gen. Virol. 95, 614–626.

Ye, Y., Hauns, K., Langland, J.O., Jacobs, B.L., Hogue, B.G., 2007. Mouse hepatitis coronavirus A59 nucleocapsid protein is a type I interferon antagonist. J. Virol. 81, 2554–2563.

Yount, B., Roberts, R.S., Sims, A.C., Deming, D., Frieman, M.B., Sparks, J., Denison, M.R., Davis, N., Baric, R.S., 2005. Severe acute respiratory syndrome coronavirus group-specific open reading frames encode nonessential functions for replication in cell cultures and mice. J. Virol. 79, 14909–14922.

Zhang, X., Wu, K., Wang, D., Yue, X., Song, D., Zhu, Y., Wu, J., 2007. Nucleocapsid protein of SARS-CoV activates interleukin-6 expression through cellular transcription factor NF-kappaB. Virology 365, 324–335.

Zhao, J., Falcon, A., Zhou, H., Netland, J., Enjuanes, L., Perez Brena, P., Perlman, S., 2009. Severe acute respiratory syndrome coronavirus protein 6 is required for optimal replication. J. Virol. 83, 2368–2373.

Zhao, J., Perlman, S., 2010. T cell responses are required for protection from clinical disease and for virus clearance in severe acute respiratory syndrome coronavirus-infected mice. J. Virol. 84, 9318–9325.

Zhao, L., Jha, B.K., Wu, A., Elliott, R., Ziebuhr, J., Gorbalenya, A.E., Silverman, R.H., Weiss, S.R., 2012. Antagonism of the interferon-induced OAS-RNase L pathway by murine coronavirus ns2 protein is required for virus replication and liver pathology. Cell Host Microbe 11, 607–616.

Zhao, L., Rose, K.M., Elliott, R., Van Rooijen, N., Weiss, S.R., 2011. Cell type-specific type I interferon antagonism influences organ tropism of murine coronavirus. J. Virol. 85, 10058–10068.

Zheng, B., He, M.L., Wong, K.L., Lum, C.T., Poon, L.L., Peng, Y., Guan, Y., Lin, M.C., Kung, H.F., 2004. Potent inhibition of SARS-associated coronavirus (SCOV) infection and replication by type I interferons (IFN-alpha/beta) but not by type II interferon (IFN-gamma). J. Interferon Cytokine Res. 24, 388–390.

Zheng, D., Chen, G., Guo, B., Cheng, G., Tang, H., 2008. PLP2, a potent deubiquitinase from murine hepatitis virus, strongly inhibits cellular type I interferon production. Cell Res. 18, 1105–1113.

Zust, R., Cervantes-Barragan, L., Habjan, M., Maier, R., Neuman, B.W., Ziebuhr, J., Szretter, K.J., Baker, S.C., Barchet, W., Diamond, M.S., Siddell, S.G., Ludewig, B., Thiel, V., 2011. Ribose 2′-*O*-methylation provides a molecular signature for the distinction of self and non-self mRNA dependent on the RNA sensor Mda5. Nat. Immunol. 12, 137–143.

Zust, R., Cervantes-Barragan, L., Kuri, T., Blakqori, G., Weber, F., Ludewig, B., Thiel, V., 2007. Coronavirus non-structural protein 1 is a major pathogenicity factor: implications for the rational design of coronavirus vaccines. PLoS Pathog. 3, e109.

OPEN ACCESS Freely available online

PLOS | PATHOGENS

Severe Acute Respiratory Syndrome Coronavirus Envelope Protein Ion Channel Activity Promotes Virus Fitness and Pathogenesis

Jose L. Nieto-Torres[1], Marta L. DeDiego[1¤], Carmina Verdiá-Báguena[2], Jose M. Jimenez-Guardeño[1], Jose A. Regla-Nava[1], Raul Fernandez-Delgado[1], Carlos Castaño-Rodriguez[1], Antonio Alcaraz[2], Jaume Torres[3], Vicente M. Aguilella[2], Luis Enjuanes[1]*

1 Department of Molecular and Cell Biology, Centro Nacional de Biotecnología (CNB-CSIC), Campus Universidad Autónoma de Madrid, Madrid, Spain, **2** Department of Physics, Laboratory of Molecular Biophysics. Universitat Jaume I, Castellón, Spain, **3** School of Biological Sciences, Division of Structural and Computational Biology, Nanyang Technological University, Singapore, Singapore

Abstract

Deletion of Severe Acute Respiratory Syndrome Coronavirus (SARS-CoV) envelope (E) gene attenuates the virus. E gene encodes a small multifunctional protein that possesses ion channel (IC) activity, an important function in virus-host interaction. To test the contribution of E protein IC activity in virus pathogenesis, two recombinant mouse-adapted SARS-CoVs, each containing one single amino acid mutation that suppressed ion conductivity, were engineered. After serial infections, mutant viruses, in general, incorporated compensatory mutations within E gene that rendered active ion channels. Furthermore, IC activity conferred better fitness in competition assays, suggesting that ion conductivity represents an advantage for the virus. Interestingly, mice infected with viruses displaying E protein IC activity, either with the wild-type E protein sequence or with the revertants that restored ion transport, rapidly lost weight and died. In contrast, mice infected with mutants lacking IC activity, which did not incorporate mutations within E gene during the experiment, recovered from disease and most survived. Knocking down E protein IC activity did not significantly affect virus growth in infected mice but decreased edema accumulation, the major determinant of acute respiratory distress syndrome (ARDS) leading to death. Reduced edema correlated with lung epithelia integrity and proper localization of Na^+/K^+ ATPase, which participates in edema resolution. Levels of inflammasome-activated IL-1β were reduced in the lung airways of the animals infected with viruses lacking E protein IC activity, indicating that E protein IC function is required for inflammasome activation. Reduction of IL-1β was accompanied by diminished amounts of TNF and IL-6 in the absence of E protein ion conductivity. All these key cytokines promote the progression of lung damage and ARDS pathology. In conclusion, E protein IC activity represents a new determinant for SARS-CoV virulence.

Citation: Nieto-Torres JL, DeDiego ML, Verdiá-Báguena C, Jimenez-Guardeño JM, Regla-Nava JA, et al. (2014) Severe Acute Respiratory Syndrome Coronavirus Envelope Protein Ion Channel Activity Promotes Virus Fitness and Pathogenesis. PLoS Pathog 10(5): e1004077. doi:10.1371/journal.ppat.1004077

Editor: Mark R. Denison, Vanderbilt University, United States of America

Received December 23, 2013; **Accepted** March 5, 2014; **Published** May 1, 2014

Funding: This work was supported by grants from the Ministry of Science and Innovation of Spain (BIO2010-16705), the European Community's Seventh Framework Programme (FP7/2007–2013) under the project "EMPERIE" EC Grant Agreement number 223498, and U.S. National Institutes of Health (NIH) (2P01AI060699 and 0258-3413/HHSN266200700010C). Financial support from Generalitat Valenciana (Prometeu 2012/069) and Fundacion Caixa Castello-Bancaixa (Project No. P1-1B2012-03) is also acknowledged. JLN received a contract from NIH. JAR and CCR received fellowships from Fundacion La Caixa. The funders had no role in study design, data collection and analysis, decision to publish, or preparation of the manuscript.

Competing Interests: The authors have declared that no competing interests exist.

* E-mail: L.Enjuanes@cnb.csic.es

¤ Current address: David H. Smith Center for Vaccine Biology and Immunology, University of Rochester Medical Center, Rochester, New York, United States of America

Introduction

Coronaviruses (CoVs) are vertebrate pathogens that cause severe diseases in a wide range of animals and infections in humans that until recently were limited to common colds [1]. Nevertheless, by the end of 2002, a novel coronavirus causing the severe acute respiratory syndrome (SARS-CoV) emerged in China and rapidly spread worldwide causing around 8000 infections leading to death in 10% of the cases [2,3]. Since then, CoVs surveillance programs were intensified, and two additional human coronaviruses, already circulating in the human population, were identified as the causative agents of several cases of pneumonia and bronchiolitis (HCoV-HKU1 and HCoV-NL63) [4]. Furthermore, in 2012 a novel coronavirus infecting humans, the Middle East Respiratory Syndrome Coronavirus (MERS-CoV) appeared in Saudi Arabia and disseminated to nine additional countries [5,6]. To date, 182 cases of MERS-CoV have been reported, which has led to 79 fatalities (http://www.who.int). Clinical presentation of infected individuals involves acute pneumonia, sometimes accompanied by renal disease [7]. CoVs similar to SARS-CoV and MERS-CoV have also been isolated from bats widely distributed throughout the world [8–13], which represents a potential reservoir for outbreaks of novel zoonoses into humans. Therefore, understanding the virulence

Author Summary

Several highly pathogenic viruses encode small transmembrane proteins with ion-conduction properties named viroporins. Viroporins are generally involved in virus production and maturation processes, which many times are achieved by altering the ion homeostasis of cell organelles. Cells have evolved mechanisms to sense these imbalances in ion concentrations as a danger signal, and consequently trigger the innate immune system. Recently, it has been demonstrated that viroporins are inducers of cytosolic macromolecular complexes named inflammasomes that trigger the activation of key inflammatory cytokines such as IL-1β. The repercussions of this system in viral pathogenesis or disease outcome are currently being explored. SARS-CoV infection induces an uncontrolled inflammatory response leading to pulmonary damage, edema accumulation, severe hypoxemia and eventually death. In this study, we report that SARS-CoV E protein ion channel activity is a determinant of virulence, as the elimination of this function attenuated the virus, reducing the harmful inflammatory cytokine burst produced after infection, in which inflammasome activation plays a critical role. This led to less pulmonary damage and to disease resolution. These novel findings may be of relevance for other viral infections and can possibly be translated in order to find therapies for their associated diseases.

mechanisms of these pathogens, will allow the development of effective therapies in order to prevent and control future outbreaks.

SARS-CoV is an enveloped virus containing a positive sense RNA genome of 29.7 kb, one of the largest viral RNA genomes known. The genome encodes a viral replicase involved in the synthesis of new genomes and in the generation of a nested set of subgenomic messenger RNAs, encoding both structural proteins present in all CoVs: Spike (S), Envelope (E), Membrane (M) and Nucleoprotein (N), and a group of proteins specific for SARS-CoV: 3a, 3b, 6, 7a, 7b, 8a, 8b, and 9b [14].

SARS-CoV E protein is a 76-amino acid transmembrane protein actively synthesized during viral infection, that mainly localizes at the ERGIC region of the cell, where virus budding and morphogenesis take place [15–18]. Different requirements of E protein during the virus cycle have been described among CoVs. Elimination of E gene in transmissible gastroenteritis coronavirus (TGEV) or MERS-CoV leads to a replication-competent propagation-deficient phenotype [19–21]. In contrast, deletion of E gene from mouse hepatitis virus (MHV) or SARS-CoV does not abolish virus production, although viral titers are significantly reduced by 1000 to 20-fold, respectively [16,22]. Interestingly, E gene deleted SARS-CoV (SARS-CoV-ΔE) was attenuated in three animal models, and confers protection against challenge with parental virus in immunized hamsters, and in young or aged mice, representing a promising vaccine candidate [16,23–27]. Cells infected with SARS-CoV-ΔE show increased stress and apoptotic markers compared to wild type virus, perhaps resulting in a decreased productivity of infection [28]. Additionally, elimination of the E gene diminishes inflammation induced by SARS-CoV through the NF-κB pathway [27].

Remarkably, SARS-CoV E protein was found to self-interact forming a pentameric structure that delimits an ion conductive pore, which may play a role in virus-host interaction [29–32]. E protein ion conductivity was also confirmed for a set of CoVs from different genera [33]. The ion channel (IC) activity of SARS-CoV E protein was mapped within the transmembrane domain of the protein by using synthetic peptides [31,34,35]. Recent studies determined that both ion conductance and selectivity of E protein ion channel were highly controlled by the charge of the lipid membranes in which the pores were assembled. This suggests that lipid head-groups are components of the channel structure facing the lumen of the pore, a novel concept for CoV E protein ion channel [34,36]. Chemically synthesized SARS-CoV E protein showed slight preference for cations over anions when reconstituted in lipids that mimicked both charge and composition of ERGIC membranes, and displayed no specific selectivity for a particular cation [34,36]. In addition, point mutations that suppressed SARS-CoV E protein IC activity (N15A and V25F) have been identified and confirmed [34,35].

Several reports have analyzed the relevance of CoV E protein transmembrane domain, which contains ion-conduction properties, in virus maturation and production. Insertion of alanine residues within the transmembrane domain of MHV E protein rendered crippled viruses that evolutionary reverted to restore a proper structure of the alpha helix within the transmembrane domain [37]. Interchanging the genus β CoV MHV E protein transmembrane domain by those of CoVs from different genera revealed that only domains belonging to genus β, and γ, but not α, functionally replaced MHV E transmembrane domain in terms of viral production. It was speculated that this effect was a consequence of the possible different ion selectivity of these domains [38]. Replacement of genus γ CoV infectious bronchitis virus (IBV) E protein transmembrane domain, which displays IC activity, for vesicular stomatitis virus (VSV) G protein transmembrane domain lacking this function, interfered with an efficient trafficking and release of the viral progeny in the infected cells [39]. In contrast, mutation of threonine at position 16 to alanine, which is the amino acid change predicted to inhibit IC activity in IBV E protein did not affect virus-like particles formation, suggesting a multifunctional role of E protein [40].

Besides the E protein, SARS-CoV encodes two other ion-conducting proteins, 3a and 8a [41,42]. In a related virus, human coronavirus 229E (HCoV-229E), novel IC activity has been described within the 4a protein [43]. The abundance and conservation of IC activity suggests an importance of influencing ion homeostasis within cells during the CoV infection cycle.

Modulation of the cellular ion balance seems to be a common issue for viruses, as a growing list of viroporins are being identified, especially within RNA viruses [44]. Highly pathogenic human viruses such as influenza A virus, human immunodeficiency virus (HIV), hepatitis C virus (HCV) and several picornaviruses, among others, encode at least one viroporin [45–49]. Viroporins have been involved in virus entry, trafficking, morphogenesis, maturation and even virulence [50–53]. Influenza virus M2 is essential for viral RNA release from infections virions within the endosome into the cell cytoplasm [45] and also for raising the pH at the trans-Golgi network lumen, which prevents premature activation of hemaglutinin, which may render non-infectious virions [54]. Similarly, HCV p7 protein equilibrates the pH at the Golgi apparatus, protecting acid-sensitive intracellular virions [51]. Coxsackievirus 2B protein alters Golgi and endoplasmic reticulum (ER) Ca^{2+} and H^+ concentrations, which in turn delay protein transport through the secretory pathway facilitating virus assembly and preventing major histocompatibility complex (MHC) molecules from reaching the cell surface [48,55,56]. A recent finding described that influenza M2 protein IC activity triggers NOD-like receptor family, pyrin domain containing 3 (NLRP3) inflammasome activation [52]. Furthermore, mutant versions of M2 protein that conduct Na^+ and K^+ ions apart from H^+ ions more strongly elicited the inflammasome response [52]. This novel mechanism of

immune system activation has also been proven for other viroporins [53,57–59].

Viral proteins with IC activity impact different aspects of the virus life cycle, however, the involvement of their IC activity in pathogenesis remain to be further explored. Previous findings demonstrated that SARS-CoV E protein is a virulence determinant. In this manuscript we analyze the contribution of E protein IC activity in pathogenesis. Two recombinant viruses, each one containing a single point mutation suppressing IC activity, were generated by reverse genetics. Mutant viruses showed a tendency to evolve and restore E protein IC architecture and activity after serial infections, and viruses with deficient IC activity were outcompeted by those displaying this function after co-infections. This highlights the importance of IC activity in virus fitness. Interestingly, infection of mice with a set of viruses lacking or displaying E protein IC activity, revealed that the activation of inflammasome pathway, and the exacerbated inflammatory response induced by SARS-CoV was decreased in infections by on channel deficient viruses. In addition, less lung damage and proper localization of Na^+/K^+ ATPase within epithelia, which prevents edema accumulation, was detected for the mice infected with the viruses lacking E protein IC activity. As a consequence, increased survival of the infected animals was observed when E protein ion conductivity was absent. Therefore, E protein IC activity is required for inflammasome activation and a novel determinant for the virulence of highly pathogenic SARS-CoV.

Results

SARS-CoV E protein IC activity is not essential for virus production in cell culture

Deletion of SARS-CoV E gene resulted in a virus that was attenuated in three animal models, as we have previously shown [16,23,24,26,27]. E gene codes for the small multifunctional E protein, which displays IC activity [31,34–36]. To specifically test the relevance of IC activity in virus virulence, residues involved in E protein ion conductance were firstly identified. To this end a set of synthetic peptides representing the transmembrane domain of E protein were evaluated for their IC activity. These peptides contained point mutations that affect different conserved residues, or residues predicted to face the lumen of the channel pore [34]. Mutations N15A and V25F within the transmembrane domain of E protein completely disrupted IC activity [34,35]. Accordingly, two recombinant viruses containing each of these two changes in the E gene, rSARS-CoV-E-N15A (N15A) and rSARS-CoV-E-V25F (V25F), were engineered (**Fig. 1**). A SARS-CoV with a mouse adapted (MA15) genetic background [27,60] was used to generate these viruses, as infection of mice with SARS-CoV MA15 accurately reproduces the symptoms of human disease [27,60]. The mutant viruses were efficiently rescued, cloned by three rounds of plaque purification, and their sequence was confirmed (data not shown). To test whether the introduced mutations may alter E protein subcellular localization affecting other functions of the protein, Vero E6 cells were infected with the wt virus, the viruses lacking IC activity (N15A and V25F) or a virus missing E gene (ΔE) as a control. Immunofluorescence analysis showed similar colocalization patterns of E protein and ERGIC, the subcellular compartment where E protein mainly accumulates during infection, for both the wt and the mutant viruses (**Fig. 2A**), indicating that other functions of E protein associated with its localization are most likely not affected.

Deletions or mutations within the E gene of several CoVs sometimes led to crippled viruses or to lower virus yields [16,20–22,37,39]. To test whether inhibition of E protein IC activity affects virus production, growth kinetics were performed in the monkey Vero E6 and mouse DBT-mACE2 cells [61]. Minor differences in growth rates were observed between the parental virus (wt), that contains E protein IC activity, and the mutant viruses that lack E protein IC activity (**Fig. 2B**), indicating that this function was not essential for virus growth in cell culture. More striking differences in plaque phenotypes were observed. Mutant viruses lacking E protein IC activity, apparently formed smaller plaques than wt virus, and V25F virus plaques were smaller than N15A virus (**Fig. 2C**). A possible explanation for all these data could be that infection foci productivity and area may be quite similar regardless of E protein IC activity, as determined by viral titration, but higher cytopathic effect may be induced when E protein IC is present, rendering bigger plaques. Elimination of full-length E protein induced more severe growth defects (**Fig. 2B and Fig. 2C**), suggesting that other functions of the protein contributing to virus production, apart from IC activity, may be affected.

SARS-CoV E protein IC activity improves viral fitness

Inhibition of E protein IC activity slightly reduced virus production in cell culture in a relatively short period of time, but these differences were not significant. To further explore whether ion conductivity could improve viral growth and fitness, a long-term competition assay was performed between the wt virus and the N15A mutant lacking IC activity, that was relative stable through passages as will be described below. Vero E6 cells were co-infected with N15A mutant and the wt virus in a proportion 7:3, and the supernatant was serially passaged for 20 times every 24 hours. The E gene was sequenced every 4 passages, revealing that the proportion of wt virus steadily increased over the passages, accompanied by a decrease in the abundance of the N15A mutant. From passage 8 on, the wt virus took and maintained majority over the N15A mutant (**Fig. 3**). These results suggested that E protein IC activity for SARS-CoV confers a selective advantage improving virus production.

SARS-CoV E protein IC activity confers virulence *in vivo*

To specifically analyze the contribution of E protein IC activity to SARS-CoV virulence, BALB/c mice were intranasally inoculated with the wt virus displaying E protein IC activity, or three independently-isolated clones of the mutant viruses N15A and V25F lacking E protein IC activity, and mice were monitored daily for 10 days (n = 5/virus clone). All infected animals showed disease symptoms at 2 days post infection (dpi), reflected by slower movements and ruffled fur (data not shown). Mice infected with the wt virus started to lose weight by day 2, and by day 5 all of them died (**Fig. 4**). Interestingly, although mice infected with the three clones of N15A mutant started to lose weight in a similar fashion, at day 4 almost all of them started to regain weight, recover from the disease, and 80–100% survived (**Fig. 4**). In contrast to N15A, mice infected with V25F virus experimented similar weight losses and survival rates (from 0 to 20%) than the wt virus (**Fig. 4**). A possible explanation for this apparent discrepancy was the reversion of the introduced mutation or the incorporation of compensatory mutations restoring E protein IC activity. To test whether this was the case, total RNA was collected from the lungs of infected mice at 2 and 4 dpi or from the lungs of mice that died after infection. The virus genome region containing E gene was sequenced, as it was the target of the point mutations inhibiting IC activity, and therefore a likely place to incorporate compensatory mutations. E genes from wt virus and N15A mutant virus remained stable during the course of the experiment, since no changes were found in viral RNA extracted either from lungs of

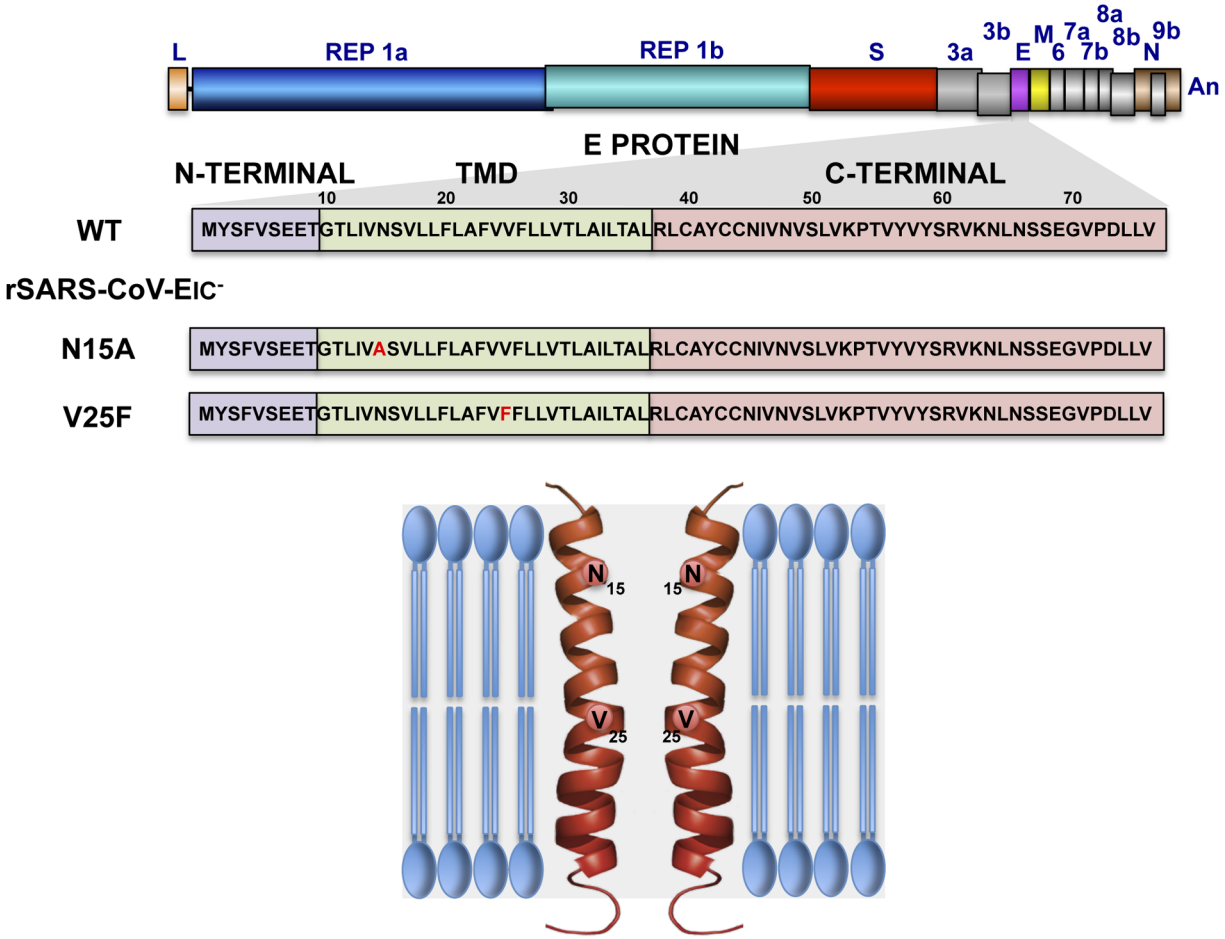

Figure 1. Engineering of rSARS-CoVs lacking E protein ion channel (IC) activity. SARS-CoV genome is represented at the top, and the region expanded shows wild type SARS-CoV E protein sequence (wt) and its different domains: amino terminal (N-terminal), transmembrane (TMD) and carboxy terminal (C-terminal). To generate viruses lacking E protein ion channel activity (rSARS-CoV-EIC^{-}) the amino acid changes N15A or V25F were introduced within viral genome to generate two recombinant viruses. The positions of the mutated residues within the transmembrane domain of a simplified E protein oligomer inserted in a lipid membrane are shown at the bottom.
doi:10.1371/journal.ppat.1004077.g001

several mice at 2 and 4 dpi or from dead mice (**Fig. 5A**). In contrast, V25F viruses incorporated mutations in the E gene that led to amino acid changes either in the same position of the mutation that abolished IC activity (F25C) or in relatively close positions within the E protein transmembrane domain: L19A, F20L, F26L, L27S, T30I and L37R (**Fig. 5A**). These evolved variants of the V25F virus appeared as early as 2 days after mice infection and, in some cases (T30I mutant), completely overgrew the original virus by day 2. The tentative compensatory mutations were also present in the viral population at 4 dpi and in dead mice (**Fig. 5A**). Overall, the data obtained with wt and N15A viruses, which were genetically stable throughout the experiment, suggest that E protein IC activity is required for a virulent phenotype.

Viruses missing E protein IC activity are prone to evolve and restore ion conductivity

To further analyze the evolution of the mutant viruses lacking E protein IC activity, two clones of the mutants N15A and V25F were serially passaged in cell culture. Throughout the 24 serial passages, E gene was sequenced at passages 0, 8, 16 and 24 for the two mutant viruses and wt as control. As observed during *in vivo* infection, the wt virus remained stable during the passages (**Fig. 5B**). V25F viruses rapidly incorporated additional mutations within E gene (L19A, L27S and T30I), reproducing our *in vivo* observations. The viruses incorporating T30I mutation completely out-competed the original V25F mutant by passage 8 (**Fig. 5B**). In contrast, N15A viruses either remained stable or incorporated a mutation in the E gene (A15D) that appeared late, at passage 24, suggesting that this mutant was more stable, confirming our *in vivo* results (**Fig. 5B**). The data obtained in cell culture or after mice infection indicate that SARS-CoVs lacking E protein IC activity incorporated mutations at the E gene that directly reverted the original mutation that suppressed IC activity (A15D and F25C) or modified residues mapping to a close position of the E protein transmembrane domain. These modified residues face the original mutation inhibiting IC activity, when the ion channel is assembled (**Fig. 6**). To analyze whether these mutations restored IC activity, synthetic peptides representing the E protein transmembrane domain containing the mutations obtained after viral evolution *in vivo* and in cell culture (N15D, V25L, V25F L19A, V25F F26C, V25F L27S, V25F T30I, V25F L37R), were synthesized. The IC activity of these peptides was evaluated in artificial lipid membranes as previously described [34]. Whereas peptides containing the original mutations N15A and V25F did not show

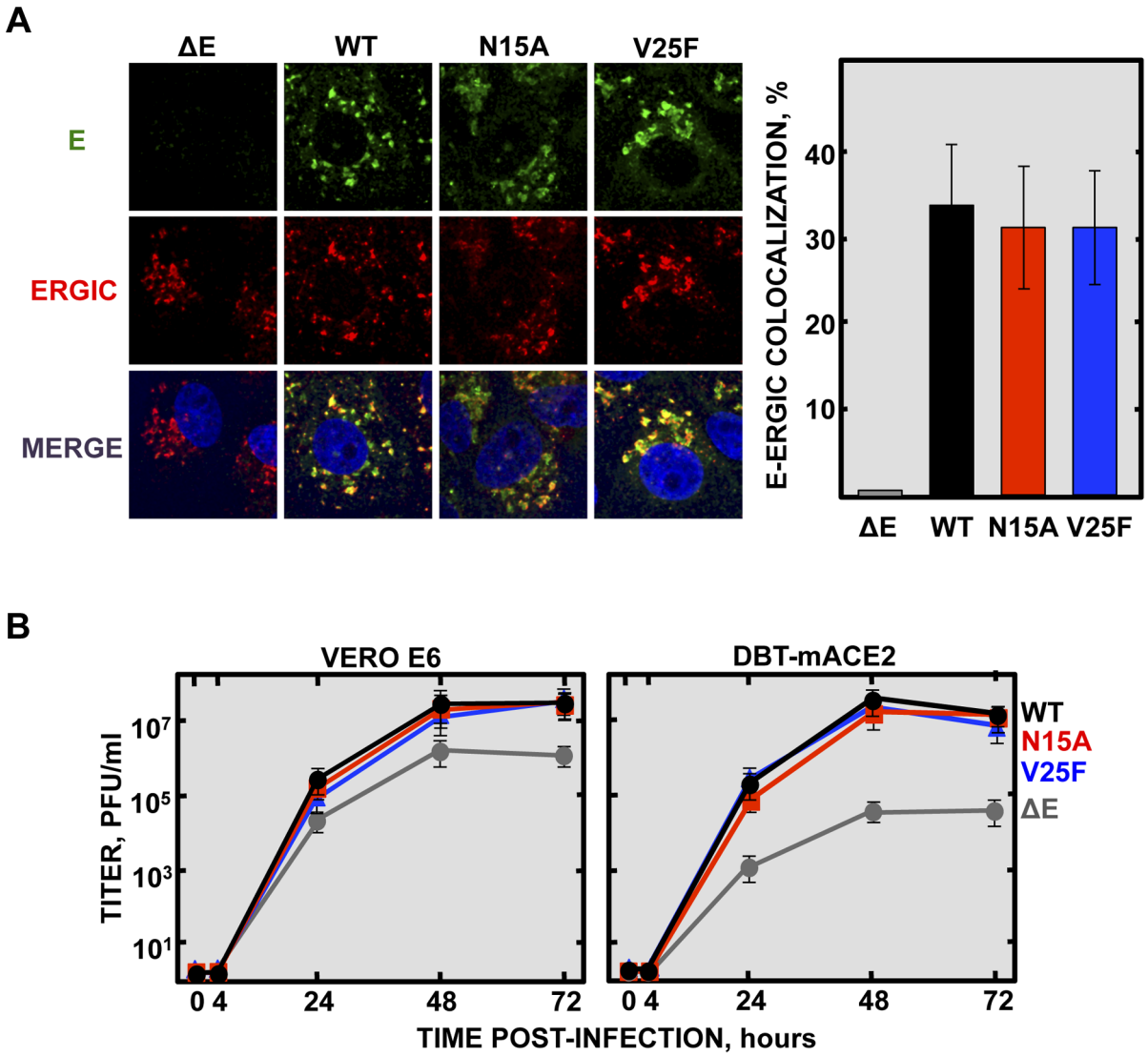

Figure 2. Subcellular localization of rSARS-CoV-EIC$^-$ E proteins, growth kinetics and plaque size. (**A**) Vero E6 cells were infected either with the mutant viruses (N15A and V25F), the parental virus (wt) or a virus lacking E gene (ΔE) at an MOI of 0.3, fixed at 24 hpi and E protein (green) and ERGIC (red) were labeled with specific antibodies. Nuclei were stained with DAPI (blue). Original magnification was 126×. Right graphic on the panel represents the percentage of colocalization between E protein and ERGIC, calculated with Leica LAS AF v2.6.0 software. (**B**) Vero E6 and DBT-mACE2 cells were infected at an MOI of 0.001 with mutant viruses lacking IC activity (N15A and V25F), the parental virus (wt) or a virus lacking E gene (ΔE), and viral progeny was titrated at the indicated times post-infection. Error bars represent the standard deviation of three independent experiments. (**C**) Plaque morphology of the parental, the mutant viruses N15A and V25F and a ΔE virus.
doi:10.1371/journal.ppat.1004077.g002

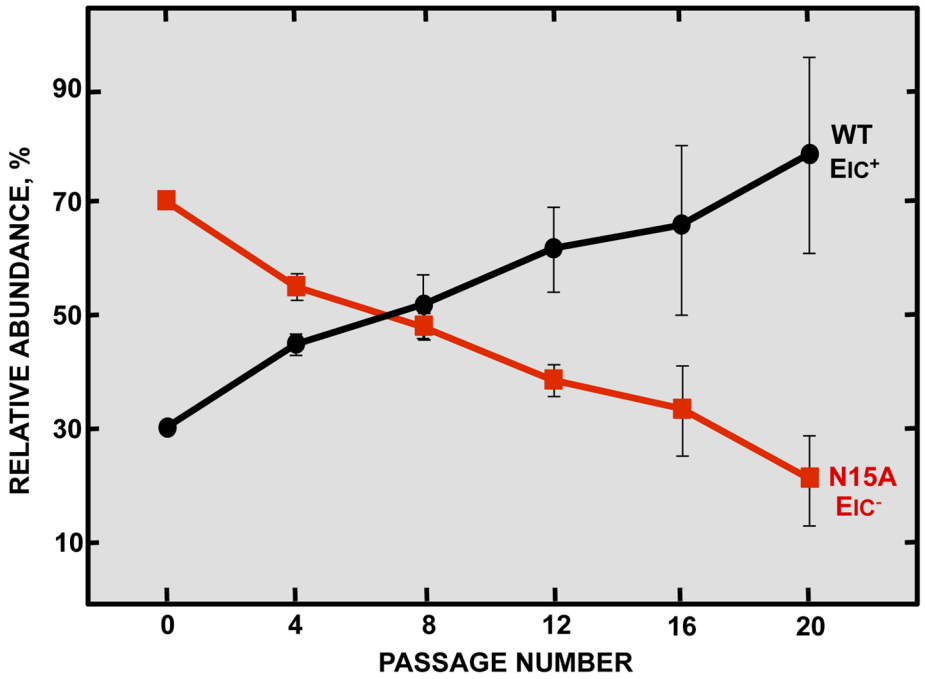

Figure 3. Effect of SARS-CoV E protein IC activity on viral fitness. Competition assays between the parental virus (wt, black circles) displaying IC activity (EIC^{+}) and a mutant virus (N15A, red squares) lacking IC activity (EIC^{-}) were performed. Vero E6 cells were co-infected with mutant and parental viruses at a ratio 7:3 and supernatants were serially passaged 20 times every 24 hours. Relative abundance of each virus was determined by sequencing E gene within viral progeny. Error bars represent the standard deviation from three independent experiments.
doi:10.1371/journal.ppat.1004077.g003

any conductance, all the peptides containing the mutations obtained after viral evolution displayed similar conductance values than a wild type peptide (**Fig. 7**), indicating that all these compensatory mutations restored E protein IC activity.

Genetically engineered revertant viruses restoring E protein IC activity show a virulent phenotype in mice

A correlation between IC activity and virulence was found *in vivo*, where N15A viruses lacking IC activity were attenuated compared to wt virus competent in IC activity. Mutant virus V25F, originally lacking ion conductivity, rapidly incorporated compensatory mutations upon infection *in vivo* that restored IC activity and thus caused pathogenicity. To test whether the recovery of IC activity was the unique determinant of virulence, and to rule out effects of other mutations arising outside of the E gene, recombinant viruses containing a set of the compensatory mutations that restored IC activity (rSARS-CoV-EIC^{rev}): rSARS-CoV-E-V25F L27S (V25F L27S), rSARS-CoV-E-V25F T30I (V25F T30I), rSARS-CoV-E-V25F L37R (V25F L37R) were engineered, rescued and tested in mice. These viruses were

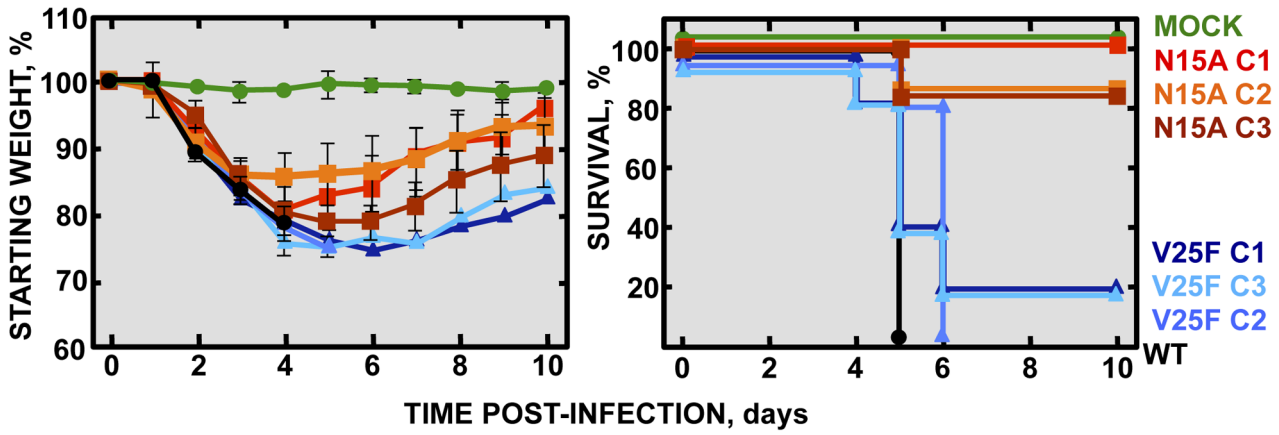

Figure 4. Pathogenesis caused by rSARS-CoV-EIC^{-} in BALB/c mice. Groups of five 16 week-old BALB/c mice were mock infected (Mock, green circles) or infected with 100000 PFU of either the parental virus (wt, black circles) or several clones of the mutant viruses missing IC activity: N15A C1, N15A C2 and N15A C3 (red, orange and deep-red squares, respectively), and V25F C1, V25F C2 and V25F C3 (dark blue, blue and light blue triangles, respectively). Mean weight losses (left graph) and survival (right graph) during 10 days following infection are represented for each group. Error bars represent the standard deviation for mice weights per experimental condition.
doi:10.1371/journal.ppat.1004077.g004

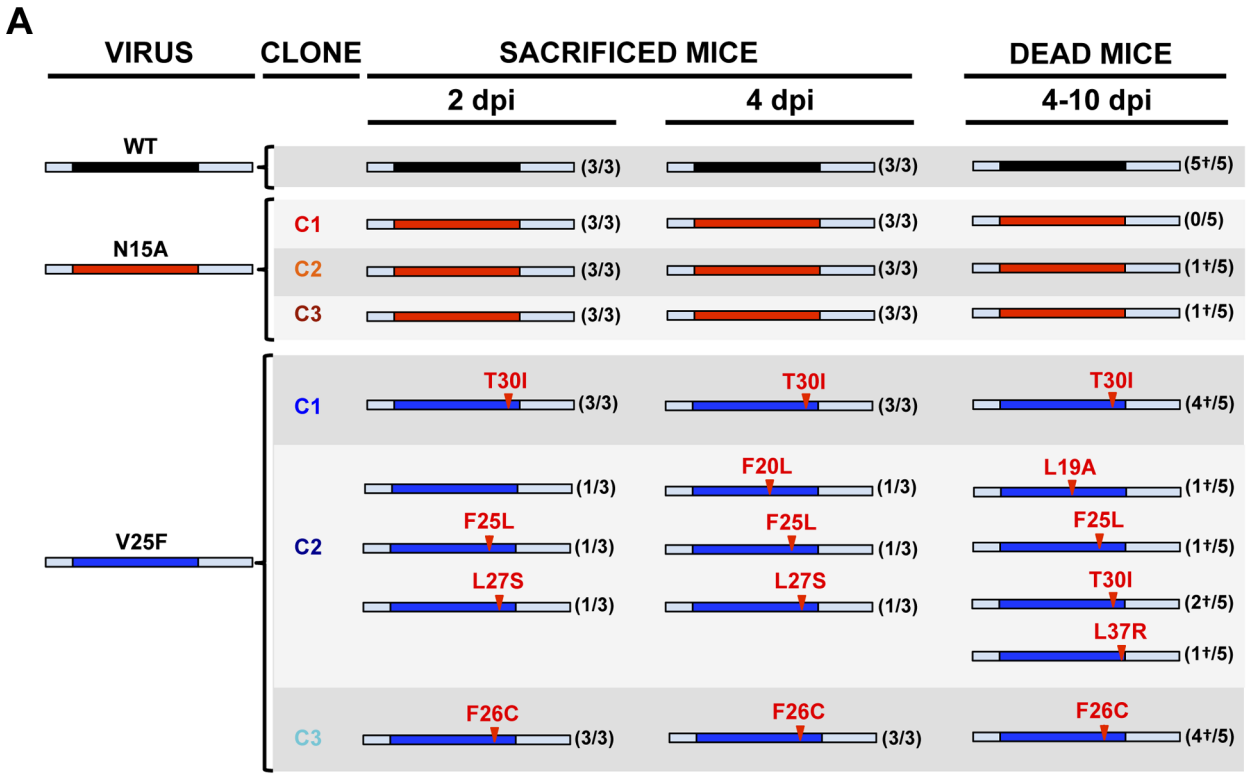

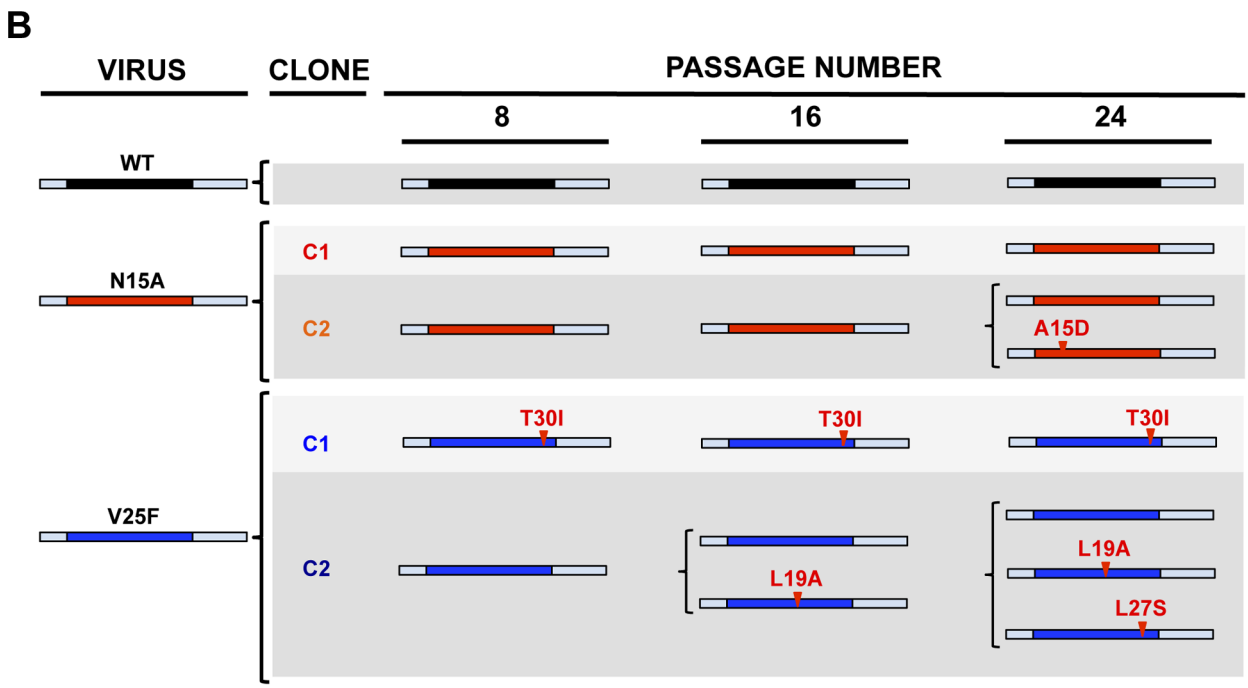

Figure 5. Stability of rSARS-CoV-EIC⁻ after serial infections. (**A**) Groups of eleven 16 week-old BALB/c mice were infected with 100000 PFU of either the parental virus (wt) or three clones of the mutant viruses missing IC activity: N15A C1, N15A C2, N15A C3, V25F C1, V25F C2 and V25F C3. At 2 dpi and 4 dpi 3 mice of each group were sacrificed, lung RNA was extracted, and E gene was sequenced. The rest of the mice (5 per group) participated in the weight-loss and survival experiment. When any mouse died, from 4 to 10 dpi, lung RNA was extracted and E gene was sequenced. Bars represent different E protein sequences, either that of parental or the mutant viruses. The central colored part represents the transmembrane domain of the protein. Letters and numbers in red represent the amino acid changes detected after viral evolution and their relative position within transmembrane domain, respectively. Numbers accompanying bars indicate from how many mice (first number) out of the total of the animals analyzed (second number) arose the indicated sequence change. Dead mice are indicated by a †. (**B**) Vero E6 cells were infected with the wt virus or the mutant clones N15A C1 and N15A C2, V25F C1 and V25F C2 at an initial MOI of 0.5, and supernatants were serially passaged for 24 times every 24 hours. E gene in the viral population was sequenced at passages 0, 8, 16 and 24. Colored bars represent the transmembrane domain of different E protein sequences and letters and numbers in red represent the amino acid mutations identified and their relative position, respectively.
doi:10.1371/journal.ppat.1004077.g005

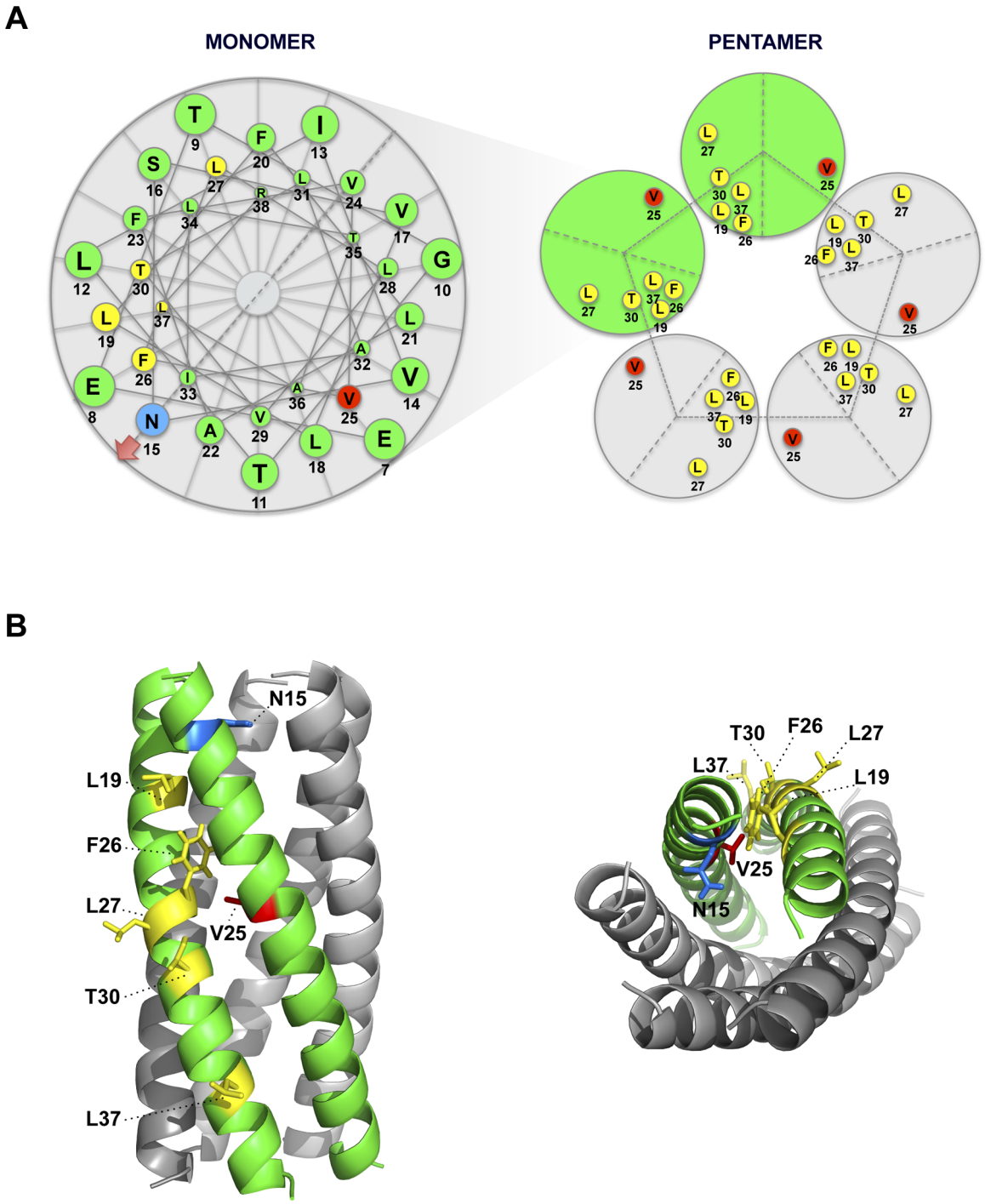

Figure 6. Spatial distribution of the mutations obtained in rSARS-CoV-EIC^{-} after serial infections. (**A**) Left diagram represents a top view of E protein transmembrane domain and the spatial distribution of the amino acids within the alpha helix. Blue and red circles correspond to amino acids N15 and V25, respectively, originally mutated to inhibit IC activity. Yellow circles surround the amino acids that changed after evolution of V25F mutant. Arrow at position 15 points the lumen of the ion channel pore. Right graphic depicts the pentamer conformation of E protein that forms the ion conductive pore and the positions of both the mutated residue at position 25 and the evolved mutations at positions 19, 25, 26, 27, 30 and 37. Evolved changes map close to the originally mutated residue in the monomer-monomer interface. (**B**) Pentameric model of SARS-CoV E protein from a lateral (left) or a top view (right). This model was first proposed from linear dichroism of isotopically labeled E protein transmembrane peptides in lipid bilayers [29,32]. The residues involved in ion channel inhibition (N15 in blue and V25 in red) or mutated after viral evolution (L19, F26, L27, T30 and L37 in yellow) are highlighted.
doi:10.1371/journal.ppat.1004077.g006

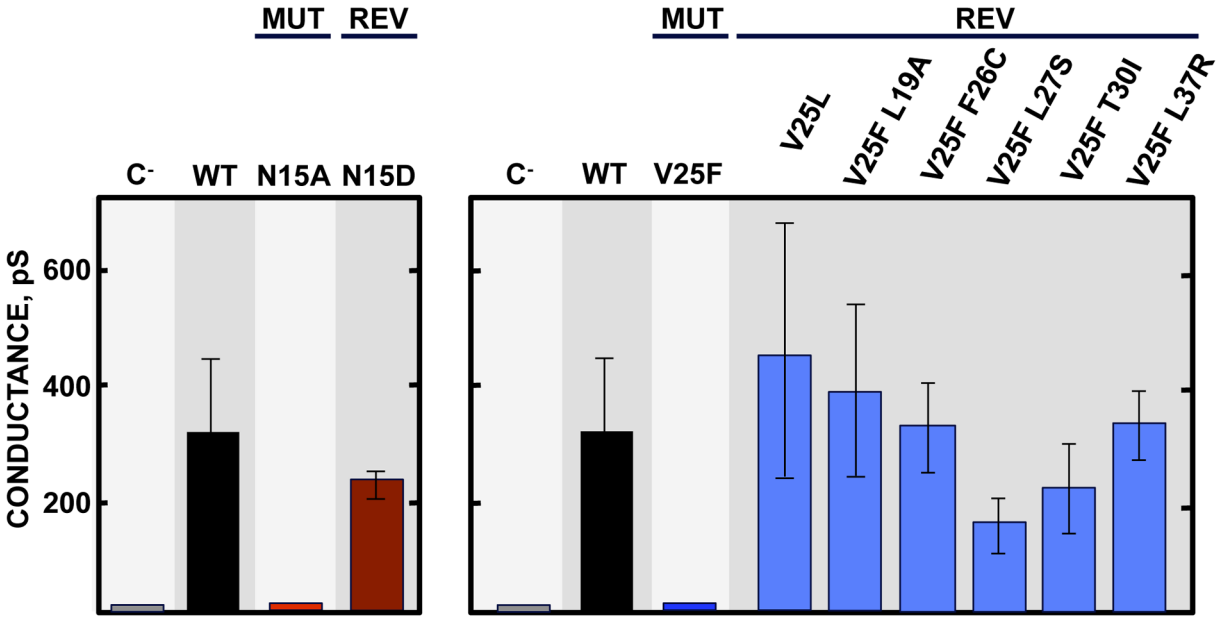

Figure 7. E protein IC activity of the rSARS-CoV-EIC^{-} evolved variants. Synthetic peptides representing E protein transmembrane domain of the parental virus (wt) the mutant viruses (MUT) lacking IC activity (N15A and V25F) and their evolved revertants (REV) obtained after infections of mice or cell culture (N15D, V25L, V25F L19A, V25F F26C, V25F L27S, V25F T30I and V25F L37R) were reconstituted in artificial lipid bilayers, and their IC activity was analyzed as mean conductance values. Negative controls (C^{-}) indicate conductance values obtained in the absence of any peptide. Error bars represent the variations obtained in 100 independent experiments.
doi:10.1371/journal.ppat.1004077.g007

virulent in mice in terms of weight loss and survival rates, causing similar disease as that caused by the wt virus (**Fig. 8**). We sought to confirm this data on another genetic background, so a recombinant SARS-CoV containing the mutation that restored IC activity in N15A mutant after cell culture passage was engineered rSARS-CoV-E-N15D (N15D) and evaluated. In agreement with the V25F revertants, the mutant N15D induced similar morbidity and mortality as wt (**Fig. 8**), confirming that E protein IC activity is a determinant of virus pathogenesis.

SARS-CoV E protein IC activity is dispensable for efficient growth *in vivo*

Although E protein IC activity is not essential for virus growth in cell culture (**Fig. 2B**), it is possible that production of virus *in vivo* further depends on ion conductivity. To test if the attenuation observed *in vivo* with IC inactive viruses is due to lower virus production, 16 week-old BALB/c mice were intranasally inoculated with the wt virus, the genetically engineered revertant viruses N15D and V25F T30I displaying IC activity, or the N15A mutant lacking IC activity. Mice lungs were collected at 2 and 4 days post

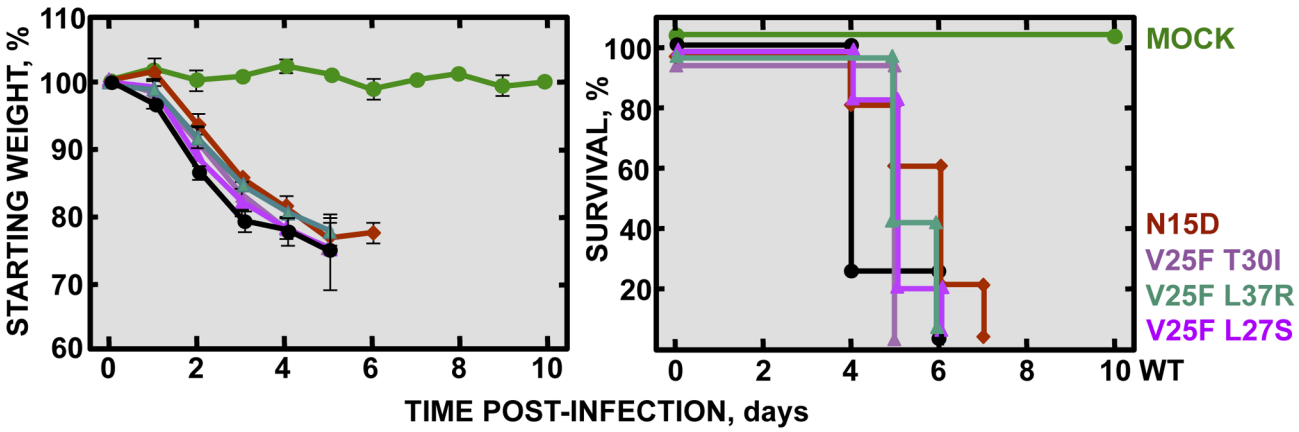

Figure 8. Pathogenesis caused by rSARS-CoV-EIC^{rev} in BALB/c mice. Groups of five 16 week-old BALB/c mice were mock infected (Mock, green circles) or infected with 100000 PFU of either the parental virus (wt, black circles) or the genetically engineered revertant viruses recovering IC activity: N15D (deep-red diamonds), V25F L27S (fuchsia triangles), V25F T30I (pink triangles) and V25F L37R (green triangles). Mean weight losses (left graph) and survival (right graph) during 10 days are represented for each group. Error bars represent the standard deviation for mice weights per experimental condition.
doi:10.1371/journal.ppat.1004077.g008

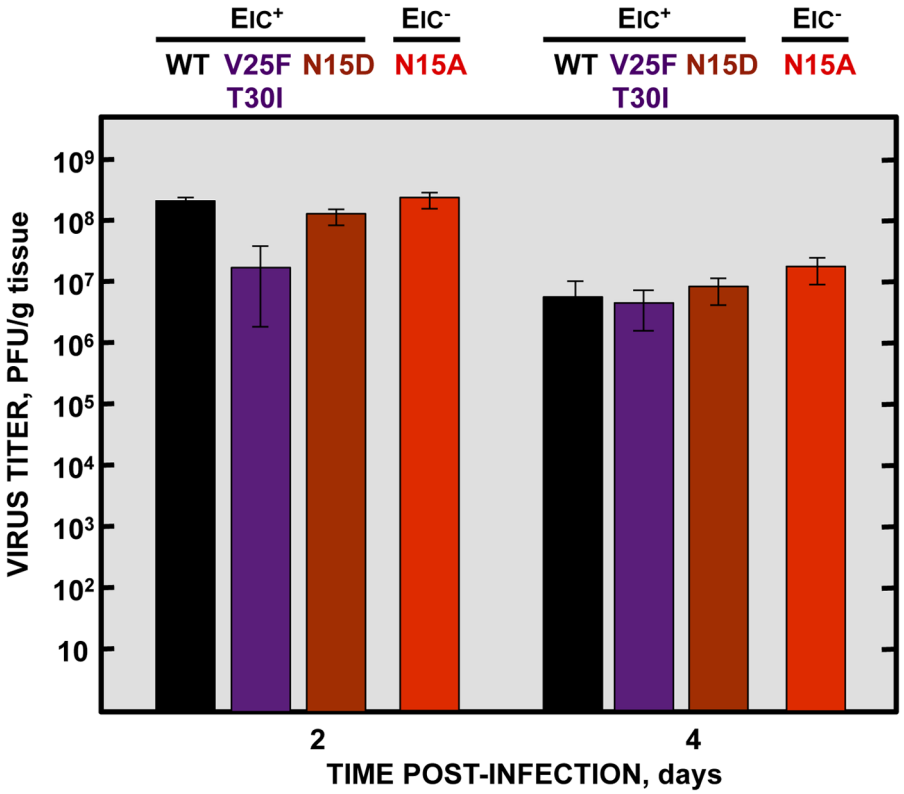

Figure 9. Effects of SARS-CoV E protein IC activity on virus growth in BALB/c mice lungs. Groups of six 16 week-old BALB/c mice were infected with 100000 PFU of viruses displaying E protein IC activity (EIC^+), either the parental virus (wt, black columns) or the genetically engineered revertant viruses V25F T30I (purple columns) and N15D (deep-red columns) or with the mutant lacking IC activity (EIC^-) N15A (red columns). At 2 and 4 days post infection (dpi) 3 mice from each group were sacrificed to determine virus titers.
doi:10.1371/journal.ppat.1004077.g009

infection, homogenized, and viral titers were determined. Interestingly, the virus lacking IC activity (N15A) grew to the same extent or even better than the wt and the revertant viruses, respectively, reaching titers higher than 10^8 and 10^7 PFU/gr of lung tissue at 2 and 4 dpi, respectively (**Fig. 9**). These data indicate that E protein IC activity does not significantly affect virus production *in vivo*, under these experimental conditions. Therefore the attenuation of the virus lacking IC activity is likely due to a host-specific effect mediated by the ion channel in the mouse, and not to a reduction in virus yields.

Viruses with E protein IC activity induced edema accumulation after SARS-CoV infection

To analyze the mechanisms by which IC inactivity confers less virulence, lung sections of mock-infected mice, or of those infected with the wt virus, IC revertants and N15A mutant were collected at 2 and 4 dpi, stained with hematoxylin and eosin and examined for histopathological changes. Mock-infected animals showed wide free alveolar and bronchiolar airways and no evidence of leukocyte infiltrates (**Fig. 10A**). Animals infected with the viruses displaying IC activity, presented swollen alveoli walls and leukocyte infiltrates in the infected areas at both time points (**Fig. 10A**). The histopathology caused by IC proficient viruses was even more dramatic at 4 dpi, where cell infiltrates were more abundant, and air spaces were collapsed by a profuse lung edema, which is the ultimate cause of acute respiratory distress syndrome (ARDS) that leads to lung failure and death (**Fig. 10A**). Edema accumulation at 4 dpi was also reflected by a marked increase (>1.5 fold) in the weight of lungs in animals infected with viruses competent in E protein ion conductivity (**Fig. 10B**). In contrast, mice infected with the virus lacking IC activity (N15A) showed moderate swollen lung epithelia and lung infiltrates that reflected a productive viral infection. However, at 4dpi, lung airways remained free from pulmonary edema, reflected by both the lung sections and in the minimal change of lung weight (**Fig. 10A and 10B**). Such moderate changes in the lung may retain efficient oxygen exchange. These data suggested that E protein IC activity contributes to SARS-CoV induced lung edema.

SARS-CoV displaying E protein IC activity induces disassembly of bronchoalveolar epithelia

ARDS caused by SARS-CoV infection originates from the accumulation of a protein rich edema, leading to severe hypoxemia and eventually to death. Lung epithelial cells create an osmotic gradient between airways and lung interstitium controlling water levels within air spaces. Damage to the epithelium is therefore a major cause of edema accumulation. To test the correlation between presence of E protein IC activity and an increase in epithelial damage leading to edema accumulation, lungs from mock-infected and from mice infected with the wt or the N15A virus were processed at 2 and 4 dpi for immunofluorescence. Epithelium integrity was evaluated using a specific antibody for Na^+/K^+ ATPase, a key factor in establishing the osmotic gradient necessary for edema clearance, and infection was tracked using an antibody specific for N protein. At 2 dpi many infected cells (around 16%) were observed in lungs of mice infected with either wt or N15A virus (**Fig. 11A and S1**), overlapping with the most productive time of viral infection. Both

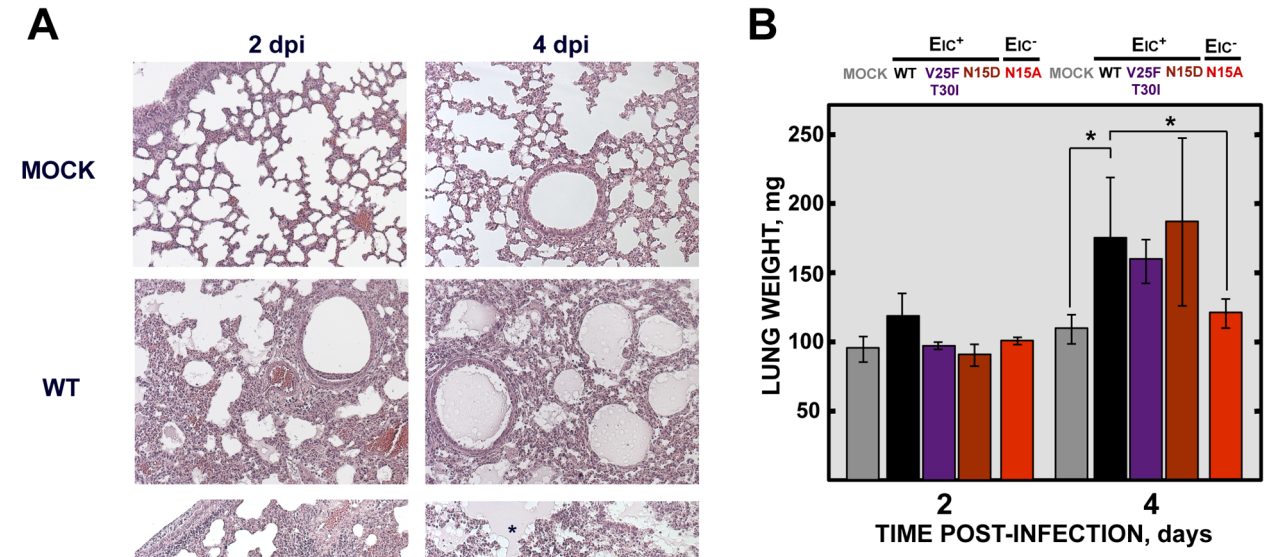

Figure 10. SARS-CoV E protein IC activity and lung pathology. Groups of six 16 week-old BALB/c mice were mock infected (Mock) or infected with 100000 PFU of viruses displaying E protein IC activity (EIC^+), either the parental virus (wt) or the genetically engineered revertant viruses V25F T30I and N15D or with the mutant lacking IC activity (EIC^-) N15A. At 2 and 4 dpi 3 mice from each group were sacrificed and their lungs were collected. (**A**) Lungs were fixed in formalin, paraffin embedded, sectioned and processed for hematoxylin and eosin staining. Asterisks indicate edema accumulation in both bronchiolar and alveolar airways. Original magnification was 20×. (**B**) When collected and prior to fixation lungs were weighted. Error bars indicate the standard deviation from 3 mice lungs per each condition. Statistically significant data are indicated with an asterisk (Student's t-test p-value<0.05).
doi:10.1371/journal.ppat.1004077.g010

viruses presented similar cell tropisms within lungs, infecting bronchiolar epithelium (between 60–70% of the cells) and alveolar epithelium (around 10% of the cells) (**Fig. 11A and S1**). Viral infections caused cell death leading to desquamation, especially at the bronchiolar barrier (**Fig. 11A**). At 4 dpi the number of infected cells was dramatically reduced (close to 1%) (**Fig. 11B and S1**), accompanying viral titer decrease. Interestingly, wt infected mice showed abundant epithelia disassembly at this time point, especially in the bronchioles. Na^+/K^+ ATPase was mislocated from its basolateral position within the plasma membrane of epithelial cells as a consequence of bronchiolar barrier destruction, and detected in desquamated cells or cell debris present at air spaces (**Fig. 11B**), where edema accumulation was also observed (**Fig. 10**). The removal of Na^+/K^+ ATPase from its native position within the epithelial barrier most likely prevented its function in edema clearance. In contrast, animals infected with N15A mutant, presented less damaged epithelia and Na^+/K^+ ATPase location was not disturbed (**Fig. 11B**), which may allow edema resolution, as no accumulation of protein rich edema was observed under these conditions (**Fig. 10**).

E protein IC activity triggers the production of IL-1β, TNF and IL-6, key inflammatory cytokines in lung damage and edema accumulation

Severe damage caused to the epithelial barrier is associated with an acute inflammatory response in the lung parenchyma along

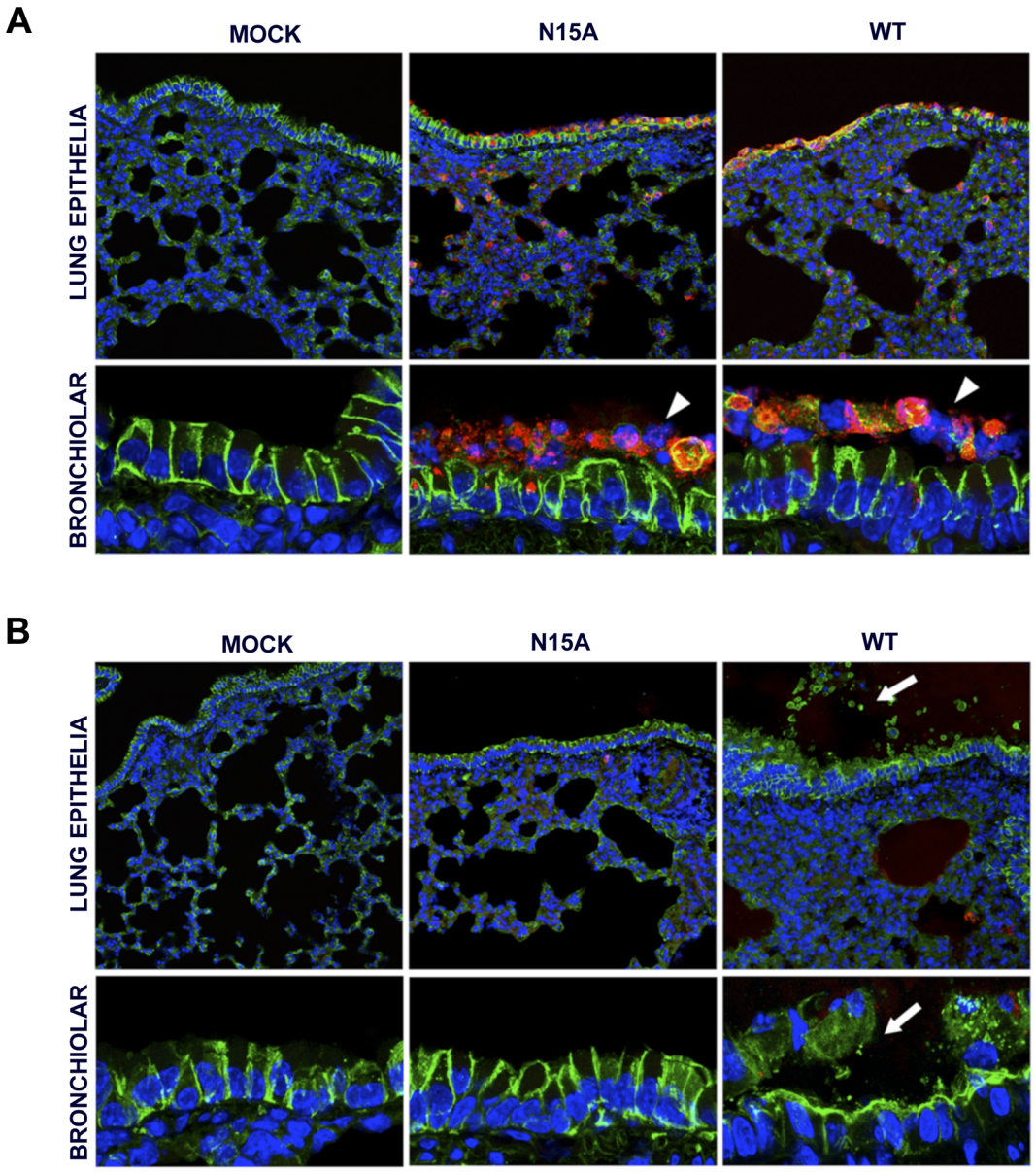

Figure 11. Lung epithelia disassembly in SARS-CoV infected BALB/c mice. 16 week-old BALB/c mice were mock infected (Mock) or infected with 100000 PFU of the parental virus (wt) displaying E protein IC activity or the mutant virus lacking IC activity N15A. At 2 (**A**) and 4 (**B**) dpi mice were sacrificed and their lungs were fixed in formalin, paraffin embedded, sectioned and processed for immunofluorescence. Na^+/K^+ ATPase was labeled in green, SARS-CoV N protein was labeled in red to detect infected cells and cell nuclei are shown in blue. A general view of lung epithelia at an original magnification of 40× is shown in the upper rows of the panels. Magnified bronchiolar epithelia at an original magnification of 189× are shown in the rows of the bottom. White arrowheads indicate cell desquamation in the bronchiolar barrier. White arrows show epithelium disassembly and mislocated Na^+/K^+ ATPase staining away from basolateral cell membranes, and present within air spaces.
doi:10.1371/journal.ppat.1004077.g011

with edema accumulation. Elevated levels of inflammatory cytokines IL-1β, TNF and IL-6 are found in the lungs of ARDS patients and play a key role in the progression of the disease [62]. IL-1β is an early response highly inflammatory cytokine that is tightly regulated. During viral infection, recognition of pathogen molecular associated patterns (PAMPs) by the cells, such as double stranded viral RNA, induces IL-1β mRNA expression and translation to generate the inactive form of the protein pro-IL-1β. Upon certain stimuli, pro-IL-1β is then cleaved by caspase-1 through inflammasome activation, generating the active form IL-1β, which is subsequently secreted to exert its function [52]. Interestingly, viral proteins with IC activity have been recently found to activate the inflammasome, which finally leads to the secretion of active IL-1β to the extracellular media [52,59]. We thus sought to test whether E protein IC activity was implicated in the production of active IL-1β in the lungs of SARS-CoV infected mice. First, the expression of pro-IL-1β mRNA and the amounts of its derived protein, inactive pro-IL-1β, were measured in wt- and N15A-infected mice at 2dpi. Infections with both wt and N15A mutant viruses induced similar overexpression of pro-IL-1β mRNA as compared with the mock-infected animals (**Fig. 12A**). The increased levels of pro-IL-1β mRNA found in infected mice,

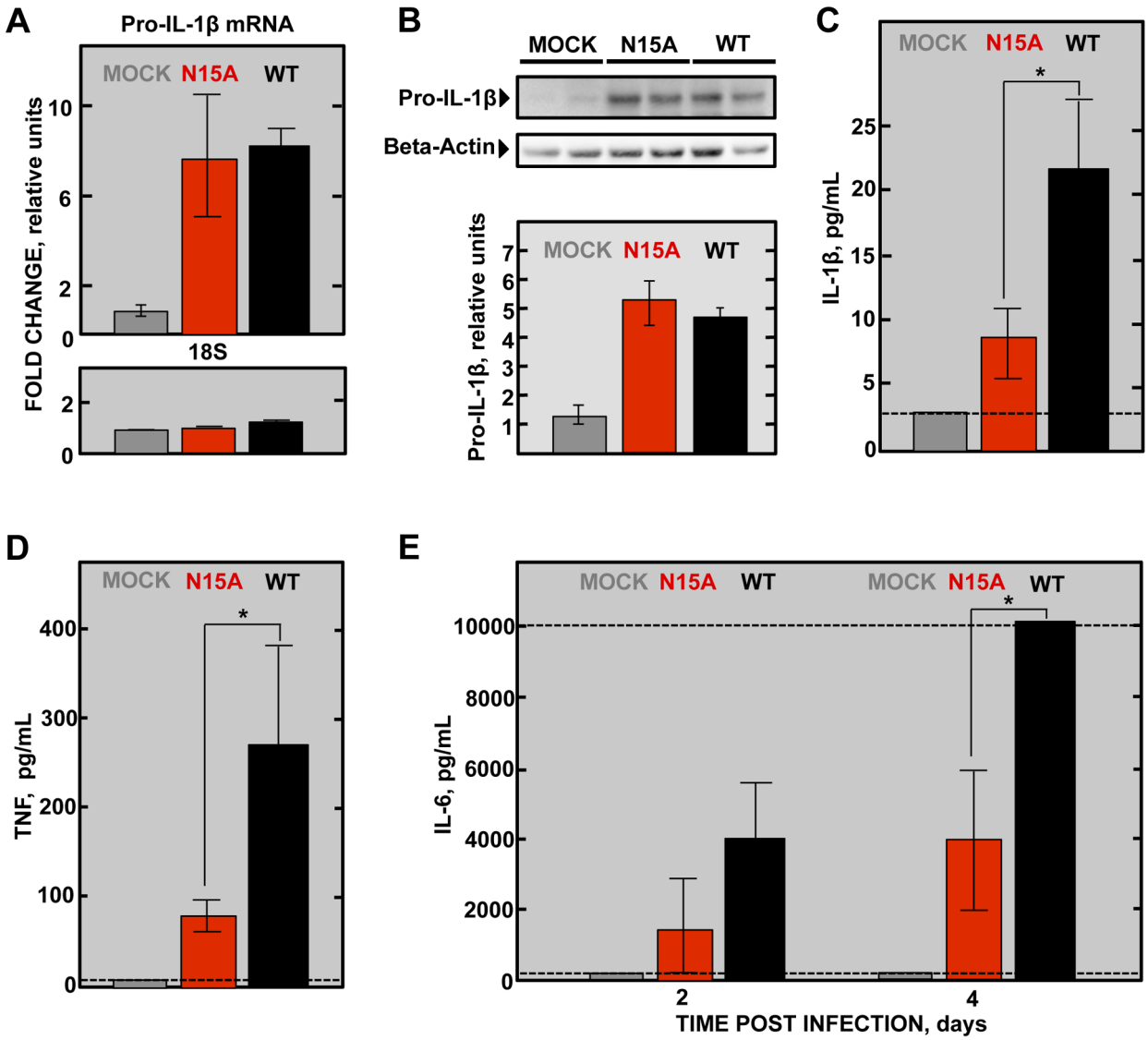

Figure 12. SARS-CoV E protein IC activity and induction of inflammatory cytokines involved in lung injury. Groups of six 16 week-old BALB/c mice were mock infected or infected with 100000 PFU of the parental virus (wt) displaying E protein IC activity or the mutant virus lacking IC activity N15A. At 2 dpi 3 mice from each group were sacrificed and their lungs were collected. (**A**) Total RNA was extracted and levels of pro-IL-1β mRNA, and 18s rRNA (18S), as a control, were analyzed by RT-qPCR. Error bars indicate the standard deviation from samples of 3 mice per experimental setting. (**B**) Lung protein extracts were prepared and levels of inactive pro-IL-1β (35 kDa) and beta-actin, as a loading control, were detected by Western blot and quantified by densitometry analysis. Bottom of the figure represents the ratio pro-IL-1β/beta-actin relative to the mock-infected animals levels, as a reference. Bronchoalveolar lavages (BAL) of infected mice were collected and the concentration of (**C**) the active form of IL-1β protein at 2 dpi, (**D**) TNF protein at 2 dpi and (**E**) IL-6 protein at 2 and 4 dpi within the lavages were determined using the Luminex technology. Error bars indicate the standard deviation from samples of 3 mice per condition. Discontinuous lines indicate the limit of the detection of the technique. Statistically significant data are indicated with an asterisk (Student's t-test p-value<0.05).
doi:10.1371/journal.ppat.1004077.g012

correlated with enhanced amounts of inactive pro-IL-1β, which reached similar values in wt and N15A infections (**Fig. 12B**). To analyze the levels of active, secreted IL-1β, bronchoalveolar lavages were performed at 2 dpi. The amount of IL-1β in the airways was significantly higher in the mice infected with the wt virus displaying E protein IC activity, over those infected with the mutant N15A missing this function (**Fig. 12C**). Collectively, these data indicated that E protein IC activity promotes the secretion of mature IL-1β, without increasing pro-IL-1β transcription or synthesis.

IL-1β enhances the production of TNF, another key early response cytokine, and IL-6, which follows a more sustained increase over time [62–64]. Therefore, it is not surprising that both TNF and IL-6 levels were more dramatically increased in wt-infected mice in comparison with the N15A-infected mice at 2 dpi (**Fig. 12D and 12E**). Furthermore, analysis of IL-6 levels in the bronchoalveolar lavages of infected mice at 4 dpi, revealed that overwhelming amounts of this cytokine, exceeding 10000 pg/mL, accumulated in wt-infected mice, whereas IL-6 levels were at least 2.5-fold lower when E protein IC activity was absent during infection (**Fig. 12E**). All these results indicate that the presence of E protein IC activity correlates with the activation of the inflammasome and an acute inflammatory response that is deleterious for lung tissue.

Discussion

Several viruses that cause severe diseases in humans encode small transmembrane proteins containing IC activity [44]. The alteration of host cell ion balance by these proteins is usually necessary for virus production and maturation, but the effect of IC activity in pathogenesis is less well understood. Coronaviruses are the causative agent of recent and likely future serious diseases. We have focused this study on SARS-CoV E protein, a virulence determinant displaying IC activity. In this manuscript, we sought to elucidate the role of E protein IC activity in virus pathogenesis by combining our knowledge of residues essential for E protein ion conductivity with the manipulation of SARS-CoV genome. To this end we used a mouse adapted genetic background (MA15) assembled in a bacterial artificial chromosome (BAC). Two rSARS-CoVs, each one containing mutation N15A or V25F in the transmembrane domain of E protein were generated to knock down its IC activity. Upon competition during several passages, the viruses lacking E protein IC activity were clearly overgrown by the parental virus, which replicated better. Nevertheless, these differences in viral growth needed several replication cycles to be amplified and detected, as only slight no significant changes in virus production were observed after 72 hours growth kinetics. In agreement with this result, when T16A mutation was introduced within IBV E protein, which represents the equivalent mutation to SARS-CoV E protein N15A, no alterations in the production of virus like particles (VLPs) were detected after 48 hours [40]. The fact that deeper alterations of CoV E protein transmembrane domain cause much more dramatic effects in virus production [37,39] may be due to additional structural or functional changes in E protein, besides their effect on ion conductivity. In conclusion, E protein IC activity, although not essential for virus production, confers and advantage to the virus by enhancing its fitness and growth. Accordingly, a selective advantage of IC activity has also been shown for influenza virus. Mutants lacking M2 protein IC activity were overgrown by the parental virus in competition assays in an even faster manner than in SARS-CoV, probably because the influenza virus lacking IC activity has more profound replication defects [65,66]. SARS-CoV encodes other two proteins, 3a and 8a, which also contain IC properties [41,42]. Therefore, an essential contribution of IC activity to virus production cannot formally be excluded for SARS-CoV, as 3a and 8a derived ion channels could functionally compensate the absence of E protein IC activity.

SARS-CoV mutant viruses lacking E protein IC activity showed a clear tendency to revert both in cell culture and *in vivo* after mice infection. N15A and V25F mutant viruses, devoid of E protein ion conductivity, incorporated additional mutations in the E gene to restore IC activity, suggesting that this function confers a selective advantage to the virus. This trend was more evident in the case of V25F virus, which evolved more quickly and frequently than the N15A mutant virus. No reversion of E protein IC activity was observed for N15A mutant in mice, at least during the first five days post infection. Attempts to sequence the viral progeny at 9 and 10 days after the inoculation were unsuccessful, probably because the virus was mostly cleared by those time points. Nevertheless, as N15A mutant restored its ion channel activity after long number (>24) of passages in cell culture, it is possible that after serial passages *in vivo* this mutant could also revert, as ion conductivity confers better fitness for the virus. Although both N15A and V25F mutations equally disrupted IC activity, the mechanisms by which this is achieved could be different. Replacement of N at position 15 to A, an amino acid predicted to be located facing the channel lumen, is not likely to affect the channel architecture. In fact, the rotational orientation in lipid bilayers of a labeled synthetic transmembrane peptide bearing this mutation was entirely consistent with that of a pentameric model [29]. In contrast, mutation at V25 implies the introduction of a larger side chain (replacement of V to F) at the monomer-monomer interface, which is likely to affect the overall structure of the homo-oligomer and therefore inhibit ion conductivity by causing larger structural changes. This may also explain the higher number of compensatory mutations found in V25F with respect to N15A virus, as the ways to recover a stable oligomer are more varied than those needed to recover channel activity. The compensatory mutations incorporated by the V25F mutant mapped to the opposite face of the transmembrane helix, although they are adjacent when the E protein pentamer is formed. Therefore, the compensatory mutations most likely restored the interaction and assembly between the mutated monomers, reinforcing our hypothesis (**Fig. 6**). IC activity restoration through virus passage suggests that this function is important for the virus. Several of the mutations restoring ion channel activity appeared both in mice and in cell culture. Therefore, it seems that reverting E protein ion conductivity, and not adaptation to mice, was its main goal. Nevertheless, the possibility that these mutations could also improve mouse adaptation through an ion channel dependent or independent mechanism cannot be fully excluded.

E protein IC activity was also involved in SARS-CoV pathogenesis as tested in the mouse model. Viruses lacking IC activity that were stable during multiple passages (N15A mutants) caused reduced mortality, whereas the wt and the mutant viruses restoring IC activity during mice infection (V25F background-evolved variants) caused high mortality rates. Furthermore, genetically engineered viruses containing the point mutations necessary to recover E protein IC activity induced similar mortality as wt virus, reinforcing that E protein IC activity contributes to SARS-CoV pathogenicity. The relevance of viroporins in virus virulence has also been shown in other viruses, such as respiratory syncytial virus SH protein, influenza A virus M2 protein and classical swine fever virus p7 protein [67–70], by deleting a large fraction of or the entire protein. Viroporins may play other critical functions apart from ion conduction. Therefore, a direct correlation between IC activity and virulence could not be formally established. To our knowledge, this is the first time in which the IC activity of a viroporin is directly linked to the virulence of the virus.

The infection with highly pathogenic respiratory viruses, including SARS-CoV, is one of the causative agents of acute lung injury (ALI) and its most severe form, ARDS [71]. Just in the United States, 200,000 ARDS cases are reported annually with a 40% mortality rate [72]. Late stages of ARDS are characterized by development of pulmonary edema that leads to an impaired gas exchange, hypoxemia and eventually death. Infection of mice with rSARS-CoV-MA15 resulted in an abundant edema accumulation both in alveolar and bronchiolar spaces at late times post infection (4 dpi), which correlated with mortality. This phenotype was reproduced upon mice infection with other highly-virulent SARS-CoVs displaying IC activity based on alternative E protein sequences (revertant viruses). On the other side, infection of mice with the attenuated mutant lacking E protein IC activity (N15A) caused significantly reduced edema accumulation, likely contributing to a majority of the animals surviving. Collectively, these data indicate that E protein IC activity *in vivo* promotes lung pathology through edema accumulation.

The pulmonary epithelia regulate water levels present within air spaces, a critical parameter for gas exchange, and play a critical role in edema clearance [72,73]. Epithelial cells create an osmotic

gradient mainly through a coordinated Na^+ transport first from the airways to the cell cytoplasm through epithelial sodium channels (ENaC), located at the apical part of the plasma membrane, and then to the interstitium by Na^+/K^+ ATPase, present at the basolateral region of the plasma membrane. This vectorial transport of Na^+ is accompanied by a water removal from the airspace and edema resolution [72,73]. The integrity of alveolar and bronchiolar epithelia was analyzed by labeling of Na^+/K^+ ATPase in the lungs of mice infected with the virus containing or lacking IC activity. Interestingly, animals infected with the wt virus presented a strong disassembly of bronchiolar epithelia and mislocalization of Na^+/K^+ ATPase from its basolateral distribution within cells at late times, coincident with edema accumulation. In contrast, epithelia integrity was clearly preserved in the lungs of animals infected with the virus missing E protein IC activity. Intact lung epithelia may be required for proper function of the main components involved in edema resolution (Na^+/K^+ ATPase and ENaC), which may explain the lack of edema and therefore the attenuation observed for this virus. As previously described for SARS-CoV, differences in viral tropism within lung cells, without affecting viral production, can induce different pathologies [74]. Nevertheless, we have observed no significant differences in the infection patterns in the presence or absence of E protein ion channel activity, suggesting that the virulence conferred by E protein IC activity does not depend on alternative tropisms.

Pulmonary epithelia damage leading to ALI and ARDS is a consequence of a cytokine burst initiated, in this case, by viral infection. One of the key early-response cytokines driving proinflammatory activity in bronchoalveolar spaces is IL-1β [75]. IL-1β is mainly produced by macrophages and dendritic cells through inflammasome activation. Ion imbalances within cells have been described as triggers of this pathway [52]. The levels of active IL-1β secreted to the airways were enhanced when E protein IC activity was conserved in SARS-CoV infection. Taking into account that the presence or absence of SARS-CoV E protein IC activity did not interfere with the production of IL-1β precursors (mRNA and protein levels of pro-IL-1β), these results suggest that E protein ion conduction may induce inflammasome triggering resulting in secretion of mature IL-1β. In agreement with this hypothesis, release of active IL-1β has recently been reported for viroporins of other viruses [52,53,57,59]. IL-1β is implicated in the development of diverse pathologies, including obesity, atherosclerosis, diabetes and several pulmonary illnesses such as asthma, pulmonary obstructive chronic disease and ARDS progression through edema accumulation [75–78]. Here, we report the implications of this cytokine in SARS-CoV pathology and E protein ion channel activity as a trigger of its production.

ARDS progression involves the production of TNF, another early response cytokine, and IL-6, which exerts its function in a more sustained manner accumulating during the disease [63]. We found that after SARS-CoV infection, these patterns of cytokine expression were clearly reproduced. TNF and IL-6 accumulated to higher levels in the lungs of animals infected with the wt virus displaying IC activity compared to the mutant lacking ion conductivity. IL-1β enhances the production of TNF, and IL-6 is stimulated by both cytokines providing an integrated amplified inflammatory response, detrimental for pulmonary function [63]. Elevated amounts of these cytokines have been reported in bronchoalveolar lavages of SARS-CoV patients [79]. Therefore, the enhanced amounts of active IL-1β found in the animals infected with the wt virus may explain the increased levels of TNF and IL-6, which leads to severe pathology. It is important to note that the increased damage found in pulmonary epithelia infected with the virus displaying E protein IC activity may not be explained by a higher virus production, as suppression of E protein IC activity rendered similar growth in mice lungs during the analyzed time points. SARS-CoV early replication may be a relevant issue in the induction of pathology. We cannot exclude early replicative defects for the N15A mutant in mice, delaying virus growth during the first hours post-infection. Nevertheless, alternative explanations are also possible, as it has been described that some mutations at SARS-CoV S gene conferred increased virulence without affecting growth within mice, even at early times. This increased pathogenesis was mainly dependent on an exacerbated host response to the viral infection [74]. Accordingly, the enhanced inflammatory response triggered by E protein ion channel proficient viruses may be a major pathology inducer.

In this study, we have shown that SARS-CoV E protein IC activity is a virulence determinant, influencing inflammatory responses, including those inflammasome-derived, pulmonary damage and disease outcome. Although not essential for virus production, E protein IC activity confers a selective advantage, as the parental virus, competent for ion conductivity, was more fit. Nevertheless, the virulence associated to E protein ion conductivity could represent a non-selectable consequence. SARS-CoV crossed species barriers from zoonotic reservoirs such as bats, palm civets and raccoon dogs to humans, causing a severe disease [71]. Possibly, in SARS-CoV infection of its natural hosts, E protein ion channel activity may not have a relevant impact in SARS-CoV pathogenesis, and therefore it was positively selected before crossing species barrier. In conclusion, this work provides several findings that may have translational relevance for other coronaviruses, such as the highly pathogenic MERS-CoV, and even on other viruses encoding proteins with IC activity.

Materials and Methods

Ethics statement

Animal experimental protocols were approved by the Ethical Committee of The Center for Animal Health Research (CISA-INIA) (permit numbers: 2011-009 and 2011-09) in strict accordance with Spanish national Royal Decree (RD 1201/2005) and international EU guidelines 2010/63/UE about protection of animals used for experimentation and other scientific purposes and Spanish national law 32/2007 about animal welfare in their exploitation, transport and sacrifice and also in accordance with the Royal Decree (RD 1201/2005). Infected mice were housed in a ventilated rack (Allentown, NJ).

Cells

The African green monkey kidney-derived Vero E6 cells were kindly provided by Eric Snijder (Medical Center, University of Leiden, The Netherlands). The mouse delayed brain tumor cells stably expressing the murine receptor for SARS-CoV (DBT-mACE2) were generated as previously described [61]. Baby hamster kidney cells (BHK-21) were obtained from American Type Culture Collection (ATCC; CCL-10). Cells were grown at 37°C with an atmosphere of 98% humidity, in Dulbecco's modified Eagle medium (DMEM, GIBCO) supplemented with 25 mM HEPES, 2 mM L-glutamine (SIGMA), 1% non essential amino acids (SIGMA) and 10% fetal bovine serum (FBS, Biowhittaker).

Mice

Specific-pathogen-free 8 week-old BALB/c OlaHsd female mice were purchased from Harlan. Mice were maintained for 8 additional weeks in the animal care facility at the National Center

of Biotechnology (Madrid). All protocols were approved by the Ethical Review Committee at the center for animal health research (CISA-INIA). For infection experiments, 16-week-old mice females were anesthetized with isoflurane and intranasally inoculated with 100000 PFU of the indicated viruses. All work with infected animals was performed in a BSL3 laboratory (CISA, INIA) equipped with a ventilated rack (Animal transport unit-Bio containment unit, Harvard) to store the animals during the experiment.

Construction of mutant rSARS-CoVs-MA15

An infectious cDNA clone encoding a mouse adapted (MA15) SARS-CoV assembled in a bacterial artificial chromosome (BAC) in our laboratory [26] was used as the background to introduce the mutations that inhibited or restored E protein IC activity. Briefly, DNA fragments representing the nucleotides 26044 to 26779 of SARS-CoV-MA15 genome, flanked by the restriction sites BamHI and MfeI, respectively, were chemically synthesized (Bio Basic Inc). These fragments contained different point mutations within the E gene, that generated amino acid changes inhibiting IC activity: N15A (AAT to GCC) and V25F (GTA to TTC) or restoring this activity: N15D (GCC to GAC), V25F L19A (GTA to TTC and CTT to GCA), V25F L27S (GTA to TTC and TTG to TCG), V25F T30I (GTA to TTC and ACA to ATA), V25F L37R (GTA to TTC and CTT to CGT). The fragments containing these mutations were digested and exchanged in the original BAC. The genetic integrity of the cloned DNA was verified by restriction analysis and sequencing.

Recovery of recombinant viruses from the cDNAs clones

BHK cells were grown to 95% confluency in 12.5 cm^2 flasks and transfected with 6 μg of the infectious cDNA clones and 18 μl of Lipofectamine 2000 (Invitrogen), according to the manufacturer's specifications. At 6 hours post transfection, cells were trypsinized, added to Vero E6 cells confluent monolayers grown in 12.5 cm^2 flasks and incubated at 37°C for 72 h. Cell supernatants were harvested, passaged once on fresh cells and the recovered viruses were cloned by three rounds of plaque purification following standard procedures.

Growth kinetics and plaque assays

Vero E6 or DBT-mACE2 cells were grown to confluency on 12.5 cm^2 flasks and infected at a multiplicity of infection (MOI) of 0.001. Cells supernatants were collected at 0, 6, 24, 48 and 72 hpi and titrated on Vero E6 cells. For virus titration and plaque detection, supernatants of infected cells were added to confluent monolayers of Vero E6 cells and incubated for 45 min at 37°C. Media was removed and cells were overlaid with DMEM containing 0.6% of low melting agarose and 2% of fetal calf serum (FCS). At 72 hpi cells were fixed with 10% formaldehyde and stained with crystal violet.

Confocal microscopy

Vero E6 cells were grown to 90% confluency on glass coverslips and infected with rSARS-CoV-ΔE, rSARS-CoV wt, rSARS-CoV-E-N15A and rSARS-CoV-E-V25F at an MOI of 0.3. At the indicated hpi, media were removed and cells were washed twice with PBS and fixed with 4% paraformaldehyde in PBS for 30 min at room temperature. Then, cells were washed twice with PBS and permeabilized for 10 min with 0.2% saponin and 10% FBS in PBS. Primary antibody incubations were performed in PBS containing 10% FBS and 0.2% saponin for 1 h 30 min at room temperature. Immunofluorescence was performed using a mouse mAb specific for ERGIC53 (dilution 1:200, Alexis Biochemicals), and a rabbit pAb specific for E protein [15] at 1:2000 dilution. Coverslips were washed four times with PBS between primary and secondary antibody incubations. Alexa 488- or Alexa 546-conjugated antibodies specific for the different species (dilution 1:500, Invitrogen) were incubated for 45 min at room temperature in PBS containing 10% FBS. Nuclei were stained using DAPI (dilution 1:200, Sigma). Coverslips were mounted in ProLong Gold anti-fade reagent (Invitrogen) and examined on a Leica SP5 confocal microscope (Leica Microsystems). Colocalization studies were performed using Leica LAS AF v2.6.0 software.

Virus genome sequencing

The genomic region including nucleotides 26017 to 26447 that contains the E gene was sequenced after RT and PCR reactions. Briefly, total RNA from infected cells or homogenized mice lungs, was collected and purified using RNeasy kit (Qiagen) according to the manufacturer's specifications. For RT reaction, 1 μg of RNA was used as template, random oligonucleotides primers and Thermoscript reverse transcriptase (Invitrogen). The product was subsequently subjected to a PCR reaction using the oligonucleotides E-VS (CTCTTCAGGAGTTGCTAATCCAGCAATGG) and E-RS (TCCAGGAGTTGTTTAAGCTCCTCAACGGTA) and the Vent polymerase (New England Biolabs), following manufacturer's recommendations. Sequence assembly and comparison with the consensus sequence of SARS-CoV-MA15 strain were performed with the SeqMan program (Lasergene, Madison, WI).

Genetic stability through serial infections of SARS-CoVs lacking IC activity

Confluent monolayers of Vero E6 cells grown in 12.5 cm^2 flasks were infected at an MOI of 0.5 with the viruses rSARS-CoV wt, rSARS-CoV-E-N15A and rSARS-CoV-E-V25F. At 24 hpi, supernatants were collected and passaged on fresh monolayers of Vero E6 cells, performed 24 times, serially. E gene sequence was analyzed at passages 0, 8, 16 and 24 as described.

For *in vivo* experiments, mice were intranasally inoculates with 100000 PFU of the viruses described above. Lungs were collected at days 2 and 4 post infection and incubated in RNAlater (Ambion) at 4°C for 48 hpi prior to −80°C freezing. To extract total RNA, lungs were homogenized in 2 ml of RLT lysis buffer (QIAGEN) containing 1% β-mercaptoethanol using gentleMACS Dissociator (Miltenyi Biotec). Samples were centrifuged at 3000 rpm during 10 min, and RNA was purified from supernatants using RNeasy kit (QIAGEN) as previously described.

Peptide synthesis and ion channel measurements in artificial lipid membranes

Synthetic peptides representing the transmembrane domain of SARS-CoV E protein (amino acids 7 to 38) encoding the point mutations that appeared after serial infections of the mutant viruses were generated by standard phase synthesis, purified by HPLC and their IC activity was tested in artificial lipid membranes, as previously described [34].

Competition assays

Total RNA from co-infected cells was isolated and E gene was sequenced as described above. Relative abundance of the rSARS-CoV wt and rSARS-CoV-E-N15A viruses within viral population was determined by quantifying the relative amounts of their

respective E gene genetic markers in the sequence obtained from the population.

Mice infection and evaluation of virus virulence

16 week-old BALB/c mice females were intranasally inoculated with 100000 PFU of the viruses rSARS-CoV wt, rSARS-CoV-E-N15A, rSARS-CoV-E-V25F, rSARS-CoV-E-N15D, rSARS-CoV-E-V25F L27S, rSARS-CoV-E-V25F T30I and rSARS-CoV-E-V25F L37R in 50 µl of DMEM containing 2% FCS. Weight loss and survival of the infected mice were monitored for 10 days. Animals reaching weight losses higher than 25% of the initial body weight were sacrificed according to the established euthanasia protocols.

Virus growth in mice lungs and lung histology

Mice were inoculated with 100000 PFU of the virus rSARS-CoV wt, rSARS-CoV-E-N15A, rSARS-CoV-E-N15D and rSARS-CoV-E-V25F T30I, sacrificed at days 2 and 4 post infection, and lungs were collected. To analyze viral growth, right lungs were homogenized in 2 ml of Phosphate Buffered Saline (PBS) containing 100 UI/ml penicillin, 100 µg/ml streptomycin, 50 µg/ml gentamicin and 0.5 µg/ml fungizone using MACS homogenizer (Miltenyi Biotec) according to manufacturer's protocols, and titered as previously described. To examine lung histopathology, left lungs of infected mice were incubated with 10% zinc formalin for 24 h at 4°C, embedded in paraffin, sectioned, and stained with hematoxylin and eosin.

Immunofluorescence in lung sections

Five micron sections of zinc formalin fixed lungs were deparaffined at 60°C and rehydrated by successive incubations in 100% xylol, 100% ethanol and 96% ethanol. Antigen unmask was performed by boiling the samples in citrate buffer (8.2 mM sodium citrate; 1.8 mM citric acid, pH 6.5) for 5 min at 110°C in a decloaking chamber (Biocare medical). Samples were then permeabilized with 0.25% Triton X-100 in PBS for 15 min and blocked with 10% bovine serum albumin (BSA) and 0.25% Triton X-100 in PBS for 30 min. Samples were labeled with a mouse monoclonal antibody specific for SARS-CoV N protein (kindly provided by Ying Fang, South Dakota State University) diluted 1:250 and a rabbit monoclonal antibody specific for Na^+/K^+ ATPase alpha subunit (Abcam) diluted 1:100 in 0.25% Triton X-100 and 10% BSA in PBS for 1 h 30 min at room temperature. Goat anti-mouse and goat anti-rabbit secondary antibodies bound to Alexa 488 and Alexa 594 fluorophores were used respectively at a dilution 1:250 in 0.25% Triton X-100 and 10% BSA in PBS for 45 min at room temperature. Cell nuclei were stained with DAPI (1:200). Tissues were mounted in ProLong antifade reagent (Invitrogen) and analyzed in a Leica TCS SP5 confocal microscope.

RT-qPCR analysis

RNA extracted from lungs of infected mice was prepared as described above, and subjected to retro transcriptase reactions using a High-Capacity cDNA transcription kit (Applied Biosystems) to generate cDNAs. PCR using Taqman assays specific for IL-1β (Mm01336189-m1) and 18S ribosomal RNA as a control (Mm03928990-g1) [80,81] (Applied Biosystems) were performed. Data were acquired with an ABI Prism 7000 sequence detection system (Applied Biosystems) and analyzed using ABI Prism 7000 SDS v1.0 software. Gene expression relative to mock-infected samples is shown.

Lung protein extracts preparation and western blot assays

Lungs from infected mice were collected at 2 dpi and the right lung was homogenized in 1.2 mL of protein lysis buffer containing Tris/HCl 10 mM, EDTA 1 mM, NaCl 150 mM, IGEPAL 1%, and complete protease inhibitor (Roche) pH8, using MACS homogenizer (Miltenyi Biotec). Samples were centrifuged for 1 h at 4°C and 13000× g and supernatants were collected. Pro-IL-1β levels were analyzed by Western blotting using a goat anti mouse IL-1β/IL-1F2 antibody (R&D systems). As a loading control, beta-actin was labeled using a mouse monoclonal antibody (Abcam). Bound antibodies were detected using a rabbit anti goat and a rabbit anti mouse HRP conjugated antibodies and the Immobilon Western chemiluminiscence substrate (Millipore), following manufacturer's specifications. Densitometric analysis was performed in non-saturated exposures of several experimental replicates using Quantity One, version 4.5.1 software (BioRad). Levels of pro-IL-1β were normalized to the levels of beta-actin.

Bronchoalveolar lavages

Following euthanasia by cervical dislocation, the trachea was exposed and cannulated through the animal mouth with a 19 gauge tube. Lungs were lavaged three times with 400 µl of cold phosphate buffered saline (PBS). Samples were centrifuged for 10 minutes at 3000× g at 4°C to separate cellular content, and supernatants were collected to analyze their cytokine levels.

Cytokine multiplex analysis

Bronchoalveolar lavages were treated with IGEPAL reaching a final concentration of 0.2%, to inactivate sample infectivity. The expression of IL-1β, TNF and IL-6 was measured using Luminex technology and a mouse cytokine antibody bead kit (Milliplex map kit, Millipore) according to the manufacturer's specifications.

Supporting Information

Figure S1 Infection efficiency and cellular tropism within mice lungs, in the presence or absence of SARS-CoV E protein IC activity. 16 week-old BALB/c mice were infected with 100000 PFU of the parental virus (wt, black columns) displaying E protein IC activity or the mutant virus lacking IC activity N15A (red columns). At 2 and 4 dpi mice were sacrificed and their lungs were fixed in formalin, paraffin embedded, sectioned and processed for immunofluorescence. SARS-CoV N protein and cell nuclei were labeled to discriminate both non-infected and infected cells. The number of alveolar (alveo), bronchiolar (bronch) and overall infected cells (total) were calculated in several representative images, and represented as percentages of their corresponding total cells (infected plus non-infected). Error bars indicate the standard deviation from the data collected from different images.
(TIF)

Acknowledgments

We thank Marga Gonzalez for her technical assistance.

Author Contributions

Conceived and designed the experiments: JLNT LE MLD. Performed the experiments: JLNT MLD CVB JMJG JARN RFD. Analyzed the data: JLNT LE MLD CVB JMJG JARN RFD CCR AA VMA. Contributed reagents/materials/analysis tools: JT. Wrote the paper: JLNT LE MLD. Revised the manuscript: JLNT MLD CVB JMJG JARN RFD CCR AA JT VMA LE.

References

1. Perlman S, Netland J (2009) Coronaviruses post-SARS: update on replication and pathogenesis. Nat Rev Microbiol 7: 439–450.
2. Rota PA, Oberste MS, Monroe SS, Nix WA, Campganoli R, et al. (2003) Characterization of a novel coronavirus associated with severe acute respiratory syndrome. Science 300: 1394–1399.
3. Drosten C, Gunther S, Preiser W, van der Werf S, Brodt HR, et al. (2003) Identification of a novel coronavirus in patients with severe acute respiratory syndrome. N Engl J Med 348: 1967–1976.
4. Pyrc K, Berkhout B, van der Hoek L (2007) The novel human coronaviruses NL63 and HKU1. J Virol 81: 3051–3057.
5. Zaki AM, van Boheemen S, Bestebroer TM, Osterhaus AD, Fouchier RA (2012) Isolation of a novel coronavirus from a man with pneumonia in Saudi Arabia. N Engl J Med 367: 1814–1820.
6. Danielsson N, Catchpole M (2012) Novel coronavirus associated with severe respiratory disease: case definition and public health measures. Euro Surveill 17: 20282.
7. Assiri A, McGeer A, Perl TM, Price CS, Al Rabeeah AA, et al. (2013) Hospital outbreak of Middle East respiratory syndrome coronavirus. N Engl J Med 369(5):407–16 doi:10.1056/NEJMoa1306742.
8. Muller MA, Paweska JT, Leman PA, Drosten C, Grywna K, et al. (2007) Coronavirus antibodies in African bat species. Emerg Infect Dis 13: 1367–1370.
9. Chu DK, Peiris JS, Chen H, Guan Y, Poon LL (2008) Genomic characterizations of bat coronaviruses (1A, 1B and HKU8) and evidence for co-infections in Miniopterus bats. J Gen Virol 89: 1282–1287.
10. Drexler JF, Gloza-Rausch F, Glende J, Corman VM, Muth D, et al. (2010) Genomic characterization of severe acute respiratory syndrome-related coronavirus in European bats and classification of coronaviruses based on partial RNA-dependent RNA polymerase gene sequences. J Virol 84: 11336–11349.
11. Quan PL, Firth C, Street C, Henriquez JA, Petrosov A, et al. (2010) Identification of a severe acute respiratory syndrome coronavirus-like virus in a leaf-nosed bat in Nigeria. MBio 1: e00208–00210.
12. Annan A, Baldwin HJ, Corman VM, Klose SM, Owusu M, et al. (2013) Human betacoronavirus 2c EMC/2012-related viruses in bats, Ghana and Europe. Emerg Infect Dis 19: 456–459.
13. Falcon A, Vazquez-Moron S, Casas I, Aznar C, Ruiz G, et al. (2011) Detection of alpha and betacoronaviruses in multiple Iberian bat species. Arch Virol 156: 1883–1890.
14. Enjuanes L, Gorbalenya AE, de Groot RJ, Cowley JA, Ziebuhr J, et al. (2008) The Nidovirales. In: Mahy BWJ, Van Regenmortel M, Walker P, Majumder-Russell D, editors. Encyclopedia of Virology, Third Edition. Oxford: Elsevier Ltd. pp. 419–430.
15. Nieto-Torres JL, Dediego ML, Alvarez E, Jimenez-Guardeno JM, Regla-Nava JA, et al. (2011) Subcellular location and topology of severe acute respiratory syndrome coronavirus envelope protein. Virology 415: 69–82.
16. DeDiego ML, Alvarez E, Almazan F, Rejas MT, Lamirande E, et al. (2007) A severe acute respiratory syndrome coronavirus that lacks the E gene is attenuated *in vitro* and *in vivo*. J Virol 81: 1701–1713.
17. Maeda J, Repass JF, Maeda A, Makino S (2001) Membrane topology of coronavirus E protein. Virology 281: 163–169.
18. Raamsman MJB, Locker JK, de Hooge A, de Vries AAF, Griffiths G, et al. (2000) Characterization of the coronavirus mouse hepatitis virus strain A59 small membrane protein E. J Virol 74: 2333–2342.
19. Ortego J, Escors D, Laude H, Enjuanes L (2002) Generation of a replication-competent, propagation-deficient virus vector based on the transmissible gastroenteritis coronavirus genome. J Virol 76: 11518–11529.
20. Ortego J, Ceriani JE, Patino C, Plana J, Enjuanes L (2007) Absence of E protein arrests transmissible gastroenteritis coronavirus maturation in the secretory pathway. Virology 368: 296–308.
21. Almazan F, Dediego ML, Sola I, Zuniga S, Nieto-Torres JL, et al. (2013) Engineering a replication-competent, propagation-defective Middle East respiratory syndrome coronavirus as a vaccine candidate. MBio 4: e00650–00613.
22. Kuo L, Masters PS (2003) The small envelope protein E is not essential for murine coronavirus replication. J Virol 77: 4597–4608.
23. DeDiego ML, Pewe L, Alvarez E, Rejas MT, Perlman S, et al. (2008) Pathogenicity of severe acute respiratory coronavirus deletion mutants in hACE-2 transgenic mice. Virology 376: 379–389.
24. Lamirande EW, DeDiego ML, Roberts A, Jackson JP, Alvarez E, et al. (2008) A live attenuated SARS coronavirus is immunogenic and efficacious in golden Syrian hamsters. J Virol 82: 7721–7724.
25. Netland J, DeDiego ML, Zhao J, Fett C, Alvarez E, et al. (2010) Immunization with an attenuated severe acute respiratory syndrome coronavirus deleted in E protein protects against lethal respiratory disease. Virology 399: 120–128.
26. Fett C, DeDiego ML, Regla-Nava JA, Enjuanes L, Perlman S (2013) Complete protection against severe acute respiratory syndrome coronavirus-mediated lethal respiratory disease in aged mice by immunization with a mouse-adapted virus lacking E protein. J Virol 87: 6551–6559.
27. Dediego ML, Nieto-Torres JL, Regla-Nava JA, Jimenez-Guardeno JM, Fernandez-Delgado R, et al. (2013) Inhibition of NF-kappaB mediated inflammation in severe acute respiratory syndome coronavirus-infected mice increases survival. J Virol 88(2):913–24 doi10.1128/JVI.02576-02513.
28. DeDiego ML, Nieto-Torres JL, Jimenez-Guardeno JM, Regla-Nava JA, Alvarez E, et al. (2011) Severe acute respiratory syndrome coronavirus envelope protein regulates cell stress response and apoptosis. PLoS pathog 7: e1002315.
29. Torres J, Parthasarathy K, Lin X, Saravanan R, Liu DX (2006) Model of a putative pore: the pentameric alpha-helical bundle of SARS coronavirus E protein in lipid bilayers. Biophys J 91: 938–947.
30. Pervushin K, Tan E, Parthasarathy K, Lin X, Jiang FL, et al. (2009) Structure and inhibition of the SARS coronavirus envelope protein ion channel. PLoS Pathog 5: e1000511.
31. Wilson L, McKinlay C, Gage P (2004) SARS coronavirus E protein forms cation-selective ion channels. Virology 330: 322–331.
32. Parthasarathy K, Ng L, Lin X, Liu DX, Pervushin K, et al. (2008) Structural flexibility of the pentameric SARS coronavirus envelope protein ion channel. Biophys J 95: 39–41.
33. Wilson L, Gage P, Ewart G (2006) Hexamethylene amiloride blocks E protein ion channels and inhibits coronavirus replication. Virology 353: 294–306.
34. Verdia-Baguena C, Nieto-Torres JL, Alcaraz A, Dediego ML, Torres J, et al. (2012) Coronavirus E protein forms ion channels with functionally and structurally-involved membrane lipids. Virology 432: 485–494.
35. Torres J, Maheswari U, Parthasarathy K, Ng L, Liu DX, et al. (2007) Conductance and amantadine binding of a pore formed by a lysine-flanked transmembrane domain of SARS coronavirus envelope protein. Protein Sci 16: 2065–2071.
36. Verdia-Baguena C, Nieto-Torres JL, Alcaraz A, Dediego ML, Enjuanes L, et al. (2013) Analysis of SARS-CoV E protein ion channel activity by tuning the protein and lipid charge. Biochim Biophys Acta 1828: 2026–2031.
37. Ye Y, Hogue BG (2007) Role of the coronavirus E viroporin protein transmembrane domain in virus assembly. J Virol 81: 3597–3607.
38. Kuo L, Hurst KR, Masters PS (2006) Exceptional flexibility in the sequence requirements for coronavirus small envelope protein (E) function. J Virol 81: 2249–2262.
39. Ruch TR, Machamer CE (2011) The hydrophobic domain of infectious bronchitis virus E protein alters the host secretory pathway and is important for release of infectious virus. J Virol 85: 675–685.
40. Ruch TR, Machamer CE (2012) A single polar residue and distinct membrane topologies impact the function of the infectious bronchitis coronavirus E protein. PLoS Pathog 8: e1002674.
41. Lu W, Zheng BJ, Xu K, Schwarz W, Du L, et al. (2006) Severe acute respiratory syndrome-associated coronavirus 3a protein forms an ion channel and modulates virus release. Proc Natl Acad Sci USA 103: 12540–12545.
42. Chen CC, Kruger J, Sramala I, Hsu HJ, Henklein P, et al. (2011) ORF8a of SARS-CoV forms an ion channel: experiments and molecular dynamics simulations. Biochim Biophys Acta 1808: 572–579.
43. Zhang R, Wang K, Lv W, Yu W, Xie S, et al. (2013) The ORF4a protein of human coronavirus 229E functions as a viroporin that regulates viral production. Biochim Biophys Acta 1838(4):1088–95 doi 10.1016/j.bbamem.2013.1007.1025.
44. Nieva JL, Madan V, Carrasco L (2012) Viroporins: structure and biological functions. Nat Rev Microbiol 10: 563–574.
45. Pinto LH, Holsinger LJ, Lamb RA (1992) Influenza virus M2 protein has ion channel activity. Cell 69: 517–528.
46. Ewart GD, Sutherland T, Gage PW, Cox GB (1996) The Vpu protein of human immunodeficiency virus type 1 forms cation-selective ion channels. J Virol 70: 7108–7115.
47. Pavlovic D, Neville DC, Argaud O, Blumberg B, Dwek RA, et al. (2003) The hepatitis C virus p7 protein forms an ion channel that is inhibited by long-alkyl-chain iminosugar derivatives. Proc Natl Acad Sci USA 100: 6104–6108.
48. de Jong AS, Visch HJ, de Mattia F, van Dommelen MM, Swarts HG, et al. (2006) The coxsackievirus 2B protein increases efflux of ions from the endoplasmic reticulum and Golgi, thereby inhibiting protein trafficking through the Golgi. J Biol Chem 281: 14144–14150.
49. Henkel M, Mitzner D, Henklein P, Meyer-Almes FJ, Moroni A, et al. (2010) The proapoptotic influenza A virus protein PB1-F2 forms a nonselective ion channel. PLoS One 5: e11112.
50. Campanella M, de Jong AS, Lanke KW, Melchers WJ, Willems PH, et al. (2004) The coxsackievirus 2B protein suppresses apoptotic host cell responses by manipulating intracellular Ca2+ homeostasis. J Biol Chem 279: 18440–18450.
51. Wozniak AL, Griffin S, Rowlands D, Harris M, Yi M, et al. (2010) Intracellular proton conductance of the hepatitis C virus p7 protein and its contribution to infectious virus production. PLoS Pathog 6: e1001087.
52. Ichinohe T, Pang IK, Iwasaki A (2010) Influenza virus activates inflammasomes via its intracellular M2 ion channel. Nat Immunol 11: 404–410.
53. McAuley JL, Tate MD, MacKenzie-Kludas CJ, Pinar A, Zeng W, et al. (2013) Activation of the NLRP3 inflammasome by IAV virulence protein PB1-F2 contributes to severe pathophysiology and disease. PLoS Pathog 9: e1003392.
54. Sakaguchi T, Leser GP, Lamb RA (1996) The ion channel activity of the influenza virus M2 protein affects transport through the Golgi apparatus. J Cell Biol 133: 733–747.

55. de Jong AS, de Mattia F, Van Dommelen MM, Lanke K, Melchers WJ, et al. (2008) Functional analysis of picornavirus 2B proteins: effects on calcium homeostasis and intracellular protein trafficking. J Virol 82: 3782–3790.
56. Cornell CT, Kiosses WB, Harkins S, Whitton JL (2007) Coxsackievirus B3 proteins directionally complement each other to downregulate surface major histocompatibility complex class I. J Virol 81: 6785–6797.
57. Triantafilou K, Kar S, Vakakis E, Kotecha S, Triantafilou M (2013) Human respiratory syncytial virus viroporin SH: a viral recognition pathway used by the host to signal inflammasome activation. Thorax 68: 66–75.
58. Zhang K, Hou Q, Zhong Z, Li X, Chen H, et al. (2013) Porcine reproductive and respiratory syndrome virus activates inflammasomes of porcine alveolar macrophages via its small envelope protein E. Virology 442: 156–162.
59. Ito M, Yanagi Y, Ichinohe T (2012) Encephalomyocarditis virus viroporin 2B activates NLRP3 inflammasome. PLoS Pathog 8: e1002857.
60. Roberts A, Deming D, Paddock CD, Cheng A, Yount B, et al. (2007) A mouse-adapted SARS-coronavirus causes disease and mortality in BALB/c mice. PLoS Pathog 3: 23–37.
61. Regla-Nava JA, Jimenez-Guardeno JM, Nieto-Torres JL, Gallagher TM, Enjuanes L, et al. (2013) The replication of a mouse adapted SARS-CoV in a mouse cell line stably expressing the murine SARS-CoV receptor mACE2 efficiently induces the expression of proinflammatory cytokines. J Virol Methods 193: 639–646.
62. Meduri GU, Headley S, Kohler G, Stentz F, Tolley E, et al. (1995) Persistent elevation of inflammatory cytokines predicts a poor outcome in ARDS. Plasma IL-1 beta and IL-6 levels are consistent and efficient predictors of outcome over time. Chest 107: 1062–1073.
63. Tisoncik JR, Korth MJ, Simmons CP, Farrar J, Martin TR, et al. (2012) Into the eye of the cytokine storm. Microbiol Mol Biol Rev 76: 16–32.
64. Martinon F, Petrilli V, Mayor A, Tardivel A, Tschopp J (2006) Gout-associated uric acid crystals activate the NALP3 inflammasome. Nature 440: 237–241.
65. Watanabe T, Watanabe S, Ito H, Kida H, Kawaoka Y (2001) Influenza A virus can undergo multiple cycles of replication without M2 ion channel activity. J Virol 75: 5656–5662.
66. Takeda M, Pekosz A, Shuck K, Pinto LH, Lamb RA (2002) Influenza a virus M2 ion channel activity is essential for efficient replication in tissue culture. J Virol 76: 1391–1399.
67. Bukreyev A, Whitehead SS, Murphy BR, Collins PL (1997) Recombinant respiratory syncytial virus from which the entire SH gene has been deleted grows efficiently in cell culture and exhibits site-specific attenuation in the respiratory tract of the mouse. J Virol 71: 8973–8982.
68. Whitehead SS, Bukreyev A, Teng MN, Firestone CY, St Claire M, et al. (1999) Recombinant respiratory syncytial virus bearing a deletion of either the NS2 or SH gene is attenuated in chimpanzees. J Virol 73: 3438–3442.
69. Watanabe S, Watanabe T, Kawaoka Y (2009) Influenza A virus lacking M2 protein as a live attenuated vaccine. J Virol 83: 5947–5950.
70. Gladue DP, Holinka LG, Largo E, Fernandez Sainz I, Carrillo C, et al. (2012) Classical swine fever virus p7 protein is a viroporin involved in virulence in swine. J Virol 86: 6778–6791.
71. Graham RL, Donaldson EF, Baric RS (2013) A decade after SARS: strategies for controlling emerging coronaviruses. Nat Rev Microbiol 11: 836–848.
72. Matthay MA, Zemans RL (2011) The acute respiratory distress syndrome: pathogenesis and treatment. Annu Rev Pathol 6: 147–163.
73. Hollenhorst MI, Richter K, Fronius M (2011) Ion transport by pulmonary epithelia. J Biomed Biotechnol 2011: 174306.
74. Rockx B, Baas T, Zornetzer GA, Haagmans B, Sheahan T, et al. (2009) Early upregulation of acute respiratory distress syndrome-associated cytokines promotes lethal disease in an aged-mouse model of severe acute respiratory syndrome coronavirus infection. J Virol 83: 7062–7074.
75. Pugin J, Ricou B, Steinberg KP, Suter PM, Martin TR (1996) Proinflammatory activity in bronchoalveolar lavage fluids from patients with ARDS, a prominent role for interleukin-1. Am J Respir Crit Care Med 153: 1850–1856.
76. Grommes J, Soehnlein O (2011) Contribution of neutrophils to acute lung injury. Mol Med 17: 293–307.
77. dos Santos G, Kutuzov MA, Ridge KM (2012) The inflammasome in lung diseases. Am J Physiol Lung Cell Mol Physiol 303: L627–633.
78. Strowig T, Henao-Mejia J, Elinav E, Flavell R (2012) Inflammasomes in health and disease. Nature 481: 278–286.
79. Wang CH, Liu CY, Wan YL, Chou CL, Huang KH, et al. (2005) Persistence of lung inflammation and lung cytokines with high-resolution CT abnormalities during recovery from SARS. Respir Res 6: 42.
80. Frieman MB, Chen J, Morrison TE, Whitmore A, Funkhouser W, et al. (2010) SARS-CoV pathogenesis is regulated by a STAT1 dependent but a type I, II and III interferon receptor independent mechanism. PLoS Pathog 6: e1000849.
81. Sheahan T, Morrison TE, Funkhouser W, Uematsu S, Akira S, et al. (2008) MyD88 is required for protection from lethal infection with a mouse-adapted SARS-CoV. PLoS Pathog 4: e1000240.

OPEN ACCESS Freely available online

PLoS PATHOGENS

Severe Acute Respiratory Syndrome Coronavirus Envelope Protein Regulates Cell Stress Response and Apoptosis

Marta L. DeDiego[1], Jose L. Nieto-Torres[1], Jose M. Jiménez-Guardeño[1], Jose A. Regla-Nava[1], Enrique Álvarez[1¤], Juan Carlos Oliveros[2], Jincun Zhao[3], Craig Fett[3], Stanley Perlman[3], Luis Enjuanes[1]*

1 Department of Molecular and Cell Biology, Centro Nacional de Biotecnología (CNB-CSIC), Campus Universidad Autónoma de Madrid, Madrid, Spain, **2** Genomics Unit, Centro Nacional de Biotecnología (CNB-CSIC), Campus Universidad Autónoma de Madrid, Madrid, Spain, **3** Department of Microbiology, University of Iowa, Iowa City, Iowa, United States of America

Abstract

Severe acute respiratory syndrome virus (SARS-CoV) that lacks the envelope (E) gene (rSARS-CoV-ΔE) is attenuated *in vivo*. To identify factors that contribute to rSARS-CoV-ΔE attenuation, gene expression in cells infected by SARS-CoV with or without E gene was compared. Twenty-five stress response genes were preferentially upregulated during infection in the absence of the E gene. In addition, genes involved in signal transduction, transcription, cell metabolism, immunoregulation, inflammation, apoptosis and cell cycle and differentiation were differentially regulated in cells infected with rSARS-CoV with or without the E gene. Administration of E protein in trans reduced the stress response in cells infected with rSARS-CoV-ΔE or with respiratory syncytial virus, or treated with drugs, such as tunicamycin and thapsigargin that elicit cell stress by different mechanisms. In addition, SARS-CoV E protein down-regulated the signaling pathway inositol-requiring enzyme 1 (IRE-1) of the unfolded protein response, but not the PKR-like ER kinase (PERK) or activating transcription factor 6 (ATF-6) pathways, and reduced cell apoptosis. Overall, the activation of the IRE-1 pathway was not able to restore cell homeostasis, and apoptosis was induced probably as a measure to protect the host by limiting virus production and dissemination. The expression of proinflammatory cytokines was reduced in rSARS-CoV-ΔE-infected cells compared to rSARS-CoV-infected cells, suggesting that the increase in stress responses and the reduction of inflammation in the absence of the E gene contributed to the attenuation of rSARS-CoV-ΔE.

Citation: DeDiego ML, Nieto-Torres JL, Jiménez-Guardeño JM, Regla-Nava JA, Álvarez E, et al. (2011) Severe Acute Respiratory Syndrome Coronavirus Envelope Protein Regulates Cell Stress Response and Apoptosis. PLoS Pathog 7(10): e1002315. doi:10.1371/journal.ppat.1002315

Editor: Volker Thiel, Kantonal Hospital St. Gallen, Switzerland

Received April 26, 2011; **Accepted** August 29, 2011; **Published** October 20, 2011

Funding: This work was supported by grants from the Ministry of Science and Innovation of Spain (BIO2007-60978 and BIO2010-16705), the European Community's Seventh Framework Programme (FP7/2007-2013) under the project "EMPERIE" EC Grant Agreement number 223498, and U.S. National Institutes of Health (R56 AI079424-01A1 and 2PO1 AI060699). Marta L. DeDiego received a contract from the project "EMPERIE" EC Grant Agreement number 223498. The funders had no role in study design, data collection and analysis, decision to publish, or preparation of the manuscript.

Competing Interests: The authors have declared that no competing interests exist.

* E-mail: L.Enjuanes@cnb.csic.es

¤ Current address: Centro de Biología Molecular Severo Ochoa (CBMSO), UAM-CSIC, Campus Universidad Autónoma de Madrid, Madrid, Spain

Introduction

Severe acute respiratory syndrome coronavirus (SARS-CoV) was identified as the etiological agent of a respiratory disease that emerged in Guandong Province, China at the end of 2002, and spread to 32 countries in a few months [1,2,3,4,5,6,7]. SARS-CoV infected 8000 people in 2002–2003, with an average mortality of 10%. After July 2003, only a few community and laboratory-acquired cases have been reported (http://www.who.int/csr/sars/en/). Nevertheless, coronaviruses similar to the one that caused the epidemic are widely disseminated in bats circulating all over the world, making a future outbreak possible [8,9,10].

SARS-CoV is an enveloped, single-stranded positive sense RNA virus, with a genome of 29.7 kb. The coronavirus replicase gene is encoded within the 5′ two thirds of the genome, and includes two overlapping open reading frames (ORFs) named ORF1a and ORF1b. Translation of both ORFs in the cytoplasm of infected cells results in the synthesis of two large polyproteins, pp1b and pp1ab, processed by two viral proteases to yield 16 non structural proteins (nsps) [11,12]. The nsps are involved in genome replication and transcription of subgenomic mRNAs (sg mRNAs) that encode structural proteins such as the nucleocapsid (N), envelope (E), membrane (M), and spike (S), and a set of group-specific proteins whose sequence and number differ among the different coronavirus species [13]. In the case of SARS-CoV, the group-specific proteins 3a, 6, 7a and 7b, are also structural proteins [14,15,16,17,18].

SARS-CoV E protein, a small integral membrane protein of 76 amino acids, contains a short hydrophilic amino-terminus followed by a hydrophobic region and a hydrophilic carboxy-terminus [19]. The hydrophobic region forms at least one amphipathic α-helix that oligomerizes to form an ion-conductive pore in membranes [19]. Furthermore, HCoV-229E, murine hepatitis virus (MHV), SARS-CoV, and infectious bronchitis virus (IBV) E proteins form ion channels permeable to monovalent cations [20,21,22]. The E protein from genus α transmissible gastroenteritis coronavirus (TGEV) is essential for the generation of propagation competent viruses [23,24,25]. In contrast, genus β MHV and SARS-CoV E

Author Summary

To identify potential mechanisms mediating the *in vivo* attenuation of SARS-CoV lacking the E gene (rSARS-CoV-ΔE), the effect of the presence of the E gene on host gene expression was studied. In rSARS-CoV-ΔE-infected cells, the expression of at least 25 stress response genes was preferentially upregulated, compared to cells infected with rSARS-CoV. E protein supplied in trans reversed the increase in stress response genes observed in cells infected with rSARS-CoV-ΔE or with respiratory syncytial virus, and by treatment with drugs causing stress by different mechanisms. Furthermore, in the presence of the E protein a subset (IRE-1 pathway), but not two others (PERK and ATF-6), of the unfolded protein response was also reduced. Nevertheless, the activation of the unfolded protein response to control cell homeostasis was not sufficient to alleviate cell stress, and an increase in cell apoptosis in cells infected with the virus lacking E protein was observed. This apoptotic response was probably induced to protect the host by limiting virus production and dissemination. In cells infected with rSARS-CoV-ΔE, genes associated with the proinflammatory pathway were down-regulated compared to cells infected with virus expressing E protein, supporting the idea that a reduction in inflammation was also relevant in the attenuation of the virus deletion mutant.

proteins are not completely essential for the generation of infectious viruses [26,27,28]. SARS-CoV lacking the E protein is attenuated in different animal models for SARS, such as hamsters and transgenic mice that express the SARS-CoV receptor, human angiotensin converting enzyme 2 (hACE-2) [26,27].

Virus infection may result in the expression of stress proteins, like heat shock proteins (hsps), glucose-regulated proteins (GRPs) and ubiquitin [29]. Some of these proteins are constitutively expressed, while others are induced by proteotoxic stresses such as protein overload, heat shock, hypoxia, ischemia, heavy metals, radiation, calcium increase, reactive oxygen species, and drugs, in addition to virus infection [30]. Stress proteins may act as molecular chaperones, participating in protein synthesis, folding, transport, cell viability [31], and modulating the immune response [32]. Increasing evidence suggests that certain hsps play a role in both innate and adaptive immunity [32,33]. Hsps can act independently of chaperoned peptides to directly stimulate innate immune responses, such as the maturation and activation of dendritic cells, and the activation of natural killer cells (reviewed in [33]).

Coronavirus infection generates double membrane vesicles [34,35] derived from the endoplasmic reticulum (ER), in which the RNA virus genome is replicated and transcribed [36]. In addition, enveloped viruses modify and perturb membranes to generate new virus particles. This extensive use of intracellular membranes for virus replication and morphogenesis likely overloads the ER during infection, causing ER stress responses and triggering the unfolded protein response (UPR). The UPR increases the production of chaperones that facilitate protein folding, promotes the synthesis of lipids that constitute cellular membranes and inhibits translation in order to reduce ER stress [37]. The UPR is mediated by three ER-resident transmembrane proteins that are activated through binding to unfolded proteins: PKR-like ER kinase (PERK), activating transcription factor 6 (ATF6), and inositol-requiring enzyme 1 (IRE-1) [38,39,40]. Upon activation, PERK dimerizes and autophosphorylates. This protein phosphorylates eIF2α, leading to the inhibition of translation. ATF6 activation involves the translocation of this protein to the Golgi compartment, where site 1 and site 2 proteases process the 90 KDa form to create a 50 KDa form, the ATF6α(C), a soluble transcription factor that translocates to the nucleus and upregulates the expression of genes involved in protein folding. IRE-1 mediates the splicing of the mRNA encoding the transcription factor X box-binding protein 1 (XBP-1), leading to a frame shift and translation of a functional XBP-1 protein. The active transcription factor (sXBP-1) can then stimulate the transcription of genes encoding proteins that promote the folding, transport, and degradation of ER proteins, and lipid biosynthesis.

The ER stress response acts to restore ER homeostasis. However, when homeostasis cannot be restored, persistent or intense ER stress can also trigger programmed cell death or apoptosis [41], a physiological mechanism to control the number of cells during development and to respond to infections. Autopsy studies have revealed signs of apoptosis in SARS-CoV-infected tissues from patients, such as lung, spleen and thyroid [42,43]. Accordingly, it has been shown that the infection by SARS-CoV triggers apoptosis in cell cultures via protein kinase R (PKR) [44] and that at least eight SARS-CoV-encoded proteins induce apoptosis [45].

The expression of genes leading to hyperinflammation has been associated with SARS-CoV-induced pathology. In fact, highly elevated expression of inflammatory mediators such as interleukin (IL)-1, -6, and -8, CXCL10/interferon-inducible protein (IP)-10, CCL2/monocyte chemoattractant protein (MCP)-1, CCL5/regulated on activation, normal T expressed and secreted (RANTES), and CXCL9/monokine induced by interferon gamma (MIG), has been described within the circulation and lungs of SARS patients [46,47,48,49,50,51].

In this study, the effect of SARS-CoV E protein on host cell responses during virus infection was analyzed for the first time by comparing the transcriptomes of rSARS-CoV-ΔE and rSARS-CoV-infected cells using microarrays and quantitative reverse transcription polymerase chain reaction (qRT-PCR). We showed that SARS-CoV E protein influenced the expression of genes associated to stress response, immunoregulation, inflammation, apoptosis, and cell cycle and differentiation. Among these changes, the effect on stress response was most robust, based on both the number of differentially expressed genes regulating this activity and on the extent of the changes observed. This downregulation of the stress response in the presence of gene E was specific as this process was reversed by providing E protein in trans. In addition, we showed that E protein reduced the cellular stress caused by another respiratory virus, respiratory syncytial virus (RSV), and two drugs (tunicamycin and thapsigargin) that induce stress by different mechanisms. Furthermore, the presence of E protein reduced the activation of the IRE-1 mediated pathway during the UPR. However, the activation of these signaling pathways in the absence of E protein was not sufficient to reverse the cellular stress induced by rSARS-CoV-ΔE since infected cells underwent apoptosis. In addition, the absence of E protein increased the expression of the double specificity phosphatases (DUSP)-1 and DUSP-10, and down regulated proinflammatory cytokines such as CCL2 and CXCL2. Therefore, the effect of E protein on the stress response, including the UPR, and on proinflammatory cytokine expression may explain the attenuation of rSARS-CoV-ΔE *in vivo*.

Results

Growth kinetics of SARS-CoV in Vero E6 and MA-104 cells

To study the host response elicited by SARS-CoV, it is essential to use cell lines, such as Vero E6, MA-104, CaCo-2, Huh7,

FRhK-4, PK15, HepG2, 293 and 293T cells, that are highly susceptible to infection with SARS-CoV [52,53,54,55]. To determine whether these cell lines were also susceptible to rSARS-CoV-ΔE, virus growth kinetics studies were performed. rSARS-CoV-ΔE passaged 16 times in Vero E6 cells (P16) was analyzed, as this virus grew with titers similar to those of rSARS-CoV, around 10-fold higher than virus passaged only once (P1). rSARS-CoV-ΔE-P16 contained only a single nucleotide substitution at amino acid 607 of the S gene (S607F) compared to the P1 virus [56]. Both rSARS-CoV-ΔE P1 and the P16 were attenuated in the highly susceptible transgenic mice model [56], showing that the deletion of the E gene, and not the amino acid substitution in S protein, was responsible for virus attenuation. All the cell lines indicated above were infected with SARS-CoV with and without E gene at a multiplicity of infection (moi) of 1, 3 and 5 and the percentage of infected cells at 24 hours post infection (hpi) was determined using an immunofluorescence assay. Similar results were obtained both in SARS-CoV and rSARS-CoV-ΔE-infected cells, so only the results obtained with SARS-CoV-infected cells are provided in Supplementary Table SI. An increase in the moi led to a higher proportion of infected cells in all cell lines. The percentage of infected cells was below 40% in all cases, except for African green monkey kidney Vero E6 and MA-104 cells (Supplementary Table S1), which have or do not have, respectively, a defect in interferon (IFN) production [57,58]. More than 90% of Vero E6 cells were infected with rSARS-CoV-ΔE or rSARS-CoV at 24 hpi, whereas in the case of MA-104 cells, more than 80% of the cells were infected with both viruses at 24 hpi (Supplementary Table S1). The growth kinetics of rSARS-CoV-ΔE and rSARS-CoV in Vero E6 cells at an moi of 2 showed similar profiles and titers for both viruses, reaching maximum titers and cytopathicity at 15 hpi (Fig. 1A). In contrast, in the case of MA-104 cells, although growth kinetics for rSARS-CoV-ΔE and the parental virus were similar, a 10-fold reduction in virus titers was observed in cells infected with rSARS-CoV-ΔE virus (Fig. 1A). This difference is not unexpected, as the ΔE virus that was used in these experiments was passaged and adapted to growth in Vero E6, but not in MA-104 cells. The cytopathic effect in MA-104 cells was evident at 48 hpi and maximum virus titers were reached at 65 hpi (Fig. 1A). The kinetics of genomic RNA and N gene sg mRNA accumulation were similar in rSARS-CoV-ΔE and rSARS-CoV-infected Vero E6 and MA-104 cells, as determined by qRT-PCR (Fig. 1B and 1C), indicating that SARS-CoV E protein had no influence on the accumulation of viral RNAs. Maximum levels of both types of viral RNA were observed at 15–22 hpi, in the case of infected Vero E6 cells and at 48 hpi in the case of MA-104 cells. These data showed that although Vero E6 and MA-104 cells were susceptible to SARS-CoV, the kinetics of the infection was slower in MA-104 than in Vero E6 cells, which needs to be considered when cellular mRNAs are collected for differential gene expression studies.

Effect of SARS-CoV E protein on host gene expression

To analyze the impact of E protein on host gene expression during SARS-CoV infection, the transcriptomes of rSARS-CoV-ΔE and rSARS-CoV-infected Vero E6 and MA-104 cells were compared. Taking into account the data obtained in Figure 1, early (7 hpi in the case of Vero E6, and 24 hpi in the case of MA-104 cells), and late (15 and 65 hpi, in Vero E6 and MA-104 cells, respectively) times post-infection (pi), were analyzed. Microarray-based studies of global gene responses were performed in triplicate in each case. As there are no commercially available microarrays specific for African green monkey species, and the sequence homology between humans and monkeys is very high [59], human U133 plus 2.0 microarrays were used. The results of the microarray analysis have been deposited in the Gene Expression Omnibus (GEO, NCBI, accession code GSE30589). Only those genes showing significant expression changes (i.e., 2.0-fold and false discovery rate (FDR)$<$0.01) at each time point were selected for further investigation. Comparison of gene expression in cells infected with rSARS-CoV with or without E gene versus mock-infected cells showed that more that 800 cellular genes were differentially expressed at late time post-infection (Fig. 2) and that the number of genes differentially expressed increased over time (i.e. in the case of Vero E6 cells, 4940 annotated genes for rSARS-CoV versus mock-infected cells at 15 hpi, compared to 1324 annotated genes at 7 hpi; for MA-104 cells, 971 annotated genes for rSARS-CoV versus mock-infected cells at 65 hpi, compared to 11 annotated genes at 24 hpi). Interestingly, the number of annotated genes differentially expressed in cells infected with rSARS-CoV-ΔE compared to rSARS-CoV, in which the only difference is the expression of E gene, was reduced to 57 (Vero E6 cells) or to 72 (MA-104 cells) at 15 or 65 hpi, respectively (Fig. 2). These genes were classified according to their most commonly accepted functions (Fig. 3). A high number of genes related to stress responses (19 out of 57 in Vero E6 cells, and 19 out of 72 in MA-104 cells) were differentially expressed, with 2- to 35-fold increases. The pattern of genes upregulated in rSARS-CoV-ΔE compared to rSARS-CoV-infected cells was very similar in Vero E6 and MA-104 cells, and included different isoforms of heat shock protein (hsp) (hsps-10, -27, -40, -60, -70, -90 and -105/110), and different genes encoding ubiquitins and chaperonins (Fig. 3). These data clearly indicated that the cellular stress induced by the infection was significantly reduced in the presence of E protein. Nevertheless, it is worthy to mention that not all cellular stress genes were differentially expressed in cells infected with SARS-CoV lacking E protein versus those infected with rSARS-CoV. In fact, a set of genes coding for different isoforms of hsp40, hsp70, and hsp 90, also modified their expression between −11.0 and and +4.0-fold but to a similar extent in rSARS-CoV-ΔE and rSARS-CoV-infected cells when compared with mock infected ones (Fig. S1).

Differentially expressed genes were also involved in signal transduction, transcription, cell metabolism, immunoregulation, inflammation, apoptosis and cell cycle and differentiation, although to a lower extent (Fig. 3). Among the genes involved in signal transduction, the upregulation of DUSP1 and DUSP10 may be relevant in rSARS-CoV-ΔE attenuation, as these genes are involved in down regulating cellular responses associated with different types of stress. Furthermore, these genes reduce the inflammatory response induced by viral infections by negatively regulating mitogen-activated protein kinase (MAPK) signaling [60]. Accordingly, the expression of the proinflammatory cytokines CCL2 and CXCL2 was reduced in rSARS-CoV-ΔE-infected, compared to rSARS-CoV-infected MA-104 cells.

Consistent with the mRNA results, we detected increases in the levels of representative stress proteins, such as hsp60 and hsp90 although differences were not as great as observed when mRNA levels were assessed (Fig. 4). Lesser effects on protein levels may reflect inhibitory effects of SARS-CoV on non-viral protein synthesis [61] or, alternatively to the presence of pre-existing stress proteins in cells prior to infection.

To better understand the biological relevance of the SARS-CoV E protein on host gene expression, all of the genes that were significantly upregulated or downregulated in rSARS-CoV-ΔE-infected compared to rSARS-CoV-infected Vero E6 and MA-104 cells were clustered in functional groups based on gene ontology (GO) classification. A summary is shown in Fig. 5. In contrast, no

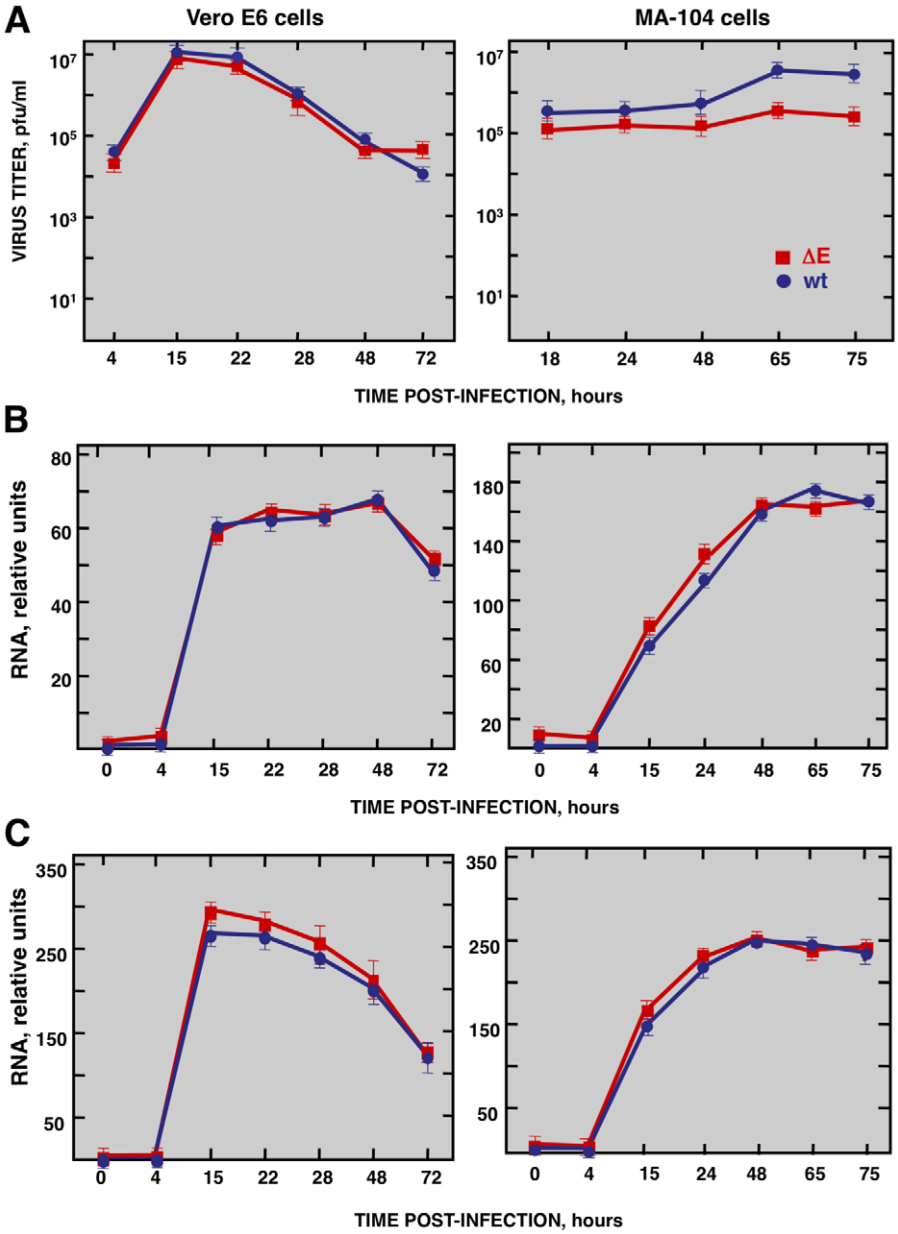

Figure 1. Characterization of infection of Vero E6 and MA-104 cells with rSARS-CoV and rSARS-CoV-ΔE. Vero E6 and MA-104 cells were infected at an moi of 2 with rSARS-CoV-ΔE or rSARS-CoV. (A) Growth kinetics curves. Virus titers in supernatants of infected cells at different times pi were determined by plaque assay. (B) Levels of intracellular genomic RNA in infected cells at different times pi as determined by qRT-PCR. (C) Levels of intracellular N gene sg mRNA in infected cells at different times pi as determined by qRT-PCR. Standard bars represent standard deviations of the mean of results from three experiments.
doi:10.1371/journal.ppat.1002315.g001

enriched GO terms were found for genes that were downregulated in MA-104-infected cells. All of the functionally enriched GO terms were related to cellular stress (chaperone binding, response to biotic stimulus, unfolded protein binding, protein folding), cellular death (anti-apoptosis), cellular transport (protein import, nucleocytoplasmic transport), transcription (transcription repressor activity) and metabolism (protein catabolic process, cellular protein catabolic process). Remarkably, similar, highly significant (FDR$<$0.01) changes in levels of genes related to cellular stress response to biotic stimulus, unfolded protein binding and protein folding were identified in both Vero E6 and MA-104-infected cells (Fig. 5).

To validate the results obtained with the cDNA microarrays, the differential expression of a wide set of cellular genes observed in cells infected with rSARS-CoV with or without the E gene was evaluated by qRT-PCR. 18S ribosomal RNA (rRNA) was used in all cases to normalize the data because differences in levels of this RNA were always lower than 1.5-fold and because the 18S rRNA has also been used successfully in similar reports [62,63]. The patterns of differential gene expression obtained by qRT-PCR analysis were similar to those observed with the microarray data (Figs. 3 and 6), validating the results obtained with both techniques. Nevertheless, in the case of genes with large differences in expression between rSARS-CoV and rSARS-CoV-ΔE-infected

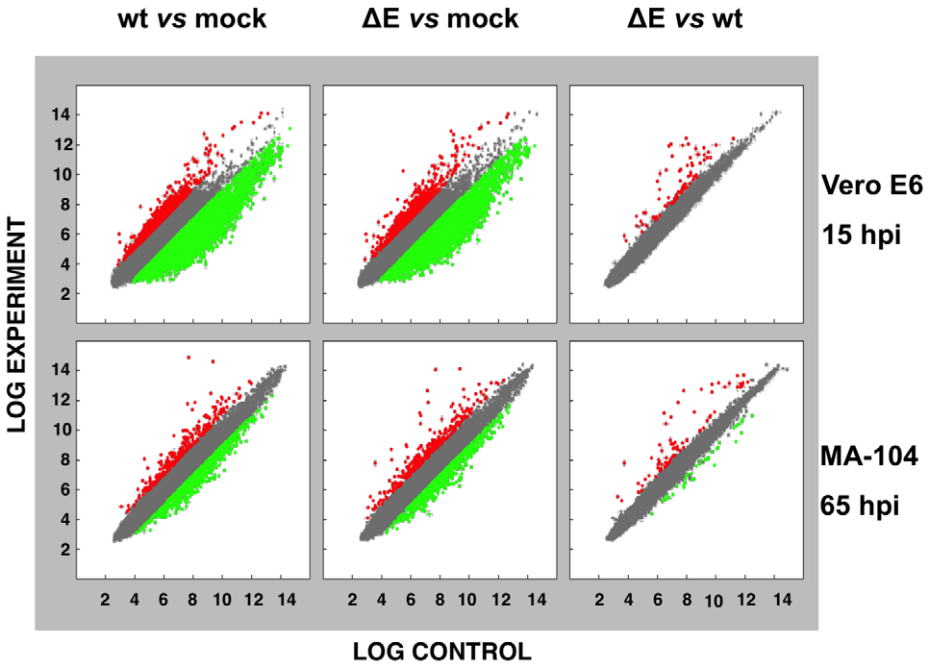

Figure 2. Effect of SARS-CoV E protein on host gene expression. Comparison of gene expression in Vero E6 (at 15 hpi) and MA-104 (at 65 hpi) cells using microarrays: rSARS-CoV versus mock-infected, rSARS-CoV-ΔE versus mock-infected and rSARS-CoV-ΔE versus rSARS-CoV-infected cells. Red spots indicate upregulated gene transcripts while green spots indicate downregulated gene transcripts. Only genes with a fold change higher than two or lower than minus two (FDR<0.01) were considered.
doi:10.1371/journal.ppat.1002315.g002

cells determined using microarrays, changes were even larger when evaluated by qRT-PCR.

Influence of SARS-CoV E protein on cell stress response

To confirm the effect of the E protein on the stress response, total RNA from infected cell cultures were analyzed at different times pi (15, 22 and 28 hpi in the case of Vero E6 cells, and 24, 48, 65 and 75 hpi, in the case of MA-104 cells) for the expression of genes related to cytosolic (hsp70 A1B and hsp90 AB1), ER (hspA5/GRP78), and mitochondrial (hsp60 D1) stress by qRT-PCR. Maximal differences in the upregulation of the three types of stress responses in rSARS-CoV-ΔE compared to rSARS-CoV were observed at 22 and 65 hpi in Vero E6 and MA-104 cells, respectively (Fig. S2). Consequently, these time points were selected to further analyze the stress responses elicited by these viruses (Fig. 6). Using microarrays, we observed that nineteen genes involved in cytosolic stress were upregulated at least 2.5-fold (FDR<0.01) in rSARS-CoV-ΔE-infected compared to rSARS-CoV-infected Vero E6 cells (15 hpi) and MA-104 cells (65 hpi). Changes in expression of these cytosolic stress genes were confirmed by qRT-PCR (Fig. 6) and shown to be highly significant (from 2.4 to 42.5-fold in Vero E6 cells, and from 3.1 to 372.3-fold in MA-104 cells). In addition, we confirmed the effect of E protein on ER (GRP78, GRP94, DNAJC3 and SERPINH1) and mitochondrial (hspA9, hsp10 E1, and hsp60 D1) stress, using infected Vero E6 and MA-104 cells (Fig. 6), with differences in gene expression that were up to 23.4 or 13.0-fold greater for ER and mitochondrial stress, respectively. These data reinforced the conclusion that SARS-CoV E protein reduced cellular stress induced by SARS-CoV, and that this reduction affected the cytosol, ER, and mitochondria.

In the experiments described above, virus without E protein was passaged 16 times, resulting in a virus with a 10-fold increase in titer, and a single point mutation in the S gene. To rule out the possibility that the mutation in the S gene was responsible for the observed increase in cellular stress, and not the absence of E protein, the induction of stress genes in cells infected with rSARS-CoV-ΔE-p1, which has an RNA genome sequence identical to that of the parental virus except for the deletion of gene E, was analyzed. Total RNA from Vero E6 cultures infected with the original viruses (P1) with or without E protein, and with the virus lacking E protein passaged 16 times, was extracted at 22 hpi. The expression of cellular genes involved in cytosolic, ER, and mitochondrial stress was evaluated by qRT-PCR. Cellular stress genes were upregulated to similar extents in cells infected with the viruses lacking the E gene (either from P1 or P16) compared to cells infected with virus expressing the E gene (Fig. S3). These data indicated that the mutation in gene S was not responsible for the observed differences in stress response, and confirmed that E protein itself down regulated the cellular stress in virus-infected cells.

To reinforce the conclusion that SARS-CoV E protein was responsible for the reduction of cellular stress, we transfected the E gene into rSARS-CoV-ΔE-infected cells together with controls. Vero E6 cells were infected with viruses lacking the E gene (P1 and P16) or with virus expressing the E gene, and 90 min later, cells were transfected with the plasmid pcDNA3.1-E, encoding the E protein, or with empty plasmid as a control. E protein was expressed in cells transfected with plasmids expressing this protein, although levels were 10-fold lower than in SARS-CoV infected cells, as shown by Western-blot analysis (Fig. 7A). As an additional control, the effect of E protein expression on the replication of SARS-CoV with or without E gene was studied (Fig. 7B). E protein added in trans had no significant effect on rSARS-CoV-P16 or rSARS-CoV-ΔE titers, indicating that the absence of E protein in rSARS-CoV-ΔE, and not the amount of virus

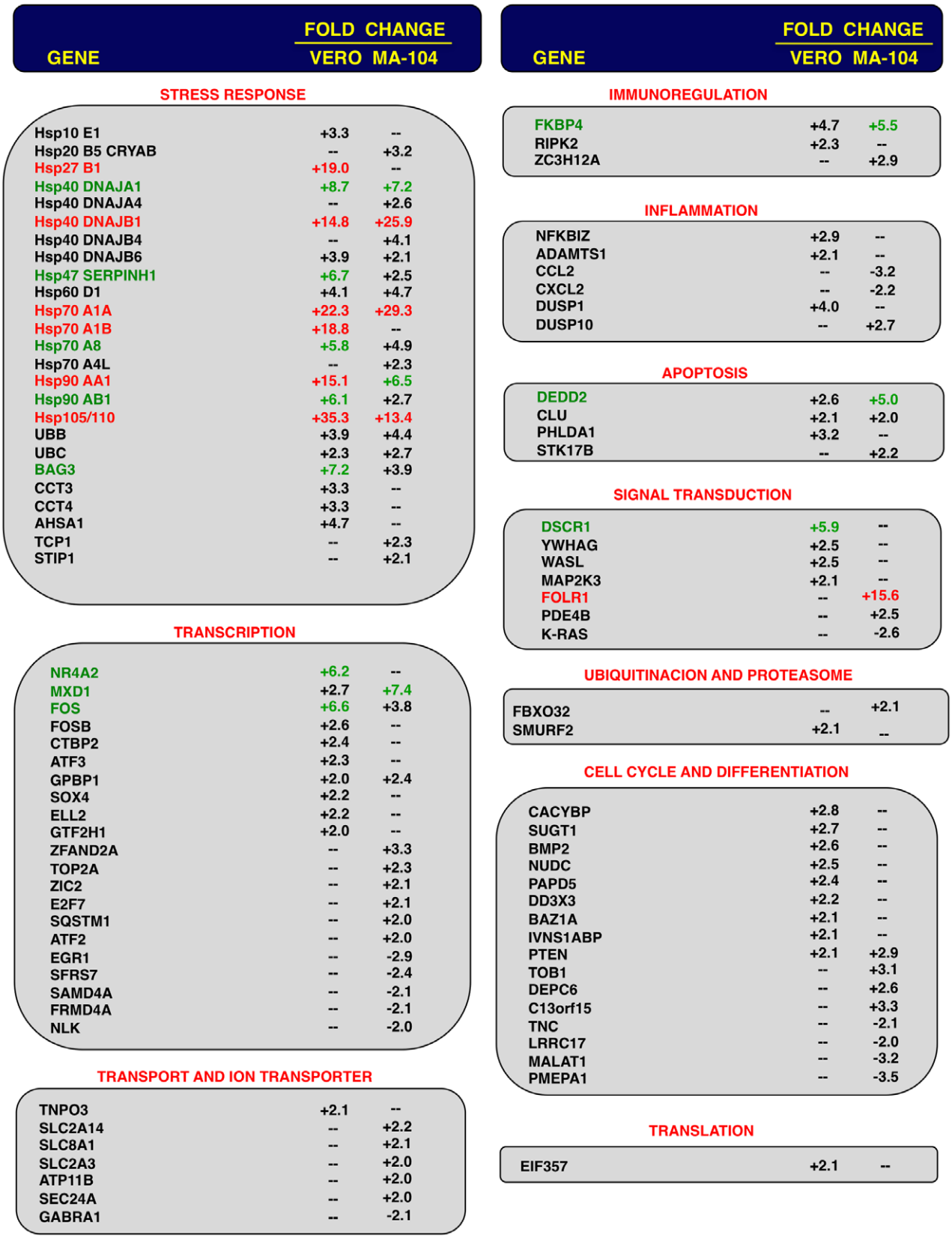

Figure 3. Host cell genes differentially expressed in rSARS-CoV-ΔE versus rSARS-CoV-infected cells using microarrays. Genes differentially expressed in rSARS-CoV-ΔE versus rSARS-CoV-infected Vero E6 and MA-104 cells, were classified according to their main biological functions. Only genes with a fold change higher than two or lower than minus two (FDR<0.01) were considered. –, indicates that the gene is not detected in the array or is not differentially expressed with a fold change higher than two or lower than minus two. Red color indicates genes

upregulated more than 10 fold. Green color indicates genes upregulated between 5 and 10 fold, at least in one cell line. For those genes recognized with more than one probe, the value corresponding to the highest upregulation or downregulation is represented.
doi:10.1371/journal.ppat.1002315.g003

produced, was responsible for the increase in cell stress response. The expression of stress genes hsp70 A1A, hsp90 AA1, hspH1, SERPINH1, and hsp10 E1 in cells infected with rSARS-CoV-ΔE viruses (P1 and P16) or rSARS-CoV, in the presence or absence of the transfected E gene, was analyzed by qRT-PCR (Figs. 7C and S4). The expression of all analyzed stress-induced genes was clearly upregulated in cells infected with virus lacking E protein, compared to those infected with rSARS-CoV. When E protein was provided in trans, the expression of these genes in rSARS-CoV-ΔE-infected cells was clearly reduced. To analyze whether the decreased expression of stress-related genes in the presence of E protein was specific, the expression of the gene encoding DNA polymerase theta (polQ) was evaluated. No significant differences were observed in the expression of polQ, irrespective of the presence or absence of E protein (Figs. 7C and S4), suggesting that the reduction of stress-related genes was specific. In addition, the expression of 18S rRNA was analyzed as an endogenous control for the amount of RNA in all samples (Figs. 7C and S4). These data indicated that E protein reduced the stress caused by SARS-CoV infection.

To analyze whether E protein alone could reduce the cellular stress caused by another virus, the effect of SARS-CoV E protein on the stress induced by RSV was analyzed. Vero E6 cells were transfected with a plasmid encoding E protein or with empty plasmid as control. At 24 hours post-transfection (hpt), Vero E6 cells were infected with RSV or left uninfected, and RNA was extracted at the indicated hpi. The expression of E protein in cells infected with RSV was confirmed by Western-blot analysis and the levels were similar to those of rSARS-CoV infected cells (Fig. 8A). In addition, no significant effect of E protein expression on RSV titers was detected. The expression of the stress response genes hsp90 AA1, UBB, hspH1, SERPINH1 and hsp10 E1 was analyzed in the presence or absence of SARS-CoV E protein by qRT-PCR (Fig. 8B). The expression of these stress response genes was significantly induced by RSV infection at almost all times (Fig. 8B). In the presence of E protein, the induction of these stress genes was significantly reduced (Fig. 8B) in a specific manner as no significant differences were observed in the expression of polQ gene, irrespective of the presence or absence of E protein (Fig. 8B). These data indicated that SARS-CoV E protein alone reduced different types of stress, such as cytosolic (genes hsp90 AA1, UBB, hspH1), ER (gene SERPINH1) and mitochondrial stress (gene hsp10 E1), produced by infection with at least two different respiratory viruses (SARS-CoV and RSV).

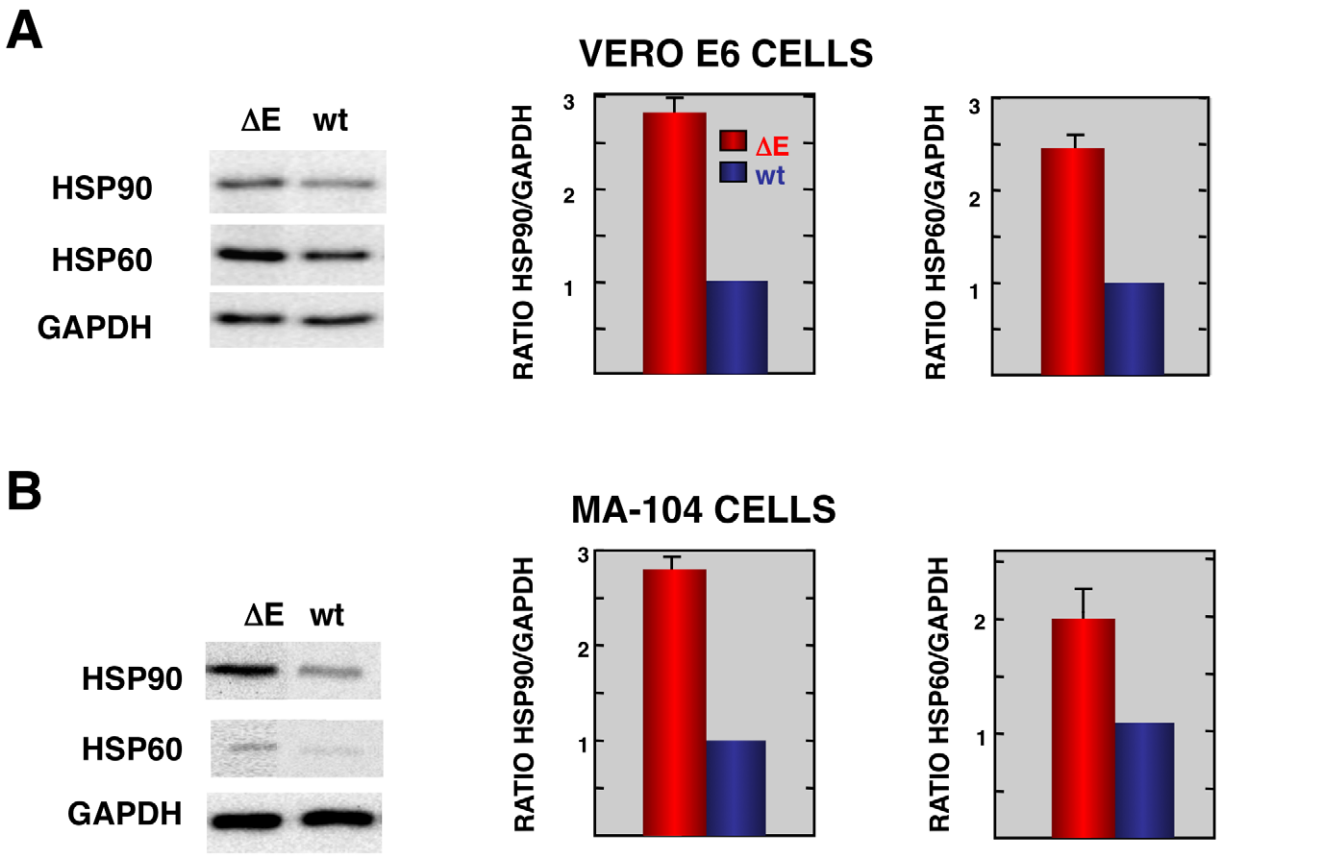

Figure 4. Stress response proteins are differentially expressed in rSARS-CoV-ΔE versus rSARS-CoV-infected cells. Total protein from Vero E6 (A) and MA104 (B) cells infected with rSARS-CoV-ΔE or SARS-CoV was extracted at 22 and 75 hpi, respectively. Levels of hsp90 and hsp60 were normalized to those of GAPDH after Western-blot assay (left panels) and densitometric analysis of the bands (right panels). Columns represent hsp90/GAPDH and hsp60/GAPDH ratios in SARS-CoV-ΔE (red) or SARS-CoV (blue) infected cells. Error bars indicate the standard deviation from three independent experiments.
doi:10.1371/journal.ppat.1002315.g004

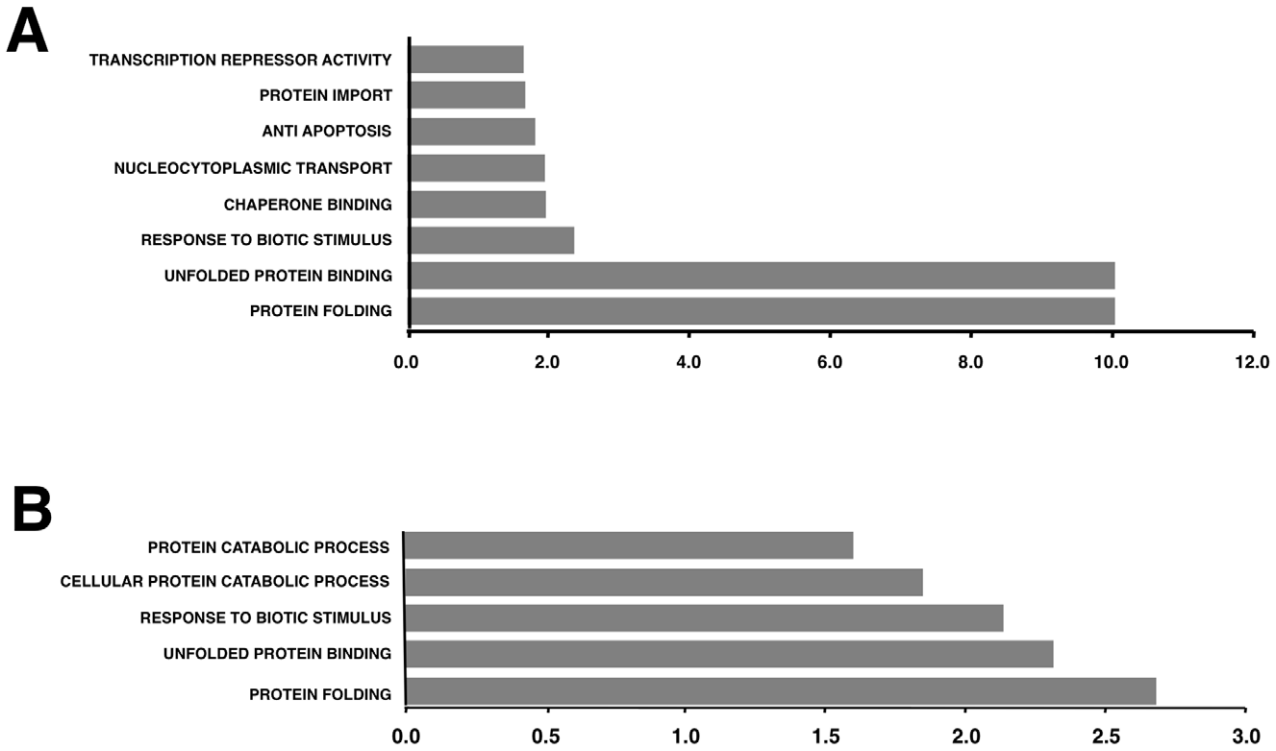

Figure 5. Upregulation of functionally associated genes in rSARS-CoV-ΔE compared to rSARS-CoV-infected cells using microarrays. Gene Sets, based on Gene Ontology terms, that correlate with upregulated genes in Vero E6 cells at 15 hpi (A) and in MA-104 cells at 65 hpi (B). X values: −log10 (FDR-q val).
doi:10.1371/journal.ppat.1002315.g005

Coronavirus infection induces ER stress [64] due to the extensive use of intracellular membranes for the generation of replication complexes and for the assembly of virus particles [36,65]. In addition, viral glycoproteins can induce ER stress during infection as a result of incomplete glycosylation and incorrect folding or accumulation in the ER lumen [66,67]. Accordingly, we decided to focus our attention on ER stress. To determine whether E protein alone was responsible for the downregulation of the ER stress response, Vero E6 and MA-104 cells were transfected with a plasmid encoding SARS-CoV E protein or with empty plasmid as a control. At 24 hpt cell cultures were treated with thapsigargin and tunicamycin, which induce ER stress by altering intracellular Ca^{++} levels or by preventing protein glycosylation, respectively [68], for 8 or 20 h, or left untreated. The levels of E protein were monitored by Western-blot analysis and were similar to E protein levels after SARS-CoV infection of Vero E6 (Fig. 9A) or MA-104 cell (data not shown). Total cellular RNAs were collected and the expression of the ER-stress inducible genes GRP78 and GRP94 was evaluated by qRT-PCR. The effect of E protein expression at the times post-induction when upregulation of these genes was highest is shown (Fig. 9B and C). Treatment with thapsigargin and tunicamycin clearly induced the expression of ER stress genes in Vero E6 and MA-104 cells transfected with the empty plasmid (Fig. 9B and C). The expression of GRP78 and GRP94 was significantly reduced in the presence of E protein (Fig. 9B and C). No decrease in the expression of polQ gene was observed in the presence of E gene, suggesting that the reduction in the expression of stress related genes was specific (Fig. 9B and C). These data indicated that E protein alone was sufficient to reduce cellular stress caused by different mechanisms.

Modulation of UPR by SARS-CoV E protein

Cells induce the UPR to reduce the burden imposed by unfolded or misfolded proteins in the ER. To analyze the mechanisms by which the E protein can reduce ER stress, the effect of E protein on the three branches of the UPR (PERK, ATF6, and IRE-1) was analyzed. The PERK pathway involves the phosphorylation and subsequent activation of this kinase. Accordingly, the levels of phosphorylated PERK in Vero E6 cells infected with rSARS-CoV-ΔE or rSARS-CoV were compared at different times pi. As a control, levels of the house-keeping gene GAPDH were measured and used for normalization. Phosphorylated PERK was detectable in rSARS-CoV-ΔE and wt-infected cells at 6 hpi, in contrast to mock-infected cells, in which no phosphorylated PERK was detected. No significant differences in the phosphorylation levels of PERK were detected between cells infected with rSARS-CoV with or without E protein (Fig. S5), suggesting that E protein had no significant influence on the phosphorylation of PERK.

To analyze whether E protein inhibited the ATF6 pathway, the extent of ATF6α processing in cells infected with rSARS-CoV with or without the E gene, or mock-infected cells was measured by Western blot using an ATF6-specific antibody that recognizes the full-length and the cleaved N-terminal domain of the protein. No significant activation of ATF6 was observed in infected cells, compared to mock-infected cells (data not shown), suggesting that SARS-CoV infection did not efficiently activate this pathway.

Activation of IRE-1 mediates cytoplasmic splicing of the mRNA encoding the transcription factor XBP-1, leading to a frame shift and subsequent translation of a functional XBP-1 transcription factor. To evaluate whether SARS-CoV E protein has an impact on the activation of this pathway, Vero E6 cells were infected with

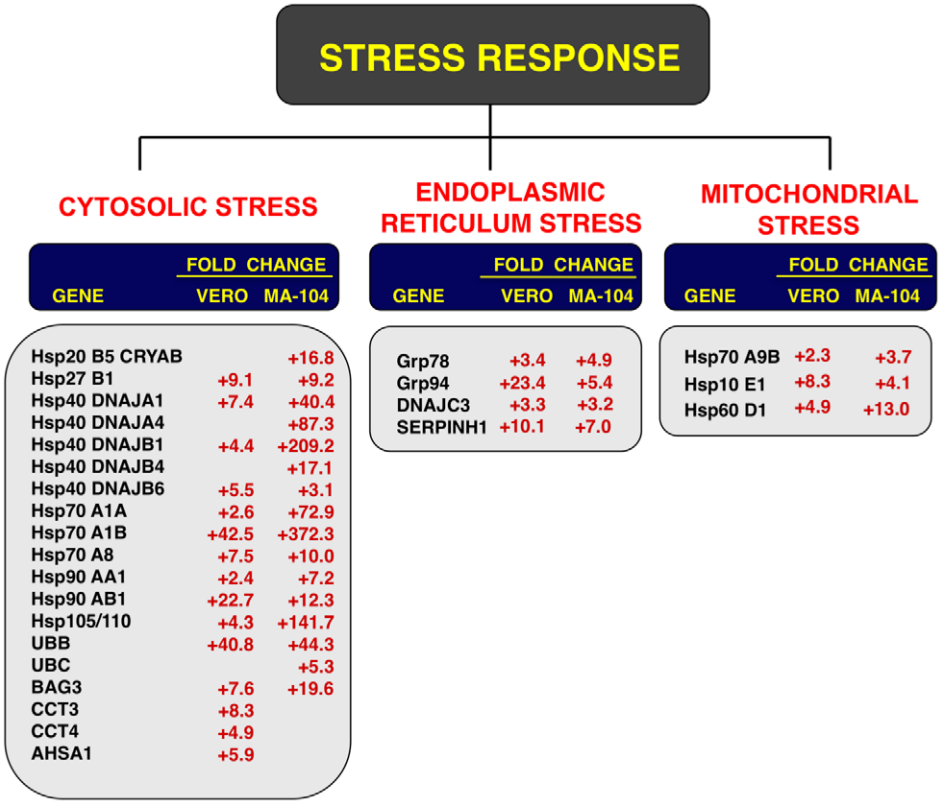

Figure 6. Cellular stress responses induced by rSARS-CoV-ΔE infection. Vero E6 and MA-104 cells were infected with rSARS-CoV-ΔE or SARS-CoV at an moi of 2. Cellular RNAs were extracted at 22 (Vero E6) and 65 (MA-104) hpi and the expression of cellular mRNAs corresponding to cytosolic, ER and mitochondrial stress genes was measured by qRT-PCR. In the case of cytosolic stress, only genes with fold increases >2.5 measured by microarrays were further evaluated by qRT-PCR. Numbers indicate the levels of gene expression in rSARS-CoV-ΔE compared to SARS-CoV-infected cells. Three independent experiments were analyzed with similar results in all cases.
doi:10.1371/journal.ppat.1002315.g006

rSARS-CoV with or without the E gene and RNA was collected at different times pi. RT-PCR was used to amplify fragments representing both the unspliced (u) and spliced (s) forms of XBP-1 mRNA, differing by 26 nt [69] (Fig. 10). The relative abundance of these XBP-1 mRNAs was independent of PCR efficiency as the corresponding mRNAs were amplified using the same primer pair. A third slowly migrating species (h), corresponding to a heterohybrid formed by the amplified unspliced and spliced forms was also detected (Fig. 10). The activation of IRE-1 was estimated as a ratio between the spliced and unspliced forms of XBP-1. Levels of spliced XBP-1 were higher in rSARS-CoV-ΔE-infected compared to rSARS-CoV infected cells from 15 to 28 hpi (Fig. 10). This result indicated that in the presence of E protein, activation of the XBP-1 pathway was reduced.

Inhibition of apoptotic cell death by SARS-CoV E protein

Persistent or intense ER stress can trigger apoptosis [41]. To analyze whether SARS-CoV E protein modulated apoptosis induced by SARS-CoV infection, the induction of apoptosis was analyzed in cells infected with rSARS-CoV lacking or expressing E gene. Cells infected either with rSARS-CoV or rSARS-CoV-ΔE were simultaneously stained with propidium iodide (PI) and Annexin V, and monitored by flow cytometry. Mock infected cells remained viable (Annexin V^-, PI^-) throughout the experiment, indicating that the treatment did not induce apoptosis by itself (Fig. 11). rSARS-CoV induced low levels of apoptosis (Annexin V^+) from 15 hpi, and a minor cell population in late apoptosis (Annexin V^+, PI^+) was evident from 24 hpi (Fig. 11). rSARS-CoV-ΔE triggered apoptosis more rapidly and to a greater extent than rSARS-CoV, with a 3 to 4-fold increase in early apoptotic cells at 4 and 15 hpi, and a 4 and 5- fold increase in late apoptotic cells between 15 and 24 hpi (Fig. 11).

Discussion

We previously showed that rSARS-CoV-ΔE is attenuated *in vivo* [26,27]. In this work, to identify possible mechanisms for this attenuation, the effect of E protein on host cell responses during virus infection was analyzed by comparing the transcriptome of rSARS-CoV-ΔE and rSARS-CoV-infected cells. Among the genes differentially expressed, a large number of genes corresponding to cellular stress were upregulated in rSARS-CoV-ΔE compared to wt virus infected cells, clearly indicating that the presence SARS-CoV E protein reduced the stress response during infection. Upregulation of the stress response was also confirmed at the protein level, as the expression of representative stress response proteins, such as hsp60 and hsp90 was also increased. The addition of E protein in trans reversed the increase in stress response gene expression observed in rSARS-CoV-ΔE-infected cells, confirming the specific suppression of the stress response by E protein. Interestingly, levels of E protein were 10-fold lower than those expressed in SARS-CoV-infected cells, but were sufficient to reduce the increase in stress response genes, indicating the robust effect of E protein. In addition, rSARS-CoV-ΔE titers were not

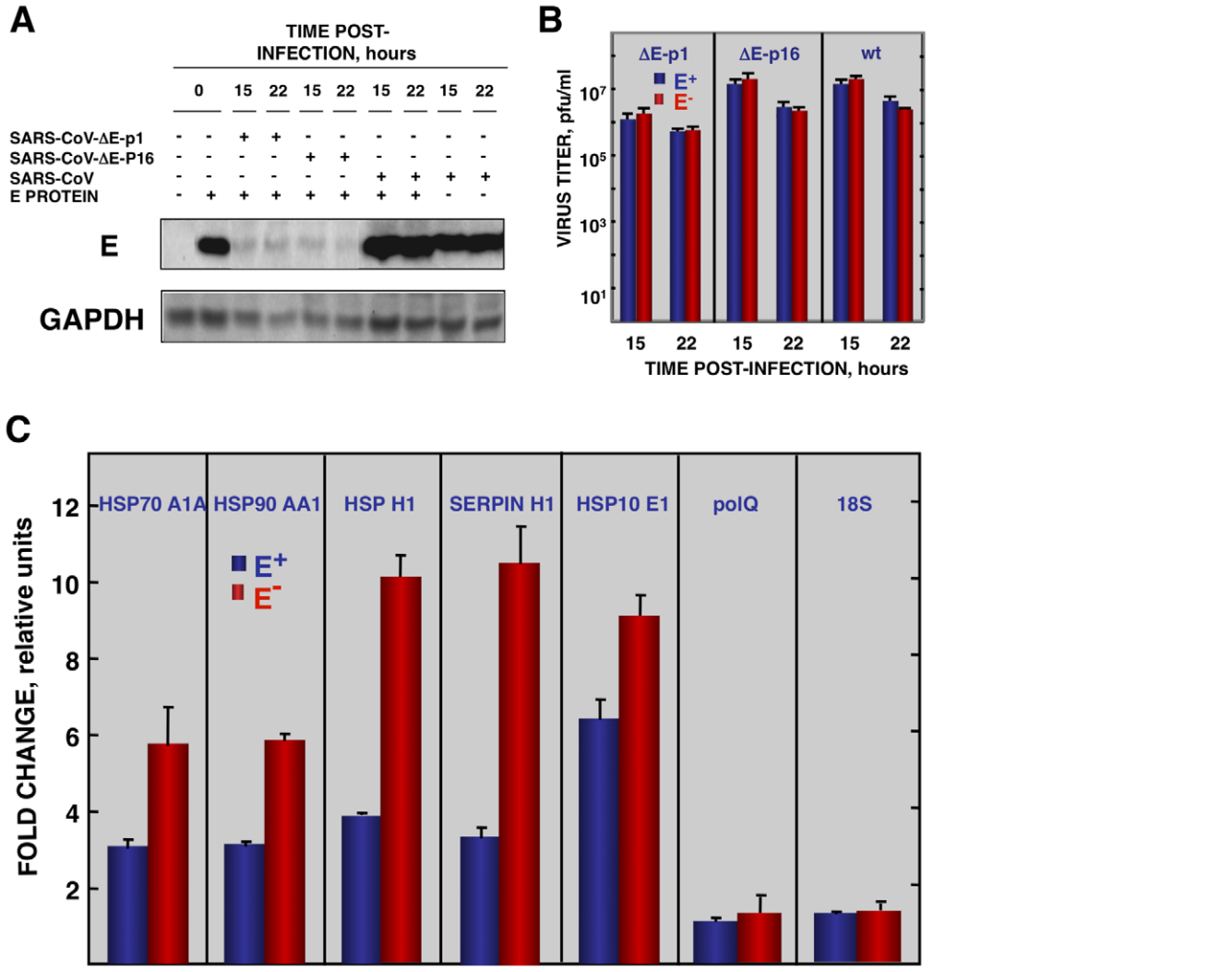

Figure 7. Effect of SARS-CoV E protein on stress induced by SARS-CoV infection. Vero E6 cells infected at an moi of 0.5 with rSARS-CoV-ΔE-P1 or rSARS-CoV were transfected with a plasmid expressing E protein (E^+) or with the empty plasmid (E^-) as control. (A) Accumulation of SARS-CoV E protein and GAPDH as a loading control, at 15 and 22 hpi were evaluated by Western blot. (B) Virus titers in the presence or absence of E protein provided in trans were evaluated at 15 and 22 hpi. (C) At 22 hpi, cellular RNAs were extracted, and the expression of the stress-induced genes hspA1A, hsp90AA1, hspH1, SERPINH1, and hspE1, and that of polQ and 18S rRNA, as controls, were analyzed by qRT-PCR. In each case, the expression levels of mRNAs encoding representative cell stress proteins were evaluated in rSARS-CoV-ΔE-P1-infected cells in relation to rSARS-CoV-infected cells. Bars represent standard deviations of the mean from three experiments.
doi:10.1371/journal.ppat.1002315.g007

significantly increased by providing E protein in trans, probably due to the low levels of E protein expressed in rSARS-CoV-ΔE infected cells, indicating that the presence or absence of E protein, and not the amount of virus, was responsible for the increase in stress response and apoptosis. In addition, stress induced by another virus, RSV, was also downregulated by SARS-CoV E protein. Furthermore, expression of E protein in the absence of virus infection reduced stress induced by tunicamycin or thapsigargin. SARS-CoV E protein also inhibited a subset of the stress response. Specifically, E protein inhibited the activation of the XBP-1-mediated pathway of the UPR, and apoptosis induced by SARS-CoV. We have shown that in MA-104 cells infected with rSARS-CoV-ΔE, two important pro-inflammatory cytokines (CCL2/MCP-1 and CXCL2/macrophage inflammatory protein 2 [MIP-2]) were downregulated, indicating that the E protein reduces virus-induced inflammation.

SARS-CoV is the most pathogenic human coronavirus known [70]. Besides pneumonia, SARS-CoV causes diarrhea [71], lymphopenia [72], haematological disorders [47], pulmonary vasculitis, and thrombosis [73,74]. In previous reports, we showed that rSARS-CoV-ΔE was attenuated in hamsters and hACE2 transgenic mice [26,27]. The relevance of virus-host interaction in virus attenuation is high as differences in virulence are frequently due to differences in host responses, rather than to virus growth kinetics [75,76].

Coronavirus infection induces an ER stress response due to the extensive use of ER membranes for RNA synthesis [35,36] and virion assembly at the ER-Golgi intermediate compartment [64,77]. Further, it has been shown that SARS-CoV structural proteins S, 6, and 3a [66,78,79,80], and the accessory protein 8ab [81] induce ER stress responses. Using genomic approaches, the upregulation of stress genes in SARS-CoV-infected Huh-7 [82],

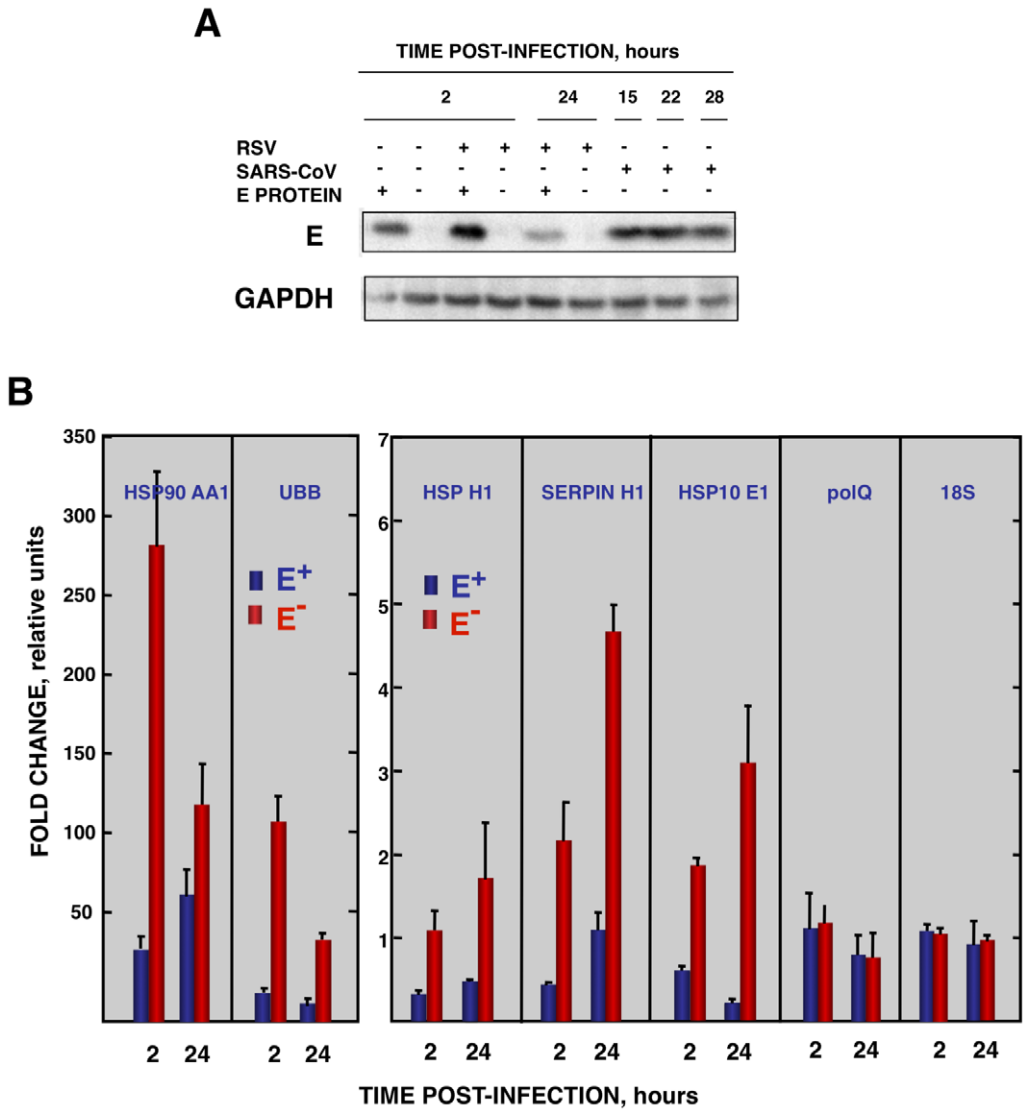

Figure 8. Effect of SARS-CoV E protein on the stress induced by RSV infection. Vero E6 cells transfected with a plasmid expressing SARS-CoV E protein (E^+) or with the empty plasmid (E^-) were infected with RSV at a moi 2. (A) Accumulation of SARS-CoV E protein and GAPDH as a loading control, at 2 and 24 hpi in the case of RSV-infected cells and at 15, 22, and 28 hpi in the case of SARS-CoV-infected cells, was evaluated by Western blot. (B) Intracellular RNA was extracted at 2 and 24 hours post-RSV infection and the expression of cellular stress genes, polQ and 18S rRNA, was measured by qRT-PCR. In each case, levels of expression in infected cells were compared to those in mock-infected ones. Bars represent standard deviations of the mean of results from three experiments.
doi:10.1371/journal.ppat.1002315.g008

Vero [59], and blood mononuclear cells [83,84] has been reported in cell cultures and also *in vivo* [75,85]. We show, for the first time, that SARS-CoV E protein limits the stress response elicited by SARS-CoV infection, which probably represents a selective advantage for the virus. In fact, we have shown that rSARS-CoV-ΔE is cleared faster than rSARS-CoV with E protein [26,27]. We observed that genes related to hsps were upregulated in rSARS-CoV-ΔE infected compared to wt virus-infected cells. The presence of hsps on the cell surface facilitates the elimination of infected cells by natural killer (NK) and T cell subsets [32]. Hsps facilitate the presentation of antigenic peptides by the major histocompatibility complex I (MHC I), helping clearance of infected cells by $CD8^+$ T cells [86].

SARS-CoV E protein expressed in trans reduced the stress response induced by rSARS-CoV-ΔE, by a heterologous virus such as RSV (without affecting the amount of virus in both cases), and by non-viral agents, such as thapsigargin and tunicamycin. Therefore, E protein limited the ER stress caused by the unbalance of ER Ca^{++} ion concentrations, and by the inhibition of N-glycosylation leading to the accumulation of misfolded or unfolded proteins. Overall, these results showed that the downregulation of the stress response by SARS-CoV E protein was a general phenomenon.

In order to analyze the specific pathways modulated by SARS-CoV E protein, the three branches of the UPR were analyzed. Only the XBP-1 pathway was significantly activated in cells infected with rSARS-CoV-ΔE compared to infection with the wt virus. Possibly, the partial activation of the UPR was not sufficient to alleviate cellular stress, and cell apoptosis was induced to help virus clearance [31,41]. The ectopic expression of coronavirus E protein induces apoptosis in the absence of infection [87,88], whereas in this manuscript we describe that the expression of E

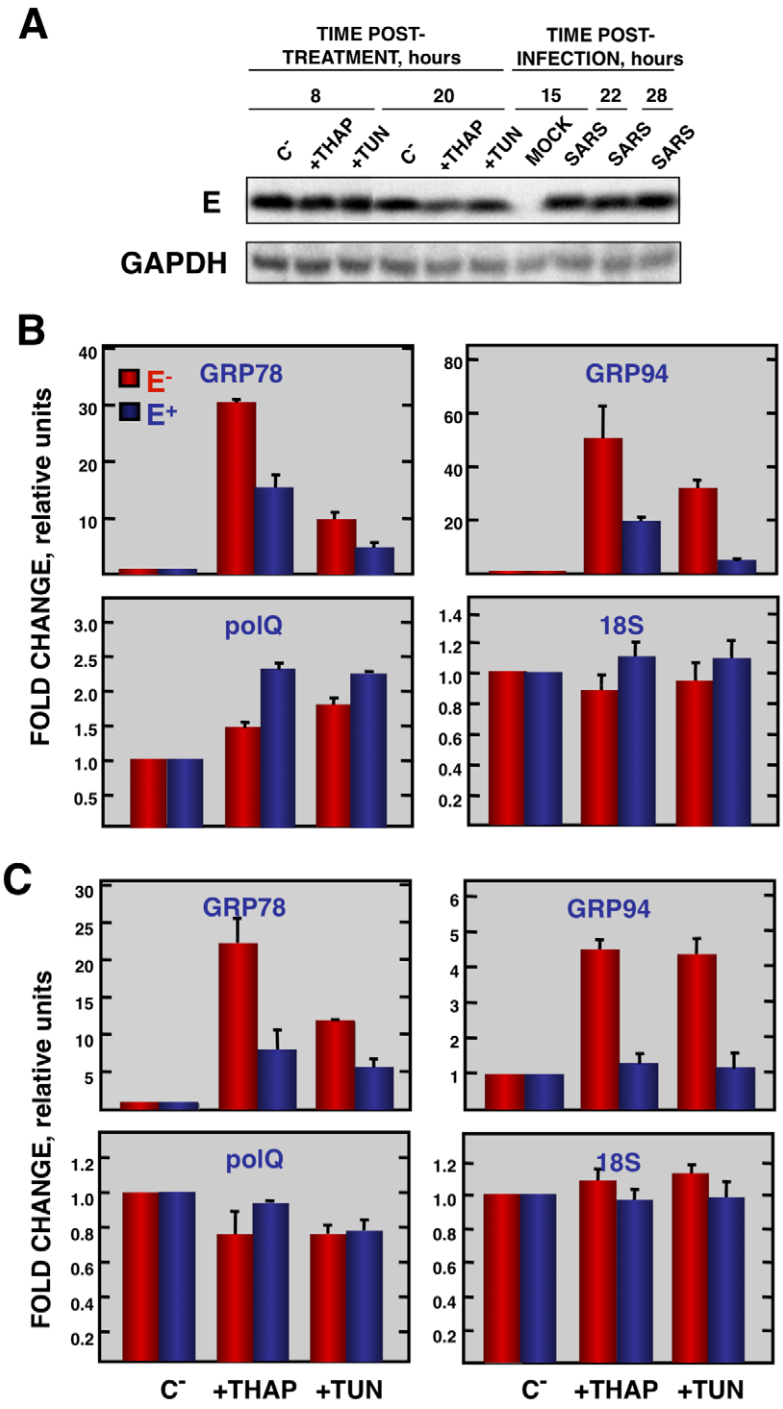

Figure 9. Effect of SARS-CoV E protein on the induction of ER stress caused by drugs. Vero E6 and MA-104 cells were transfected with a plasmid expressing SARS-CoV E protein (E^+) or with the empty plasmid (E^-). At 24 hpt, the cells were treated with 1000 nM thapsigargin (+thap), 2 μg/ml of tunicamycin (+tun) or left untreated (−). (A) Levels of SARS-CoV E and GAPDH (loading control) at 8 and 20 h post treatment in Vero E6 cells were determined by Western blot. The expression of the stress induced genes, GRP78 and GRP94 ER and that of polQ and 18S rRNA was evaluated by qRT-PCR in Vero E6 (B) or MA-104 (C) cells. In each case, levels of expression in treated cells were compared to non-treated cells. Bars represent the standard deviations from the mean in three independent experiments.
doi:10.1371/journal.ppat.1002315.g009

protein in the context of SARS-CoV infection, limited the levels of apoptosis in infected cells, which may represent an advantage for virus production and dissemination [89]. This is not surprising, as previous experiments were performed in transfected cells and not in the context of viral infection, and as many other viral proteins such as 3C-like protease, spike, membrane, nucleocapsid, 3a, 3b, and 7a (reviewed by Tan et al. in [45]), and proteins 6, 7b, and 8a [78,90,91] also elicit apoptosis. Removal of the E gene from SARS-CoV led to an increase in stress responses and UPR. Nevertheless, the stress and UPR responses were not able to balance the homeostasis of the system and apoptosis was increased as a defense mechanism that may have contributed to the

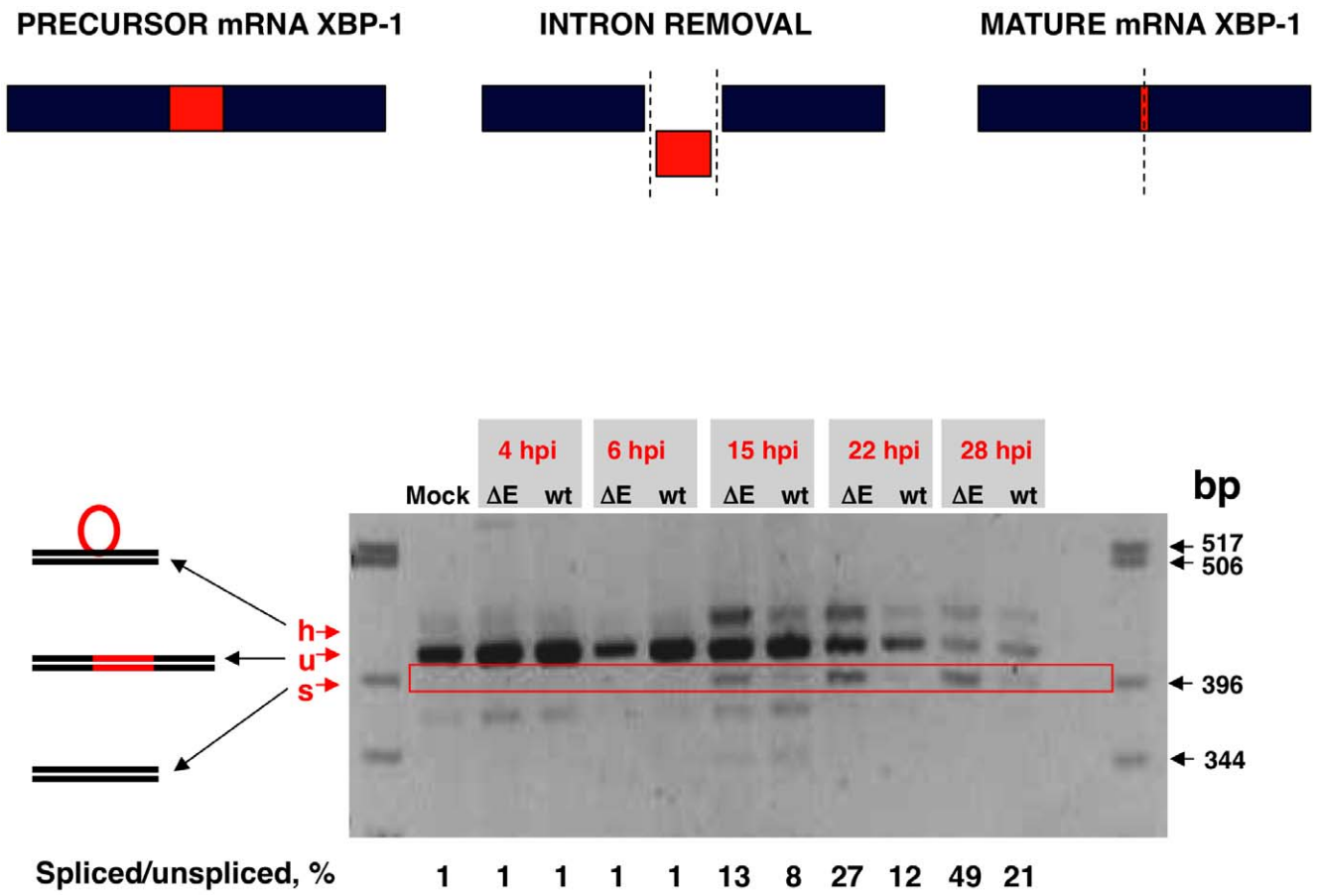

Figure 10. Activation of the IRE-1 pathway in rSARS-CoV-ΔE-infected cells. Vero E6 cells were infected with rSARS-CoV-ΔE or rSARS-CoV at an moi of 2. Splicing of XBP-1 mRNA was analyzed at different times pi using oligonucleotides flanking the splicing region. Numbers below the gel represent the percentage of spliced/unspliced forms of XBP-1.
doi:10.1371/journal.ppat.1002315.g010

attenuation observed in rSARS-CoV-ΔE-infected hamsters and mice [26,27]. Overall, these data indicate that the regulatory influence of E protein on signaling pathways leading to apoptosis still needs further clarification. The control of the stress response and apoptosis by a viral protein has also been observed in infections by human cytomegalovirus, in which the UL38 protein suppresses ER stress-induced death, preventing premature cell death and facilitating efficient virus replication [92,93].

The expression of genes leading to exuberant inflammation has been associated with SARS-CoV-induced pathology [75,76]. The upregulation of stress genes observed in SARS-CoV-infected cells when the E gene was deleted probably diminished proinflammatory processes, leading to a decrease in pathology [94,95]. In fact, we have observed that MAPK phosphatases DUSP1 and DUSP10 were upregulated in rSARS-CoV-ΔE-infected cells when compared to wt virus-infected cells. DUSP proteins are critical regulators of innate immune responses [96]. Using DUSP1 and DUSP10 knock out cell cultures and mice, it has been shown that these genes limit the expression of inflammatory genes such as TNF, IL-6, CCL2/MCP-1, CCL3, CCL4 and CXCL2/MIP-2 [60,97,98,99]. Interestingly, we observed a decrease in the expression of CXCL2/MIP-2 and CCL2/MCP-1 in rSARS-CoV-ΔE infected MA-104 cells compared to wt virus-infected cells, probably contributing to the reduction of lung inflammation that we observed *in vivo* [26,27]. In human SARS, increases in IL-6, CCL2/MCP-1 and CXCL10/IP-10 expression were detected in the lungs of human patients with fatal SARS [48,49,100]. Furthermore, persistent expression of CCL2/MCP-1, CXCL9/MIG and CXCL10/IP-10 was observed in the blood of SARS patients with fatal disease [48,49,100], reinforcing the idea that elevated expression of proinflammatory cytokines significantly contributes to the pathogenicity of the virus.

In summary, we found that deletion of the E gene from SARS-CoV increased the expression of host genes involved in stress response and immunoregulation, among others, and decreased those involved in inflammation. Further, SARS-CoV E protein reduced the stress caused by two viruses, SARS-CoV and RSV, and by drugs. E protein may represent a novel strategy used by SARS-CoV to increase its virulence and may also serve as a potential therapeutic target in outbreaks of SARS-CoV or other coronaviruses.

Materials and Methods

Virus

rSARS-CoV and rSARS-CoV-ΔE were rescued from infectious cDNA clones as previously described [26,101]. rSARS-CoV-ΔE was passaged 16 times in Vero E6 cells and characterized *in vitro* and *in vivo* (rSARS-CoV-ΔE-P16) [56]. Remarkably, only a single mutation, at position 23312, which resulted in a serine to phenylalanine mutation in the gene S, was detected in the rSARS-CoV-ΔE passaged 16 times [56]. All work with infectious

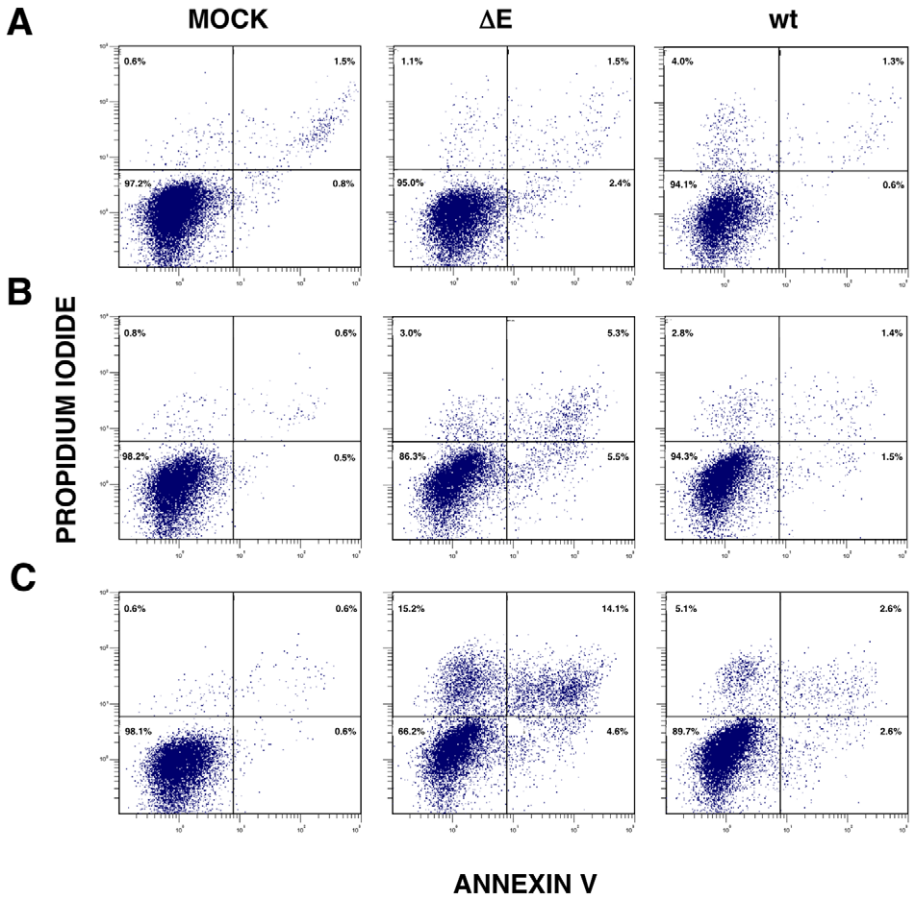

Figure 11. rSARS-CoV-ΔE-induced apoptosis. Apoptosis levels in mock, rSARS-CoV-ΔE and rSARS-CoV-infected cells were evaluated at 4 (A), 15 (B) and 24 (C) hpi by flow cytometry. Annexin V-PI double staining was performed to differentiate cells in early apoptosis (Annexin V^+, PI^-) from those in late apoptosis (Annexin V^+, PI^+).
doi:10.1371/journal.ppat.1002315.g011

viruses was performed in biosafety level (BSL) 3 facilities by personnel wearing positive-pressure air purifying respirators (3M HEPA AirMate, St. Paul, MN).

Cells

African Green monkey kidney-derived Vero E6 cells were kindly provided by Eric Snijder (Medical Center, University of Leiden, The Netherlands). African monkey kidney-derived MA-104 cells were kindly provided by J. Buesa (Universidad de Valencia, Valencia, Spain). Human colon carcinoma-derived CaCo-2 cells were obtained from the *European Collection of Cell Cultures* (EACC 86010202). Human hepatocarcinoma-derived Huh7 cells were provided by R. Bartenschlager (Department for Molecular Biology, University of Heidelberg, Germany). Rhesus monkey kidney-derived FRhK-4 cells were obtained from the *American Type Culture Collection* (ATCC CRL-1688). Porcine kidney-derived PK15 cells were provided by A. Carrascosa (Centro de Biología Molecular, Madrid, Spain). Human hepatocarcinoma-derived HepG2 cells were provided by M. Esteban (Centro Nacional de Biotecnología, Madrid, Spain). Human kidney-derived 293 cells were obtained from the *American Type Culture Collection* (ATCC CRL-1573). The 293-derived clone 293T, which expresses the SV40 T antigen, was obtained from the *American Type Culture Collection* (ATCC CRL-11268). In all cases, cells were grown in Dulbecco's modified Eagle's medium (GIBCO) supplemented with 25 mM HEPES and 10% fetal bovine serum (Biowhittaker). Virus titrations were performed in Vero E6 cells following standard procedures using closed flasks or plates sealed in plastic bags, as previously described [26].

rSARS-CoV growth kinetics

Subconfluent monolayers (90% confluency) of Vero E6 and MA-104 cells were infected at an moi of 2 with rSARS-CoV-ΔE, or rSARS-CoV. Culture supernatants were collected at different hpi and virus titer was determined as previously described [26].

Indirect immunofluorescence assay

Subconfluent Vero E6, MA-104, CaCo-2, Huh7, FRhK-4, PK15, HepG2, 293 and 293T cells grown in 9 cm^2 flasks were infected at an moi of 1, 3 or 5. At different times pi, cells were washed in ice-cold phosphate-buffered saline (PBS) and fixed with 4% paraformaldehyde for 30 min at room temperature. The cells were then permeabilized with 0.2% saponin in blocking solution (PBS, pH 7.4, containing 10% FBS) for 1 h at room temperature and incubated with a SARS-CoV N protein-specific monoclonal antibody (SA46-4), kindly provided by Ying Fang (Center for Infectious Disease Research and Vaccinology, Brookings, South Dakota, USA) for 90 min at room temperature. Cells were then washed three times with PBS, incubated with Alexa 488-conjugated mouse antibodies (Molecular Probes) at 1:500 dilution in blocking solution for 30 min at room temperature and washed five times with PBS. The slides were removed, mounted with glass

coverslips and analyzed with a Zeiss Axiophot fluorescence microscope.

Microarray analysis

Vero E6 or MA-104 cells were mock-infected or infected at an moi of 2 with rSARS-CoV or rSARS-CoV-ΔE. Total RNA was extracted using a RNeasy mini kit (Qiagen) according to the manufacturer's instructions and RNA integrity was measured in a bioanalyzer (Agilent Technologies, Inc.). RNAs were biotin-labeled using the *One cycle target-labeling kit* (Affymetrix, Santa Clara, CA). Briefly, cDNA was synthesized from 5 μg total RNA using an oligo-dT primer with a T7 RNA polymerase promoter site added to the 3′ end. After second-strand synthesis, *in vitro* transcription was performed using T7 RNA polymerase to produce biotin-labeled cRNA. cRNA preparations (15 μg) were fragmented at 94°C for 35 min into 35–200 bases in length and added to a hybridization solution (100 mM 4-morpholinopropanosulfonate acid, 1 M Na^+, 20 mM EDTA and 0,01% Tween-20). The cRNAs (10 μg) were hybridized to Human Genome U133 plus 2.0 Arrays (Affymetrix, Santa Clara, CA) at 45°C for 16 hours. The arrays were stained with streptavidin-phycoerythrin and read at 1.56 μm in a GeneChip Scanner 3000 7G System (Affymetrix, Santa Clara, CA). Three independent microarrays were hybridized for each experiment.

Microarray data analysis

Data analysis was performed with the system affylma GUI R [102]. Robust Multi-array Analysis (RMA) algorithm was used for background correction, normalization and presentation of the expression levels [103]. Next, analysis of differential expression was performed with the Bayes t-statistics using microarray data (limma) linear models, included in the affylmGUI package. P-values were corrected for multiple-testing using the Benjamini-Hochberg's method (False Discovery Rate) [104,105]. Genes were considered differentially expressed if the FDR were <0.01. In addition, only genes with a signal log ratio of more than one or less than minus one were considered for further analysis.

Gene Set Enrichment Analysis of DNA microarray results

To understand the biological significance underlying the gene expression data, gene set enrichment analysis (GSEA) was used [106]. This method analyzes all of the gene expression data to identify genes coordinately regulated in predefined gene sets. GSEA was applied independently to gene expression results obtained at 15 hpi and to those obtained at 65 hpi. Gene expression results were sorted by their logRatios. Gene Sets based on Gene Ontology keywords as defined in the subset C5 of Molecular Signatures Database (MSigDB v2.5) [106] were used. 1402 Gene Sets containing more than 4 and less than 501 members were considered. 1000 permutations were performed. In each case, the top 20 Gene Sets showing positive correlation with upregulated genes in our data were further analyzed.

RNA analysis by qRT-PCR

Total RNA from Vero E6, or MA-104-infected cells was extracted using the Qiagen RNeasy kit according to the manufacturer's instructions and used to determine N gene subgenomic (sg) mRNA and genomic RNA levels by qRT-PCR. Reactions were performed at 37°C for 2 h with a High Capacity cDNA transcription kit (Applied Biosystems) using 100 ng of total RNA and the antisense primers Q-NsgSARS-RS (5′-TGGGTCCACCAAATGTAATGC-3′), complementary to nt 44 to 64 of N gene; and Q-SARS-2015-RS (5′-ATGGCGTCGACAAGACGTAAT-3′), complementary to nt 1995 to 2015 of genomic RNA. cDNAs were amplified by PCR using the Power SYBR Green PCR Master Mix (Applied Biosystems) and oligonucleotides Q-NsgSARS-VS (5′-AAGCAACCAACCTC-GATCTC-3′), complementary to the virus leader sequence, and Q-SARS-1931-VS (5′-ACCACTCAATTCCTGATTTGCA-3′), complementary to nucleotides 1931 to 1952 of genomic RNA, and the oligonucleotides RS previously described [1]. All the primers were designed using Primer Express software (Applied Biosystems). Data were acquired with an ABI PRISM 7000 sequence detection system (Applied Biosystems) and analyzed with ABI PRISM 7000 SDS version 1.0 software. Levels of viral RNAs are represented in comparison to reference levels from cells infected with rSARS-CoV at 0 hpi.

For qRT-PCR of cellular genes, total RNA from Vero E6, and MA-104-infected cells was extracted as described above. Reactions were performed at 37°C for 2 h using a High Capacity cDNA transcription kit (Applied Biosystems) using 100 ng of total RNA and random hexamer oligonucleotides. Cellular gene expression was analyzed using TaqMan gene expression assays (Applied Biosystems) specific for human or monkey genes (Table 1). Data were acquired with an ABI PRISM 7000 sequence detection system (Applied Biosystems) and analyzed with ABI PRISM 7000 SDS version 1.0 software. Gene expression in rSARS-CoV-ΔE and rSARS-CoV-infected cells were compared. Alternatively, gene expression in rSARS-CoV-ΔE or SARS-CoV-infected cells was compared to mock-infected cells. Quantification was achieved using the $2^{-\Delta\Delta Ct}$ method, which is a convenient way to analyze relative changes in gene expression in qPCR experiments [107]. The data represent the average of three independent experiments.

Transfection of pcDNA3.1-E and infection with rSARS-CoV

Vero E6 cells grown to 90% confluence in M24 wells, were infected at an moi of 0.5 with rSARS-CoV-ΔE-P1 and -P16 and rSARS-CoV. Ninety min after infection, cells were transfected with 1 μg of the plasmid pcDNA3.1-E expressing the SARS-CoV E protein [77], or empty plasmid as control, using 1 μg of Lipofectamine 2000 (Invitrogen) according to manufacturer's instructions. Total RNA from mock- infected or rSARS-CoV-infected cultures was extracted at different times pi as described above and used to quantify the expression of the stress-response genes hspA1A, hsp90AA1, hspH1, SERPINH1 and hspE1 by qRT-PCR as described.

Transfection of pcDNA3.1-E and infection with RSV

Vero E6 cells grown to 90% confluence in M24 multiwell plates were transfected with 1 μg of the plasmid pcDNA3.1-E, or empty plasmid as control, using 1 μg of Lipofectamine 2000 (Invitrogen) according to the manufacturer's instructions. After an incubation period of 5 h at 37°C, the transfection media were replaced and cells were incubated at 37°C for 24 h. Then, the cells were infected at an moi of 2 with RSV, Long strain [108]. RSV was provided by Dr. Blanca Garcia-Barreno (National Institute of Microbiology, Madrid), and titrated on Hep-2 cells as previously described [109]. Total RNA from mock-infected or RSV-infected cultures was extracted at different times pi as described above and used to quantify the expression of the stress-response genes hspAA1, UBB, hspH1, SERPINH1 and hspE1 by qRT-PCR as described.

Transfection of pcDNA3.1-E and treatment with thapsigargin and tunicamycin

Vero E6 and MA-104 cells were transfected with plasmid pcDNA3.1-E or empty plasmid as above. Twenty-four hpt, cells

Table 1. Taqman assays used to analyze the expression of cellular genes by quantitative RT-PCR.

Gene name	Taqman assay*	Description
DNAJA1	hs0266011-m1	DnaJ (Hsp40) homolog, subfamily A, member 1
DNAJA4	hs00388055-m1	DnaJ (Hsp40) homolog, subfamily A, member 4
DNAJB1	hs00428680-m1	DnaJ (Hsp40) homolog, subfamily B, member 1
DNAJB4	hs00199826-m1	DnaJ (Hsp40) homolog, subfamily B, member 4
DNAJB6	hs00369717-m1	DnaJ (Hsp40) homolog, subfamily B, member 6
DNAJC3	hs00534483-m1	DnaJ (Hsp40) homolog, subfamily C, member 3
SERPINH1	hs01060397-g1	serpin peptidase inhibitor, clade H (heat shock protein 47), member 1
hspA1A	hs00271229-s1	heat shock 70 kDa protein 1A
hspA1B	hs01040501-sH	heat shock 70 kDa protein 1B
hspA5/GRP78	hs99999174-m1	heat shock 70 kDa protein 5 (glucose-regulated protein, 78kDa)
hspA8	hs00852842-gH	heat shock 70 kDa protein 8
hspA9B	hs00269818-m1	heat shock 70 kDa protein 9B, mortalin
hsp90AA1	rh02791406-gH	heat shock protein 90 kDa alpha (cytosolic), class A member 1
hsp90AB1	hs00607336-gH	heat shock protein 90 kDa alpha (cytosolic), class B member 1
hsp90B1/GRP94	hs00427665-g1	heat shock protein 90 kDa beta (glucose-regulated protein, 94 KDa)
hspB1	hs03044127-g1	heat shock 27 kDa protein 1
hspD1	hs01036746-g1	heat shock 60 kDa protein 1 (chaperonin)
hspE1	hs00950982-gH	heat shock 10 kDa protein 1 (chaperonin 10)
hspH1	hs00971475-m1	heat shock 105 kDa/110 kDa protein 1
UBB	hs00430290-m1	ubiquitin B
UBC	hs01871556_s1	ubiquitin C
CCT3	hs00195623-m1	chaperonin containing TCP1, subunit 3 (gamma)
CCT4	hs00272345-m1	chaperonin containing TCP1, subunit 4 (delta)
BAG3	hs00188713-m1	BCL2-associated athanogene 3
AHSA1	hs00201602-m1	AHA1, activator of heat shock 90 kDa protein ATPase homolog 1 (yeast)
CRYAB	hs00157107-m1	crystallin, alpha B
18S	hs99999901-s1	Ribosomic RNA 18S
polQ	Hs00198196-m1	DNA polymerase, theta
TNF	Mm00443258-m1	Tumor necrosis factor
CCL2/MCP-1	Mm00441242-m1	Monocyte chemotactic protein 1
CCL5/RANTES	Mm01302428-m1	Regulated upon Activation, Normal T-cell Expressed, and Secreted
CXCL1/NAP-3	Mm04207460-m1	Neutrophil activating protein 3
CXCL2/MIP-2	Mm00436450-m1	Macrophage inflammatory protein 2
CXCL10/IP-10	Mm00445235-m1	Interferon inducible protein 10
IL-1α	Mm00439620-m1	Interleukin 1α
IL-1β	Mm01336189-m1	Interleukin 1β
IL-6	Mm00446190-m1	Interleukin 6
IFNγ	Mm01168134-m1	Interferon γ

*hs, means *homo sapiens*. rh, means rhesus (*Macaca mulatta*). Mm, means *Mus musculus*.
doi:10.1371/journal.ppat.1002315.t001

were cultured in media containing 1000 nM thapsigargin, or 2 μg/ml of tunicamycin and incubated for another 8 or 20 hours, before analysis of expression of the UPR-induced genes, GRP78 and GRP94.

Western blotting

Cell lysates were analyzed by sodium dodecyl sulfate-polyacrylamide gel electrophoresis (SDS-PAGE). Proteins were transferred to a nitrocellulose membrane with a Bio-Rad mini protean II electroblotting apparatus at 150 mA for 2 h in 25 mM Tris-192 mM glycine buffer, pH 8.3, containing 20% methanol. Membranes were blocked for 1 h with 5% dried skim milk in TBS (20 mM Tris-HCl, pH 7.5, 150 mM NaCl) and incubated with antibodies specific for hsp60 (Cell Signaling, Ref. 4870), hsp90 (Cell Signaling, Ref. 4877), SARS-CoV E protein (kindly provided by Shen Shuo, Institute of Molecular and Cellular Biology, Singapore), phospho-PERK (Santa Cruz Biotechnology, Ref. sc-32577), GAPDH (Abcam, Ref. ab9485), and ATF-6 (Abcam, Refs. ab11909 and ab37149). Bound antibodies were detected with horseradish peroxidase-conjugated goat anti-rabbit or anti-mouse antibodies (Cappel) and the ECL detection system (Amersham Pharmacia Biotech).

RT-PCR analysis of XBP-1 mRNA

Total RNA from mock-infected or rSARS-CoV or rSARS-CoV-ΔE-infected cells was used for RT-PCR analysis of XBP-1 mRNA. cDNA was prepared using the specific oligonucleotide XBP1-RS (5′-CTGGGTCCTTCTGGGTAGAC-3′). cDNAs were amplified by PCR using the sense primer XBP1-VS (5′-CTGGAACAGCAAGTGGTAGA-3′), and XBP1-RS, flanking the splicing region of XBP-1 mRNA [69]. The RT-PCR products were resolved by electrophoresis in 2% agarose gels.

Analysis of apoptosis in rSARS-CoV-infected cells

Vero E6 cells were grown to confluence in 12.5 cm^2 flasks and infected at an moi of 4 with rSARS-CoV or rSARS-CoV-ΔE. At 4, 15 and 24 hpi, cells were treated with fluorescein isothiocyanate (FITC)-conjugated annexin V (Southern Biotech) to identify apoptotic cells measured by flow cytometry, as previously described [110]. Cells were then treated with 1 volume of 4% paraformaldehyde in PBS to inactivate virus. At the end of the process, propidium iodide (PI) staining was performed to differentiate cells in early apoptosis (Annexin V^+, PI^-) from those in late apoptosis (Annexin V^+, PI^+) stage.

Supporting Information

Figure S1 Cellular stress genes with expression levels similarly modified in rSARS-CoV-ΔE and rSARS-CoV infected cells versus mock-infected cells. The differential expression of stress genes in rSARS-CoV-ΔE (X axis) and rSARS-CoV (Y axis) infected cells versus mock infected Vero E6 cells (blue symbols) and MA-104 cells (red symbols) studied using micro-arrays is represented. Symbol numbers correspond to the following genes: 1, CIP29; 2, DNAJC19; 3, DNAJA2; 4, DNAJC10; 5, hspA9; 6, DNAJC7; 7, hspA14; 8, DNAJB14; 9, DNAJB12; 10, hspA4; 11, DNAJC18; 12, DNAJC8; 13, DNAJC13; 14, DNAJC6; 15, DNAJC3; 16, DNAJC1; 17, DNAJB5; 18, hsp90B1; 19, DNAJB13.
(TIF)

Figure S2 Cellular stress responses induced by rSARS-CoV-ΔE infection. Vero E6 (A) and MA-104 (B) cells were infected with rSARS-CoV-ΔE or rSARS-CoV at an moi of 2. Cellular RNAs were extracted at 15, 22 and 28 (A) and at 24, 48, 65 and 75 (B) hpi, and the expression of cellular mRNAs corresponding to cytosolic, ER and mitochondrial stress was measured by qRT-PCR. Numbers indicate the level of gene expression in rSARS-CoV-ΔE compared to rSARS-CoV-infected cells. Three independent experiments were analyzed with similar results in all cases. Two commonly used acronyms of each protein are indicated at the bottom of the figure.
(TIF)

Figure S3 Effect of S607F mutation in S protein on cellular stress responses induced by rSARS-CoV-ΔE infection. Vero E6 cells were infected with the viruses lacking E gene passaged one or sixteen times (rSARS-CoV-ΔE-p1 and -p16, respectively) or with rSARS-CoV at an moi of 0.5. Cellular RNAs were extracted at 22 hpi and the expression of cellular mRNAs corresponding to cytosolic, ER and mitochondrial stress genes was measured by qRT-PCR. Numbers indicate the levels of gene expression in rSARS-CoV-ΔE-p1 or -p16-infected cells compared to rSARS-CoV-infected cells. Three independent experiments were analyzed with similar results in all cases. Two commonly used acronyms of each protein are indicated at the bottom of the figure.
(TIF)

Figure S4 Effect of SARS-CoV E protein on the stress induced by infection with SARS-CoV. Vero E6 cells infected at an moi of 0.5 with rSARS-CoV-ΔE-P16, or with SARS-CoV, were transfected with a plasmid expressing E protein (E^+) or with empty plasmid (E^-) as a control. At 22 hpi, cellular RNAs were extracted, and the expression of the stress-induced genes hsp10 A1A, hsp90 AA1, hsp H1, SERPIN H1, and hsp10 E1, and that of polQ and 18S rRNA, as controls, was analyzed by qRT-PCR. In each case, the corresponding mRNA expression levels in rSARS-CoV-ΔE-P16-infected cells were compared to those of rSARS-CoV-infected cells. Standard bars represent standard deviations of the mean of results from three experiments.
(TIF)

Figure S5 Effect of SARS-CoV E protein on PERK activation. Vero E6 cells were infected at an moi of 2 with rSARS-CoV-ΔE and rSARS-CoV. Cell extracts were collected at different times post-infection and the levels of the phosphorylated form of PERK, and of GAPDH as a reference control protein were analyzed by Western blot with antibodies specific for these proteins. pPERK levels in rSARS-CoV-ΔE or rSARS-CoV-infected cells, related to the levels of the housekeeping gene GAPDH are shown.
(TIF)

Table S1 Level of cell infection by rSARS-CoV. Human, porcine or monkey cells were infected at different mois, and the percentage of infected cells was measured by analyzing the presence of SARS-CoV N protein by immunofluorescence.
(DOC)

Acknowledgments

We thank Dr. Isidoro Martinez for his advice on RSV biology. We thank Marga Gonzalez for technical assistance.

Author Contributions

Conceived and designed the experiments: MLDD LE. Performed the experiments: MLDD. Analyzed the data: MLDD LE. Contributed reagents/materials/analysis tools: JLNT JMJG JARN EA JCO JZ CF SP. Wrote the paper: MLDD LE SP.

References

1. Drosten C, Gunther S, Preiser W, van der Werf S, Brodt HR, et al. (2003) Identification of a novel coronavirus in patients with severe acute respiratory syndrome. N Engl J Med 348: 1967–1976.
2. Fouchier RA, Kuiken T, Schutten M, van Amerongen G, van Doornum GJ, et al. (2003) Aetiology: Koch's postulates fulfilled for SARS virus. Nature 423: 240.
3. Ksiazek TG, Erdman D, Goldsmith C, Zaki S, Peret T, et al. (2003) A novel coronavirus associated with severe acute respiratory syndrome. N Engl J Med 348: 1953–1966.
4. Kuiken T, Fouchier RAM, Schutten M, Rimmelzwaan GF, van Amerongen G, et al. (2003) Newly discovered coronavirus as the primary cause of severe acute respiratory syndrome. Lancet 362: 263–270.
5. Marra MA, Jones SJM, Astell CR, Holt RA, Brooks-Wilson A, et al. (2003) The genome sequence of the SARS-associated coronavirus. Science 300: 1399–1404.
6. Peiris JSM, Lai ST, Poon LLM, Guan Y, Yam LYC, et al. (2003) Coronavirus as a possible cause of severe acute respiratory syndrome. Lancet 361: 1319–1325.
7. Rota PA, Oberste MS, Monroe SS, Nix WA, Campganoli R, et al. (2003) Characterization of a novel coronavirus associated with severe acute respiratory syndrome. Science 300: 1394–1399.
8. Lau SK, Woo PC, Li KS, Huang Y, Tsoi HW, et al. (2005) Severe acute respiratory syndrome coronavirus-like virus in Chinese horseshoe bats. Proc Natl Acad Sci U S A 102: 14040–14045.

9. Li W, Shi Z, Yu M, Ren W, Smith C, et al. (2005) Bats are natural reservoirs of SARS-like coronaviruses. Science 310: 676–679.
10. Woo PC, Lau SK, Li KS, Poon RW, Wong BH, et al. (2006) Molecular diversity of coronaviruses in bats. Virology 351: 180–187.
11. Ziebuhr J (2005) The coronavirus replicase. In: Enjuanes L, ed. Coronavirus replication and reverse genetics. Berlin Heidelberg, Germany: Springer-Verlag. pp 57–94.
12. Ziebuhr J, Snijder EJ, Gorbalenya AE (2000) Virus-encoded proteinases and proteolytic processing in the *Nidovirales*. J Gen Virol 81: 853–879.
13. Enjuanes L, Gorbalenya AE, de Groot RJ, Cowley JA, Ziebuhr J, et al. (2008) The Nidovirales. In: Mahy BWJ, Van Regenmortel M, Walker P, Majumder-Russell D, eds. Encyclopedia of Virology, Third Edition. Oxford: Elsevier Ltd. pp 419–430.
14. Huang C, Ito N, Tseng CT, Makino S (2006) Severe acute respiratory syndrome coronavirus 7a accessory protein is a viral structural protein. J Virol 80: 7287–7294.
15. Huang C, Peters CJ, Makino S (2007) Severe acute respiratory syndrome coronavirus accessory protein 6 is a virion-associated protein and is released from 6 protein-expressing cells. J Virol 81: 5423–5426.
16. Ito N, Mossel EC, Narayanan K, Popov VL, Huang C, et al. (2005) Severe acute respiratory syndrome coronavirus 3a protein is a viral structural protein. J Virol 79: 3182–3186.
17. Schaecher SR, Mackenzie JM, Pekosz A (2007) The ORF7b protein of SARS-CoV is expressed in virus-infected cells and incorporated into SARS-CoV particles. J Virol 81: 718–731.
18. Shen S, Lin PS, Chao YC, Zhang A, Yang X, et al. (2005) The severe acute respiratory syndrome coronavirus 3a is a novel structural protein. Biochem Biophys Res Commun 330: 286–292.
19. Torres J, Parthasarathy K, Lin X, Saravanan R, Liu DX (2006) Model of a putative pore: the pentameric alpha-helical bundle of SARS coronavirus E protein in lipid bilayers. Biophys J 91: 938–947.
20. Torres J, Maheswari U, Parthasarathy K, Ng L, Liu DX, et al. (2007) Conductance and amantadine binding of a pore formed by a lysine-flanked transmembrane domain of SARS coronavirus envelope protein. Protein Sci 16: 2065–2071.
21. Wilson L, Gage P, Ewart G (2006) Hexamethylene amiloride blocks E protein ion channels and inhibits coronavirus replication. Virology 353: 294–306.
22. Wilson L, McKinlay C, Gage P (2004) SARS coronavirus E protein forms cation-selective ion channels. Virology 330: 322–331.
23. Curtis KM, Yount B, Baric RS (2002) Heterologous gene expression from transmissible gastroenteritis virus replicon particles. J Virol 76: 1422–1434.
24. Ortego J, Ceriani JE, Patino C, Plana J, Enjuanes L (2007) Absence of E protein arrests transmissible gastroenteritis coronavirus maturation in the secretory pathway. Virology 368: 296–308.
25. Ortego J, Escors D, Laude H, Enjuanes L (2002) Generation of a replication-competent, propagation-deficient virus vector based on the transmissible gastroenteritis coronavirus genome. J Virol 76: 11518–11529.
26. DeDiego ML, Alvarez E, Almazan F, Rejas MT, Lamirande E, et al. (2007) A severe acute respiratory syndrome coronavirus that lacks the E gene is attenuated in vitro and in vivo. J Virol 81: 1701–1713.
27. DeDiego ML, Pewe L, Alvarez E, Rejas MT, Perlman S, et al. (2008) Pathogenicity of severe acute respiratory coronavirus deletion mutants in hACE-2 transgenic mice. Virology 376: 379–389.
28. Kuo L, Masters PS (2003) The small envelope protein E is not essential for murine coronavirus replication. J Virol 77: 4597–4608.
29. Sullivan CS, Pipas JM (2001) The virus-chaperone connection. Virology 287: 1–8.
30. Santoro MG (2000) Heat shock factors and the control of the stress response. Biochem Pharmacol 59: 55–63.
31. Nollen EA, Morimoto RI (2002) Chaperoning signaling pathways: molecular chaperones as stress-sensing 'heat shock' proteins. J Cell Sci 115: 2809–2816.
32. Moseley P (2000) Stress proteins and the immune response. Immunopharmacology 48: 299–302.
33. Robert J (2003) Evolution of heat shock protein and immunity. Dev Comp Immunol 27: 449–464.
34. Gosert R, Kanjanahaluethai A, Egger D, Bienz K, Baker SC (2002) RNA replication of mouse hepatitis virus takes place at double-membrane vesicles. J Virol 76: 3697–3708.
35. Snijder EJ, van der Meer Y, Zevenhoven-Dobbe J, Onderwater JJ, van der Meulen J, et al. (2006) Ultrastructure and origin of membrane vesicles associated with the severe acute respiratory syndrome coronavirus replication complex. J Virol 80: 5927–5940.
36. Knoops K, Kikkert M, Worm SH, Zevenhoven-Dobbe JC, van der Meer Y, et al. (2008) SARS-coronavirus replication is supported by a reticulovesicular network of modified endoplasmic reticulum. PLoS Biol 6: e226.
37. Ron D, Walter P (2007) Signal integration in the endoplasmic reticulum unfolded protein response. Nat Rev Mol Cell Biol 8: 519–529.
38. Wang XZ, Harding HP, Zhang Y, Jolicoeur EM, Kuroda M, et al. (1998) Cloning of mammalian Ire1 reveals diversity in the ER stress responses. EMBO J 17: 5708–5717.
39. Harding HP, Zhang Y, Ron D (1999) Protein translation and folding are coupled by an endoplasmic-reticulum-resident kinase. Nature 397: 271–274.
40. Chen X, Shen J, Prywes R (2002) The luminal domain of ATF6 senses endoplasmic reticulum (ER) stress and causes translocation of ATF6 from the ER to the Golgi. J Biol Chem 277: 13045–13052.
41. Boyce M, Yuan J (2006) Cellular response to endoplasmic reticulum stress: a matter of life or death. Cell Death Differ 13: 363–373.
42. Wei L, Sun S, Xu CH, Zhang J, Xu Y, et al. (2007) Pathology of the thyroid in severe acute respiratory syndrome. Hum Pathol 38: 95–102.
43. Zhang QL, Ding YQ, He L, Wang W, Zhang JH, et al. (2003) Detection of cell apoptosis in the pathological tissues of patients with SARS and its significance. Di Yi Jun Yi Da Xue Xue Bao 23: 770–773.
44. Krahling V, Stein DA, Spiegel M, Weber F, Muhlberger E (2009) Severe acute respiratory syndrome coronavirus triggers apoptosis via protein kinase R but is resistant to its antiviral activity. J Virol 83: 2298–2309.
45. Tan YJ, Lim SG, Hong W (2007) Regulation of cell death during infection by the severe acute respiratory syndrome coronavirus and other coronaviruses. Cell Microbiol 9: 2552–2561.
46. Huang KJ, Su IJ, Theron M, Wu YC, Lai SK, et al. (2005) An interferon-gamma-related cytokine storm in SARS patients. J Med Virol 75: 185–194.
47. Wong RS, Wu A, To KF, Lee N, Lam CW, et al. (2003) Haematological manifestations in patients with severe acute respiratory syndrome: retrospective analysis. BMJ 326: 1358–1362.
48. Tang NL, Chan PK, Wong CK, To KF, Wu AK, et al. (2005) Early enhanced expression of interferon-inducible protein-10 (CXCL-10) and other chemokines predicts adverse outcome in severe acute respiratory syndrome. Clin Chem 51: 2333–2340.
49. Jiang Y, Xu J, Zhou C, Wu Z, Zhong S, et al. (2005) Characterization of cytokine/chemokine profiles of severe acute respiratory syndrome. Am J Respir Crit Care Med 171: 850–857.
50. Zhang Y, Li J, Zhan Y, Wu L, Yu X, et al. (2004) Analysis of serum cytokines in patients with severe acute respiratory syndrome. Infect Immun 72: 4410–4415.
51. Reghunathan R, Jayapal M, Hsu LY, Chng HH, Tai D, et al. (2005) Expression profile of immune response genes in patients with Severe Acute Respiratory Syndrome. BMC Immunol 6: 2.
52. Gillim-Ross L, Taylor J, Scholl DR, Ridenour J, Masters PS, et al. (2004) Discovery of novel human and animal cells infected by the severe acute respiratory syndrome coronavirus by replication-specific multiplex reverse transcription-PCR. J Clin Microbiol 42: 3196–3206.
53. Hattermann K, Muller MA, Nitsche A, Wendt S, Donoso Mantke O, et al. (2005) Susceptibility of different eukaryotic cell lines to SARS-coronavirus. Arch Virol 150: 1023–1031.
54. Lu W, Zheng BJ, Xu K, Schwarz W, Du L, et al. (2006) Severe acute respiratory syndrome-associated coronavirus 3a protein forms an ion channel and modulates virus release. Proc Natl Acad Sci U S A 103: 12540–12545.
55. Mossel EC, Huang C, Narayanan K, Makino S, Tesh RB, et al. (2005) Exogenous ACE2 expression allows refractory cell lines to support severe acute respiratory syndrome coronavirus replication. J Virol 79: 3846–3850.
56. Netland J, DeDiego ML, Zhao J, Fett C, Alvarez E, et al. (2010) Immunization with an attenuated severe acute respiratory syndrome coronavirus deleted in E protein protects against lethal respiratory disease. Virology 399: 120–128.
57. Emeny JM, Morgan MJ (1979) Regulation of the interferon system: evidence that Vero cells have a genetic defect in interferon production. J Gen Virol 43: 247–252.
58. McKimm-Breschkin JL, Holmes IH (1982) Conditions required for induction of interferon by rotaviruses and for their sensitivity to its action. Infect Immun 36: 857–863.
59. Leong WF, Tan HC, Ooi EE, Koh DR, Chow VT (2005) Microarray and real-time RT-PCR analyses of differential human gene expression patterns induced by severe acute respiratory syndrome (SARS) coronavirus infection of Vero cells. Microbes Infect 7: 248–259.
60. Zhang Y, Blattman JN, Kennedy NJ, Duong J, Nguyen T, et al. (2004) Regulation of innate and adaptive immune responses by MAP kinase phosphatase 5. Nature 430: 793–797.
61. Narayanan K, Huang C, Lokugamage K, Kamitani W, Ikegami T, et al. (2008) Severe acute respiratory syndrome coronavirus nsp1 suppresses host gene expression, including that of type I interferon, in infected cells. J Virol 82: 4471–4479.
62. Frieman MB, Chen J, Morrison TE, Whitmore A, Funkhouser W, et al. (2010) SARS-CoV pathogenesis is regulated by a STAT1 dependent but a type I, II and III interferon receptor independent mechanism. PLoS Pathog 6: e1000849.
63. Sheahan T, Morrison TE, Funkhouser W, Uematsu S, Akira S, et al. (2008) MyD88 is required for protection from lethal infection with a mouse-adapted SARS-CoV. PLoS Pathog 4: e1000240.
64. Bechill J, Chen Z, Brewer JW, Baker SC (2008) Coronavirus infection modulates the unfolded protein response and mediates sustained translational repression. J Virol 82: 4492–4501.
65. Salanueva IJ, Carrascosa JL, Risco C (1999) Structural maturation of the transmissible gastroenteritis coronavirus. J Virol 73: 7952–7964.
66. Chan CP, Siu KL, Chin KT, Yuen KY, Zheng B, et al. (2006) Modulation of the unfolded protein response by the severe acute respiratory syndrome coronavirus spike protein. J Virol 80: 9279–9287.
67. He B (2006) Viruses, endoplasmic reticulum stress, and interferon responses. Cell Death Differ 13: 393–403.

68. Wang Y, Shen J, Arenzana N, Tirasophon W, Kaufman RJ, et al. (2000) Activation of ATF6 and an ATF6 DNA binding site by the endoplasmic reticulum stress response. J Biol Chem 275: 27013–27020.
69. Shang J, Lehrman MA (2004) Discordance of UPR signaling by ATF6 and Ire1p-XBP1 with levels of target transcripts. Biochem Biophys Res Commun 317: 390–396.
70. Weiss SR, Navas-Martin S (2005) Coronavirus pathogenesis and the emerging pathogen severe acute respiratory syndrome coronavirus. Microbiol Mol Biol Rev 69: 635–664.
71. Cheng VC, Hung IF, Tang BS, Chu CM, Wong MM, et al. (2004) Viral replication in the nasopharynx is associated with diarrhea in patients with severe acute respiratory syndrome. Clin Infect Dis 38: 467–475.
72. Peiris JS, Yuen KY, Osterhaus AD, Stohr K (2003) The severe acute respiratory syndrome. N Engl J Med 349: 2431–2441.
73. Ding Y, Wang H, Shen H, Li Z, Geng J, et al. (2003) The clinical pathology of severe acute respiratory syndrome (SARS): a report from China. J Pathol 200: 282–289.
74. Nicholls JM, Poon LL, Lee KC, Ng WF, Lai ST, et al. (2003) Lung pathology of fatal severe acute respiratory syndrome. Lancet 361: 1773–1778.
75. Rockx B, Baas T, Zornetzer GA, Haagmans B, Sheahan T, et al. (2009) Early upregulation of acute respiratory distress syndrome-associated cytokines promotes lethal disease in an aged-mouse model of severe acute respiratory syndrome coronavirus infection. J Virol 83: 7062–7074.
76. Smits SL, de Lang A, van den Brand JM, Leijten LM, van IWF, et al. (2010) Exacerbated innate host response to SARS-CoV in aged non-human primates. PLoS Pathog 6: e1000756.
77. Nieto-Torres JL, DeDiego ML, Alvarez E, Enjuanes L (2010) Cellular localization and topology of severe acute respiratory syndome coronavirus (SARS-CoV) envelope protein. Virology 415: 69–82.
78. Ye Z, Wong CK, Li P, Xie Y (2008) A SARS-CoV protein, ORF-6, induces caspase-3 mediated, ER stress and JNK-dependent apoptosis. Biochim Biophys Acta 1780: 1383–1387.
79. Minakshi R, Padhan K, Rani M, Khan N, Ahmad F, et al. (2009) The SARS Coronavirus 3a protein causes endoplasmic reticulum stress and induces ligand-independent downregulation of the type 1 interferon receptor. PLoS One 4: e8342.
80. Versteeg GA, van de Nes PS, Bredenbeek PJ, Spaan WJ (2007) The coronavirus spike protein induces endoplasmic reticulum stress and upregulation of intracellular chemokine mRNA concentrations. J Virol 81: 10981–10990.
81. Sung SC, Chao CY, Jeng KS, Yang JY, Lai MM (2009) The 8ab protein of SARS-CoV is a luminal ER membrane-associated protein and induces the activation of ATF6. Virology 387: 402–413.
82. Tang BS, Chan KH, Cheng VC, Woo PC, Lau SK, et al. (2005) Comparative host gene transcription by microarray analysis early after infection of the Huh7 cell line by severe acute respiratory syndrome coronavirus and human coronavirus 229E. J Virol 79: 6180–6193.
83. Yu SY, Hu YW, Liu XY, Xiong W, Zhou ZT, et al. (2005) Gene expression profiles in peripheral blood mononuclear cells of SARS patients. World J Gastroenterol 11: 5037–5043.
84. Shao H, Lan D, Duan Z, Liu Z, Min J, et al. (2006) Upregulation of mitochondrial gene expression in PBMC from convalescent SARS patients. J Clin Immunol 26: 546–554.
85. Zhang L, Zhang ZP, Zhang XE, Lin FS, Ge F (2010) Quantitative proteomics analysis reveals BAG3 as a potential target to suppress severe acute respiratory syndrome coronavirus replication. J Virol 84: 6050–6059.
86. Callahan MK, Garg M, Srivastava PK (2008) Heat-shock protein 90 associates with N-terminal extended peptides and is required for direct and indirect antigen presentation. Proc Natl Acad Sci U S A 105: 1662–1667.
87. Yang Y, Xiong Z, Zhang S, Yan Y, Nguyen J, et al. (2005) Bcl-xL inhibits T-cell apoptosis induced by expression of SARS coronavirus E protein in the absence of growth factors. Biochem J 392: 135–143.
88. An S, Chen CJ, Yu X, Leibowitz JL, Makino S (1999) Induction of apoptosis in murine coronavirus-infected cultured cells and demonstration of E protein as an apoptosis inducer. J Virol 73: 7853–7859.
89. Brune W (2010) Inhibition of programmed cell death by cytomegaloviruses. Virus Res 157: 144–150.
90. Chen CY, Ping YH, Lee HC, Chen KH, Lee YM, et al. (2007) Open reading frame 8a of the human severe acute respiratory syndrome coronavirus not only promotes viral replication but also induces apoptosis. J Infect Dis 196: 405–415.
91. Schaecher SR, Touchette E, Schriewer J, Buller RM, Pekosz A (2007) Severe acute respiratory syndrome coronavirus gene 7 products contribute to virus-induced apoptosis. J Virol 81: 11054–11068.
92. Terhune S, Torigoi E, Moorman N, Silva M, Qian Z, et al. (2007) Human cytomegalovirus UL38 protein blocks apoptosis. J Virol 81: 3109–3123.
93. Xuan B, Qian Z, Torigoi E, Yu D (2009) Human cytomegalovirus protein pUL38 induces ATF4 expression, inhibits persistent JNK phosphorylation, and suppresses endoplasmic reticulum stress-induced cell death. J Virol 83: 3463–3474.
94. Chen Y, Voegeli TS, Liu PP, Noble EG, Currie RW (2007) Heat shock paradox and a new role of heat shock proteins and their receptors as anti-inflammation targets. Inflamm Allergy Drug Targets 6: 91–100.
95. Johnson BJ, Le TT, Dobbin CA, Banovic T, Howard CB, et al. (2005) Heat shock protein 10 inhibits lipopolysaccharide-induced inflammatory mediator production. J Biol Chem 280: 4037–4047.
96. Wang X, Liu Y (2007) Regulation of innate immune response by MAP kinase phosphatase-1. Cell Signal 19: 1372–1382.
97. Hammer M, Mages J, Dietrich H, Servatius A, Howells N, et al. (2006) Dual specificity phosphatase 1 (DUSP1) regulates a subset of LPS-induced genes and protects mice from lethal endotoxin shock. J Exp Med 203: 15–20.
98. Zhao Q, Shepherd EG, Manson ME, Nelin LD, Sorokin A, et al. (2005) The role of mitogen-activated protein kinase phosphatase-1 in the response of alveolar macrophages to lipopolysaccharide: attenuation of proinflammatory cytokine biosynthesis via feedback control of p38. J Biol Chem 280: 8101–8108.
99. Salojin KV, Owusu IB, Millerchip KA, Potter M, Platt KA, et al. (2006) Essential role of MAPK phosphatase-1 in the negative control of innate immune responses. J Immunol 176: 1899–1907.
100. Cameron MJ, Ran L, Xu L, Danesh A, Bermejo-Martin JF, et al. (2007) Interferon-mediated immunopathological events are associated with atypical innate and adaptive immune responses in patients with severe acute respiratory syndrome. J Virol 81: 8692–8706.
101. Almazan F, DeDiego ML, Galan C, Escors D, Alvarez E, et al. (2006) Construction of a SARS-CoV infectious cDNA clone and a replicon to study coronavirus RNA synthesis. J Virol 80: 10900–10906.
102. Wettenhall JM, Simpson KM, Satterley K, Smyth GK (2006) affylmGUI: a graphical user interface for linear modeling of single channel microarray data. Bioinformatics 22: 897–899.
103. Irizarry RA, Bolstad BM, Collin F, Cope LM, Hobbs B, et al. (2003) Summaries of Affymetrix GeneChip probe level data. Nucleic Acids Res 31: e15.
104. Benjamini Y, Hochberg Y (1995) Controlling the false discovery rate: a practical and powerful approach to multiple testing. J Roy Stat Soc B 57: 289–300.
105. Reiner A, Yekutieli D, Benjamini Y (2003) Identifying differentially expressed genes using false discovery rate controlling procedures. Bioinformatics 19: 368–375.
106. Subramanian A, Tamayo P, Mootha VK, Mukherjee S, Ebert BL, et al. (2005) Gene set enrichment analysis: a knowledge-based approach for interpreting genome-wide expression profiles. Proc Natl Acad Sci U S A 102: 15545–15550.
107. Livak KJ, Schmittgen TD (2001) Analysis of relative gene expression data using real-time quantitative PCR and the 2(−Delta Delta C(T)) Method. Methods 25: 402–408.
108. Martinez I, Lombardia L, Herranz C, Garcia-Barreno B, Dominguez O, et al. (2009) Cultures of HEp-2 cells persistently infected by human respiratory syncytial virus differ in chemokine expression and resistance to apoptosis as compared to lytic infections of the same cell type. Virology 388: 31–41.
109. Martinez I, Lombardia L, Garcia-Barreno B, Dominguez O, Melero JA (2007) Distinct gene subsets are induced at different time points after human respiratory syncytial virus infection of A549 cells. J Gen Virol 88: 570–581.
110. van Engeland M, Ramaekers FC, Schutte B, Reutelingsperger CP (1996) A novel assay to measure loss of plasma membrane asymmetry during apoptosis of adherent cells in culture. Cytometry 24: 131–139.

Virology 415 (2011) 69–82

Contents lists available at ScienceDirect

Virology

journal homepage: www.elsevier.com/locate/yviro

Subcellular location and topology of severe acute respiratory syndrome coronavirus envelope protein

Jose L. Nieto-Torres [a], Marta L. DeDiego [a], Enrique Álvarez [a,1], Jose M. Jiménez-Guardeño [a], Jose A. Regla-Nava [a], Mercedes Llorente [b], Leonor Kremer [b], Shen Shuo [c], Luis Enjuanes [a,*]

[a] Department of Molecular and Cell Biology, Centro Nacional de Biotecnología (CNB-CSIC), Darwin 3, Campus Universidad Autónoma de Madrid, 28049 Madrid, Spain
[b] Protein Tools Unit, Centro Nacional de Biotecnología (CNB-CSIC), Madrid, Spain
[c] Institute of Molecular and Cell Biology, 61 Biopolis Drive, Proteos, Singapore 138673, Singapore

ARTICLE INFO

Article history:
Received 18 February 2011
Returned to author for revision
10 March 2011
Accepted 31 March 2011
Available online 27 April 2011

Keywords:
SARS
Coronavirus
Envelope protein
Antibodies
Location
Ion channel
Topology

ABSTRACT

Severe acute respiratory syndrome (SARS) coronavirus (CoV) envelope (E) protein is a transmembrane protein. Several subcellular locations and topological conformations of E protein have been proposed. To identify the correct ones, polyclonal and monoclonal antibodies specific for the amino or the carboxy terminus of E protein, respectively, were generated. E protein was mainly found in the endoplasmic reticulum-Golgi intermediate compartment (ERGIC) of cells transfected with a plasmid encoding E protein or infected with SARS-CoV. No evidence of E protein presence in the plasma membrane was found by using immunofluorescence, immunoelectron microscopy and cell surface protein labeling. In addition, measurement of plasma membrane voltage gated ion channel activity by whole-cell patch clamp suggested that E protein was not present in the plasma membrane. A topological conformation in which SARS-CoV E protein amino terminus is oriented towards the lumen of intracellular membranes and carboxy terminus faces cell cytoplasm is proposed.

Introduction

The etiologic agent of severe acute respiratory syndrome (SARS) is a coronavirus (CoV), which is the responsible for the most severe human disease produced by a CoV (van der Hoek et al., 2004; Weiss and Navas-Martin, 2005). SARS-CoV emerged in Guangdong province, China, at the end of 2002 and during 2003 rapidly spread to 32 countries causing an epidemic of more than 8000 infected people with a death rate of around 10% (Drosten et al., 2003; Rota et al., 2003). Since then, only a few community-acquired and laboratory-acquired SARS cases have been reported (http://www.who.int/csr/sars/en/). Nevertheless, CoVs similar to SARS-CoV have been found in bats distributed in different regions all over the planet (Chu et al., 2008; Drexler et al., 2010; Muller et al., 2007; Quan et al., 2010), making the reemergence of SARS possible.

SARS-CoV is an enveloped virus with a single-stranded positive-sense 29.7 kb RNA genome, which belongs to *Coronavirinae* subfamily, genus β (Enjuanes et al., 2008) (http://talk.ictvonline.org/media/g/vertebrate-2008/default.aspx). Several proteins are embedded within the SARS-CoV envelope: spike (S), envelope (E), membrane (M), and the group specific proteins 3a, 6, 7a and 7b (Huang et al., 2006, 2007; Schaecher et al., 2007; Shen et al., 2005). Protected by the viral envelope, there is a helicoidal nucleocapsid, formed by the association of the nucleoprotein (N) and the viral genome (gRNA). The CoV infectious cycle begins when the S protein binds the cellular receptor, which in the case of SARS-CoV is the human angiotensin converting enzyme 2 (hACE-2) (Li et al., 2003; Wong et al., 2004), and the virus enters into the cell. Then, the virus nucleocapsid is released into the cytoplasm, and ORFs 1a and 1b are translated directly from the gRNA, generating two large polyproteins, pp1a and pp1ab, which are processed by viral proteinases yielding the replication–transcription complex proteins (Ziebuhr, 2005; Ziebuhr et al., 2000). This complex associates with double membrane vesicles (Gosert et al., 2002; Snijder et al., 2006) and is involved in viral genome replication and in the synthesis of a nested set of subgenomic messenger RNAs (sgmRNAs) through negative polarity intermediaries in both cases (Enjuanes et al., 2006; Masters, 2006; Sawicki and Sawicki, 1990; van der Most and Spaan, 1995; Zuñiga et al., 2010). CoV proteins M, S and E are synthesized and incorporated in the endoplasmic reticulum (ER) membrane, and transported to the pre-Golgi compartment where M protein recruits S protein and binds E protein (de Haan et al., 1999; Lim and Liu, 2001; Nguyen and Hogue, 1997). In parallel, N protein binds gRNA to

* Corresponding author at: Department of Molecular and Cell Biology, Centro Nacional de Biotecnología (CNB-CSIC), Darwin 3, Cantoblanco, 28049 Madrid, Spain.
E-mail address: L.Enjuanes@cnb.csic.es (L. Enjuanes).
[1] Present address: Centro de Biología Molecular Severo Ochoa (CBMSO), UAM-CSIC, Nicolás Cabrera 1, Campus Universidad Autónoma de Madrid, 28049 Madrid, Spain.

0042-6822/$ – see front matter © 2011 Elsevier Inc. All rights reserved.
doi:10.1016/j.virol.2011.03.029

generate the nucleocapsid that is incorporated into virions through the interaction of N and M proteins during an intracellular budding process (Narayanan et al., 2000). Assembled virions accumulate in vesicles that progress through the secretory pathway, and fuse with the plasma membrane to release viruses into the extracellular media (Tooze et al., 1987).

CoV E protein is a small integral membrane protein whose sequence varies between 76 and 109 amino acids (Arbely et al., 2004; Raamsman et al., 2000). Based on primary and secondary structure, the E protein can be divided into a short hydrophilic amino terminal stretch of between 7 and 12 amino acids, a hydrophobic zone of around 25 amino acids with an α-helix secondary structure that constitutes the transmembrane region of the protein, and a carboxy terminal domain, that comprises the majority of the protein (Torres et al., 2007). Nevertheless, a variety of E protein topologies have been described for different CoVs. Mouse hepatitis virus (MHV) and infectious bronchitis virus (IBV) E proteins expose their carboxy terminal region towards the cell cytoplasm, whereas the amino terminal domain is located towards the luminal side of intracellular membranes for IBV or towards the cytoplasm for MHV (Corse and Machamer, 2000; Raamsman et al., 2000). Transmissible gastroenteritis virus (TGEV) E protein adopts a carboxy terminus luminal, amino terminus cytosolic conformation (Godet et al., 1992). In the case of SARS-CoV two alternative topologies have been proposed. In one of them, the transmembrane region forms a helical hairpin, with the amino and carboxy termini oriented towards the cytoplasm (Arbely et al., 2004; Yuan et al., 2006). In the other one, E protein establishes a single-pass transmembrane conformation with the carboxy terminal domain oriented towards the luminal side and the amino terminal domain remaining oriented towards the cytoplasm (Yuan et al., 2006). Therefore, the precise intracellular topology of SARS-CoV E protein is still under debate and needs to be clarified.

Only a small fraction of the pool of CoV E protein generated during infection is incorporated in virions (Maeda et al., 2001; Raamsman et al., 2000), which suggests an important role of E protein within the cell. Apparently, CoV E protein is mainly distributed in intracellular membranes between ER and Golgi compartments (Lim and Liu, 2001; Nal et al., 2005; Raamsman et al., 2000), where it participates in virus assembly, budding and intracellular trafficking through a not fully understood mechanism. In the case of SARS-CoV, it has been shown that E protein is located in the ER or in the Golgi apparatus using cells expressing tagged versions of the protein (Liao et al., 2006; Nal et al., 2005), however, no studies have been performed using infected cells. Recently it has been reported that E protein displays ion channel activity in the plasma membrane when expressed in mammalian cells (Pervushin et al., 2009), which indirectly suggests the presence of SARS-CoV E protein on the cell surface. These data reinforce the need to clearly determine the subcellular location of SARS-CoV E protein in infected cells and specifically, to clarify whether this protein is located at the plasma membrane.

Different requirements of E protein for virus production have been described among different CoVs. TGEV (an α genus CoV) E protein is essential for the maturation and secretion of recombinant infectious viruses (Ortego et al., 2007, 2002). In contrast, a recombinant MHV (β genus CoV) lacking E gene was infectious although it showed lower titers in cell culture than the recombinant wild type virus (Kuo and Masters, 2003). Similarly, in the case of SARS-CoV, the E gene is not essential, although recombinant SARS-CoV lacking the E gene (rSARS-CoV-ΔE) grew from 20- to 200-fold lower than the wild-type virus (rSARS-CoV *wt*) in monkey or human cells, respectively (DeDiego et al., 2007). In addition, SARS-CoV lacking the E gene was attenuated in two animal models (DeDiego et al., 2007, 2008; Netland et al., 2010) indicating that SARS-CoV E gene may be a virulence factor.

Of the CoV E protein activities, the ion channel activity is one of the most remarkable. Several viral proteins with ion channel activity have been described for other RNA viruses, such as M2 from influenza A virus, p7 from hepatitis C virus, Vpu from human immunodeficiency virus (HIV), or 2B from enterovirus (de Jong et al., 2006; Ewart et al., 1996; Pinto et al., 1992; Wozniak et al., 2010). Nevertheless, the relevance of the SARS-CoV E protein ion channel activity and its possible relationship with virus trafficking and assembly is not known. In vitro studies using artificial lipid bilayers showed that HCoV-229E, MHV, SARS-CoV and IBV E proteins behaved as cation-selective ion channels (Torres et al., 2007; Wilson et al., 2006, 2004). A recent report determined that SARS-CoV E protein expressed in mammalian cells, displayed ion channel activity at the plasma membrane as determined by whole-cell patch clamp (Pervushin et al., 2009). Nevertheless, contradictory results have also been reported indicating that SARS-CoV E protein does not behave as an ion channel at the cell surface (Ji et al., 2009).

The clarification of the cellular localization and topology of the SARS-CoV E protein is a crucial issue to understand the activities of E protein. In this article, we report the generation and characterization of monoclonal and polyclonal antibodies specific for the SARS-CoV E protein as essential tools to address E protein subcellular location and topology. The data presented in this study showed that the SARS-CoV E protein essentially accumulated in the endoplasmic reticulum-Golgi intermediate compartment (ERGIC) when expressed both alone or after SARS-CoV infection. No evidence of E protein presence in the plasma membrane was found using immunofluorescence, immunoelectron microscopy or cell surface protein labeling and purification. In addition, whole-cell patch clamp assays revealed decreased current intensity in the plasma membrane of cells expressing E protein, which is not compatible with an E protein mediated voltage gated ion channel at the cell surface. All these data indicated that the E protein would carry out its direct functions from intracellular membranes. By using the specific antibodies generated in this work and selective permeabilization of plasma or intracellular membranes, we propose a topological conformation for SARS-CoV E protein in which this protein spans intracellular membranes only once, with the E protein amino terminus oriented towards the lumen of intracellular membranes and the E protein carboxy terminus exposed towards the cytoplasm.

Results

Generation and characterization of antibodies specific for SARS-CoV E protein

To determine the cellular localization and topology of SARS-CoV E protein, five independently derived hybridomas producing mAbs specific for SARS-CoV E protein were generated. SARS-CoV E protein is mainly hydrophobic and poorly immunogenic (Fig. 1A). Nevertheless, in silico analysis of the E protein amino acid sequence revealed the presence of two regions located in the amino (Ent) and carboxy terminus (Ect) of the protein with higher probability of inducing an immune response (Fig. 1A). To obtain mAbs recognizing different regions of the protein, three pairs of BALB/c mice were each immunized with affinity chromatography purified full-length SARS-CoV E protein expressed in bacteria, or in a baculovirus system, or with chemically synthesized E protein. Sera from immunized mice were analyzed by ELISA using the three sources of purified E protein, and by immunofluorescence using rSARS-CoV *wt*-infected Vero E6 cells and cells infected with a recombinant virus lacking E gene (rSARS-CoV-ΔE) as a negative control. ELISA and immunofluorescence assays showed that the sera from all immunized animals contained antibodies specific for SARS-CoV E protein (data not shown). However, three of the six mice (one of each pair), which developed the highest titers to E protein died or became sick prior to hybridoma generation. The remaining seropositive mice were boosted with the same antigen used in previous immunizations, and sacrificed to collect their spleens to generate hybridomas. Five hybridomas that produced mAbs positive by ELISA, immunofluorescence and Western

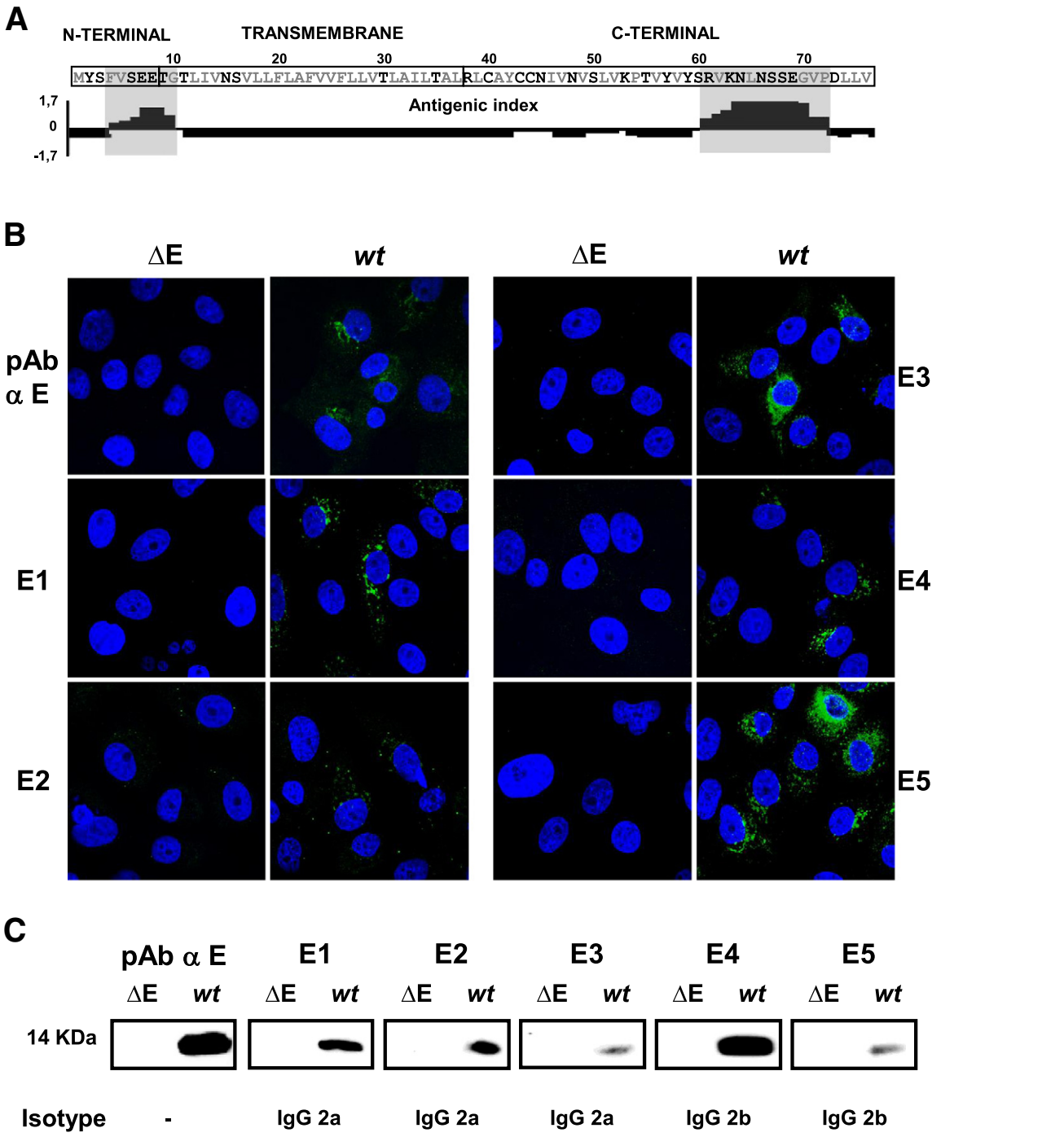

Fig. 1. Characterization of mAbs specific for SARS-CoV E protein. (A) E protein sequence is divided into three domains: the amino terminal (N-terminal), the transmembrane and the carboxy terminal (C-terminal). Gray letters represent hydrophobic amino acids, and black letters indicate hydrophilic amino acids. Jamesson–Wolf antigenic index (DNA-STAR, Lasergene) is shown below the amino acid sequence. Positive values in the graph represent high antigenicity indexes whereas negative values represent low antigenicity indexes. The highest antigenic regions of the protein are shown in gray boxes. (B) Immunofluorescences of SARS-CoV-infected Vero E6 cells. Vero E6 cells were grown on coverslips and infected at an moi of 0.3 with rSARS-CoV *wt* (*wt*) or with rSARS-CoV-ΔE (ΔE) as a control. At 24 hpi cells were fixed with 4% paraformaldehyde, and labeled with E protein specific antibodies (green). Rabbit polyclonal antibody specific for E protein (pAb α E) was used as a control. mAbs are numbered from E1 to E5. (C) Western blot analysis of SARS-CoV-infected Vero E6 cells. Vero E6 cells were infected at an moi of 0.3 with rSARS-CoV *wt* (*wt*) or with rSARS-CoV-ΔE (ΔE) as a control. At 24 hpi cell lysates were collected and probed with mAbs specific for E protein (E1 to E5) or with a polyclonal antibody used as a control (pAb α E). mAbs isotype is indicated bellow Western blot results (C). (For interpretation of the references to color in this figure legend, the reader is referred to the web version of this article.)

blot assays were selected and mAbs were purified by G protein affinity chromatography. All the selected hybridomas were derived from a mouse immunized with the SARS-CoV E protein produced in bacteria. The corresponding purified mAbs (E1, E2, E3, E4 and E5) specifically recognized E protein by immunofluorescence assays on Vero E6 cells infected with rSARS-CoV *wt* but did not bind to the control rSARS-CoV-ΔE infected cells (Fig. 1B). The mAbs showed a staining pattern consistent with a perinuclear distribution of E protein, similar to that observed with a rabbit polyclonal antibody specific for E protein (pAb α E) used as a positive control. Nevertheless, some differences in the staining could be observed. mAb E5 showed the strongest signal and the lowest background in the immunostaining (Fig. 1B). Western blot analysis using protein extracts of rSARS-CoV infected Vero E6 cells showed that all mAbs and the rabbit pAb specific for E protein

recognized a band of approximately 14 kDa, corresponding to E protein. mAb E4 showed the strongest binding by Western blot (Fig. 1C). To analyze the immunoglobulin subclass of each antibody, mAbs were subjected to an ELISA using specific secondary antibodies recognizing the heavy chain of mouse immunoglobulins (IgG1, IgG2a, IgG2b, IgG3 and IgM). Three of the selected mAbs matched to IgG2a isotype and two to IgG2b isotype (Fig. 1C).

To identify the region of E protein recognized by the mAbs, a PEPSCAN epitope mapping was performed. A total of 34 peptides of 10 amino acids covering SARS-CoV E protein full-length sequence were synthesized on a cellulose membrane. Contiguous peptides had eight overlapping amino acids. All mAbs recognized the same two consecutive peptides L_{65}NSSEGVPDL$_{74}$ and S_{67}SEGVPDLLV$_{76}$, representing the end of SARS-CoV Ect domain, although different staining intensities for one or the other peptide were observed with the different mAbs (Fig. 2A). Therefore, these mAbs should recognize the overlapping peptide S_{67}SEGVPDL$_{74}$. The E protein specific polyclonal antibody used as a positive control recognized the same two peptides as the mAbs (L_{65}NSSEGVPDL$_{74}$ and S_{67}SEGVPDLLV$_{76}$) and, in addition, three consecutive peptides, N_{45}IVNVSLVKP$_{54}$, V_{47}NVSLVKPTV$_{56}$ and V_{49}SLVKPTVYV$_{58}$, which are also located in the Ect domain (Fig. 2A). These results indicated that all the antibodies recognized the end of the Ect, suggesting that this domain was the most immunodominant E protein region.

Since all selected mAbs bound the Ect domain, to perform E protein topology studies, polyclonal antibodies specific for Ent domain were generated. To this end, two rabbits were immunized with a peptide corresponding to the first 19 amino acids of the E protein (MYSFVSEETGTLIVNSVLC) coupled to an eight branched polylysine core by a carboxy terminal cysteine. Sera from the two immunized rabbits bound purified E protein produced in bacteria, chemically synthesized E protein, and a peptide containing the Ent domain of the E protein (MYSFVSEETGTL) in an ELISA test (data not shown). Immunofluorescence analysis showed a specific staining of cells transfected with a plasmid expressing E protein (pcDNA-E) or rSARS-CoV *wt*-infected cells but not of cells transfected with the

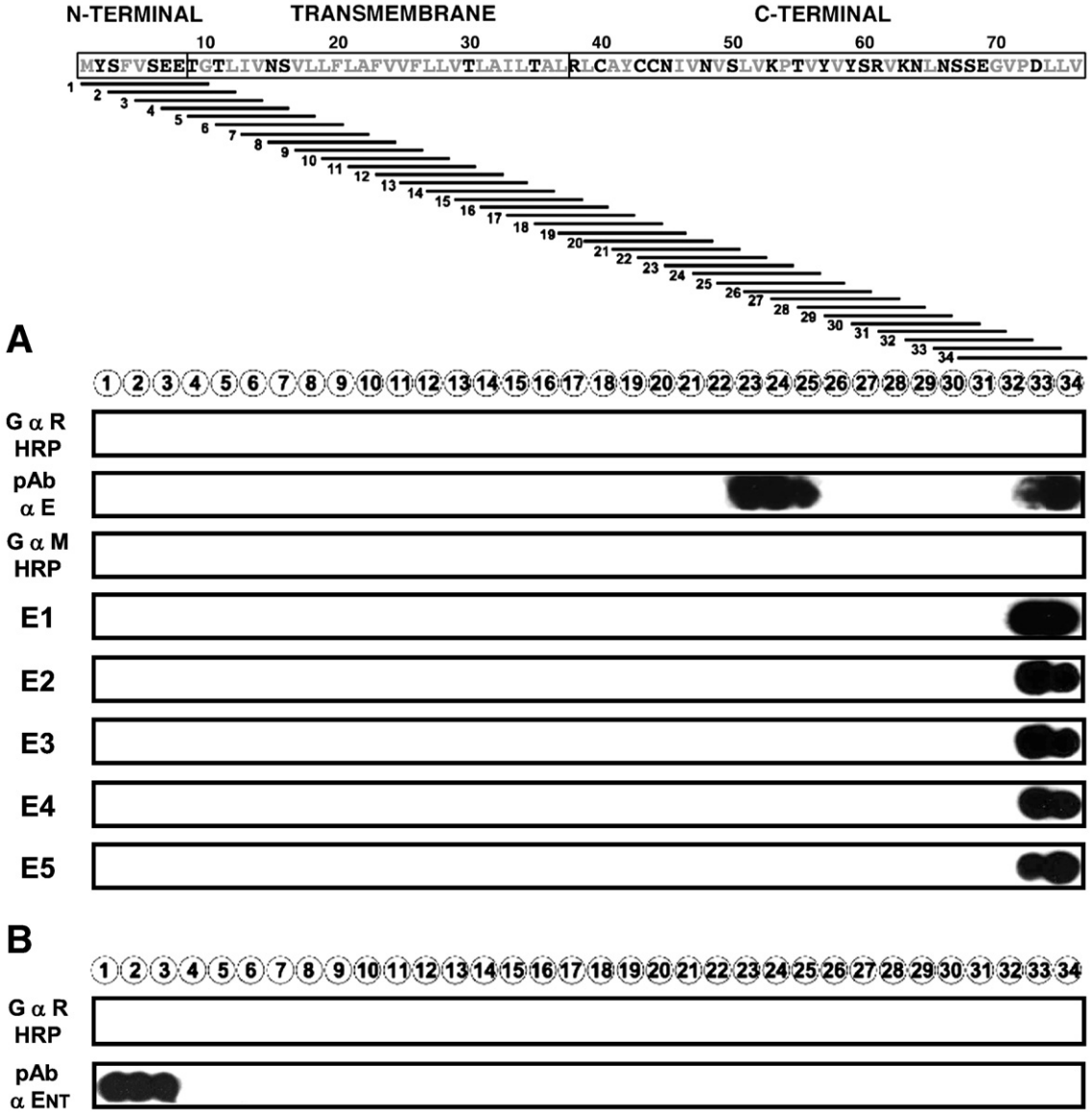

Fig. 2. Epitope mapping of SARS-CoV E protein specific mAbs and pAbs by PEPSCAN. (A) 34 peptides of 10 amino acids each covering the full length SARS-CoV E protein were synthesized on a cellulose membrane. The peptides overlapped contiguous peptides by 8 amino acids. (A) E protein derived peptides were probed by Western blot using a rabbit polyclonal antibody specific for E protein (pAb α E) or using the specific mAbs (E1 to E5). As controls, primary antibodies were omitted and goat secondary antibody coupled to HRP specific for rabbit (G α R HRP) and rabbit secondary antibody coupled to HRP specific for mouse (R α M HRP) were used alone. (B) Epitope mapping of rabbit polyclonal antibody specific for E protein amino terminal domain (pAb α Ent). As a control, a rabbit specific secondary antibody coupled to HRP (G α R HRP) was probed alone.

empty plasmid or infected with the deletion mutant rSARS-CoV-ΔE (data not shown). The serum showing the lowest background in immunofluorescence was analyzed by PEPSCAN epitope mapping. The rabbit antiserum recognized the first three peptides M_1YSFVSEETG$_{10}$, S_3FVSEETGTL$_{12}$ and V_5SEETGTLIV$_{14}$ in which amino terminal domain of SARS-CoV E protein is included. Therefore this pAb most likely recognized the oligopeptide V_5SEETG$_{10}$ (Fig. 2B).

SARS-CoV E protein subcellular localization

The subcellular localization of SARS-CoV E protein was studied in virus-infected cells and in cells transfected with a plasmid encoding the E protein (pcDNA-E). Special focus was devoted to the potential presence of E protein in the plasma membrane, a place where it might display ion channel activity, a remarkable function of this protein. To this end, Vero E6 cells were either infected with rSARS-CoV *wt* or with rSARS-CoV-ΔE as a control, or transfected with the pcDNA-E plasmid or the empty plasmid as a control. Cells were fixed at different hours post infection (hpi) or transfection (hpt), permeabilized, and the subcellular localization of E protein was determined by immunofluorescence, using the E protein specific antibodies previously described and antibodies for the cellular proteins PDI (ER marker), ERGIC53 (ERGIC marker) and cadherin (plasma membrane marker). Confocal microscopy analysis showed similar patterns of E protein distribution in transfected and infected cells at different time points (Fig. 3), suggesting that none of the other viral proteins significantly influenced the subcellular localization of SARS-CoV E protein. At 8 and 16 hpt or hpi E protein mainly colocalized with the ERGIC marker, whereas essentially no colocalization was observed with the ER (in some infected cells a reduced number of colocalization points could be seen), and no colocalization with plasma membrane marker was detected (Fig. 3 and data not shown). Between 24 and 48 hpt or hpi, when the cytopathic effect became evident in infected cells, E protein showed a broader staining pattern in part of the cells (30–40%), which partially overlapped with ERGIC marker, whereas no colocalization was observed with the ER, or with the plasma membrane (Fig. 3 and data not shown). These data showed that SARS-CoV E protein was mainly accumulated within the ERGIC and was not detected at the plasma membrane. To further analyze whether SARS-CoV E protein is present at the plasma membrane, immunofluorescence studies were also performed using non-permeabilized transfected and infected cells, in order to better preserve plasma membrane structure, and antibodies specific for E protein amino and carboxy terminal domains. No specific labeling was detected at the plasma membrane level, reinforcing the previous observations (see below, in SARS-CoV E protein topology section).

To complement the studies on the subcellular localization of SARS-CoV E protein by immunofluorescence, and to further analyze whether E protein was located in the plasma membrane, immunoelectron microscopy analysis was used to determine the presence of SARS-CoV E protein in Vero E6 cells infected with rSARS-CoV *wt* or with rSARS-CoV-ΔE as a control. E protein specific mAb E5 was used in the immunostaining with its corresponding gold-labeled secondary antibody. Gold labeling was analyzed in the plasma membrane and near the viral factories of infected cells. Around 800 gold dots on several micrographs were counted for either rSARS-CoV *wt* or rSARS-CoV-ΔE-infected cells, and gold labeling was referred as gold dots per surface units, considering 12 nm the width of the plasma membrane. Differential gold staining was found in the viral factories of rSARS-CoV *wt*-infected cells as compared with rSARS-CoV-ΔE-infected cells, whereas no specific labeling was found at the plasma membrane as determined by Student's t-test statistical analysis (Fig. 4), what indicated that SARS-CoV E protein was not present at the plasma membrane of rSARS-CoV *wt*-infected cells.

The potential presence of SARS-CoV E protein within the plasma membrane was further studied by biotinylation and purification of cell surface proteins. To this end, Vero E6 cells were infected with either rSARS-CoV *wt* or rSARS-CoV-ΔE as a control. In parallel, cells were transfected with either a pcDNA-E or with the empty plasmid as a control. Plasma membrane proteins were biotin-labeled by incubating cells with Sulfo-NHS-SS-Biotin. This compound is not internalized into cells through the plasma membrane and binds to primary amines of the proteins exposed in cell surface. Cells were lysed and biotinylated proteins were purified by affinity chromatography through a neutravidin Sepharose resin. Cell surface proteins should be biotinylated and captured (B fraction) whereas intracellular proteins should not be biotin-labeled and, therefore, should be present in the chromatography flow through (FT fraction). Complete cell lysates, captured B and flow through FT fractions were analyzed by Western blot using an E protein specific antibody (Fig. 5). In parallel, antibodies recognizing the cytosolic protein β-actin, the endoplasmic reticulum luminal protein GRP78 and the plasma membrane protein cadherin where used as controls of the biotinylation process. Intracellular proteins β-actin and GRP78 were only present in cell lysates and FT fractions but not in B fractions (Fig. 5). In contrast, the plasma membrane protein cadherin was observed in cell lysates, FT fractions and also in B fractions, as expected. E protein was detected in cell lysates and FT fractions of rSARS-CoV wt infected cells and in pcDNA-E transfected cells (Fig. 5), but it was not found in the B fractions, indicating that E protein was not biotinylated, suggesting that this protein was not accumulated at the plasma membrane (Fig. 5).

All together, these data indicated that SARS-CoV E protein is located intracellularly, mainly in the ERGIC, when expressed alone or in a SARS-CoV infection. No evidence of E protein presence in the plasma membrane was found using three complementary assays.

Whole-cell patch clamp assays

To complement and reinforce location studies of E protein in the plasma membrane, ion channel activity measurements were performed by using whole-cell patch clamp. This technique would determine any potential increase in ion currents due to the presence of minor quantities of E protein derived ion channels at the plasma membrane. HEK-293T cells were mock transfected, transfected with an empty plasmid or with a plasmid expressing SARS-CoV E protein (pcDNA-E). At 24 hpt cells were analyzed by the patch-clamp technique in a whole-cell configuration, which allow to measure voltage activated currents corresponding to voltage gated ion channels distributed all over the plasma membrane. Interestingly, control cells without E protein showed high intensity voltage activated currents, whereas cells expressing E protein revealed a significant decrease in current intensities (Fig. 6). These data suggested that E protein was not acting as a voltage gated ion channel present at the plasma membrane, because, that being the case, an increase in voltage activated currents intensity should have been observed in cells expressing E protein as compared with control cells. This finding reinforces our previous conclusion on the absence of E protein within the cell plasma membrane. The observed decrease in current intensity could be due to an indirect effect of E protein on plasma membrane proteins involved in ion transport. In fact we performed E protein pull down assays (Fig. 7), and demonstrated the interaction of SARS-CoV E protein with Na^+/K^+ ATPase alpha 1 subunit and stomatin, that were identified by mass spectrometry with significant Mascot scores (301/80 and 251/70 respectively). Na^+/K^+ ATPase is the main cellular ion pump involved in ion homeostasis control (Kaplan, 2002) and stomatin has been described as an ion channel regulator (Price et al., 2004). These interactions might be responsible for the decrease in the intensity of voltage activated currents in cells expressing E protein.

SARS-CoV E protein topology

It has previously been shown that E protein is an integral transmembrane protein (Liao et al., 2006). To further analyze the topology

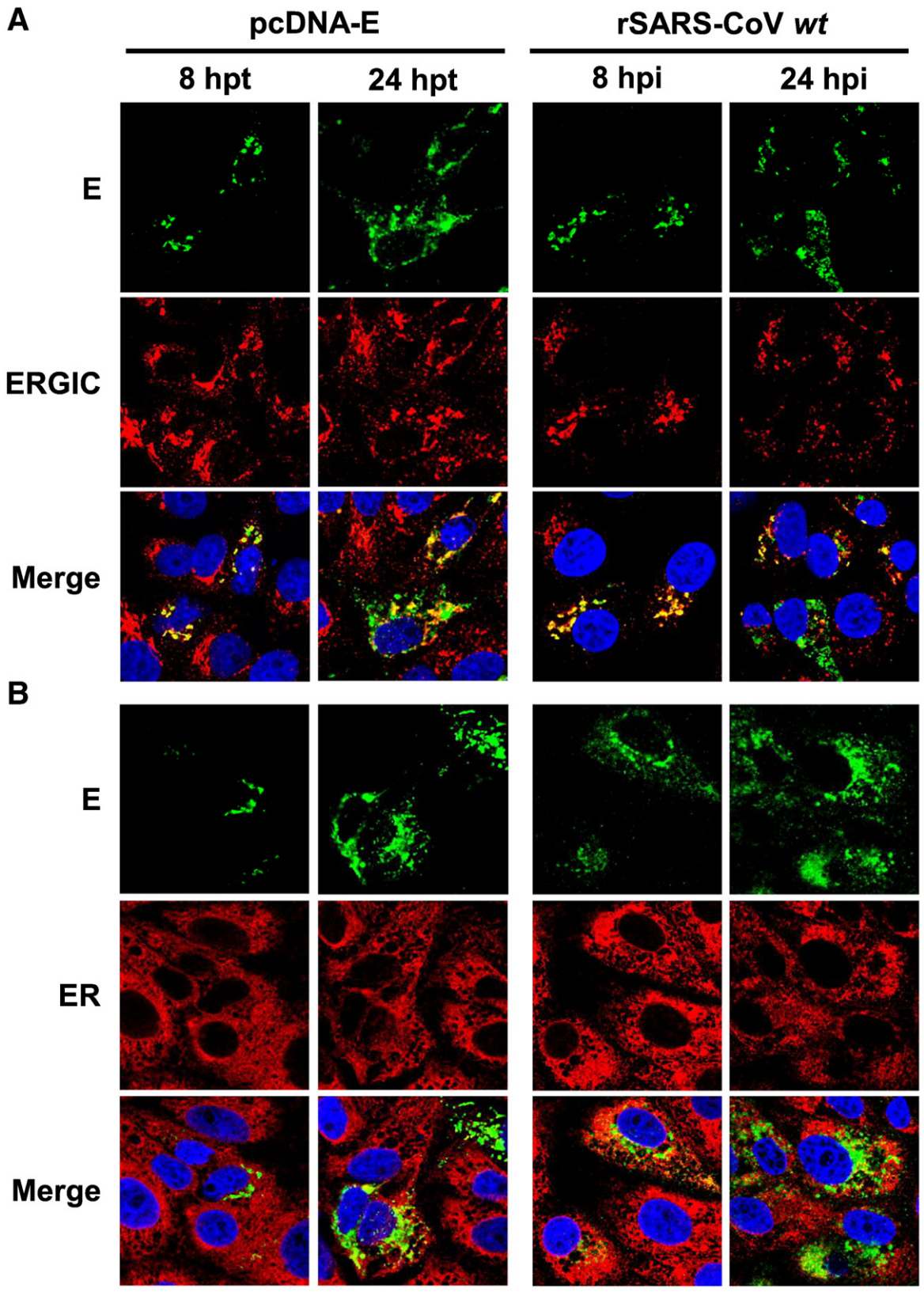

Fig. 3. Subcellular localization of SARS-CoV E protein analysis by immunofluorescence. Vero E6 cells were grown on coverslips and transfected with a plasmid encoding E protein (pcDNA-E) or infected with rSARS-CoV *wt*. Cells were fixed with 4% paraformaldehyde at 8 and 24 h post transfection (hpt) or post infection (hpi). (A) Cells were labeled with E protein (green) or ERGIC53 ERGIC marker (red) specific antibodies. (B) Cells were labeled with E protein (green) or PDI ER marker (red) specific antibodies. (C) E protein was labeled in green and plasma membrane (cadherin) was labeled in red using specific antibodies. Nuclei were stained with DAPI in all cases (blue).

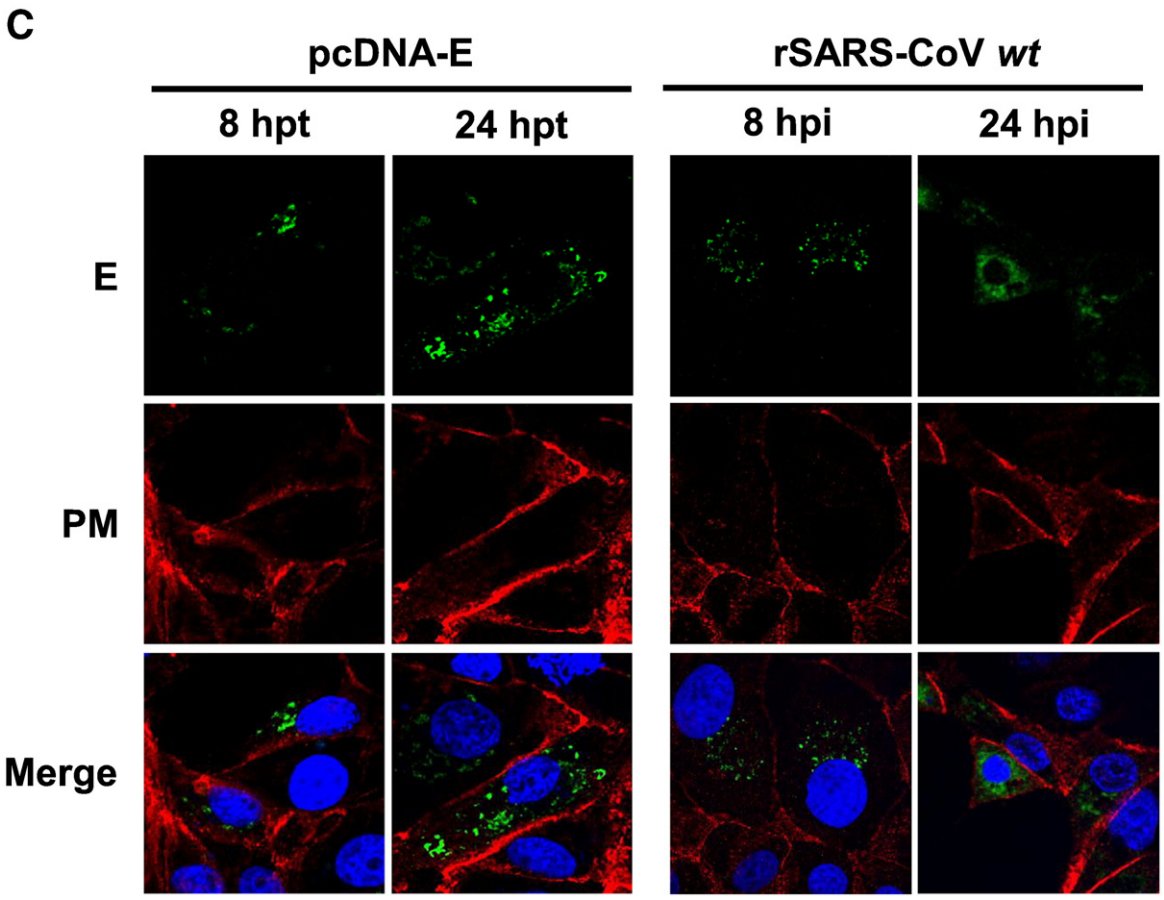

Fig. 3 (*continued*).

of SARS-CoV E protein within cell membranes, antibodies specific for the Ent or Ect domains were used in immunofluorescence assays on detergent permeabilized cells. Vero E6 cells transfected with plasmids expressing E protein or infected with SARS-CoV *wt* were processed either without permeabilization, after permeabilizing their plasma membrane by using digitonin, or after permeabilizing plasma and intracellular membranes by using Triton X-100. An antibody recognizing the cytoplasmic protein β-tubulin, and another one specific for the luminal endoplasmic reticulum protein PDI were used as controls of permeabilization of the plasma membrane or intracellular membranes. The selective permeabilization of the plasma membrane by using digitonin led to the detection of SARS-CoV Ect domain in cells transfected with a plasmid encoding E protein and in SARS-CoV *wt*-infected cells (Fig. 8). Under these conditions, the cytosolic protein β-tubulin was also detected, in contrast to the luminal ER protein PDI that was not accessible, as expected (Fig. 8). Permeabilization of plasma and intracellular membranes with Triton X-100 allowed the detection of SARS-CoV Ect domain, β-tubulin and PDI, as expected (Fig. 8). These experiments were repeated several times with identical results indicating that SARS-CoV Ect domain was exposed towards the cell cytoplasm. In contrast, SARS-CoV Ent domain was only detected when transfected or infected cells were permeabilized with Triton X-100, indicating that this domain must only be exposed towards the luminal side (Fig. 8). Overall, these data indicated that SARS-CoV E protein has a topological conformation spanning the intracellular membranes only once exposing its carboxy terminal domain towards the cell cytoplasm and the amino terminal domain towards the lumen of intracellular membranes.

Discussion

A polyclonal antiserum specific for the SARS-CoV E protein amino terminus, and a set of monoclonal antibodies specific for the SARS-CoV E protein carboxy terminus have been generated. Using these antibodies, SARS-CoV E protein was shown to localize essentially in the ERGIC when expressed alone or in the context of SARS-CoV infection. No evidence for the presence of the SARS-CoV E protein at the plasma membrane has been found by using four complementary approaches. In addition, a topological model for SARS-CoV E protein in which E protein spans intracellular membranes only once and exposes the amino terminal domain towards the lumen of intracellular membranes and the carboxy terminal domain towards the cytoplasm has been proposed.

CoV E protein is involved in virus budding, morphogenesis and intracellular trafficking and possesses ion channel activity (DeDiego et al., 2007; Ortego et al., 2007; Wilson et al., 2006). In previous publications, different authors have proposed alternative cellular locations (ER, Golgi membranes, and plasma membrane) or topologies (spanning membranes once or twice) for SARS-CoV E protein (Liao et al., 2006; Nal et al., 2005; Pervushin et al., 2009; Yuan et al., 2006). To clarify this point, we focused on the subcellular location and topology of SARS-CoV E protein in transfected and infected cells.

In this work, using mAbs specific for the SARS-CoV E protein, and Vero E6 cells, susceptible to SARS-CoV infection, it was shown that E protein was mainly located in the ERGIC at early times (8 and 16 hpi or hpt). Moreover, it was shown that this distribution was extremely similar when E protein was expressed alone from a DNA plasmid or

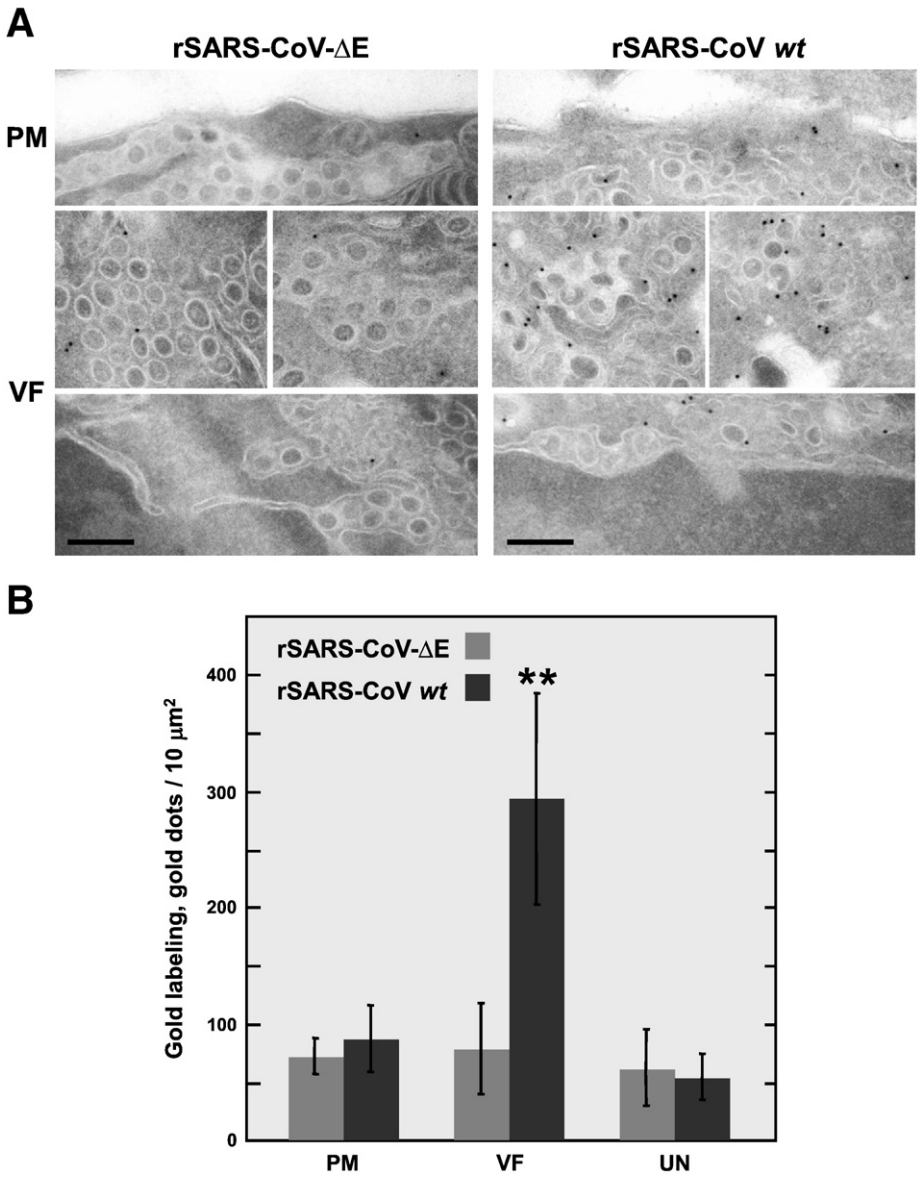

Fig. 4. Analysis of SARS-CoV E protein subcellular localization by immunoelectron microscopy. Vero E6 cells were infected with rSARS-CoV *wt* or rSARS-CoV-ΔE. At 16 hpi cells were fixed with 4% paraformaldehyde and 0.125% glutaraldehyde, scrapped and pelleted. Pellets were processed and sectioned. (A) Ultrathin cryosections were incubated with mAb E5 and an anti-mouse secondary antibody labeled with 10 nm colloidal gold. PM (plasma membrane), VF (Viral factories). Bars 200 nm. (B) Around 800 gold dots were counted in several images of rSARS-CoV-ΔE or rSARS-CoV *wt*-infected cells. Gold labeling is represented as gold dots per surface units (10 μm^2) at the plasma membrane (PM), the viral factories (VF) and at unspecific locations (UN) such as the cell nucleus or mitochondrion, which represent the background displayed by the antibody. Statistically significant data are indicated with two asterisks (Student's t-test p-value$<$0.01).

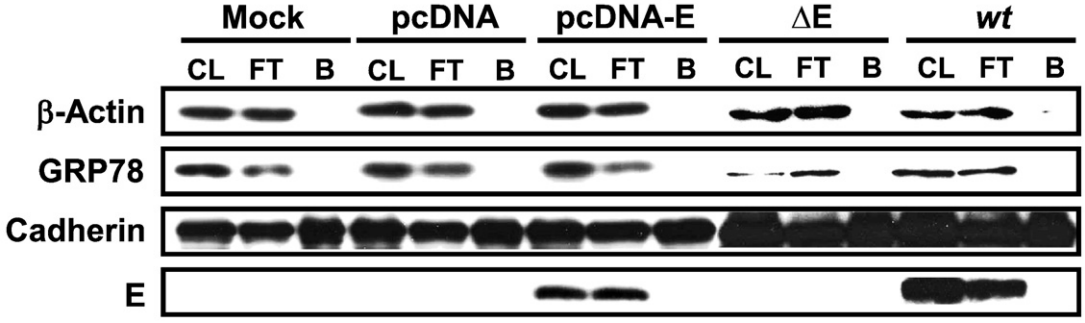

Fig. 5. Analysis of SARS-CoV E protein presence at the plasma membrane by cell surface protein biotinylation and purification assay. Vero E6 cells were either mock transfected, transfected with a plasmid encoding E protein (pcDNA-E) or with an empty plasmid as a control (pcDNA), or infected with rSARS-CoV *wt* (*wt*) or with rSARS-CoV-ΔE (ΔE) as a control. Plasma membrane proteins were biotin labeled and cells were lysed. Cell lysates (CL) were incubated with an avidin resin, and biotinylated cell surface proteins were isolated (B). Non-biotinylated proteins were discarded and eluted in the flow through (FT). CL, FT and B fractions were analyzed by Western blot using antibodies specific for the intracellular proteins β-actin and GRP78, the plasma membrane protein cadherin and SARS-CoV E protein.

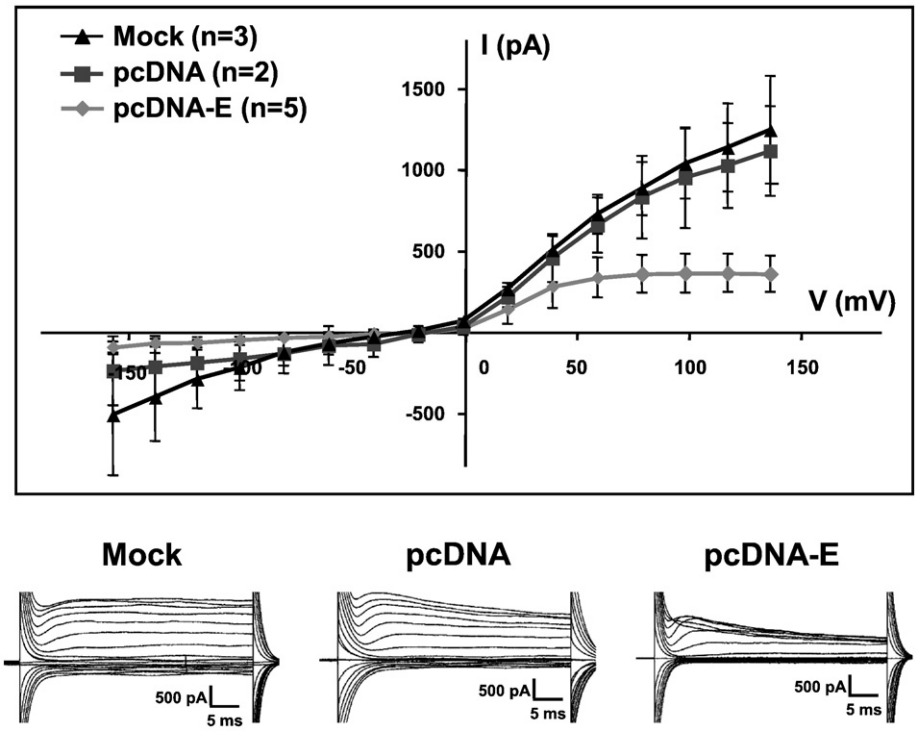

Fig. 6. Whole-cell patch clamp. HEK-293T cells were mock transfected (Mock), transfected with an empty plasmid (pcDNA) or transfected with a plasmid encoding SARS-CoV E protein (pcDNA-E). At 24 hpt cells were voltage clamped, and stepped from −160 mV to +140 mV in 20 mV increments with pulses of 40 ms from a resting potential of −40 mV. Current intensity was plotted against voltage. Currents values were measured at 30 ms, standard deviations are shown. Lower panels show examples of original recordings from each cell type.

after SARS-CoV infection, indicating that other viral proteins did not significantly affected the subcellular location of E protein. At late times, (between 24 and 48 hpi or hpt) 30 to 40% of the cells expressing E protein showed a broader distribution, possibly involving other cell compartments apart from the ERGIC, which might correspond to Golgi modified membranes, similarly to what has been described previously (Liao et al., 2006). The accumulation of E protein at the ER was only found occasionally in infected cells. These data indicated that E protein did not accumulate within this compartment. In contrast to our observations, other reports described that SARS-CoV E protein colocalized with ER and Golgi markers (Liao et al., 2006; Nal et al., 2005). The apparent discrepancies between our results and previous publications, may be explained by the strength of the expression system used, by the use of different cell lines, by performing the studies at different time points and by the use of different tagged versions of E protein. Nevertheless, in the publications by other authors, E protein location was not analyzed in cells infected with SARS-CoV, as done in this paper.

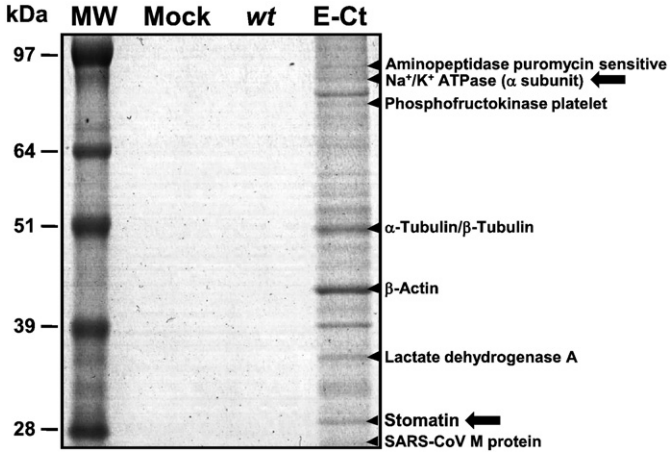

Fig. 7. Identification of proteins interacting with SARS-CoV E protein. Vero E6 cell extracts from mock-infected cells (Mock) or cells infected with rSARS-CoV *wt* or rSARS-CoV-EtagCt (E-tag) were used in a double affinity chromatography. Purified proteins were detected by using Coomassie blue gels. Bands were excised from gels and identified by mass spectrometry. Arrows point Na^+/K^+ ATPase alpha 1 subunit and stomatin protein bands.

It has been reported that E protein displays ion channel activity in the plasma membrane of mammalian cells (Pervushin et al., 2009), which has indirectly suggested that E protein is present on the cell surface. Nevertheless, neither our results shown in this manuscript nor other published work (Nal et al., 2005; Yuan et al., 2006) have provided direct evidence showing the presence of SARS-CoV E protein in the plasma membrane. In fact, special attention was paid in this study to analyze whether SARS-CoV E protein was located in the plasma membrane. Immunofluorescence analysis of cells transfected with a plasmid encoding E protein and SARS-CoV-infected cells, revealed that E protein did not accumulate at the plasma membrane neither at early (8 and 16 hpt or hpi) nor at late time points (24 and 48 hpt or hpi). In addition, immunofluorescence using non-permeabilized cells and antibodies specific for the amino or carboxy terminal domains of E protein did not reveal any specific staining at the cell surface. To reinforce these data immunoelectron microscopy was performed. E protein was identified intracellularly in infected cells, close to viral factories, whereas no significant labeling was observed at the plasma membrane. To further study the possible presence of E protein in the plasma membrane, cell surface proteins were biotinylated and isolated. Protein biotinylation was achieved by using a compound that binds covalently to primary amines, present in lysines side chain and in the protein N-terminal amino acid. If SARS-CoV E protein would be displayed in the plasma membrane, it should expose its amino terminal domain towards the outside of the cell, taking into account our purposed topological conformation. No lysine residues are contained within SARS-CoV E protein amino terminal domain. Nevertheless, the amino group of the

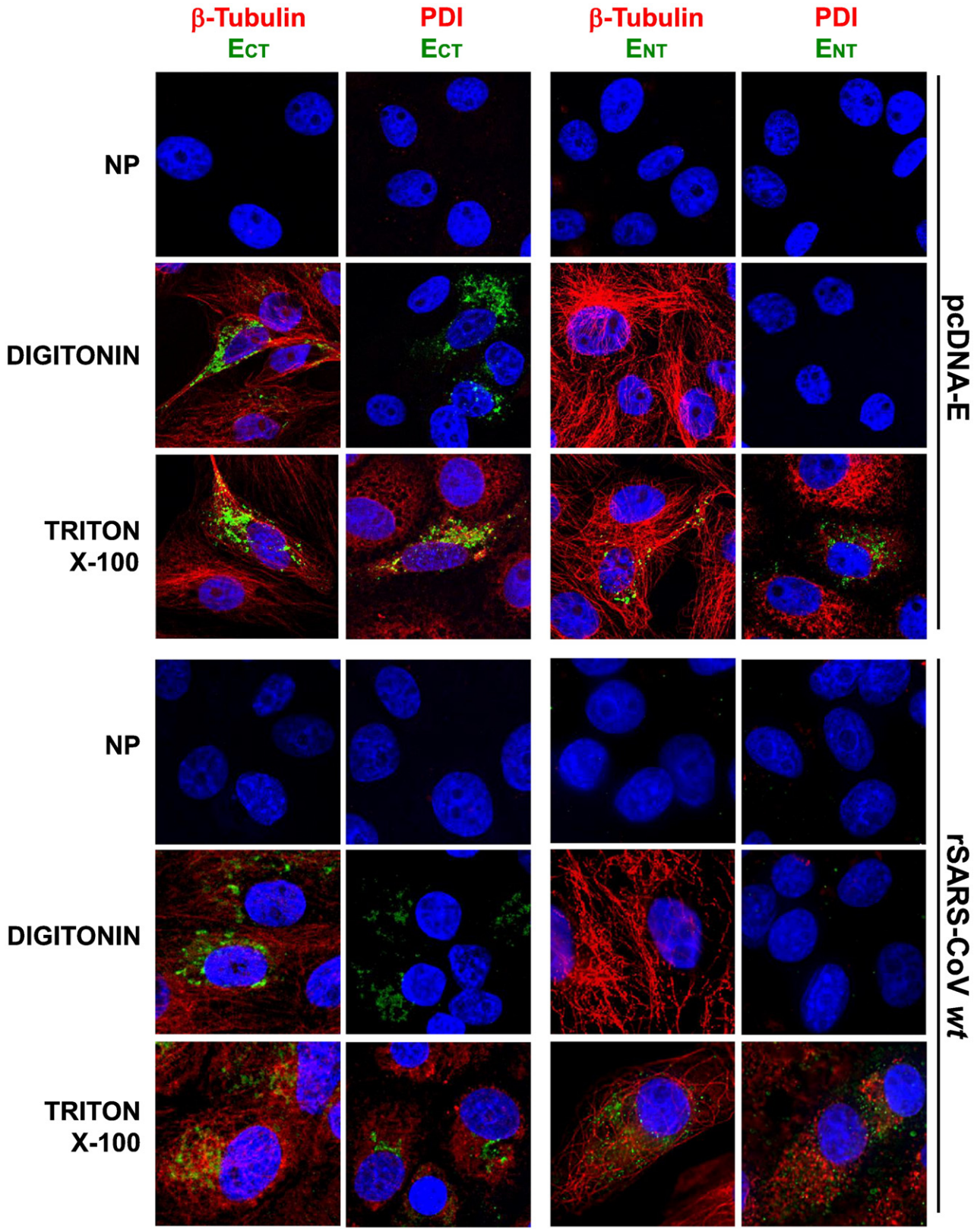

Fig. 8. SARS-CoV E protein topology. Vero E6 cells expressing E protein alone (pcDNA-E) or in an infection context (rSARS-CoV *wt*) were alternatively processed with no permeabilization (NP), selectively permeabilizing plasma membrane by using digitonin or permeabilizing all cell membranes by using Triton X-100. Specific antibodies were used to label the E protein carboxy terminal domain (ECT, green), E protein amino terminal domain (ENT, green), the cytosolic protein β-tubulin (red) and the luminal ER protein PDI (red). Nuclei were stained with DAPI (blue). (For interpretation of the references to color in this figure legend, the reader is referred to the web version of this article.)

N-terminal amino acid would be a potential site of biotinylation. No evidence of biotinylated E protein was detected, indicating that E protein did not accumulate in the plasma membrane.

In order to investigate potential ion channel activity due to the presence of E protein at the cell surface, whole-cell patch clamp assay was performed as a functional approach to alternatively determine

whether SARS-CoV E protein is located at the plasma membrane. If E protein were acting as an ion channel activated by voltage in the plasma membrane, an increase in current intensities displayed by cells expressing E protein, as compared with control cells, would be expected. Interestingly, cells expressing E protein showed a decrease of current intensities as compared with control cells not expressing E protein, suggesting that this protein was not acting as an ion channel at the plasma membrane, and reinforcing the observation that E protein was not physically located within the plasma membrane. The fact that E protein decreased ion currents in the plasma membrane might be explained by an indirect influence of E protein on other cellular proteins involved in ion transport. Recently, in our laboratory, two cellular proteins involved in ion transport: Na^+/K^+ ATPase alpha 1 subunit and stomatin, have been identified as interacting partners of SARS-CoV E protein. Possibly, these interactions could lead to partial relocalization of these proteins and therefore to the observed reduction of ion transport, which may explain decreased voltage activated currents intensity detected by whole-cell patch clamp assays. Importantly, in agreement with our work, it has been shown that E protein does not display ion channel activity in a different experimental system, the plasma membrane of *Xenopus* oocytes (Ji et al., 2009) but decreases the levels and activity of human epithelial sodium channels, affecting ion transport at the plasma membrane level.

Overall, our results from four complementary approaches strongly suggest that SARS-CoV E protein did not accumulate at the plasma membrane during SARS-CoV infection, or when expressed alone, suggesting that the intrinsic activities of E protein should be displayed in the inner organelles and that plasma membrane permeabilization to monovalent ions (Pervushin et al., 2009) or to small weight compounds in E protein expressing cells (Liao et al., 2004, 2006; Madan et al., 2008), is most likely due to indirect effects. In fact, similar interpretations have been made for the increased plasma membrane permeability to small weight compounds by another viral protein with ion channel activity such as coxsackievirus 2B protein (Cornell et al., 2007; de Jong et al., 2006). This protein also locates in intracellular membranes, from where it alters protein trafficking by enhancing endocytosis processes resulting in the entry of small weight compounds. In other viral systems the intrinsic ion channel activity of specific viral proteins such as p7 protein of hepatitis C, was also restricted to intracellular membranes (Wozniak et al., 2010).

Two alternative SARS-CoV E protein topological conformations have been suggested. Studies using tagged versions of SARS-CoV E protein, suggested that this protein may have a cytosolic amino terminal domain and a carboxy terminal domain also facing the cytoplasm, or alternatively, in a minor proportion, an amino terminal cytosolic, and carboxy terminal luminal conformation, in intracellular membranes (Yuan et al., 2006). These topology models would correspond to the hairpin or to the single transmembrane pass conformations defined for SARS-CoV E protein transmembrane domain respectively (Arbely et al., 2004; Torres et al., 2006). In this work, by using highly specific antibodies for E protein amino terminal and carboxy terminal domains in selective permeabilization assays, we have clearly shown that E protein adopted an amino terminus luminal carboxy terminus cytosolic conformation in intracellular membranes of transfected and infected cells. The discrepancies on E protein amino terminus orientation with previous published data, could be due to the use of amino terminal tagged versions of E protein, which may affect the correct association of the protein with cell membranes. The model proposed here is only compatible with the single transmembrane pass described for SARS-CoV E protein, but in intracellular membranes.

Materials and methods

Viruses

The recombinant parental virus (rSARS-CoV *wt*) and a virus that lacks E gene (rSARS-CoV-ΔE) derived from the Urbani strain, were rescued from infectious cDNA clones and titrated as previously described (Almazan et al., 2006; DeDiego et al., 2007). Infections were performed in biosafety level 3 containment facilities by personnel wearing positive-pressure air-purifying respirators (HEPA AirMate; 3M, Saint Paul, MN).

Cells

The African green monkey kidney-derived Vero E6 cells were kindly provided by Eric Snijder (Medical Center, University of Leiden, The Netherlands). The human embryonic kidney-293T cells (HEK-293T) were kindly provided by Juan Ortín (CNB, Madrid, Spain).

Cells were grown at 37 °C with an atmosphere of 98% humidity, in Dulbecco's modified Eagle medium (DMEM, GIBCO) supplemented with 25 mM HEPES, 2 mM L-glutamine (SIGMA), 1% non-essential amino acids (SIGMA) and 10% fetal bovine serum (FBS, Biowhittaker).

Plasmids

The plasmid pcDNA 3.1 (+) was purchased from Invitrogen. The plasmid pcDNA-E, used to express SARS-CoV E protein, was engineered by inserting a PCR product containing the open reading frame (ORF) of SARS-CoV E gene, digested with the restriction endonucleases EcoRI and XhoI in the same sites of the pcDNA 3.1 (+) plasmid. A kozak sequence (GCCGCC) was placed immediately before the E protein ATG start codon, to improve protein translation efficiency.

Generation of monoclonal antibodies (mAbs) specific for SARS-CoV E protein

Three pairs of BALB/c mice females were respectively immunized with purified SARS-CoV E protein from one of the following sources: recombinant histidine-tagged SARS-CoV E protein, expressed using a baculovirus system; *Escherichia coli* purified E protein, obtained through the NIH Biodefense and Emerging Infections Research Resources Repository, NIAID, NIH: NR-4284; or chemically synthesized E protein, which was a gift from Jaume Torres (School of Biological Sciences, Nanyang Technological University, Singapore). Mice were immunized with three doses of 100, 50 and 50 μg of one source of protein at days 0, 21 and 35, respectively. Antigen was delivered intraperitoneally with complete Freund's adjuvant in the first immunization and with incomplete Freund's adjuvant in the following ones. Ten days after the last immunization, sera were analyzed by enzyme-linked immunosorbent assay (ELISA) using purified E protein from the three origins and by immunofluorescence using rSARS-CoV-infected Vero E6 cells. Mice that developed an antibody response to SARS-CoV E protein were selected and boosted with two consecutive doses of 40 μg of antigen. Three days later, animals were sacrificed, and spleens were collected and dissociated. Cell fusion with the murine myeloma cell line X63-Ag8.653 (Kearney et al., 1979) using the polyethylene glycol method was performed (Galfre and Milstein, 1981) and hybridomas were generated. Hybridomas were cultured in 96 multiwell plates using ClonaCell®-HY medium E (StemCell Technologies) supplemented with 10 μM azaserine. Ten days after seeding, culture supernatants were analyzed by ELISA, using the three sources of purified SARS-CoV E protein, and by immunofluorescence and Western blot, using SARS-CoV-infected cells. Hybridomas secreting specific antibodies were selected and cloned twice by limit dilution. Supernatants were analyzed 10–14 days after seeding as described above. mAbs purification from hybridoma culture supernatant was achieved by G protein affinity chromatography in HiTrap™ Protein G HP columns (GE Healthcare), and dialyzed against phosphate-buffered saline (PBS). Immunoglobulin subclass was determined by ELISA using specific antibodies against heavy chain of mouse immunoglobulins (IgG1, IgG2a, IgG2b, IgG3 and IgM) (Southern Biotech).

Generation of polyclonal antibodies (pAbs) specific for the amino terminal domain of SARS-CoV E protein

A synthetic peptide corresponding to the first 19 residues of SARS-CoV E protein (MYSFVSEETGTLIVNSVLC) was coupled to an eight branched polylysine core via a carboxy terminal cysteine to prepare multiple antigenic peptides (MAP) as described (Wilson et al., 2004). Two rabbits were immunized by Biogenes (Berlin, Germany) with 1, 0.5, 0.25 and 0.25 mg of the coupled peptide at days 1, 7, 14 and 28, respectively. Sera were collected and evaluated by ELISA, using the three sources of purified SARS-CoV E protein described above, and a peptide containing the amino terminal domain and four amino acids of the transmembrane domain of E protein (MYSFVSEETGTL). Sera were also analyzed by immunofluorescence and Western blot using pcDNA-E-transfected or SARS-CoV-infected Vero E6 cells. Rabbits producing E protein specific antibodies were boosted with 0.25 mg of coupled peptide at days 50 and 57. Final bleed sera of immunized animals were collected at day 64 and evaluated as previously described.

Confocal microscopy

Vero E6 cells were grown to 90% confluency on glass coverslips and infected with rSARS-CoV-ΔE or rSARS-CoV *wt* at a multiplicity of infection (moi) of 0.3. Alternatively, Vero E6 cells were grown to 70% confluency in 1 cm^2 wells and transfected with 1 μg of DNA using 1 μl of Lipofectamine 2000 (Invitrogen) according to the manufacturer's indications. At the indicated hours post infection (hpi) or post transfection (hpt), media were removed and cells were washed twice with PBS and fixed with 4% paraformaldehyde in PBS for 30 min at room temperature. Then, cells were washed twice with PBS and permeabilized for 10 min with 0.1% Triton X-100 in PBS. Primary antibody incubations were performed in PBS containing 10% FBS for 1 h 30 min at room temperature. Immunofluorescence was performed using mouse mAbs specific for E protein (dilution 1:5000), ERGIC53 (dilution 1:200, Alexis Biochemicals), protein disulfide isomerase (PDI, dilution 1:500, Abcam), β-tubulin (dilution 1:200, Sigma) and cadherin (dilution 1:500, Abcam). Rabbit pAbs specific for E protein (Alvarez et al., 2010), E protein amino terminal domain and PDI were used at 1:2000, 1:1000 and 1:500 dilution, respectively. Coverslips were washed four times with PBS between primary and secondary antibody incubations. Alexa 488- or Alexa 546-conjugated antibodies specific for the different species (dilution 1:500, Invitrogen) were incubated for 45 min at room temperature in PBS containing 10% FBS. Nuclei were stained using DAPI (dilution 1:200, Sigma). Coverslips were mounted in ProLong Gold anti-fade reagent (Invitrogen) and examined on a Leica SP5 confocal microscope (Leica Microsystems).

Western blot analysis

Proteins were resolved by sodium dodecyl sulfate-polyacrylamide gel electrophoresis (SDS-PAGE), transferred to a nitrocellulose membrane by wet immunotransfer and processed for Western blotting. The blots were probed using mouse mAbs specific for E protein (dilution 1:500), β-actin (dilution 1:10,000, Abcam), cadherin (dilution 1:1000, Abcam) and rabbit pAbs against E protein (dilution 1:6000) and GRP78 (1:1000, Abcam). Horseradish peroxidase-conjugated antibodies against the different species (dilution 1:40,000, Sigma) and the Immobilon Western chemiluminiscence substrate (Millipore) were used to detect bound antibodies. Chemiluminiscence was detected by exposure to Agfa X-ray film.

PEPSCAN analysis

SARS-CoV E protein sequence was represented in 34 peptides of 10 amino acids each, which overlapped in 8 amino acids with contiguous peptides. Peptides were synthesized on a cellulose membrane using the SPOT technique (Frank, 2002) at the CNB proteomics facility (Madrid, Spain). Membranes were processed as previously described for Western blot assays.

Immunoelectron microscopy

Vero E6 cells were grown to 90% confluency and infected with rSARS-CoV-ΔE or rSARS-CoV *wt* at an moi of 1. At 16 hpi, cells were fixed by adding 1 volume of fixative 2× (4% paraformaldehyde, 0.25% glutaraldehyde in sodium phosphate buffer [PB] 0.2 M pH 7.2) to the culture medium for 30 min at room temperature. Medium and fixative 2× mixture were replaced by a fixative 1× solution (2% paraformaldehyde, 0.125% glutaraldehyde in PB 0.1 M pH 7.2), and incubated for 1 h 30 min at 4 °C. Fixative was removed, and cells were scrapped and pelleted. After washing with PB containing 50 mM glycine, cells were embedded in 12% gelatine and infused in 2.3 M sucrose. Mounted gelatine blocks were frozen in liquid nitrogen. Thin sections were prepared in an ultracryomicrotome (Leica EM Ultracut UC6/FC6, Vienna, Austria). Ultrathin cryosections were collected with 2% methylcellulose in 2.3 M sucrose. Cryosections were incubated at room temperature on drops of 2% gelatin in PBS for 20 min at 37 °C, followed by 50 mM glycine in PBS during 15 min, 10% FBS in PBS during 10 min and 5% FBS in PBS 5 min. Then, cryosections were incubated with SARS-CoV E protein specific mAb E5 (dilution 1:250) in PBS containing 5% FBS for 30 min at room temperature. After three washes with drops of PBS for 10 min, sections were incubated for 20 min using mouse IgG specific antibody coupled to 10 nm diameter colloidal gold particles using a 1:100 dilution in 5% FBS/PBS. Cryosections were washed three times with drops of PBS for 10 min and twice with distilled water. As a control for non-specific binding of the colloidal gold-conjugated antibody, the primary antibody was omitted. Cells were observed using a Jeol Electron Microscope (JEM 1020) with a CCD camera SIS Megaview III.

Plasma membrane protein biotinylation

Vero E6 cells were grown to 70% confluency in 75 cm^2 flasks and either mock transfected, or transfected with 37.5 μg of empty pcDNA 3.1 (+) or pcDNA-E plasmids using 37.5 μl of Lipofectamine 2000 (Invitrogen) according to manufacturer's instructions. In parallel, Vero E6 cells were grown to 90% confluency and infected with rSARS-CoV-ΔE or rSARS-CoV *wt* at an moi of 0.3. At 24 hpt or hpi, cell surface proteins were biotin labeled using the Cell Surface Protein Isolation Kit (Pierce) following the manufacturer's indications. Briefly, cells were rinsed twice with ice-cold PBS, and incubated with EZ-link Sulfo-NHS-SS-biotin for 15 min at 4 °C to biotinylate surface proteins. Reaction was quenched, cells were washed twice with PBS and scrapped. Cells were pelleted, lysed and cell extracts were clarified by centrifugation. Biotin labeled proteins were purified using affinity chromatography, by incubating cell extracts for 1 h with a neutravidin Sepharose resin. Resin was washed three times, and bound proteins were eluted by adding SDS-sample buffer.

Whole-cell patch clamp

HEK-293T cells were grown to 70% confluency in 12.5 cm^2 flasks and transfected with 12.5 μg of DNA using 37.5 μl of Lipofectamine 2000 (Invitrogen) according to manufacturer's indications. At 8 hpt cells were trypsinized and seeded onto poly-L-lysine coated glass coverslips. At 24 hpt whole-cell currents were recorded at room temperature using an Axopatch 1D amplifier (Axon instruments). Cells were placed in a bath solution containing (in mM): 5 KCl, 135 NaCl, 1 $MgCl_2$, 2 $CaCl_2$, 10 Glucose, 10 HEPES, and BSA 0.001% pH 7.4 and filled through the electrode with a solution containing (in mM): 110 KCl, 5 NaCl, 0.5 $CaCl_2$, 5 EGTA, 2 $MgCl_2$ and 10 HEPES pH 7.2. The voltage clamp protocol consisted of rectangular voltage steps of 40 ms

duration from −160 mV to +140 mV in 20 mV increments applied from a holding potential of −40 mV.

Pull-down assays

Vero E6 cells were grown to 90% confluence and mock infected, infected at an moi of 0.1 with rSARS-CoV *wt* or with a virus containing a tagged E protein (rSARS-CoV-ETagCt) for further purification of associated protein complexes (Alvarez et al., 2010). Cell extracts, tandem affinity purification and mass spectrometry were performed as previously described to identify SARS-CoV E bound proteins (Alvarez et al., 2010).

Plasma membrane selective permeabilization assays

Prior to fixation, cells were placed on ice and rinsed twice with KHM buffer (110 mM potassium acetate, 2 mM magnesium acetate, and 20 mM HEPES pH 7.2). After that, the plasma membrane of cells was selectively permeabilized with 25 μg/ml of digitonin (Sigma) in KHM buffer for 5 min at 4 °C. Then, cells were washed twice with KHM buffer, fixed with 4% paraformaldehyde in PBS for 30 min at room temperature and subjected to immunofluorescence as described before.

Acknowledgments

This work was supported by grants from the Ministry of Science and Innovation of Spain (BIO2007-60978 and BIO2010-16705), the European Community's Seventh Framework Programme (FP7/2007–2013) under the project "EMPERIE" EC Grant Agreement number 223498, U.S. National Institutes of Health (ARRA-W000151845) and Consejo Superior de Investigaciones Cientificas (CSIC) of Spain (CSIC-200920I016 and CSIC-201120E007). JLN received a fellowship from CSIC. We thank Monica Garcia-Gallo and Laura Martin for help in monoclonal antibody production and purification (Protein tools, CNB), Fernando Roncal (CNB, Proteomics facility) for his advice on PEPSCAN assays, Cristina Patiño and Javier Bueno for advise in immunoelectron microscopy assays (CNB, Electron Microscopy facility), Pedro de la Villa, Javier Vicente and Laura Ramirez (Physiology department, UAH, Madrid) for help in patch-clamp assays, Jaume Torres for provide reagents, Alberto Perez (Physiology department, UAM, Madrid) for the discussion of the manuscript and Marga Gonzalez for her technical assistance.

References

Almazan, F., DeDiego, M.L., Galan, C., Escors, D., Alvarez, E., Ortego, J., Sola, I., Zuñiga, S., Alonso, S., Moreno, J.L., Nogales, A., Capiscol, C., Enjuanes, L., 2006. Construction of a SARS-CoV infectious cDNA clone and a replicon to study coronavirus RNA synthesis. J. Virol. 80, 10900–10906.

Alvarez, E., DeDiego, M.L., Nieto-Torres, J.L., Jimenez-Guardeno, J.M., Marcos-Villar, L., Enjuanes, L., 2010. The envelope protein of severe acute respiratory syndrome coronavirus interacts with the non-structural protein 3 and is ubiquitinated. Virology 402, 281–291.

Arbely, E., Khattari, Z., Brotons, G., Akkawi, M., Salditt, T., Arkin, I.T., 2004. A highly unusual palindromic transmembrane helical hairpin formed by SARS coronavirus E protein. J. Mol. Biol. 341, 769–779.

Chu, D.K., Peiris, J.S., Chen, H., Guan, Y., Poon, L.L., 2008. Genomic characterizations of bat coronaviruses (1A, 1B and HKU8) and evidence for co-infections in Miniopterus bats. J. Gen. Virol. 89, 1282–1287.

Cornell, C.T., Kiosses, W.B., Harkins, S., Whitton, J.L., 2007. Coxsackievirus B3 proteins directionally complement each other to downregulate surface major histocompatibility complex class I. J. Virol. 81, 6785–6797.

Corse, E., Machamer, C.E., 2000. Infectious bronchitis virus E protein is targeted to the Golgi complex and directs release of virus-like particles. J. Virol. 74, 4319–4326.

de Haan, C.A.M., Smeets, M., Vernooij, F., Vennema, H., Pottier, P.J.M., 1999. Mapping of the coronavirus membrane protein domains involved in interaction with the spike protein. J. Virol. 73, 7441–7452.

de Jong, A.S., Visch, H.J., de Mattia, F., van Dommelen, M.M., Swarts, H.G., Luyten, T., Callewaert, G., Melchers, W.J., Willems, P.H., van Kuppeveld, F.J., 2006. The coxsackievirus 2B protein increases efflux of ions from the endoplasmic reticulum and Golgi, thereby inhibiting protein trafficking through the Golgi. J. Biol. Chem. 281, 14144–14150.

DeDiego, M.L., Alvarez, E., Almazan, F., Rejas, M.T., Lamirande, E., Roberts, A., Shieh, W.J., Zaki, S.R., Subbarao, K., Enjuanes, L., 2007. A severe acute respiratory syndrome coronavirus that lacks the E gene is attenuated in vitro and in vivo. J. Virol. 81, 1701–1713.

DeDiego, M.L., Pewe, L., Alvarez, E., Rejas, M.T., Perlman, S., Enjuanes, L., 2008. Pathogenicity of severe acute respiratory coronavirus deletion mutants in hACE-2 transgenic mice. Virology 376, 379–389.

Drexler, J.F., Gloza-Rausch, F., Glende, J., Corman, V.M., Muth, D., Goettsche, M., Seebens, A., Niedrig, M., Pfefferle, S., Yordanov, S., Zhelyazkov, L., Hermanns, U., Vallo, P., Lukashev, A., Muller, M.A., Deng, H., Herrler, G., Drosten, C., 2010. Genomic characterization of severe acute respiratory syndrome-related coronavirus in European bats and classification of coronaviruses based on partial RNA-dependent RNA polymerase gene sequences. J. Virol. 84, 11336–11349.

Drosten, C., Gunther, S., Preiser, W., van der Werf, S., Brodt, H.R., Becker, S., Rabenau, H., Panning, M., Kolesnikova, L., Fouchier, R.A., Berger, A., Burguiere, A.M., Cinatl, J., Eickmann, M., Escriou, N., Grywna, K., Kramme, S., Manuguerra, J.C., Muller, S., Rickerts, V., Sturmer, M., Vieth, S., Klenk, H.D., Osterhaus, A.D., Schmitz, H., Doerr, H.W., 2003. Identification of a novel coronavirus in patients with severe acute respiratory syndrome. N. Engl. J. Med. 348, 1967–1976.

Enjuanes, L., Almazan, F., Sola, I., Zuniga, S., 2006. Biochemical aspects of coronavirus replication and virus–host interaction. Annu. Rev. Microbiol. 60, 211–230.

Enjuanes, L., Gorbalenya, A.E., de Groot, R.J., Cowley, J.A., Ziebuhr, J., Snijder, E.J., 2008. The Nidovirales, Third Edition. In: Mahy, B.W.J., Van Regenmortel, M., Walker, P., Majumder-Russell, D. (Eds.), Encyclopedia of Virology, 5 vols.. Elsevier Ltd., Oxford, pp. 419–430.

Ewart, G.D., Sutherland, T., Gage, P.W., Cox, G.B., 1996. The Vpu protein of human immunodeficiency virus type 1 forms cation-selective ion channels. J. Virol. 70, 7108–7115.

Frank, R., 2002. The SPOT-synthesis technique. Synthetic peptide arrays on membrane supports—principles and applications. J. Immunol. Methods 267, 13–26.

Galfre, G., Milstein, C., 1981. Preparation of monoclonal antibodies: strategies and procedures. In: Langone, J.J., Van Vunakis, H. (Eds.), Immunochemical Techniques, Vol. 73. Academic Press, New York, pp. 3–46.

Godet, M., L'Haridon, R., Vautherot, J.F., Laude, H., 1992. TGEV coronavirus ORF4 encodes a membrane protein that is incorporated into virions. Virology 188, 666–675.

Gosert, R., Kanjanahaluethai, A., Egger, D., Bienz, K., Baker, S.C., 2002. RNA replication of mouse hepatitis virus takes place at double-membrane vesicles. J. Virol. 76, 3697–3708.

Huang, C., Ito, N., Tseng, C.T., Makino, S., 2006. Severe acute respiratory syndrome coronavirus 7a accessory protein is a viral structural protein. J. Virol. 80, 7287–7294.

Huang, C., Peters, C.J., Makino, S., 2007. Severe acute respiratory syndrome coronavirus accessory protein 6 is a virion-associated protein and is released from 6 protein-expressing cells. J. Virol. 81, 5423–5426.

Ji, H.L., Song, W., Gao, Z., Su, X.F., Nie, H.G., Jiang, Y., Peng, J.B., He, Y.X., Liao, Y., Zhou, Y.J., Tousson, A., Matalon, S., 2009. SARS-CoV proteins decrease levels and activity of human ENaC via activation of distinct PKC isoforms. Am. J. Physiol. Lung Cell. Mol. Physiol. 296, L372–L383.

Kaplan, J.H., 2002. Biochemistry of Na,K-ATPase. Annu. Rev. Biochem. 71, 511–535.

Kearney, J.F., Radbruch, A., Liesegang, B., Rajewsky, K., 1979. A new mouse myeloma cell line that has lost immunoglobulin expression but permits the construction of antibody-secreting hybrid cell lines. J. Immunol. 123, 1548–1550.

Kuo, L., Masters, P.S., 2003. The small envelope protein E is not essential for murine coronavirus replication. J. Virol. 77, 4597–4608.

Li, W., Moore, M.J., Vasilieva, N., Sui, J., Wong, S.K., Berne, M.A., Somasundaran, M., Sullivan, J.L., Luzuriaga, K., Greenough, T.C., Choe, H., Farzan, M., 2003. Angiotensin-converting enzyme 2 is a functional receptor for de SARS coronavirus. Nature 426, 450–454.

Liao, Y., Lescar, J., Tam, J.P., Liu, D.X., 2004. Expression of SARS-coronavirus envelope protein in *Escherichia coli* cells alters membrane permeability. Biochem. Biophys. Res. Commun. 325, 374–380.

Liao, Y., Yuan, Q., Torres, J., Tam, J.P., Liu, D.X., 2006. Biochemical and functional characterization of the membrane association and membrane permeabilizing activity of the severe acute respiratory syndrome coronavirus envelope protein. Virology 349, 264–265.

Lim, K.P., Liu, D.X., 2001. The missing link in coronavirus assembly. Retention of the avian coronavirus infectious bronchitis virus envelope protein in the pre-Golgi compartments and physical interaction between the envelope and membrane proteins. J. Biol. Chem. 276, 17515–17523.

Madan, V., Castello, A., Carrasco, L., 2008. Viroporins from RNA viruses induce caspase-dependent apoptosis. Cell. Microbiol. 10 (2), 437–451.

Maeda, J., Repass, J.F., Maeda, A., Makino, S., 2001. Membrane topology of coronavirus E protein. Virology 281, 163–169.

Masters, P.S., 2006. The molecular biology of coronaviruses. Adv. Virus Res. 66, 193–292.

Muller, M.A., Paweska, J.T., Leman, P.A., Drosten, C., Grywna, K., Kemp, A., Braack, L., Sonnenberg, K., Niedrig, M., Swanepoel, R., 2007. Coronavirus antibodies in African bat species. Emerg. Infect. Dis. 13, 1367–1370.

Nal, B., Chan, C., Kien, F., Siu, L., Tse, J., Chu, K., Kam, J., Staropoli, I., Crescenzo-Chaigne, B., Escriou, N., van der Werf, S., Yuen, K.Y., Altmeyer, R., 2005. Differential maturation and subcellular localization of severe acute respiratory syndrome coronavirus surface proteins S, M and E. J. Gen. Virol. 86, 1423–1434.

Narayanan, K., Maeda, A., Maeda, J., Makino, S., 2000. Characterization of the coronavirus M protein and nucleocapsid interaction in infected cells. J. Virol. 74, 8127–8134.

Netland, J., DeDiego, M.L., Zhao, J., Fett, C., Alvarez, E., Nieto-Torres, J.L., Enjuanes, L., Perlman, S., 2010. Immunization with an attenuated severe acute respiratory syndrome coronavirus deleted in E protein protects against lethal respiratory disease. Virology 399, 120–128.

Nguyen, V.-P., Hogue, B.G., 1997. Protein interactions during coronavirus assembly. J. Virol. 71, 9278–9284.

Ortego, J., Escors, D., Laude, H., Enjuanes, L., 2002. Generation of a replication-competent, propagation-deficient virus vector based on the transmissible gastroenteritis coronavirus genome. J. Virol. 76, 11518–11529.

Ortego, J., Ceriani, J.E., Patino, C., Plana, J., Enjuanes, L., 2007. Absence of E protein arrests transmissible gastroenteritis coronavirus maturation in the secretory pathway. Virology 368, 296–308.

Pervushin, K., Tan, E., Parthasarathy, K., Lin, X., Jiang, F.L., Yu, D., Vararattanavech, A., Soong, T.W., Liu, D.X., Torres, J., 2009. Structure and inhibition of the SARS coronavirus envelope protein ion channel. PLoS Pathog. 5, e1000511.

Pinto, L.H., Holsinger, L.J., Lamb, R.A., 1992. Influenza virus M2 protein has ion channel activity. Cell 69, 517–528.

Price, M.P., Thompson, R.J., Eshcol, J.O., Wemmie, J.A., Benson, C.J., 2004. Stomatin modulates gating of acid-sensing ion channels. J. Biol. Chem. 279, 53886–53891.

Quan, P.L., Firth, C., Street, C., Henriquez, J.A., Petrosov, A., Tashmukhamedova, A., Hutchison, S.K., Egholm, M., Osinubi, M.O., Niezgoda, M., Ogunkoya, A.B., Briese, T., Rupprecht, C.E., Lipkin, W.I., 2010. Identification of a severe acute respiratory syndrome coronavirus-like virus in a leaf-nosed bat in Nigeria. MBio 1, e00208–e00210.

Raamsman, M.J.B., Locker, J.K., de Hooge, A., de Vries, A.A.F., Griffiths, G., Vennema, H., Rottier, P.J.M., 2000. Characterization of the coronavirus mouse hepatitis virus strain A59 small membrane protein E. J. Virol. 74, 2333–2342.

Rota, P.A., Oberste, M.S., Monroe, S.S., Nix, W.A., Campganoli, R., Icenogle, J.P., Peñaranda, S., Bankamp, B., Maher, K., Chen, M.-H., Tong, S., Tamin, A., Lowe, L., Frace, M., DeRisi, J.L., Chen, Q., Wang, D., Erdman, D.D., Peret, T.C.T., Burns, C., Ksiazek, T.G., Rollin, P.E., Sanchez, A., Liffick, S., Holloway, B., Limor, J., McCaustland, K., Olsen-Rassmussen, M., Fouchier, R., Gunther, S., Osterhaus, A.D.M.E., Drosten, C., Pallansch, M.A., Anderson, L.J., Bellini, W.J., 2003. Characterization of a novel coronavirus associated with severe acute respiratory syndrome. Science 300, 1394–1399.

Sawicki, S.G., Sawicki, D.L., 1990. Coronavirus transcription: subgenomic mouse hepatitis virus replicative intermediates function in RNA synthesis. J. Virol. 64, 1050–1056.

Schaecher, S.R., Mackenzie, J.M., Pekosz, A., 2007. The ORF7b protein of SARS-CoV is expressed in virus-infected cells and incorporated into SARS-CoV particles. J. Virol. 81, 718–731.

Shen, S., Lin, P.S., Chao, Y.C., Zhang, A., Yang, X., Lim, S.G., Hong, W., Tan, Y.J., 2005. The severe acute respiratory syndrome coronavirus 3a is a novel structural protein. Biochem. Biophys. Res. Commun. 330, 286–292.

Snijder, E.J., van der Meer, Y., Zevenhoven-Dobbe, J., Onderwater, J.J., van der Meulen, J., Koerten, H.K., Mommaas, A.M., 2006. Ultrastructure and origin of membrane vesicles associated with the severe acute respiratory syndrome coronavirus replication complex. J. Virol. 80, 5927–5940.

Tooze, J., Tooze, S.A., Fuller, S.D., 1987. Sorting of progeny coronavirus from condensed secretory proteins at the exit from the trans-golgi network of atT20 cells. J. Cell Biol. 105, 1215–1226.

Torres, J., Parthasarathy, K., Lin, X., Saravanan, R., Liu, D.X., 2006. Model of a putative pore: the pentameric alpha-helical bundle of SARS coronavirus E protein in lipid bilayers. Biophys. J. 91, 938–947.

Torres, J., Maheswari, U., Parthasarathy, K., Ng, L., Liu, D.X., Gong, X., 2007. Conductance and amantadine binding of a pore formed by a lysine-flanked transmembrane domain of SARS coronavirus envelope protein. Protein Sci. 16, 2065–2071.

van der Hoek, L., Pyrc, K., Jebbink, M.F., Vermeulen-Oost, W., Berkhout, R.J., Wolthers, K.C., Wertheim-van Dillen, P.M., Kaandorp, J., Spaargaren, J., Berkhout, B., 2004. Identification of a new human coronavirus. Nat. Med. 10, 368–373.

van der Most, R.G., Spaan, W.J.M., 1995. Coronavirus replication, transcription, and RNA recombination. In: Siddell, S.G. (Ed.), The Coronaviridae. Plenum Press, New York, pp. 11–31.

Weiss, S.R., Navas-Martin, S., 2005. Coronavirus pathogenesis and the emerging pathogen severe acute respiratory syndrome coronavirus. Microbiol. Mol. Biol. Rev. 69, 635–664.

Wilson, L., McKinlay, C., Gage, P., 2004. SARS coronavirus E protein forms cation-selective ion channels. Virology 330, 322–331.

Wilson, L., Gage, P., Ewart, G., 2006. Hexamethylene amiloride blocks E protein ion channels and inhibits coronavirus replication. Virology 353, 294–306.

Wong, S.K., Li, W., Moore, M.J., Choe, H., Farzan, M., 2004. A 193-amino acid fragment of the SARS coronavirus S protein efficiently binds angiotensin-converting enzyme 2. J. Biol. Chem. 279, 3197–3201.

Wozniak, A.L., Griffin, S., Rowlands, D., Harris, M., Yi, M., Lemon, S.M., Weinman, S.A., 2010. Intracellular proton conductance of the hepatitis C virus p7 protein and its contribution to infectious virus production. PLoS Pathog. 6, e1001087.

Yuan, Q., Liao, Y., Torres, J., Tam, J.P., Liu, D.X., 2006. Biochemical evidence for the presence of mixed membrane topologies of the severe acute respiratory syndrome coronavirus envelope protein expressed in mammalian cells. FEBS Lett. 580, 3192–3200.

Ziebuhr, J., 2005. The coronavirus replicase. In: Enjuanes, L. (Ed.), Coronavirus Replication and Reverse Genetics, Vol. 287. Springer, pp. 57–94.

Ziebuhr, J., Snijder, E.J., Gorbalenya, A.E., 2000. Virus-encoded proteinases and proteolytic processing in the *Nidovirales*. J. Gen. Virol. 81, 853–879.

Zuñiga, S., Cruz, J.L., Sola, I., Mateos-Gomez, P.A., Palacio, L., Enjuanes, L., 2010. Coronavirus nucleocapsid protein facilitates template switching and is required for efficient transcription. J. Virol. 84, 2169–2175.